



Energy Storage with Energy Efficient Buildings and Districts: Optimization and Automation



Fariborz Haghghat
Operating Agent



Executive summary

The building sector accounted for 32% of the global energy consumption in 2010 which escalated up to 40% in 2018. This change in the trend of energy consumption in buildings not only increased the energy demand, but also increased the greenhouse gas (GHG) emissions (CO₂ from 19% in 2010 to 39% in 2017). To resolve this, efficient utilization of renewable energy sources is considered to be a potential alternative to meet the increasing energy demand in buildings. Statistical data conveys that the power generation from renewables grew by 17% in 2017, contributing to 8% of the global electricity. In addition, the concepts of district level generation, cogeneration systems together with the energy storage technologies and energy-efficient buildings have also been accepted globally by the building community to achieve the future goal of energy roadmap defined by the international energy agency (IEA).

At present, the energy requirements in buildings are majorly met from non-renewable sources where the contribution of renewable sources is still in its initial stage. Meeting the peak energy demand by non-renewable energy sources is highly expensive for the utility companies and it critically influences the environment through GHG emissions. In addition, renewable energy sources are inherently intermittent in nature. Therefore, to make both renewable and non-renewable energy sources more efficient in building/district applications, they should be integrated with energy storage systems.

Nevertheless, determination of the optimal operation and integration of energy storage with buildings/districts are not straightforward. The real strength of integrating energy storage technologies with buildings/districts is stalled by the high computational demand (or even lack of) tools and optimization techniques. Annex 31 aims to resolve this gap by critically addressing the challenges in integrating energy storage systems in buildings/districts from the perspective of design, development of simplified modeling tools and optimization techniques.

There are several well-established modeling approaches available at the building level. These include approaches such as heating degree day, energy use intensity and load factor, comprehensive (using simulation software) and simplified modeling, etc. Many of the existing simulation software (including but not limited to TRNSYS and Modelica) now have built-in options/libraries to accommodate energy storage in buildings. However, most of the existing models consider buildings as standalone systems, barely representing the complexity of an urban/district setting. This leads to over-simplification of the building model and less accuracy in

the results. In Annex 31 (Chapter 3), advanced concepts for effective modeling of buildings in urban setting are proposed. Moreover, innovative ideologies on simplified modeling of buildings (such as multiple linear regression) and their components (e.g. PCM heat exchangers, electrically heated floor, thermally activated walls, etc.) are presented as examples. Furthermore, the potential of PCM-based free cooling over the conventional district heating and cooling system is emphasized in terms of annual primary energy savings.

On the other hand, modeling a district not only includes several buildings, but also the interactions amongst them, with at least one heating/cooling network and at least one energy resource. If energy storage is also utilized, it should be included, too. Therefore, modeling at the district level is much more complicated and computationally intense, which requires sacrificing some accuracy compared to the building level. That is why simplified models have received considerable attention at the district level. Several tools have also been developed to achieve different objectives with diverse features and various levels of complexity. In this regard, Annex 31 recommends that screening of existing tools should be conducted (prior to modeling) to select and use the best one for that specific case. Note that the developed tools are often criticized for their limitations in terms of accuracy and frustrating computational time. To resolve this, a 4-step procedure has been developed in Annex 31 (Chapter 4) to accurately predict the demand profile of different types of district systems with high resolution (hourly interval) and in a timely manner. In addition, two levels of model validation (for the 4-step procedure) at the district level are illustrated as examples.

Once developed and validated, building/district models can then be used for system optimization based on various criteria. Generally, objective functions can be classified in two major categories of environmental (including GHG and pollutant production, energy efficiency, life cycle analysis, and thermal comfort) and cost. Multi-objective optimization at the district level is very common which (due to the complexity and size of the system) suffers from long computational time. Therefore, some methods have been introduced in Annex 31 (Chapter 5) to reduce this period for instance by the parallelism of the models, surrogating modeling and utilization of satisfaction functions. Besides, state-of-the-art optimization examples at the building/district levels are presented.

From the viewpoint of design as well as guidelines, standards and policy development, it is important to ensure that the value of a storage is correctly captured. In this way, the storage can be appropriately adopted to enhance the system performance and achieve the aims of resilient energy

systems with minimum emissions. To evaluate the effectiveness of energy storage technologies in building/district applications, key performance indicators (KPIs) can represent important methods for analyzing interactions among economic, human activity, energy consumption and reduction of GHG emissions. Despite the importance of KPIs, the lack of clear definition (even for well-known metrics such as efficiency) hinders their widespread application and prevents comparability of the obtained results. Therefore, ten main KPIs (i.e. storage capacity, recharging energy, maximum charging and discharging power, depth of discharge, durability, specific cost of storage, maximum self-discharge rate, storage size/weight, energy storage factor and generated energy/cost saving) are hereby developed (in Chapter 6) and used to evaluate the Annex 31 case studies. Ten case studies have been carried out in several participating countries including Canada, France, Italy, Japan, Turkey and UK. This international effort as part of Annex 31 revealed the potentials and challenges to use these KPIs.

The main contributions of Annex 31 lie on addressing the existing hindrance in developing simplified models, optimization tools and performance evaluation criteria related to energy efficient buildings/districts with energy storage. The results disseminated by this publication in terms of given examples in each domain (application of energy storage in buildings/districts, optimization techniques, etc.) and the ideology of representing KPIs for evaluating the effectiveness of energy storage in buildings and districts will benefit researchers in identifying and reducing the existing research gaps in designing, modeling and optimizing energy efficient buildings and districts with energy storage systems.

FARIBORZ HAGHIGHAT, Ph.D., P. Eng.
Professor,
Concordia University, Montreal, Canada
Operating Agent

Acknowledgements

The material presented in this publication has been collected, developed and prepared within the Annex 31 of the IEA Technology Collaboration Programs (TCPs), Energy Conservation through Energy Storage, “Energy storage with energy efficient buildings and districts: Optimization and automation”.

This report is the outcome of an international joint effort conducted in 11 countries (nine member countries and two associate member countries). All those have contributed to the project are gratefully acknowledged. The list of participating institutes can be found on pages IX and X. The Task Leaders have taken the lead of collecting information and writing the preliminary draft of the following chapters in this report. They are:

Authors

Chapter 3: Application to buildings

*Professor Paul Tuohy
Energy Systems Research Unit
Mechanical and Aerospace Engineering
University of Strathclyde*

Chapter 4: Application to districts

*Professor Paul Tuohy
Energy Systems Research Unit
Mechanical and Aerospace Engineering
University of Strathclyde*

Chapter 5: Optimization

*Professor Gilles Fraisse
LOCIE - CNRS UMR 5271
Polytech'Annecy-Chambéry - Université Savoie Mont Blanc
Campus Scientifique Savoie Technolac
INES - Bâtiment HELIOS*

Chapter 6: Key performance indicators

*Professor Claudio Del Pero
Politecnico Di Milano
Dept. of Architecture, Built Environment and Construction Engineering*

Special thanks to Dr. Mahmood Mastani Joybari and Dr. Karthik Panchabikesan for their help in the preparation of the final draft and their valuable suggestions.

The Operating Agent would like also to acknowledge the contributions of the following individuals to the work of this Annex:

■ Australia

- University of Tasmania
Saeid Seddegh

■ Canada

- Concordia University
Mahmood Mastani Joybari, Amine Lazrak, Dave Olsthoorn, Karthik Panchabikesan, Mohammad Sameti, Behrang Talebi, H el ene Thieblemont

■ Denmark

- Aalborg University
Alessandro Maccarini

■ France

- Universit  de Savoie
Ioannis Axaopoulos, Simon Rouchier, Bernard Souyri
-  cole Nationale des Travaux Publics de l' tat,
Letizia Roccamena, Nikolaos Stathopoulos

■ Italy

- Politecnico di Milano,
Samuele Grillo, Fabrizio Leonforte, Parsa Salehi Azari
- Politecnico di Torino
Maria Ferrera

■ Japan

- University of Tokyo
Wonjun Choi and Shintaro Ikeda

■ Slovenia

- University of Ljubljana
Rok Stropnik

■ Turkey

-  ukurova University
Kemal Cellat

■ UK

- University of Strathclyde
John Allison, Andrew Cowie, Graeme Flett, Nicolas Kelly, Andrew Lyden, Russell Pepper
- University of Cambridge
Bryn Pickering

The Operating Agent would like to express his gratitude to the Dean of Faculty of Engineering and the Office of VP research for providing support for his participation at the Exco meetings and the final report preparation.

Preface

The International Energy Agency (IEA) supports research and development projects for energy security, economic growth and environmental protection through Technology Collaboration Programs (TCPs). Energy Conservation through Energy Storage (ECES) - one of the 38 TCPs operating today - was established in 1978. To date, the following projects have been initiated by the executive committee of ECES (ongoing, planned and not materialized projects are identified by *, # and ^, respectively):

- Annex 1: Large scale thermal storage systems evaluation
- Annex 2: Lake storage demonstration plant in Mannheim
- Annex 3: Aquifer storage demonstration plant in Lausanne Dorigny
- Annex 4: Short term water heat storage systems
- Annex 5: Full scale latent heat storage installations
- Annex 6: Environmental and chemical aspects of thermal energy storage in aquifers and research and development of water treatment methods
- Annex 7: Innovative and cost effective seasonal cold storage applications
- Annex 8: Implementing underground thermal energy storage systems
- Annex 9: Electrical energy storage technologies for utility network optimization
- Annex 10: Phase change materials and chemical reactions for thermal energy storage
- Annex 12: High-temperature underground thermal energy storage (HT UTES)
- Annex 13: Design, construction and maintenance of UTES wells and boreholes
- Annex 14: Cooling with TES in all climates
- Annex 15[^]: Applying thermal and electrical energy storage in ultra-low energy buildings
- Annex 16[^]: Deployment of energy storage technologies
- Annex 17: Advanced TES techniques: Feasibility studies and demonstration projects
- Annex 18: Transportation of thermal energy utilizing thermal energy storage technology
- Annex 19: Optimised industrial process heat and power generation with thermal energy storage
- Annex 20: Sustainable cooling with thermal energy storage
- Annex 21: Thermal response test for underground thermal energy storages
- Annex 22: -----
- Annex 23: Applying energy storage in ultra-low energy buildings
- Annex 24: Material development for improved thermal energy storage systems
- Annex 25: Surplus heat management using advanced TES for CO₂ mitigation
- Annex 26: Electric energy storage: Future energy storage demand
- Annex 27^{*}: Quality management in design, construction and operation of borehole TES systems
- Annex 28^{*}: Distributed energy storages for the integration of renewable energies
- Annex 29: Compact Thermal Energy Storage
- Annex 30^{*}: Thermal Energy Storage for Cost-Effective Energy Management & CO₂ Mitigation
- Annex 31^{*}: Energy storage with energy efficient buildings and districts: Optimization and automation
- Annex 32[#]: Modeling of energy storage for simulation/optimization of energy systems
- Annex 33^{*}: Material and component development for thermal energy storage
- Annex 34[#]: Flexible sector coupling by energy storage implementation
- Annex 35[#]: Accelerating development for affordable domestic combined heat pump and storage systems

The mission of TCP Energy Conservation and Energy Storage (TCP ECES) is to facilitate integral research, development, implementation and integration of energy-storage technologies, to optimize the energy efficiency of all kinds of energy system and to enable the increasing use of renewable energy instead of fossil fuels.

Storage technologies are a central component in energy-efficient systems. Since energy storage is a cross-cutting issue, expert knowledge of many disciplines (energy supply and all end-use sectors, as well as distribution) must be taken into account. To use this widespread experience efficiently and gain benefits from the resulting synergies, high-level coordination is needed to develop suitable working plans and research goals. TCP ECES is responsible for fulfilling this important task. TCP ECES' strategic plan therefore includes research activities (strategies for scientific research and development, dissemination and market deployment), as well as coordination activities (aims and administration).

National contacts

MEMBER COUNTRIES:

■ Canada

- **Concordia University**
Fariborz Haghighat (*Operating Agent*)
Email: fariborz.haghighat@concordia.ca
- **Hydro-Quebec**
Alain Moreau
Email: moreau.alain2@ireq.ca

■ China

- **Hunan University**
Zhun (Jerry) Yu
Email: zhunyu@hnu.edu.cn

Guoqiang Zhang
Email: gqzhang@188.com
- **Southeast University**
Shuhong Li
Email: equart@163.com

■ Denmark

- **Aalborg University**
Alireza Afshari
Email: ala@sbi.aau.dk

■ France

- **Université de Savoie**
Gilles Fraisse (*Leader of Subtask B*)
Email: gilles.fraisse@univ-savoie.fr
- **École Nationale des Travaux Publics de l'État**
Mohamed El Mankibi
Email: elmankibi@entpe.fr

■ Italy

- **Politecnico di Milano**

Niccolo Aste

Email: niccolo.aste@polimi.it

Claudio Del Pero (*Leader of Subtask D*)

Email: claudio.delpero@polimi.it

- **Politecnico di Torino**

Enrico Fabrizio

Email: enrico.fabrizio@polito.it

■ Japan

- **University of Tokyo**

Ryozo Ooka

(*Leader of Subtask C*)

Email: ooka@iis.u-tokyo.ac.jp

■ Slovenia

- **University of Ljubljana**

Uroš Stritih

Email: uros.stritih@fs.uni-lj.si

■ Turkey

- **Çukurova University**

Halime Paksoy

Email: hopaksoy@cu.edu.tr

■ UK

- **University of Strathclyde**

Paul Tuohy

(*Leader of Subtask A*)

Email: paul.tuohy@strath.ac.uk

- **University of Cambridge**

Ruchi Chaudhary

Email: rc488@cam.ac.uk

- **University of Nottingham**

Parham A. Mirzaei

Email: parham.mirzaei_ahranjani@nottingham.ac.uk

ASSOCIATE MEMBERS:

■ Czech Republic

- **Brno University of Technology**

Milan Ostrý

Email: ostry.m@fce.vutbr.cz

Pavel Charvát

Email: charvat@fme.vutbr.cz

■ Estonia

- **Tallinn University of Technology**

Jarek Kurnitski

Email: ostry.m@fce.vutbr.cz

Table of contents

Executive summary	I
Acknowledgements	IV
Preface	VI
National contacts	VIII
Table of contents	XI
List of figures	XVI
List of tables	XXII
List of abbreviations	XXVI
Chapter 1: Introduction	1
1.1 Energy in buildings and districts	1
1.2 Necessity of energy storage	1
1.2.1 Profile smoothing	1
1.2.2 Time of use tariffs.....	2
1.2.3 Efficiency improvements.....	2
1.2.4 Seasonal variations	2
1.3 Content organization.....	2
Chapter 2: Energy storage technologies	4
2.1 Thermal energy storage	4
2.1.1 Sensible.....	5
2.1.2 Latent	6
2.1.3 Thermochemical	7
2.2 Electrical energy storage.....	8
2.2.1 Thermal.....	8
2.2.2 Chemical	8
2.2.3 Mechanical.....	9
2.2.4 Superconducting magnet	10
Chapter 3: Application to buildings	11
3.1 Fundamentals	14
3.1.1 Heating degree day	15
3.1.2 Energy use intensity and load factor.....	15
3.1.3 Comprehensive models.....	16

3.1.4	Simplified simulation models	16
3.1.5	Predictive models	16
3.2	Available tools	18
3.2.1	TRNSYS	18
3.2.2	eQUEST	19
3.2.3	EnergyPlus	19
3.2.4	Modelica	20
3.3	Examples	21
3.3.1	Simplified building load prediction	21
3.3.2	Electrically heated floor	27
3.3.3	Triplex tube heat exchanger with PCM	31
3.3.4	Shell and tube heat exchanger with PCM	37
3.3.5	Air-PCM heat exchanger	48
3.3.6	Water-PCM heat exchanger	51
3.3.7	Thermally activated wall panels containing PCM	54
3.3.8	High-temperature cooling system with PCM	57
3.3.9	Borehole heat exchanger	62
Chapter 4:	Application to districts	68
4.1	Elements	69
4.1.1	Energy resources	69
4.1.2	Distribution network	76
4.1.3	End-users	80
4.2	Fundamentals	80
4.2.1	Energy resources	81
4.2.2	Distribution network	81
4.2.3	User demand profile	86
4.3	Simplified 4-step prediction model	89
4.3.1	Limitations of current models	89
4.3.2	Model development	90
4.4	Available tools	94
4.4.1	Initial tool screening	94
4.4.2	Categorization of capabilities	98

4.4.3	Tool selection process	111
4.4.4	Shortcomings of available tools	115
4.5	Examples.....	116
4.5.1	Simplified district load prediction: inter-model comparison.....	116
4.5.2	Simplified district load prediction: case study	122
Chapter 5:	Optimization	131
5.1	Types of methods.....	133
5.1.1	Deterministic	133
5.1.2	Stochastic.....	134
5.1.3	Hybrid.....	135
5.2	Algorithms	135
5.2.1	Mixed-integer linear programming	135
5.2.2	Mixed-integer nonlinear programming	137
5.2.3	Dynamic programming.....	137
5.2.4	Quasi-Newton method.....	140
5.2.5	Nelder-Mead simplex method	140
5.2.6	Genetic algorithms.....	140
5.2.7	Particle swarm optimization	143
5.3	Objective functions	145
5.3.1	Environmental	146
5.3.2	Cost.....	149
5.3.3	Multi-objective	153
5.4	Decision parameters.....	155
5.4.1	Building and district optimization	157
5.4.2	Constraints	161
5.5	Available tools	169
5.5.1	AIMMS.....	169
5.5.2	GAMS.....	170
5.5.3	CPLEX.....	170
5.5.4	AMPL	170
5.5.5	Xpress	170
5.5.6	MATLAB/Simulink.....	170

5.5.7	LINGO.....	170
5.5.8	HOMER.....	170
5.5.9	SynCity	170
5.5.10	Neplan.....	171
5.5.11	MODEST.....	171
5.5.12	GenOpt.....	171
5.6	Problem classification.....	173
5.6.1	Optimal superstructures	177
5.6.2	Operation and planning	178
5.6.3	Distributed integration.....	179
5.6.4	Subsystem building blocks	180
5.7	Computational time deduction.....	180
5.7.1	Simulated period reduction.....	181
5.7.2	Parallelism models.....	183
5.7.3	Surrogate modeling.....	184
5.7.4	Satisfaction functions	185
5.8	Examples.....	186
5.8.1	Building level	186
5.8.2	District level	203
Chapter 6: Key performance indicators		225
6.1	Review of existing KPIs	226
6.2	Main KPIs.....	227
6.2.1	Storage capacity.....	227
6.2.2	Recharging energy	227
6.2.3	Maximum charging and discharging power	228
6.2.4	Depth of discharge.....	228
6.2.5	Durability.....	228
6.2.6	Specific cost of the storage	228
6.2.7	Maximum self-discharge rate	229
6.2.8	Storage size/weight.....	229
6.2.9	Energy storage factor.....	229
6.2.10	Generated energy/cost saving.....	230

6.3	Related KPIs	231
6.3.1	Fastest charge/discharge durations	231
6.3.2	Charging efficiency	231
6.3.3	Discharging efficiency.....	231
6.3.4	Total charging/discharging efficiency	232
6.3.5	Mass and volume densities of energy.....	232
6.3.6	Specific cost of the stored energy.....	232
6.4	Schematic representation	232
6.5	Advanced KPIs	234
6.5.1	KPIs capturing storage advantages.....	235
6.5.2	KPIs capturing storage disadvantages	239
6.6	Description of case studies	240
6.6.1	HIKARI project, France	241
6.6.2	LOCCIONI project, Italy.....	244
6.6.3	Electrically heated floor, Canada.....	245
6.6.4	PCM wall, Turkey	246
6.6.5	KOMCEE, Japan	249
6.6.6	Integral solar collector, France	250
6.6.7	WWHC District, UK	253
6.6.8	Tsukuba-Mirai, Japan	258
6.6.9	Nagoya University, Japan.....	259
6.6.10	T-building, Japan.....	260
6.7	KPI calculation for the Annex 31 case studies	261
Chapter 7: Conclusion.....		275
7.1	Concluding remarks.....	275
7.2	Achievements	276
7.3	Recommendations for the future work	276
References.....		277

List of figures

Figure 2.1: Common energy storage technologies and their storage mechanisms	4
Figure 3.1: Storage temperature and systems options	12
Figure 3.2: Taxonomy of FITS for coupled storage systems.....	13
Figure 3.3: Taxonomy of FITS for semi-decoupled and decoupled storage systems.....	14
Figure 3.4: Simulation (blue) versus prediction (red) graphs for heating demand profile [kWh] of B1 showing a one-month (Dec.) period (top) and an 8-day (in mid-Dec.) period (bottom)	24
Figure 3.5: Results for B1 showing residual against fitted values (left) and error histogram (right)	25
Figure 3.6: Simulation (blue) versus prediction (red) graph for heating demand profile [kWh] of B2 including the heating season (top) and 10 days period in late Dec. till early Jan. (bottom)	26
Figure 3.7: Results for B2 showing residual against fitted values (left) and error histogram (right)	26
Figure 3.8: Conventional configuration of a room in TRNSYS (left) and configuration with the added fictitious zone in TRNSYS (right).	28
Figure 3.9: Conventional configuration of an EHF (electrically heated floor) (left) and configuration of the floor in TRNSYS with the added fictitious zone and the wall gain (right)	28
Figure 3.10: Experimental building including its picture (left), and its zones (right)	29
Figure 3.11: Discretization of thermal mass around electric heating cables	30
Figure 3.12: Temperature distribution within the zone after 10 hours of continuous heating.....	30
Figure 3.13: Schematic representation of the triplex tube heat exchanger	33
Figure 3.14: Comparison of the steady solid-liquid interface for pure conduction model (left half) and combined conduction and natural convection model (right half) for the phase change material	37
Figure 3.15: Schematic representation of the STHXs	39
Figure 3.16: Schematic representation of two separate melting fronts for upper and lower halves	42
Figure 3.17: Flowchart of the novel front tracking method.....	43
Figure 3.18: Variation of the upper half liquid fraction versus PC model liquid fraction.....	44

Figure 3.19: Variation of the upper half liquid fraction versus the developed correlation.....	45
Figure 3.20: Liquid fraction variation for Case 17	45
Figure 3.21: Variation of the modified lower half liquid fraction versus modified PC model liquid fraction.....	47
Figure 3.22: Variation of the modified lower half liquid fraction versus the developed correlation	47
Figure 3.23: Verification of the developed correlations for the upper half (left) and modified lower half (right) liquid fractions	48
Figure 3.24: Schematic of the investigated heat storage unit (left) and the unit without the front and top walls revealing CSM panels (right).....	49
Figure 3.25: Schematics of the numerical model (left) and a computational domain (right).....	50
Figure 3.26: Effectiveness of an air-PCM heat exchanger in peak-shaving of ventilation air temperature	51
Figure 3.27: Latent heat thermal storage material package or gel pack (left), plastic case filled with gel packs (middle), and typical installation of the plastic cases into the isolated tank (right)	52
Figure 3.28: Schematic representation of the thermal storage system.....	52
Figure 3.29: Comparison of the temperature curves for the same point using MATLAB Simulink and ANSYS	53
Figure 3.30: Schematic representation of the experimental prototype	54
Figure 3.31: Comparison of the temperature curves for the same point between the experimental and the MATLAB Simulink results for the solidification (left) and melting (right) processes	54
Figure 3.32: Schematic representation of the thermally activated wall panel	55
Figure 3.33: Base plates with attached plastic tubes.....	56
Figure 3.34: Schematic of the wall panel model.....	56
Figure 3.35: Thermally activated panel on an external wall.....	57
Figure 3.36: Model validation (left) and thermal imaging results (right).....	57
Figure 3.37: Assembly of the PCM-based heat exchanger.....	58
Figure 3.38: Schematic representation of the computational domain for the PCM-based heat exchanger showing cells and direction of fluids and heat transfer.....	59

Figure 3.39: Modelica model of the thermal plant configuration including a reversible heat pump and a PCM-based heat exchanger.....	60
Figure 3.40: Annual primary energy use for the four configurations	61
Figure 3.41: Calculation domain, geometry of BHE, and boundary conditions.....	63
Figure 3.42: The coupled simulation scheme and data transfer among the simulation models ...	64
Figure 3.43: Schematic of heat balance on ground surface and flux components.....	65
Figure 3.44: Temperature distribution of horizontal sections at different depths at 6:00 PM on the 221st day in the 10th year: (a) $z = -2$ m, (b) $z = -10$ m, (c) $z = -50$ m, and (d) $z = -100$ m .	66
Figure 3.45: Temperature distribution of vertical sections at different y coordinates; (a) $y = 0$ m, and (b) $y = 6$ m ($y = -6$ m showed almost the same distribution).....	67
Figure 4.1: Share of low temperature heat demand in Europe met by DHSs [162]	68
Figure 4.2: Heat flow in the piping system.....	83
Figure 4.3: Predicting the heating demand schedule	93
Figure 4.4: The algorithm used to generate Districts 1-3	117
Figure 4.5: Simulation (blue) versus prediction (red) graphs for heating demand profile [kWh] of District 1 showing an 11-day (end of Dec.) period (top) and error histogram (bottom)...	119
Figure 4.6: Simulation (blue) versus prediction (red) graphs for heating demand profile [kWh] of District 2 showing an 11-day (end of Dec.) period (top) and error histogram (bottom)...	120
Figure 4.7: Simulation (blue) versus prediction (red) graphs for heating demand profile [kWh] of District 2 showing an 11-day (end of Dec.) period (top) and error histogram (bottom)...	121
Figure 4.8: Hybrid community-district heating system layout in Whitlawburn, Cambuslang, Scotland	123
Figure 4.9: Monthly consumption of individual units in Tower#1 (Arran tower).....	124
Figure 4.10: Outdoor temperature and HDD for the 2016-17 heating season (Nov 2016 to Feb 2017).....	125
Figure 4.11: Optimal number of archetypes	126
Figure 4.12: Clustering results for Tower#1	127
Figure 4.13: Energy demand from model prediction (orange) versus measured (blue) for Tower#2	128
Figure 4.14: Operational temperature of the underground network	128
Figure 4.15: Water flow rate versus outdoor temperature in the distribution network.....	129

Figure 4.16: Monthly heat loss projection of the distribution network	129
Figure 4.17: Accumulated predicted energy delivered versus actual generated energy in the boiler house.....	130
Figure 5.1: An exemplary Pareto approach for a 2D optimization.....	132
Figure 5.2: A framework for optimization at district level.....	133
Figure 5.3: Implicit calibration process	133
Figure 5.4: Optimization methods applied in building energy optimization studies [400]	135
Figure 5.5: Schematic representation of branch-and-bound method.....	136
Figure 5.6: Backward algorithm on the first step	138
Figure 5.7: Forward algorithm on all time intervals during one cycle	140
Figure 5.8: Coding of a chromosome using the genetic algorithms	141
Figure 5.9: One-point (top) and two-point crossover (bottom)	142
Figure 5.10: Common objective functions for building level optimization [400].....	146
Figure 5.11: Global approach for the optimized design of buildings over their lifetime [462]..	148
Figure 5.12: Organization of costs included in the global cost objective function [466].....	150
Figure 5.13: Illustration of the final value concept according to EN 15459 [467].....	152
Figure 5.14: Inputs and outputs for a system optimization.....	155
Figure 5.15: An example of cost function for slab insulation in the French market	158
Figure 5.16: Example of cost function for window packages in the Italian market	159
Figure 5.17: Classification of constraints in programming building and district energy optimization	162
Figure 5.18: TRNSYS-GenOpt coupling framework.....	173
Figure 5.19: Classification of district optimization problems	174
Figure 5.20: Flowchart of the general optimization process and the interaction between the computation and management units	181
Figure 5.21: Representation of the two approaches for system optimization (the only difference is the period of boundary conditions data, note that the solutions are different).....	182
Figure 5.22 Representation of a master-slave model and the interaction between the units	183
Figure 5.23 Master-slave model: parallelism approach based on dividing tasks according to optimization algorithms.....	184
Figure 5.24: Illustration of decision making aid with satisfaction functions.....	186

Figure 5.25: The future climate change scenarios [576].....	188
Figure 5.26: The heat demand (kWh) and internal temperature (max and mean) variations	188
Figure 5.27: General presentation of the adaptive sequential design (LHS: Latin hypercube sampling)	190
Figure 5.28: The satisfaction functions [0, 1] for all the optimal solutions.....	192
Figure 5.29: Links between the 62 individuals of the Pareto front and the performance criteria where a short distance between an individual node and criterion node means that high level of satisfaction.....	193
Figure 5.30: The 62 optimal solution nodes linked to the corresponding values of the decision parameters where variation range was divided into 3 partitions of +/++/+++	194
Figure 5.31: Comparison of solutions 1 and 2.....	194
Figure 5.32: Pictures of the reference building.....	197
Figure 5.33: Representation of parameters on the south front and section.....	198
Figure 5.34: All the resulted cost-optimal clouds, with indicated cost optimal levels	202
Figure 5.35: Simultaneous charging and discharging configuration	206
Figure 5.36: Step-wise charging and discharging configuration	207
Figure 5.37: Graphical representation of the case study district network.....	213
Figure 5.38: Graphical representation of SOS2 piecewise linearization where $f(x)$ is the sum of weighted values $\alpha_i f(x_i)$ and $\alpha_{i+1} f(x_{i+1})$, with all other values of α being zero	215
Figure 5.39: Graphical representation of 3D piecewise linearization where $f(\bar{x}, \bar{y})$ is the sum of weighted decision variables λ and μ applied to $f(x_i, y_j)$, $f(x_{i+1}, y_{j+1})$ and $f(x_{i+1}, y_j)$	216
Figure 5.40: Application of bounding a technology nonlinear curve under multiple straight lines to create a piecewise linear curve where (a) shows its effective use on a curve of continuously decreasing gradient, while (b) shows its ineffectiveness when applied to a more complex curve	217
Figure 5.41: Comparison of different methods to describe electricity consumption of an EC, from nonlinear to SVE where (a) shows consumption curve and piecewise linearization with five breakpoints, (b) shows root-mean-square error between the methods and the nonlinear curve	218

Figure 5.42: Comparison of different methods for describing the primary fuel consumption of an AHP and HRAR, from nonlinear to SVE, at different load rates where piecewise curves have five breakpoints	218
Figure 5.43: Comparison of different methods for describing the gas consumption and heat output of a CHP, from nonlinear to SVE, at different load rates where five breakpoints are given for piecewise curves	219
Figure 5.44: Configurations of modeling runs.....	219
Figure 5.45: Graphical representation of the simplified case study district network	220
Figure 5.46: Root-mean-square error between linearization methods and the nonlinear characteristic curve of CHP HTP, for full range of breakpoints	221
Figure 5.47: Technology output histograms for SVE and optimized piecewise model runs where full and zero loads are given as single points, with all other part load operation given in 10% increments.....	223
Figure 5.48: Energy supply technology investment portfolios at each location and in each season	224
Figure 6.1: Schematic representation of an energy storage system and the main KPIs	233
Figure 6.2: HIKARI project description with surface sharing.....	243
Figure 6.3: Picture of test buildings for demonstration of the novel composite walls in Adana, Turkey.....	247
Figure 6.4: Thermal camera images of mFDM panel (left) and the reference case (right)	248
Figure 6.5: Picture of the considered university building, (left) and process flow diagram (right)	250
Figure 6.6: The new concept of integral collector storage.....	251
Figure 6.7: Picture of the integral collector storage.....	252
Figure 6.8: Temperature and solar radiation profile (from May 24 to 29)	252
Figure 6.9: Current biomass and thermal storage operation	254
Figure 6.10: Temperature levels in thermal storage	255
Figure 6.11: Picture of WWHC multi-story flats.....	255
Figure 6.12: Picture of Viessman Pyrotec (740 kW).....	256
Figure 6.13: Picture of the thermal storage with 50,000 liters capacity (left) and the boiler house (right).....	256

List of tables

Table 1.1: Modeling requirements for different levels and domains.....	3
Table 2.1: Comparison of sensible heat and latent heat storages	7
Table 2.2: Chemical storage materials and reactions [39].....	8
Table 3.1: Characteristics of the buildings	22
Table 3.2: Statistical index to compare energy consumptions of the reference and modified buildings	29
Table 3.3: Thermophysical properties of RT31 [109]	33
Table 3.4: Geometrical properties of the STHXs [127].....	39
Table 3.5: Thermophysical properties of the PCMs [128]	40
Table 3.6: List of dimensionless parameters.....	40
Table 3.7: The investigated values of Stefan and shell-to-tube radius ratios	41
Table 3.8: Constants of Equation (3.24) for the upper half liquid fraction	45
Table 3.9: Constants of Equation (3.28) for the modified lower half liquid fraction	47
Table 3.10: Properties of the PCM (PureTemp 18).....	60
Table 3.11: Thermal properties used in the numerical model	63
Table 4.1: Recent case studies of available energy resources for district heating networks	70
Table 4.2: District heating system projects utilizing sensible seasonal heat storage.....	79
Table 4.3: Summary of the recent DHS modeling studies.....	85
Table 4.4: Parameters considered to model the demand profiles	88
Table 4.5: Summary of the method used for load prediction in DHS and type of building stocks	89
Table 4.6 Summary of the methods used for load prediction in DHS.....	90
Table 4.7: Summary of the accuracy level of the previous studies	90
Table 4.8: Initial tool screening process	96
Table 4.9: Tool input data characteristics	98
Table 4.10: Supply system technologies.....	100
Table 4.11: Design optimization, outputs, controls and DSM controls capabilities.....	101
Table 4.12: Storage and DSM general capabilities and underlying models	105
Table 4.13: Electrical and thermal storage technologies and models.....	106
Table 4.14: Practical considerations	110

Table 4.15: Output from application of tool selection process	114
Table 4.16: Description of District 1	118
Table 4.17: Description of District 2	118
Table 4.18: Description of District 3	118
Table 5.1: Recent studies of district heating systems classified by optimized variable	154
Table 5.2: Classification of optimization problems according to the criteria of decision parameters	156
Table 5.3: Decision parameters for energy systems in high performing buildings: energy production systems	160
Table 5.4: Decision parameters for energy systems in high performing buildings: storage, terminal units, ventilation	161
Table 5.5: Formulation for some common inequality constraints at district level: component inequality constraints.....	163
Table 5.6: Formulation for some common inequality constraints at district level: Network inequality constraints.....	164
Table 5.7: Some common constraints employed in recent district optimization studies.....	164
Table 5.8: Feasibility of combinations of decision parameters among energy systems in high-performance buildings: energy production systems.....	166
Table 5.9: Feasibility of combinations of decision parameters among energy systems in high-performance buildings: storage, terminal units, ventilation systems	167
Table 5.10: Feasibility of combinations of decision parameters among energy systems in high-performance buildings	168
Table 5.11: Some tools for optimization of buildings [502].....	169
Table 5.12: Summary of optimization approach in some recent district optimization studies...	175
Table 5.13: Summary of technologies under consideration in some recent district optimization studies	176
Table 5.14: The objective functions.....	191
Table 5.15: The decision parameters	191
Table 5.16: Definition, variability range and step for parameters of the envelope systems.....	198
Table 5.17: Description of window types used for parameters WT, WTR and WTS	198
Table 5.18: Energy efficiency measures concerning building technical systems (TSs).....	199

Table 5.19: Combination of envelope and technical systems.....	199
Table 5.20: Investment, installation and replacement costs of the technical systems	200
Table 5.21: Annual costs calculation assumptions	200
Table 5.22: Set of parameter values related to relevant cost optimal points	203
Table 5.23: Optimization results for Scenario 1	210
Table 5.24: Fraction of the occupants' types in different scenarios	210
Table 5.25: Performance of the optimized system under new demand profile load.....	211
Table 5.26: Optimization results for Scenario 2	211
Table 5.27: Comparison of the equipment size, cost for different design strategies	211
Table 5.28: Model supply technologies and their consumption/production energy.....	213
Table 5.29: Characteristics of the buildings in the case study district.....	214
Table 5.30: Objective function value in GBP for all run configurations.....	221
Table 5.31: Model runtime in seconds for all configurations, including pre-processing and subsequent MILP solving in CPLEX	222
Table 5.32: Capacity of distribution network to, and storage at, both demand locations.....	224
Table 6.1: Short-term demand response KPIs	236
Table 6.2: Load shaping for demand to supply optimization KPIs	237
Table 6.3: Local building or district supply optimization KPIs.....	238
Table 6.4: Plant optimization KPIs.....	239
Table 6.5: Enhanced service KPIs	239
Table 6.6: HIKARI surface sharing between buildings and activities.....	243
Table 6.7: KPI values for HIKARI project, France, storage 1: chilled water storage (thermal storage)	262
Table 6.8: KPI values for HIKARI project, France, storage 2: electrical energy storage (electrochemical storage).....	263
Table 6.9: KPI values for LOCCIONI project, Italy	264
Table 6.10: KPI values for electrically heated floor, Canada	265
Table 6.11: KPI values for PCM wall, Turkey	266
Table 6.12: KPI values for KOMCEE, Japan	267
Table 6.13: KPI values for integral solar collector, France	268
Table 6.14: KPI values for biomass district heating with thermal storage, UK	269

Table 6.15: KPI values for Tsukuba-Mirai, Japan	270
Table 6.16: KPI values for Nagoya University, Japan.....	271
Table 6.17: KPI values for T-building, Japan.....	272
Table 6.18: Percentage of the case studies in which the KPI was correctly calculated using the available information.....	273

List of abbreviations

Abbreviation	Description
<i>3GDHS</i>	Third generation district heating system
<i>4GDHS</i>	Fourth generation district heating system
<i>AHP</i>	Air source heat pump
<i>AI</i>	Artificial intelligence
<i>ANN</i>	Artificial neural network
<i>APF</i>	Advanced pulverized fuel
<i>AR</i>	Autoregressive
<i>ARMA</i>	Autoregressive moving average
<i>ASHRAE</i>	American society of heating, refrigeration and air conditioning engineers
<i>ATES</i>	Aquifer thermal energy storage
<i>BHE</i>	Borehole heat exchanger
<i>BSM</i>	Building stock model
<i>BTES</i>	Borehole thermal energy storage
<i>CAES</i>	Compressed air energy storage
<i>CCHP</i>	Combined cooling, heat and power
<i>CCNC</i>	Combined conduction and natural convection
<i>CCGT</i>	Combined cycle gas turbine
<i>CFB</i>	Circulation fluidized bed
<i>CFD</i>	Computational fluid dynamics
<i>CHP</i>	Combined heat and power
<i>CHTF</i>	Cold heat transfer fluid
<i>COP</i>	Coefficient of performance
<i>CPEA</i>	Clustering Pareto evolutionary algorithm
<i>CSHPSS</i>	Central solar heating plants with seasonal storage
<i>CSB</i>	Case study building
<i>CSM</i>	Compact storage module
<i>DC</i>	Dry cooler
<i>DDM</i>	Degree-day method
<i>DH</i>	District heat
<i>DHC</i>	District heating/cooling
<i>DHS</i>	District heating system
<i>DHW</i>	Domestic hot water
<i>DOD</i>	Depth of discharge
<i>DOE</i>	Department of energy
<i>DP</i>	Dynamic programming
<i>DR</i>	Demand response
<i>DSM</i>	Demand side management
<i>EA</i>	Evolutionary algorithms

<i>EEM</i>	Energy efficiency measure
<i>EER</i>	Energy efficiency ratio
<i>EHF</i>	Electrically heated floor
<i>ESS</i>	Energy storage system
<i>EUI</i>	Energy use intensity
<i>FC</i>	Fuel cell
<i>FES</i>	Flywheel energy storage
<i>FITS</i>	Fabric integrated thermal storage
<i>FNN</i>	Fuzzy neural network
<i>GA</i>	Genetic algorithms
<i>GDHS</i>	Geothermal district heating system
<i>GHE</i>	Ground heat exchanger
<i>GHG</i>	Greenhouse gas
<i>GIS</i>	Geographic information system
<i>GSHP</i>	Ground source heat pump
<i>H-CDHS</i>	Hybrid community district heating system
<i>HDD</i>	Heating degree day
<i>HHTF</i>	Hot heat transfer fluid
<i>HOB</i>	Heat-only boilers
<i>HP</i>	Heat pump
<i>HRAR</i>	Heat recovery absorption refrigerator
<i>HTF</i>	Heat transfer fluid
<i>HTP</i>	Heat to power
<i>HVAC</i>	Heating ventilation and air conditioning
<i>ICS</i>	Integrated collector storages
<i>KPI</i>	Key performance indicator
<i>KR</i>	Kriging
<i>LCA</i>	Life cycle analysis
<i>LCC</i>	Life cycle cost
<i>LF</i>	Load factor
<i>LHS</i>	Latent heat storage
<i>LSDHS</i>	Large-scale district heating system
<i>LTDHS</i>	Low temperature district heating system
<i>LZCT</i>	Low or zero carbon technologies
<i>MAES</i>	Metal-air energy storage
<i>MARS</i>	Multivariate adaptive regression splines
<i>MB</i>	Moving boundary
<i>MCDA</i>	Multi-criteria decision making analysis
<i>MILP</i>	Mixed-integer linear programming
<i>MINLP</i>	Mixed-integer nonlinear programming

<i>MLR</i>	Multiple linear regression
<i>MNLR</i>	Multiple nonlinear regression
<i>MSW</i>	Municipal solid waster
<i>NGCC</i>	Natural gas combined-cycle
<i>NSGA</i>	Non-dominated sorting genetic algorithm
<i>NTU</i>	Number of transfer units
<i>nZEB</i>	Nearly zero energy building
<i>NZEB</i>	Net zero energy building
<i>O&M</i>	Operation and management
<i>PC</i>	Pure conduction
<i>PCM</i>	Phase change material
<i>PES</i>	Primary energy saving
<i>PHS</i>	Pump hydro storage
<i>PSO</i>	Particle swarm optimization
<i>PV</i>	Photovoltaic
<i>PWF</i>	Present worth factor
<i>RES</i>	Renewable energy sources
<i>SCD</i>	Simultaneous charging and discharging
<i>SDHW</i>	Solar domestic hot water
<i>SF</i>	Solar fraction
<i>SH</i>	Space heating
<i>SHREC</i>	Smart hybrid renewable energy for communities
<i>SHS</i>	Sensible heat storage
<i>SM</i>	Surrogate models
<i>SMES</i>	Superconducting magnetic energy storage
<i>SPECO</i>	Specific exergy and cost method
<i>SSM</i>	Simple storage model
<i>STHX</i>	Shell and tube heat exchanger
<i>SVE</i>	Single value for efficiency
<i>SVM</i>	Support vector machine
<i>SVR</i>	Support vector regression
<i>TCES</i>	Thermochemical energy storage
<i>TES</i>	Thermal energy storage
<i>TMY</i>	Typical meteorological year
<i>TOU</i>	Time of use
<i>TRL</i>	Technology readiness level
<i>TSP</i>	Thermal solar plant
<i>TTHX</i>	Triplex tube heat exchanger
<i>UTES</i>	Underground thermal energy storage
<i>WWHC</i>	West Whitlawburn housing co-operative

Chapter 1: Introduction

1.1 Energy in buildings and districts

Sustainable development is the ability to fulfill the requirements of current generation without disturbing the future generations to sustain theirs [1]. Most traditional forms of energy such as coal, petroleum and natural gas are non-renewable sources of energy and will be depleted in the near future [2, 3]. Use of renewable energy and an increase in energy efficiency are two essential solutions to address the current energy crisis [4].

In the recent years, substantial energy is spent in building sector where 46% of the total worldwide energy demand can be attributed to heating and cooling [5]. In addition to the availability of nonrenewable energy forms, environmental impacts associated with power production from these nonrenewable energies stresses the development of more efficient and sustainable heating/cooling and energy distribution strategies. District heating systems (DHSs) are found to be a promising technology to address sustainability in building-related energy production and distribution [6].

1.2 Necessity of energy storage

As energy systems become more complex (in both supply and demand), mechanisms are being sought by which greater control for variability and unpredictability can be adopted. At the district level, where heating and/or cooling networks can exist, energy storage can provide such control. Such districts vary in size, from tens of buildings connected to a small gas engine in London, UK [7], through hundreds of properties in Lieni, Italy [8] and Southern Austria [9], to a 974 km district network within Vienna, Austria [10] or even a 1,300 km district heating network connecting 19 energy centers in Berlin, Germany [11]. New thermal energy storage (TES) vessels are often the focus, but innovative methods are also considered for storing thermal energy, using the existing building stock thermal mass [12] and district heating pipework [10]. This section discusses the necessity of energy storage within building and district energy systems.

1.2.1 Profile smoothing

Renewable energy is becoming globally more prevalent as a source of heat and electricity; however, it is also inherently intermittent with time and space. To smoothen this varying supply, it is possible to use energy storage as a buffer. Electrical or thermal storage can be used indirectly, by using peaks in renewable supply to operate electric heaters/chillers [13] or by operating combined heat and power (CHP) plants in renewable supply troughs without wasting the resultant heat output [14, 15]. Solar thermal systems also tend to be optimized with storage in mind, either at high temperature preceding use through a Rankine engine (as is the case for concentrated solar power [16]) or at low temperature for direct use in a heating network [17].

Less intermittent than renewables (but equally variable) is the demand for electricity, heating, and cooling. Supply technologies are conventionally designed to meet the peak demand,

but could be sized smaller with the installment of storage [18-20]. By operating the supply to meet average demand, excess energy can be stored for use during peak demands, reducing the pressure on supply.

1.2.2 Time of use tariffs

Profile smoothing is beneficial to allow for intermittency and to reduce capacity requirements of the supply technologies. However, the same capability provided by storage to decouple supply from demand can be used purely for operational economic gain. Given a large enough swing in electricity wholesale price, significant economic gain can be achieved from operating CHP plants at the right time of day and selling the produced electricity to the grid [7, 21-24]. In fact, some argue that thermal storage in a district system is only beneficial with sufficient variation in wholesale electricity price [7, 22, 25]. Conversely, electricity can be purchased at off-peak times to operate chillers, reducing operating costs [18].

1.2.3 Efficiency improvements

Off-peak electricity wholesale pricing hours tend to be overnight, when the temperatures are lower. By operating cooling systems at this time, not only the electricity purchasing is cheaper, but also enhancement in efficiency can be realized directly in the technologies and via the cooling towers [26]. Thermal storage is then utilized to meet cooling demands when temperature increases during the day and buildings are occupied.

Loading of a given technology also affects its efficiency, with certain cooling technologies operating more efficiently at partial load rates, which can be maintained if supply is decoupled from demand by use of storage [27]. Avoiding excessive cycling (to meet varying demands) can also have the added benefit of extending technology lifetime and reducing maintenance requirements [28].

1.2.4 Seasonal variations

Short-term storage is widely found in actual and modeled systems; however, seasonal storage could also be used. Cooling in summer can be matched to heating in winter for potentially greater economic gain than considering the systems separately in the short-term [29].

1.3 Content organization

Energy storage technologies can be generally classified in two major categories of thermal and electrical energy storage. These technologies and their mechanisms are covered in Chapter 2, introducing storage systems.

To support the optimum integration of TES into future building energy systems, benefits of TES should be quantified during decision making processes at policy, strategy, concept design and detailed design stages. Modeling has a key role in providing this quantification and underpinning future standards, regulations, guidance and design methods for effective TES integration. In general, modeling can be viewed as supporting three different domains with different requirements on modeling outputs (see Table 1.1):

- (1) Policy, scoping and concept design, regulation compliance
- (2) Detailed system design
- (3) System automation design and operation.

Table 1.1: Modeling requirements for different levels and domains

Scale	Component	Building	District	Regional
Policy, scoping/concept design, regulatory compliance	✓	✓	✓	✓
Detailed system design	✓	✓	✓	
System automation design and operation	✓	✓	✓	

The integration of TES primarily requires that materials, components, and local interactions are characterized, and their behavior are captured in models which allow these to represent TES systems in the design process. Thereafter, these TES system characteristics must be appropriately integrated within constructions or plant models for their behavior to be correctly comprehended within building or district models in the higher-level design processes. In turn, the TES characteristics at building level should be comprehended in district or regional level models. Therefore, energy storage applications in buildings (including component level) are discussed in Chapter 3, while Chapter 4 is devoted to the district level. These chapters cover the fundamentals of energy storage, introduce available tools, provide state-of-the-art examples, etc. Note that this publication is not focused on the regional or national level.

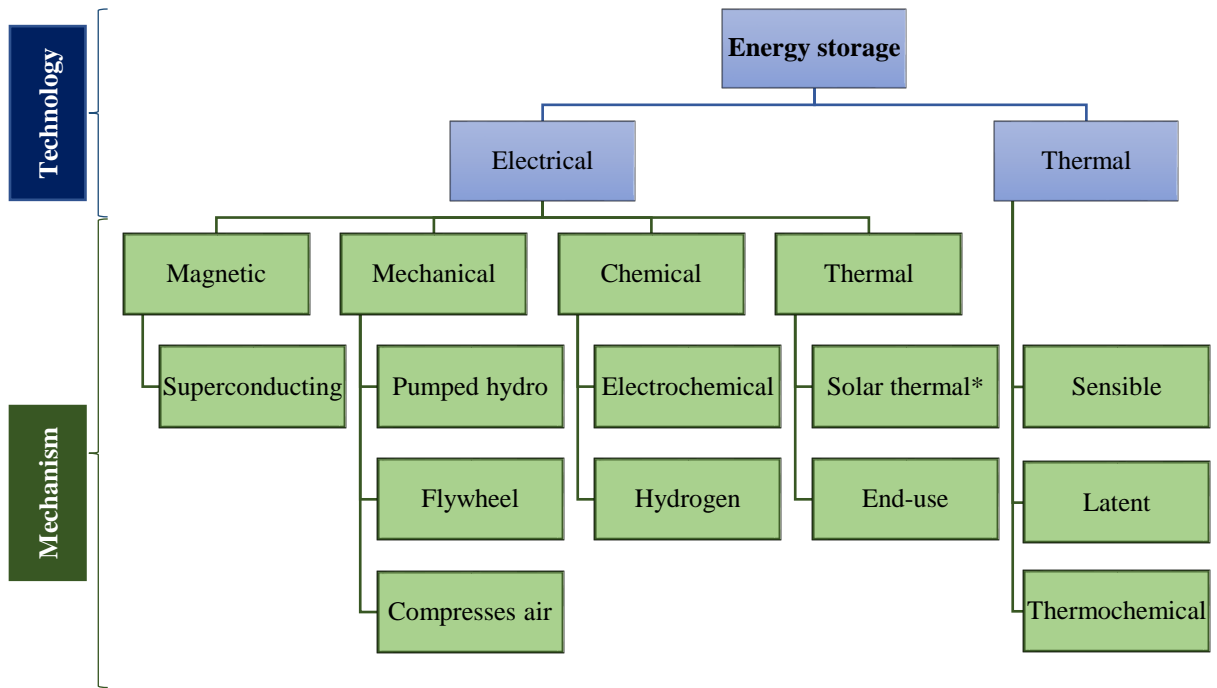
Once a system is modeled, optimization can be carried out based on several criteria. This is the subject of Chapter 5 with a focus on energy storage. First, common optimization methods and algorithms are explained. Then, common objective functions and decision parameters for energy storage are presented. Existing tools for optimization at building and district levels are elaborated. Thereafter, due to the complicated nature of district level optimization, some computational time deduction methods are covered. Further, examples based on some recent studies are provided to illustrate how optimization can be applied to energy storage in buildings and districts.

In order to evaluate the effectiveness of energy storage technologies in building/district applications, key performance indicators (KPIs) are important for analyzing the interactions among economic, human activity, energy consumption and GHG emissions [30]. Therefore, Chapter 6 first reviews the existing KPIs and then introduces ten KPIs in detail which are later used at the end of Chapter 6 to evaluate Annex 31 case studies. The chapter also introduces some other advanced KPIs.

Finally, Chapter 7 concludes the publication by explaining the achievements of Annex 31 as well as providing recommendations for the future work.

Chapter 2: Energy storage technologies

Energy storage technologies store energy at the time of availability of excess energy for later use. The most common storage technologies for building applications can be divided into two categories of electrical energy storage devices [31, 32] and TES devices [33]. These energy storage technologies as well as their common mechanisms are shown in Figure 2.1. In this chapter, each category is presented in detail.



*Solar thermal power plants

Figure 2.1: Common energy storage technologies and their storage mechanisms

Note that since sensible and latent thermal energy storages received considerable attention, this chapter primarily focuses on these types of TES. Therefore, their fundamentals and applications are also presented.

2.1 Thermal energy storage

The main energy demands in buildings are related to supplying power for heating, ventilation and air conditioning (HVAC) systems and hot water tanks. The occurrence of these demands varies considerably and can depend upon the time of day or night and season, particularly in regions with extreme weather conditions. Any change in energy demand results in peak and off-peak energy usage of the grid, leading to a variation in energy prices offered by most utility companies. According to time of use tariffs, higher electricity rates are imposed during peak-power demand (reflecting the cost of electricity generation during peak periods) compared to off-peak power demand. The disparity between the available energy supply and the consumed energy necessitates the need for integrating TES in different building applications such as

providing hot water, HVAC and utilizing waste heat. This also highlights the need to store excess energy which would otherwise be wasted as well as shifting peak power demand. In addition, TES not only improves the performance and reliability of energy systems, but also plays a key role in energy conservation and reducing the time mismatch between energy supply and demand. The following sections briefly introduce four modes of TES, namely sensible, latent and thermochemical energy storages.

2.1.1 Sensible

Sensible heat storage (SHS) is the energy stored in a material within fixed temperature ranges without phase change.

2.1.1.1 Fundamentals

In SHS, thermal energy is normally stored by raising the temperature of a liquid, such as water (temperature levels range from 0 to 100 °C), or a solid, such as bricks, concrete, sand, soil and metals such as aluminum and steel. SHS systems utilize the heat capacity and change in temperature of the material during the process of charging and discharging. Water is used as the storage medium in most of the low temperature applications. In such systems, when the energy is stored or released in/from the storage medium, its temperature either increases or decreases. The amount of stored heat can be calculated by Equation (2.1):

$$Q_{SHS} = mC_p(T_2 - T_1) \quad (2.1)$$

where Q_{SHS} is the amount of stored sensible heat (J), m is the storage mass (kg), C_p is the specific heat capacity at constant pressure (J/kg.°C), and T_1 and T_2 are the lower and upper temperatures (°C) between which heat storage occurs.

2.1.1.2 Applications

In buildings, the use of SHS involves various applications such as the provision of domestic hot water (DHW) which is mostly provided by electric or gas heaters. In this case, sensible heat is stored by a temperature change of water using heating devices.

The main advantage of using SHS lies in the simplicity of its system design. The disadvantages are its typical very low efficiency in terms of energy usage and low storage capacity which means that large size of TES systems must often be used in practice. The water heater is one fine example for the SHS. Its performance depends mostly on the position and number of thermal elements, inlet design, size and aspect ratio of the tank, and location of the inlet and outlet of the water heater.

Another example for SHS is the underground thermal energy storage (UTES) which uses underground as the storage medium for heat or cold storage. The shallow geothermal energy is regarded as one of the most stable renewable energy sources (RES). When this renewable energy is utilized in building sector, the ground can be utilized as a heat source/sink or a medium for heat storage depending on the hydrological and thermal properties of the ground. In UTES, a ground heat exchanger (GHE) is the key component, connecting the demand and source sides.

Aquifer thermal energy storage (ATES) is also a SHS system as it uses underground water in an aquifer for heat storage and is referred to as an open loop system. This technique is limited by the geological parameters and is normally used for seasonal energy storage. On the other hand, when the heat is transferred indirectly via a closed fluid loop without a direct mass transfer, it is referred to as a closed loop system. Generally, the closed loop configuration is more common since the direct use of groundwater is often strictly restricted by local regulations. Among the several types of closed loop GHEs, the most favorable type is the vertical closed-loop GHE, also known as borehole heat exchanger (BHE). Basically, borehole thermal energy storage (BTES) needs much less space than other types of GHEs and can utilize the thermal capacity of the ground to its maximum.

2.1.2 Latent

Latent heat storage (LHS) is the energy stored or released when a storage material undergoes a phase change process from solid to liquid or liquid to gas or solid to gas (and vice versa), or is the energy needed to change the phase of a material without temperature change. Typical examples of latent heat are melting of ice (solid to liquid) and boiling of water (liquid to gas).

2.1.2.1 Fundamentals

Materials used for their latent heat thermal storage capacity are called phase change materials (PCMs) which have received considerable interest in recent years. The substance used as a storage medium in latent heat storage applications is often water/ice or PCMs usually based on paraffin, hydrated salts or fatty acids. The stored latent heat for a given mass of a substance can be calculated by Equation 2.2:

$$Q_{LHS} = mL \quad (2.2)$$

where Q_{LHS} is the amount of stored latent heat during the phase change of the substance (J), m is its mass (kg) and L is its latent heat (J/kg).

2.1.2.2 Applications

During the past decade, LHS has received wide attention from building engineers, researchers, architects and designers and has been applied to HVAC systems and building envelopes, etc. The economic aspect of LHS is particularly evident for buildings in which there is a significant demand for cooling. A typical example is the usage of PCMs in wallboards and water heaters.

One major advantage of LHS systems is their relatively large heat storage capacity, compared with SHS, which is due to the high enthalpy change during phase change. This can be illustrated by the huge amount of energy requirement during the phase change of water. As an example of LHS, the energy required to melt 1 kg of ice at 0 °C is 333 kJ/kg. The same amount of energy is required to heat up 1 kg water from 0 °C to up 80 °C (by SHS). Some other operational advantages are smaller temperature swing between day indoors and night outdoors, smaller size and lower weight per unit of storage capacity with high energy storage density [34]. Setterwall

[35] reported that PCM storage (i.e. LHS) is very compact compared to SHS and it allows for greater flexibility in choosing a location for the storage system.

In Table 2.1, SHS in a rock bed and a water tank is compared to LHS using organic and inorganic compounds. In summary, while most of practical applications utilize SHS methods, LHS provides a much higher storage density, with very little temperature variation during the charging/discharging processes with higher efficiency in storing thermal energy.

Table 2.1: Comparison of sensible heat and latent heat storages

Property	Sensible heat storage		Latent heat storage	
	Rock	Water	Organic PCM	Inorganic PCM
Density (kg/m ³)	2,240	1,000	800	1,600
Specific heat (kJ/kg)	1.0	4.2	2.0	2.0
Latent heat (kJ/kg)	N/A	N/A	190	230
Latent heat (kJ/m ³)	N/A	N/A	368	368
Storage mass required for 106 J (kg)	67,000	16,000	5,300	4,350
Storage volume required for 106 J (m ³)	30	16	6.6	2.7
Relative storage mass*	15	4	1.25	1.0
Relative storage volume*	11	6	2.5	1.0

* Relative to the inorganic PCM

It can be seen from Table 2.1 that the use of LHS results in storage densities which are typically five to ten times higher than that of SHS and that the PCM storage volume is twice smaller than that of water [36, 37]. The table also shows that inorganic compounds, such as hydrated salts, have a greater volumetric thermal storage density than most organic compounds due to their higher latent heat and density [38].

2.1.3 Thermochemical

Thermochemical energy storage (TCES) systems rely on the energy absorbed and released by breaking and reforming molecular bonds in a completely reversible chemical reaction. As such, the stored heat depends on the amount of storage material, endothermic heat of reaction, and extent of conversion. For example, in a TCES system, thermal energy from a solar collector is commonly used to initiate an endothermic chemical reaction in a storage medium and the constituents of the storage medium are then stored for later use. The chemical reactions selected for the storage system should necessarily be completely reversible. Compared with sensible and latent heat storages, TCES benefits from higher storage capacity. The main principle of TCES can be generally described by the reaction in Equation (2.3):



where Z is a thermochemical material, and X and Y are reactants (X can be a hydrate, hydroxide or ammoniate and Y can be CO_2 or water).

The main advantages of using chemical reactions as storage systems are the potentially high energy density and the possibility of indefinitely long duration of storage near ambient temperatures. Some typical TCES materials and chemical reactions are listed in Table 2.2.

Table 2.2: Chemical storage materials and reactions [39]

Compound	Reaction	Energy density	Reaction temperature
Hydroxides [40]	$\text{Ca}(\text{OH})_2 \rightleftharpoons \text{CaO} + \text{H}_2\text{O}$	3 GJ/m ³	500 °C
Ammonia [41]	$\text{NH}_3 + \Delta\text{H} \rightleftharpoons 1/2 \text{N}_2 + 3/2 \text{H}_2$	67 kJ/mol	400-500 °C
Calcium carbonate [42]	$\text{CaCO}_3 \rightleftharpoons \text{CaO} + \text{CO}_2$	4.4 GJ/m ³	800-900 °C
Iron carbonate [43]	$\text{FeCO}_3 \rightleftharpoons \text{FeO} + \text{CO}_2$	2.6 GJ/m ³	180 °C
Methanolation [44]	$\text{CH}_3\text{OH} \rightleftharpoons \text{CO} + 2\text{H}_2$	N/A	200-250 °C

2.2 Electrical energy storage

The principle of electrical energy storage is to store electrical energy as mechanical energy, chemical energy or other forms such that it can be converted back to electrical energy again when the demand is high.

2.2.1 Thermal

TES systems for electrical energy generation are usually contained in high temperature TES plants. There are two types of TES systems for electrical energy storage, namely those which are applicable to solar thermal power plants and end-use TES. Application of TES for solar thermal power plants consists of a synthetic oil or molten salt which stores solar energy in the form of heat collected by solar radiation. End-use TES uses hot or cold storage in underground aquifers, water or ice tanks, or other materials and uses this energy to reduce the electricity consumption of buildings.

2.2.2 Chemical

2.2.2.1 Electrochemical

There are various types of devices which use chemical energy to store electrical energy. The most common technique is the well-known electrochemical battery which converts the chemical energy contained in its active materials directly into electrical energy by an electrochemical oxidation-reduction (redox) reaction. The basic electrochemical unit is a cell. A battery consists of one or more cells, connected in series or parallel, or both, depending on the desired output voltage or capacity. The cells consist of three major components: the anode, the cathode and the electrolyte. These components are placed in the same container.

A variety of electrolytes are used including lead-acid, nickel-cadmium (Ni-Cd), lithium-ion (Li-ion), sodium-sulfur (Na-S), zinc-bromide (Zn-Br), nickel-metal hydride (Ni-MH), etc. Another battery type, called flow batteries or redox flow batteries, uses an electrolyte which is stored in a separate container outside of the battery cell container. Thus, in a flow battery, the reactants flowing across the electrodes come from containers outside the electrochemical cell and are prevented from mixing by a specially chosen membrane: an ion selective membrane or a micro-porous separator.

Another type of electrochemical energy storage is metal-air energy storage (MAES) which holds out great promise in terms of its intrinsic specific energy density. This type of battery uses the electrochemical coupling of a reactive metal anode to an air electrode. Several types of metal-air battery have been successfully developed, including zinc-air, aluminum-air, magnesium-air,

iron-air and lithium-air configurations, all operating in alkaline or neutral aqueous electrolytes. The MAES technology is very promising but its future usefulness in the development of electrical energy storage, especially renewable energy storage, depends largely on the successful development of bi-functional air electrodes.

2.2.2.2 Hydrogen

The fuel cell (FC) technology is one of the most promising new electric power technologies. Fuel cell power systems have attracted attention due to their potential for high efficiency, low emission, flexible use of fuels and quietness. FCs are electrochemical devices which convert the chemical energy of a fuel directly into usable energy, electricity and heat, without combustion. They can be operated as either a generator or storage device. FCs can be regarded as similar to batteries containing electrodes and electrolytic material to accomplish the electrochemical production of electricity. An FC uses oxidation-reduction reaction between hydrogen and oxygen to produce electricity and heat. It includes (1) electrolysis which consumes off-peak electricity to produce hydrogen, (2) the fuel cell which uses that hydrogen and oxygen from air to generate peak-hour electricity, and (3) a hydrogen buffer tank to ensure adequate resources in periods of need.

There are many types of FCs, such as alkaline fuel cell (AFC), proton exchange membrane fuel cell (PEMFC), direct methanol fuel cell (DMFC), phosphoric acid fuel cell (PAFC), molten carbonates fuel cell (MCFC) and solid oxide fuel cell (SOFC). The last two operate at high temperatures, while the rest are low temperature FCs.

2.2.3 Mechanical

2.2.3.1 Pumped hydro

Pumped hydro storage (PHS) utilizes off-peak electricity to pump water from a lower reservoir into another one at a higher elevation. When the water stored in the upper reservoir is released, it passes through hydraulic turbines to generate electricity. Thus, the key elements of a PHS include turbine/generator equipment, a water way, an upper reservoir and a lower reservoir. The turbine/generator is similar to equipment used for normal hydroelectric power plants with no storage. The off-peak electrical energy used to pump the water to a higher elevation can be stored indefinitely as gravitational energy in the upper reservoir. Thus, two reservoirs in combination can be used to store electrical energy for a long period of time and in large quantities.

2.2.3.2 Flywheel

A conventional flywheel energy storage (FES) system is a cylinder which spins at very high speed storing kinetic energy. A flywheel can be combined with a device operating as an electric motor which produces electricity from the energy stored in the flywheel. The faster the flywheel spins, the more energy it retains. Energy can be drawn off as needed by slowing the flywheel. Modern flywheels use composite rotors made with carbon-fiber materials [45].

The rotors have a very high strength-to-density ratio and rotate in a vacuum chamber to minimize aerodynamic losses. Moreover, a magnet levitates the cylinder limiting friction-related

losses and wear. The amount of energy stored in a flywheel depends upon the linear speed of rotation and the mass of the disk. Short discharge time flywheels are suitable for stabilizing voltage and frequency, while longer duration flywheels may be suitable for damping load fluctuations.

2.2.3.3 Compressed air

Compressed air energy storage (CAES) uses off-peak electricity to power a motor/generator which drives compressors to force the air into a storage reservoir such as rock caverns, salt formations or depleted natural gas fields for large CAES plants. For smaller CAES plants, compressed air is stored in tanks or large pipes such as those designed for high pressure natural gas transmission. When the demand for electric power peaks, the process is reversed. The compressed air is released, heated by natural gas in combustors and run through high-pressure and low-pressure expanders to power the motor/generator producing electricity. In a traditional gas turbine, the air which drives the turbine is compressed and heated using natural gas. CAES technology needs less gas to produce power because it uses air which has already been compressed.

2.2.4 Superconducting magnet

Superconducting magnetic energy storage (SMES) systems store energy in the magnetic field created by the flow of direct currents through a large coil of superconducting material which has been super-cooled. In low-temperature superconducting materials, electric currents encounter almost no resistance, greatly enhancing their storage capacity. The coil with many windings of superconducting wire should be cooled to a temperature below the temperature needed for superconductivity. SMES charging or discharging causes a corresponding increase or decrease in the current flow. Thus, energy is added or extracted from the magnetic field of the inductor by increasing or decreasing the current in the windings. Moreover, power is available almost instantaneously and very high output power can be provided for a short period of time. The lack of moving parts results in high reliability and minimal maintenance. However, superconductors require refrigeration systems which induce energy losses and contain moving parts.

Chapter 3: Application to buildings

The overall aim of this publication is to address the existing challenges in the integration of TES in buildings and districts. To support the design and optimization of systems incorporating TES, this chapter is dedicated to buildings and their components. Clearly, there is no distinguishable boundary between buildings and districts as many of the models and tools developed for buildings can be used (with some modification) for districts. Keeping that in mind, the building level is covered in this chapter and next chapter focuses on the district level.

The integration of TES in buildings can temporally decouple when devices such as heat pumps or chillers should operate and when the heating or cooling should be provided to the end users. This can radically alter the timing of building energy demand, potentially enhancing the use of renewable energy resources [46]. TES allows potentially cheaper off-peak energy supplies to be exploited [47] and it can also act as a means to collect local energy resources [48]. However, many obstacles exist with regards to integration and operation of heat storage systems in buildings. One of the most significant is competition for space. As dwelling sizes reduce, floor area is at a premium and the space penalty associated with conventional technologies such as hot water storage can act as a barrier to its uptake. This problem becomes more acute if the operation of future networks necessitates the need for heat to be stored over longer time periods than is done at present [49]. Storage in the future may need to migrate away from the traditional hot water tank, towards media such as PCMs and storages which make better use of the existing space and thermal mass in and around buildings, including large-scale community storage.

Fabric integrated thermal storage (FITS) systems store heat in structural or constructional elements; therefore, they do not compromise internal space. However, the effective operation of FITS, within a building, possibly featuring multiple heterogeneous heat sources and active energy network participation, raises significant engineering and social challenges. For example, the heat stored in building fabric should be effectively insulated to prevent excessive losses as well as overheating which could be a problem in modern, well-insulated dwellings. Moreover, FITS should be integrated and operated with existing energy systems. Finally, operating local storage to improve the operation of external energy networks (in addition to servicing the needs of the local building) would not be attractive to building owners if they were financially disadvantaged or subject to increased discomfort.

Depending on the storage temperature, FITS can be coupled to or decoupled from the building interior according to insulation level and its location inside the building. The storage temperature is a key element in a FITS system and has multiple implications on the system design since the available charging and discharging options, as well as working fluid, are dependent on this (Figure 3.1). Charging and discharging of FITS, can be passive or active. Generally, active systems provide the opportunity to operate with higher and greater range of storage temperatures than passive systems. With passive storage, the heat is stored without mechanical input, instead by using solar gains, convection or temperature difference. On the other hand, active systems require

a system for heat generation and transfer to/from the storage. Passive storage systems or technologies are normally integrated as part of the building structure. This is the case in sun spaces, exposed thermal mass or shading devices [50]. In an active storage system, the heat is transferred using a distribution medium (such as air or water) with forced convection [50] or using electricity. Air and water-based systems can either be used for cooling or heating, while direct electric systems are used for heating. In some cases, charging and discharging can be a combination of active charging and passive discharging or vice versa, and the thermal energy can be stored in a HVAC system, in the building fabric or outside the building structure [51]. The comprehensive taxonomy of coupled FITS systems is illustrated in Figure 3.2. It uses parameters such as storage location, temperature, material and charge/discharge options, and it includes passive and active systems. In this figure, passive systems use storage temperatures ranging from ambient to low temperature up to 30 °C and are presented as sensible or latent storage systems. Besides, active coupled systems include low storage temperatures up to around 40 °C and are presented according to the storage activation process and, therefore, organized by distribution medium, such as air and water, and electricity. A taxonomy for semi-decoupled and decoupled systems is presented in Figure 3.3. Note that the semi-decoupled systems use medium storage temperatures up to 70 °C with electric activation, while the decoupled systems are best used with temperatures greater than 70 °C.

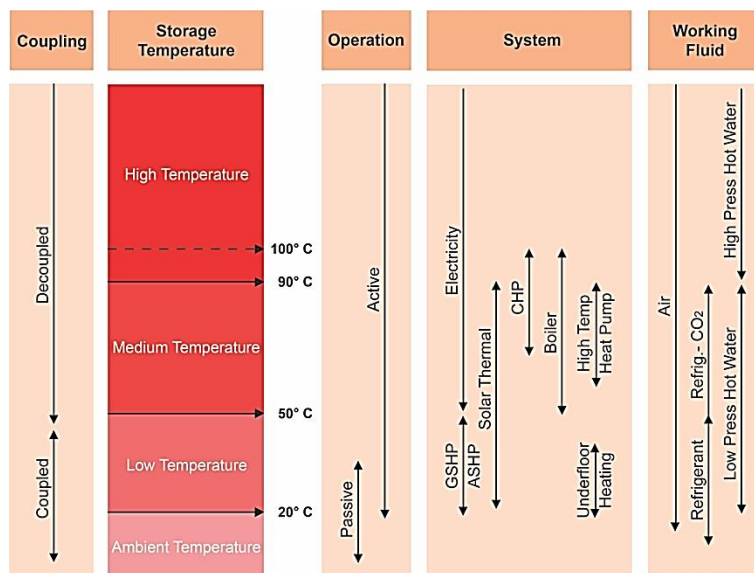
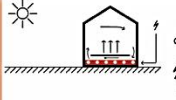
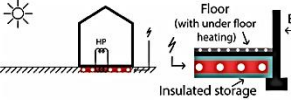
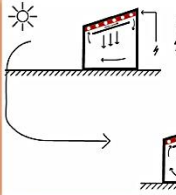
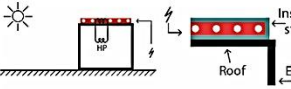

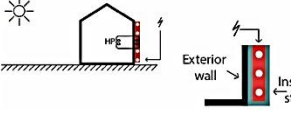
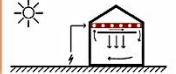
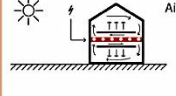
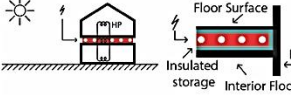
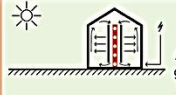
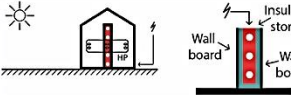
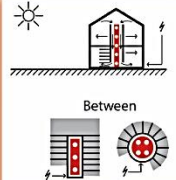
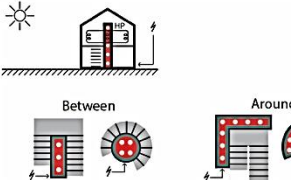




Figure 3.1: Storage temperature and systems options

Storage Location	Passive Charge & Discharge			Hybrid Charge & Discharge	Active Charge & Passive Discharge
	Passive FITS Systems			Active FITS Systems Distribution medium: air or water	Active FITS Systems Charge with electricity
	Sensible Storage		Latent Storage	Sensible or latent Storage	Sensible or Latent Storage
	Solid	Liquid	PCM	Solid or PCM	Solid or PCM
	Ambient to Low Temperature up to 30°C			Low Temperature up to 40°C	Low Temperature up to 40°C
Floor					
Roof					
Exterior Wall					
Trompe Wall/ Double Facade					
Ceiling					
Interior Floor					
Interior Wall					
Staircase & lift areas (wall, column or void areas)					
Window					
Shading Device					

Passive FITS systems locations based on previous taxonomies
 Active FITS systems locations based on reviewed studies
 Potential active FITS systems locations

Figure 3.2: Taxonomy of FITS for coupled storage systems

Storage Location	Active Charge & Passive or Active Discharge		Active Charge & Discharge	
	Active FITS systems charge with electricity		Active FITS systems charge with electricity	
	Sensible or latent storage semi-decoupled from the living areas		Sensible storage decoupled from the living areas	
	Solid or PCM		Solid	
	Medium Temperature up to 70°C		Medium to High Temperature above 70°C	
Floor		The floor surface can be suspended over a semi-insulated storage. The warm air can be introduced into the living areas through floor openings. PCM floor surfaces such as tiles can be used to avoid overheating.		Total insulated storage decoupled from the thermal zone.
Roof		Roof semi-insulated thermal storage with suspended ceiling to avoid overheating. The use of fans is necessary to distribute the heat. PCM ceiling boards can be used to avoid overheating.		A Roof total insulated storage decoupled from the thermal zone.
Exterior Wall		A wall panel separates the semi-insulated storage from the living zones to avoid burnings or overheating. The heated air can be stopped from entering the rooms by closing the wall vents. PCM boards can be used to avoid overheating.		Total insulated storage decoupled from the thermal zone.
Ceiling		Similar to the Roof system. PCM boards can be used to avoid overheating.		
Interior Floor		PCM tiles can be used to avoid overheating of the floor surface. PCM ceiling boards can be used to avoid overheating near the ceiling.		Total insulated storage decoupled from the thermal zone.
Interior Wall		Similar to the Exterior Walls. The storage can be semi-isolated from the living areas. This allows higher temperature storage. With or without PCM wallboards.		Total insulated storage decoupled from the thermal zone.
Staircase & lift areas (wall, column or void areas)		Similar to Interior Walls. The semi-insulated storage is detached from the stairs. Wall boards with air gap and with air circulation. Possible positions: around, between or below the stairs. With or without PCM wall boards.		Total insulated storage decoupled from the thermal zone.
Foundation pile & retaining wall		FITS System with Water Base Distribution Ambient to Lower Temperature		

Active FITS systems locations based on reviewed studies
 Potential active FITS systems locations and concept designs

Figure 3.3: Taxonomy of FITS for semi-decoupled and decoupled storage systems

In this chapter, fundamentals of some well-established modeling approaches at the building level are presented. In addition, introduction of some available tools along with state-of-the-art examples for component and building levels are illustrated.

3.1 Fundamentals

Accurate prediction of the energy demand profile of users in smaller time interval (such as hourly basis) can affect the efficiency of a system as well as its optimization procedure [52]. It is thus essential to predict the heating demand profiles of the users to determine the appropriate sizing of the heating equipment. Regardless of the method used, the heating demand profile of each user

consists of three major parts of (1) physical and environmental characteristics of the building (i.e. R-value, infiltration rate, ambient air temperature, solar radiation, and humidity), (2) human-related factors or social behavior of the occupants, and (3) random factors which account for uncertainties. Different techniques have been developed to predict user demand profiles considering all or one of the mentioned factors, including historical approaches [52, 53], deterministic method and times series predictive methods [54]. While the deterministic methods (also known as simulation-based models) use the mathematical representation of the buildings physical behavior, the numerical predictive time series methods rely on the mathematical curve fitting relation(s) to predict user demand profiles. The predictive models themselves are further categorized to classical approaches and artificial intelligence (AI) methods.

3.1.1 Heating degree day

Heat loss in buildings (Q_{loss}) is proportional to the difference between indoor and outdoor ambient temperature. This concept is used in the development of the heating degree day (HDD) method [55]:

$$Q_{loss} = (UA)_{overall} \times HDD \quad (3.1)$$

where $(UA)_{overall}$ is the overall heat loss coefficient which is determined based on the infiltration rate and the summation of the UA values for all different envelope assemblies of the building. The infiltration rate can be defined either in hourly rate or as an average [55].

Online and free historical weather data are mainly assumed as reliable sources to obtain the HDD values [56-58]. This method is widely used to model small buildings in whose envelope the main source of energy is unclear. HDD method has been compared with a historical method known as the BIN method [59]. Unlike HDD method, the BIN method is mainly used for larger scale buildings in which the internal load generation has a significant effect, rendering the HDD method unfeasible. In both cases, the main concern in modeling is the ambient condition of the buildings and the average envelope thermal resistance. The fact that factors such as the social behavior of occupants and buildings thermal mass are not considered results in predominantly low-accuracy findings [52]. In addition, the low frequency of available data results in inaccurate outcomes.

3.1.2 Energy use intensity and load factor

Energy use intensity (EUI) and load factor (LF) is another technique to estimate the users demand profile where the historical supply data is provided. EUI is the rate of energy use per unit area [60] and LF is the ratio of energy consumption over the maximum possible energy generation of the supply side (the product of peak demand and time) [61, 62].

Knowing the EUI and LF of different users [63], it is possible to calculate the total energy and peak heating demand required for each consumer. The supply energy demand provides the annual average LF per area of different users. Mainly, the values are accessible based on region or reference archetype [58, 63]. As an example, this method can be used for load prediction based on

different user sectors of a DHS whose summation provides the heating demand profile of the users [64]. One of the main problems with this method is the lack of separated factors for ambient conditions.

3.1.3 Comprehensive models

Simulation software (such as EnergyPlus [65] and TRNSYS [66]) are widely used for predicting the energy consumption pattern of various buildings. Although they yield highly accurate demand profiles, the main disadvantage of these models is their dependency on data and high computational cost for modeling each building [53, 67, 68]. For small-scale systems consisting of a limited number of buildings, using the comprehensive method can increase the accuracy of the simulation. Nevertheless, the data and time required to model many buildings in a city-wide scale is computationally expensive. As an example, a comprehensive method was utilized to model the demand profile of 95,817 buildings in Westminster, UK [69, 70].

3.1.4 Simplified simulation models

Simplified methods are adopted when the comprehensive method is computationally expensive for a large-scale community. Moreover, they can be used for cases where computational speed prevails its accuracy. These methods simplify the buildings physical characteristics to predict their demand profile. For example, parameters including shape, orientation and occupancy type were considered to model the end-user profiles [71]. Besides, the average energy required per square meter of a dwelling area of a building was used based on its monthly/yearly outdoor design temperature. Two sets of coefficients can be used to consider the shape and orientation of buildings [67]: (1) the ratio of the outdoor surface to volume of the building (the shape factor) and (2) the orientation relative to the south (orientation factor). A simplified physical method can also be used to predict the demand profile load of a residential building, with a lower internal heat gain density [72]. Inversely, this method is unsuitable for larger buildings with higher internal heat gain density.

3.1.5 Predictive models

3.1.5.1 ARMA type

Autoregressive moving average (ARMA) time series predict end-user profiles by implementation of a linear combination between the previous value along with previous and current noise values. For demand profile prediction [73]:

$$z(t) = Y_p(t) + Y(t) \quad (3.2)$$

where $Y_p(t)$ represents the day and the normal weather condition for the design day, and $Y(t)$ indicates the effect of deviation from the normal weather pattern.

With slight difference from the general form, different kinds of ARMA-type models can be developed, e.g. Box-Jenkins [74], time series [75], ARIMA [76].

3.1.5.2 Kalman filter

Similar to other predictive methods, this technique estimates the future time step values ($t + \Delta t$) based on the current time step values (t). To make the best estimation, Kalman filter determines the best variable set, which minimizes the source function using the residual sequence method. In each step, Kalman filter checks the difference between the measurements and model output and selects the variable, minimizing the difference. Since the deviation from the measurement can be positive or negative, two different sets of residual sequences could be assumed; residual for the hot side as well as residual for the cold side of the profile [77].

3.1.5.3 Regression-based methods

One of the most common methods to predict the demand profile of buildings is the regression-based methods. These models are usually divided into two subcategories of multiple linear regression (MLR) and multiple nonlinear regression (MNL) models. While the main objective of the MLR is to find a linear relationship between some independent variables and one dependent variable, the nonlinear regression methods assume nonlinear behavior between the dependent variable and independent variables:

$$Y = \alpha_0 + \alpha_1 X_1 + \alpha_2 X_2 + \dots + \alpha_n X_n \quad \text{MLR} \quad (3.3)$$

$$Y = \alpha_0 + \alpha_{1,1} X_1 + \alpha_{2,1} X_1 + \dots + \alpha_{1,2} X_1^2 + \alpha_{2,2} X_2^2 + \dots + \alpha_{n,n} (X_1 X_2 \dots X_n) \quad \text{MNL} \quad (3.4)$$

In some cases, the results of the dependent variable at the time t is highly influenced not only by the value of the independent variables at the time t , but also by some previous time steps. In these cases, such as a building with high thermal mass, the dependent variable is predicted based on the previously observed set of independent variables. Due to its usefulness in predicting the dependent variable, this method received attention to forecast future results [78]. There are different types of time series methods among which the simple exponential smoothing is the most common one [79]. Besides, the autoregressive (AR) method is a predictive time series method which works based on the simple exponential smoothing method.

3.1.5.4 Artificial intelligence

Using predictive methods such as AI is another approach to predict building demand profiles. The most common AI methods used for load prediction are artificial neural network (ANN), fuzzy neural network (FNN) and support vector machine (SVM). The ANN has been widely used for load prediction, particularly in forecasting the electricity consumption of buildings [80]. In most cases, the ANN shows superior prediction performance compared with other simulation-based methods. This higher accuracy of the ANN method is usually due to its higher adaptability as it considers the social parameters in load prediction by integration of real case data into the system training [80, 81]. Despite the high accuracy of the predictive methods, their main drawbacks are the over-fitting problem as well as the data requirements for the training purposes. Requirement

of accurate, comprehensive archives of data for ANN is one of its main drawbacks. For cases where the data archive used for training the system is small, the SVM methods [82] show a better performance. However, SVM was scarcely used in the last few years; therefore, there is limited information regarding the utilization of this model.

3.2 Available tools

Available building simulation tools have already been contrasted [83] and it is beyond the scope of this publication to go through their details. Nevertheless, in this section, some common tools which are later discussed in this publication are introduced.

3.2.1 TRNSYS

TRNSYS is a program with a modular structure which was designed to solve complex energy system problems by breaking them down into a series of smaller components. TRNSYS components (referred to as types) may be as simple as a pump or pipe, or as complicated as a multi-zone building model. The components are configured and assembled using a fully integrated visual interface known as TRNSYS Simulation Studio, and building input data are entered through a dedicated visual interface. The simulation engine then solves the system of algebraic and differential equations which represent the entire system. In building simulations, all HVAC system components are simultaneously solved with the building envelope thermal balance as well as the air network at each time-step.

As the building model is developed separately from the other parts of the model, the process to obtain a complete TRNSYS simulation model requires the creation of two separate files. The file concerning the building has a “bui” extension, while the Simulation Studio file, containing data related to the boundary conditions, energy systems, equation components and output management, has a “tpf” extension. As the “bui” file is called as an external file in the “tpf” file, it is possible to use the same “tpf” file for different “bui” files. This means that it is easy and fast to evaluate and compare the performance of different buildings in the same context of climate and energy system.

The modular nature of TRNSYS facilitates the addition of new mathematical models to the software. Components can be easily shared between users without recompiling the program. Simple components, control strategies or pre and post-processing operations can also be implemented directly in an input file using simple equation(s) supporting the usual mathematical and logical operators and can use the (optionally delayed) outputs of other components. In addition to the ability to develop new components in any programming language, the program allows to directly embed the components implemented using other software (such as MATLAB/Simulink, Excel/VBA and Engineering Equation Solver).

The TRNSYS library includes many common components found in the thermal and electrical energy systems such as solar thermal and photovoltaic systems, low energy buildings and HVAC systems, renewable energy systems, cogeneration, and hydrogen systems. It also

provides component routines to handle input of weather data or other time-dependent forcing functions and output of simulation results.

The standard library includes a popular vertical cylindrical storage tank model. In addition, the TES storage tank library contains spherical, rectangular and horizontally cylindrical tank models. It also features a wrap-around heat exchanger tank, aquastats, a heat pump water heater, and a water heater.

3.2.2 eQUEST

The U.S. department of energy developed a free building energy simulation engine, known as DOE-2. To include graphical features in DOE-2, eQUEST (the QUick Energy Simulation Tool) has been developed based on the DOE engine and it is a free software. eQUEST includes configurations, wizards and industry standard defaults. With its extra added feature, the application of eQUEST can now be extended from both basic/simple energy analysis to detailed life cycle cost (LCC) analysis. eQUEST was developed to enable users to conduct detailed comparative analysis of building designs and technologies by applying sophisticated building energy simulation techniques. The main advantage of eQUEST is that it is not necessary for users to have extensive expertise in building performance modeling.

eQUEST can be used for (1) basic energy modeling and comparative runs, (2) intermediate energy modeling, (3) LCC analysis and (4) advanced energy modeling and complex comparative runs. eQUEST has three built-in wizards of schematic design (SD), design development (DD) and energy efficiency measure (EEM). The first two are used for building design purposes, while the latter is for energetic comparison of models.

Using the SD wizard, the user can create an energy model. SD wizard is used in the initial stage/earliest design phase and hence basic details of the building (shape of the building, HVAC system, DHW, occupancy schedules, energy usage data, internal loads, etc.) are fed as input. Once all the required inputs in SD wizard are provided, the user can enter into the main eQUEST window.

In DD wizard, additional information regarding the developed building model (more details on complicated structures, internal loads, schedules, HVAC system assignments, etc.) can be provided. The EEM wizard is the most powerful feature of eQUEST as it allows users to create modified energy models in a faster and easier way. The energy comparison (individual or cumulative) can be performed in the EEM wizard. The energy efficient measurement category, type, details pertaining to LCC analysis can also be provided in the EEM wizard.

3.2.3 EnergyPlus

EnergyPlus is a building energy simulation program developed with support from the U.S. department of energy. It was originally developed using Fortran 90, but was changed to C ++ on its way with open source code.

EnergyPlus receives the input data describing the building to calculate the thermal load conducted in the heat and mass balance engine. The resultant conditions of zones are then transferred to the building system simulation part to calculate the heat and mass transfer in the HVAC system. The result of building system simulation is again transferred to the heat and mass balance engine in a ping pong coupling way which updates the state of a zone.

In EnergyPlus, a node represents a quantity state of a zone or some point in a system loop. Generally, a zone air node has only one representative temperature and humidity information since the zone air node assumes fully mixed state. However, since each component of the system in EnergyPlus has a module structure, a system can be configured as a multi-node system. For example, the temperature stratification in a TES system can be reproduced using multiple nodes and the resultant information is exchanged with the heat and mass balance engine.

EnergyPlus is more of a simulation engine (with minimal graphic user interface) than a complete simulation program such as TRNSYS. Therefore, there are many third-party programs such as OpenStudio, a plug-in of Google SketchUp, where all the building geometry, and system configuration can be easily defined with full graphical interface. Then, the specified information in OpenStudio can be exported to an “idf” extension file which can be imported to EnergyPlus.

EnergyPlus also has its own language, the EnergyPlus runtime language (ERL), to allow users to perform various controls internally. Additionally, there is a middleware building controls virtual test bed (BCVTB) which enables EnergyPlus to be coupled with other programs such as MATLAB and Modelica.

3.2.4 Modelica

In 1997, an international effort was carried out to design Modelica [84], a freely available, object-oriented equation-based language for modeling large, complex, and heterogeneous physical systems. In the last two decades, Modelica has been used especially in the design of multi-domain engineering systems such as mechatronic, automotive and aerospace applications involving mechanical, electrical, hydraulic and control subsystems. The use of Modelica has recently been extended to the building energy research community due to the increasing need for analysis of more complex and efficient systems.

Modelica is an open language, and not a dedicated computer program. Equations in this language are encapsulated into models, which can be graphically assembled through connectors to define the architecture of larger and more complex models. To assemble models and perform simulations, a simulation environment (e.g. Dymola or OpenModelica) is needed.

The Modelica code behind a graphical model is automatically converted into executable code. Therefore, a separation exists between the code defining the physical equations and the executable code. This separation makes it easier to implement new component and system models than in traditional tools.

Modelica models are typically structured into libraries. There are numerous libraries available (both commercial and free) ranging from thermodynamics and chemical processes to automotive and space applications. Currently, several Modelica libraries exist for building components and HVAC systems, which are continuously being updated [85-87]. Moreover, the International Energy Agency (IEA) undertook a large-scale international project (IEA ECB Annex 60 [88]) to develop a new generation of computational tools for building energy systems based on Modelica. The continuation of Annex 60 is currently being conducted by the International Building Performance Simulation Association (IBPSA), known as IBPSA Project 1, focused on designing and operation of building and community energy systems [89].

3.3 Examples

In this section, some sample applications are presented for building as well as component level modeling. Ideally, each modeling level would feed characteristics into the next level of modeling so that systems are easily adopted in modeling frameworks. Modeling at all levels should support robust design methodologies which incorporate uncertainties such as user behaviors and weather conditions in determining optimal solutions for system design and their control automation algorithms.

3.3.1 Simplified building load prediction

Districts are made up of several individual buildings. Although district systems are thoroughly covered in Chapter 4, individual building modeling lies within the scope of this chapter. There are several challenges in the design, construction, and operation of energy-efficient DHSs. Simulation tools are addressed among one of the essential lacks when such systems are designed and implemented. Building simulation tools are broadly used to investigate the effectiveness of integrating energy storage and renewable energy resources [90-93]. Nonetheless, only limited simulation tools have been developed to predict the energy demand at the district level [94, 95]. Furthermore, detailed building simulation tools (e.g. TRNSYS, EnergyPlus) can also be utilized for the energy analysis of the district energy networks; however, other tools (such as HOMER, explained further in Chapter 4) utilize the predicted demand profile from other software or measured data as an input to the DHS. In both scenarios, existing tools cannot satisfy the current need for a dynamic, reliable and accurate tool which can envisage the demand profile prediction of large-scale district networks in a timely manner. As a result, simplified methods emerged for prediction of demand profile of district networks.

3.3.1.1 Background

Three primary sources of discrepancies can be identified for existing models which are occupant behavior, neighborhood interference and scaling effect. The first two are further explained here. Since most of the models do not directly consider the occupant behavior influence, the accuracy of the prediction, particularly at the building level, is observed to show a much lower value in many cases. In contrast, the accuracy is significantly higher at the district level with more diverse building types since several building influencing parameters at the district level overlap one another; therefore, they compensate the accumulated error at some points. As a consequence

of this misleading schedule prediction, most studies focused only on one type of building to improve their simulation accuracy.

The unmeasured effects of the district/community on buildings (such as shared walls between them and also the solar blockage by the adjacent shadow casted from surrounding buildings) significantly impact on the prediction of the heating demand schedules. Most of the existing models are designed as a standalone building, barely representing the complexity of an urban/district setting. Indeed, the first assumption in the modeling of a standalone building is that the entire building shell receives solar radiation and exchanges heat with the surrounding environment.

In this example, an MLR model (described in Section 3.1.5.3) was used to predict the heating demand profile of the individual buildings. A simplified building load prediction approach based on MLR was validated. Then, the obtained results were compared with those predicted by a comprehensive software model.

3.3.1.2 System description

The first step in defining the new procedure to predict the heading demand profile of a district is to identify the entire building stock and to segment it into different building archetypes. To have different building archetypes, a reference building was defined for each archetype, which represents all the buildings within that category. Using the geometrical properties and actual demand schedule of the reference building, an MLR model was developed to predict the demand profile of an entire district. Using the MLR model, the heating demand of two buildings (B1 and B2) were predicted. These buildings were developed using some verified models. The buildings were first modeled in eQUEST, by changing some of the parameters (see Table 3.1). Since one of the identified source of discrepancy in predicted results was the common wall, building B1 assumed to have a common wall on the east side.

Table 3.1: Characteristics of the buildings

Building	Area [m ²]	Stories	Window/wall ratio	Set point	Note
Reference	1,858	4	30	25 °C	Detached with no shading
B1	2,044	4	35	24 °C	Common wall on east
B2	1,998	4	35	Schedule 1*	20° rotation to east

*Schedule 1

Month	Nov	Dec	Jan	Feb	Mar	Apr
Average temperature [°C]	2.61	-6.82	-9.83	-9.43	-2.72	6.49
Set point [°C]	22	23	24	24	22	21

3.3.1.3 Methodology

The heating demand profiles of the buildings were obtained using MLR approach and were compared with those obtained from the eQUEST simulation. Moreover, to check the model accuracy under different circumstances, two different air set-point temperature scenarios were defined (see Table 3.1) and the accuracy of the results was compared with those obtained from the comprehensive modeling. In the first scenario (B1), a constant set-point air temperature was

defined for the entire year. In the second scenario (B2), two different heating and cooling seasons were defined. It was assumed that there is no heating load during the cooling season, even if the indoor air temperature drops below the thermostat set-point. On the other hand, different set-points were defined based on the average outdoor temperature of that month. The heating season was assumed to start from November, lasting until the end of April.

In some MLR cases, the results of the dependent variable at the time t is highly influenced by the value of the independent variables at the time t as well as some previous time steps. In these cases (such as buildings with high thermal mass), the dependent variables are predicted based on the previously observed set of independent variables. Due to its effectiveness in predicting the dependent variable, this method is common to forecast future results [78]. The autoregressive (AR) method is a linear prediction time series method which works based on the simple exponential smoothing method, and was use in this example:

$$\begin{aligned}
 Y(t) = & \alpha_1 X_1(t) + \alpha_2 X_1(t-1) + \alpha_3 X_1(t-2) \dots + \alpha_n X_1(t-n-1) + \\
 & \beta_1 X_2(t) + \beta_2 X_2(t-1) + \beta_3 X_2(t-2) \dots + \beta_n X_2(t-n-1) + \\
 & \dots + \\
 & \gamma_1 X_n(t) + \gamma_2 X_n(t-1) + \gamma_3 X_n(t-2) \dots + \gamma_n X_n(t-n-1) + C
 \end{aligned} \tag{3.5}$$

where α , β and γ are the coefficients obtained from auto regression, C is a constant and X_k are the input parameters of the system. For instance, for a low-rise multifamily residential building, this value was determined to be 4. To determine the best fit, two criteria were checked; having the highest R -value while maintaining the P -value within 95% confident interval.

3.3.1.4 Results

From the regression analysis, for a low-rise multifamily residential building the best-fit results for $t = 4$ were the same value of 0.9966 for both multiple R and adjusted R^2 . These results indicated a high correlation between the input file and target values (heating demand profile). Having the coefficients of the regression analysis of the reference building, further simulations were performed using MLR method to predict the heating demand profile of B1 and B2 buildings. As shown in Table 3.1, building B1 had a common wall with another building on the east side and a constant set-point temperature of 24 °C.

Figure 3.4 compares the results of B1 for the simplified model and the comprehensive simulation for December, showing an acceptable agreement. The R -value and standard error of the prediction (MSE) were found to be 0.9971 and 6.996, respectively.

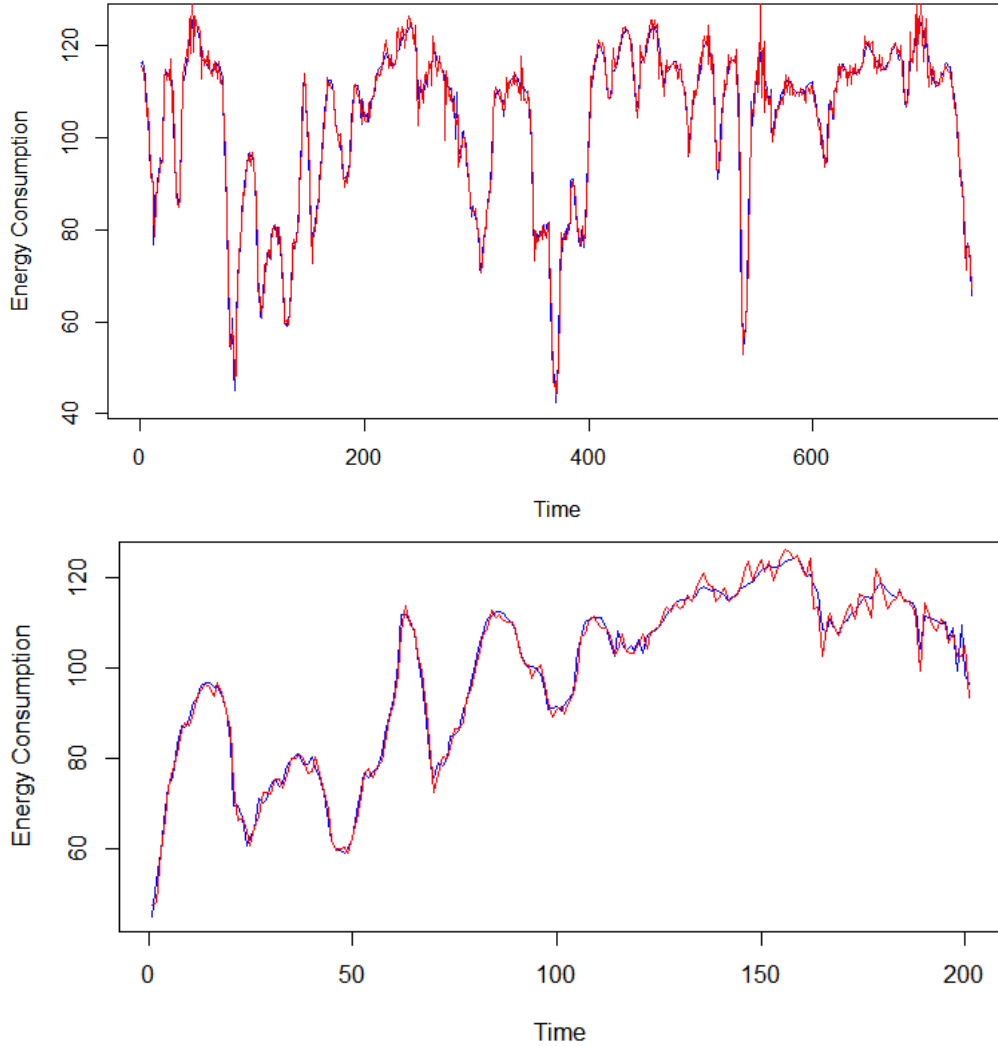


Figure 3.4: Simulation (blue) versus prediction (red) graphs for heating demand profile [kWh] of B1 showing a one-month (Dec.) period (top) and an 8-day (in mid-Dec.) period (bottom)

Since MLR method mainly assumes that there is a linear relation between load at the time t and inputs, the linearity assumption was also checked. According to the left graph in Figure 3.5, the red line shows almost a linear relationship between predicted values and simulated ones. Furthermore, the magnitude of the errors between predicted and simulated profile is shown by the histogram as depicted on the right.

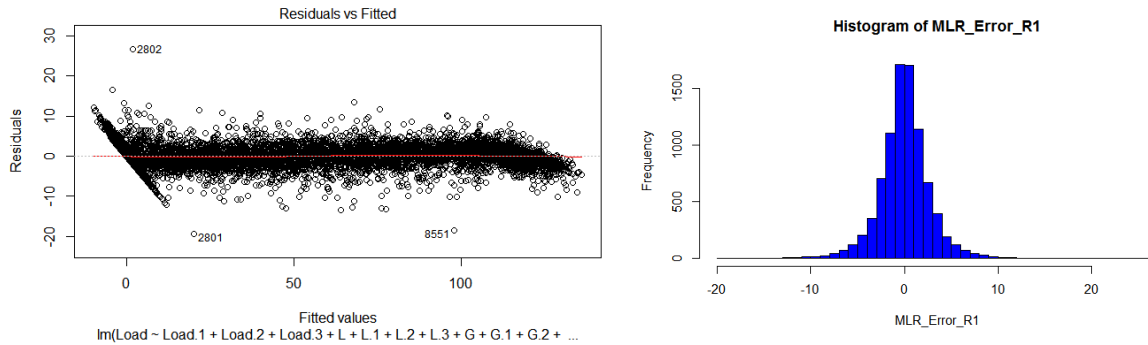


Figure 3.5: Results for B1 showing residual against fitted values (left) and error histogram (right)

In the second scenario, the demand profile of building B2 was predicted only for the defined heating season. Unlike the previous scenario, based on the average outdoor temperature, the set-point was varied between 21-24 °C. Figure 3.6 shows the predicted demand profile against the simulated profile of B2. Similar to B1, an acceptable agreement exists between the MLR predicted and simulated demand profiles. For B2, the R -value and standard error of the prediction (MSE) were 0.9947 and 5.462, respectively. The predicted heating demand profile for B2 showed slightly lower correlation with the demand profile obtained from detailed simulation. However, note that the duration of simulation was different for the two cases (i.e. 8,760 hours for B1 and 4,341 hours for B2). Figure 3.7 also proves the linearity assumption made earlier in proposing the MLR methods. It also illustrates the error histogram for B2.

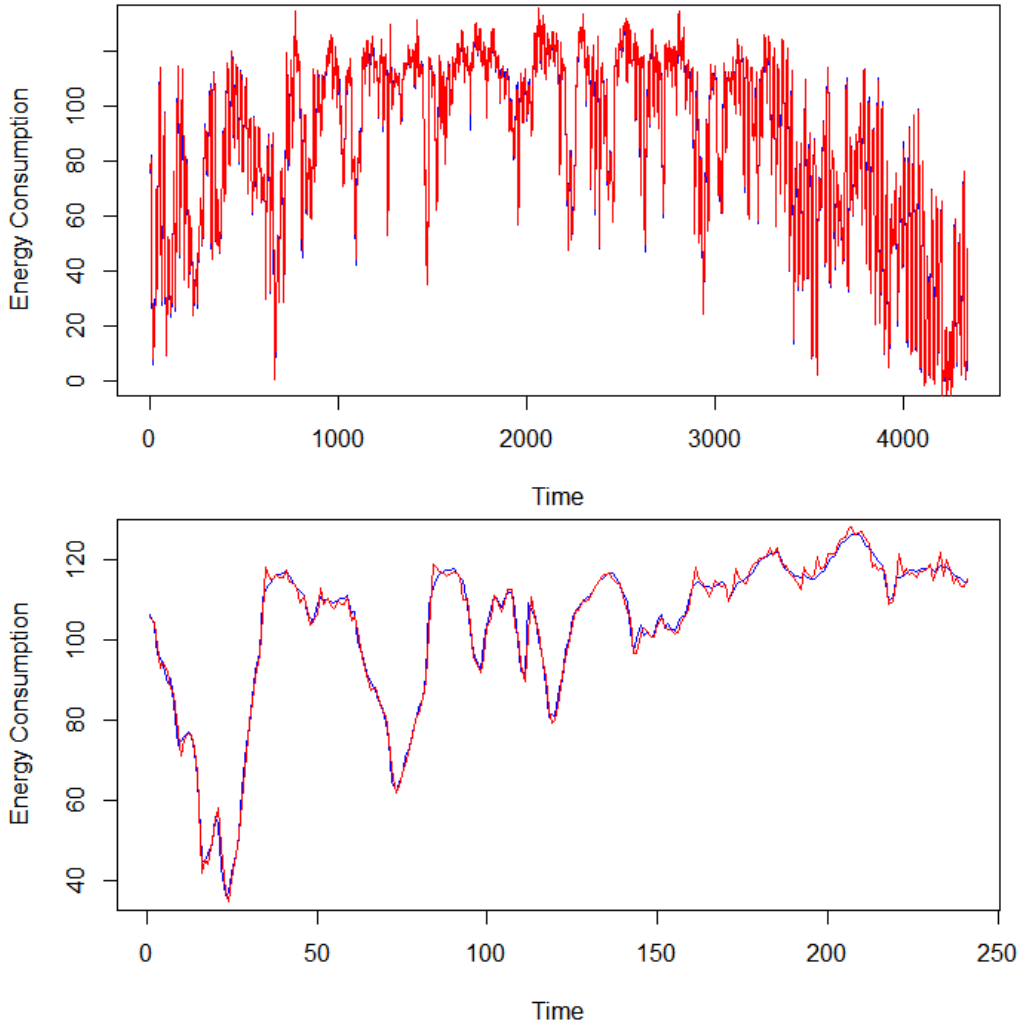


Figure 3.6: Simulation (blue) versus prediction (red) graph for heating demand profile [kWh] of B2 including the heating season (top) and 10 days period in late Dec. till early Jan. (bottom)

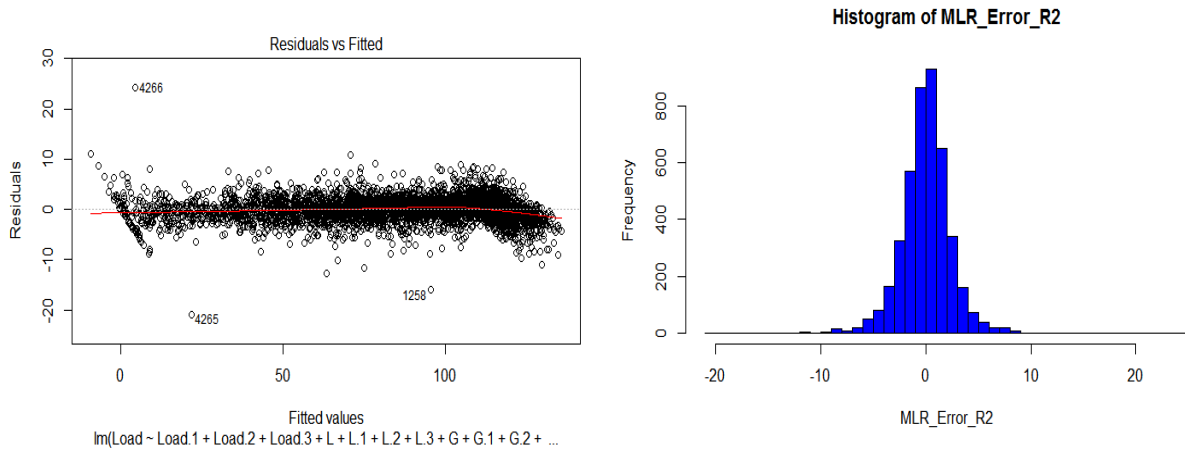


Figure 3.7: Results for B2 showing residual against fitted values (left) and error histogram (right)

3.3.2 Electrically heated floor

In cold climates, electricity demand for space heating becomes a critical issue for utility companies during certain periods of the day. Shifting a portion or all the demand to off-peak periods can help reduce peak demand and reduce stress on the electrical grid. Sensible TES systems, particularly electrically heated floors (EHF), can store thermal energy in buildings during the off-peak periods and release it during the peak periods while maintaining occupants' thermal comfort.

3.3.2.1 Background

To improve the performance of floor heating systems, it is important to understand the behavior and the importance of each layer of the assembly on their performance. The insulation layer between the ground and the floor heating system has a considerable influence on its performance. A thicker insulation layer is required to reduce heat losses to the ground for a floor heating system compared to a conventional system [96, 97]. Moreover, the concrete thickness affects the system performance. Using a hydronic floor heating system with concrete, the impact of the concrete layer on the performance of hydronic heating system was assessed where the floor surface temperature was found to be higher when the concrete layer was thin [98].

Although floor heating systems can shift part of or the entire space-conditioning load from peak periods to off-peak periods, they may not be able to provide the required thermal comfort, especially with intermittent heating mode. This can be investigated using a building simulation software, such as TRNSYS. However, the existing models for an EHF in TRNSYS do not allow the consideration of the thermal mass on the top of the EHF. Therefore, in this example, a procedure was developed for the integration of an EHF in TRNSYS. Then, the developed model was validated using experimental data.

3.3.2.2 Methodology

To model an EHF in TRNSYS, two methods can be used. The first method consists of using the *wall gain* which is defined as “an energy flux to the inside wall surface”. Considering that in TRNSYS the term “wall” is used whether it is positioned as an actual wall, floor or roof, the *wall gain* is thus analogous to simply defining a given heat flux on a surface. However, the *wall gain* can only be defined on the top of the surface and not within it, and consequently may change the storage system behavior.

The other method is to use the *active layer* in TRNSYS, which is designed for hydronic floor heating systems. By choosing a high water flow rate, a constant water temperature can be assumed, which can then behave as an EHF. However, the use of the active layer requires determination of the relationship between the parameters of the active layer (flow, pipe diameter, pipe conductivity, water temperature, etc.) and the EHF power. Moreover, to use this type of layer, some hypotheses should be verified [99], which may limit the parametric study.

In this example, the *wall gain* method was selected, with some modifications to go beyond the presented limit. Few modifications must be made in the floor assembly to use the wall gain for

an EHF integrated in a building. In an EHF, heating elements are uniformly placed within the concrete. Thus, the power is evenly distributed, and the concept of constant power gain can be applied to EHF. Then, to model the heat flux, a wall gain was used. To apply this surface gain for such application, a fictitious zone was created below the room zone, as presented in Figure 3.8. By having the size of the air volume of this fictitious zone infinitesimally small and assuming a high heat transfer coefficient for the fictitious zone, a perfect contact between the two layers can be assumed. In addition, the perimeter heat losses were neglected since the height of the air node of the fictitious zone is very small.

As depicted in Figure 3.8, the fictitious zone has one floor (connected to the ground) and one ceiling (connected to the room zone). Coupled together, these two zones represent all layers of the floor assembly. The wall gain, used as a surface gain (the EHF), is added on the upper-surface of the lower-wall (between the Floor_1 and Floor_2 as shown in Figure 3.9) to model the wires. The total thickness of each material (insulation, concrete and plywood) is the same in the two configurations.

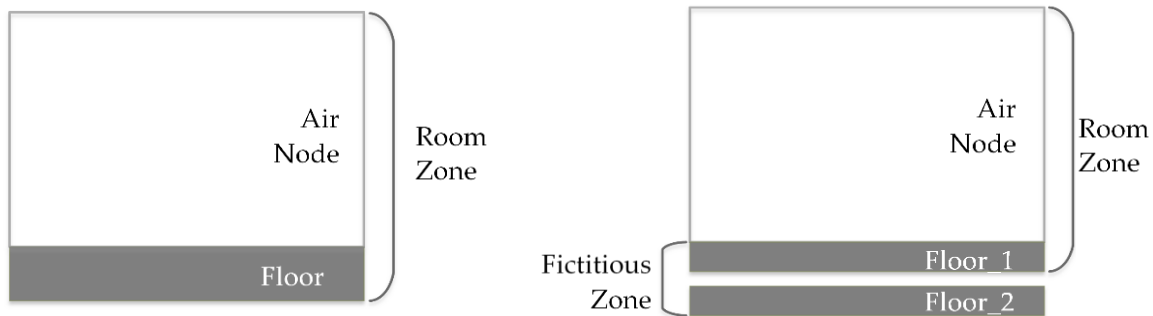


Figure 3.8: Conventional configuration of a room in TRNSYS (left) and configuration with the added fictitious zone in TRNSYS (right).



Figure 3.9: Conventional configuration of an EHF (electrically heated floor) (left) and configuration of the floor in TRNSYS with the added fictitious zone and the wall gain (right)

3.3.2.3 System description

The developed model was applied to a residential building in Montreal, Canada (Figure 3.10), which had been previously validated for electric baseboard with field measurement data [100] and used in previous studies [101]. To validate the model, the main concern was to make sure that the fictitious zone was properly created, and the proposed wall gain approach simulates the behavior of the system accurately.

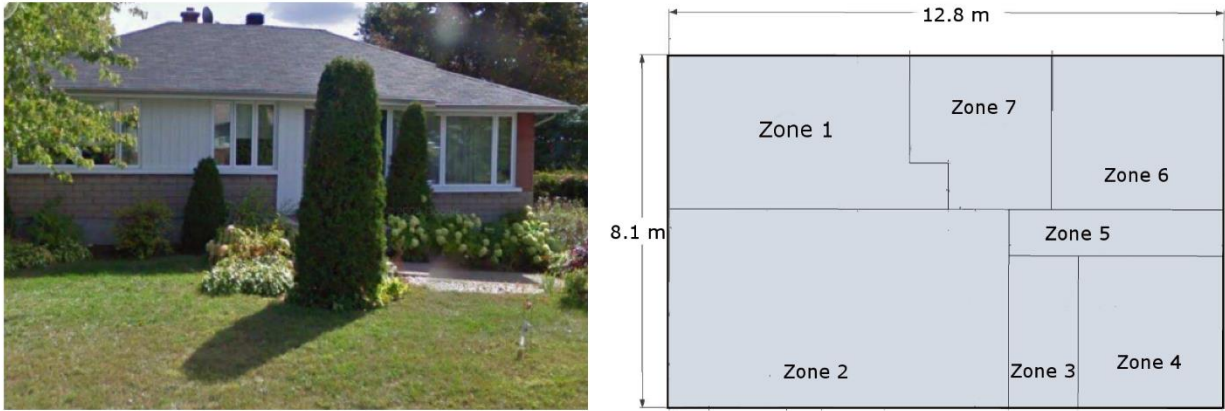


Figure 3.10: Experimental building including its picture (left), and its zones (right)

3.3.2.4 Results

In this section, the results for energy validation, temperature validation and inter-model comparison are presented. To validate the integration of the fictitious zone, the *wall gain* was set to zero, and electrical baseboards were used to heat the building with the same control strategy as the one used earlier (operating all day as a function of the indoor temperature with a set-point at 21 °C). Simulations were performed for one month (January), for the reference building (equipped with electrical baseboards only) and the modified one (with electrical baseboards and the EHF structure with the *wall gain* set to zero). The energy consumption of the two heating systems was compared by calculating the normalized mean bias error (NMBE). Details about the calculation procedure for this statistical index are accessible in the ASHRAE Guideline 14-2014 [102]. The results are presented in Table 3.2 where the passive EHF model is shown not to have any adverse effect on the building performance.

Table 3.2: Statistical index to compare energy consumptions of the reference and modified buildings

Statistical index	Monthly	Hourly
NMBE	0.20%	1.91%

To validate the assumption of perfect contact between the two concrete layers, the temperature on the bottom of Floor_1 was compared to the temperature on the top of Floor_2 (see Figure 3.8). These temperatures were obtained from TRNSYS simulation. The temperature difference between the upper side of Floor_2 and the lower side of Floor_1 was calculated for ten days. To ignore the initial condition effect, only the last eight days were considered for the analysis. The results showed an NMBE of less than 1%.

The inter-model comparison was conducted through the development of a finite-element mathematical model in MATLAB and validated using LISA, a CFD software. The radiant floor in the MATLAB environment is analyzed in two dimensions with the electric heating cables running perpendicular to the two considered axes. The objective was to analyze the temperature of the cable as well as the concrete in proximity to the cables. The size of the analyzed wires was 6.25 mm. The cable was assumed to be a square, with dimensions of 6.25 mm × 6.25 mm. The

dimensions governed the size of the elemental volumes around the cable. The discretization of the concrete around the wire is shown in Figure 3.11.

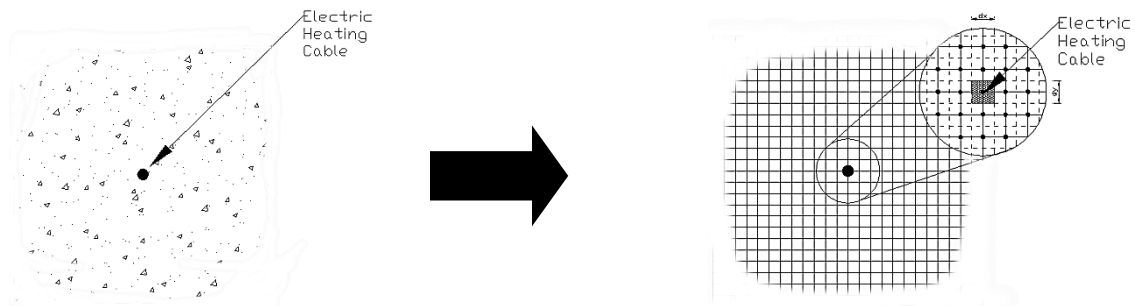


Figure 3.11: Discretization of thermal mass around electric heating cables

The model was validated by comparing its prediction to LISA. This simulation software is designed for matrix analyses using finite element analysis for complicated geometries of many types such as structural, heat flow and acoustics. The discretization of the thermal mass and cables in the LISA graphical interface was executed to achieve much smaller elemental volumes. In addition, the arrangement of the nodes was performed in a way to have the nodes much closer to one another near the cable. There was an acceptable agreement between the predictions made by the two models. Error values of 0.2% and 3.6% were observed for the floor surface temperature and electrical cable temperature, respectively. The temperature distribution from the MATLAB interface is shown in Figure 3.12 for an initial concrete temperature of 20 °C and a charging duration of 10 hours.

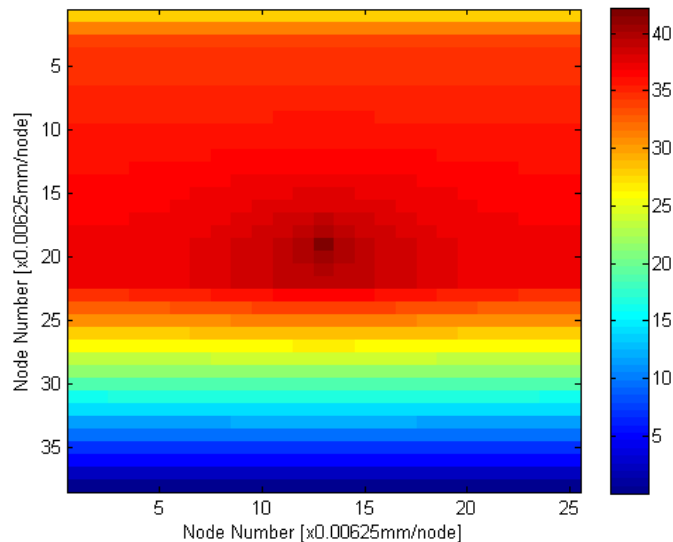


Figure 3.12: Temperature distribution within the zone after 10 hours of continuous heating

The predicted temperature at the heating cable height from an equivalent TRNSYS study was 32.38 °C, while the 2D MATLAB model predicted a temperature of 35.48 °C in close proximity to the cables. This shows that for this type of system, a 1D analysis (TRNSYS model)

underestimated the temperature of the cables. However, the average temperature along the height of the cables from the 2D model output was 31.11 °C, which is very close to the 1D model. The average surface temperature of the 2D model was 24.26 °C. The floor surface was almost isothermal due to the concrete thickness in the assembly. Nonetheless, the same quantity of heat was stored in both models, with a difference of only 0.312%. The TRNSYS simulation overestimated the surface temperature by approximately 1 °C.

3.3.3 Triplex tube heat exchanger with PCM

PCMs received considerable attention for building and district TES applications in recent years. This is mainly due to the high thermal storage capacity of PCMs compared to the sensible heat storage methods.

The ultimate goal of charging any thermal storage system is to use the stored heat when needed. Generally, PCM storages could be classified into two major categories based on their charging/discharging capabilities. The first category includes those storages which are consecutively charged and discharged by the same heat transfer fluid (HTF) path. For instance, the same tube first carries the hot HTF to charge the storage and then the cold HTF is flown through to discharge it. In essence, such storages are not capable of simultaneous charging and discharging (SCD) due to the restricted configuration. An insulated shell and tube heat exchanger (STHX) is an example of such storages. In contrast, the second category is capable of SCD due to the separate HTF paths. Thus, based on the control strategy, occupant behavior, etc. the PCM could undergo charging or discharging or a combination of both.

Storages of the first category are the most common ones and are not able to efficiently handle continuous operation, when the storage needs to be simultaneously charged and discharged. In real life applications, PCMs might go through SCD several times. In such scenarios, a PCM undergoes charging from one hand, while it simultaneously faces discharging from the other. Specifically, SCD can happen when dealing with unpredictable occupant behavior or intermittent consumption. For instance, in the case of solar domestic hot water (SDHW), water consumption might occur during sunshine hours; i.e. at the same time when the thermal storage is being charged.

Despite the applicability of the second type storages, the issue of simultaneous charging and discharging did not receive enough attention from the research community especially because it is not an efficient and desirable way of heat transfer. Besides, researchers face several challenges for such systems regarding the thermal conductivity enhancement of the PCM and optimizing the heat exchange area.

For efficient integration of TES systems with PCM in buildings and districts, storage systems should be able to handle different charging and discharging scenarios. Understanding and investigating the heat transfer mechanisms inside thermal storage systems of the second category is necessary to develop simple and reliable models of such systems, which can be used to optimize the integration.

3.3.3.1 Background

According to the literature, the numerical analysis of the phase change process of PCMs could generally be classified into two major categories based on the considered heat transfer mechanism: the pure conduction (PC) model and the combined conduction and natural convection (CCNC) model. Early numerical modeling of the process considered only conduction as the dominant heat transfer mechanism during the melting and solidification processes [103]. This is equivalent to a circular (or cylindrical in 3D) PCM melting front shape around a tube [104, 105]. However, during the phase change process, the density changes create buoyancy forces resulting in natural convection in the melted PCM, which affects the heat transfer. The effect of natural convection on the phase change process has been reported experimentally [106, 107]. Nevertheless, some simple approaches (such as the well-known ϵ -NTU approach for heat exchanger design) ignore the effect of natural convection. Ignoring this effect resulted in the underestimation of effectiveness values during melting and solidification processes [108]. Therefore, it is important to compare the results of the real process considering the effect of natural convection with those of the pure conduction assumption in order to understand the deviation of such an assumption from the reality.

The literature about phase change process of PCMs had a routine trend over the course of these years. This trend includes investigation of a PCM under a one-time charging or one-time discharging process or considering consecutive charging and discharging periods. Therefore, it is assumed that the PCM is initially completely melted/solidified and then it undergoes solidification/melting. This ideal assumption ignores the fact that in real life applications, PCMs might, as presented earlier, go through SCD. In this example, the results of a numerical study related to a triplex tube heat exchanger (TTHX) under SCD is presented.

3.3.3.2 System description

Certain configurations have the capability of providing SCD such as TTHXs. Basically, a TTHX is a concentric configuration of three tubes. For thermal storage applications, the middle tube is filled with a PCM while the inner and outer ones carry the HTFs. Therefore, the PCM is surrounded in an annulus as shown in Figure 3.13. The heat exchanger had inner and middle tubes with nominal diameters of 2 and 5 inches, respectively. Thus, the inner tube had a radius (r_i) of 25.51 mm and a thickness of 1.47 mm. The middle tube had a radius (r_o) of 62.32 mm with 4.32 mm of thickness.

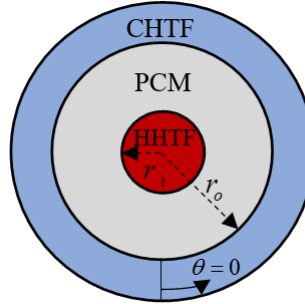


Figure 3.13: Schematic representation of the triplex tube heat exchanger

A commercial PCM (RT31, Rubitherm Technologies GmbH) was considered for the investigation. Table 3.3 shows the thermophysical properties of the PCM, which filled the middle space in the TTHX as shown in Figure 3.13.

Table 3.3: Thermophysical properties of RT31 [109]

Property	Symbol	Value
Solidus temperature	T_s	300.15 K (27 °C)
Liquidus temperature	T_l	306.15 K (33 °C)
Solid density	ρ_s	880 kg/m ³
Liquid density	ρ_l	760 kg/m ³
Specific heat capacity	C_p	2,000 J/kg.K
Latent heat of fusion	λ	170,000 J/kg
Thermal conductivity	k	0.2 W/m.K
Thermal expansion coefficient	β	0.00076 1/K
Dynamic viscosity	μ	0.002508 kg/m.s

3.3.3.3 Methodology

In this section, the modeling procedure and its assumptions as well as the initial and boundary conditions are presented.

According to the physics of the problem as well as the common assumptions used in the literature, the following assumptions were made for the PCM phase change modeling:

- The flow of the liquid PCM was considered as laminar, incompressible Newtonian fluid flow,
- Viscous dissipation was neglected since large velocity gradients were not present,
- No-slip boundary condition was present,
- At the boundaries, heat transfer occurred with the corresponding HTF (Dirichlet boundary condition),
- Liquid fraction variation was assumed to be linear with temperature, and
- Phase-wise constant thermophysical properties for the PCM except for the density, which was evaluated based on Boussinesq approximation to account for the buoyancy forces.

Since the problem was symmetric ($\theta=0$), half of the annulus was modeled to save computational time. The governing equations were developed as follows:

3.3.3.3.1 Continuity equation

Based on the assumptions, the continuity equation is:

$$\frac{\partial \rho}{\partial t} + \frac{1}{r} \frac{\partial}{\partial r} (\rho r v_r) + \frac{1}{r} \frac{\partial}{\partial \theta} (\rho v_\theta) = 0 \quad (3.6)$$

3.3.3.3.2 Momentum balance

To develop momentum balance equations, Darcy's law was used to account for the flow of the mushy PCM due to the natural convection. The law appears as a source term in the momentum balance [110]:

$$S_i = \frac{C(1-\gamma)^2}{\gamma^3 + \varepsilon} u_i \quad (3.7)$$

where γ is the liquid fraction of the melted PCM, which will be presented later. To avoid division by zero, ε is added to the denominator with the value of 0.001 [111]. The mushy zone parameter C in Equation (3.7) is a measure that indicates the steepness of reaching zero velocity during solidification. In this example, a value of $10^5 \text{ kg.m}^{-3}.\text{s}^{-1}$ was considered for this parameter. The following equations were developed for the two velocity components:

$$\begin{aligned} \frac{\partial(\rho v_r)}{\partial t} + \frac{1}{r} \frac{\partial(\rho r v_r v_r)}{\partial r} + \frac{1}{r} \frac{\partial(\rho v_r v_\theta)}{\partial \theta} = \\ -\frac{\partial p}{\partial r} + \mu \left[\frac{\partial}{\partial r} \left(\frac{1}{r} \frac{\partial}{\partial r} (r v_r) \right) + \frac{1}{r^2} \frac{\partial^2 v_r}{\partial \theta^2} - \frac{2}{r^2} \frac{\partial v_\theta}{\partial \theta} \right] + \rho g \cos \theta - \frac{C(1-\gamma)^2}{\gamma^3 + \varepsilon} v_r \end{aligned} \quad (3.8)$$

$$\begin{aligned} \frac{\partial(\rho v_\theta)}{\partial t} + \frac{1}{r} \frac{\partial(\rho r v_r v_\theta)}{\partial r} + \frac{1}{r} \frac{\partial(\rho v_\theta v_\theta)}{\partial \theta} = \\ -\frac{1}{r} \frac{\partial p}{\partial \theta} + \mu \left[\frac{\partial}{\partial r} \left(\frac{1}{r} \frac{\partial}{\partial r} (r v_\theta) \right) + \frac{1}{r^2} \frac{\partial^2 v_\theta}{\partial \theta^2} + \frac{2}{r^2} \frac{\partial v_r}{\partial \theta} \right] - \rho g \sin \theta - \frac{C(1-\gamma)^2}{\gamma^3 + \varepsilon} v_\theta \end{aligned} \quad (3.9)$$

Boussinesq approximation was introduced to account for the natural convection process in the melted PCM [111, 112]:

$$\rho = \rho_l [1 - \beta(T - T_l)] = \frac{\rho_l}{C_p} [1 - \beta(h - h_l)] \quad (3.10)$$

where β is the thermal expansion coefficient.

3.3.3.3.3 Energy balance

Enthalpy method was adopted for the problem since it has been proven to prevent the difficulties of phase change front tracking of the normal energy balance equation [111]. Energy balance in terms of enthalpy variations is:

$$\frac{\partial(\rho h)}{\partial t} + \frac{1}{r} \frac{\partial(\rho r v_r h)}{\partial r} + \frac{1}{r} \frac{\partial(\rho v_\theta h)}{\partial \theta} = \frac{k}{C_p} \left[\frac{1}{r} \frac{\partial}{\partial r} \left(r \frac{\partial h}{\partial r} \right) + \frac{1}{r^2} \frac{\partial^2 h}{\partial \theta^2} \right] - S_h \quad (3.11)$$

where the source term is:

$$S_h = \frac{\partial(\rho \Delta H)}{\partial t} + \frac{1}{r} \frac{\partial(\rho r v_r \Delta H)}{\partial r} + \frac{1}{r} \frac{\partial(\rho v_\theta \Delta H)}{\partial \theta} \quad (3.12)$$

In these equations h and ΔH account for sensible and latent heat, respectively. Furthermore:

$$\Delta H = \gamma \lambda \quad (3.13)$$

where γ is the liquid fraction whose variation was assumed to be linear during the phase change process:

$$\gamma = \begin{cases} 0 & T < T_s \\ \frac{T - T_s}{T_l - T_s} & T_s < T < T_l \\ 1 & T > T_l \end{cases} \quad (3.14)$$

3.3.3.3.4 Initial and boundary conditions

According to the previous assumptions and Figure 3.13, the PCM was heated by the inner tube carrying hot heat transfer fluid (HHTF), while it was simultaneously cooled down by the cold heat transfer fluid (CHTF). Therefore, initial and boundary conditions for inside heating/outside cooling mode were defined as:

$$\begin{aligned}
t = 0 &\longrightarrow T = T_i \\
r = r_i &\longrightarrow \begin{cases} v_r = 0 \\ v_\theta = 0 \\ T = T_{HHTF} \end{cases} \\
r = r_o &\longrightarrow \begin{cases} v_r = 0 \\ v_\theta = 0 \\ T = T_{CHTF} \end{cases} \\
\theta = 0, \pi &\longrightarrow \begin{cases} \frac{\partial v_r}{\partial \theta} = 0 \\ v_\theta = 0 \\ \frac{\partial T}{\partial \theta} = 0 \end{cases}
\end{aligned} \tag{3.15}$$

while for outside heating/inside cooling only the HTF temperatures were swapped at inner and outer boundaries. Constant wall temperature values of 40 °C and 20 °C were assumed for the HHTF and CHTF, respectively. The PCM was assumed to be initially fully melted or solidified depending on the case under investigation.

3.3.3.3.5 Software tools

There is several commercial software available for numerical analysis of the melting/solidification process. However, according to a recent review [113], ANSYS Fluent is the most widely accepted and utilized software among researchers. Therefore, numerical study of the developed model was conducted using ANSYS Fluent v16.2. ANSYS Fluent uses the enthalpy-porosity approach in which the mushy zone is considered as a porous medium where the liquid fraction is its porosity.

A step-by-step approach was taken in ANSYS Workbench to simulate the process. First, the 2D symmetric half of the annulus was sketched in the DesignModeler environment. Thereafter, ANSYS Meshing generated the mesh. Then, the simulation was set up in ANSYS Fluent environment. To solve the equations, pressure-based solver was used since it is the only option in the software for solving melting/solidification processes. Semi-implicit pressure-linked equation (SIMPLE) method was used for pressure-velocity coupling. For spatial discretization of pressure and momentum, PRESTO (pressure staggering option) and QUICK schemes were adopted, respectively.

3.3.3.4 Results

This section presented the numerical investigation results for simultaneously charged and discharged PCM with different heat transfer modes and different initial conditions. Eight cases were compared showing the effect of natural convection on the phase change process (see Figure 3.14). The most important findings are:

- For the case of internal heating/external cooling, the natural convection did not affect the lower half of the system since it had almost similar temperature distribution; however, the top half was greatly affected by the buoyancy forces and natural convection of the melted PCM. On the other hand, for the case of internal cooling/external heating, the upward PCM motion affected the entire domain.
- Depending on the initial condition of the PCM, different liquid fraction, temperature, and solid-liquid interface locations were observed, which was totally different from the results obtained from the pure conduction model. This shows how far from reality such an assumption could be and to have accurate modeling of SCD, natural convection should be considered.
- Comparing the average temperature and liquid fraction results, it was found that the pure conduction model could be applied to the initially fully melted PCM under SCD with a small error, but for the initially solidified PCM neglecting the natural convection would result in an unacceptably high error.

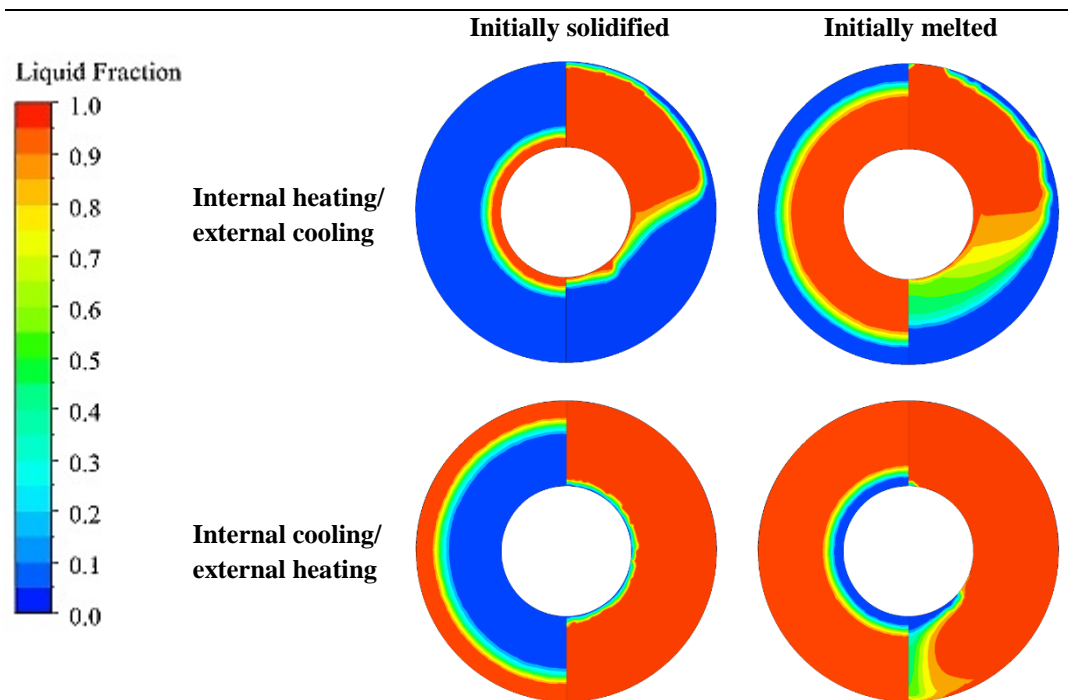


Figure 3.14: Comparison of the steady solid-liquid interface for pure conduction model (left half) and combined conduction and natural convection model (right half) for the phase change material

3.3.4 Shell and tube heat exchanger with PCM

Shell and tube heat exchangers (STHXs) are used in several engineering applications particularly due to their manufacturing simplicity and economic feasibility [114]. Agyenim et al. reviewed the materials, heat transfer and phase change problem formulation for latent heat TES units [115]. It was concluded that the most intensely studied unit was the shell and tube storage,

accounting for about 70% of publications. Latent heat storage STHXs have found application in solar domestic hot water systems [114], solar thermal plants [116], solar collectors [117], etc.

The possible heat transfer mechanisms in PCMs are conduction, convection or a combination of both. Therefore, the simulation methods in the literature are based on the considered heat transfer mechanism: the pure conduction (PC) model and the combined conduction and natural convection (CCNC) model. Due to the complexity of the CCNC model, to account for the buoyancy effect during the melting process, effective thermal conductivity was introduced in order to have better accuracy in the ε -NTU method. Comparing the results of the ε -NTU method (1D) and CFD (3D) with experimental data [108], it was found that the 1D ε -NTU method could be utilized for PCM heat exchanger design instead of the complicated time-consuming 3D CFD if the natural convection is accurately accounted by the effective thermal conductivity. It is common to develop power law effective thermal conductivity correlations as a function of Rayleigh number; i.e. $c(Ra)^n$ [118-120]. Nevertheless, the main disadvantages of effective thermal conductivity are: (1) experimental data should be available *a priori* to evaluate the effective thermal conductivity; (2) derivation of effective thermal conductivity is a tedious task since several thermal conductivity values should be examined to find the one that has similar heat transfer rate as that of the experimental data; (3) a constant value cannot be designated to the effective thermal conductivity of a fluid with varying temperature [121]; and (4) despite all the complexity, it cannot provide information about the melting front location since it is essentially a conduction model.

3.3.4.1 Background

During the phase change process, knowing the location of melting front is greatly important since it shows what portion of the storage has gone through the phase change (also known as the liquid fraction) as well as the speed of the front propagation. However, this knowledge has been proven to be hard to obtain, particularly experimentally. Calculation of liquid fraction from experimental data was formerly conducted by interruption of the process at various stages to remove the remaining solid part [122]. However, in recent years, utilization of transparent tubes for direct visual observation [123] or digital high resolution photography [124], which might include image processing [125], replaced the old technique. Due to such complexities, it is preferred to obtain liquid fraction values from numerical analysis.

In early numerical studies, front tracking was a great challenge. The problem was the complexity of simultaneously solving the conventional energy equation for solid and liquid domains together with the energy balance at the melting front (i.e. a moving-boundary problem). However, the introduction of enthalpy method significantly improved numerical studies by replacing the simultaneous solving approach with a single enthalpy-based energy equation for the whole domain [111]. Nevertheless, melting front tracking by enthalpy method is a two-step process, where first the enthalpy values are calculated and then the location of the melting front is determined from the respective temperature values [126]. Furthermore, as of today, the numerical analysis is still complicated and computationally intense and requires expertise to develop in-house codes or familiarity with commercial software.

Therefore, several studies developed correlations to characterize the phase change process within PCMs. According to the literature, most of the old studies focused on the phase change time by developing correlations for Fourier number (Fo), whereas liquid fraction (γ) correlations received attention more recently. Besides, absence of Rayleigh number (Ra) in many correlations shows that the effect of natural convection was neglected. Overall, despite separate correlation developments for natural convection as well as pure conduction model, no study has focused on a correlation between these two models.

Therefore, it is desirable to develop a simplified method, which (1) can provide the results of the CCNC model from PC model results and (2) can approximate the melting front location (outperforming the effective thermal conductivity method).

3.3.4.2 System description

In the horizontal STHXs, the PCM filled the shell side forming an annulus as shown in Figure 3.15. Three different geometries were used in this study to generate the required data. Table 3.4 shows the geometrical properties of the investigated STHXs. The shell diameter was fixed whereas tube diameter was altered.

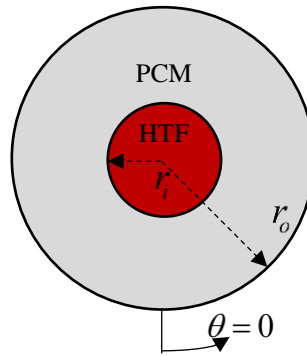


Figure 3.15: Schematic representation of the STHXs

Table 3.4: Geometrical properties of the STHXs [127]

Geometry	Radius (mm)				Shell-to-tube radius ratio
	Tube		Shell		
	Inner	Outer	Inner	Outer	
Geometry 1	25.51	26.98	62.32	65.09	2.31
Geometry 2	37.86	39.69	62.32	65.09	1.57
Geometry 3	49.97	52.38	62.32	65.09	1.19

Commercial paraffin-based PCMs (from Rubitherm Technologies GmbH) were considered for the investigation whose thermophysical properties are tabulated in Table 3.5. It should be noted that the highlighted PCM (RT35HC) was not included in the model development phase to be used later for verification purposes.

Table 3.5: Thermophysical properties of the PCMs [128]

Property	Dimension	Symbol	RT31	RT35	RT35HC	RT44HC
Solidus temperature	K (°C)	T_s	300.15 (27)	302.15 (29)	307.15 (34)	314.15 (41)
Liquidus temperature	K (°C)	T_l	306.15 (33)	309.15 (36)	309.15 (36)	317.15 (44)
Solid density	kg/m ³	ρ_s	880	860	880	800
Liquid density	kg/m ³	ρ_l	760	770	770	700
Specific heat capacity	J/kg.K	C_p	2,000	2,000	2,000	2,000
Latent heat of fusion	J/kg	λ	170,000	160,000	240,000	250,000
Thermal conductivity	W/m.K	k	0.2	0.2	0.2	0.2
Thermal expansion coefficient	1/K	β	0.00076	0.00076	0.00076	0.00076
Dynamic viscosity	kg/m.s	μ	0.002508	0.002500	0.002700	0.003300

3.3.4.3 Methodology

The modeling approach has already been introduced and validated in an earlier study [129]. Nevertheless, the non-dimensionalized form of the equations are presented here. The dimensionless parameters are listed in Table 3.6. Moreover, modified pressure (P) is defined in a way that:

$$\frac{\partial P}{\partial r} = \frac{\partial p}{\partial r} - \rho g \cos \theta \quad (3.16)$$

where p is the pressure.

Table 3.6: List of dimensionless parameters

Name	Formula	Name	Formula
Dimensionless time (Fo)	$Fo = \frac{\alpha t}{D_i^2}$	Dimensionless radius	$r^* = \frac{r}{D_i}$
Dimensionless velocity (r)	$U = \frac{v_r D_i}{\alpha}$	Dimensionless velocity (θ)	$V = \frac{v_\theta D_i}{\alpha}$
Dimensionless pressure	$P^* = \frac{PD_i^2}{\rho \alpha^2}$	Dimensionless Darcy coefficient	$C^* = \frac{C(1-\gamma)^2 D_i^2}{(\gamma^3 + \delta) \rho \alpha}$
Prandtl number	$Pr = \frac{\nu}{\alpha}$	Rayleigh number	$Ra = \frac{g \beta (T - T_s) D_i^3}{\nu \alpha}$
Dimensionless enthalpy	$h^* = \frac{h}{\lambda}$	Stefan number	$Ste = \frac{C_p (T - T_s)}{\lambda}$

Substitution of these parameters in the governing equations yields where the continuity equation is:

$$\frac{\partial \rho}{\partial Fo} + \frac{1}{r^*} \frac{\partial}{\partial r^*} (\rho r^* U) + \frac{1}{r^*} \frac{\partial}{\partial \theta} (\rho V) = 0 \quad (3.17)$$

The momentum balances in r and θ directions are:

$$\frac{\partial U}{\partial Fo} + U \frac{\partial U}{\partial r^*} + \frac{V}{r^*} \frac{\partial U}{\partial \theta} - \frac{V^2}{r^*} = -\frac{\partial P^*}{\partial r^*} + Pr \left[\frac{\partial}{\partial r^*} \left(\frac{1}{r^*} \frac{\partial}{\partial r^*} (r^* U) \right) + \frac{1}{(r^*)^2} \frac{\partial^2 r^*}{\partial \theta^2} - \frac{2}{(r^*)^2} \frac{\partial V}{\partial \theta} \right] - \frac{Ra \cdot Pr}{Ste} (h^* - h_{ref}^*) \cos \theta - C^* U \quad (3.18)$$

$$\frac{\partial V}{\partial Fo} + U \frac{\partial U}{\partial r^*} + \frac{V}{r^*} \frac{\partial V}{\partial \theta} + \frac{UV}{r^*} = -\frac{1}{r^*} \frac{\partial P^*}{\partial \theta} + Pr \left[\frac{\partial}{\partial r^*} \left(\frac{1}{r^*} \frac{\partial}{\partial r^*} (r^* V) \right) + \frac{1}{(r^*)^2} \frac{\partial^2 V}{\partial \theta^2} + \frac{2}{(r^*)^2} \frac{\partial U}{\partial \theta} \right] + \frac{Ra \cdot Pr}{Ste} (h^* - h_{ref}^*) \sin \theta - C^* V \quad (3.19)$$

Finally, the energy balance is:

$$\left(\frac{\partial h^*}{\partial Fo} + U \frac{\partial h^*}{\partial r^*} + \frac{V}{r^*} \frac{\partial h^*}{\partial \theta} \right) + \left(\frac{\partial \gamma}{\partial Fo} + U \frac{\partial \gamma}{\partial r^*} + \frac{V}{r^*} \frac{\partial \gamma}{\partial \theta} \right) = \frac{1}{r^*} \frac{\partial}{\partial r^*} \left(r^* \frac{\partial h^*}{\partial r^*} \right) + \frac{1}{(r^*)^2} \frac{\partial^2 h^*}{\partial \theta^2} \quad (3.20)$$

To conduct simulations, each PCM (see Table 3.5) was used within each storage (see Table 3.4). Table 3.7 shows the combination of Stefan numbers and shell-to-tube radius ratios (R). It should be noted that the three cases designated by ‘‘Ver’’ indicate the cases used for verification purpose. Since simulations were required for both PC and CCNC models, a total of 42 simulations were carried out.

Table 3.7: The investigated values of Stefan and shell-to-tube radius ratios

Case	Ste	R	Case	Ste	R	Case	Ste	R
Case 1	0.16	2.31	Case 7	0.25	2.31	Case 13	0.47	2.31
Case 2	0.16	1.57	Case 8	0.25	1.57	Case 14	0.47	1.57
Case 3	0.16	1.19	Case 9	0.25	1.19	Case 15	0.47	1.19
Case 4	0.24	2.31	Case 10	0.32	2.31	Case 16	0.50	2.31
Case 5	0.24	1.57	Case 11	0.32	1.57	Case 17	0.50	1.57
Case 6	0.24	1.19	Case 12	0.32	1.19	Case 18	0.50	1.19
Ver 1	0.17	2.31	Ver 2	0.17	1.57	Ver 3	0.33	1.19

In this example, the intent is to use the PC model liquid fraction as a measure of time to be able to link the PC and CCNC models. Therefore, instead of time, the liquid fraction of the CCNC model would be a function of that of the PC model.

When dealing with the PC model, the melting front departs from the HTF tube towards the outer shell forming a circular shape (i.e. cylindrical in 3D). This is due to the fact that gravity has no effect on the results of this model. Therefore, the upper and lower halves of the system have equal liquid fraction values, which is equal to that of the PC model:

$$\gamma_{PC} = \gamma_{PC}^L = \gamma_{PC}^U \quad (3.21)$$

However, in reality, buoyancy forces create an upward melted PCM motion affecting the upper half of the system. The logic behind the method is to assume that the difference between the results of the CCNC and PC models is due to the natural convection:

$$\gamma_{Conv} = \gamma_{CCNC} - \gamma_{PC} \quad (3.22)$$

At the initial stages of melting, conduction is the dominant heat transfer mechanism. This is due to the lack of enough melted PCM to create an upward buoyancy-driven motion. As soon as enough PCM is melted, convection establishes, which later dominates the heat transfer. Based on this, the simplified method assumes that the lower half of the system remains the same as that of the PC model. This assumption is not far from reality, which has been reported in detail [130]. Therefore, the lower half would have a semi-circular (or semi-cylindrical in 3D) front. On the other hand, the effect of natural convection is designated solely to the upper half of the system. Thus, the difference between the CCNC and PC models is only attributed to the melting front propagation at the upper half, as long as the liquid fraction of the upper half is lower than unity. In other words, the upper and lower halves of the system would have two semi-circular (or semi-cylindrical in 3-D) front shapes where the radius of the upper half's front is larger than that of the lower half (see Figure 3.16). A correlation (f_1) is developed to map the PC model liquid fraction to that of the upper half.

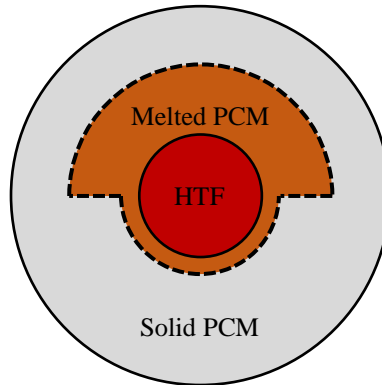


Figure 3.16: Schematic representation of two separate melting fronts for upper and lower halves

Once the upper half of the PCM is fully melted (i.e. when its liquid fraction reaches one), the rest of the melting is attributed to the lower half, differing it from the PC model. The melting process continues until the maximum liquid fraction value is reached. In such conditions, another correlation (f_2) is developed to map the PC model liquid fraction to that of the lower half. When there are two separate melting fronts for the upper and lower halves, the overall liquid fraction value would be the average of the two:

$$\gamma = \frac{\gamma^U + \gamma^L}{2} \quad (3.23)$$

Therefore, the developed correlations are independent of time (i.e. Fourier number) and instead dependent on the liquid fraction of the PC model. Figure 3.17 shows the flowchart of the method for users. In order to generalize the flowcharts, the first decision symbol (i.e. the first diamond) compares the liquid and solid density values of the PCM. This is to make sure that the natural convection is designated to the correct half of the system. For several materials with lower liquid density, the buoyancy-induced motion is upward. However, for other materials such as water, the flow is downward.

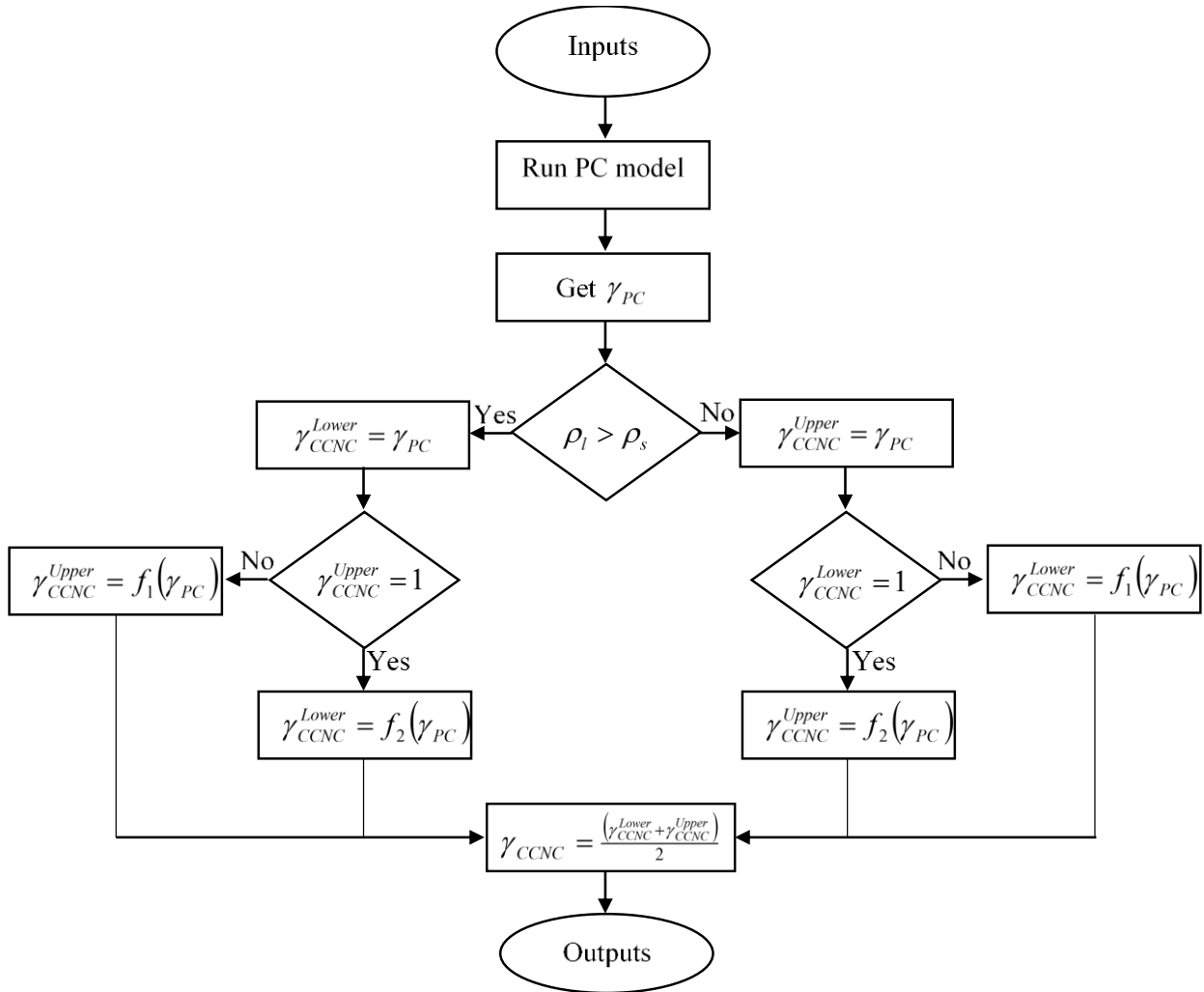


Figure 3.17: Flowchart of the novel front tracking method

3.3.4.4 Results

Figure 3.18 shows the variation of upper half liquid fraction values versus those of the pure conduction model. Despite showing the results for different PCMs, the figure is dominated by

three separate lines, each of which representing a geometry as presented in Table 3.4. Interestingly, the data for each geometry almost coincide, which confirms that the only effective parameter for the upper half liquid fraction versus that of the PC model is the geometrical properties of the system. In other words, the thermophysical properties of the PCMs have negligible effect. Therefore:

$$\gamma^U = c(R)^m (\gamma_{PC})^n \quad (3.24)$$

where c , m and n are the three constants of the equation and R is the shell-to-tube radius ratio:

$$R = \frac{r_o}{r_i} \quad (3.25)$$

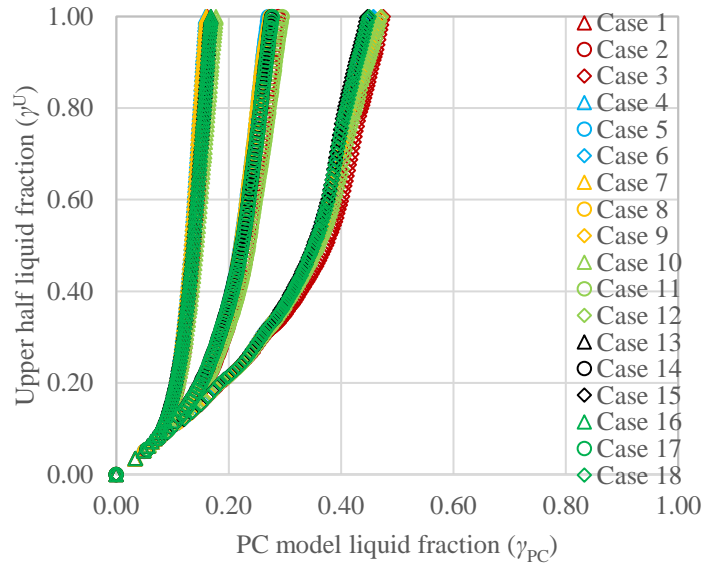


Figure 3.18: Variation of the upper half liquid fraction versus PC model liquid fraction

The multiple variable regression analysis was applied to the to the upper half liquid fraction data. Regression results with 95% confidence level using least-squares method for all the cases are graphically shown in Figure 3.19 and the constants are tabulated in Table 3.8. The figure also shows that the majority of the data points (about 95%) lie within the range of $\pm 15\%$ discrepancy from the linear curve.

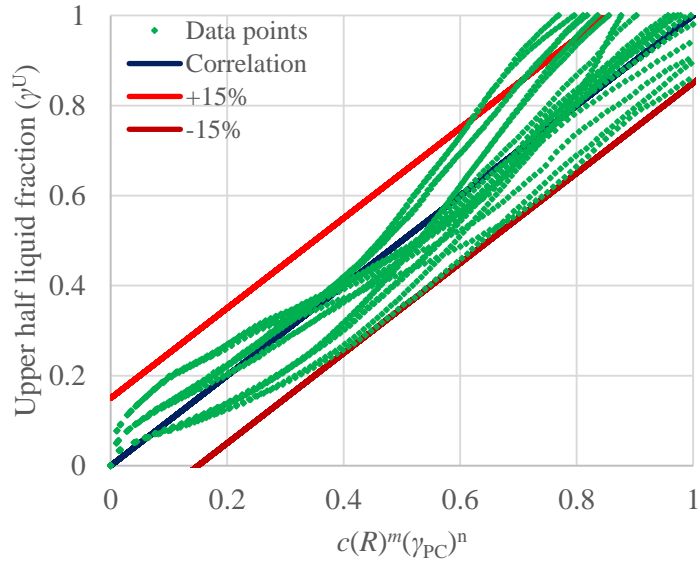


Figure 3.19: Variation of the upper half liquid fraction versus the developed correlation

Table 3.8: Constants of Equation (3.24) for the upper half liquid fraction

C	m	n	R^2	Range
3.981	3.747	2.553	0.9209	$R = 1.19 - 2.31$

Correlation development for the lower half is not as straightforward as the upper half. First of all, in order to use the same correlation format for the lower half, some modifications are required. The reason is graphically shown in Figure 3.20 for Case 17 (see Table 3.7) as an example.

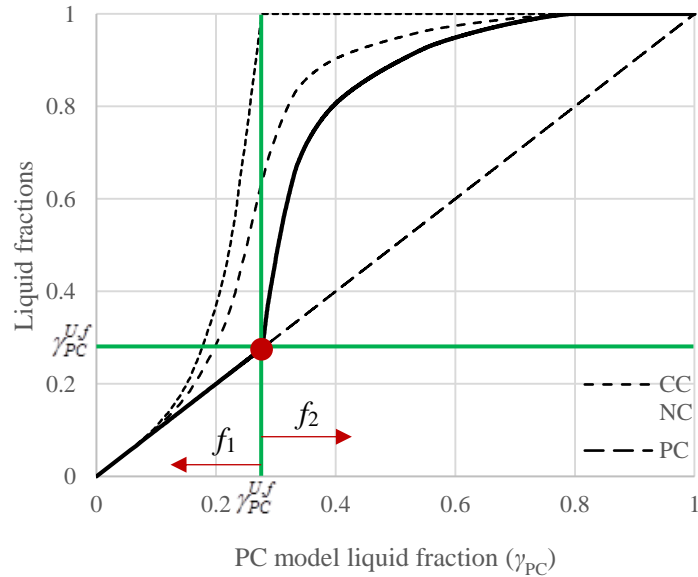


Figure 3.20: Liquid fraction variation for Case 17

According to Figure 3.20, since the lower half correlation (f_2) should initiate upon completion of melting in the upper half (shown by the vertical green line), its initial PC model liquid fraction value would be the last one of the upper half correlation (f_1). In other words, for each case, there is a different liquid fraction value of the PC model ($\gamma_{PC}^{U,f}$), upon which the upper half is completely melted, which is the starting point for the lower half correlation. To have consistency with the upper half, the coordinate of the origin should be transformed to that point (shown by a red dot). Consequently, for the horizontal and vertical axes, the values are modified so that the initial value for all the cases is zero, which would otherwise be different for each case, making the regression meaningless:

$$\gamma_{PC}^{mod} = \gamma_{PC} - \gamma_{PC}^{U,f} \quad (3.26)$$

$$\gamma^{L,mod} = \gamma^L - \gamma_{PC}^{U,f} \quad (3.27)$$

Another modification is related to the nature of conduction heat transfer. As the melting front propagates, the thermal resistance between the hot HTF tube and the melting front increases. Therefore, the heat transfer rate and consequently the rate of liquid fraction change decreases with time. Since this liquid fraction is used as the horizontal axis, whereas that of the lower half (which considers the effect of natural convection) is used as the vertical axis, after a certain period, the graph would become more and more vertical. The time when this happens (if any) depends on the thermophysical properties of the PCM, the geometrical properties of the thermal storage and the boundary conditions. To prevent complexity of the method and upon careful examination of the PC model data, it was found that prior to a certain time when the slope of PC model liquid fraction versus time is higher than 10^{-5} , a format close to that of the upper half could be utilized.

The variation of the modified lower half liquid fraction values versus the modified PC model results is shown in Figure 3.21. Again, three main separate lines exist in the figure per geometry; however, due to the vicinity of the data points, they are barely distinguishable. Therefore, a similar format to that of the upper half is adopted:

$$\gamma^{L,mod} = c(R)^m (\gamma_{PC}^{mod})^n \quad (3.28)$$

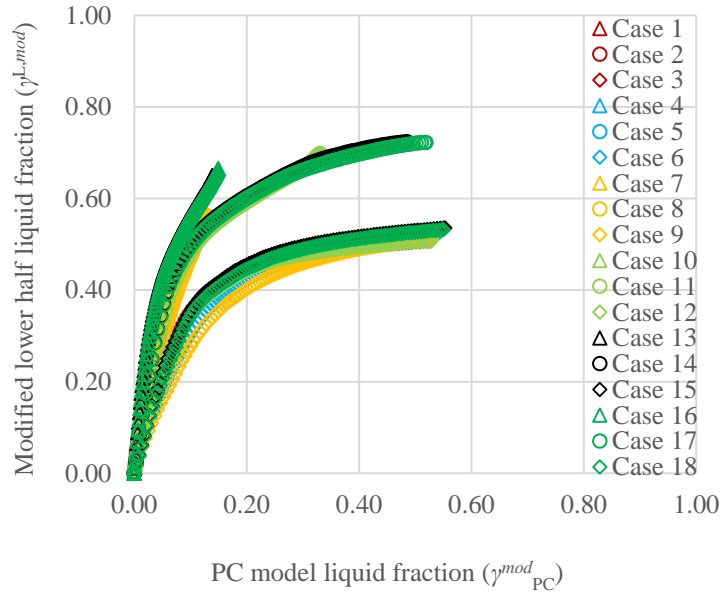


Figure 3.21: Variation of the modified lower half liquid fraction versus modified PC model liquid fraction

Figure 3.22 shows the regression results for all the cases and the obtained constants are shown in Table 3.9. The figure also shows that the majority of the data points (about 96%) lie within the range of $\pm 10\%$ discrepancy from the linear curve.

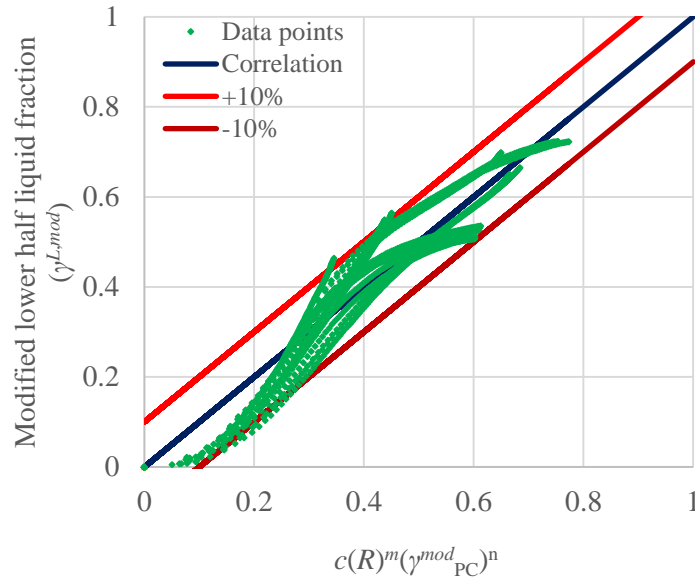


Figure 3.22: Variation of the modified lower half liquid fraction versus the developed correlation

Table 3.9: Constants of Equation (3.28) for the modified lower half liquid fraction

C	m	n	R^2	Range
0.6558	0.9259	0.3857	0.8999	$R = 1.19 - 2.31$

Finally, since the method was developed using the three PCMs presented in Table 3.5, its application should be verified by a new PCM. To examine the developed method, the correlations

were used for a new PCM, RT35HC. For the three verification cases (see Table 3.7), the left and right graphs in Figure 3.23 show the verification of the developed correlations for the upper and lower halves, respectively. According to the figure, all data points of the upper half correlation lie within the range of $\pm 15\%$ discrepancy from the linear curve (the correlation). For the lower half there is also an acceptable agreement between the results from the correlation and the data points, which lie within the range of $\pm 10\%$ discrepancy.

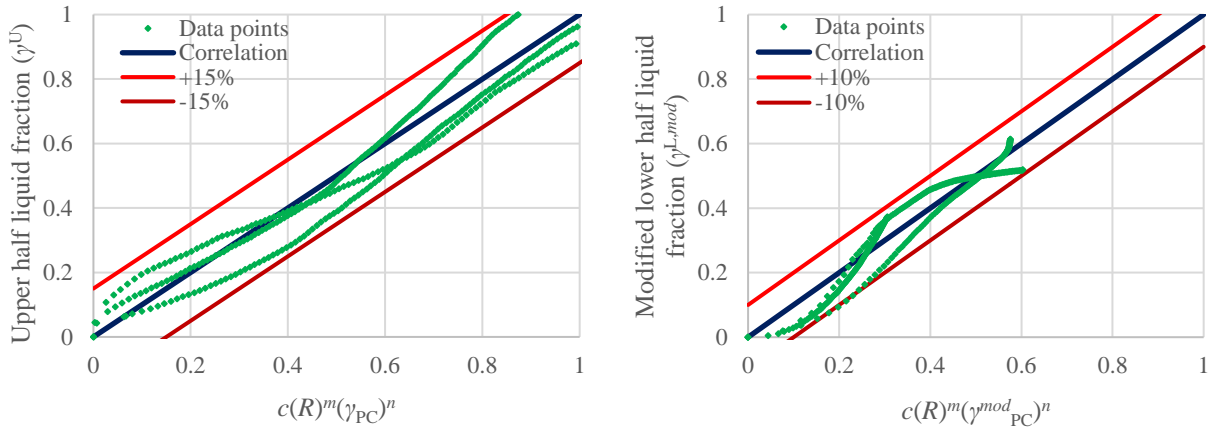


Figure 3.23: Verification of the developed correlations for the upper half (left) and modified lower half (right) liquid fractions

3.3.5 Air-PCM heat exchanger

On certain days, especially in spring and autumn, space heating or ventilation air heating may not be required during the daytime when the outdoor temperature is relatively high and solar radiation is available but that need usually arises after the sunset. In addition, some residential buildings do not need to be ventilated or heated to the comfort level during the day since occupants are not at home. These are the situations where a day-cycle thermal storage unit can be used in air-based solar systems. Solar heat can be stored in the heat storage unit during the day when the heat supply exceeds the heating demand and it can be released later when otherwise. For that purpose, the latent heat of phase change can favorably be utilized. The main advantage of thermal storage with PCMs is the amount of heat which can be stored in a small temperature interval around the melting temperature. That amount of heat stored in a PCM is generally larger than in the case of sensible heat storage operating in the same temperature range.

A general problem with most solar thermal systems is the need for thermal storage to balance the supply and demand of heat over a certain period. Numerous ways of integrating the PCM-based heat storage with air-based solar thermal systems have been reported. One of the simplest ways is the integration of PCMs directly with the solar air collector.

Compact storage module (CSM) panels provide a rather easy and flexible approach to building thermal storage units of a desired thermal storage capacity. The CSM panels can be arranged in several ways in the units. The basic arrangement is a row of parallel CSM panels with an air channel between the two adjacent panels. In order to increase the capacity of the heat storage

unit, the CSM panels can be added in all three spatial directions. However, even if the storage unit has the desired thermal capacity, that capacity may not be available in operation due to various heat transfer constraints. The simplified energy balance calculations may underestimate the problems with heat transfer between the HTF and the heat storage materials.

3.3.5.1 Background

Several numerical studies have been carried out on latent heat thermal storage with air as the HTF. However, many of the models neglect the heat exchange between the thermal storage unit and the ambient environment [131, 132]. Such simplification can be justified for thermal storage in passive cooling applications where the temperature difference between the PCM and the ambient air is rather small (usually less than 10 °C) and the heat storage cycles are relatively short. In the case of thermal storage for space heating, the temperature difference between the PCM and the ambient air can exceed 30 °C, resulting in a non-negligible heat loss over a certain period. Another assumption often made in modeling of the storage units with PCM slabs is the equal air flow rate in all air channels. This flow pattern can be achieved in laboratory experiments, but it is less likely in the case of the thermal storage units in actual building energy systems.

Therefore, in this example, a simulation model was developed for the heat storage units comprising CSM panels filled with PCMs. The simulation model allowed considering the distribution of air flow rates in different air channels as well as the heat exchange with the ambient environment.

3.3.5.2 System description

A schematic of the air-PCM heat exchanger is shown in Figure 3.24. The air-PCM heat exchanger consists of several rows of CSM panels. The CSM panels are aluminum containers filled with a PCM. The model was validated with the experimental data for the air-PCM heat exchanger containing 100 CSM panels (5 rows of 20 panels) but the model is not limited to this number or this arrangement of the CSM panels.

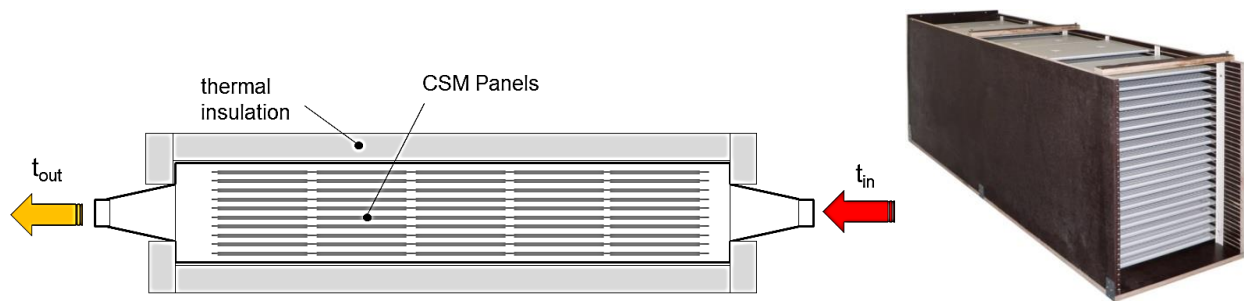


Figure 3.24: Schematic of the investigated heat storage unit (left) and the unit without the front and top walls revealing CSM panels (right)

3.3.5.3 Methodology

The model of the air-PCM heat exchanger was formulated with the numerical solution of 1D heat conduction including an internal heat source representing the PCM:

$$\rho C_p \frac{\partial T}{\partial t} = \frac{\partial}{\partial x} \left(k \frac{\partial T}{\partial x} \right) + \dot{Q} \quad (3.29)$$

$$\rho C_p \frac{\partial T}{\partial t} = \frac{\partial}{\partial x} \left(k \frac{\partial T}{\partial x} \right) + \rho \lambda \frac{\partial \gamma}{\partial t} \quad (3.30)$$

where ρ , C_p , k , T , x , λ and γ are the density, specific heat, thermal conductivity, spatial coordinate (in the direction of the PCM layer thickness), latent heat of fusion and liquid fraction, respectively.

The effective heat capacity method was adopted for latent heat modeling. The control volume method using the explicit scheme for the time derivative was utilized to solve the problem numerically. The detail of one of the sections (a sample computational domain) is shown in Figure 3.25. The initial condition was the uniform temperature of the entire heat storage unit. The convective heat flux according to Newton's law of cooling was used as the boundary condition at the surfaces of the panels. The number of nodes used for the calculations could be specified in the model together with the number of sections which should be solved for each panel. Regardless of the number of sections, each of them was solved as a 1D heat transfer problem. The model accounted for the heat loss to the ambient environment. Several versions of the model were developed with different level of details. Understandably, the more detailed the model is the more calculation time is required for the simulation.

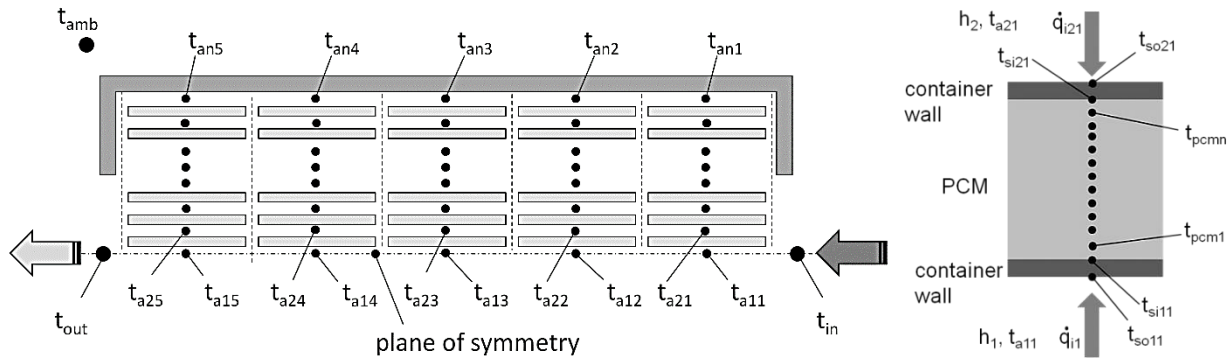


Figure 3.25: Schematics of the numerical model (left) and a computational domain (right)

3.3.5.4 Results

The TRNSYS model of the PCM heat exchanger was used for a parametric study aimed at the reduction of peak air temperatures of ventilation air. The goal of the study was to investigate the potential of LHS in reducing the peak temperatures of outdoor air supplied to the ventilated space; thus, reducing the ventilation cooling load. The study was conducted for the typical meteorological year (TMY) of the city of Brno, Czech Republic. The simulated time period was from June 15 to August 31. The air-PCM heat exchanger containing 100 CSM panels (approximately 50 kg of PCM) was considered in the study. The study was performed for 4 phase change temperatures of PCM (22, 24, 26 and 28 °C) and 4 air flow rates of ventilation air (200,

100, 50 and $25 \text{ m}^3\text{h}^{-1}$). The results for the phase change temperature of $24 \text{ }^\circ\text{C}$ and the ventilation air volumetric rate of $50 \text{ m}^3\text{h}^{-1}$ is shown in Figure 3.26.

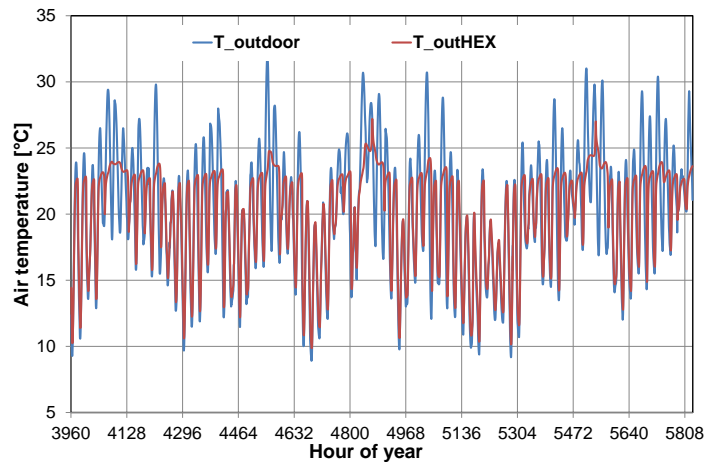


Figure 3.26: Effectiveness of an air-PCM heat exchanger in peak-shaving of ventilation air temperature

3.3.6 Water-PCM heat exchanger

Despite the fact that TES has been a main topic in research for the last 30 years (particularly PCMs [133]), the release to market of efficient technologies for the cold storage systems using these materials is quite recent [134]. Due to the high costs of experimental tests in the real conditions of buildings, numerical simulation, developed analytical methods and different modeling are needed to predict the behavior and results of TES usage in buildings. These tools are necessary to optimize this technique and to make it more efficient and cost-effective.

The system presented in this example will be part of the multi-energy production and storage systems of HIKARI project (details in Section 6.6.1), a positive energy district located in Lyon, France consisting of three buildings, combining commercial, residential and office usage. The exchanger will help to optimize and improve the performance of HIKARI's absorption chiller.

3.3.6.1 Background

The aim of this example is to develop and validate a numerical model of an innovative water-PCM heat exchanger for cooling purposes. This model was validated and then integrated into a building model to optimize the behavior of this innovative energy storage technology when coupled to other multi-source energy architectures.

3.3.6.2 System description

The system is an innovative thermal storage system at low temperature. In particular, it consists of 60 m^3 of PCM (subject to a phase change between 8 and $9 \text{ }^\circ\text{C}$) processed into a gelatinous form and enclosed in multilayer film with both water and oil resistance for ease of use. According to Figure 3.27, the gel is enclosed in cylindrical stick packages that are inserted in plastic cases, which are subsequently inserted in four insulated thermal storage tanks.



Figure 3.27: Latent heat thermal storage material package or gel pack (left), plastic case filled with gel packs (middle), and typical installation of the plastic cases into the isolated tank (right)

A flow of water runs into each tank, entering in the system from tubes situated on the top of the tank, passing from little holes. The plastic cases have large apertures so as not to impede the water flow which runs into the tank when they are stacked in it. After passing through the gel sticks layer (PCM), the water exits the system passing through some openings present in other tubes located at the bottom of the tanks.

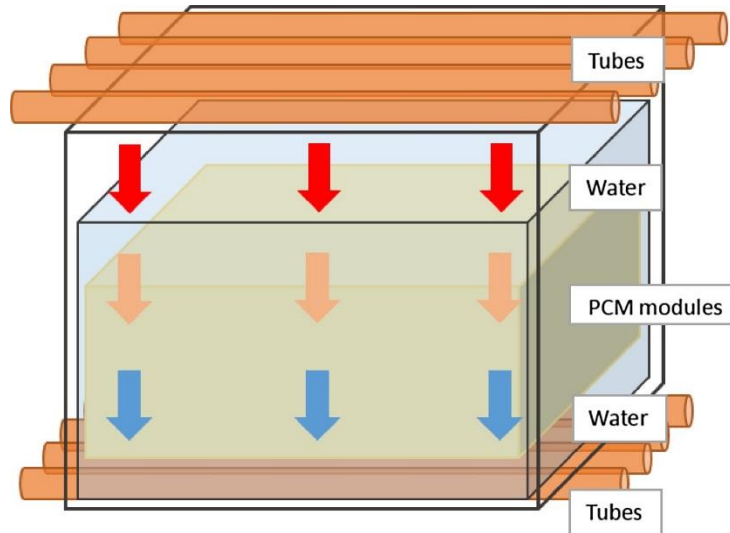


Figure 3.28: Schematic representation of the thermal storage system

3.3.6.3 Methodology

The model of the system was developed using MATLAB Simulink to analyze the heat transfer between a cylinder of PCM and water. To obtain the dynamic model, the heat balance approach was chosen. It was based on the division of the analyzed system into a defined number of volume elements and the subsequent application of the energy balance equations for each of them. The first step was to analyze all the relevant energy flows present in the system to write the energy balance equation (i.e. conduction, convection and advection).

The phase change problem of the heat storage medium was modeled using the apparent heat capacity method. It represents the phase change through an apparent increase of the PCM heat capacity value for a certain temperature range where the increase represents the corresponding latent heat absorption/release.

Once the energy balance equations were written, the finite difference method was employed to approximate the partial differential equations.

3.3.6.4 Results

Two validation studies were considered in this example (1) a CFD model designed using ANSYS Fluent and (2) an experimental prototype of the cold storage system, designed and constructed in laboratory conditions. The first (numerical) validation shows that there is a time difference between the two software's results, even if the behavior can be considered similar (Figure 3.29). It could be caused by some input errors that cause the delay between the curves or by some assumptions made in the energy balance equations that are far from reality.

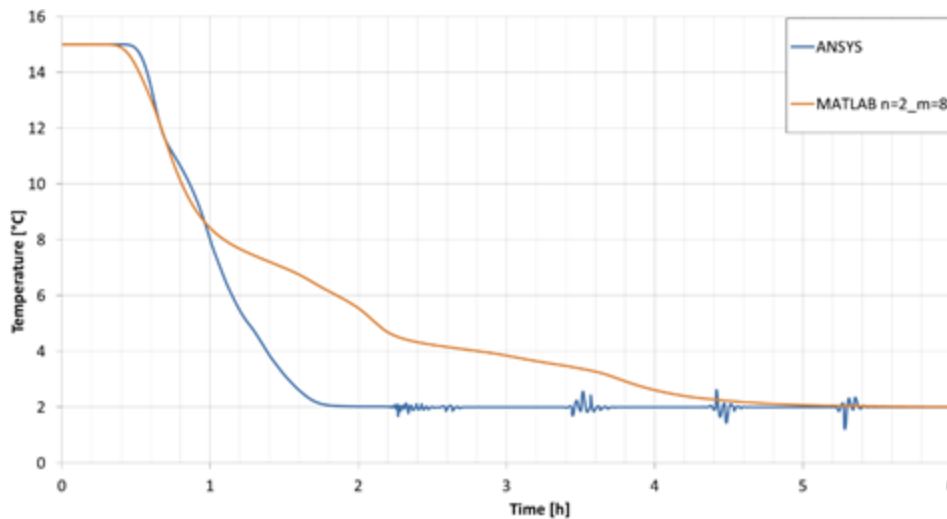


Figure 3.29: Comparison of the temperature curves for the same point using MATLAB Simulink and ANSYS

For the second validation, the results obtained from MATLAB Simulink were compared with the results obtained using an experimental prototype which reproduces the real system. It consisted of two Plexiglas tanks filled with water inside one of which plastic case filled with the PCM sticks was inserted. The water temperature in Tank 1 was regulated by an external cryostat and then sent to Tank 2, crossing the PCM modules layer, enabling the heat exchange (see Figure 3.30). The second comparison, between the experimental results obtained from the prototype and the values obtained from MATLAB Simulink, shows a very similar behavior. As shown in Figure 3.31, there is no delay as was found in the comparison with the CFD model in the freezing and melting processes, respectively.

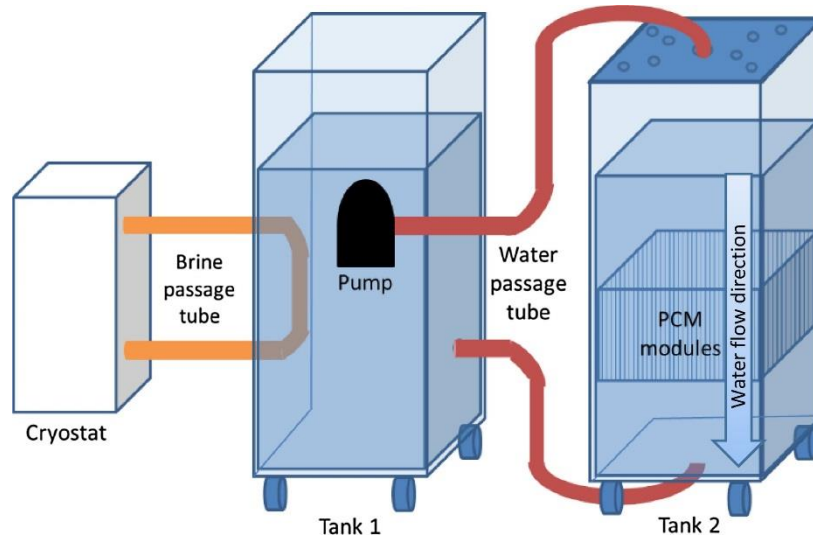


Figure 3.30: Schematic representation of the experimental prototype

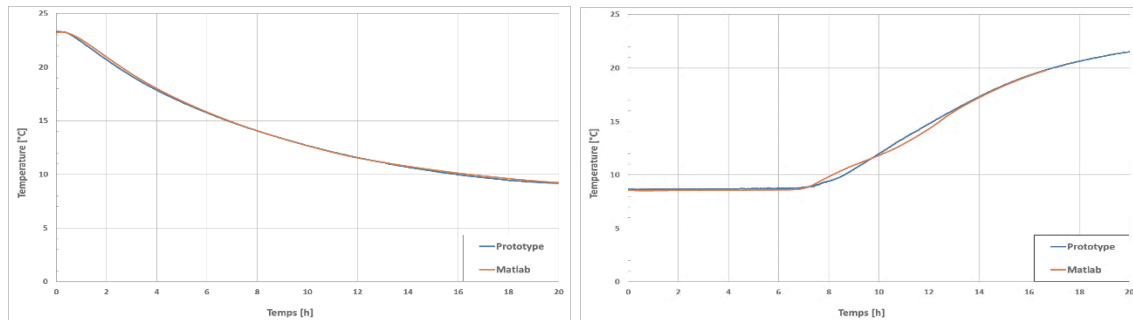


Figure 3.31: Comparison of the temperature curves for the same point between the experimental and the MATLAB Simulink results for the solidification (left) and melting (right) processes

3.3.7 Thermally activated wall panels containing PCM

Thermally activated building structures (TABS) such as floor or wall heating or ceiling radiant cooling have received much attention in the past decade. An advantage of TABS is their large surface area which allows for lower temperature difference between the heat carrier and the ambient environment. Such conditions are favorable for enhancing the efficiency of the heat and cold sources (e.g. the COP of heat pumps). Another advantage of TABS is radiant heat transfer which makes it possible to achieve an acceptable level of occupant thermal comfort at lower indoor air temperatures during the heating season and higher indoor air temperatures in the cooling season.

The heating and cooling capacity of TABS per unit area is limited; thus, these systems are not suitable for spaces with high heating or cooling loads. Moreover, radiant cooling systems alone are not suitable for climates or indoor spaces with high latent heat cooling loads as the moisture condensation on surfaces of TABS can result in mold growth and other problems.

TABS can be extended with integrated latent heat storage in the form of PCMs [135] and thus be employed for other energy saving measures such as peak shaving, shifting of cooling load

or even nighttime cooling (under favorable climatic conditions). The increasing use of energy simulations in design and operation of buildings and HVAC systems brought about the development of the models of various HVAC system components including TABS [136]. TABS have high thermal inertia and therefore respond relatively slowly to changes in heating or cooling demand [137].

3.3.7.1 Background

Simulation of buildings or HVAC systems performance usually covers a period of several weeks, months or even a year. Therefore, the computational demand for simulation models of buildings or HVAC systems can be quite constraining for their practical application. A substantial simplification of the simulated problem is usually necessary to reduce the computational demand. In this example, a quasi 1D model was developed for a thermally activated layer with PCM.

3.3.7.2 System description

Experimental data for model validation were acquired from an experimental room located at the Faculty of Civil Engineering of Brno University of Technology, Czech Republic. The thermally activated panels, shown in Figure 3.32, consisted of oriented strand boards (OSB) with gypsum plaster containing a microencapsulated PCM on one side and thermal insulation on the other. The plastic tubes for liquid HTF were embedded in the plaster. There were 17 U-shape plastic tubes in each panel (Figure 3.33). The tubes had an inner diameter of 2.35 mm, a wall thickness of 0.5 mm and were placed 15 mm from each other. The supply and return piping for the HTF was on one side of the panels; thus, the tubes were connected in a U-shape manner (with both the inlet and outlet at the same side of the panel). Four heights of the panels were experimentally tested (0.9 m, 1.25 m, 1.5 m and 2.0 m).

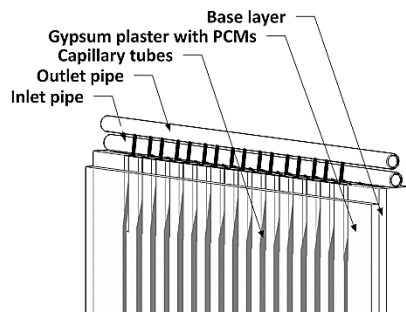


Figure 3.32: Schematic representation of the thermally activated wall panel



Figure 3.33: Base plates with attached plastic tubes

3.3.7.3 Methodology

A quasi 1D model of thermally activated wall panels containing PCM was developed to obtain the average surface temperatures on each side of the panel and the outlet water temperature. The model was developed in MATLAB and subsequently implemented as a TRNSYS type. A schematic of the numerical model of a wall panel is shown in Figure 3.34. It was assumed that the HTF mass flow rate was the same in all 17 tubes. Besides, the following parameters were assumed to be constant: thermophysical properties of the plaster with PCM, the plaster thickness, the capillary tubes thickness and the overall thermal resistance of base plate with thermal insulation. The effective heat capacity method was used to account for enthalpy change of the PCM in the plaster. The heat conduction with a heat source was considered in the layer of plaster containing the PCM and a simple energy balance was used for the calculation of water temperature along the length of the tube.

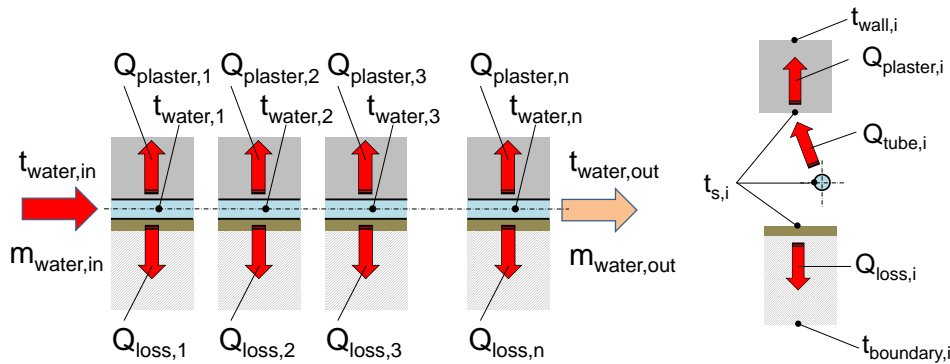


Figure 3.34: Schematic of the wall panel model

The developed model (TRNSYS type) can be used as a stand-alone component or in combination with Type 56 (multi-zone building). The use of the panel with Type 56 is more complicated. As the model of wall panel is a separate type not integrated in Type 56, the input and output data need to be exchanged between Type 56 and the model of the panel (Figure 3.35).

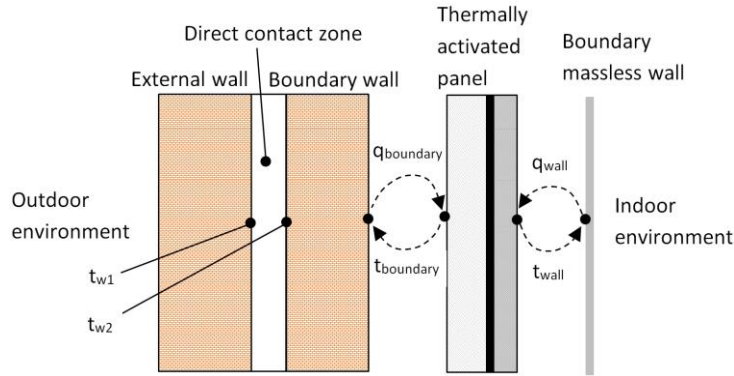


Figure 3.35: Thermally activated panel on an external wall

3.3.7.4 Results

The hot/cold water for thermal activation of the panels was provided by a reversible air-to-water heat pump. Thermal imaging was used to acquire the surface temperatures of the panels. The average temperature of the plaster (the surface facing the room) was acquired in 5-minute intervals. The comparison of the experimental and simulation results for the panel with the height of 2 m is shown in Figure 3.36. Initially, the test room was cooled down to 18 °C and later it was heated up to 30 °C with thermally activated wall panels. The wall panels were installed on all surfaces of the experimental room (Figure 3.36). As the hot water was provided by the air-to-water heat pump, the water temperature was not constant but gradually increased during the experiment. The heat pump went through a defrosting mode about 1.5 hours into the experiment and as a result both the water temperature and the surface temperature of the panels decreased.

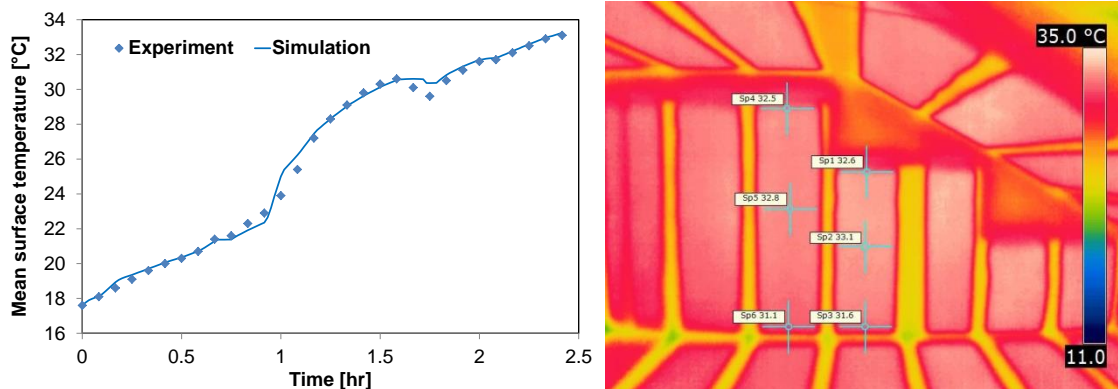


Figure 3.36: Model validation (left) and thermal imaging results (right)

3.3.8 High-temperature cooling system with PCM

Free cooling can be defined as that amount of cooling which can be obtained from existing, additional or modified system components during low ambient conditions and used to partly or fully offset the load on mechanical refrigeration plant [138]. In building applications, there are two free cooling approaches: water-side free cooling and air-side free cooling. The water-side free cooling often adopts dry coolers or evaporative cooling towers to cool down the chilled water

without the need of mechanical cooling. The air-side free cooling uses fresh air and/or recirculated indoor air to cool down the building.

3.3.8.1 Background

It is noted that most of the applications found in the literature regarding PCM-based free cooling techniques used the air-side approach [139-141]. Conversely, a PCM-based heat exchanger can take advantage of free cooling conditions by using the water-side approach. The possibility of using the water-side approach effectively depends on two factors. First, the PCM-based heat exchanger should be integrated into high-temperature cooling systems with chilled water at about 18-20 °C. Second, the PCM-based heat exchanger should be used in buildings located in cold climates, where ambient air temperature during summer nights falls below 16 °C (e.g. Scandinavian climate).

3.3.8.2 System description

A conceptual design of the PCM-based heat exchanger assembly is illustrated in Figure 3.37. It consisted of PCM layers embedded in a heat exchanger, a fan to enhance heat transfer and lamellas.

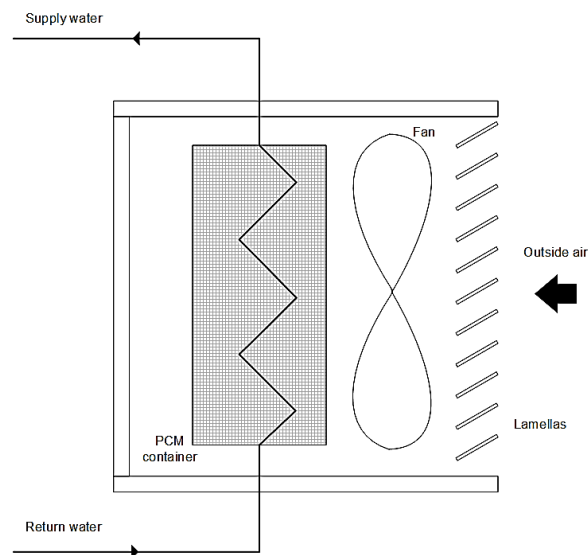


Figure 3.37: Assembly of the PCM-based heat exchanger

The working principle had two operation modes of charging and discharging. The charging process occurred during nighttime when lamellas were opened, and the fan blew the ambient air to solidify the PCM layers (store cooling energy). The discharging process occurred during daytime when lamellas were closed, isolating the heat exchanger from the outdoor. The return water flowing through the heat exchanger was at a temperature higher than the PCM melting point. Therefore, PCM layers absorbed heat, and the material melted.

3.3.8.3 Methodology

The model of the PCM-based heat exchanger was developed in Modelica [84] using models from the “Buildings” library [85]. The computational domain is shown in Figure 3.38, which can be divided into water flow, wall, PCM slab and air flow cells.

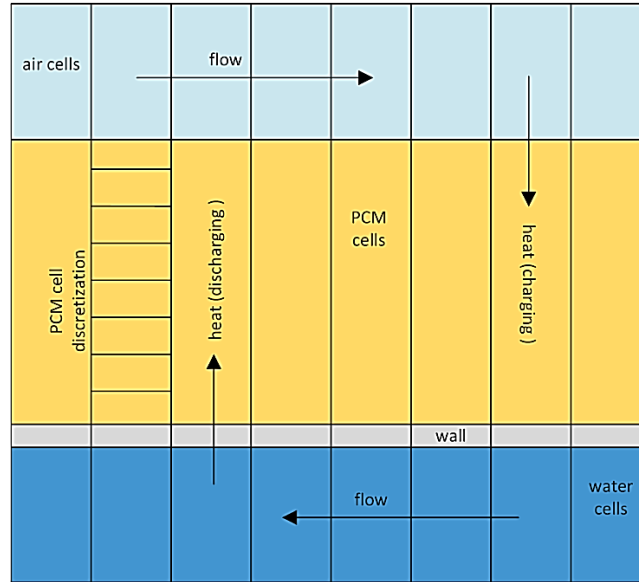


Figure 3.38: Schematic representation of the computational domain for the PCM-based heat exchanger showing cells and direction of fluids and heat transfer

The energy in the water flow was carried from fluid cell to fluid cell diffusing into the adjacent wall cell by heat transfer using a convective heat transfer coefficient (h_i), which is defined as:

$$h_i = \frac{Nuk_w}{d_h} \quad (3.31)$$

where Nu is the Nusselt number calculated with the Dittus-Boelter correlations [142], k_w is the thermal conductivity of water and d_h is the hydraulic diameter. The convective heat transfer coefficient was calculated at every time-step according to the actual water mass flow rate.

The wall cell transmitted energy to the adjacent PCM cell. Each PCM cell was further discretized into layers parallel to the wall where energy was transferred one dimensionally:

$$\rho \left[\frac{\partial u(y,t)}{\partial t} \right] = k_{PCM} \left[\frac{\partial^2 u(y,t)}{\partial y^2} \right] \quad (3.32)$$

where u is specific internal energy, k_{PCM} is the thermal conductivity of the PCM and y is the vertical location.

The Modelica model of the PCM-based heat exchanger is illustrated in Figure 3.39. The PCM slab was thermally connected to the air flow (ambient environment) through a convective heat transfer coefficient that varied according to the actual air mass flow rate between 25 W/m²K

- **DHC:** District heating/cooling (baseline)
- **HP:** Reversible air-source heat pump
- **HP_DC:** Reversible air-source heat pump with dry cooler
- **HP_PCM:** Reversible air-source heat pump with PCM-based heat exchanger

Simulations were performed for a fifteen-zone building model which is representative of the medium office building prototype, as described by the U.S. Department of Energy [144]. Annual simulations were run for the four thermal plant configurations. Figure 3.40 shows the annual primary energy use in terms of heating, cooling and auxiliary devices, such as circulating pumps and fans included in the configurations HP_DC and HP_PCM. The configuration HP_PCM has the best energy performance with an annual primary energy use of 6.3 kWh/m², followed by the configuration HP_DC with 7.7 kWh/m², the configuration HP with 10.9 kWh/m² and the configuration DHC with 19.2 kWh/m².

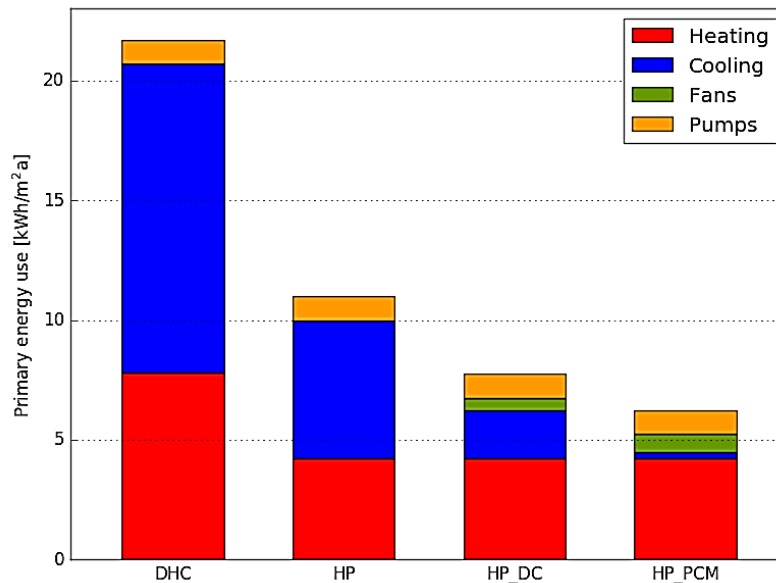


Figure 3.40: Annual primary energy use for the four configurations

When comparing thermal plant configurations with the baseline configuration DHC, energy savings of approximately 67%, 60% and 43% were achieved respectively for the configurations HP_PCM, HP_DC and HP.

Since the configurations DHC and HP do not implement any free cooling strategy, mechanical cooling was required almost all over the year. Note that in large office buildings, interior zones tend to overheat due to the waste heat generated by internal factors (e.g. people, lighting and equipment) even during the coldest day. Therefore, cooling might be required in winter, too.

The configuration HP_DC allowed avoiding the use of mechanical cooling for most of the year. Whenever ambient air temperature was suitable, the building cooling load could be rejected to the ambient by activating the fan in the dry cooler. However, the dry cooler could only be used

during operating hours of the system (daytime), meaning that ambient air temperatures were favorable for free cooling, especially during summer. Conversely, the configuration HP_PCM allowed avoiding mechanical cooling energy even during summer, except for very few days where ambient conditions during nighttime were not cold enough for a complete solidification of the PCM.

3.3.9 Borehole heat exchanger

To utilize the thermal capacity of the ground, the most favorable type of ground heat exchanger (GHE) is the vertical closed-loop GHE, also known as the borehole heat exchanger (BHE). To accurately design BHEs, or optimize system operation, including ground source heat pump (GSHP), a reliable thermal response model is essential.

Modeling of BHEs is about the prediction of fluid temperature in the BHE loop or subsurface temperature distribution. Ground thermal response can be predicted using either analytical models or numerical models. There are some accuracy issues in different response time scales. They can be categorized into the short-term accuracy and long-term accuracy problems. The former problem is caused by the geometry simplification of GHE which is extremely slender, and the latter is caused by the simplified boundary condition of top and bottom-end of the ground.

As stated, either a numerical or analytical approach can be used to predict the thermal response of a BHE. When examining the temperature response of a BHE, an analytical solution is a quick and convenient option to choose. However, in the process of deriving an analytical solution, many assumptions and simplifications are needed, specifically, the simplification of boundary conditions and geometry of a BHE. Those simplifications cause some accuracy problems, especially in short-term and long-term predictions. The validity range of classical analytical models at different time-scales, such as the infinite line source [145, 146], the infinite cylindrical source [145, 147], and the finite line source [148-151] can be found in the literature [152-154] hence detailed discussions are not provided here.

A typical problem is the inaccurate short-time transient behavior in which the temperature response of BHE itself is important. Additionally, in a long-term simulation of temperature response, the axial heat transfer near the ground surface and the bottom-end of BHE has a significant impact on the accuracy. Although, research has been actively conducted to overcome the drawbacks of classical analytical solutions, a time-varying ground surface boundary condition is very difficult to consider in an analytical solution. Most analytical solutions which consider the axial effect assign a constant Dirichlet boundary condition to the ground surface. However, this is far from the actual condition where the ground surface temperature is affected by BHE operation.

3.3.9.1 Background

Although a numerical model is computationally more intensive compared to analytical models, a numerical approach is easier to achieve the required accuracy at all time scales than the analytical approach because the numerical models use fewer assumptions and have flexibility in imposing the boundary conditions. However, the advantages of numerical approach have not been

fully exploited in this field. In particular, although boundary conditions in a numerical model can have a time-varying form for a realistic consideration of the heat balance at ground surface, such study has not been reported yet. This is especially important in a long-term prediction.

To address the mentioned issues, in this example, a numerical model is presented based on the finite element method. The geometric shape of a BHE was fully discretized and the heat balance model of the ground surface was also integrated into the numerical model to examine the impact of the ground surface boundary condition on the long-term prediction. The developed model was coupled with a building simulation program, and the coupled simulation was conducted for 10 years to examine the long-term performance of a GSHP and subsurface thermal state.

3.3.9.2 System description

Figure 3.41 shows the boundary condition and geometry of the numerical BHE model. The thermal properties of each component are listed in Table 3.11. To generate the load profile assigned to a BHE, EnergyPlus 8.0 was used [155]. Weather data generated by the expanded AMeDAS (EA) method [156] were used for the load calculation and ground heat flux model integrated in the numerical BHE model. The coupling scheme is shown in Figure 3.42.

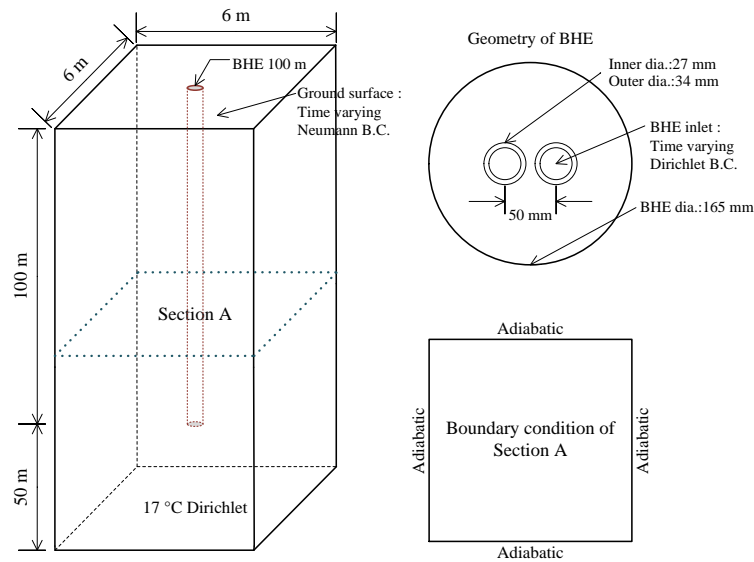


Figure 3.41: Calculation domain, geometry of BHE, and boundary conditions

Table 3.11: Thermal properties used in the numerical model

Properties	Fluid	U-tube	Backfill	Ground
Volumetric heat capacity [MJ/(m ³ K)]	4.2	1.8	2.8	2.8
Thermal conductivity [W/(mK)]	0.6	0.38	1.72	1.72

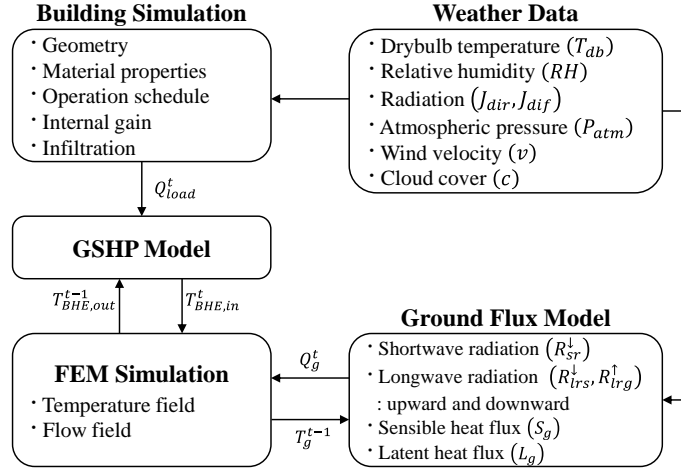


Figure 3.42: The coupled simulation scheme and data transfer among the simulation models

3.3.9.3 Methodology

The ground was modeled from a macroscopic view. Except for the fluid flow in the U-tube, the model considered neither the advective heat transfer by groundwater flow nor the natural convection in the porous medium. Therefore, all thermal properties of components were considered as bulk properties. The fluid flow in the U-tube was simplified using a one-dimensional (1D) flow element based on the law of Hagen–Poiseuille flow [156-158]. Except for the 1D flow element, the entire numerical model domain is governed by the following equation of energy conservation:

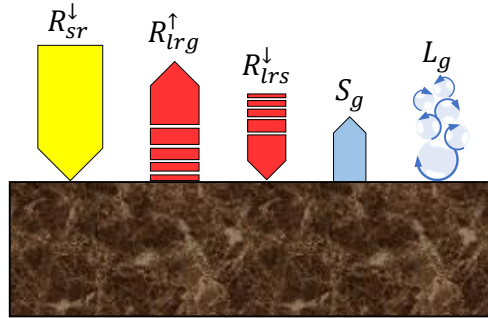
$$(\rho c)_b \frac{\partial T}{\partial t} - \nabla(\lambda_b) \nabla T = Q_T \quad (3.33)$$

The initial temperature of the entire calculation domain was 17 °C. The adiabatic boundary condition was assigned to the sides of a section. A Dirichlet condition of 17 °C was set to the bottom surface ($z = -150$ m) and a time-varying Neumann boundary condition was assigned to the top surface. For the inlet and outlet of the U-tube (represented using a 1D-flow element) a volumetric flow rate of 17 L/min was assigned and the inlet had an additional time-varying Dirichlet boundary condition to describe the change in the fluid temperature in terms of the heat exchange between the circulating fluid and heat pump. The time-varying boundary condition for BHE inlet is defined by:

$$T_{f,in}^t = T_{f,out}^{t-1} + \frac{Q_{load}^t \left(1 + \frac{1}{COP}\right)}{C_f \dot{V}_f} \quad (3.34)$$

The heat balance of ground surface can be expressed as Equation (3.35) [159] whose schematic is depicted in Figure 3.43. The net heat flux Q_g is a time-varying value and assigned to the ground surface in the calculation model.

$$Q_{gs} = R_{sr}^{\downarrow} + R_{lrs}^{\downarrow} - R_{lrg}^{\uparrow} + S_g + L_g \quad (3.35)$$



Keys: R_{sr} : absorbed global solar irradiation, R_{lrg} : longwave radiation from ground to sky, R_{lrs} : longwave radiation from sky to ground, S_g : sensible heat transfer on the ground surface, and L_g : latent heat transfer on the ground surface. All the components have the unit W/m^2

Figure 3.43: Schematic of heat balance on ground surface and flux components

3.3.9.4 Results

The simulation was conducted for 10 years. The temperature distribution across the horizontal and vertical cross-sections for the 221th day (at 6 PM) in the tenth year of operation (when the peak fluid temperature occurred) are shown in Figure 3.44 and Figure 3.45, respectively. The maximum entrance fluid temperature was $43.22\text{ }^{\circ}\text{C}$. Overall, the ground temperature had risen compared with the initial temperature ($17\text{ }^{\circ}\text{C}$) due to the dominated cooling load. The ground temperature was approximately $23\text{ }^{\circ}\text{C}$ and $18\text{ }^{\circ}\text{C}$ at the depths of 100 m and 120 m, respectively. This indicated the importance of the thermal diffusion in axial direction in long-term simulation. The steep axial temperature gradient can also be observed below the depth of 100 m in Figure 3.45. This steep vertical temperature gradient below the BHE indicated a large heat flux in the vertical direction. If this effect were not considered, the subsurface temperature under conditions dominated by the cooling load would be overestimated.

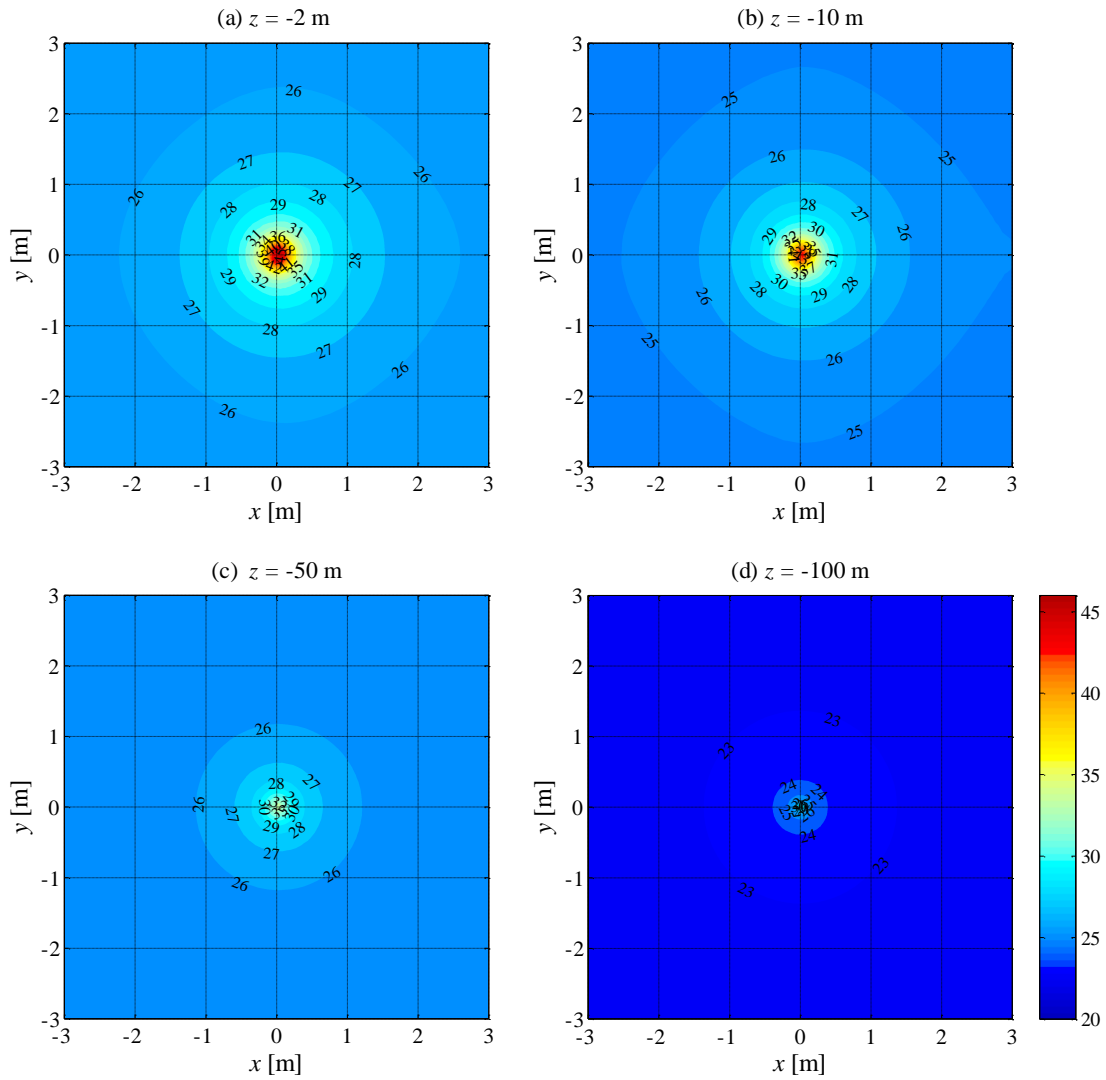


Figure 3.44: Temperature distribution of horizontal sections at different depths at 6:00 PM on the 221st day in the 10th year: (a) $z = -2$ m, (b) $z = -10$ m, (c) $z = -50$ m, and (d) $z = -100$ m

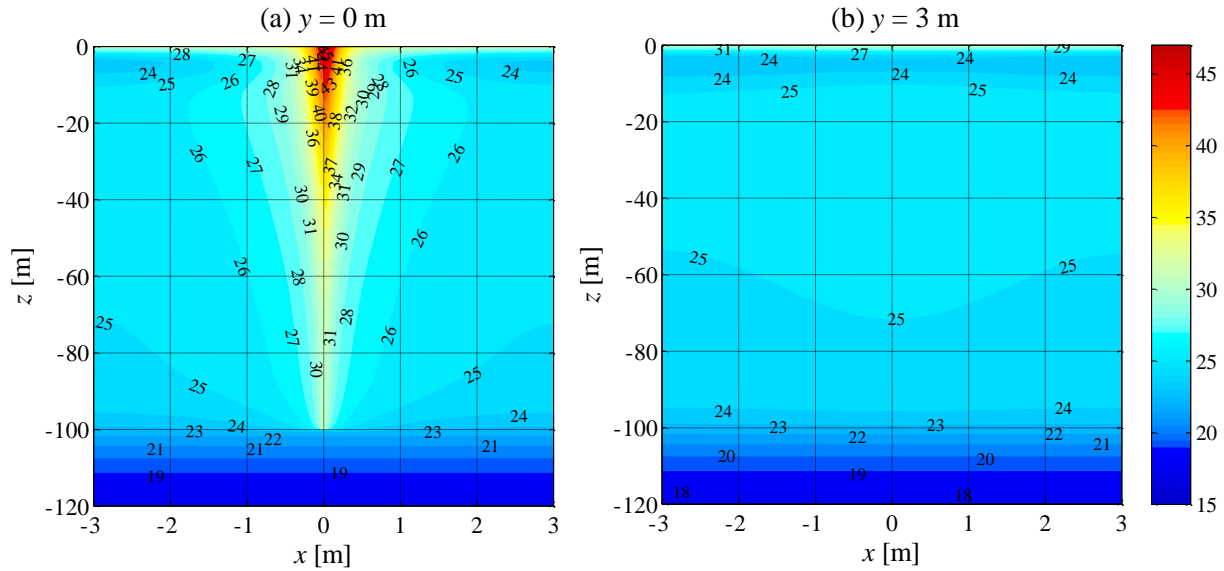


Figure 3.45: Temperature distribution of vertical sections at different y coordinates; (a) $y = 0$ m, and (b) $y = 6$ m ($y = -6$ m showed almost the same distribution)

The vertical temperature distribution presents some interesting features. Near the ground surface, the highest temperature is visible, because in July the global solar irradiation is strong (around $1,000 \text{ W/m}^2$). However, below the shallow part, a convex shaped vertical temperature distribution can be observed around $z = -5$ m, with lower temperature (about $24 \text{ }^\circ\text{C}$) than the surrounding area. This indicates the cooling effect from the ground surface boundary during winter and spring still influences the ground temperature due to the large heat capacity of the ground. Such a heat storage effect by the time-varying boundary condition is difficult to consider in analytical models. Especially, when a ground heat exchanger is installed in shallow ground of which the depth is less than -20 m (e.g. a horizontal heat exchanger or energy piles) considering the effect of the time-varying surface boundary can be a very important factor for predicting the long-term operation. Based on the results, it was concluded that the ground surface boundary and the axial effect should be considered for a better long-term simulation of ground thermal response.

Chapter 4: Application to districts

In recent years, many countries have benefited from a rapid growth in the number of the installed DHSs [160]. In many cities, the requirements for space heating (SH) and domestic hot water (DHW) can be entirely supplied by a DHS. Figure 4.1 shows the percentage of DHSs utilized in Europe by 2012. Many long and short-term plans have also been developed to fully take advantage of RES. An example is a plan in Denmark to employ 100% of the energy demand from renewable sources [2, 3]. In addition to energy efficiency, DHSs help to minimize several safety and fuel transportation issues due to the absence of any combustion system for the space heating at the end-user level. The absence of boilers also elevates the available usable floor area. Moreover, individual users restrain from dependency on installation and maintenance of boilers, furnaces, chillers and/or air conditioning [161].

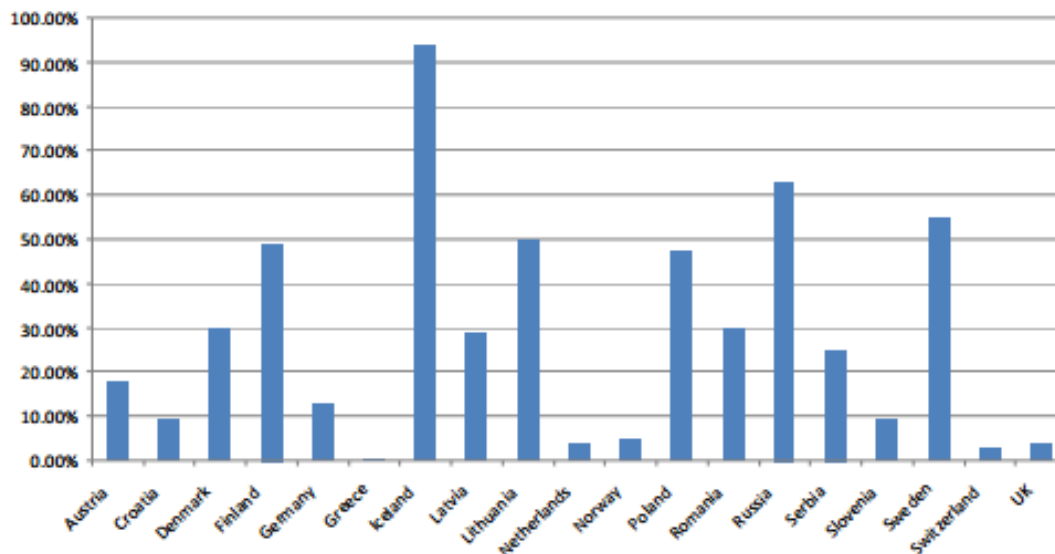


Figure 4.1: Share of low temperature heat demand in Europe met by DHSs [162]

Nevertheless, DHS implementation requires a high level of management, especially in regions with a high share of renewable energy systems (e.g. Germany, Sweden and Denmark). In that case, most end-users have to remain connected to the electrical grid to import/export excess electricity during the fluctuations of power and heat demand in the operation period [161]. Note that cost optimization is necessary to justify the fluctuations in heating and electricity consumption in accordance with peak and off-peak tariffs from electrical distribution companies [161].

In this chapter, the main elements of a DHS along with its fundamentals are presented. Furthermore, the available tools for modeling a DHS are briefly discussed and a tool selection process is proposed. Finally, two unique examples are illustrated for DHS modeling.

4.1 Elements

DHSs are broadly designed to be localized to mainly make use of the excess heat in a specific area. The supply of heat depends on the available local energy sources, topography of suppliers/end-users and DHW needs [163]. The design of such systems requires a case-by-case approach to fully take advantage of the available local energy. Nonetheless, in all DHSs, three main elements can be identified (1) an energy source, (2) a distribution network and (3) more than one end-user. The DHS design (as opposed to stand-alone individual building heating/cooling systems) should consider the energy requirements of all the end-users, the energy resources available locally as well as the spatial distribution of the energy suppliers with respect to the energy consumers.

4.1.1 Energy resources

Most DHSs employ several energy resources. Some focus on increasing the fuel utilization factor where the main electricity production comes from coal or natural gas [164] and waste heat energy [165]. Other systems integrate renewable technologies such as solar energy [166]. The renewable technologies can be located on the energy supplier side, in the actual distribution network or be installed on individual buildings. The selected energy type can vary region by region as it highly depends on the locally available resources and the associated climate. Table 4.1 shows some recent studies of the DHS and sorts them in terms of type of energy resource.

Table 4.1: Recent case studies of available energy resources for district heating networks

Source	Type of system	Ref.	Modeling	Location	Remarks
CHP	CFB ¹ gasification from biomass and plastic in coal-fired CHP	[167]	ECLIPSE	UK	<ul style="list-style-type: none"> Up to 20% of coal can be replaced by biomass and plastic without decreasing electrical efficiency or increasing CO₂ emissions.
	Combined cycle gas turbine CHP with biomass	[168]	Epsilon Professional 7.0 and Aspen Plus v7.1	Spain	<ul style="list-style-type: none"> CCGT CHP with biomass gasification can have up to 3% higher efficiency when biomass is dried from the flue gas.
		[169]	Aspen Plus [®] with Fortran sub-models	Güssing, Austria	<ul style="list-style-type: none"> Detailed modeling of a wood biomass CCGT CHP connected to a DHS. When considering processes to clean the syngas for the gas engine, the electrical and heat efficiencies can be expected to reach 27% and 39%.
		[170]	EnergyPlan	Jiangsu, China	<ul style="list-style-type: none"> CCGTs are more flexible plants compared to nuclear and coal.
		[171]	Deterministic energy model for combustion and heat transfer	Liège, Belgium	<ul style="list-style-type: none"> CHP coupled to DHS is identified as an effective way to integrate RES. Gas emissions from incomplete combustion and thermal storage were not included in this study.
		[172]	EU Directive CHP Method	Netherlands	<ul style="list-style-type: none"> NGCC CHP coupled to DHSs are more energy efficient than natural gas condensing boilers, which are widely used in the Netherlands.
	Coal-fired CHP	[173]	Hysys v7.3	China	<ul style="list-style-type: none"> The minimum extraction ratio can be used as an indicator when choosing a CHP for a DHS.
	CCGT ³ , CFB and APF ⁴	[174]	EnergyPlan	Denmark	<ul style="list-style-type: none"> The CCGT CHP plant is the best type of the three analyzed plants for large-scale DHSs and for the integration of RES.
	-	[175]	Deterministic energy and exergy model	-	<ul style="list-style-type: none"> CHP plants combining exergy and thermal energy was analyzed using a novel approach.
	Renewable	Geothermal systems and heat pumps	[176]	Energy and exergy	Afyonkarahisar, Turkey
[177]			balance equations to train		
[178]			an artificial neural network		
		[179]	Deterministic energy and exergy model	Salihli, Turkey	<ul style="list-style-type: none"> Exergoeconomic analysis of a GDHS was conducted.
		[180]	TERMIS	Aarhus, Denmark	<ul style="list-style-type: none"> A 100% renewable scenario for Denmark was developed.
		[181]	EnergyPlan	Frederikshavn	
		[182]			
		[183]		Aalborg, Denmark	
	[184]	Deterministic model	Gonen, Turkey	<ul style="list-style-type: none"> Results show that the energy losses in the pipes and the initial investment of the system are the costliest part of the implementation of the GDHS. 	
	[185]	Deterministic model based on mass, energy and exergy balance equations	Izmir, Turkey	<ul style="list-style-type: none"> Energy and exergy efficiencies must be calculated based on a reference temperature that is more realistic. Energy and exergy efficiencies could vary between 38-49% and 45-47%, respectively by changing reference temperatures within 0-25 °C. 	

Waste to energy	[186]	Simple deterministic model	Hurning and Aarhus, Denmark	<ul style="list-style-type: none"> Integration of waste incineration to coal-fired CHP was analyzed. It is insufficient to only consider plant efficiency since heat and electricity production are interlaced in CHP.
	[187]	EnergyPlan	Denmark	<ul style="list-style-type: none"> Syngas is the waste to energy technology which has the lowest CO₂ emission (i.e. negative) and both biogas and syngas are interesting waste incineration technologies.
	[188]	-	China	<ul style="list-style-type: none"> Incineration of municipal solid waste (based on technological advancements) is now considered a renewable energy source in China.
	[189]	EnergyPlan	Denmark	<ul style="list-style-type: none"> Producing syngas as a waste source for CHP was identified as an approach to reduce dependence on fossil fuels. The dynamic effects of heat supply and demand were investigated.
	[190]	R1 formula	Europe	<ul style="list-style-type: none"> Application of R1 formula by country was found.
Solar	[191]	TRNSYS	Chemnitz, Germany	<ul style="list-style-type: none"> Conversion of a 3GDHS to a 4GDHS with solar collector bay was investigated.
	[192]	TRNSYS	Europe	<ul style="list-style-type: none"> Application of a system and methodology from Okotoks study to five other cities in Europe was studied.
	[193]	TRNSYS	Okotoks, Canada	<ul style="list-style-type: none"> 52 residences entirely heated by a solar collector bay were equipped with thermal storage above 90% solar fraction.
	[194]	Deterministic heat, cost and electricity model	Spain	<ul style="list-style-type: none"> Addition of a TSP⁵ to a DHS for heating and cooling increases payback period, but considerably decreases production of CO₂.
	[195]	TRNSYS	Denmark	<ul style="list-style-type: none"> Over 70% solar fraction can be achieved for most large-scale DHS.
	[196]	Deterministic	-	<ul style="list-style-type: none"> Using CuO nanofluid as a heat transfer medium can increase energy efficiency of solar collector bays for low temperature CHP plants.
Industrial excess energy	[197]	Method for analysis of industrial energy systems (MIND)	Sweden	<ul style="list-style-type: none"> Excess industrial heat is economically more competitive in small to medium sized DHSs than in large DHSs due to the potential for biomass CHP and low temperature output.
	[165]	-	China	<ul style="list-style-type: none"> Excess industrial output temperature is mainly lower than 200 °C.
	[198]	-	UK	<ul style="list-style-type: none"> Not all of the excess industrial heat is economically viable because of the location of the industry with respect to the end-users.

¹ CFB: circulation fluidized bed

² NGCC: natural gas combined-cycle

³ CCGT: combined-cycle gasification turbine

⁴ APF: advanced pulverized fuel

⁵ TSP: Thermal solar plant

4.1.1.1 Combined heat and power plants

Cogeneration plants coupled with DHSs have been proposed as a solution to maximize the fuel utilization factor [160]. Centralized heat and power plants provide the necessary heat to meet the thermal energy demand of the end-users as well as electrical power needs. A key advantage to such thermal energy distributions is the considerable reduction in the pollutant and waste thermal energy emissions [160]. However, these plants are most efficient when operated at full capacity [164]. Knowing that heat and electricity demands are non-uniform and not synchronized, operating these plants at their optimal efficiency can be a very challenging problem. Therefore, CHP plants can be employed to provide 50-60% of the heat demand while boilers, being more efficient when trying to meet the peak demand, provide the remainder of the heat [186]. Another option to tackle the time mismatch is by benefiting from energy storage.

CHP plants have been reported to be efficient for meeting both electrical and heating demands. Overall, the flexibility in CHP plants is important for the integration of wind and other RES [170]. Note that to maximize the economic, environmental and energetic efficiencies of a CHP connected to a DHS, both the electrical and heating demands should be simultaneously analyzed [171]. Energetic and exergetic analyses of a coal-fired CHP revealed that the minimum extraction ratio can be used as a reliable indicator to design or select a CHP for a DHS [173]. Fuel burning and tax credits can be optimized for CHP plants to help the decision making process [199]. However, it is highly insufficient to analyze the efficiency of CHP plants without considering the configuration of the district heating network [186].

4.1.1.2 Industrial excess energy

The attention to energy efficiency in the building sector is not equally seen in the energy intensive industrial sector [165]. For example, in the United States, where the industrial sector accounts for one third of the energy demand, it is estimated that 20-50% of this energy is dumped to the environment as heat [200]. With the increased awareness about global warming and the energy crisis, the industrial excess energy serves as a potential source to be recovered and reused in DHSs [198].

Overall, excess industrial heat is economically more competitive in small to medium sized DHSs than in large DHSs due to the potential for a biomass CHP [197]. However, utilization of excess heat has its difficulties as most of the excess heat is below 200 °C and most often unstable as it depends on the production and related processes [165]. Besides, not all of the excess industrial heat can be used in DHSs due to the industry location with respect to heat consumers, which would not be economically viable in all the scenarios [198].

4.1.1.3 Renewable sources

The integration of RES into DHSs mainly results in low-temperature outputs, meaning that it is lower than most supply temperatures of DHS distribution networks. A thorough discussion of low temperature district heating system (LTDHS) is provided in Section 4.1.2. Designing a DHS for full integration of RES requires considerable initial investment, which can be as much as 30%

of total expenditures over 30 years. However, such a system is sustainable from socioeconomic and environmental viewpoints [61].

4.1.1.3.1 Solar energy

Integration of solar energy into DHSs has seen a considerable increase in the past few years in many countries such as Austria and Germany [166]. The main challenge for the use of solar energy in DHSs is the time lag between the solar irradiance and the heat demand peak [201]. Hence, this technology needs to be coupled to a TES system, being often a vessel/tank filled with a high thermal density material such as water or a PCM [202]. The size of the collector, tank and thermal panel should be carefully designed to avoid panel overheat during the off-heating season. If the heat can be dissipated into a heat sink such as a pool, then the collector area as well as the storage capacity can be increased. Otherwise, either seasonal storage is installed or the remainder of the energy is supplied through another technology during the heating season [201]. Studies have shown that small-scale storage is inefficient as the volume to surface area ratio of the storage vessel is very low, resulting in considerable thermal losses [202]. In this regard, large-scale district heating systems (LSDHSs) are proposed with collectors installed on each individual building, and a central thermal storage, serving the whole district.

In Europe, most of the solar thermal systems are coupled with biomass boilers, which can utilize residual wood chips from the wood industry. In response to this, the framework SOLLET was put in place to standardize the combined solar thermal-biomass heating systems [166]. This includes 10 plants across Europe (Austria, Germany, Sweden, Luxembourg and Greece), currently being monitored. Moreover, the installed collector area is now more than 340,000 m² in eight European countries (Germany, Austria, France, Netherlands, Switzerland, Sweden, Denmark and Norway) [203].

Another challenge when using solar energy in DHSs is the very low solar irradiation in most of the developed countries. For instance, the average sun irradiance in southern Germany is 130 W/m² [204]. Maximum values are attained in summer months when the demand for heating is less. To use the heat available in the summer for winter heating, seasonal storage is often required.

The integration of solar collectors to DHSs can represent a high economic risk [205]. Despite considerable research in the design of LSDHS and seasonal storage [206-208], implementation of these systems are very costly [205]. Nonetheless, in many countries such as Denmark, tax credits on alternative fuels make solar collectors a more economically viable alternative.

Since 1996, several central solar heating plants with seasonal storage (CSHPSS) projects have been established in Germany mainly aligned with “SolarThermie 2000” and “SolarThermie 2000plus” frameworks [206]. For example, a DHS with a CHP plant was economically justified in Chemnitz, located in eastern Germany, due to a need to restructure a part of the town [191]. Up to 2010, solar energy in eastern Germany stood against low cost of the CHP heat from coal, power demand management of CHP developing excess heat and the high service temperature of the DHS. The new design of this part of the town included a solar thermal plant as opposed to being

connected to the CHP. Despite the low solar fraction (11.1%), its development is an improvement towards a sustainable DHS.

Most of the large-scale solar heating plants are built in Northern or Mid-Europe, in countries such as Sweden, Denmark, Germany and Austria [209]. It is economically advantageous to build larger scaled solar plants as it reduces the relative initial investment per kWh. Such systems equipped with short-term storage (diurnal) typically supply 15-20% of the energy required for SH and DHW. Systems with long-term storage (seasonal) have typical solar fractions (SF) of 50% [206] for systems installed in the late 1990's and early 2000's.

The Drake Landing Solar Community in Alberta, Canada is a DHS with a large-scale solar collector bay which reaches an SF of over 90% [193]. However, it was shown that this solar fraction was only met after the fifth year of the DHS operation [193]. Based on the promising results of the Drake Landing Solar Community, various cities across Europe were assessed in terms of achievable SF in various geographical locations: Helsinki, Hohhot, Dublin, Oviedo and Perpignan (with HDD of 4598, 4634, 3009, 2118 and 1608, respectively) [192]. Based on a series of simulations using TRNSYS, it was possible to obtain SF values above 90% for all five cities, but not all without building modifications. For instance, houses in Helsinki had to be insulated to PassiveHaus standards.

The combination of large solar plants with seasonal storage and heat pumps is very attractive due to the flexibility of power and heat generation as well as the high SF which can be obtained [210]. The effective use of such combinations was the main objective of Task 45 of IEA-SHC [211]. In the current market, the investment cost of solar collectors is still high compared to fuel-based technologies, but it is prone to be decreased with additional market penetration [212].

Solar collectors can also be integrated to CHP plants for instance to pre-heat the production of steam for the turbines [196]. Besides, changing the heat transfer medium to a mixture of water and copper oxide (CuO) nanofluid increases the daily thermal and exergy efficiencies, and decreases the total production costs for all CHP operating fluids.

4.1.1.3.2 Geothermal systems and heat pumps

Geothermal energy is often proposed as a renewable, sustainable, simple, safe and adaptive source of energy [185]. Geothermal district heating system (GDHS) can be a sustainable replacement to fossil and fissile fuels [213]. Heat is mainly extracted from or exhausted to the ground with the use of heat pumps, achieving coefficient of performance (COP) values of approximately four [214]. GDHSs produce negligible CO₂, SO_x and NO_x and particulate matters. Some systems use an air duct in the ground as a way to extract heat from the earth as opposed to a heat pump [215].

There is a large potential for more exploitation of geothermal energy in many regions. For instance, since its first geothermal installation in 1964, Turkey has had a large development in the installation of geothermal systems. By 2004, there were 10 city-based GDHSs [179]. However,

implementation and development of GDHSs is very low compared to the availability and potential of geothermal energy in Turkey [216, 217]. In Sweden, 12% of the heat supplied to DHSs comes from heat pumps connected to seawater or sewage sludge [218]. Inversely, geothermal energy adoption is likely to decrease in such countries due to the competition to CHP and waste incineration energy systems unless considerable investments and political incentives are directed towards this technology. On a short-term basis, GDHSs are in competition to biofuel/gas heat-only boilers (HOB) and gas-steam cycle/oil CHP [218].

Denmark, in particular, established a new policy for reducing dependency on fossil fuels by achieving a 30% utilization of RES by 2025 and 100% by 2050, which includes an increase in use of geothermal energy [183]. These policies are tremendously supported by many municipal incentives such as in Aalborg, Samso, Arhus [180], Frederikshavn [181, 182], Thisted and Margretheholm [183]. As an example, Thisted plant is a currently active geothermal plant in Denmark which produces more than 15.4 GWh of heat per year. Geothermal wells in Denmark have the potential of supplying water at 40 °C which can be integrated to fourth generation DHSs where with an absorption heat pump they can easily be integrated to current third generation DHS (DHS generations are explained in Section 4.1.2) [181]. They can also be combined to solar collectors for a higher renewable energy fraction [219].

Many energy and exergy studies have been conducted on GDHSs [220]. For example, it was shown that a control strategy based on exergy rather than energy can increase the heat production of the Afyon GDHS by up to 13% with a payback period as low as 3.8 years [221]. An ANN model was developed to predict future exergy efficiencies of the Afyon GDHS and an economic analysis was simulated. A system composed of proportional-integral-derivative (PID) controllers coupled with an ANN model for exergy efficiency was developed and recognized to be more efficient than conventional manual ON/OFF control [176]. It was shown that the installation of a GDHS was profitable when the present worth factor (PWF) is higher than 7.9.

Note that energy and exergy efficiencies of GDHSs must be calculated based on a more realistic reference temperature. For instance, reference temperature of 11.4 °C as the average local temperature of a GDHS in Balcova, Turkey was found to be more realistic than the previously used 13.4 °C [185]. Besides, energy and exergy efficiencies could vary between 38-49% and 45-47%, respectively, by changing the reference temperatures within 0-25 °C. Moreover, the design of any DHS should have a supply temperature as high as possible to increase the exergy efficiencies of the heat exchangers and the total exergy content. Note that the total energy efficiency increases as the ambient temperature decreases.

Furthermore, exergy and energy efficiency as well as LCC of GDHSs were evaluated in locations such as Afyon [178], Balcova [185], Bigadic [222], Gonen [184], Dikili [223] and Salihli [224]. Interestingly, all these systems have an average cost of 1.47 million USD/kW of useful energy, varying only by 0.03 million USD/kW.

4.1.1.3.3 Solid waste to energy

Another source of energy for DHSs is solid waste material, which is identified as a RES [214]. Waste heat is a possible solution for many countries to achieve policies regarding GHG emissions reduction [225]. Municipal solid waste (MSW) in Denmark accounts for 20% of the district heating and 4% of electricity production [186]. Efficiencies of 20-30% for electricity and 70-80% for heat production can be achieved with modern waste material incinerators. The combustion of residual solid waste, as a sustainable energy production approach, is still reluctantly seen by many European Union members. This is due to the fact that early incinerator designs emitted a considerable quantity of toxic gases and heavy metals [190]. However, recent technology advances enabled MSW to reduce its footprint on the environment and health risks [226].

A major challenge with MSW is the composition of the utilized fuel, which is constantly changing while the emissions must always be kept under an acceptable environmental and health associated concentration [227]. Incineration is a costly energy production approach, but it still remains less expensive than recycling and more sustainable than landfilling [228]. This is due to the fact that preparing the waste material for incineration requires several stages of preparation, including drying and degassing, pyrolysis and gasification [229]. Sewage waste, for example, usually comes with a high water content and requires a considerable amount of drying and sometimes addition of a second fuel to assure a proper combustion. More research advancements are needed to render MSW as a more economical competitor to fossil fuels [230].

4.1.2 Distribution network

The distribution network links the energy supplier(s) and end-user(s) and is mainly designed on a case-by-case basis. Parameters involved in the design of distribution networks include the distance between energy supply and end-users, distance between end-users, quantity of available/required energy, temperature of supply and return, sizing of pipes and flow rate of liquid in pipes. In this sense, there is a considerable number of possible configurations when it comes to linking energy supplier(s) and end-user(s). Many studies presented the methodologies for the design of such networks [6, 231]. Heat is delivered to the end-users through a hot water supply line from which end-users collect the required heat through heat exchangers. A challenge behind designing such a system is the temperature change of the supply line throughout the system where users at the end of the supply line have access to a lower temperature with respect to other users.

4.1.2.1 First to third generation DHS

The first generation DHS (between 1880 and 1930) used steam at temperatures over 200 °C in concrete conduits to provide energy to end-users. Such systems were replaced due to the high thermal losses and the risk of conduit explosions [232]. The second generation DHS (between 1930 and 1980) had pressurized water at temperatures higher than 100 °C in concrete conduits. They were replaced by the third generation DHS (3GDHS), being constructed by lighter prefabricated insulated components and operated at temperatures lower than 100 °C.

4.1.2.2 Low temperature DHS

The more recent DHSs, the fourth generation DHS (4GDHS), is commonly referred to low temperature district heating system (LTDHS). An extensive differentiation of all four generations of DHSs has been performed by Lund et al. [232]. It has been shown through case studies that LTDHSs are more exergy efficient than medium or high temperature DHSs [233]. Super low supply temperatures (40-45 °C) are also utilized where the temperature is raised near the end user with heat pumps [234]. The problem with lowering supply temperatures of the DHS piping is the risk for *Legionella* bacteria, enforcing the temperature needs to be higher than 55 °C [234].

A comparison between 3GDHSs and 4GDHSs was conducted to assess the impact of introducing LTDHSs to the current and future (2025) Danish context [235]. The new generation of DHS showed reduced levels in heat losses, CO₂ emissions and costs. Moreover, consumers' costs could possibly be lower if the temperature of the system is high enough so that booster heat pumps are not required. Challenges in justifying the cost of 4GDHSs were also discussed with respect to the cost of the piping and various insulation layers [236].

Newer or refurbished buildings with lower energy demand can be entirely supplied in energy by LTDHSs with an adequate control of the substations. In the cases where the demand cannot be met during peak periods, the supply temperature can temporarily be increased with limited negative impact on exergy efficiency given the short duration of the increased load [237]. Different configurations of the pipe distribution of a LTDHS was studied and it was found that the addition of a buffer tank at each substation can help to considerably diminish the pipe size [238]. The DHW tank can also be used as a DHS substation reservoir for energy accumulation coupled to the LTDHSs [239].

4.1.2.3 Heat storage

The intermittent nature of low temperature heat production from industrial excess heat, solar collectors and heat pumps justifies the need of storage technologies in LTDHSs. The embedded heat storage can be divided into two types: (1) diurnal heat storage, designed to cover 10-20% of the yearly heat load and usually used for hospitals, hostels and apartment buildings and (2) seasonal storage [209].

Currently, latent and chemical seasonal heat storage applications are at the stage of laboratory-scale prototypes, whereas sensible seasonal heat storage has been used for large-scale demonstration plants [240]. Table 4.2 shows a list of the current DHS projects using seasonal storage. Nearly all CHP plants in Sweden and Denmark have short-term sensible storage tanks to cover peak demand periods, to achieve smaller plant design and to run at full capacity [241].

Hot water tanks (for SHS) can be made of concrete and can be completely or partly buried. Steel liners can be placed inside them to limit vapor diffusion [209]. They can also be built from stainless steel [241], but their size is often not sufficient for seasonal storage.

A comparison of German solar collector plants equipped with seasonal storage was conducted based on experience from operation and construction of 11 plants through the

‘SolarThermie 2000’ and ‘SolarThermie 2000plus’ programs [206]. Tank and pit thermal storage are found to be feasible, but considerable improvements need to be done with respect to insulation and material vapor resistance. It has been reported that hot water storages have the lowest storage volume to solar collector area ratio (1.5-3.0) in comparison to gravel pits (2.81-14.81) [206].

Aquifer heat storages are reserves of hydraulically porous materials filled with groundwater. One half is used as a cold well and the other as a hot well. Charging can be carried out by extracting water from the cold well and passing it through a heat exchanger to later be injected in the hot well. Discharging is done by reversing the flow direction. The first solar heat plant with an aquifer heat storage connected to a DHS was built in 2000 [209]. The highest obtained solar fraction was 57% in 2005, which is close to the planned SF (62%) [206]. Note that the temperature of the system is limited to 500 °C, above which there is a change in soil chemical properties. Moreover, it was reported that fuel energy savings could be reduced [241]; for instance, by 90-95% [242].

Other types of sensible seasonal storage include pit TES, consisting of a pit dug out and lined with an impermeable liner and filled with water. In some applications, the pit can be filled with gravel. The advantage of this storage application is associated to less effort to build structural components since the retaining walls of the reservoirs are mounds of soil [241]. This approach is particularly attractive in the Danish market since a major income for CHP plants is the regulation of electricity production [243]. Cities where seasonal storage has been constructed include Marstal, Braedstrup and Dronninglund of which two have pit thermal storage. Pilot plants with pit seasonal storage have also been constructed in Germany as part of the ‘SolarThermie2000’ and ‘SolarThermie Plus 2000’ programs [244].

Borehole heat exchangers can also be used in conjunction to a DHS. They consist of holes dug in the ground and a U-tube with operative fluid to transfer heat. A borehole heat exchanger can have many rows of holes with the U-tubes connected in series or parallel arrangements. Recent modifications have been made to this configuration while two U-tubes are inside the hole to simultaneously charge and discharge the heat [245]. The efficiency of borehole heat storage increases as the quantity of boreholes increases, since this reduces the surface to volume ratio of the apparatus in the ground [241]. The most recent example of this technology is the Drake Landing Solar Community in Canada where a 144 borehole heat storage could enable a 52 house community to have solar fractions above 90% [193].

Table 4.2: District heating system projects utilizing sensible seasonal heat storage

Project location	No. of buildings	DHS demand	System type	System size	Storage volume	Reference
Rise, Denmark	115 buildings		Solar collector	3,575 m ²	5,000 m ³	[246]
Marstal, Denmark	1,300 houses		Solar collector	26,000 m ²	70,000 m ³	[247]
Ingelstad, Sweden	50 houses		Solar collector	1,320 m ²	5,000 m ³	[246]
Lambohov, Sweden	50 houses		Solar collector	2,700 m ²	10,000 m ³	[246]
Westway Beacons, UK	130 apartments		Solar collector			[246]
Attenkirchen, Germany	30 homes	1,386 GJ/year	Solar collector	836 m ²	500 m ³	[244]
Anneberg, Sweden	50 residential units	1,980 GJ/year	Solar collector	2,400 m ²	60,000 m ³	[248]
Izmir, Turkey	4,000 residences		Geothermal		356 m aquifer horizon	[185, 223]
Aalborg, Denmark *	-	7,380 GJ/year	Geothermal, CHP			[183]
Frederikshavn, Denmark *	-	194,400 GJ/year	Solar collector	8,000 m ²	1,500 m ³	[181]
Salihli, Turkey	5,470 residences		Geothermal		40-513 m depth	[179, 224]
Afyonkarahisar, Turkey	4,613 residences	173,988 GJ/year	Geothermal			[176]
Balikesir, Turkey	2,200 residences	132,388 GJ/year	Geothermal		429 m and 307 m depth	[184, 222]
Okotoks, Canada	52 homes		Solar collector	2,293 m ²	34,000 m ³ , 144 boreholes	[193]
Braedstrup, Denmark	500 residences		Solar collector	37,500 m ²	500 m ³	[243]
Dronninglund, Denmark	-	144,000 GJ/year	Solar collector	35,000 m ²	50,000 m ³	[243]

* 2050 scenario, 100% renewable energy

4.1.3 End-users

DHSs can accommodate a variety of different end-users, which consume the produced energy for their space heating and DHW. In some cases, especially when end-users are sparse in distance, connecting buildings to a DHS is not justified since it can be beneficial for the users to be heated through an alternative energy. An example is the Turin DHS where the potential of a community heated with groundwater heat pump systems was investigated based on a thermoeconomic optimization [57]. An optimal configuration was established for this application with regards to the distance between end-users and the piping distribution network.

From the end-user's perspective, DHSs are much safer (heat exchangers as opposed to boilers), there is an increase in floor space (no boiler needed anymore), and often the heating costs are reduced [214]. However, buildings are often not designed for DHS; therefore, their conversion demands a considerable retrofit program. The responsibility of the operation and maintenance is mainly given to a third party, taking a burden off the homeowners. On the other hand, specialized maintenance technicians are required to be trained, turning a DHS to a more complex system [249].

There is also a potential for end-users to be an integral part of the heat supply of DHSs. In this case, the end-user is referred to as a 'prosumer' [250] where one of the biggest challenges is dealing with the intermittent power production associated with prosumers. The decentralization of district heat (DH) production has been studied and it was shown that prosumers reinjecting heat in the system create daily temperature variations in the pipes [251].

The control of a DHS integrated with prosumers (smart DHS) is very different from a DHS with a centralized heat production [252]. A control strategy that includes metering of the prosumer's heat production takes more advantage of the available solar thermal heat. Using this approach, integrated solar collectors could supply 108% of the yearly thermal needs, whereas standalone systems could only provide 27.7%. The Hyllie Swedish case study is another example that highlights the prosumer concept. The potential for prosumers in the city of Hyllie was studied with a deterministic energy balance model integrated with the software NetSim [253]. It was shown that a DHS has prosumer potential in areas with a mixed building stock.

4.2 Fundamentals

Accurate modeling and design of each DHS component plays an important role in its efficacy and efficiency. To shed light on the recent achievements in modeling of DHSs, this section aims to summarize the fundamentals of modeling.

Unlike building demand profiles, the heating demand profile of a DHS is defined as the summation of (1) the heating demand profile of the individual users of the system, (2) the heating demand profile of the distribution network, and (3) the heat loss of distribution network. Therefore, predicting the demand heat profile of the individual users of the DHS is similar to the one presented earlier for buildings (in Chapter 3). However, due to the unmeasured effects of the district/community on the buildings (e.g. shared walls or solar blockage by the adjacent shadow

casted from surrounding buildings), building methods should be modified for demand load prediction at the district level.

4.2.1 Energy resources

In general, heat sources in DHSs are modeled based on their efficiency and heat generation output. A minimum efficiency index has been defined depending on the type of the heat source. For example, the primary energy saving (PES) index has been defined to evaluate the efficiency of a CHP heat source [8]:

$$PES = \left(1 - \frac{1}{\frac{\eta_{H,CHP}}{\eta_{H,Ref}} + \frac{\eta_{E,CHP}}{\eta_{E,Ref}}} \right) \times 100\% \quad (4.1)$$

where $\eta_{H,CHP}$ is the heat efficiency in cogeneration production, $\eta_{H,Ref}$ is the efficiency in separated heat generation, $\eta_{E,CHP}$ is the electricity efficiency in cogeneration production, and $\eta_{E,Ref}$ is the efficiency in separated electricity generation.

The minimum PES value for a CHP heat source with the nominal size of smaller than 1 MW should be a positive value, whilst this value is more than 0.1 for sources above 1 MW [8]. Similar types of indices have been defined for other types of heat sources [254].

4.2.2 Distribution network

A DHS distribution network is mainly designed in accordance with the system scale, geographical considerations, type of the users and utilized heat generations sources. Beside the role of the distribution network in linking the generation side with demand side of the cycle and defining the inter communication between different components of the system, the distribution network affects the energy consumption of the system as well. In general, the total energy required to be fed to the system is:

$$Q = Q_{loss} + \int_1^n Q_i \quad (4.2)$$

where Q is the total energy consumption of the DHS, Q_i is the demand profile of each user and Q_{loss} is the heat loss of the system. Since most distribution networks operate within a specific temperature range, the heat loss from the system could be considered as a function of the network size and not a function of time. As a result, the total energy requirement of the system is equal to the summation of the profiles of different users in addition to the heat loss per network length. Since a DHS is a type of hydronic system, the modeling technique to design the distribution system can be either based on hydraulic or thermal equilibrium.

4.2.2.1 Hydraulic equilibrium

The distribution system in the DHS operates based on heat transfer through a heated fluid. Therefore, it should be designed based on the requirements of the hydraulic system regardless of the flow rate and energy level of the fluid.

4.2.2.1.1 Mass balance

The mass flow balance could be written for each point of the system as [255, 256]:

$$\sum_{in} Q_{in} - \sum_{out} Q_{out} - \sum_{user} Q_{user} = 0 \quad (4.3)$$

where Q_{in} is the mass flow rate entering the point, Q_{out} is the mass flow rate exiting the point, and Q_{user} is the mass flow rate required by the utility. Depending on the type of the system (i.e. open or closed loop), Q_{user} could be considered as zero. It is important to note that the system and network are assumed to be leak free without any loss of the fluid mass.

4.2.2.1.2 Energy balance

The energy balance could be written between any two points in the system as [160]:

$$\Delta H_{ij} - (H_i - H_j) = 0 \quad (4.4)$$

where ΔH_{ij} represents the energy loss between points i and j and H_i and H_j are the energy content of the fluid at points i and j , respectively. Considering the DHS as a closed system and without any loss in the liquid mass, the energy loss in the system could be written as a correlation to the pressure loss in the system represented in two different ways:

$$\Delta H = f \cdot \frac{L}{D} \cdot \rho \cdot \frac{V^2}{2} \quad \text{Distribution pressure drop} \quad (4.5)$$

$$\Delta H = \beta \cdot \rho \cdot \frac{V^2}{2} \quad \text{Concentrated pressure drop} \quad (4.6)$$

In the distribution pressure drop, the friction loss due to viscous effect, generated by the pipe surface, is the governing parameter. The hydraulic diameter of the pipe, mass flow rate of the system and roughness of the pipe surface are the parameters affecting the distribution pressure loss of the system [256]. Additionally, in concentrated pressure loss, head loss due to fittings and changes in pipe diameter are taken into the account [160].

4.2.2.2 Thermal equilibrium

Thermal equilibrium can be represented as either a steady-state or dynamic equation. A DHS with operational temperature lower than 70 °C or with low heat propagation (well insulated) can be represented as a steady state system. Inversely, a DHS operating with temperatures higher than 110 °C or with high heat propagation can be considered as a dynamic system [232, 257]. The thermal model could be written based on two major sources of the temperature drop in the system,

including temperature drop across the users and due to the system heat loss. The temperature drop across the users can be modeled based on a simple convection heat transfer equation [258, 259]:

$$Q = U \cdot \Delta T \quad (4.7)$$

where Q is the amount of the energy flux required by the system, U is the heat transfer coefficient and ΔT is the temperature drop across the users.

On the other side, the temperature drop due to heat loss in the system occurs in both longitudinal and radial directions. The longitudinal heat loss is along the system between different locations, whereas the radial heat loss occurs in the surrounding environment. Both types of the heat transfer in the system could simply be modeled by the enthalpy balance between any two points [260, 261]:

$$\frac{\partial(mh)}{\partial t} = \sum_{in} h_{in} - \sum_{out} h_{out} - \sum_{loss} h_{loss} \quad (4.8)$$

$$\frac{\partial(mh)}{\partial t} = \dot{Q}_c(x) - \dot{Q}_c(x + dx) - d\dot{Q}_1 \quad (4.9)$$

where \dot{Q}_c is the convective heat flow and $d\dot{Q}_1$ is the radial heat flow:

$$d\dot{Q}_1 = k \cdot dx \cdot (T - T_{earth}) \quad (4.10)$$

$$\dot{Q}_c(x) = q_{mx} \cdot T_x \cdot C_p \quad (4.11)$$

where k is the radial heat transmission coefficient and q_{mx} is the flow rate. By replacing $d\dot{Q}_1$ and $\dot{Q}_c(x)$ in Equation (4.9), the temperature at any point can be calculated as (see Figure 4.2):

$$T_i^{n+1} = T_i^n + \frac{\Delta t}{m_i C_p} (q_{m_{i-1}} C_p T_{i-1}^n - q_{m_i} C_p T_i^n - d\dot{Q}_1) \quad (4.12)$$

where C_p is heat capacity, T^n is the temperature, Δt is the time step and m_i is the water mass.

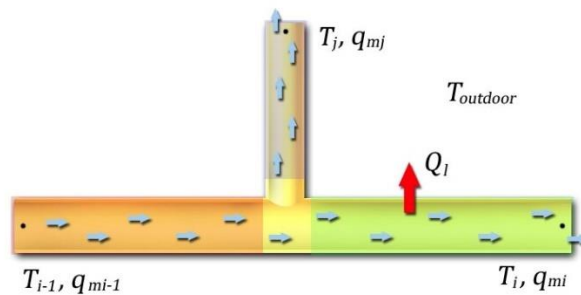


Figure 4.2: Heat flow in the piping system

Based on the definition of the $d\dot{Q}_1$, one of the main factors influencing the amount of heat loss is the earth's temperature. In systems with higher operating temperature, the higher differences in temperature could result in higher amounts of heat loss in the system. Similarly, the increased heat losses in a system could result in increased surrounding temperatures over time, consequently decreasing the heat loss over time.

4.2.2.3 Holistic modeling

Physical and black box models are the approaches conducted in holistic DHS modeling [262]. The network has been considered as a package in the black box models where individual design of the components is disregarded. The whole system is then modeled by techniques such as the transfer function or ANN [176]. On the other hand, in physical models, each component of the DHS has been designed separately and as a set of equations describing the flow and pressure losses of that element. For instance, the physical modeling has been categorized as the link flow (Q), the loop corrective flow (ΔQ), the nodal heads (H) and finally the mixed node-loop approaches [263].

Due to the high number of the elements which should be considered, solving such a system can be computationally expensive. Therefore, numerical approaches have been widely developed for solving the system of equations of the hydraulic distribution networks. Some of these approaches are categorized as [263]:

- **Numerical minimization method:** finding the minimum value of the nonlinear function subjected to linear constrained
- **Hardy-Cross method:** solving the system of nonlinear equations [264]
- **Newton-Raphson method:** solving the system of nonlinear equations [265]
- **Linear theory method:** solving the system of nonlinear equations [266]

The most frequently used method is a combination of Newton-Raphson and nodal head methods [263]. This is due to the simplicity of the input data, the number of equations and the size of equation matrix [267] as well as the accuracy of the results. Furthermore, due to the weak convergence of the nodal equation algorithm for networks with low flow rate, another approach has been suggested (called the loop equation method), which is a combination of the loop corrective and Newton-Raphson methods [263].

Further to the abovementioned studies, several commercial software (explained in Section 4.4) has been developed based on the loop equation method using the graph theory such as TERMIS [268] or spHeat [269]. Table 4.3 summarizes some of the current DHS modeling studies.

Table 4.3: Summary of the recent DHS modeling studies

No.	Description	Country/	Modeling level			Scale	Energy source	Utilized tool	Validation	Ref.
		Climate	Source	Building	System					
1	34 Users	Italy		GD	P	M	CHP	ODS	TERMIS	[160]
2	Combined sources		SM			M	Combined	UC		[161]
3	Multi-unit apartment building			GD	P	S	CHP	UC		[259]
4	8 units, different supply temperature	Geneva	SM	GD		M	CHP	UC		[270]
5	7 users with $L_p > 13.5$ km	Germany		GD	P/T	L	Biomass	ODS		[260]
6	Compares HT and LT supply	Ottawa		LF	P/T	L	CHP	Logster	TERMIS	[62]
7	Effect of human behavior	Denmark		LF	P	M	HP	IDA-ICE	TERMIS	[61]
8	Thermal storage	Stuttgart		GD	P/T	L	CHP/Biomass		spHeat	[255]
9	Solar district heating		SM	GD		M	Solar/CHP	UC		[271]
10	Solar thermal heating network	Sonnenberg	SM	Software	P/T	M	Geothermal/Solar		spHeat	[272]
11	CHP with thermal storage for 100 units	Flanders	SM	Measurement	P	M	CHP	UC		[273]
12	Biomass fired CHP with storage	Leini/Turin	SM	Measurement		L	CHP/Biomass	UC		[8]
13	For 50% heating load calculation	Zaragoza	SM	TRNSYS		L	Solar	UC		[68]
14	Source optimization	Estonia	SM			L	CHP	UC		[274]
15	Different flow control strategy			GD	P/T	M	CHP/HP	UC		[261]
16	Different control strategy	Wales		HDD	TPL	M	CGP	PSS SINCAL		[56]
17	City level	Yazd	SM	GD		L	Combined	EMD		[275]
18	Neighborhood	Turin		HDD						[57]

Keys: SM: source modeling, GD: given data, LF: load factor, HDD: heating degree day, P: pressure model, T: thermal model, ODS: own developed software, UC: user code, L: large, M: medium.

4.2.3 User demand profile

Accurate prediction of the energy demand profile of users in smaller time intervals (such as hourly basis) can affect the efficiency of a network as well as its optimization procedure [53]. Building heterogeneity in each district system is elevated, particularly in the urban setting, and each building has its own properties and demand profile. Therefore, developing a model which could predict the demand profile of the entire district with acceptable accuracy is essential. Most of the existing models used for demand prediction of DHSs have been developed based on the assumption of a standalone building, barely representing the complexity of an urban/district setting. Indeed, the first assumption in the modeling of a standalone building is that the entire building shell receives solar radiation and exchanges heat with the surrounding environment. Moreover, since the demand profile of a building varies as a function of time, this variation has a stochastic behavior (and not a deterministic behavior). As a result, the level of model complexity is increased [270, 276, 277], especially for large district systems with more varying occupant behaviors. In general, the methods suggested to model and predict the demand profile of DHSs (similar to Chapter 3 for buildings), can be categorized as (1) deterministic methods, (2) historical methods [52, 53], and (3) time series predictive methods [54]. Nevertheless, regardless of the prediction methods used by designers to predict the heating demand profile of the districts, these methods could be divided into two general categories:

- Comprehensive modeling using more detailed information and specifications of the buildings such as using commercial simulation software for modeling every individual user within a district
- Simplified numerical methods adopting times series predictive or historical methods to predict the district demand profile using some limited properties of individual users of the network

4.2.3.1 Comprehensive models

A common way to predict the district heating demand profile is to use the deterministic methods. Similar to building modeling, the deterministic methods are divided into two categories of (1) comprehensive modeling using commercial simulation software and (2) simplified deterministic methods. Over the past few decades, many simulation tools have been developed for predicting the energy demand profile of buildings such as EnergyPlus, TRNSYS, eQUEST, etc. These simulation tools are broadly used for modeling various type of buildings. At district level, although they yield highly accurate demand profiles, their main disadvantages are the dependency on data quantity and high computational cost for modeling each individual building [53, 68]. For small-scale districts consisting of a limited number of buildings, using comprehensive models can increase the accuracy of the simulation. Nevertheless, providing the data and time required for modeling several buildings in a city-wide scale is very expensive. As a result, simplified methods emerged as a popular option for prediction of demand profile of district networks.

4.2.3.2 Simplified simulation models

Deterministic methods have been widely used at the building level, while historical/time series methods are more favorable at the district level with a more stochastic behavior. This is

due to their high level of dependency to data for training purposes, especially for large DHSs with diverse building type [94]. These methods have mainly been adopted to predict buildings total energy consumption and maximum demand rather than predicting the actual demand of the system in a smaller interval such as an hourly basis [278].

At the district level, to simplify the prediction process and increase the prediction accuracy, the community building stock is segmented into “building archetypes” (i.e. a building which can represent a group of similar buildings). In this method, buildings with similar occupancy type are divided into subcategories while a reference building is defined for each category. The demand profile of other buildings located within each category is later defined based on the reference building with some adjustment. The number of building categories used in this method as well as the number of adjustments required for modeling the entire demand profiles are the key parameters of the simplified method. The most commonly utilized technique is the regression method.

Usually, segmentation of the building stock is carried out based on the type of parameter picked. Although different sets of parameters can be used to generate building archetypes, generally, these parameters are divided into three major categories:

- Physical properties of the building
- Usage and occupational behavior of the building
- Climatological properties of the region

To conduct the segmentation, the first step is to investigate the existing building stock to define different types of occupancy behavior and to categorize the buildings with similar occupancy type. After categorizing the buildings based on their occupancy behavior, they are further grouped based on their physical properties and/or the type of their mechanical systems. Due to existence of different climates at different regions in national level, these archetypes could be further grouped based on climatological properties of the region in the case of defining the archetypes at national level. Table 4.4 shows a summary of the previous studies.

Table 4.4: Parameters considered to model the demand profiles

		Building archetype								
Level	Ref.	Country	Statistics		Parameters					
			No. of buildings	No. of archetype	Shape	Area	Age	Use	System	Climate
Urban level	[279]	Japan	1,128	20	✓	✓				
	[280]	USA		30	✓		✓	✓	✓	
	[281]	England	267,000	144	✓		✓			
	[282]	Italy	1,320	7			✓			
	[283]	Italy		56	✓		✓	✓		
	[284]	Netherlands	300,000	26	✓		✓			
	[280]	USA	200	12	✓		✓	✓	✓	
	[285]	Switzerland	20,802	20	✓		✓	✓		
National level	[286]	England	115,751	47	✓		✓			
	[287]	Italy	11 M	96	✓		✓			✓
	[288]	Greece	2.5 M	24	✓		✓			✓
	[288]	Greece	2.5 M	5	✓		✓	✓	✓	
	[287]	Italy	877,144	3,168	✓		✓		✓	✓
	[289]	Ireland*	40,000	13						
	[290]	France	14.9 M	92	✓		✓		✓	✓
	[290]	Spain	9.8 M	120	✓		✓		✓	✓
	[290]	Germany	18 M	122	✓		✓		✓	✓
	[290]	UK	20.5 M	252	✓		✓		✓	✓
[291]	Finland	36,000	12			✓	✓			

* Ireland: construction, thermal

Although the building shape has been widely used in defining building archetypes, different studies considered different parameters to define the shape. For instance, in a study, the correlation of the building with surrounding buildings was used as the main parameters to define the building shape and shading effect, categorizing them as detached, semi-detached, townhouse [284]. However, in another study, the height of the buildings was considered as well [290]. Having the number of building archetypes, as well as the number of buildings within each archetype, the demand profile of the users can be predicted using the scaling methods. The two most common scaling methods are (1) area weighted in which the demand profile of a reference building is multiplied by the total district area over reference building area ratio and (2) number based in which the demand profile of a reference building is multiplied by the number of buildings within an archetype.

Table 4.5: Summary of the method used for load prediction in DHS and type of building stocks

Country	Year	Method	Scaling	Type	Output	Ref.
Japan	2004	Archetype/ survey	Number per archetype	Residential	Total EUI	[279]
USA	2008	eQUEST/ comprehensive modeling/ archetype	Area weighted	Mixed	Hourly/ total consumption	[280]
Italy	2012	Regression analysis of measured data	Area weighted	Residential	Total consumption	[282]
Finland	2014	Archetype/ linear development using REMA	Number per archetype	Mixed	Total consumption	[291]
Italy	2013	Archetype/ comprehensive modeling	Area weighted	Mixed	Total consumption	[283]
Italy	2014	Simplified equivalent resistance	Area weighted	Residential	Total consumption	[292]
Greece	2011	Archetype/ comprehensive modeling	Area weighted	Residential	Hourly/ total consumption	[288]
Germany	2014	Simplified/ equivalent resistance/ HDD	Building by building	Mixed	Total consumption	[269]
Switzerland	2015	Archetype/ simplified model/ adjusted HDD	Area weighted	Residential	Total consumption	[293]

In such approaches, the level of simplification in the representation of the building stock modeling is observed to be very high. For example, the orientation and other geometrical diversity of the buildings are mainly neglected compared to the reference building within a defined archetype. These shortcomings in demand profile prediction are more magnified in the case of having larger DHSs with more uniform building type. In district systems with more diverse building types, several influencing parameters overlap one another at the district level, compensating the accumulated error at some points. For instance, in the case of the Japanese district [279], German district [294] or Swiss district [293], with more homogeneous building types, the simulation accuracy is presumably much lower compared with the Italian district [283] which has more heterogeneous building archetypes.

4.3 Simplified 4-step prediction model

4.3.1 Limitations of current models

The main limitations of the methods to predict the DHS demand profile include:

- **Feasibility of expanding one model to the entire district level:** The first limitation of the presented methods is related to the limitation of these models in prediction of the total energy consumption of the entire district. Especially, in the case of a larger district system where the heterogeneity of the buildings is elevated, this problem becomes more amplified. For instance, HDD should be only used for prediction of small residential buildings while the BIN method is more suitable for larger buildings with much higher internal heat generation density. As a result, an archetype method with a combination of these methods should be used to predict the total energy load of the entire network.
- **Type of prediction:** Most of the presented methods has been adapted to predict the total energy consumption. Although at the design stage DHSs are designed based on the total energy consumption as well as the maximum peak demand of the system, detailed profile of the network is further required to improve the system efficiency and enhance the energy distribution management. Table 4.6 summarizes different prediction methods that has been used to predict the consumption load of DHSs. According to the table, most of the studies focused only on the total energy consumption of the networks and not the detailed profile.

- **Accuracy:** Prediction accuracy is the next limitation of the previous models. In the case of load prediction for district systems, two different types of error could be defined; the first type is the error associated with the entire district model, while the second one is associated to the modeling at the building level. As illustrated in Table 4.7, the simulation error is mainly much lower at the district level in comparison with the building level one, which is mainly related to behavior of the users.
- **Computational time:** The long computational time of the stock modeling is one of the major limitations of the current DHS models.

Table 4.6 Summary of the methods used for load prediction in DHS

Ref.	Year	Prediction	Prediction type/resolution	Method
[293]	2015	Annual	Total energy demand	Simplified modeling/adjusted HDD
[295]	2014	Daily	One day forecasting	NARX*, ANN
[291]	2014	Annual	Total energy demand	Linear development using REMA
[292]	2014	Annual	Total energy demand	Simplified equivalent RC
[296]	2014	Annual	Total energy demand	Simplified equivalent RC
[297]	2013	Daily	Average daily and hourly variation	Time series
[283]	2013	Annual	Total energy demand	Comprehensive modeling
[294]	2013	Annual	Total energy demand	Quasi-state monthly energy balance
[282]	2012	Annual	Total energy consumption	Linear regression analysis
[298]	2011	Annual	Peak load and total demand	Multi-variant regression
[299]	2011	Annual	Total energy demand	Gray box model
[288]	2011	Annual	Annual peak demand	Comprehensive modeling
[300]	2010	Monthly	Peak load forecasting	Linear regression and clustering
[301, 302]	2009	Annual	Annual heating degree day	Linear regression
[303]	2008	Annual	Linearized peak day profile	Linear regression
	2008	Annual	Total energy demand	Gray box
[280]	2008	Annual	Hourly/total energy demand	Software modeling using eQUEST
[304]	2006	Annual	Profile	Gray box
[305]	2008	Annual	Peak demand	Stochastic method
	2005	Annual	Total energy demand	Gray box
	2004	Annual	Total energy demand	Multi-variant regression
[279]	2004	Annual	Total EUI/total energy demand	Software modeling using SCHEDULE
[306]	2004	Annual	Total energy demand	Simplified equivalent RC
[52]	2002	Annual	Profile	Linear regression

*Nonlinear autoregressive network with exogenous inputs

Table 4.7: Summary of the accuracy level of the previous studies

Prediction error for district				Prediction error for individual buildings			
Year	Country	Error	Ref.	Year	Country	Error	Ref.
2004	Japan	18%	[279]	2014	USA	11-23%	[307]
2008	USA	10-13%	[280]	2011	Greece	12-55%	[288]
2012	Italy	10%	[282]	2013	Germany	5-50%	[294]
2013	Italy	4%	[283]	2013	Germany	18-31%	[294]
2014	Italy	8%	[292]	2014	Germany	1-60%	[308]
2013	Germany	21%	[294]	2014	Switzerland	6-88%	[309]
2013	Germany	7%	[294]	2015	Switzerland	8-99%	[293]
2014	Switzerland	8%	[309]				
2015	Switzerland	9-66%	[293]				

4.3.2 Model development

Due to the mentioned limitations, a 4-step procedure has been developed to accurately predict the heating demand profile of different type of district system with a high resolution, hourly interval, in a timely manner. The procedure is based on the multiple linear regression (MLR) and multiple nonlinear regression (MNLR) methods. In this 4-step procedure, the

heating demand profile of the entire district is predicted by modeling each individual unit in the community using its physical and geometrical characteristics, the regions' meteorological information, and the occupants' general behavior.

- **Step 1:** In the first step, a sample building stock model (BSM) is segmented into different archetypes, and a reference building is defined for each archetype. The initial segmentation is completed by considering the building construction method, physical and geometrical properties, and construction period [278]. Once the initial archetypes are determined, each archetype is further divided into sub-archetypes based on the occupancy schedule (e.g. residential user with high, medium and low usage) of the building within that archetype. Different methods are used for segmenting the BSM based on the occupancy schedule. While some researchers only segment the BSM based on major occupancy types (e.g. residential, commercial, or office types), others segment it following the user energy profile. This study presents a more detailed approach for defining the number of archetypes as well as the reference building for each archetype. A hierarchical clustering method was adopted for this end. In this method, the data set is split into a prefixed number of clusters. The building closest to the centroid of that cluster is defined as a reference building for that cluster. To define the number of clusters required for a given data set, prefixed number of clusters, the optimal number of cluster is defined using the elbow method.
- **Step 2:** The second step involves building the model input files. These files are constructed based on the physical properties of individual units, regional meteorological data, and occupant behavior. In order to determine the input file of the model, extensive sensitivity analysis has been done to identify the most influential parameter on the heating demand profile of the buildings. Based on the results obtained from sensitivity analysis, four different input files were constructed for this study.
 - ✓ **Input 2.1:** The first input file is the solar dependent variable. This variable is determined using the weather station closest to the district site and defines each unit envelope assembly solar heat gain. The solar components obtained from the weather file are translated on each envelope assembly using the incident angle, orientation, and albedo of that assembly.
 - ✓ **Input 2.2:** The second input file is the thermal dependent file. The thermal dependent file is defined based on the average heat transfer from the unit exterior façade, considering its average thermal resistance of the exterior façade of the unit and the indoor-outdoor temperature difference.
 - ✓ **Input 2.3:** The third input file is the unit internal gain. Should specific data about unit internal heat generation be unavailable, the general household average heat generation can be used.
 - ✓ **Input 2.4:** Finally, the fourth input file constructed based on the daily HVAC system on/off cycles.
- **Step 3:** In the third step, a reference building heating demand profile is initially defined using the data obtained from the measured data. An ANN model is then trained and tested using the reference building input file as well as the heating profile of them to obtain the regression coefficients.

- **Step 4:** Finally, in the fourth step, once the MNL model is trained separately for each archetype, using the reference building, each individual unit heating demand profile is predicted by adopting the input file of them [278]. This procedure can predict the heating demand profile of both individual building whereas entire district network.

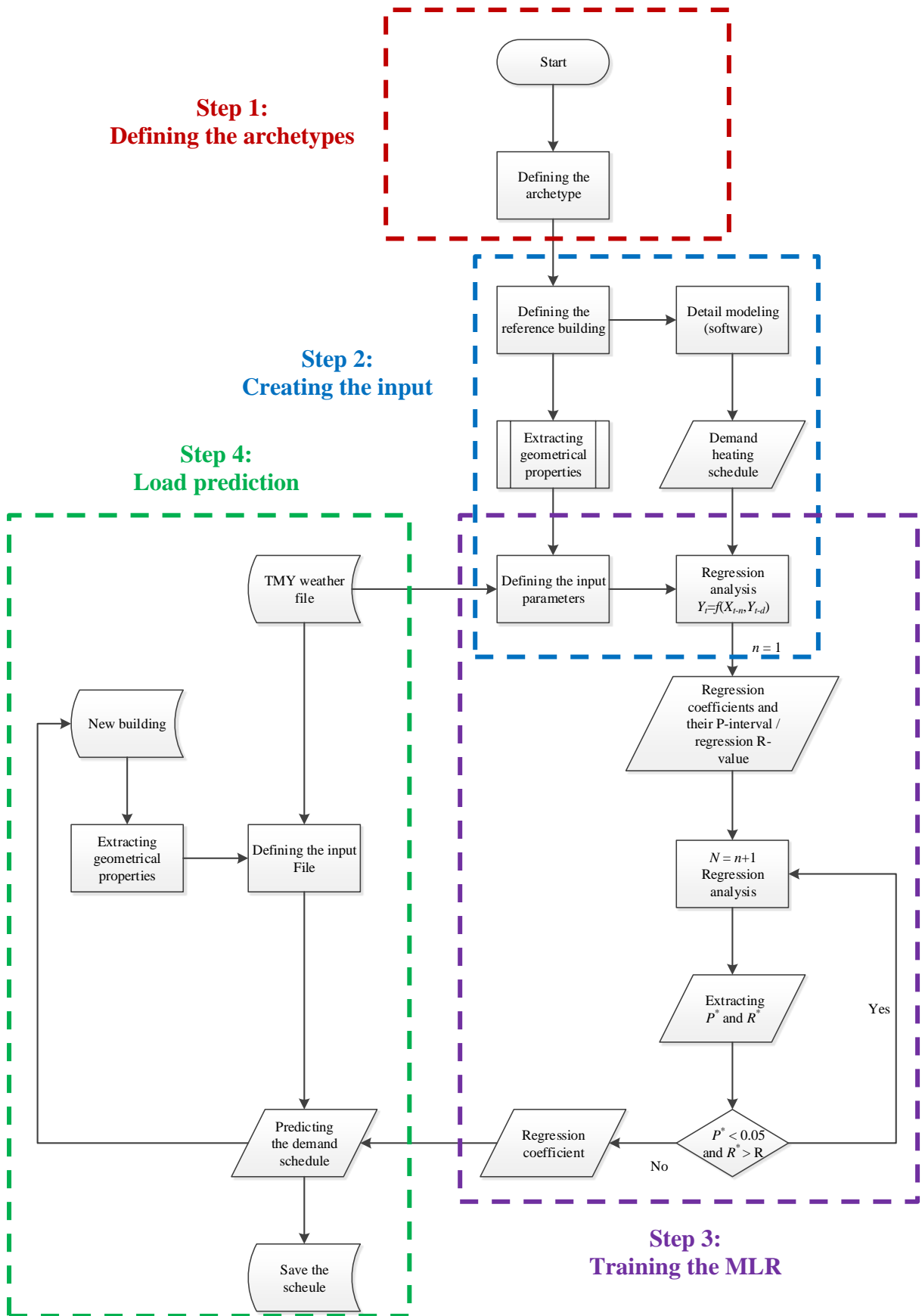


Figure 4.3: Predicting the heating demand schedule

4.4 Available tools

Storage and demand side management (DSM) are key in integrating RES into community energy systems. Many modeling tools are available which support design of such systems. To select an appropriate tool, it is essential to understand tool capabilities and assess how they match the requirements for a specific situation. The specific aims of this section are (1) to categorize and document the capabilities of tools suitable for modeling community systems for the planning design stage with focus on incorporation of storage and DSM, and (2) to develop a selection process based on these documented capabilities to identify the appropriate tools suitable for modeling a specific situation. This will be achieved through:

- Initial screening process to identify potentially suitable tools
- Categorization and tabulation of modeling tool capabilities and characteristics
- Development of a tool selection process using the tables
- Demonstration of the selection process for a case study and discussion of the findings

4.4.1 Initial tool screening

An initial list of 51 tools with some ability to model an energy system was derived from (1) literature including reviews and studies describing the development and application of tools, (2) tool user manuals/websites and (3) communication with tool providers. Tools not capable of modeling community scale energy systems were excluded. For example, Envi-met is a microclimate and landscaping tool [310], and Radiance is used in daylight prediction [311]; therefore, they were excluded.

A set of criteria were applied to the selected 51 tools to determine their potential suitability in more detail. A tool was considered to pass the criteria if it (1) could be used at community scale (i.e. was defined as such or had a case study demonstrating this capability), (2) was appropriate for the planning stage, incorporated renewable and low carbon technologies and storage as well as DSM, (3) had hourly or sub-hourly time step, and (4) could cover either thermal or electrical energy supply.

This process resulted in the identification of 15 tools suitable for modeling community scale energy systems incorporating RES, storage and DSM, for use at planning design stages. Two of the 15 tools (i.e. MODEST and Mesup/PlaNET) were excluded due to lack of accessible information required for more detailed analysis. This left 13 tools to be carried forward into the categorization of capabilities and tool selection process. The following criteria were examined for the initial screening process shown in Table 4.8:

- **Community scale:** This criterion was met if the tool manual, guidance documentation or associated publications had specifically described the tool as applicable at community scale.
- **Community scale case study:** If some tools identified as being primarily for ‘national’ or ‘regional’ planning rather than for community scale had available case studies or other documentation demonstrating application at community scale, they were included.
- **Planning-level design:** Tools capable of modeling for planning-level design were deemed to be in scope and to pass this criterion. More detailed building or system design

tools, which require very detailed user inputs to describe each individual building and system component were deemed not to meet the criteria.

- **Low or zero carbon technologies (LZCT):** Modeling of at least one low-carbon or renewable technology was imposed as a minimum.
- **Storage and DSM functionality:** Modeling of at least one form of storage and DSM was imposed as a minimum.
- **Time step:** Criterion met if capable of a time step of one hour or less.
- **Electrical and/or thermal modeling:** The imposed criterion was the ability to model either electrical or thermal networks. Community systems can consist of (1) electrical, thermal and transport demands, (2) electrical and thermal generating components, (3) microgrid networks, (4) transport fuel systems, (5) thermal networks, and (6) various DSM technologies interacting across the spectrum. Integration of these energy sectors can provide synergistic benefits, often resulting in a higher penetration of renewable supply [312, 313]. While an ideal energy system tool would combine all these energy vectors, it was recognized that many community system design tasks utilize just one; therefore, this was set as the minimum requirement.

Table 4.8: Initial tool screening process

No.	Tools	Criteria met?	Community scale	Case study	Planning-level design	LZCT	Storage/DSM	Time step	Electrical	Thermal	Ref.
1	AEOLIUS		National/regional		✓	✓	✓	Minutes	✓		[314]
2	Balmorel				✓	✓	✓	Hourly	✓	✓	[315]
3	BCHP Screening Tool				✓		✓	Hourly	✓	✓	[314, 316]
4	Biomass decision support tool	✓	✓	-	✓	✓	✓	Hourly		✓	[317]
5	CitySim		✓	-		✓	✓	Hourly	✓	✓	[318-320]
6	COMPOSE	✓	✓	-	✓	✓	✓	Hourly	✓	✓	[313, 314]
7	DECC 2050 Calculator				✓	✓	✓	Yearly	✓	✓	[321]
8	DER-CAM	✓	✓	-	✓	✓	✓	5 mins	✓	✓	[322, 323]
9	E4Cast				✓	✓	✓	Yearly	✓	✓	[314]
10	EMPS				✓	✓	✓	Weekly	✓		[314, 324]
11	EnergyPlan	✓	National/regional	✓	✓	✓	✓	Hourly	✓	✓	[325, 326]
12	EnergyPRO	✓	✓	-	✓	✓	✓	Minutes	✓	✓	[327, 328]
13	ENPEP-BALANCE		National/regional		✓	✓		Yearly	✓	✓	[313, 314, 329]
14	ESP-r		✓	-		✓	✓	Seconds	✓	✓	[330, 331]
15	ETEM/Markal-lite		✓	-	✓	✓	✓	Yearly	✓	✓	[329, 332, 333]
16	eTransport	✓	✓	-	✓	✓	✓	Hourly	✓	✓	[334, 335]
17	GTMMax				✓	✓	✓	Hourly	✓	✓	[314, 336]
18	H2RES	✓	✓	-	✓	✓	✓	Hourly	✓	✓	[325, 337, 338]
19	HOMER	✓	✓	-	✓	✓	✓	Minutes	✓	✓	[339-341]
20	Hybrid2	✓	✓	-	✓	✓	✓	Minutes	✓		[342, 343]
21	HYDROGEMS		✓	-		✓	✓	Minutes	✓		[314, 344]
22	IDA-ICE					✓	✓	Minutes		✓	[318]
23	iHOGA	✓	✓	-	✓	✓	✓	Minutes	✓		[345-347]
24	IKARUS				✓	✓	✓	5 years	✓	✓	[314, 329]
25	INFORSE				✓	✓	✓	Yearly	✓	✓	[314]
26	Invert		National/regional	✓	✓	✓		Yearly	✓	✓	[314, 348]
27	KULeuven OpenIDEAS Framework		✓	-		✓	✓	Minutes	✓	✓	[314, 349, 350]
28	LEAP				✓	✓	✓	Yearly	✓	✓	[329, 351]
29	MARKAL/TIMES	✓	✓	-	✓	✓	✓	Hourly	✓	✓	[352, 353]
30	MERIT	✓	✓	-	✓	✓	✓	Minutes	✓	✓	[354]
31	Mesap/PlaNet	✓	✓	-	✓	✓	✓	Minutes	✓	✓	[314, 329, 355]
32	MESSAGE				✓	✓	✓	5 years	✓	✓	[314, 329, 334, 356]
33	MiniCAM		National/regional		✓	✓	✓	15 years	✓	✓	[314]
34	MODEST	✓	✓	✓	✓	✓	✓	Hourly	✓	✓	[314, 357, 358]

35	NEMS			✓		✓	Yearly	✓	✓	[314]	
36	Nepplan	✓	-		✓	✓	Minutes	✓	✓	[359]	
37	NetSim	✓	-		✓		Hourly		✓	[95, 360]	
38	ORCED			✓	✓	✓	Hourly	✓		[355, 361]	
39	PERSEUS			✓	✓	✓	36-72/year	✓	✓	[314]	
40	Polysun			✓	✓	✓	15 mins	✓	✓	[362, 363]	
41	PRIMES			✓	✓	✓	Yearly	✓	✓	[95, 364]	
42	ProdRisk	✓	-	✓	✓	✓	Hourly	✓		[314, 365]	
43	RAMSES			✓	✓	✓	Hourly	✓	✓	[314, 366]	
44	RETScreen	✓	-	✓	✓	✓	Monthly	✓	✓	[312, 314, 329, 367]	
45	SimREN	✓	✓	-	✓	✓	Minutes	✓	✓	[314, 368]	
46	STREAM		National/regional		✓	✓	✓	Hourly	✓	✓	[369]
47	Termis	✓	-		✓		Minutes		✓	[160, 268]	
48	TRNSYS	✓	-		✓	✓	Seconds	✓	✓	[313, 314, 318, 346, 370, 371]	
49	UniSyD3.0			✓	✓	✓	Bi-weekly	✓	✓	[314]	
50	WASP	✓	-	✓	✓	✓	12/year	✓	✓	[314]	
51	WILMAR Planning Tool			✓	✓	✓	Hourly	✓	✓	[314]	

4.4.2 Categorization of capabilities

In this section, tool capabilities are contrasted for the 13 modeling tools based on:

- Input data requirements and input support capabilities
- Electrical and thermal supply technology modeling capabilities including district heating
- Design optimization and outputs capabilities
- Controls and DSM modeling capabilities
- Storage modeling capabilities and underlying storage models
- Practical considerations

These comparisons are intended to be useful in the tool selection process (described later in Section 4.4.3) by providing information on the capability of tools to be assessed against requirements for a specific community system analysis.

4.4.2.1 Input requirements

Tools have various levels of input data requirements. Some tools require the energy demand profiles, local climate, system characteristics or generation profiles to be explicitly input directly by the user as time series. Other tools have embedded functions and libraries which provide support in generating detailed datasets from simple inputs, and/or support a mix of both directly entered and tool generated calculation inputs. This functionality could be essential, desirable, or not applicable depending on availability of data or expertise. The key characteristics related to data input requirements for the various tools are tabulated in Table 4.9 and further described in this section.

Table 4.9: Tool input data characteristics

Tool	Demand profile generator	Resource assessor *	Supply profile generator
Biomass decision support tool	Yes	No	Modeler
COMPOSE	No	No	Database and input
DER-CAM	No	S, T, W	Modeler
EnergyPlan	No	No	Database and input
EnergyPRO	Yes	B, H, S, T, W	Modeler
eTransport	Yes	Yes	Modeler
H2RES	No	B, H, S, W	Modeler
HOMER	Yes	B, H, S, T, W	Modeler
Hybrid2	Yes	S, W	Modeler
iHOGA	Yes	H, S, W	Modeler
MARKAL/TIMES	No	B, H, S, T, W	Modeler
MERIT	Yes	S, T, W	Modeler
SimREN	Yes	Yes	Modeler

Resource assessor keys: B: Biomass, H: Hydro, S: Solar radiation, T: Temperature, W: Wind
 * “Yes” indicates that specific resources assessed by the tool were unable to be confirmed

4.4.2.1.1 Demand profile generator

Tools were deemed to contain a demand profile generator (‘Yes’ in Table 4.9) if functionality exists to support synthesis of electrical, thermal or fuel demand profiles in hourly or sub-hourly time steps from simple inputs such as monthly or annual bill data or descriptions of building numbers and types, demographics, etc. Others in which either explicit half hourly or hourly metered data needs to be obtained, or potentially generated using a secondary

modeling process (e.g. using building performance simulation tools) were categorized as ‘No’ for this category.

4.4.2.1.2 Resource assessor

A resource assessor gives access to weather and other resources (e.g. solar radiation, wind, water, biogas and biomass) in a suitable data input format (e.g. from national or international datasets) based on simple inputs (e.g. location). The resources covered were identified for each tool.

4.4.2.1.3 Supply profile generator

A supply profile generator provides electric, thermal or fuel-producing system outputs to be used in the modeling. ‘Modeler’ describes a tool which generates the supply profile from the resource input (e.g. climate) and the device specifications. For example, in HOMER, local wind speeds (the resource input) and a specific wind turbine specification (a power curve and other details) are used to calculate the wind turbine supply profile. ‘Database and input’ describes a tool in which the hourly or sub-hourly supply profiles are directly fed as inputs requiring the user to carry out some outside tool calculations or source such datasets.

4.4.2.2 Supply technology modeling capabilities

Tools vary with respect to the range of supply technologies which can be directly modeled. Table 4.10 presents information about available supply technologies within the tools. A wide range of electrical supply systems can be modeled where most tools support modeling of connection to the external electricity grid. Two categories have been assigned for modeling of the grid connection. First, ‘Grid simple’ allows for limitless import and export, with static pricing. Second, more complex ‘Grid’ models include features such as connection limits and charges, complex time-based import, export tariffs, etc.

DHS modeling (if available) is considered only as an estimated heat loss. This is a continuous heat loss as a percentage of peak load in the Biomass Decision Support Tool, or a percentage of real-time load as in EnergyPRO. The heat demand density, distribution temperature and other factors such as controls which have a large effect on ancillary energy use and losses in DHSs are not directly considered and are required to be the input provided by the user for thermal demand profiles.

4.4.2.3 Output capabilities

Two important attributes in supporting design tasks are (1) capability of the tool to aid the identification of optimum design solutions, and (2) ability of the tool to directly provide outputs required to support decision making. Key capabilities of the 13 tools in these areas are presented in the first two columns of Table 4.11 and further discussed in this section.

Table 4.10: Supply system technologies

Tools	Electrical supply	Thermal supply	District heating
Biomass decision support tool	No	FB	Yes
COMPOSE	B, C, CHP, G, Gr, PV, Wi	CHP, EB, FB, HP, ST	No
DER-CAM	CHP, D, G, Gr, PV, Wi	CHP, EB, FB, Geo, HP, ST	No
EnergyPlan	B, C, CHP, D, G, Geo, Gr, GrS, H, N, PP, PV, T, Wa, Wi	CHP, EB, FB, Geo, HP, I, ST, Was	Yes
EnergyPRO	B, C, CHP, D, G, Gr, H, PV, Wi	CHP, EB, FB, HP, ST	Yes
eTransport	CHP, Gr, PP	CHP, FB, HP	Yes
H2RES	B, C, D, G, GrS, H, PV, Wa, Wi,	EBo, FB	No
HOMER	B, C, CHP, D, G, Gr, H, PV, Wi	CHP, FB	No
Hybrid2	D, PV, Wi,	None	No
iHOGA	D, G, Gr, H, PV, Wi	None	No
MARKAL/TIMES	B, C, CHP, D, G, Geo, Gr, GrS, H, N, PP, PV, T, Wa, Wi	CHP, EB, FB, Geo, HP, I, ST, Was	No
MERIT	C, CHP, G, GrS, PV, Wi,	CHP, HP, ST	No
SimREN	Geo, H, PP PV, Wi	CHP	No

Electrical supply keys: B: Biomass power plant, C: Coal power plant, CHP: Combined heat and power plant, D: Diesel plant, G: Gas plant, Geo: Geothermal plant, Gr: Grid, GrS: Grid simple, H: Hydro, N: Nuclear, PP: Power plant (generic), PV: Photovoltaic, T: Tidal, Wa: Wave, Wi: Wind

Thermal supply keys: CHP: Combined heat and power, EB: Electric boiler, FB: Fuel boiler, Geo: Geothermal, HP: Heat pump, I: Industrial surplus, ST: Solar thermal, Was: Waste incineration

Table 4.11: Design optimization, outputs, controls and DSM controls capabilities

Tools	Optimization/Function	Outputs	Controls	DSM control
Biomass decision support tool	S	E, EP, FA, FC, RP, SA	FO, NO	FO
COMPOSE	E, F	E, EP, FA, FC, SA	MO, OO (F)	OO (F)
DER-CAM	E, F	A, E, EP, FA, FC, SA	DC, EV, LS, MO, OO (F, E)	DC, EV, LS, OO (F, E)
EnergyPlan	No	E, EP, FA, FC, SA, RP	FO, LS, MO, OO (F)	FO, LS, OO (F)
EnergyPRO	No	E, EMI, EP, FA, FC, SA	EV, MO, NO, OO (F), UO	EV, OO (F)
eTransport	F	E, EMI, EP, FA, FC, SA	MO, OO (F)	OO (F)
H2RES	No	EP, FC, RP, SA	FO, MO	FO
HOMER	F	A, E, EP, FA, FC, RP, SA	AC, LS, MO, NO, OO (F), UO	LS, OO (F)
Hybrid2	No	EP, FA, SA	FO, LS, MO, NO	FO, LS
iHOGA	Single: F Double/triple: combination of A, E, F, H, J, N	A, E, EP, FA, FC, HDI, JC, RP, SA	FO, MO, NO, OO (F)	FO, OO (F)
MARKAL/TIMES	F	E, EMI, EP, FA, FC, RP, SA	MO, NO, OO (F)	OO (F)
MERIT	No	EP, FC, M, SA	FO, LS, MO	FO, LS
SimREN	No	EMI, EP, SA	-	-

Design optimization keys: A: autonomy, E: emissions, F: financial, H: human development index, J: job creation, S: system

Outputs keys: A: Autonomy, E: Emissions, EMI: Energy market interaction, EP: Energy production, FA: Financial analysis, FC: Fuel consumption, HDI: Human development index, JC: Job creation, M: Demands/supply match, RP: Renewable penetration, SA: System analysis

Control/ DSM control keys: AC: Advanced control, CC: Cycle charging, DC: demand curtailment, EV: electric vehicle, FO: fixed order, LS: load shifting, MO: modulation output, NO: non-modulating output, OO: operational optimization (with objective function in brackets), UO: User-defined order

4.4.2.3.1 Design optimization

Optimization tools find the minima (or maxima) for a defined objective function by systematically searching a defined modeling space according to a mathematical algorithm (details in Chapter 5). Design optimization involves a search for the optimal system with respect to combination and sizing of components. Most of the reviewed tools which support optimization use a full factorial deterministic approach based on user defined inputs to solve the optimization problem and use a simple financial and/or carbon emissions objective. For example, HOMER used to execute a grid search based on user defined inputs specifying the system options to be included, but recently provided an update allowing users to only input upper and lower limits to the grid search. iHOGA was the only identified tool with multi-objective function capability. It includes a choice of available objective functions and embedded genetic algorithms [372]. The Biomass Decision Support Tool can optimize the size of TES. Tools which do not directly support mathematical optimization could be used within an external mathematical optimization process by an iterative approach; however, this can be logistically complex or require advanced software skills to automate.

4.4.2.3.2 Outputs

The outputs have a key role in assessing system performance. Different tools focus on different aspects of the system performance. Most tools provide financial analysis such as cost/kWh of energy produced or information on energy market interactions. Some tools are purely technical and focus on the energy production, system analysis, demand/supply match, or fuel consumption. Others assess emission and renewable penetration, while some others consider social factors such as job creation and the human development index. Specific tool outputs can be used in external calculations to generate a wider range of analysis outputs but only the built-in capabilities are documented here.

4.4.2.4 Control modeling capabilities

The ability to correctly capture the controls is also important to assess the performance of community scale energy systems and particularly when assessing the impacts of storage and DSM in such systems. Modeling tools often have built-in control logics intended to mimic real or idealized controls. It is important to comprehend and assess the control regime underpinning each of the models.

Controls regulate how supply, storage and DSM technologies meet loads by determining the control logic and applied constraints. A simple community scale system control strategy can include (1) an order of dispatch for the different resources, and (2) a set of constraints.

4.4.2.4.1 Operational optimization

Operational optimization (OO) control is defined as the tool which optimizes (at each time step) the order of dispatch of supply, storage and DSM technologies to satisfy an objective function which may relate to cost, emissions, etc. There are differences among the tools in terms of logical implementation; nevertheless, a general description is provided in this section.

Most tools use OO control chronologically where calculations are performed at each individual time step to establish an optimum based on prevailing conditions at that time step only, before the next time step is considered. Storage is generally charged and discharged when

it is deemed favorable to do so according to the specific logical implementation and objective function. Typically, charging occurs when there is excess energy from renewable or non-modulating supply where storage is deemed to have benefit over export or curtailment, or where grid parameters (e.g. tariff) make charging from grid advantageous. Discharging from available storage is generally treated as a dispatchable supply option. The value attached to storage charge and discharge considers characteristics of the storage system (e.g. efficiencies and costs, plus parameters such as tariffs and carbon contents). For example, in HOMER, the discharge energy cost includes average charge energy cost, efficiencies, and battery wear, lifetime and replacement costs.

OO control is applied non-chronologically in some tools (e.g. in EnergyPRO) where the whole calculation period is scanned for energy supply costs. An optimized supply schedule is determined, with excess low-cost generation charging storage and discharge occurring to meet demand in subsequent favorable high cost time steps. These OO control functionalities may replicate real control systems for situations where local renewable consumption is prioritized or where a set tariff structure is established for energy import and export. The non-chronological OO implementation may in some circumstances provide a somewhat optimistic view of system performance as perfect foresight is implied.

4.4.2.4.2 Fixed order

Fixed order (FO) control is where there is an available set of functions with predefined order of dispatch of supply, and fixed conditions for the use of storage and DSM technologies. Dispatchable supply is dispatched in an FO in periods where non-dispatchable (typically renewable) supply is below demand. EnergyPLAN, H2RES and MERIT charge electrical storage in periods of excess renewable production and prioritize discharging from electrical storage over generators and power plants. In MERIT, TES discharging is prioritized over other thermal supply options. In EnergyPLAN, TES charging is prioritized to absorb excess electricity or heat production and discharged to avoid nonrenewable generation. In iHOGA, batteries can charge/discharge at fixed, user input tariff values. In the Biomass Decision Support Tool, excess heat from the biomass boiler is stored in a TES and discharged when demand exceeds supply. EnergyPLAN includes several selectable functions for excess electricity production. Hybrid2 contains embedded functionality for 13 predefined FO controls relating to the practical performance of electric systems [373].

4.4.2.4.3 User-defined order

User-defined order (UO) control is where the order of dispatch (for at least some part of the supply) is defined by the user. For example, UO in EnergyPRO requires all supply options to be given an order of preference, which can also include separate priorities for production to satisfy different loads (i.e. peak, high, low). In this tool, storage priority setting is not an option and storage operation always follows the OO control strategy.

4.4.2.4.4 Modulating output

Application of modulating output (MO) control to a dispatchable supply allows modulation of output to match the load above certain minimum supply output level. In all tools, the grid connection (if enabled) can modulate output to follow electrical load with a minimum

supply level of zero. HOMER can only designate grid or generator supplies to this control, while in EnergyPRO, DER-CAM and eTransport any dispatchable supply can be assigned.

4.4.2.4.5 Non-modulating output

Non-modulating output (NO) control sets the constraint that a designated supply must operate at a fixed output whenever it is operating. In the Biomass Decision Support Tool, the designated supply is the biomass boiler. In EnergyPRO, the user selects the supplies. In iHOGA and HOMER, the designated supplies are the generators. In these two tools, a set state of charge can be specified, and the designated supply will continue operating (regardless of renewable generation availability) until reaching the set point. It mimics a common feature in real systems used to maximize battery life but reducing the potential for renewable inputs to the storage.

4.4.2.4.6 Advanced control

HOMER offers the capability to use advanced control (AC) strategies where users can define more complex control operating regimes than those previously outlined by interfacing with externally written codes in MATLAB [374].

4.4.2.5 Storage modeling capabilities

This section looks at relevant capabilities of the 13 screened tools and underlying models with respect to storage functionality. Such functionality enables DSM and, in the reviewed tools, is used with the operational optimization and fixed order controls.

Storage capabilities are presented in two tables for use in tool selection process. Table 4.12 describes the range of storage modeling capabilities available in each tool and Table 4.13 gives a summary of the models. In this section, a summary of each capability and underlying model is provided.

Table 4.12: Storage and DSM general capabilities and underlying models

Tools	Electrical *	Thermal *	DSM *	Fuel synthesis *	Fuel storage *
Biomass decision support tool	No	MB	No	No	B
COMPOSE	KiBaM	SSM, CS	No	No	No
DER-CAM	SSM, FB	MB	LS, DR, DCL, EV	No	No
EnergyPlan	SSM, PH, CAES	SSM, STS	LS	BF, BG, H, EF, GtL	G, O, M
EnergyPRO	SSM, PH	MB, CS	EV	BF, BG, H, EF, GtL	G, O, M
eTransport	Yes	Yes	No	Yes	Yes
H2RES	Yes	Yes	No	No	Yes
HOMER	SSM, PH, KiBaM, MKiBaM, FB	No	DCL	H	H
Hybrid2	EKiBaM	No	LS	No	No
iHOGA	SSM, KiBaM, MKiBaM	No	No	H	H
MARKAL/TIMES	Yes	Yes	Yes	Yes	Yes
MERIT	EKiBaM	SSM	LS	No	No
SimREN	Yes	No	No	No	No

Electrical keys: SSM: Simple storage model, KiBaM: Kinetic battery model, MKiBaM: Modified kinetic battery model, EKiBaM: Extended kinetic battery model, FB: Flow battery model, PH: Pumped hydro model, CAES: Compressed air energy storage model
Thermal keys: SSM: Simple storage model, MB: Moving boundary model, STS: Seasonal thermal storage model, CS: Cold storage model
DSM keys: DCL: Directly controllable load, DR: Demand response, EV: Electric vehicles, LS: Load shifting
Fuel synthesis keys: BF: Biofuel, BG: Biogas, EF: Electrofuel, GtL: Gas to liquid, H: Hydrogen
Fuel storage keys: B: Biomass, G: Gas, H: Hydrogen, M: Methanol, O: Oil
* “Yes” indicates that the tool has a certain capability, but specific models used were not able to be confirmed. These tools were assumed to have SSM as minimum electrical and thermal storage models

Table 4.13: Electrical and thermal storage technologies and models

Electrical storage	Models used	Thermal storage	Models used
Lead-acid battery	SSM, KiBaM, EKiBaM, MKiBaM	Hot water tank	SSM, MB
Li-ion battery	SSM, KiBaM, KiBaM, MKiBaM	Cold storage	SSM, CS
Flow battery	SSM, FB	Seasonal thermal storage	SSM, STS
Pumped hydro	SSM, PH		
CAES	SSM, CAES		

4.4.2.5.1 Electrical storage

Electrical storage is a general term used here to include electrochemical (li-ion, flow, lead-acid batteries), electromagnetic (supercapacitors) and mechanical (CAES, hydro, flywheels) forms. Electrical storage can be represented using several different mathematical models, the different models used in the tools are described in this section. The level of detail required at the planning stage depends on the specifics of the system being modeled and the outputs to be derived from the modeling.

4.4.2.5.1.1 Simple storage model

A tool possessing the SSM, which can interact with supply and load, can model any storage technology. EnergyPLAN and EnergyPRO use the SSM to define all types of storage, including all electrical storage types. iHOGA, DER-CAM and HOMER support the use of the SSM, e.g. for high-performance batteries [366]. HOMER also recommends its use for simple pumped hydro storage systems. The SSM consists of a simple energy in/out balance via an energy storage. Energy can enter the storage below a threshold maximum charging rate, up to a maximum storage capacity. There can be self-discharge from the storage (e.g. a percentage or other function at each time step). Energy can be discharged from the storage below a threshold maximum discharging rate. For charging and discharging there are associated efficiencies, which combine with self-discharge to give a round-trip efficiency. Charging and discharging efficiencies are both generally fixed values. The SSM has fixed maximum charging and discharging rates independent of the state of the system. This approximation may be sufficient for some analyses but may not be realistic in other cases. Storage life cycle analysis is included in some tools with the SSM. For instance, in HOMER lifetime is modeled as both an energy throughput and time. However, performance degradation effects are only included in the MKiBaM model described later.

4.4.2.5.1.2 Kinetic battery model

The kinetic battery model (KiBaM) was first developed for modeling lead-acid batteries in hybrid energy systems [375]. It is described as a two tank model [376], where one tank holds the available energy to directly support charging and discharging and the other holds the bound energy which transfers energy to and from the available tank according to a defined exchange function representing the chemical process. The model supports charge/discharge rates as functions of stored energy in the two tanks. The underpinning electronic mechanisms are still somewhat simplified with voltage modeled only as a linear function of energetic state, etc. iHOGA and HOMER both possess this model and have libraries of electrochemical batteries with parameters established from test data.

4.4.2.5.1.3 Extended kinetic battery model

The KiBaM was improved in terms of modeling voltage behavior [377]. These models are denoted here as extended kinetic battery models (EKiBaM). Hybrid2 includes such an improved model [378], with voltage, charging and discharging efficiencies and current as nonlinear functions of the state of charge. MERIT also contains a different but similar model with improved voltage modeling [354].

4.4.2.5.1.4 Modified kinetic battery Model

A further modified kinetic battery model (MKiBaM) is used by HOMER and iHOGA to provide deeper insights. This includes a thermal model component whereby the resistive properties of the battery produce heat, affecting temperature, capacity and lifetime. iHOGA offers customized models for lead-acid batteries [379, 380] and Li-ion batteries [381-383].

4.4.2.5.1.5 Flow battery model

Flow batteries can also be modeled explicitly with models which account for the independence between capacity and charge/discharge and other flow cell characteristics. Flow battery specific models based on manufacturers data are included in DER-CAM [384] and HOMER [376].

4.4.2.5.1.6 Pumped hydro model

Pumped hydro is often modeled using the SSM by factoring in the capacity and efficiency of the pump and generator as well as the capacity of the reservoir. EnergyPLAN and HOMER include pumped hydro as a technology using the SSM. Only EnergyPRO includes an explicit pumped hydro model and includes inputs such as reservoir volume, friction factors and head difference.

4.4.2.5.1.7 Compressed air energy storage model

A simple CAES model is included in EnergyPLAN, with a focus on the possible economic trading [385].

4.4.2.5.2 Thermal storage

The investigated tools use only the least complex models, some of the limitations associated with this are discussed later. The categorization of TES models found in the tools is presented in Table 4.12 and Table 4.13 and is described in this section.

4.4.2.5.2.1 Simple storage model

The SSM model for thermal storage does not consider temperatures but only accounts for energy and was described earlier for electrical storages. EnergyPLAN uses the SSM to model all TES technologies.

4.4.2.5.2.2 Moving boundary model

The most common model for TES in the examined tools is the moving boundary (MB) model, where the additional inputs over the SSM are top and bottom tank temperatures. It assumes that there is no mixing between the upper hot zone and the lower cold zone and the thermocline boundary layer is infinitesimally small. This is again an energy balance model

with inflows and outflows of energy moving the boundary layer up and down the storage and stored energy is calculated based on the thermocline position. The model does not explicitly capture temperature variation due to losses and destratification. This model is incorporated in the Biomass Decision Support Tool, DER-CAM, EnergyPRO and MERIT. The model can be adjusted in EnergyPRO using a utilization factor reducing the useful energy which can be used for supply. DER-CAM allows for different high temperature and low temperature storages within the system to allow for different heat generation devices [386]. EnergyPRO also uses the MB model for cold storage and was the only tool identified to have electrical, heat and cold storage modeling capability.

4.4.2.5.2.3 Seasonal model

A seasonal TES model is included in EnergyPLAN. It is simplified and only two inputs are required (1) capacity, and (2) days of optimizing storage, which allows for the model to identify inter-seasonal variations in demand. In general, this functionality is not supported in the tools analyzed here apart from EnergyPLAN.

4.4.2.5.2.4 Modeling of fuel synthesis and storage

Fuel synthesis is the production of fuels within a system creating a new energy vector which can be used across a range of energy sectors, and acts as storage to be used later [387]. EnergyPLAN, EnergyPro, iHOGA and HOMER can model hydrogen synthesis. This is produced using electricity with an electrolyzer to form hydrogen, stored in a hydrogen tank, and then converted to meet transport, heat or electricity demands. All three technical components can be modeled within these tools. EnergyPRO contains a simple model for the synthesis of any fuel. EnergyPLAN allows for synthesis of different fuel types including biofuel, biogas, and hydrogen from electrolysis, electrofuel and gasification to liquid transport fuel. These fuels are used to form interactions between energy sectors and ensure high-value energy is used for high-value processes.

These fuels must then be kept in storage. The Biomass Decision Support Tool can size biomass fuel storage, while iHOGA and HOMER can model hydrogen storage tanks. EnergyPLAN can model gas, oil and methanol storages, and EnergyPRO can model any fuel storage as a generic model.

4.4.2.6 Practical considerations

Table 4.14 sets out practical considerations associated with selecting a tool including cost, access, support, whether it is academic or commercial, and user-friendliness. Cost may be a vital factor in choosing an energy system tool and depends on the resources available to users. A student is likely to choose a free tool, e.g. Biomass Decision Support Tool, COMPOSE, DER-CAM, EnergyPLAN, iHOGA, Hybrid2, MERIT and MODEST. Often tools are available at discounted prices for students. A government agency or an engineering consultancy may have the resources available to afford the cost for a tool such as 3,000+ EUR for EnergyPRO, 500-1,500 USD for HOMER, or 1,275-3,130 EUR to manipulate the code for MARKAL/TIMES.

Accessibility is defined in terms of availability, purchase requirement, and if the tool is downloadable or browser-based. Available support as indicated by tool websites are listed, and

includes user manual, available contact details, videos, training and an online forum. The tools are classed as academic or commercial based on the development and ownership of the tools through either a university/research group or a private company, respectively. User friendliness was judged on the provision of an intuitive model-building pathway which was subjectively graded at a low, medium, or high level.

Table 4.14: Practical considerations

Tools	Cost	Access	Support	Academic/commercial	User friendliness
Biomass Decision Support Tool	Free	Download	UM, V, OC	Commercial	High
COMPOSE	Free	Download	V, F	Academic	Medium
DER-CAM	Free	Browser	UM, V, F	Academic	Medium
EnergyPlan	Free	Download	UM, C, V, T, OC	Academic	High
EnergyPRO	3,000+ EUR for all modules	Purchase	UM, C, T	Commercial	High
eTransport	-	Not available	-	Academic	High*
H2RES	-	Not available	None	Academic	Not available
HOMER	Free 2-week trial, 500–1,500 USD	Purchase	UM, C, V, F	Academic/commercial	High
Hybrid2	Free	Download	UM, C	Academic	Not available
iHOGA	Educational free, 500 EU for 1 year	Purchase	UM, F, C	Academic	Medium
MARKAL/TIMES	1,275-3,130 EUR to manipulate source code	Download	UM, F, PS	Academic	Low*
MERIT	Free	Download	T	Academic	Medium
SimREN	-	Not available	Not available	Commercial	Not available

Support keys: UM: user manual, V: videos, OC: online courses, F: forum, C: contact, T: training, PS: paid support

* From Beuzekom et al. [313]

4.4.3 Tool selection process

In this section, a typical stepwise tool selection process is developed to aid identifying an appropriate tool for a particular analysis for planning-level design of a community energy system incorporating storage and DSM, based on the process of Sandia National Laboratories [388].

4.4.3.1 Determination of requirements

The first process step is to establish which of the modeling tool capabilities are essential, desirable or not applicable and to assign values of 2, 1 and 0 respectively to each of these tool capabilities. This process requires that each of the capabilities described in the column headings and associated keys of the tables are individually considered against the requirements for the intended analysis. For example, according to Table 4.9, the three tool capabilities captured are demand profile generator, resource assessor and supply profile generator. If the user requires the tool to provide demand profiles, weather data and renewable generation supply profiles from simple input data (such as location and demographics), then these capabilities would be considered essential and each of these capabilities would be assigned a value of 2. Alternatively, if the user has available data for demand, weather and renewable generation and supply (e.g. from monitored data), then these capabilities are not applicable so would be assigned a value of 0 and can be eliminated from further consideration. If the user can potentially source information and generate the demand, weather and renewable generation input data but this would need significant effort, then this capability could be ranked as desirable and allocated a value of 1. Similarly, according to Table 4.10, it may be essential to have the capability to model electrical generation with both PV and wind, so each of these capabilities would be allocated a 2, while if there is no potential for hydro, then this capability would be allocated a 0. When this process is complete, the essential and desirable capability requirements have been established. This process for a case study is described in the following sections.

4.4.3.2 Scoring of tools against requirements

Once the requirements have been established, each of the tools can be scored against them. The first consideration is whether all the essential capabilities are available. If a given modeling tool has all the essential capabilities it can be further considered. Those which do not pass this check can be discounted. For the tools which pass, their scores for the essential plus desirable capabilities are summed into an overall score and ranked with the most suitable tools having the highest scores. Table 4.15 illustrates this process for a simple case study which is described in more detail in the following section.

4.4.3.3 Example application of the modeling tool selection process

Findhorn is an ecovillage in the northeastern Scotland with an ambition to transition to a local, low-carbon energy system. It consists of about 75 buildings, with a private wire electrical network, wind and solar generation, a grid connection, micro-district heating from biomass, and individual household heat pumps and solar thermal systems. The community could be said to be net zero carbon but has large electricity surpluses and shortfalls due to stochastic demands and renewable production. The community has an interest in the use of thermal and electrical

storage with advanced controls as a potential route to achieving their aims. The community had previously been monitored as a research and demonstration site for advanced DSM [389].

The overall objective is to increase the energy autonomy and use of local RES. The community has some concerns over the sustainability of biomass. To help achieve their objective, an initial scoping process identified 2 initial future illustrative scenarios to be investigated (1) increased electrical generation plus battery storage, and (2) increased electrical generation plus heat pumps and large hot water tanks replacing the micro-district biomass heat source. The modeling tool selection process was then applied to identify suitable software to be used for the investigation.

The first step was to review the tool capability requirements. Demand profile generator, resource assessor, and supply profile modeler capabilities (Table 4.9) were all deemed to have zero value (i.e. not applicable) since multi-year sub-hourly data was readily available from monitoring.

Electrical supply technologies from wind, grid and solar PV were deemed to be essential (Table 4.10). Thermal supply modeling of fuel boiler (biomass fuel in this case) and heat pumps were also deemed essential. Capability to model solar thermal and district heating in detail were scored desirable but not essential at this stage as the primary focus was on the electrical supply system and the available monitoring data included heat delivery from existing heat production units net of solar inputs and distribution losses.

Design optimization capability (Table 4.11) was deemed desirable but not essential as the view was that the relatively simple range of options to be investigated could be covered through a full factorial deterministic investigation and modeling outputs analyzed outside of the tool to establish potential optima. The output of hourly data allowing either autonomy, emissions or renewable penetration to be established was deemed essential. This level of system performance parameter output would then allow the other required outputs to be calculated outside of the tool.

For control capabilities (Table 4.11), either FO or OO control was deemed essential to support the required ordering for dispatch of supply and storage, in addition to the MO control inherent in all the tools for representing the grid. DSM specific control functionality was not required in this example.

Storage modeling capability was deemed essential for both electrical and thermal storage (Table 4.12 and Table 4.13, respectively). It was deemed that the SSM was sufficient but that it would be desirable for more complex models to be available. Fuel synthesis and fuel storage were not required in this simple illustrative study.

These technical requirements are tabulated in the top rows of Table 4.15. Each of the tools assessed against these requirements, where a tool has an essential or desirable capability then it scores 2 or 1 respectively against that capability, otherwise it scores 0. Once all the potentially capable tools have been assessed, they are ranked by (1) the tools which do not have all the essentials are deemed to 'fail' to meet the essential requirements and discounted and only those that 'pass' this test are further considered, (2) the remaining tools are then ranked

based on their cumulative score. This process is illustrated in Table 4.15, with the result in this case that 6 tools are capable with similar scores of either 20 or 21. Note that this example was relatively simple for reasons of clarity and brevity. More complex situations follow the same process.

Table 4.15: Output from application of tool selection process

Tool	Design optimization	Outputs	Control	Supply technologies								Electric battery SSM	Electric battery > SSM	Hot water tank SSM	Hot water tank MB+	Pass/fail	Score
			FO or OO	WT	PV	FB	GR	DH	ST	HP							
Desirable/Essential	D	E	E	E	E	E	E	D	D	E	E	D	E	D			
Value	1	2	2	2	2	2	2	1	1	2	2	1	2	1			
COMPOSE	1	2	2	2	2	2	2	0	1	2	2	1	2	0	Pass	21	
DER-CAM	1	2	2	2	2	2	2	0	1	2	2	0	2	1	Pass	21	
EnergyPRO	0	2	2	2	2	2	2	1	1	2	2	0	2	1	Pass	21	
EnergyPlan	0	2	2	2	2	2	2	1	1	2	2	0	2	0	Pass	20	
MERIT	0	2	2	2	2	2	2	0	1	2	2	1	2	0	Pass	20	
MARKAL/TIMES	1	2	2	2	2	2	2	0	1	2	2	0	2	0	Pass	20	
eTransport	1	2	2	0	0	2	2	1	0	2	2	0	2	0	Fail	16	
H2RES	0	2	2	2	2	2	2	0	0	0	2	0	2	0	Fail	16	
HOMER	1	2	2	2	2	2	2	0	0	0	2	1	0	0	Fail	16	
iHOGA	1	2	2	2	2	0	2	0	0	0	2	1	0	0	Fail	14	
Biomass Decision Support Tool	1	2	2	0	0	2	0	1	0	0	0	0	2	1	Fail	11	
Hybrid2	0	0	2	2	2	0	0	0	0	0	2	1	0	0	Fail	9	
SimREN	0	0	0	2	2	0	0	0	0	0	2	0	0	0	Fail	6	

Keys: WT: wind turbine, PV: photovoltaic, FB: fuel boiler, GR: grid, DH: district heating, ST: solar thermal, HP: heat pump

4.4.4 Shortcomings of available tools

The categorization and documentation of tool capabilities revealed that there are many differences between the available tools. Some tools (such as EnergyPLAN) combine all energy sectors based on the view that holistic consideration across sectors leads to optimal solutions. Other tools are primarily single domain focused. For instance, iHOGA has strong capabilities for electrical analysis with a wide range of storage models but no thermal capability.

Design optimization capabilities in the tools is generally focused on financial or technical considerations. Only iHOGA optimizes human considerations (e.g. human development index and job creation) and two tools optimize environmental considerations. Much work has been carried out regarding external optimization in a two-step process. This may influence the lack of embedded optimization options in the tools. Another factor is the preference for the simplicity and transparency in full factorial parametric analysis.

There is also a lack of detailed DHS modeling capability in any of the community-scale tools. With only a heat loss parameter as input, factors such as the heat demand density, distribution temperatures, network layouts and controls which have a large effect on ancillary energy use and losses in DHSs are not directly addressed.

Analysis of control capabilities in the tools showed a wide range including operational optimization, fixed order, and user-defined orders, for dispatch of supply and storage. Operational optimization control is usually used with a cost based objective function, other possible objective functions such as maximizing local use of renewable generation, minimizing grid imports or minimizing emissions generally are not directly supported, with DER-CAM being a notable exception. More advanced predictive controls based on weather forecast and demand prediction are not supported. However, the non-chronological operational optimization in EnergyPRO and the deferrable load functionality in HOMER, etc. can represent this type of control but with significant simplifications. The option to run tools in combination with external control algorithms in separate software packages is one way around this limitation.

The analysis of storage functionality and modeling revealed the frequent use of SSM. More complex models exist for electrochemical storage particularly for lead-acid, li-ion and flow batteries. TES is limited to simple energetic models which do not directly consider temperature variations other than in assessing capacity. These may be suitable for initial planning design stages but have limitations. Consideration of temperatures, heat transfer rates, stratification and phase change in TES systems necessitates more complex models. These will be required in the future to support realistic modeling of the hybrid systems and advanced controls for which these parameters have critical importance.

There were few tools found to be directly capable of analyzing the fuel synthesis technologies. However, such technology is currently unlikely to be at the community scale

in the short-term. For this reason, tools developed for regional scale have the most capability.

The wide range of available tools and their differing capabilities make a categorization and tool selection process valuable for the end user of such tools. The abundance of available tools and rapidly developing field dictated that it was impossible to include everything. However, their selection is reasonably representative of the state-of-the-art in tools for planning-level design at community scale. The presented categorization and selection process is not limited to the tools identified here but is intended to provide a framework which can be used in the future to refresh the capabilities categorization or be applied to further tools. The review of required capabilities as the first part of the selection process can also form a guide for modelers to ensure that relevant factors are considered.

The tool selection process does not consider the potential for multiple tools to be used together to analyze the system under consideration. Such work is recommended for future studies. The more detailed simulation modeling tools currently used in building and system domains have the potential to be developed for community scale energy systems in the future. This would allow more physical detail to be captured in planning level design studies, their capabilities could also be assessed, and tools selected using the same process.

An element not considered here is the validation of the modeling tools. So far in the available literature, case studies are largely based on design and do not include monitored data on completed schemes which include DSM and storage. Experience in the buildings industry has found that performance gaps are common [390] and identified that industry process needs to evolve to address these gaps [391]. It is critical that similar issues are addressed to avoid performance gaps in future community scale energy systems.

4.5 Examples

In the following two examples, two levels of model validation are presented at the district level for the 4-step prediction model using the simplified procedure mentioned earlier (Section 3.3.1).

4.5.1 Simplified district load prediction: inter-model comparison

A DHS is designed to distribute the heat generated by different means of heating sources within the network of users at higher efficiency and lower CO₂ production. Although some evidence of DHS use can be observed over the span of several centuries, it was not until the last two decades that it has become an established method to design green and energy efficient heating for buildings.

4.5.1.1 Background

As explained in Section 3.3.1, three primary sources of discrepancies can be identified for existing models which are occupant behavior, neighborhood interference and scaling effect. Regarding the latter, scaling methods (Section 4.2.3.2) are used to represent

the entire housing stocks (see Table 4.5 and Table 4.7). In this example, the results of the developed method for predicting the heating demand profile of a district are compared with those obtained from detailed modeling using eQUEST.

4.5.1.2 System description

The following three districts were considered for the inter-model comparison:

- **District 1:** comprised of 95 residential buildings
- **District 2:** consisting of 82 office buildings
- **District 3:** includes a mixture of 84 residential and 28 office buildings

Two validated reference buildings were selected to study these districts. The geometric parameters (i.e. number of stories, aspect ratio, orientation, net area and window to wall ratio) were altered in accordance to these buildings to define the districts (Figure 4.4). In other words, the geometric parameters from the reference buildings were utilized to define the range of the parameters of every other building in the district. These ranges were based on the likelihood of the characteristics for the archetypes within each district. Subsequently, the parameters of each building were given a random value within each of the defined ranges as shown in Table 4.16 to Table 4.18. Note that other than the reference buildings (which provide realistic values) and the ranges of the geometric parameters (which have been determined based on the likelihood within their specific district), all other values were randomly constructed. To construct the buildings within District 2 and District 3, similar patterns of assigning random values were applied.

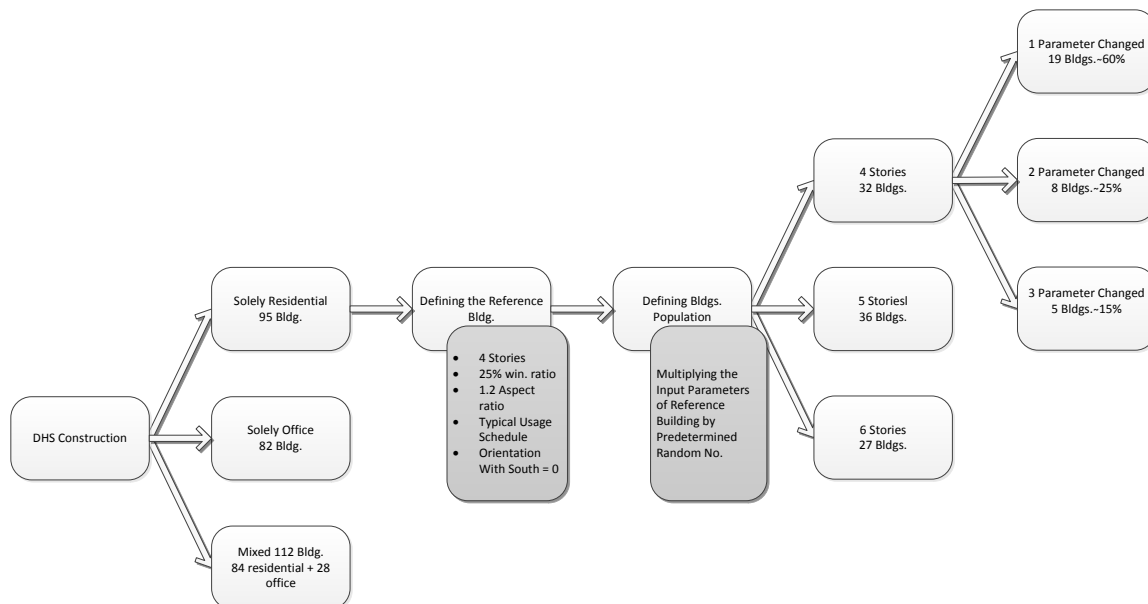


Figure 4.4: The algorithm used to generate Districts 1-3

Table 4.16: Description of District 1

Stories	Buildings	Area [m ²]	Window/wall	Aspect ratio	Orientation*	Set point [°C]
4	32	3,500-4,500	20-45%	0.75-1.3	± 25°	24
5	36	3,800-5,000	20-45%	0.75-1.3	± 25°	24
6	27	3,500-5,500	20-45%	0.75-1.3	± 25°	24

*Orientation with respect to south

Table 4.17: Description of District 2

Stories	Buildings	Area [m ²]	Window/wall	Aspect ratio	Orientation*	Set point [°C]
4	21	10,200-12,000	20-40%	0.75-1.3	± 25°	24/20
5	37**	10,200-13,000	20-35%	0.75-1.3	± 25°	24/20
6	24	11,500-14,000	20-35%	0.75-1.3	± 25°	24/20

*Orientation with respect to south

**5 buildings assumed to have common wall on east or west side

Table 4.18: Description of District 3

Type	Stories	Buildings	Area [m ²]	Window/wall	Aspect ratio	Orientation*	Set point [°C]
Residential	4	25	3,500-4,500	20-40%	0.75-1.3	± 20°	24
	5	32	3,800-5,000	20-40%	0.75-1.2	± 25°	24
	6	27	3,500-5,500	20-40%	0.75-1.3	± 20°	24
Office	4	12	10,200-12,000	20-35%	0.75-1.3	± 25°	24/20
	5	10	10,200-13,000	20-35%	0.75-1.3	± 25°	24/20
	6	6	11,500-14000	20-35%	0.75-1.1	± 25°	24/20

*Orientation with respect to south

4.5.1.3 Methodology

After defining the buildings within each district, the heating demand profile of each individual building was obtained using the simplified MLR approach as well as eQUEST. Since the office buildings were assumed to be operating for a limited period of time in each day, two different occupancy set point temperatures were defined. To have more consistency in the results, all buildings were assumed to use electrical heating systems. A similar approach was used for the office buildings. Note that the reference building used for modeling of the residential buildings in this example is the same as the one used earlier (in Section 3.3.1).

4.5.1.4 Results

Figure 4.5 presents the MLR predicted against simulated heating demand profiles for District 1 as well as the error histogram. Comparing the total heating demand load of District 1 (solely residential) with the schedule obtained from the summation of the profiles of the individual buildings using eQUEST shows high agreement between them.

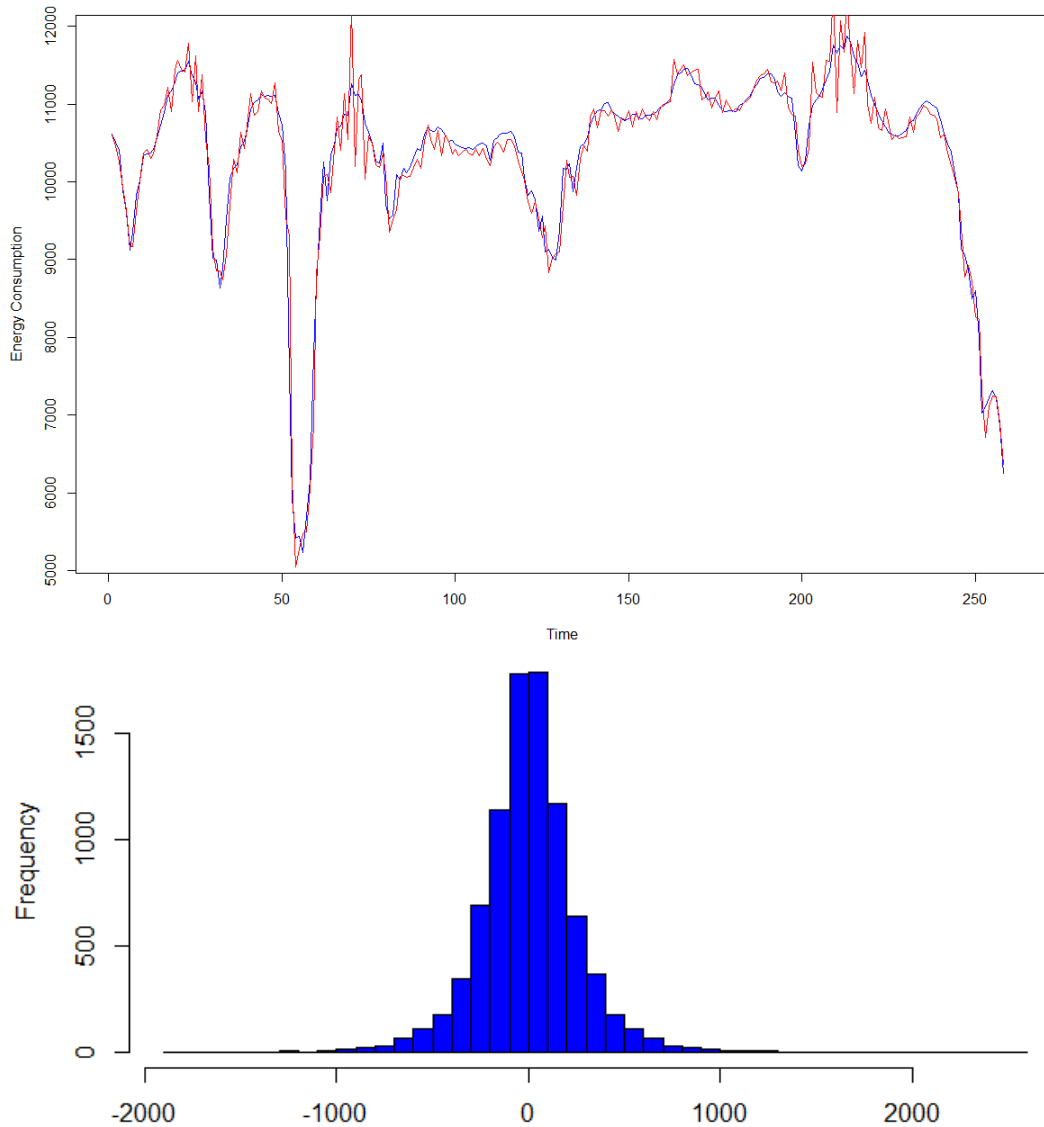


Figure 4.5: Simulation (blue) versus prediction (red) graphs for heating demand profile [kWh] of District 1 showing an 11-day (end of Dec.) period (top) and error histogram (bottom)

Based on the reference office building, the average predicted heating demand schedule of the office buildings within District 2 are presented in Figure 4.6. Due to higher daily fluctuation of the heating demand schedule of the office buildings (especially in early morning and late afternoon) switching between occupied and unoccupied periods, the average standard error for office buildings was higher (about 20.16 kW). Considering average office building area and average maximum pick, this value was slightly higher for office buildings, 1.6%.

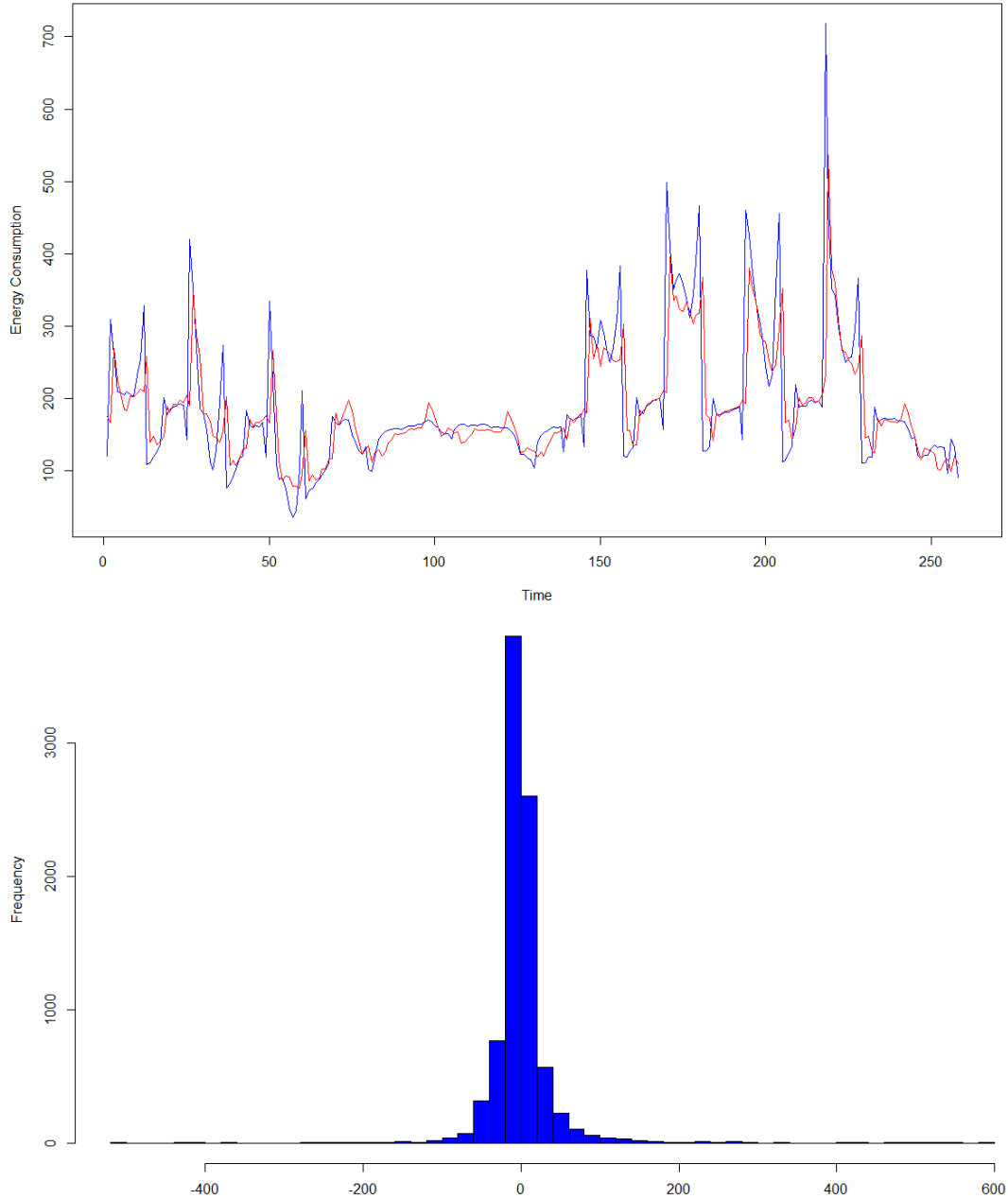


Figure 4.6: Simulation (blue) versus prediction (red) graphs for heating demand profile [kWh] of District 2 showing an 11-day (end of Dec.) period (top) and error histogram (bottom)

Finally, the results obtained for District 3 (Figure 4.7) showed that due to higher number of the residential buildings within the community, the MLR predicted profile was better fitted with simulated schedule. The R-value for District 3 was about 0.9856 and the average error was about 5.2%, which is quite close to the one obtained for District 1 (4.67%).

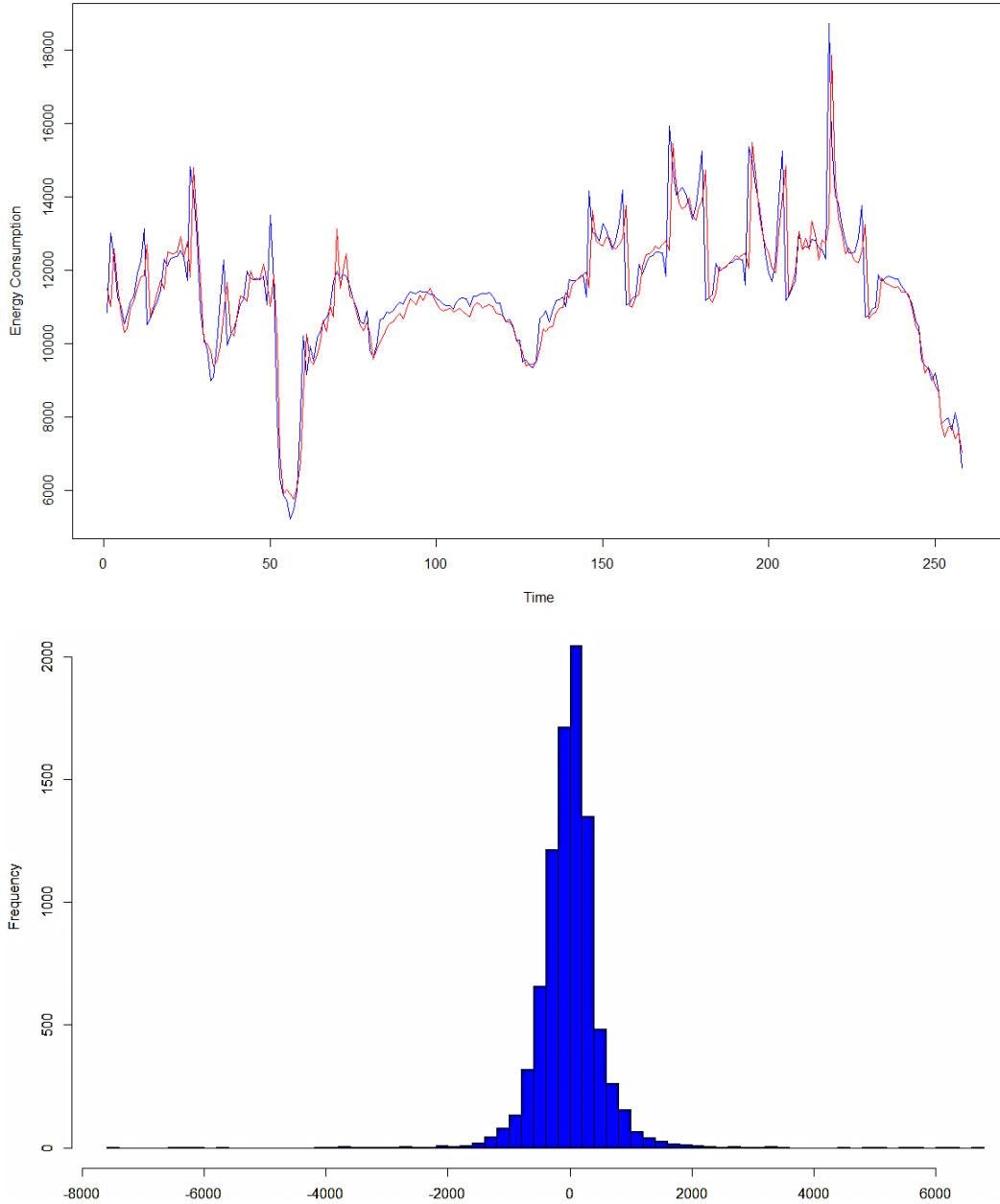


Figure 4.7: Simulation (blue) versus prediction (red) graphs for heating demand profile [kWh] of District 2 showing an 11-day (end of Dec.) period (top) and error histogram (bottom)

Due to the characteristics of the office buildings, having different daily usage schedule as well as set point temperature for occupied and unoccupied periods, the results for District 2 showed a lower correlation $R = 0.9401$ compared with 0.9966 obtained for District 1. This lower correlation was due to the higher daily heating load variation in the office buildings in District 2 compared with the residential buildings in District 1.

4.5.2 Simplified district load prediction: case study

Numerous building energy conservation strategies have been tested using energy storage [91, 129] and user-demand [392] methods. A hybrid community district heating system (H-CDHS) is a unique energy management alternative given its storage and renewable systems are integrated in the district thermal energy system. Since the energy generated by RES is not uniform throughout the day, a TES unit allows the system to synchronize with the supply and demand. To implement this system effectively, it is essential to predict the H-CDHS detailed energy demand profile [393].

4.5.2.1.1 Background

This example endorses the 4-step prediction model (described in Section 4.3) to predict the energy demand profile of an H-CDHS. The previous example covered model validation using the inter-model comparison, while in this example using measured data, the heating demand profile of a real case scenario was defined. Using the 4-step procedure, the district energy demand profile was predicted, and compared with both the measured data and the initial prediction.

4.5.2.2 System description

In this example, a mid-size community district heating system was picked. The field measurement data from the West Whitlawburn Housing Co-operative (WWHC) H-CDHS, Cambuslang, Scotland were used. The WWHC community (details in Section 6.6.7) consists of more than 640 dwellings with four types of buildings. Figure 4.8 shows the location of buildings connected to the H-CDHS with respect to the boiler house:

- Newly renovated towers with 12 stories (6 towers)
- Newly built duplex detached houses (50 buildings)
- 4-story terrace buildings (10 buildings)
- Community buildings (5 buildings)

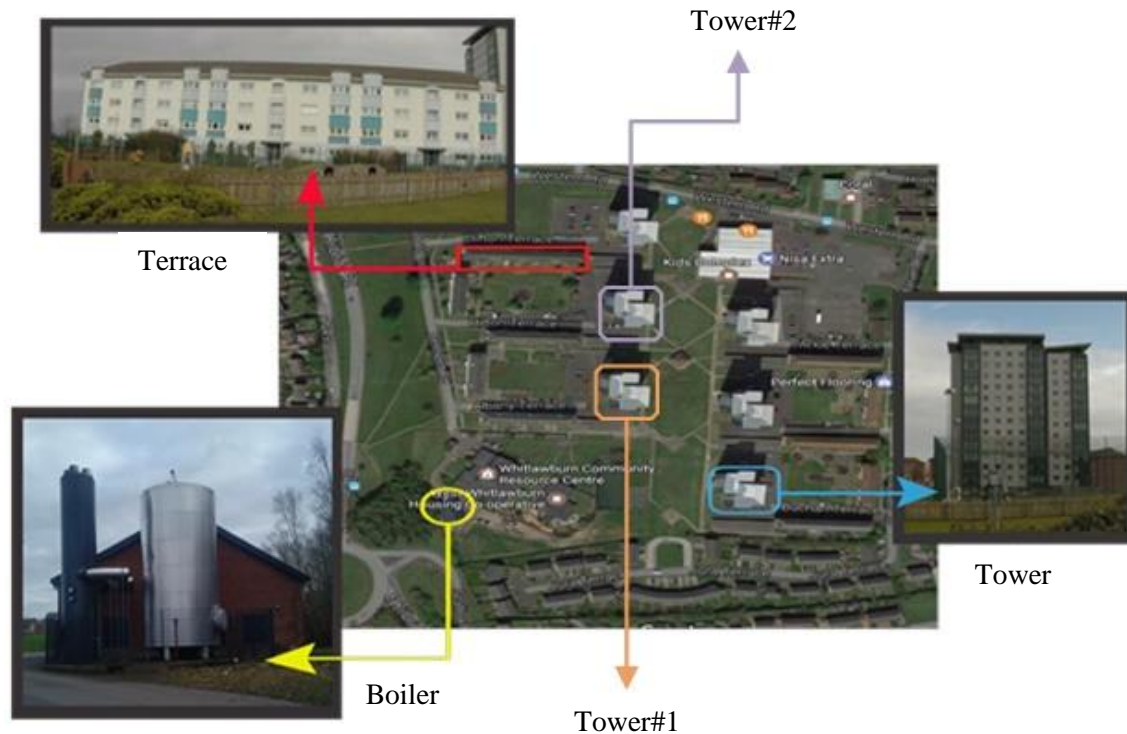


Figure 4.8: Hybrid community-district heating system layout in Whitlawburn, Cambuslang, Scotland

Unlike the inter-model comparison, in the WWHC community, the district network provided not only the heating energy required for space heating, but also the energy required for domestic usage. A dual pipe network transferred the heated water from the boiler house to the building units, where a dual heat exchanger was installed to provide energy for space heating and DHW purposes.

4.5.2.3 Methodology

A wide range of users with different socio-economic levels and behavior demands were connected to the system. Since many users were lower income families, their energy consumption (consequently their annual energy demand) were highly dependent on their economic state and the financial support received. Thus, a prepaid energy credit system allowing each tenant to buy a credit in advance has been installed. The prepaid system was connected to a meter in each unit recording the costs associated with the energy consumed every half hour, which tenants could use to monitor their energy usage over time. To ensure the accuracy of the measurements, cross validation between different data have been performed. To do so, in the first step, tenant occupancy was verified and any changes in unit occupancy was eliminated from results to avoid errors in the unit energy demand profile. After eliminating units with different tenants (between November 2016 and February 2017), the monthly energy demand of the remaining units was calculated using the data collected by smart meters. The monthly energy demand in units with similar

tenants was expected to correlate with the monthly outdoor temperature. Therefore, the monthly usage of a unit in months with similar average outdoor temperatures should remain almost constant.

Figure 4.9 and Figure 4.10 represent the cross data validation for one of the towers (Arran tower). As illustrated in Figure 4.9, in units 12, 37 and 39 there was a higher monthly consumption fluctuation during the four months compared with other units. Further investigation showed that units 37 and 39 were vacant for a short period of time (probably due to holidays), while for the other unit, the tenant has been changed. As a result, the data for unit 12 were considered as false and removed from data set.

To apply the 4-step prediction model (presented in Section 4.3) for predicting the heating load, the first step was to define the number of required clusters. To do so, all the units were initially divided (based on their built form and construction type) into two archetypes (1) newly renovated high-rise buildings, and (2) partially renovated old terrace buildings. The units within each archetype were further segmented based on their occupancy behavior. A sample population dataset was selected to define the optimal number of archetypes associated with the occupant behavior in each construction type. The total energy demand [kWh], the number of inter-unit heat exchanger ON/OFF cycles per month, the peak monthly load [kW], the monthly HDD, and average monthly outdoor temperature were determined as effective parameters to define the number of archetypes.

For large-scale communities with numerous users such as WWHC, using all monitored data from every individual unit to determine the parameters required for defining the optimal cluster number is computationally intensive. Therefore, instead of calculating the required parameters of all units, the parameters of a smaller sample data which could represent the same distribution as the whole community were considered (Arran tower, 72 units). The results were extrapolated to the entire dataset (Arian tower and the whole district).

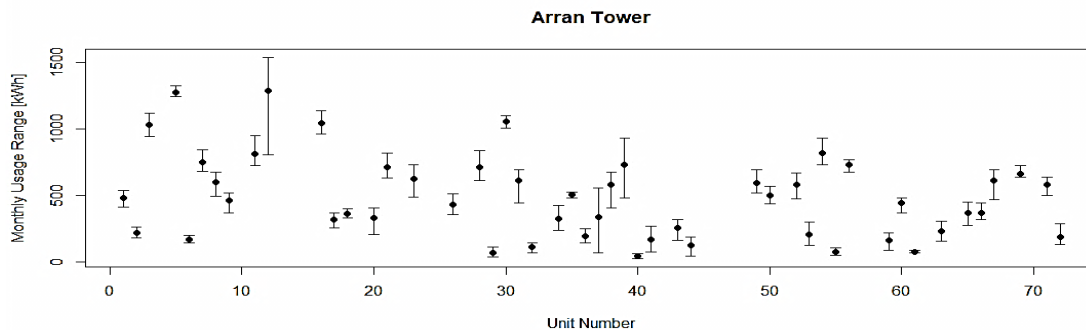


Figure 4.9: Monthly consumption of individual units in Tower#1 (Arran tower)

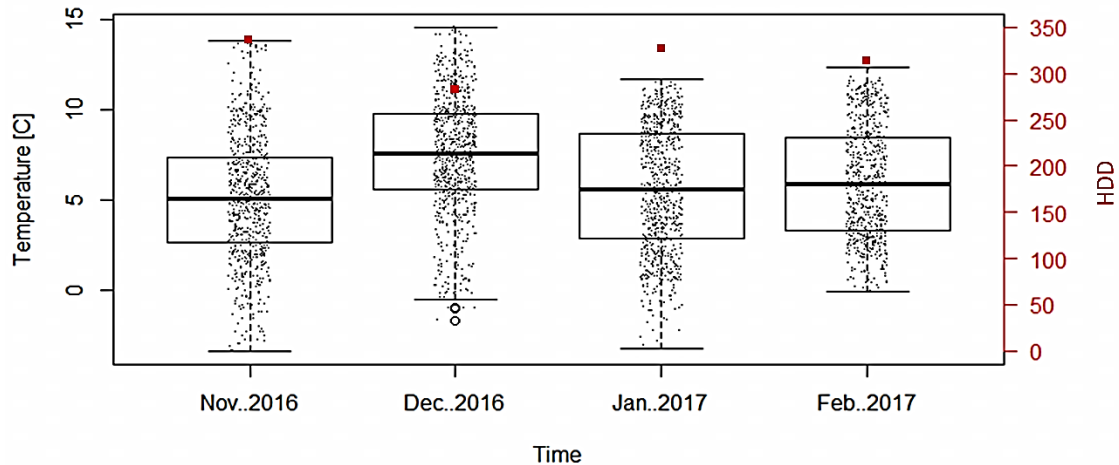


Figure 4.10: Outdoor temperature and HDD for the 2016-17 heating season (Nov 2016 to Feb 2017)

Figure 4.9 shows the average monthly energy demand (for all dwelling units) of Arran tower for both DHW and SH, between November 2016 and February 2017. This figure shows the range of energy demand fluctuation when outdoor temperatures and monthly HDD do not vary considerably. Variations between 5.17 and 5.98 °C for outdoor temperature and from 312 to 331 for monthly HDD (Figure 4.10) are not significant for most units. The results obtained for all individual units in the Arran tower show that the monthly energy demand remains almost constant, with unit-to-unit variation generally being much greater than that of a unit (except units 12, 37 and 39). Hence, the monthly average demand profile of most units is expected to remain almost constant (Figure 4.9).

4.5.2.4 Results

Using the five parameters (monthly consumption, number of inter-unit heat exchanger ON/OFF cycles per month, monthly peak demand, monthly HDD and monthly outdoor average temperature), the k-means (number of clusters) was varied between 1 and 20 to construct different numbers of clusters. Using R software for each value of k, the square metric distance [m^2] of residual (R) from a reference point was determined to find the optimal number of archetypes (clusters) for simulation. This value was selected when the difference between the residual of two consecutive clusters became negligible. The number of clusters should be selected so that adding another cluster does not significantly increase the dataset presentation. The results are plotted in Figure 4.11, and it can be concluded that four to seven archetypes can be chosen as the optimal number. Here, k-means 4 was selected as the optimal number for demonstrating the method with adequate accuracy while maintaining computational costs low.

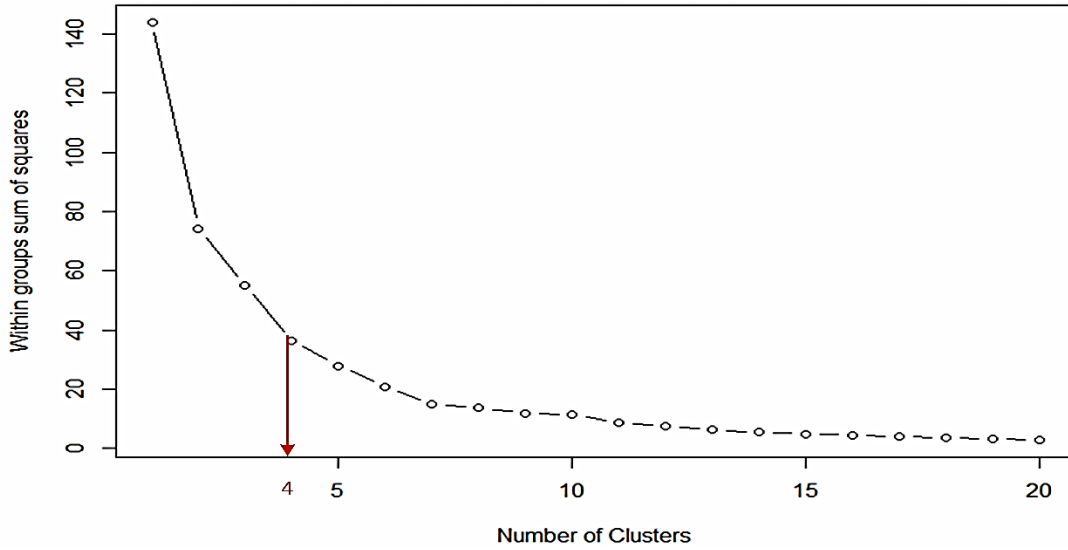


Figure 4.11: Optimal number of archetypes

Given the hierarchical clustering approach, all units in the sample dataset (Tower#1) were divided into four different archetypes of non-typical high usage (NTHU) in cluster 1, non-typical low usage (NTLU) in cluster 2, typical thermostat control usage (TTCU) in cluster 3, and non-typical medium usage (NTMU) in cluster 4 (see Figure 4.12). The percentage ratio of units within each archetype is shown in Figure 4.12.

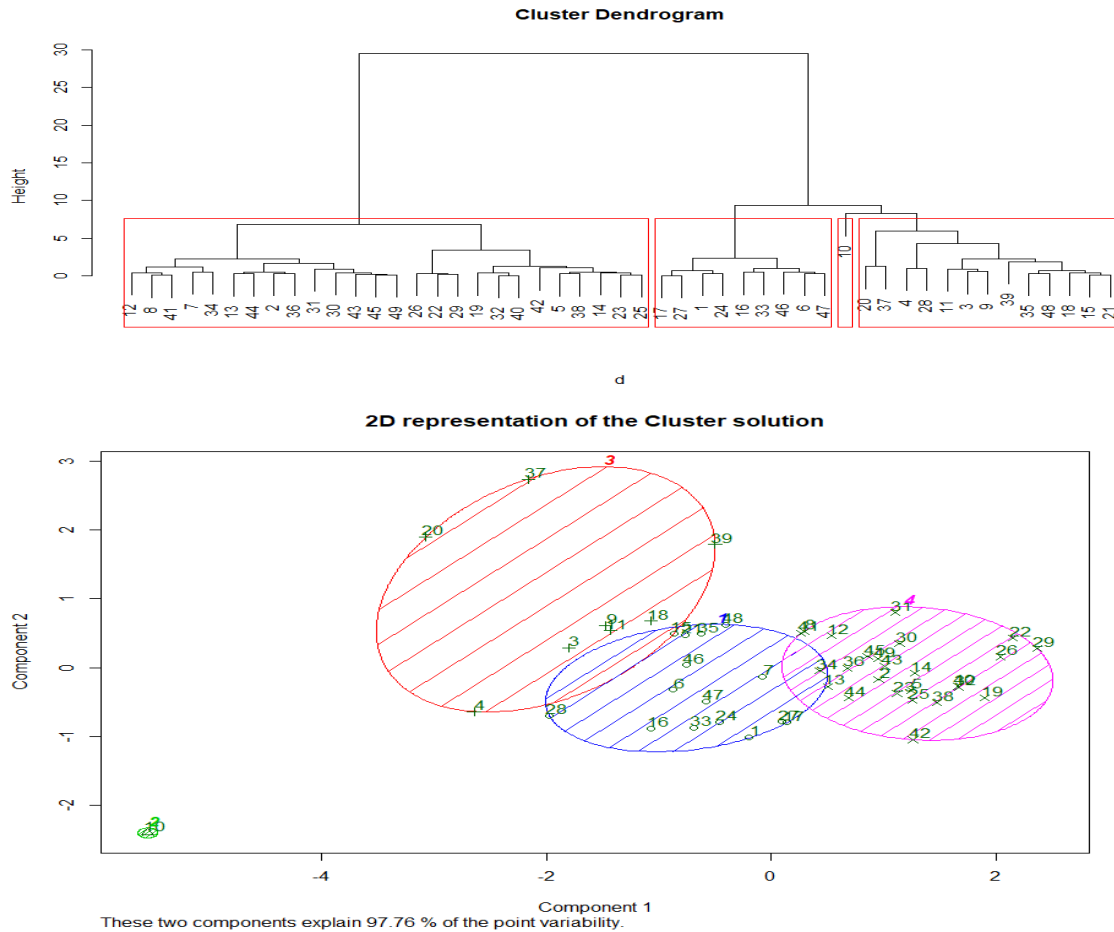


Figure 4.12: Clustering results for Tower#1

The results obtained from the clustering of Tower#1 revealed that only 5% of units were of the TTCU archetype. This value was assumed to be 100% in the CDHS design stage. The percentage of users in other archetypes were 16% (NTLU), 24% (NTMU), and 53% (NTHU). Similar distribution was extrapolated to the entire district.

Extracting the heating demand profile of the reference building of each cluster, the MLR model was trained. After training the model, and defining the input file for the remaining units, the heating demand profile of the district was predicted. To predict the demand profile in future hours, previously predicted values and input files were used at the same time. Using the trained model and the properties of the remaining units, the heating demand profile of another tower and then the monthly consumption of the entire district were predicted.

Figure 4.13 illustrates the results obtained from prediction of the heating demand profile of the Arian tower for the first 10 days of November 2016 as well as the measured data for the same period. An acceptable agreement can be observed between prediction and measurement (calculated *MSRE* was about 11.2% for the entire year and 8.2% for the

heating season). The general trend of the predicted demand matches the measured demand. Considering that the data used to generate the demand profile model was based on that of occupants in a different tower, the result is remarkably good.

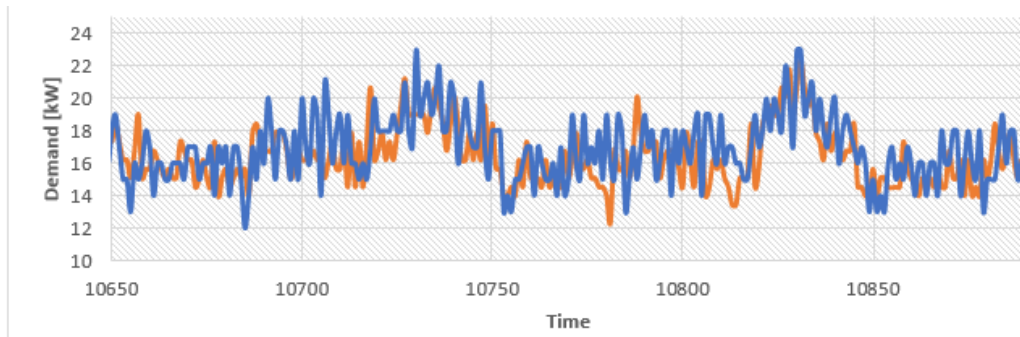


Figure 4.13: Energy demand from model prediction (orange) versus measured (blue) for Tower#2

In the next step, the monthly energy consumption of the entire district including the losses from the underground distribution network were predicted. The underground piping network was an insulated dual pipe network transferring hot water at a flow temperature of 85 °C and a return temperature of 70 °C with a total length of 2.4 km (1.2 km supply and 1.2 km return). Figure 4.14 shows the operational temperature of the underground piping network.

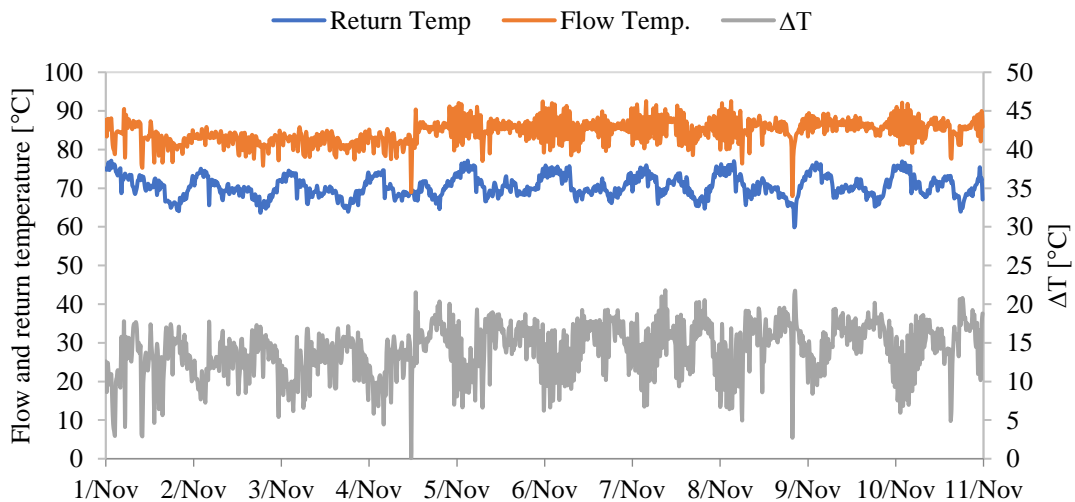


Figure 4.14: Operational temperature of the underground network

Instead of changing the room operational temperature, the network underground operational temperature remains relatively constant during the year to control the amount of heat transfer from the boiler house to the consumers. This causes the system mass flow rate to continuously vary during a day. Figure 4.15 shows the fluctuating water flow rate in the first 10 days of November 2016.

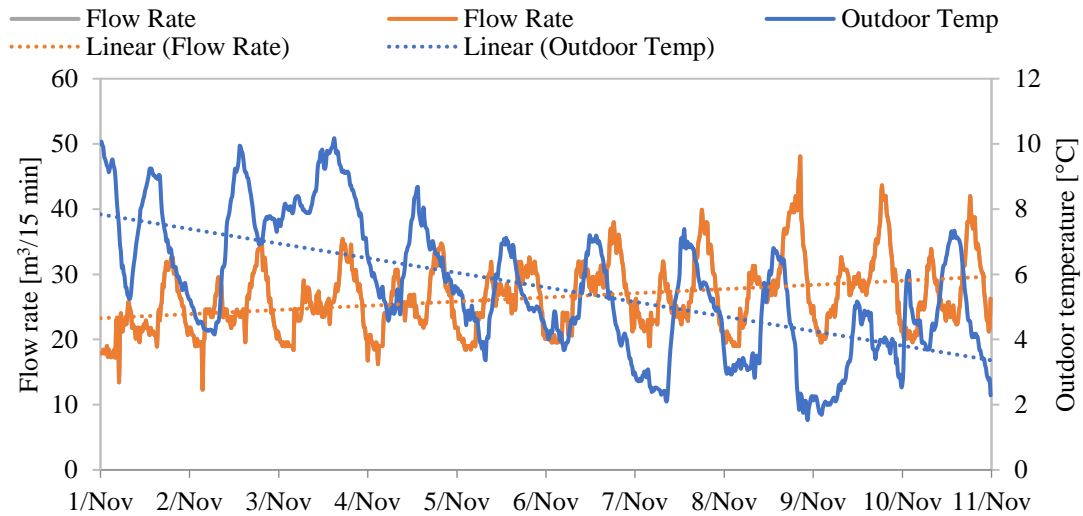


Figure 4.15: Water flow rate versus outdoor temperature in the distribution network

Having the total length for the underground network alongside its operational temperature, the supply and return water mass flow rates, the outdoor temperature, the thermal properties of the soil and pipe insulations, and the distribution network total heat loss can be determined. To simplify the prediction process, a linear relation for the temperature difference between the operational temperature and surrounding environment temperatures was assumed. Figure 4.16 shows the predicted heat loss for the underground distribution network.

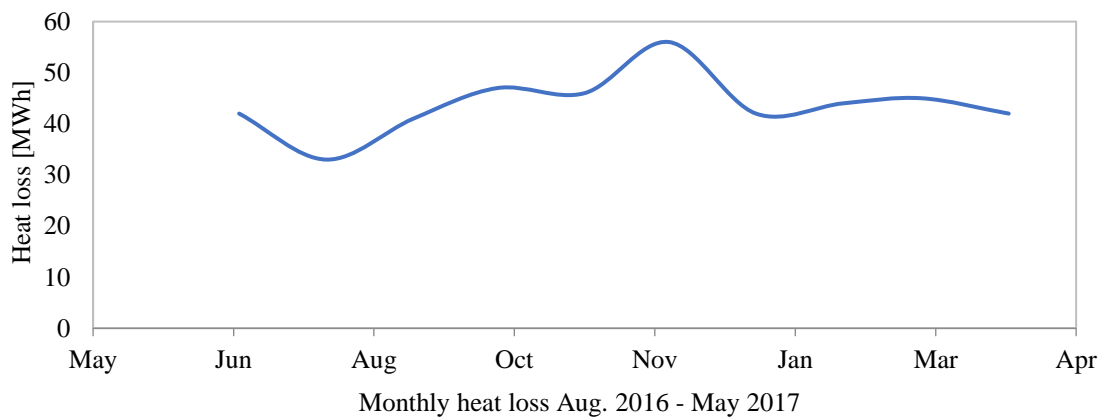


Figure 4.16: Monthly heat loss projection of the distribution network

Since for many units in the WWHC community the demand profiles were not available, the predicted energy demand for the entire system was compared with the total energy generated by the boiler house. Note that the boiler house sensor measured only the accumulated amount of fuel consumed and the energy generated by each boiler in fifteen-minute intervals. Figure 4.17 shows the predicted accumulated energy demand of the district against the energy generated by the boiler house.

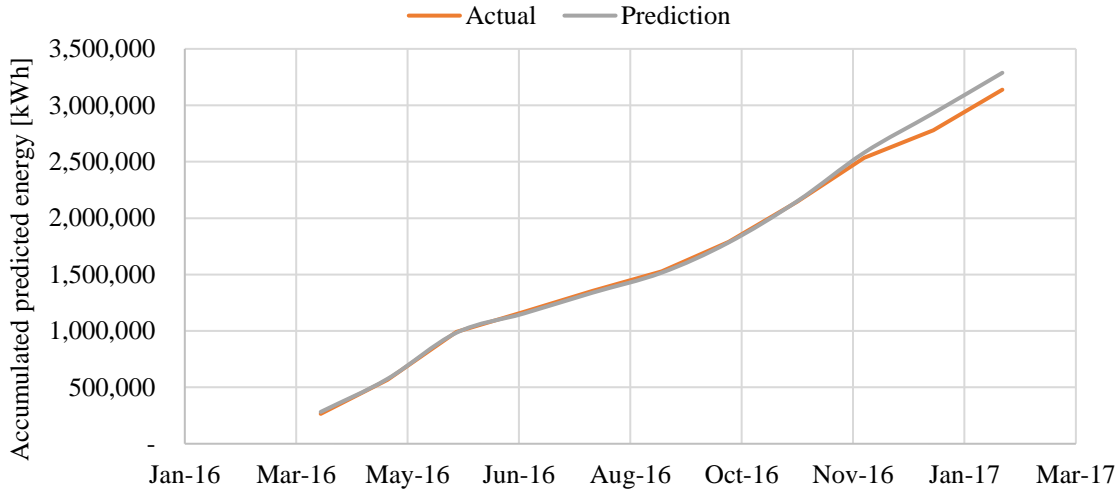


Figure 4.17: Accumulated predicted energy delivered versus actual generated energy in the boiler house

The results showed high agreement between the predicted and actual energy demand with a monthly discrepancy between -4 to 6%, except in January 2017, when the error was approximately 30%. This error was due to a relatively high heat loss in the distribution network. In January 2017, due to two faulty bypass valves in two different towers, the system mass flow rate increased. Over a year, the predicted accumulated energy demand (3,288,340 kWh) showed a discrepancy of about 5% compared with the actual energy generated by the boiler house (3,138,431 kWh). The underestimation of the total energy demand of the district was mainly due to the heat loss from buildings, especially the older 4-story terrace building with higher envelope deterioration. However, in the training process (Step 3), the reference profile obtained from the Arran tower (which was better renovated compared to the terrace buildings), was used with a relatively lower heat loss. Note that in the training stage, the MLR model was once trained using the reference building obtained from the Arran tower. These trained models were later used to predict the heating demand profile of the remaining units, only by adopting their input file. Moreover, the ratio of the occupant behavior considered in TTCU in terrace buildings was slightly higher.

Chapter 5: Optimization

The term “optimization” is often used instead of heuristic approach which is a technique to solve a problem more quickly when classical methods are too slow, or for finding an approximate solution when classic methods fail to find any exact solution. On the other hand, deterministic approaches theoretically guarantee that the reported solution is indeed the global optimum. Mathematical formulation of an optimization problem is stipulated as minimization of an objective function subject to a set of constraints:

$$\min_{x \in X} f(x) \quad (5.1)$$

where the vector $x \in X$ is called design parameter, $f: x \rightarrow \mathbb{R}$ is called objective function, and $X \in \mathbb{R}^n$ is the set of constraints. Prior to further details, some definitions for the correct interpretation of this chapter are presented:

- **Objective function:** the optimization objective, which is computed as a function of the set of parameter values.
- **Decision parameter:** also known as design variable, optimization variable or optimization parameter, denotes a component of the system which can affect the system performance, expressed by the optimization objective function through the variation of its value (see the definition of parameter value).
- **Parameter value:** one of the alternatives defined for that specific parameter in a range of variation. Such value may directly represent a physical property (e.g. thickness of a layer, thermal transmittance of a glass) or it may be the name of the alternatives (e.g. the decision variable “heating system” can have two values of “1” or “2” which refer to a gas condensing boiler and a heat pump, respectively).
- **Design option:** a combination of parameter values (one value for each decision parameter).
- **Design space:** the set of all possible design options, depending on the set of decision parameters and the range of parameter values.
- **Multi-period vs. dynamic optimization:** The term “multi-period” optimization is used if time is a discontinuous variable, otherwise “dynamic optimization” is the correct term. For simplicity, multi-period optimization is generally used with the assumption of linearity while dynamic optimization generally does not involve binary variables.
- **Single vs. multi-objective optimization:** When there is more than one objective function for optimization then a multi-objective (or multi-criteria) optimization problem arises. This is common in building design problems and these functions are often contradictory. Two popular approaches are typically adopted by researchers to solve multi-objective problems in building engineering: (1) weighted sum functions, and (2) Pareto approach. In the former approach, each of the

objective functions is normalized, multiplied by a weight factor (sum of weight factors should be 1) and a new function is formed by adding up the sub-objectives. Typical optimization techniques can then be applied to find the optimal solution. Although the method is efficient and easy to apply, interference and compromise of different sub-objective functions cannot be identified and needs prior knowledge. Another problem is associated with processing time since the approach requires testing different values of weight factors which increases the number of computation processes. The Pareto approach leads to a set of non-dominated solutions called Pareto frontier. For a 2D optimization problem, an illustrative graphical representation is shown in Figure 5.1. A Pareto optimal (or non-dominated) solution is any solution which leads to better value of the function without deteriorating the result for other function(s). In Figure 5.1, solutions A and B are non-dominated, but C is not an optimal solution. This approach is useful to exploit the diversity of the solutions, but often raises issues of inadequate effectiveness and efficiency.

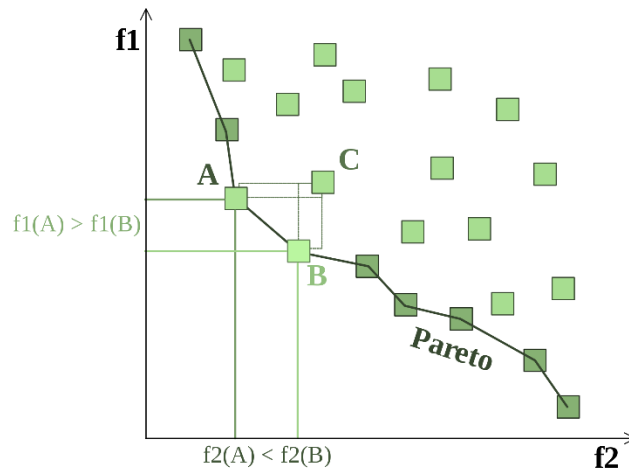


Figure 5.1: An exemplary Pareto approach for a 2D optimization

Optimization at building level has been widely investigated in the literature [394, 395]; therefore, this chapter is more focused on the district level optimization. A general framework of the optimization procedure at district level is given in Figure 5.2. This overview is applicable to a wide range of district configurations and conditions which can be represented by a group of input parameters. These are comprised of available resources (renewable and conventional), detailed neighborhood data (e.g. distances, roof area, load profiles), climatic conditions (e.g. ambient and soil temperatures, global solar irradiation, humidity) and technological parameters (e.g. efficiencies, generation capacities, investment, operating and maintenance costs). Moreover, the applicable legislative framework, including permission to sell the electricity, green certificates, and FITs (feed-in tariffs) for PV production and CHP systems, is regarded as part of the input parameters. Financial exchange of local electricity is another kind of legislative framework.

Optimization can also be used for calibration of proposed models at the district level. Implicit calibration (Figure 5.3) refers to problems which are formulated and solved by using an optimization technique coupled with a steady-state thermal simulation model.

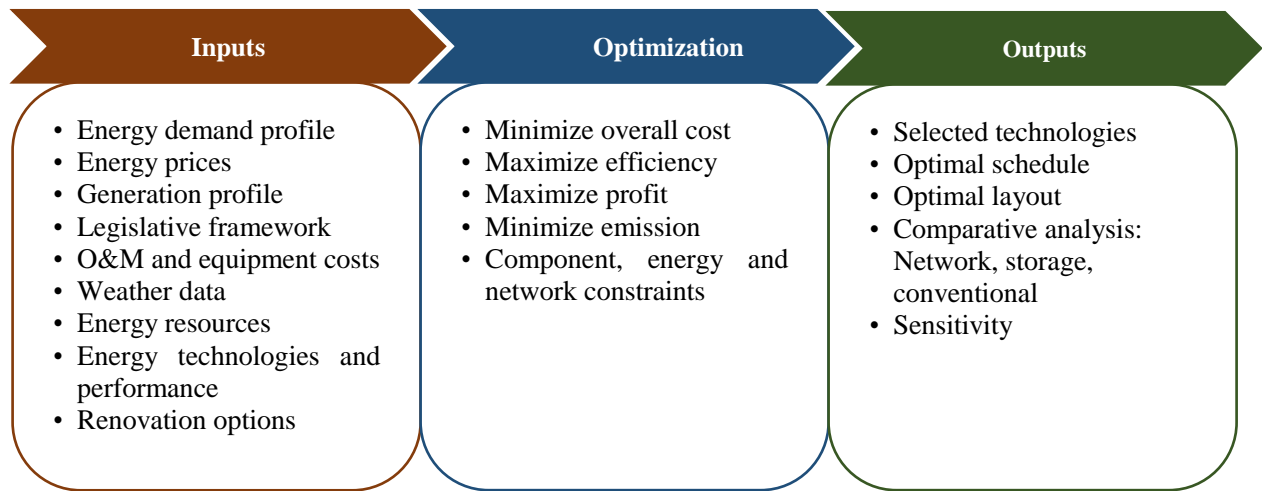


Figure 5.2: A framework for optimization at district level

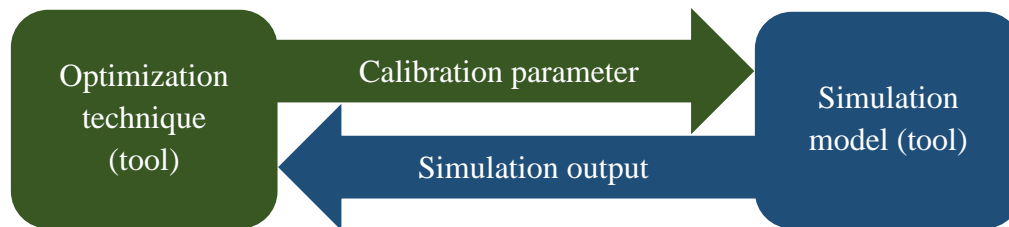


Figure 5.3: Implicit calibration process

5.1 Types of methods

Although several optimization algorithms are available, they can be classified in two main categories of deterministic and stochastic methods. Moreover, some algorithms have been developed which share the characteristic of both stochastic and deterministic methods, which are here denoted by hybrid methods.

5.1.1 Deterministic

The deterministic methods (also known as mathematical programming) use mathematical approaches, such as the gradient information of functions and include the Newton, quasi-Newton, steepest decent and the Simplex methods. Deterministic methods can obtain the exact optimal solution when the applied problem is simple; i.e. linear and convex problems. However, solving large complicated problems requires large computational load. Although most of physical phenomena are nonlinear, in many cases, engineering systems are modeled by linear functions since they can be solved mathematically. Even if a system is not modeled as a linear function, it is easy to mathematically find a minimum/maximum value from a convex function. However, it is not easy to obtain an optimal solution for nonlinear or nonconvex functions.

Deterministic methods are often used for problems with a precise relationship between decision variables and objective function values. However, these methods present some difficulties in solving a problem when the relationship between the candidate and the solution is complex, or if the search space is large [396]. Unlike stochastic methods, deterministic algorithms do not contain a random component that determines orientation in the search space.

5.1.2 Stochastic

Compared to deterministic methods, some authors affirm that stochastic techniques are advantageous since better results can be obtained [397]. Within this category, the subcategory of metaheuristic methods, such as genetic algorithms (GA) and particle swarm optimization (PSO) methods, follow a different approach to deterministic methods. The difference is clarified when considering that “meta” means “beyond” or “higher level” and “heuristics” means “to find” or “to discover by trial and error” [398]. Therefore, metaheuristic methods iteratively find the optimal solution. Their advantage is that the solution can be obtained easily with lower computational load compared to deterministic methods. However, the solution obtained from metaheuristic methods is approximate and is not necessarily the exact solution. Thus, users must monitor the accuracy.

Evolutionary algorithms (EA), such as genetic algorithms [399], are population-based metaheuristic optimization algorithms that use principles of biology such as mutation, crossing, selection natural and survival of the fittest to find a solution. In Figure 5.4, the application of various types of stochastic algorithms in building simulation and optimization studies is reported from a comprehensive review [400]. It is shown that GA are by far the most commonly used.

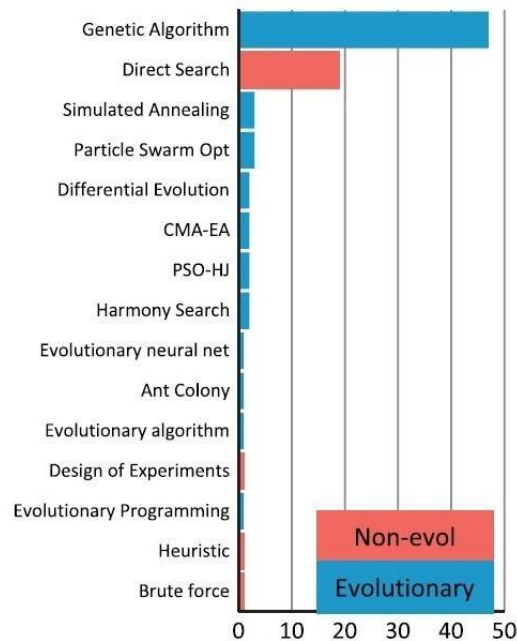


Figure 5.4: Optimization methods applied in building energy optimization studies [400]

5.1.3 Hybrid

As presented, stochastic and deterministic methods have their own limitations. Gradient based deterministic methods initially have rapid convergence; however, their convergence drops as they get closer to the optimum value. On the other hand, stochastic methods can be computationally intense when they search randomly. To benefit from the advantages of both methods simultaneously, hybrid methods have been introduced. Hybrid methods speed up the optimization process by partially solving the problem deterministically and the rest stochastically.

5.2 Algorithms

In this section, the common optimization algorithms are introduced. Note that the tools mentioned here will be explained later in Section 5.5.

5.2.1 Mixed-integer linear programming

The mixed-integer linear programming (MILP) model is composed of a linear objective function, linear constraints and one or more integer variables. Many previous research efforts [20, 271, 401-406] adopted MILP to optimize the operating schedules of an energy system with TES. Although the numerical values of continuous variables can be rounded to meet integer constraints, it cannot always guarantee an optimal solution. Therefore, developing a suitable method for MILP has received attention.

The use of MILP first involves the transformation of integer variables to continuous variables, a process which is referred to as continuous relaxation. Then, linear programming is conducted on the relaxation model to produce the optimal solution. If the

optimal solution unexpectedly meets the integer constraints, it is an optimal solution of the original problem, which means it is a non-relaxation problem. However, these cases are rare in practice. Thus, it is necessary to formulate the continuous variables which violate the constraints of an integer-to-integer number transformation. The branch-and-bound method [407, 408] is known as the most useful and powerful method which employs an MILP algorithm and is presented schematically in Figure 5.5.

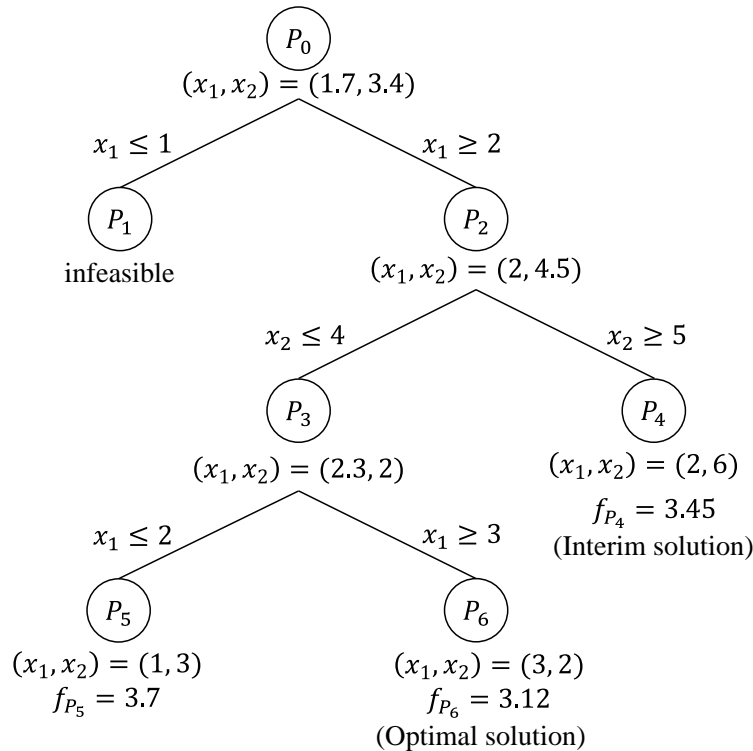


Figure 5.5: Schematic representation of branch-and-bound method

In the figure, the optimal solution $(x_1, x_2) = (1.7, 3.4)$ was obtained by linear programming of a continuous relaxation problem P_0 which originally had two decision variables with integer constraints. First, P_0 is divided into $P_1 = \{x \in P_0: x_1 = 1\}$ and $P_2 = \{x \in P_0: x_1 = 2\}$. If P_1 does not have any feasible solutions, division of the P_1 node terminates at this phase, leaving P_2 to obtain the optimal solution $(x_1, x_2) = (2, 4.5)$. Then, P_2 is divided into $P_3 = \{x \in P_2: x_2 = 4\}$ and $P_4 = \{x \in P_2: x_2 = 5\}$. Then, the optimal solution is obtained to be $(x_1, x_2) = (2, 6)$ with objective value $f_{P_4} = 3.45$ on P_4 . However, this solution is designated as the interim solution since both variables meet the integer constraint. Then, P_3 is used to obtain the optimal solution $(x_1, x_2) = (2.3, 2)$, P_3 by getting split into $P_5 = \{x \in P_3: x_1 = 2\}$ and $P_6 = \{x \in P_3: x_1 = 3\}$. If the optimal solution of P_5 is $f_{P_5} = 3.7$ at $(x_1, x_2) = (1, 3)$, it is not the optimal solution of the original problem because f_{P_5} is inferior to f_{P_4} . Finally, if the optimal solution $f_{P_6} = 3.12$ is obtained at $(x_1, x_2) = (3, 2)$, it is determined as the optimal solution of the original problem because f_{P_6} is superior to f_{P_4} , concluding the calculation of all the branches.

Although MILP is widely used to obtain optimal solution (e.g. active TES control), it has two main disadvantages. First, the objective function must be a linear function. As most of features of equipment and physical phenomena are nonlinear, they should be modeled as linear functions. Second, in some cases, it is difficult to solve the matrix employed in MILP exactly. Furthermore, for a complex system with several variables, the computational load rapidly increases. Other methods which have been used with MILP include presolving [409], cutting planes [410] and heuristic methods. Besides, in some solvers (e.g. GAMS, CPLEX, and MATLAB) a combination of these methods is applied.

5.2.2 Mixed-integer nonlinear programming

The mixed-integer nonlinear programming (MINLP) models have a nonlinear objective function and/or constraint and one or more integer constraints. MINLP has found application in optimization of operating schedules of an energy system with TES [26]. The MINLP algorithm is similar to that of MILP except for its nonlinear conditions. First, integer constraints are relaxed to continuous conditions. Then, nonlinear programming is carried out on the relaxed problems. Note that relaxed problems are often assumed to be convex functions for obtaining the global optimum. The methods employed in MINLP include the branch-and-bound method, generalized benders decomposition (GBD) method [411] and outer approximation (OA) method [412]. In particular, the OA method forms the core algorithm of commercial solvers, e.g. AIMMS. However, optimization of nonconvex functions is challenging. Therefore, research is being carried out to address this problem [413].

5.2.3 Dynamic programming

Dynamic programming (DP), which is another type of mathematical programming, was proposed by Bellman [414] in 1957. DP has been adopted to optimize the operating schedule of TES systems [415-418]. For instance, this method was applied to a cooling plant with an ice storage tank to minimize the operating cost [416]. The performances of chiller-priority control, storage-priority control and optimal control were compared, and the optimal control provided the highest operating cost savings. DP can be applied to almost all optimization problems which follow to the “principle of optimality” described as [414]: “An optimal policy has the property that whatever the initial state and the initial decisions are, the remaining decisions must constitute an optimal policy with regard to the state resulting from the first decision.”

Most scheduling problems which include energy system optimization or network modeling [419] rely on the above theorem since it is composed of multi-stage decisions. Two algorithms have been used with DP, the backward and forward algorithms. The backward algorithm is depicted in Figure 5.6.

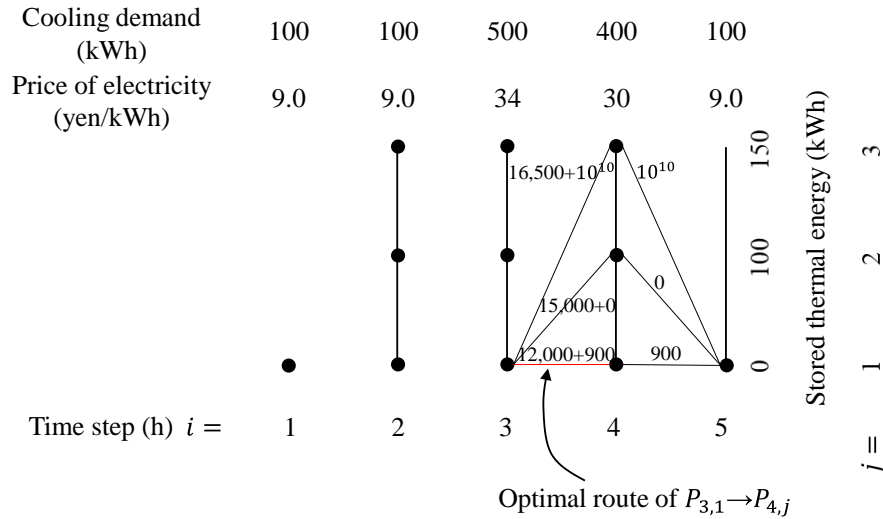


Figure 5.6: Backward algorithm on the first step

Consider an optimization problem consisting of one heat source and TES in an energy system. The capacity of TES is set to 200 kWh and the heat source price is considered to be 1 yen/kWh to generate cooling. The decision variable is the amount of energy stored in the TES and the analyzed time horizons are set to five steps (hours). The price of electricity per kWh of each time interval varies according to the cooling demand (i.e. a dynamic pricing model is used). In the first ($i = 1$) and last ($i = 5$) time steps, the stored thermal energy (kWh) is specified to be zero as the initial condition. For simplification purposes, the operation of pumps is not considered.

In the backward algorithm, the routes of all the grid points from the fourth to the last time step are considered first. $P_{i,j}$ denotes a grid point of the j -th discrete point of the i -th time step.

$P_{4,1} \rightarrow P_{5,1}$: In this route, since the amount of stored thermal energy does not vary, a charging/discharging process is not conducted. In this time step the cooling demand is 100 kWh; therefore, the operating cost is 900 yen ($100 \text{ kWh} \times 9.0 \text{ yen/kWh}$).

$P_{4,2} \rightarrow P_{5,1}$: The discharging process (100 kWh) is carried out on this route. The operating cost is zero yen since the amount of discharged cooling heat is sufficient to meet the cooling demand. Therefore, no work is required from the heat source.

$P_{4,3} \rightarrow P_{5,1}$: This route contains an applied penalty value, because the amount of discharged heat (200 kWh) exceeds the cooling demand (100 kWh). The penalty value is set to 10^{10} and the calculation of the objective function, which determines the operating cost of the heat source, is not evaluated because this route is not feasible.

Next, the routes of all grid points from the third to the fourth time step are evaluated:

$P_{3,1} \rightarrow P_{4,1}$: The charging/discharging process is not carried out along this route. Therefore, 400 kWh of cooling should be generated to meet the demand. The operating cost is $400 \text{ kWh} \times 30 \text{ yen/kWh} = 12,000 \text{ yen}$. Moreover, the operating cost of route $P_{4,1} \rightarrow P_{5,1}$, which has already been determined as 900 yen, should also be considered. Thus, the combined cost of $P_{3,1} \rightarrow P_{4,1}$ and $P_{4,1} \rightarrow P_{5,1}$ is 12,900 yen.

$P_{3,1} \rightarrow P_{4,2}$: In this route, the charging process (100 kWh) is carried out. Thus, 500 kWh of cooling should be generated. Therefore, the combined cost of $P_{3,1} \rightarrow P_{4,2}$ and $P_{4,2} \rightarrow P_{5,1}$ is $500 \text{ kWh} \times 30 \text{ yen/kWh} + 0 \text{ yen} = 15,000 \text{ yen}$.

$P_{3,1} \rightarrow P_{4,3}$: The amount of charging thermal energy is 200 kWh. Thus, 600 kWh of cooling needs to be generated. Therefore, the total cost of $P_{3,1} \rightarrow P_{4,3}$ and $P_{4,3} \rightarrow P_{5,1}$ is $600 \text{ kWh} \times 30 \text{ yen/kWh} + 10^{10} \text{ yen} \approx 10^{10} \text{ yen}$ (not feasible).

Based on the calculation flow described above, the operating costs of all the routes from $P_{3,1} \rightarrow P_{4,j}$ are obtained. In DP, it is only necessary to remember the minimum route at each grid point according to the principal of optimality. Therefore, $P_{4,1} \rightarrow P_{5,1}$ is determined as the optimal route of all the routes from $P_{3,1} \rightarrow P_{4,j}$.

The optimal route and operating costs of the grid point of each time step are determined by the calculation flow as explained above. Therefore, as shown in Figure 5.7, using a forward algorithm, the straight red line ($P_{1,1} \rightarrow P_{2,1} \rightarrow P_{3,1} \rightarrow P_{4,1} \rightarrow P_{5,1}$) is determined to be the optimal route of all time steps. The charging process is carried out when the price of electricity is low in the second time step, whereas the discharging process is carried out when it is high in the third time step.

DP benefits from two main advantages of (1) versatility in terms of problems to which it can be applied and (2) the ability to reduce computational complexity. For example, in the optimization problem discussed above, the number of full searches is 3^5 . On the other hand, the number of searches for DP is 3×5 . Therefore, the DP algorithm is capable of transforming problems with a computational complexity of $O(j^i)$ into problems of a lesser complexity, i.e. $O(i \times j)$. However, DP requires an exponential amount of time when the number of decision variables n of each time interval exceeds two, in which case the computational complexity becomes $O(i \times j^n)$.

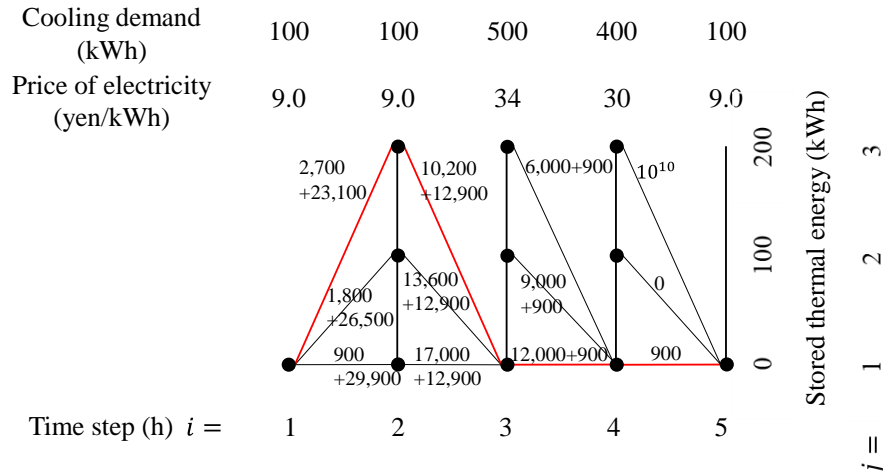


Figure 5.7: Forward algorithm on all time intervals during one cycle

5.2.4 Quasi-Newton method

The quasi-Newton method [18, 420], is a gradient-based optimization algorithm, such as the steepest decent and Newton methods. The Newton method is a famous optimizer which requires the second order differential (Hessian) of an objective function; however, its computations are time consuming. On the other hand, the quasi-Newton method assumes a Hessian value by using an approximation method, such as the symmetric rank one trust region method [421], the Berndt-Hall-Hall-Hausman (BHHH) algorithm [422] and Broyden-Fletcher-Goldfarb-Shanno (BFGS) method [423-426]. Therefore, it is possible to use the quasi-Newton method to efficiently obtain the optimal solution for a convex function.

5.2.5 Nelder-Mead simplex method

The Nelder-Mead simplex method [427] (a downhill simplex method) has been used as a direct search complex method [428, 429]. This method does not use the derivative information; instead, it uses functional comparisons to obtain the optimal solution. Thus, it is applied to almost all functions regardless of characteristics such as convexity, differentiability and continuity. This method uses $n + 1$ vertices (n is the number of decision variables). Each vertex moves iteratively to obtain the optimal solution. There are four moving step algorithms of reflection, expansion, contraction and shrink. Although this method cannot avoid being trapped in a local optimum in nonconvex functions, it is capable of effectively obtaining the optimal solution on convex functions.

5.2.6 Genetic algorithms

The origin of GA dates back to the mid-1950s, when biologists [430] and computer scientists [431] began applying computer-assisted simulations to better understand genetic processes, the evolution and natural selection. Basics of such approaches were developed by Holland [432] in the late 1960s at the University of Michigan. GA is a subclass of evolutionary algorithms where search space elements are typically binary or discrete

values. The reproduction operations apply to the (binary) genotypes of individuals while the values of the objective functions are calculated on the basis of their phenotypes (real values) in the search space. GA is a relatively new approach of solving optimization problems and is currently very widely used.

GA has been applied to optimize energy systems control which include TES [433-435]. For instance, the total cost (including the capital investment cost, operational cost and the penalty cost for CO₂ emission) of an air conditioning system with an ice storage tank in a commercial building has been optimized [434]. The results of the conventional system (without ice storage) and optimized system (with ice storage) were compared and the validity of the optimization method was confirmed.

The expression for individual modeling of GA is composed of two types, bit string and real-coded, as shown in Figure 5.8. The bit string GA is suitable for discrete optimization, whereas real-coded GA (RCGA) is suitable for continuous optimization.

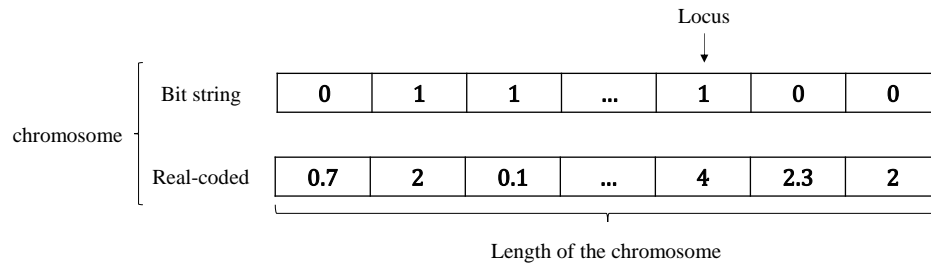


Figure 5.8: Coding of a chromosome using the genetic algorithms

The bit string GA uses the selection, crossover and mutation operators to find the optimal solution. The algorithm first conducts an initialization of the population, composed of individuals (assume the same value for the decision variables as shown in Figure 5.8). The individuals are scattered across the entire search space by using uniformly allocated random numbers. Second, some individuals are selected as parent individuals to create new solutions, the so-called child individuals. This selection is performed using a selection method such as roulette-wheel selection, tournament selection or elitist selection. The roulette-wheel selection method involves the calculation of the selected probability of each individual:

$$p_i = \frac{f_i}{\sum_{k=1}^{N_{pop}} f_k} \quad (5.2)$$

where $p_i \in [0,1]$ denotes the selected probability of the i -th individual, f_i denotes the objective function value of the i -th individual and N_{pop} denotes the number of populations.

The elitist selection method leads to the preferential selection of the individual with the preferred value. This selection method can always locate the optimum point near the current best individual but is likely to be trapped in a local optimum.

Third, the crossover method uses the crossover probability (p_c) and employs methods such as one-point or two-point crossover, as illustrated in Figure 5.9.

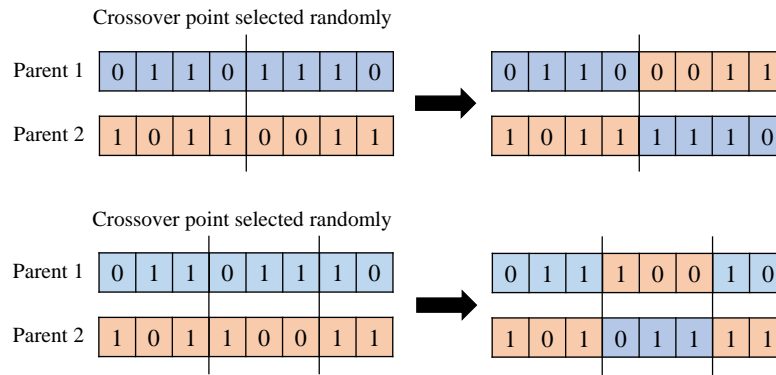


Figure 5.9: One-point (top) and two-point crossover (bottom)

Finally, the mutation method is performed for all individuals with the mutation probability (p_m) by employing methods such as bit string mutation, flip bit and uniform. The crossover probability is usually high and lies in the range of 0.7 – 0.9, which is larger than the mutation probability, for which the range is 0.001 – 0.05. The advantage of the mutation method is that individuals can easily be retrieved from the local optimum.

The RCGA uses the same approach as the bit string GA when using the crossover method for selection. In particular, the selection procedure is referred to as the “generation alternation model”, which is based on methods such as the minimal generation gap (MGG) [436] and just generation gap (JGG) [437]. In the MGG method, parent individuals are randomly selected, after which child individuals are generated using the crossover method. Then, the elitist method is used to replace the parent individuals by the top layer of individuals, which includes both parents and children. The advantage of the MGG method is its ability to obtain an optimal solution in the proximity of the preferred individuals; however, undesirably the solution is often a local optimum. Therefore, the JGG method was developed to resolve this problem. In the JGG method, all parent individuals are replaced by child individuals who have superior objective values compared to those of the other children. This strategy maintains the diversity of the population. Although there are many crossover methods for use with the RCGA, the real-coded ensemble crossover (REX) [438] and adaptation of expansion rate REX (AREX) [437, 438] are common. REX generates child individuals as:

$$x_i^c = \langle y \rangle + \alpha \sum_{j=1}^{N_p} \varepsilon_{i,j} (x_j^p - \langle y \rangle) \quad (5.3)$$

$$\varepsilon_{i,j} \sim \varphi(0, \sigma^2) \quad (5.4)$$

$$\sigma^2 = \frac{1}{N_p - 1} \quad (5.5)$$

where x_i^c ($1 \leq x_i^c \leq N_c$) denotes the i -th child individual, $\langle y \rangle$ denotes parent individuals x_j^p ($1 \leq x_j^p \leq N_p$) around the center, N_p and N_c are the number of parent and child individuals, respectively, $\varepsilon_{i,j}$ denotes certain distributed random numbers with the average 0 and the variance σ^2 , and α indicates the expansion rate (equal to 1). On the other hand, AREX (an updated version of REX) adopts REX and changes the way the value of α is updated as:

$$\alpha^{(g+1)} = \max \left[\alpha^{(g)} \sqrt{(1 - c_\alpha) + c_\alpha \frac{L_{cdp}}{L_{avg}}}, \alpha^{(0)} \right] \quad (5.6)$$

$$L_{cdp} = \alpha^2 (N_p - 1) \left[\sum_{j=1}^{N_p} \langle \varepsilon_j \rangle_{N_{c_\alpha}}^2 - \frac{1}{N_p} \left(\sum_{j=1}^{N_p} \langle \varepsilon_j \rangle_{N_{c_\alpha}} \right)^2 \right] \quad (5.7)$$

$$\langle \varepsilon_j \rangle_{N_{c_\alpha}} = \sum_{i=1}^{N_{p_\alpha}} \frac{\varepsilon_{i:N_{c_\alpha},j}}{N_{c_\alpha}} \quad (5.8)$$

$$L_{avg} = \alpha^2 \sigma^2 \frac{(N_p - 1)^2}{N_{c_\alpha}} \quad (5.9)$$

where $\alpha^{(g)}$ denotes the α value for the g -th generation, c_α denotes the learning rate parameter for the expansion rate update, L_{cdp} denotes the length of the crossover descent path, $i:N_c$ denotes i -th higher rank individual of the top child individuals, N_{c_α} denotes the number of top individuals of all child individuals, and L_{cdp} as well as L_{avg} represent the Mahalanobis distance to handle the ill-scale problem efficiently.

Due to its powerful mathematical theory, the RCGA can be applied to continuous optimization problems with a high degree of accuracy. However, it results in a long calculation time when the problem has a complicated objective function, such as an energy system, due to the large number of population and generated child individuals.

5.2.7 Particle swarm optimization

Particle swarm optimization (PSO) was developed in 1995 [439] and used to optimize an operating energy system including TES. For instance, PSO has been applied to an air conditioning system with ice storage tank in an office building to minimize the LCC [440]. This method has also been applied to the heating and power generation system

with water storage tank in a hotel building to minimize combination of primary energy saving ratio, annual total cost and CO₂ emission [441].

Performance comparison between PSO and GA has been conducted and it was inferred that PSO could find more effective solution compared to GA [441]. PSO mimics the collective behavior of birds or fish. An individual uses three types of vector when it moves to other positions; the current velocity vector (\vec{v}_i^g), the best position vector for all particles (\vec{xgb}), and the past best position vector for itself (\vec{xpb}_i). Each individual x_i^g moves iteratively as:

$$x_i^{g+1} = x_i^g + v_i^{g+1} \quad (5.10)$$

$$v_i^{g+1} = v_i^g + c_1 r_1 (xpb_i - x_i^g) + c_2 r_2 (xgb - x_i^g) \quad (5.11)$$

$$v_i^{g+1} = w v_i^g + c_1 r_1 (xpb_i - x_i^g) + c_2 r_2 (xgb - x_i^g) \quad (5.12)$$

$$v_i^{g+1} = \begin{cases} v_i^{g+1} & v_i^{g+1} \leq v_{\max} \\ v_{\max} & v_i^{g+1} > v_{\max} \end{cases} \quad (5.13)$$

where w is an inertia weight factor to control the velocity, and has the same meaning as the step length, c_1 and c_2 are acceleration constants, r_1 and r_2 are uniform random numbers [0, 1], and v_{\max} is the maximum velocity. Although the inertia weight factor w was not included when the method was first proposed [439], it was later added to the PSO method in 1998 [442]. Recently, a simplified version of the PSO was defined to include weight factor as:

$$w = w_{\max} - \frac{w_{\max} - w_{\min}}{g_{\max}} g \quad (5.14)$$

Although PSO has the advantage of high calculation and convergence speeds, it has a tendency to get trapped in a local optimum in multi-modal functions, a disadvantage which can be avoided by adding a mutation method to PSO [443]:

$$x_{i,j} = x_{i,j} (1 + N(0, \sigma)) \quad (5.15)$$

$$\sigma = 0.1 \times L(n_j) \quad (5.16)$$

where $x_{i,j}$ denotes the j -th vector component value of the i -th individual, $L(n_j)$ denotes a range of j -th decision variables and N represents normal distributed random number.

In addition, modification of the velocity has been proposed as [444]:

$$v_i^g = \begin{cases} -\frac{v_{\max}}{2}U_i & \text{initialization}(g = 0) \\ v_{\max}U_i & v_i^g > v_{\max} \\ v_i^g & \text{Otherwise} \end{cases} \quad (5.17)$$

where $U_i \in [0,1]$ denotes a uniformly distributed random number.

Evolutionary PSO (EPSO) [445] is a hybrid PSO method with an evolutionary strategy where the inertia weight factor w_i^g and the best position vector of all particles xgb^g are updated:

$$w_i^{g+1} = w_i^g + \tau N(0,1) \quad (5.18)$$

$$xgb^{g+1} = xgb^g + \tau' N(0,1) \quad (5.19)$$

where $\tau \in [0,1]$ denotes a learning dispersion constant, which is determined at the initial iteration by a uniformly distributed random number and τ' denotes the noise dispersion parameter, which is a small value.

5.3 Objective functions

Different objective functions can be applied in building and district optimization problems. The evaluation criteria are generally based on cost, energy, occupant satisfaction (thermal comfort) and life cycle analysis (LCA). In buildings, the most commonly used objective functions are energy consumption comprising 60% of cases, followed by various cost estimates (construction, operation, life cycle) and finally the set of objectives related to the comfort of the occupants (see Figure 5.10). Nevertheless, the objective functions can be categorized in two main categories of environmental and cost. Moreover, some studies considered a combination of these objective functions (multi-objective optimization). A summary of the studies on DHSs is provided in Table 5.1.

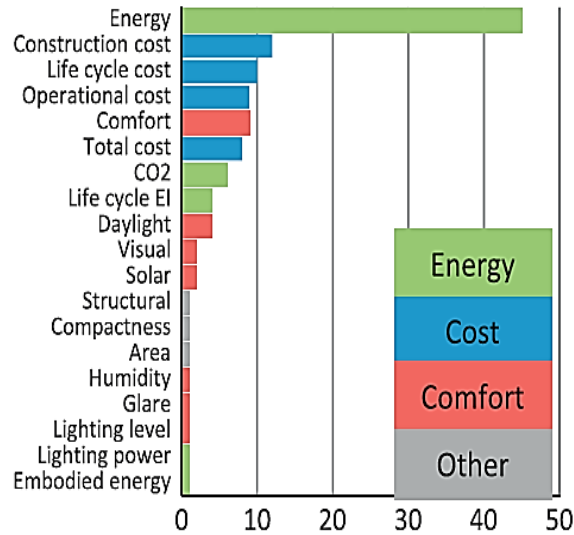


Figure 5.10: Common objective functions for building level optimization [400]

5.3.1 Environmental

The interaction between buildings or districts with the environment has triggered several optimization studies. More specifically, minimization of GHG and pollutant production as well as maximization of energy efficiency are presented in this section. Besides, LCA considers interaction with the environment. In addition, interior environment in terms of thermal comfort of occupants can also be classified in this category.

5.3.1.1 GHG and pollutant production

Efforts from many nations with regards to reduction of GHG emissions can be found such as the agreement of the European Union and other industrialized countries to reduce CO₂ levels by 5% between 2008 and 2012 [446]. An additional incentive was introduced by the European Union where GHG emissions need to be reduced by 20% by 2020 compared to 1990 levels [447].

DHSs are reported to reduce the GHG emissions [448-450] as they allow the use of CHP in addition to other technologies. Even in Norway where 60% of electricity production is hydroelectric, DHSs can be installed to make use of biomass from waste handling sectors and wood industries. Results of studies related to DHSs often present impacts on the environment in terms of reducing the total emitted CO₂ (i.e. the assessed GHG) by knowing the type of fuel used and the quantity of energy produced. Although CO₂ is most commonly used as the indicator of GHG emissions, some studies focused on other pollutants. For instance, energy and environmental aspects of replacing current heating systems with DHSs using CHP plants by monitoring pollutants such as sulfur oxides (SO_x), nitrogen oxides (NO_x) and particulate matters (PM) have been investigated [451, 452].

5.3.1.2 Energy efficiency and exergy

Reducing of energy consumption in the building sector is very important in the fight against climate change and the improvement of supply security [453]. Indeed, buildings account for about 40% of global energy consumption, and savings can be achieved relatively easily by reducing the needs (e.g. insulation, solar shading in the summer), improving the efficiency of the systems and using renewable energies.

Energy is generally calculated by considering the primary energy to consider all forms of energy (e.g. electricity and wood). A balance must be made between production and consumption to meet the needs (e.g. heating, cooling, ventilation, hot water, lighting, and specific electricity) over the period. This usually corresponds to the year, or even the lifetime, for instance consideration of the embodied energy associated with the building construction.

However, energy analysis does not consider irreversibility in thermal processes. Instead, exergy is often employed to identify less efficient components of a system and to optimize thermal energy systems. Exergy is typically known as the amount of available work that can be obtained when a system reaches thermodynamic equilibrium with its surroundings through reversible processes [177]. It determines the thermodynamic efficiency of the system and also the quantity of entropy generation [4]. In comparison to energy efficiency analysis, exergy efficiency analysis methods can identify inefficient processes within a thermal system [454]. Analyzing the quality of energy is a key aspect in optimization process of DHSs. For instance, to find when and where RES (such as geothermal wells and solar collectors) can be connected to a DHS or what the temperature of the supply and return for the brine should be.

Energy analysis has been applied to investigate the performance of a small DHS [455] where among the four considered scenarios, the final energy efficiency was almost the same for all scenarios (within 1% difference). The exergy analysis, however, demonstrated that a low temperature DHS (50 °C) with two heat exchangers (one for hot water and one for space heating) was 25% more exergy efficient than a single heat exchanger coupled to a medium temperature supply line (100 °C). In another study, exergy assessment of an educational building equipped with a boiler and a central heating system was conducted [456]. Presenting the building characteristics, the main energy losses were determined. Exergy efficiency analysis was also demonstrated to be superior to the R1 formula in evaluating CHP waste incinerating plants as the R1 formula fails to consider climatic conditions and the size of the plant, while exergy assesses both the quantity and quality of the produced energy [190]. A novel evaluation parameter for exergy has been introduced [163]. Instead of analyzing exergy levels based on reference temperature or exterior temperature, the utilization rate was introduced, which is defined as the ratio of the final consumer exergy demand over the exergy input into the system.

5.3.1.3 Life cycle analysis

There is a very complex interaction between a building and the environment. LCA is a comprehensive approach to assess building-related environmental impacts throughout its life [457-461].

A complete life cycle assessment method has been described for buildings and associated systems considering LCA, global cost (life cycle cost), and optimization [462]. This makes it possible to deal with the complexity of a global design approach by considering multiple evaluation criteria in an iterative manner (Figure 5.11).

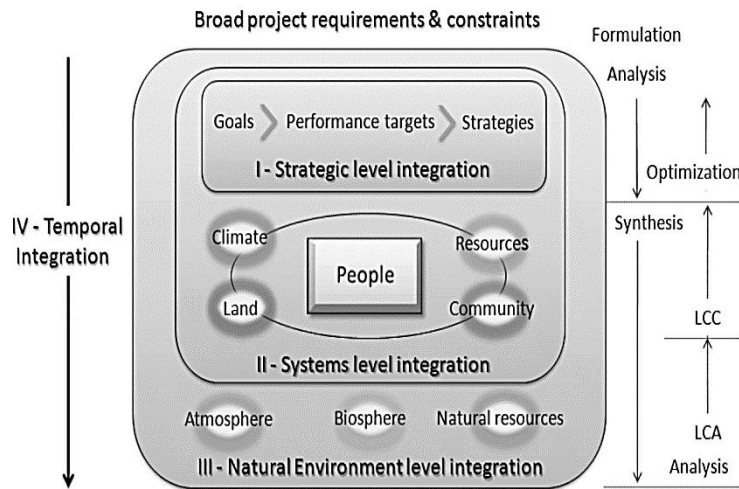


Figure 5.11: Global approach for the optimized design of buildings over their lifetime [462]

5.3.1.4 Thermal comfort

The study of the thermal interactions between an individual and the indoor environment is complex and requires the intervention of several disciplines:

- The mechanism of internal heat generation and the reactions of the human body to external climatic conditions are in the realm of physiology.
- Comfort and the qualification of indoor environments are subject to psychological behavior.
- Heat exchange between the human body and the environment are managed by physical laws.

To assess thermal comfort, two methods can be applied, static or adaptive.

5.3.1.4.1 Static

The static approach considers the individual as a passive receiver of thermal stimulations. The principle of this approach is based on the fact that the thermal effects of an ambiance are felt at the level of the skin by phenomena of heat and mass transfer. These exchanges are conditioned by physiological responses necessary to maintain the internal temperature of the human body around 37 °C. The most commonly used comfort indexes

which are based on this method are the predicted mean vote (PMV) and the predicted percentage of dissatisfied (PPD).

5.3.1.4.2 Adaptive

The adaptive approach of thermal comfort is based on the following principle: "If a change of ambiance induces a degradation of comfort, the occupant reacts so as to find the comfort" [463]. Therefore, the principle of the adaptive approach considers that the individual can adapt to an environment (within certain limits) by implementing (consciously or not) physiological, psychological and behavioral mechanisms. The comfort temperature is then calculated as a function of the running mean of outdoor temperature.

5.3.2 Cost

The European directive on the energy performance of buildings (EPBD – 2010/31/EU) introduced the key-concept of nearly zero energy building (nZEB), of which the energy performance level should be set according to cost optimality criteria [464]. This means that, in an nZEB, the cost-optimal balance between the involved investments and the saved energy costs throughout the life cycle of the building should be reached.

The specifications of the so-called cost optimal methodology can be found in the guidelines accompanying the regulation related to the EPBD recast. The objective of such cost-optimal analysis is to minimize the global cost (life cycle cost), as defined in the European Standard EN 15459.

Calculation of global cost considers the initial investment C_I and for every component or system j the annual costs for every year i (referring to the starting year) and the final value. Global cost is directly linked to the duration of the calculation period τ as [465]:

$$C_G(\tau) = C_I + \sum_j \left[\sum_{i=1}^{\tau} (C_{a,i}(j)R_d(i)) - V_{f,\tau}(j) \right] \quad (5.20)$$

where $C_G(\tau)$ represents the global cost referred to starting year τ_0 , C_I is the initial investment cost, $C_{a,i}(j)$ is the annual cost for component j at the year i (including running costs and periodic or replacement costs), $R_d(i)$ is the discount rate for year i , and $V_{f,\tau}(j)$ is the final value of component j at the end of the calculation period (referred to the starting year τ_0).

In order to refer the costs to the starting year, the present value factor f_{pv} or the discount rate R_d are used. The discount rate coefficient R_d depends on the interest rate R_R :

$$R_d = \frac{1}{(1 + R_R)^p} \quad (5.21)$$

However, for annual costs it is necessary to consider the present value factor, which depends on the real interest rate (R_R) and on the number of years (n) as:

$$f_{pv}(n) = \frac{(1 + R_R) - 1}{R_R(1 + R_R)^n} \quad (5.22)$$

In particular, for the replacement costs and the final value, the discount rate coefficient R_d is utilized, while for running costs the present value factor f_{pv} is used. The composition of the global cost objective function is shown in Figure 5.12.

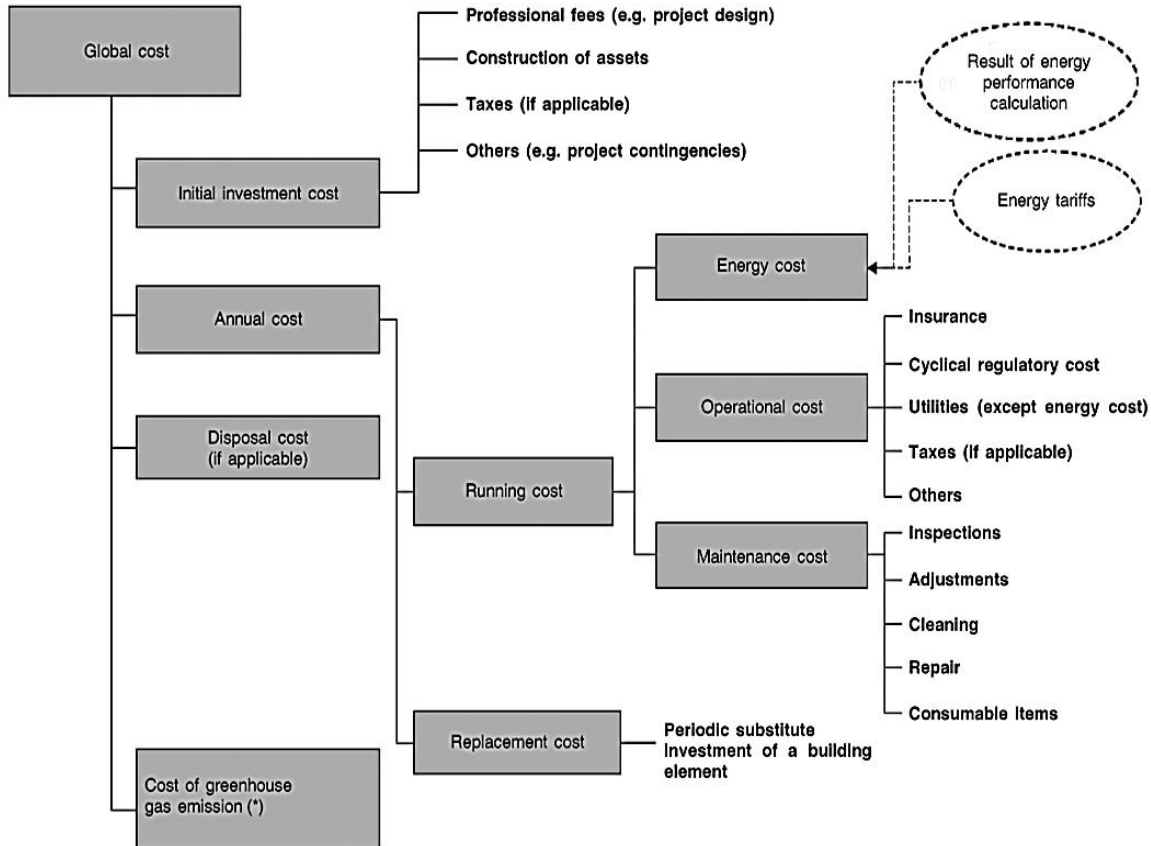


Figure 5.12: Organization of costs included in the global cost objective function [466]

To be able to calculate the global cost objective function, it is necessary to follow a step by step procedure. First, it is necessary to gather some financial and project data. Then, cost regarding components, systems and energy should be valued. Finally, the global cost of the different energy efficiency measures can be calculated.

- **Step 1: Gathering financial data**

The financial data consist of duration of calculation and discount rate. The duration of calculation represents the number of years which are considered for the global cost calculation method. According to the guidelines [466], considering a 50 years lifetime for building, the calculation period is usually set to 30 years. The discount rate depends on the market interest rate and the inflation rate and should consider a medium/long-term vision. This is usually set to 4.5%; however, it may vary according to the context and the objective

of the calculation. For the cost optimal analysis purpose, such interest rates are subject to sensitivity analysis.

- **Step 2: Gathering project data**

The project data are (1) information about the environment of the project, (2) meteorological data and (3) constraints/opportunity related to energy.

- **Step 3: Evaluating components and systems costs**

Data concerning components and systems should be collected and, if needed, information about their lifespan, maintenance and operation can be found in the Annex A of EN 15459 [467].

The investment costs should be calculated considering materials and installation costs of each of the components of the building which may affect its energy performance (envelope, energy system, RES). The running costs which may be considered are those for maintenance and repairs of systems, insurance and taxes.

- **Step 4: Evaluation of energy costs**

According to standard EN 15459 [467], energy costs should be separated into two parts. The first part is directly related to energy consumption according to meters or fuel consumption of the building. The method for determination of energy consumption can be coupled to the energy content of the fuel according to data from the provider. The second part is fixed according to the quantity of energy subscribed with energy utilities or rental for energy systems (e.g. gas tank, electricity transformation). The selected tariff for electricity should be coupled with energy consumption of the building which are estimated by dynamic simulation or other calculation methods.

- **Step 5: Global cost calculation**

Replacement costs throughout the calculation period should be calculated based on timing of and costs for replacement of systems and components. Present value factor or discount rate must be used to refer costs to the starting year. The final value at the end of the calculation period ($V_{f,\tau}$) is determined by summing up the final value of all systems and envelope components. The final value of a specific system or component is calculated from its remaining lifetime (by the end of the calculation period) from the last replacement, assuming linear depreciation over its lifespan. The final value is determined as remaining lifetime divided by lifespan and multiplied by the last replacement cost and refers to the starting year with an appropriate discount rate. Figure 5.13 illustrates the concept of the final value given by the EN 15459 [467].

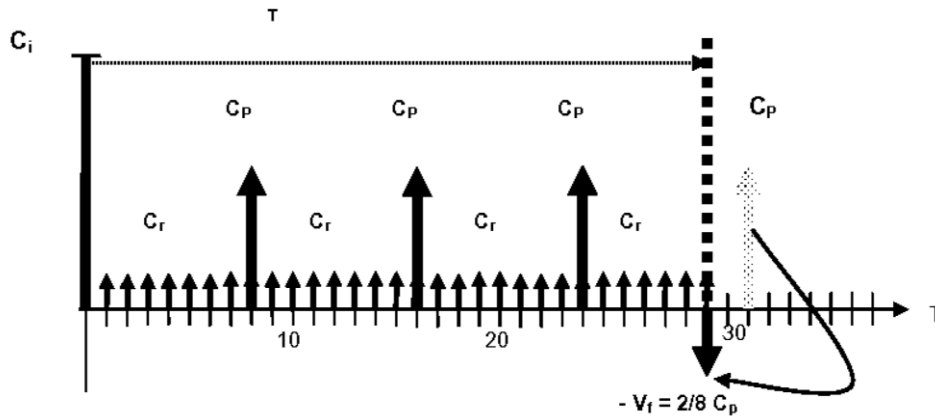


Figure 5.13: Illustration of the final value concept according to EN 15459 [467]

Finally, according to Equation (5.20), the total global cost can be determined by summing up the global costs of initial investment costs, periodic and replacement costs, annual costs and energy costs and subtracting the global cost of the final value.

The investment cost (capital cost) in heat production, operation, maintenance, heat transmission and distribution can be the driving force behind the design of a DHS. The potential of a DHS installation is measured by the difference between the economic savings in terms of the energy consumption and investment to construct and operate the system. A DHS is less cost effective in countries such as Canada [62] and Norway [449] where heating and electricity is relatively cheap. In most developed countries, heating, cooling and electricity are available in all buildings, hence, cost is often a driver to determine if replacing individual end-user systems by a DHS is a viable solution. In areas where buildings are sparse, a DHS may not offer any economic advantage. The concept of linear heat density is often used to determine the potential economic viability of a DHS such as in the analysis of a DHS in Denmark and its growth potential [468]. In Canada, DHSs are not economically viable below the linear heat density of 1.5 MWh/m.yr [62].

Many studies are available showing the methodology behind such an analysis. One approach (established in Denmark) takes advantage of the publicly available heat production, fuel costs, investment costs and heat distribution costs [468]. This information combined with a map of the DHS across Denmark can help render a cost density map of DHS. Besides, an MILP model for the design of a DHS has been developed [469]. The model identifies scenarios that are cost efficient and also identifies the potential for integrating photovoltaic systems. It also shows the optimal operation and size of elements of the system such as turbines, chillers, PV units and piping. It should be noted that DHS cost optimization has a non-continuous objective function; therefore, GA perform better for such applications [165].

Another approach for DHS cost analysis is to develop an extensive energy model of a DHS to obtain the energy consumption of all components of the system in operation

[161]. Based on known DHS cost per energy unit, the total operation cost of the system can be obtained. However, this scenario is a non-convex mixed integer problem; therefore, the regular branch-and-bound optimum solving approach cannot be used. The applied method was a bi-level approach where integer variables are determined by GA and continuous variables are solved with linear programming (a hybrid method as mentioned in Section 5.1.3).

5.3.3 Multi-objective

Multi-objective optimization does not produce a single optimal solution, but a variety of near optimal solutions, which then have to be narrowed down based on the situation and experience of the decision-making process [470]. For instance, an MILP optimization was carried out to minimize both the GHG emissions and the LCC of building energy systems and envelopes at the community level [471]. Another study took three objectives into account (energy savings, costs and indoor thermal comfort) and applied GA to define the optimal energy measures of a building as a whole, including both energy systems and envelope [472]. According to the literature, it is less common to optimize more than three objective functions simultaneously [472].

Among multi-objective optimization studies, exergoeconomic/thermoeconomic analysis received considerable attention. An exergoeconomic/thermoeconomic analysis is an approach where an economic value is assigned for various energy/exergy inefficiencies and it has been extensively applied over the last 30 years [473]. Two types of such analyses are cost accounting and optimization methods [454]. The first type includes the exergy cost method, the average cost approach and the last-in-first-out method (the specific exergy costing method), while the second type includes thermoeconomic and engineering functional analysis [178].

In DHSs, many processes of exergy destruction/energy reduction such as heat production, heat transportation through pipes, heat exchange between the distribution network and end-users as well as heat utilization by end-users can be attributed as a monetary value. For instance, an exergoeconomic analysis of a central heating system of a dormitory has been conducted [474]. It was found that although most of the building energy losses are through the envelopes, the highest exergy loss is at the generation and primary energy transformation stage. Moreover, an exergy analysis of a GDHS was conducted and a cost to the useful energy of the system was obtained [184]. Besides, an exergoeconomic analysis of a GDHS using the specific exergy costing (SPECOC) approach was conducted, and cost flows for all components of the system were displayed [178]. A detailed comprehensive review of exergoeconomic analysis of GDHS has been presented [475]. Some other examples of multi-objective optimization are tabulated in Table 5.1.

Table 5.1: Recent studies of district heating systems classified by optimized variable

Optimization variable	Ref.	Optimization approach/ software	Location	Remarks
Greenhouse gas and pollutant production	[186]	Sensitivity analysis	Denmark	Models of DHS with CHP and waste incinerators need to include heat and electricity production as well as the local configuration of the DHS as this influences the efficiencies and CO ₂ production rates of the system.
	[476]	EnergyPlan	Denmark	Potential for a 100% renewable energy system in Denmark is studied. In this situation, it is environmentally and economically beneficial for buildings not connected to the DHS to be equipped with heat pumps rather than other technologies.
Energy efficiency and exergy	[477]	Exergetic analysis and parametric study	Turkey	Component inefficiencies are acknowledged to have an influence on other components upstream.
	[478]	MINLP	Northeastern US	5-11% increase of energy efficiency with proposed modeling approach with respect to the reference case.
	[62]	Parametric study	Ottawa, Canada	Investigation of the potential of renewable energy integration to a DHS in Ottawa, Canada.
Cost	[468]	GIS mapping of DHS	Denmark	Future building energy demands as well as government incentives affect the economic viability of the system.
	[161]	MINLP	Northeast US	Other optimization methods such as branch-and-bound do not guarantee a global optimum while a computationally expensive bi-level method does.
	[469]	MILP	Teheran, Iran	It was found that MILP is very well suited for determining optimal operation of a DHS.
	[360]	MILP	Italy	Study of the feasibility of reducing CHP run time with solar collector bay and storage. With respect to cost, the objective function only uses solar energy in summer.
	[479]	GA	-	Smart metering can be used as input into static energy models and with GA, optimum operating conditions can be calculated for multiple CHPs simultaneously.
	Exergoeconomic and thermoeconomic	[474]	Annex 49 tool	Izmir, Turkey
[178]		SPECO	Afyon, Turkey	Specific components of a system can be evaluated based on exergy destruction or cost efficiency and the influence of specific components on the cost or efficiency of the system can be identified.
[454]		SPECO	-	Four CHP technologies were analyzed using energy, exergy and exergoeconomic analysis. Exergy efficiencies are higher for gas turbines than for steam turbines. Gas turbines and biomass integrated gasification combined cycle (BIGCC) CHP have a lower exergy cost.
Multi-objective	[480]	CPEA	Switzerland	The application of multi-objective optimization showed that a centralized heat pump is slightly more expensive than decentralized heat pumps but produces considerably less CO ₂ .
	[481]	Deterministic with MILP	model Switzerland	A trade-off between energy efficiency, CO ₂ emissions and annual costs can be made such that environmental impacts can be reduced by 50-65%, annual costs by 22-27%, with an efficiency of 75%. Exergy was not taken into consideration in this study.
	[482]	GA (NSGA)	-	Multi-objective GA is well adapted for the optimization of a hybrid organic Rankine plant employing low-grade energy sources.
	[196]	GA (NSGA)	-	Creating a Pareto front considerably reduces near optimal solutions and makes it easier for decision makers to select a solution based on experience.
	[470]	GA (NSGA)	China	An operation strategy which follows the thermal demand always performs better than a strategy which follows electrical demand.

5.4 Decision parameters

Decision parameters can shape the nature of optimization problems. The input parameters for a system optimization can be divided in two categories [483] of environment parameters and decision parameters, as shown in Figure 5.14.

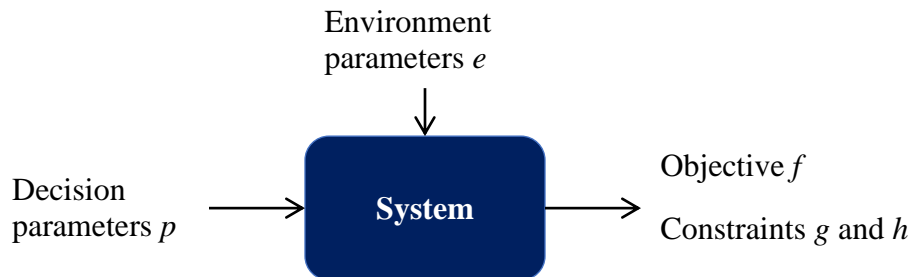


Figure 5.14: Inputs and outputs for a system optimization

The environment parameters create the scenario in which the optimization is performed. For building and district optimization problems, the environment parameters usually include the climate conditions (e.g. hourly, daily, monthly or annual profiles of temperature, humidity, solar radiation, wind speed), the market characteristic (e.g. cost evolution of materials and technologies, energy prices, discount rates) and the available technologies in the project location. Although such parameters may have a significant impact on the system performance, they cannot be controlled by system designers nor be optimized. However, they should be considered as the boundary conditions creating the scenario in which the system is optimized. Such a scenario is often fixed prior to optimization, but it may be subject to uncertainty, especially when optimizing the system performance in the medium/long-term. However, the uncertainty may be considered by running multiple optimization processes with different sets of environment parameters [484].

On the other hand, system designers can control the decision parameters by optimizing their values according to the objective function(s). The features of optimization problems are strictly correlated to the choice of decision parameters, as they are the main inputs to the system to be optimized. When defining optimization problems related to the component/building/district energy efficiency, the choice of decision parameters should be made coherently with the scale and the objective of the problem. In fact, as shown in Table 5.2, the number, nature and type of decision parameter influence the nature of the optimization problem itself by determining its complexity and therefore the selection of the most suitable solving method [394].

Table 5.2: Classification of optimization problems according to the criteria of decision parameters

Criteria	Categories of optimization problems
Number of decision parameters	Depending on the number of decision parameters: <i>One-dimensional</i> or <i>multi-dimensional</i> optimization
Nature of decision parameters	Decision parameters can be independent or mutually dependent: <ul style="list-style-type: none"> • <i>Static/dynamic</i> optimization if decision parameters are independent/are functions of other parameters • <i>Deterministic optimization</i> if decision parameters are subject to small/no uncertainty • <i>Probabilistic-based design optimization</i> in presence of uncertainty
Types of decision parameters	Decision parameters can be: <ul style="list-style-type: none"> • <i>Continuous</i> (accept any real value in a range) • <i>Discrete</i> (accept only integer values or discrete values) • <i>Both continuous and discrete</i>

Depending on the number of the selected decision parameters (n) the design space of the optimization problem is n -dimensional. Each decision parameter is constrained to certain values within its defined range and step of variation. Clearly, the greater the number of defined variables, the more complex the problem is. However, when the number of decision variables is high, it increases the potential for minimization of objective function, due to the higher potential for exploitation of synergies of decision parameters given by their mutual relationships.

The involved decision parameters may be related to different scales and therefore defined in different ways [400]. Such variables may be related to different parts of a same component, as it is for the parameters related to the thicknesses of each wall layer, or to the length and the number of fins of heat exchangers inside a thermal storage. Other variables may represent a set of different packages of building and system components with the related set of physical properties, as it is for the parameters related to the choice of a window type, which may include defined packages of thermal and visual properties of the glass and frame. Other variables may be chosen among different alternatives of complex systems which require additional components. For instance, the heating system alternatives include not only the heat generator but also the defined set of appropriate pipes, pumps and other components of the distribution and regulation system, or a parameter related to the PV array may represent the choice among different PV panel technologies with the required set of circuits and batteries.

Overall, the optimization problems related to energy efficient buildings and districts, regardless of the optimization objective, must be solved in adherence with the reality, which is the technical feasibility of the resulting optimal design of building and system components and coupling among components. In this perspective, the decision parameters should be selected based on their market availability and should be optimized to the order of their variability on the market. Moreover, their variability should consider the uncertainty scale of the variable itself due to the manufacturing and construction process and the marginal improvement of the building energy performance produced by the variable variations. In this context, most optimization problems in the field of energy efficient buildings and districts deal with discrete variables [485].

5.4.1 Building and district optimization

In energy efficient buildings and districts optimization problems, various decision parameters may be interrelated on multiple levels. The first interrelation is on their impact on the performance of the whole system, which is considered in the objective function. In fact, the same value of a parameter may have a different impact on the objective function according to the value of other parameters to which it is combined [486].

5.4.1.1 Passive parameters

The decision parameters related to the building envelope mostly affect the building/district performance in terms of passive reduction of energy needs for heating, cooling and lighting. In most optimization studies related to building and district energy efficiency, construction of opaque envelopes is referred to in terms of material and thickness of each layer and/or wall package alternatives, and to the type and dimension of window packages (glass and frame) [487-489].

According to the mentioned principle of feasibility, the insulation thickness of the opaque envelope components, depending on the material properties, can vary with a step of 1-2 cm, in a range imposed by construction feasibility (e.g. the technology solution for installing a 60 cm-thick layer of insulation is not commonly available on the market) and energy performance benefit. A sensitivity analysis for studying the variation impact of each parameter can be useful for determining the range. For instance, depending on the building location and the related energy need repartition in heating and cooling, the marginal improvement in energy performance tends to decrease when increasing insulation.

When performing optimization with financial objectives, it is common to assign each decision parameter a dedicated cost function [490]. In Figure 5.15, an example of cost function for a slab insulation is illustrated [491]. As shown, the specific cost of an insulation (expressed in terms of thermal resistance unit) decreases when the overall thermal resistance increases following an exponential function (the black curve). In the figure, the derived cost function representing the specific cost of 1 m² of slab insulation as a function of thermal resistance is shown in red.

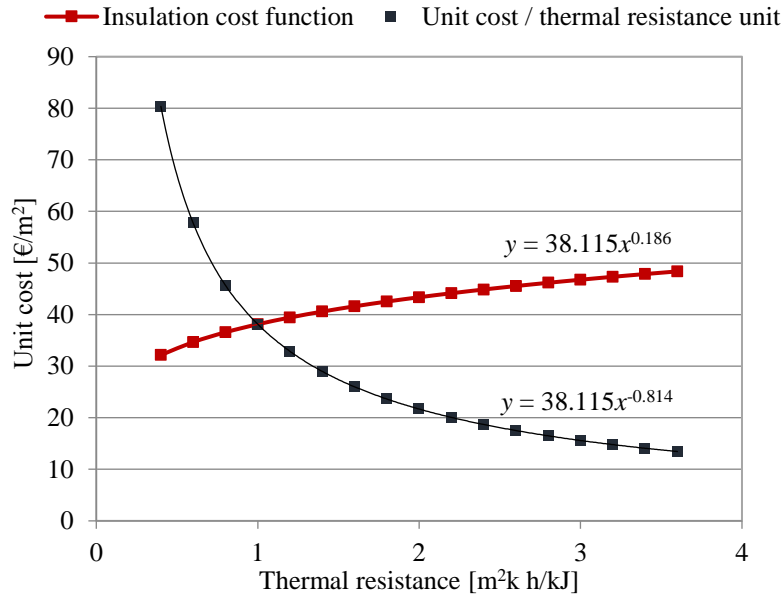


Figure 5.15: An example of cost function for slab insulation in the French market

Concerning the window type, it is known that the glazing overall impact on energy performance is based on the combination of its thermal and visual performances. If these properties were optimized independently, the result would probably be a glazing type which is not available on the market, as these properties are interdependent, and it is technically hard to create glazing with the entire set of desired characteristics. Since the glazing types available on the market are different packages with defined physical properties, the window type variables are usually composed of a set of different window packages selected from the market.

As shown in Figure 5.16, for a given window type it is possible to create linear cost functions which have different gradients according to the type of glazing and frame. However, constraints to the variability range should be imposed based on building layout, regulations (e.g. minimum amount of daylight), and the step of variation should account for the standard dimension of modular glass panels available on the market.

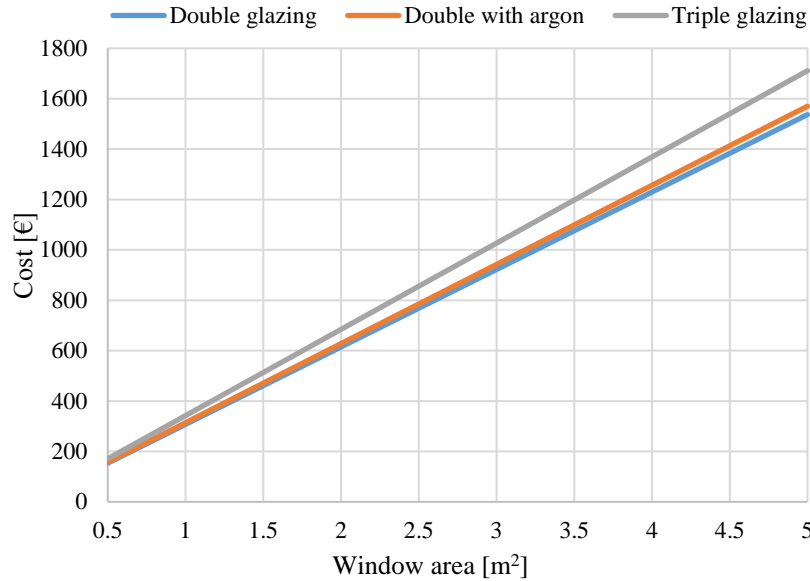


Figure 5.16: Example of cost function for window packages in the Italian market

Other variables (usually set in preliminary design studies when the building geometry is not determined yet) are related to the building orientation, the ratio between transparent and opaque envelope, the depth and orientation of shadings, etc.

It is important to note that the number and variability of the parameters related to building envelopes depend on the scale of the optimization problem. The decision parameters described so far are usually defined for the building scale optimization problems. They may also be used at the district level, but often the district level requires some simplifications to maintain the problem complexity to a manageable order. Therefore, instead of defining the thickness of each layer of each wall in each building of the district as a different decision parameter, the average thermal transmittance of each building opaque envelope is set as a decision parameter in a district scale optimization problem.

Other typical decision parameters at the district level are those affecting the urban heat island, such as the type and color of reflecting surfaces, or those affecting the cast shadows of different buildings and ability of the district to catch and use the solar energy for instance by the building geometry and orientation, and roof area.

5.4.1.2 Active parameters

Concerning energy systems in optimization problems, one or several alternatives can be evaluated (e.g. heat pump, gas condensing boiler, wood boiler) with their cost of investment, maintenance, replacement and the related energy costs according to the required type of energy. It has to be noted that some of these costs can vary according to the size of the system required to match the maximum building energy load, which is in turn related to the building envelope configuration. Therefore, the energy and cost models should account for this variability [492, 493].

For each energy system alternative which can be selected for each energy use (level 1 of decision parameters), several level 2 decision parameters may be identified. A summary of the most common “active” decision parameters is presented for energy production systems (Table 5.3) as well as the storage systems, energy use systems (terminals) and ventilation systems (Table 5.4).

Table 5.3: Decision parameters for energy systems in high performing buildings: energy production systems

Decision parameters				
	Level 1: type of system		Level 2: features of the system components	
Energy production system	Heating	Combined solar heating system	<ul style="list-style-type: none"> • Area of solar thermal panel • Type of solar thermal panel • Volume of the water storage • Orientation of the solar panels • Type and power of energy supply integration (electric resistance, gas boiler, heat pump, biomass, etc.) 	
		Boiler	<ul style="list-style-type: none"> • Type (electric, gas condensing, biomass, pellets, etc.) • Operating temperature (depending on terminals) • Efficiency 	
		Heat pump	<ul style="list-style-type: none"> • Type (electric, absorption, etc.) • Efficiency • Source temperature • Operating temperature (depending on terminals) • Type of geothermal boreholes (if present) • Length of geothermal boreholes (if present) 	
		Electric resistances	<ul style="list-style-type: none"> • Heating capacity 	
		District heating	<ul style="list-style-type: none"> • Operating temperature • Energy source (solar, biomass, fossil, etc.) • Maximum available power 	
		Cooling	Reversible heat pump	<ul style="list-style-type: none"> • Efficiency • Maximum capacity • Operating temperatures (condenser and evaporator)
			Absorption chiller	<ul style="list-style-type: none"> • Source type (solar or not) • Source temperature • Operating temperatures (condenser and evaporator)
	Adsorption chiller		<ul style="list-style-type: none"> • Source type (solar or not) • Source temperature • Operating temperatures (condenser and evaporator) 	
	Desiccant cooling		<ul style="list-style-type: none"> • Heating source (usually solar) • Dimension and efficiency of solar field 	
	District cooling		<ul style="list-style-type: none"> • Operating temperature • Energy source (solar, biomass, fossil, etc.) 	
	Electricity		PV	<ul style="list-style-type: none"> • Area of PV panels • Type of PV panels • Orientation of PV panels
			Micro wind turbines	<ul style="list-style-type: none"> • Maximum power • Surface of blades
		Grid	<ul style="list-style-type: none"> • Demand distribution over time 	

Table 5.4: Decision parameters for energy systems in high performing buildings: storage, terminal units, ventilation

Decision parameters			
	Level 1: type of system	Level 2: features of the system components	
Storage systems	Thermal	Water storage (sensible heat)	<ul style="list-style-type: none"> • Temperature • Insulation level • Volume • Length and geometry of heat exchangers
		Geothermal storage (sensible heat)	<ul style="list-style-type: none"> • Type of ground • Thermally activated volume
		Phase change materials (latent)	<ul style="list-style-type: none"> • Phase change temperature • Insulation level
		Thermo-chemical	<ul style="list-style-type: none"> • Type of material • Coverage ratio
Terminal units	Electric	Batteries	<ul style="list-style-type: none"> • Type of batteries • Capacity of batteries
	Heating	Electric radiators	<ul style="list-style-type: none"> • Capacity
		Water radiators	<ul style="list-style-type: none"> • Capacity
		Radiant surfaces	<ul style="list-style-type: none"> • Area (floor, ceiling, walls, etc.)
		Fan coil units	<ul style="list-style-type: none"> • Capacity
	Cooling	Cold surfaces (floor, walls, beams, ceiling)	<ul style="list-style-type: none"> • Area (floor, ceiling, beams, walls, etc.)
		Fan-coils	<ul style="list-style-type: none"> • Capacity
Lighting	Type of lighting (bulbs, LED, etc.)	<ul style="list-style-type: none"> • Power 	
Ventilation systems	Natural		<ul style="list-style-type: none"> • Openings dimension and location
		Mechanical	<ul style="list-style-type: none"> • Efficiency • Flow rate • Temperature
	Double-flux		<ul style="list-style-type: none"> • Efficiency • Air tightness of the conduits • Flow rate • Temperature
		Canadian wells	<ul style="list-style-type: none"> • Dimension • Depth

5.4.2 Constraints

The constraints applied in optimization of districts can be classified in three major groups [301] as illustrated in Figure 5.17. Note that the first two categories can also be applied to buildings. Component constraints usually state input/output energy for each module. Constraints for energy balances ensure that the amount of input energy is equal to the output, for each time interval and for each node (site) including supply and demand sides. Some common inequality constraints for different components are tabulated in Table 5.5. Equality constraint are highly dependent to the model; however, for some components such as TES, similar models are typically employed. Network constraints only apply to DHSs, stipulating various kinds of constraints related to energy distribution such as energy losses through wires and pipes (see Table 5.6). Table 5.7 summarizes the constraints used in recent studies for optimization of district energy systems.

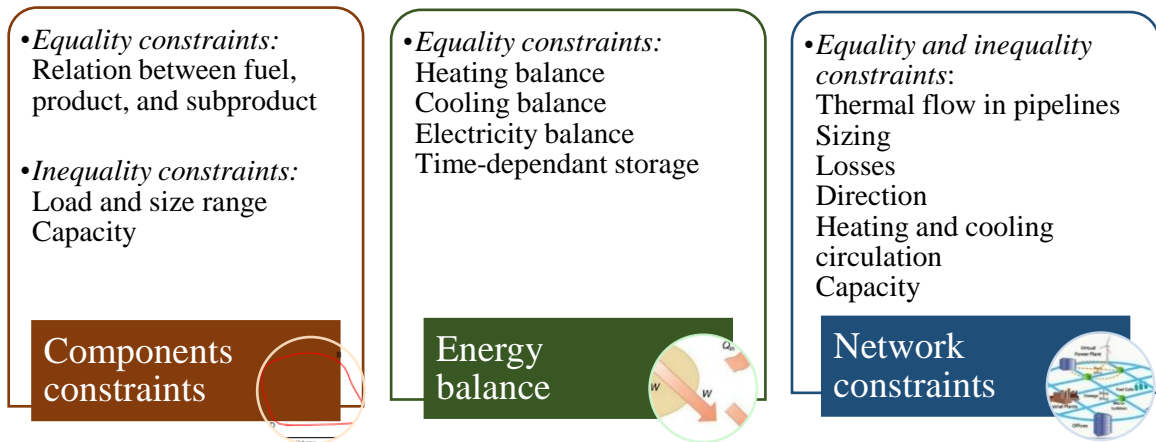


Figure 5.17: Classification of constraints in programming building and district energy optimization

Table 5.5: Formulation for some common inequality constraints at district level: component inequality constraints

Number of components	$y_i \leq n_i \leq n_{max} y_i$	The component number n_i should be lower than a maximum value n_{max} where y_i is a binary variable
Power and heat generation	$P_{GT} \leq P_{GT}^{max} y_{GT}$ $Q_B \leq Q_B^{max} y_B$	The generated power by gas turbines P_{GT} and the produced heat of boilers Q_B are less than their maximum capacity at each point of the operation time. y_{GT} and y_B are binary variables showing ON and OFF modes
Supply heat and flowrate	$G_{SA}^{min} y_{SA} \leq G_{SA} \leq G_{SA}^{max} y_{SA}$ $P_{EC}^{min} y_{EC} \leq P_{EC} \leq P_{EC}^{max} y_{EC}$	G_{SA} is steam flowrate and P_{EC} is supplied electricity.
Energy storage	$S_{TES}^{min} \leq S_{TES} \leq S_{TES}^{max}$ $S_{EES}^{min} \leq S_{EES} \leq S_{EES}^{max}$	TES: thermal energy storage EES: electrical energy storage
Power ramping	$\frac{P_{CHP}^t - P_{CHP}^{t-1}}{P_{CHP}^{t-1}} \leq \varepsilon$	Power by the plant between two successive time points are P_{CHP}^t and P_{CHP}^{t-1} .
Charging and discharging	$y_{in} + y_{out} \leq 1$	Battery or some TES cannot be simultaneously charged and discharged. Therefore, two binary variables of y_{in} and y_{out} for charging and discharging are introduced, respectively.
Charging supply	$\sum_{i=1}^n E_{sto,i} \leq M y_{in}$	The storage may be allowed to be charged from certain systems. $E_{sto,i}$ is the energy flow delivered by component i among n allowable units.
Grid interaction	$y_{in} + y_{out} \leq 1$	Supplying electrical energy to the grid or its withdrawal cannot be implemented at the same time.
PV area on the roof	$\sum_{i=1}^n n_i A_{PV,i} \leq A_{roof}$	Total PV area (n_i number of $A_{PV,i}$) which cannot violate the available roof surface area A_{roof} .
Solar absorption chiller	$\frac{P_{abs}}{COP} \leq P_{solar}$	P_{abs} is the chiller required energy with COP as the coefficient of performance and P_{solar} as the generated solar heat.
Up-time and down-time	$y_{ON}^{t+1} = \begin{cases} 0 & T_{up}^t \geq T_{up} \\ 1 & T_{down}^t \leq T_{down} \end{cases}$	The running time of a power or heat generation unit can be controlled by a binary variable y_{ON}^{t+1} at instant $t + 1$ based on the instant t .
Priority operation	$P_i^t \leq P_i^{t+1}$	Priority for the operation of the power or heating engines p_i^t at point t may be considered to prevent generation of multiple solutions.
Allowable modes	$y_{tr}^t + y_{tr}^{t+1} = 1$	In the case of successive permitted and unpermitted operation modes of a component, especially a CHP, a binary transition variable is defined as y_{tr} .

Table 5.6: Formulation for some common inequality constraints at district level: Network inequality constraints

Energy flow direction	$E_{j,i} \leq My_{j,i}$	Binary variables $y_{i,j}$ and $y_{j,i}$ for two buildings
Delivery capacity	$E_{j,i} \leq My_{j,i}$	Maximum delivery capacity is M for energy flow $E_{j,i}$
Thermal energy circulation	$OR_j = OR_i + 1 - i (1 - y_{i,j})$	Creation of a loop results in production and circulation of energy which is not demanded. For example, CHP can operate at a higher rate in order to sell electricity while the actual buildings demand is lower. OR is the order of a building.

Table 5.7: Some common constraints employed in recent district optimization studies

Constraint	[494]	[495]	[469]	[496]	[17]	[360]	[496]	[497]	[498]	[499]
Number of each/all equipment	✓			✓			✓	✓	✓	
CHP/boiler/chiller capacity (min/max)	✓	✓	✓	✓	✓	✓	✓		✓	
Storage capacity	✓					✓			✓	✓
PV area	✓	✓	✓	✓						
PV rated capacity	✓	✓	✓	✓			✓			
Storage flow capacity	✓				✓					
One-direction energy flow	✓	✓	✓	✓						
Maximum pipeline capacity	✓									
Heating/ cooling circulation	✓	✓		✓			✓			
Electricity balance	✓		✓				✓		✓	✓
Heating balance	✓		✓			✓	✓		✓	✓
Storage balance	✓	✓				✓			✓	✓
CHP/PGU/Boiler relationship	✓		✓			✓				
Grid interaction		✓	✓	✓		✓	✓			✓
Pipe heat interchange (capacity)		✓	✓							
Input energy limitations			✓							
Up/down time						✓				

The mentioned constraints are generally applicable to both district and building levels. Focusing on the component constraints, another important constraint is related to the combination feasibility of the different technologies for the different energy uses. Therefore, constraints on level 1 parameters (type of the system) should be defined according to such feasibility.

Here, some tables provide a summary of the most commonly used technologies with the feasibility evaluation of the combination of each level 1 parameter to the others. Table 5.8 reports the evaluation of the technical feasibility of the combinations among the different energy production systems for heating, cooling and electricity. Table 5.9 reports the same information for storage systems, the terminal units for electricity, heating, cooling and lighting, and the ventilation systems. Table 5.10 analyzes the possible combinations among the energy production systems, the terminal units, the storage systems and the ventilation systems.

For all these systems, the relevance of the coupling among components has been evaluated. It is shown that the number of optimally feasible combinations is strongly reduced compared to all possible combinations. The selection of the feasible combination of decision parameters related to energy systems should be conducted considering the following general principles:

- Multifunction systems are characterized by integrating several complementary systems. Compact systems (double flow, heat pump, DHW and heating sometimes including solar thermal), combined solar systems, PVT solar panels (thermal photovoltaic), cogeneration and reversible heat pumps are considered [500].
- Among the other combinations which were considered as feasible, the high-performance systems in middle seasons (air heat pumps, solar thermal) can be advantageously combined with systems whose performances degrade at low power (conventional boilers, stoves).
- The sorption cooling systems can be advantageously combined with solar systems (thermal and PV) to match the demand with the resource. If cooling is needed in the absence of sunshine, cogeneration systems can provide the heat while generating electricity [501].
- Low temperature heat terminal units (radiant floor, fan coil) are recommended for some heat production systems (solar thermal, heat pump). In addition, the air heat diffusion can be optimally combined with double flow ventilation systems.
- Canadian wells can improve the performance of all air systems. Air-source heat pumps can take advantage of the exhaust air heat of some ventilation systems.
- It is also recommended to couple moderately electricity-consuming systems (heat pumps) with local production systems (PV, wind, micro-hydro).
- The need for storage systems (thermal or electrical) appears for most systems, especially if the resource or demand is intermittent.

Table 5.9: Feasibility of combinations of decision parameters among energy systems in high-performance buildings: storage, terminal units, ventilation systems

		Storage systems					Terminal units								Ventilation systems								
		Thermal					Heating				Cooling												
		Water storage (sensible heat)	Geothermal storage (sensible)	Phase change materials (latent)	Thermo-chemical	Electric batteries	Electric radiators	Water radiators	Radiant surfaces	Fan coil units	Cold surfaces	Fan-coil units	Domestic hot water	Electric lighting	Natural	Controlled mechanical	Controlled hygro-adjustable	Double-flux	Double-flux hygro-adjustable	Controlled mechanical insufflation	Distributed mechanical	Canadian wells	
Storage systems	Thermal	Water storage (sensible heat)																					
		Geothermal storage (sensible)																					
		Phase change materials (latent)																					
		Thermo-chemical																					
		Electric batteries																					
Terminal units	Heating	Electric radiators																					
		Water radiators																					
		Radiant surfaces																					
	Cooling	Fan coil units																					
		Cold surfaces																					
		Fan-coil units																					
		Domestic hot water																					
Electric lighting																							
Ventilation systems	Natural																						
	Controlled mechanical																						
	Controlled hygro-adjustable																						
	Double-flux																						
	Double-flux hygro-adjustable																						
	Controlled mechanical insufflation																						
	Distributed mechanical																						
	Canadian wells																						

Legend	
	Unfeasible combination
	Non-optimal but feasible combination
	Optimally feasible combination

5.5 Available tools

Application of an optimization tool is vital for the performance analysis of a building or district energy system both in the design stage and real-time operation. According to the U.S. Department of Energy, some tools for optimization of buildings/systems, dedicated to economic, energy and environmental performance are shown in Table 5.11.

Table 5.11: Some tools for optimization of buildings [502]

Tool	Capabilities
AFT Mercury	Optimization, pipe optimization, pump selection, duct design, duct sizing, chilled water systems, hot water systems
BEopt	Residential buildings, energy simulation, optimization, retrofit, new construction
CHP Capacity Optimizer	CHP, cogeneration, capacity optimization, distributed generation
EA-QUIP	Building modeling, energy savings analysis, retrofit optimization (work scope development), investment analysis, online energy analysis tool, multifamily building analysis
EnerCAD	Building energy efficiency, early design optimization, architecture oriented, LCA
HAMLab	Heat air and moisture, simulation laboratory, hygrothermal model, PDE model, ODE model, building and systems simulation, optimization
HOMER	Remote power, distributed generation, optimization, off-grid, grid-connected, stand-alone
TOP Energy	Simulation and optimization of energy systems, energy efficiency, time series analysis, variant comparison, Sankey diagrams, material and energy flow analysis, process optimization
Umberto	Material and energy flow analysis, process optimization, environmental impact assessment, material flow cost accounting, life cycle assessment, life cycle costing
MyVerdafero	Utility optimization, building performance, portfolio analysis
GenOpt	System optimization, parameter identification, nonlinear programming, optimization methods, HVAC systems

Overall, the optimization tools for building applications have been deeply reviewed in the literature [395]. Therefore, this section is mainly focused on district level tools. The models representing a district energy system or a poly-generation system are generally developed within a mathematical programming tool rather than a compact separate software package. In this section, some optimization tools and their capabilities are briefly introduced. Most tools used for district energy optimization consist of algebraic modeling language (AML) which means they are high-level languages and usually have similar mathematical notation to describe optimization problems.

5.5.1 AIMMS

Advanced interactive multidimensional modeling system (AIMMS) includes algebraic modeling language and graphical user interface. Multiple solvers are included in the tool and it can tackle a wide range of problems including robust, stochastic and constraints programming. AIMMS has integrated development environment tools which allows software development. AIMMS provides free license for academic applications.

5.5.2 GAMS

General algebraic modeling system (GAMS) is another AML tool used to model and solve linear, nonlinear, MILP and MINLP problems. Similar to AIMMS, GAMS provides programmers with an environment for software development.

5.5.3 CPLEX

CPLEX can solve linear and MILP problems. CPLEX can also deal with certain types of problems where the objective function is nonlinear but quadratic whether the problem is constrained or not. It includes free license for academic applications.

5.5.4 AMPL

AMPL is an AML tool used to handle linear and nonlinear convex quadratic problems with both integer and continuous variables. The tool supports a variety of optimization problems such as semidefinite programming and is suitable for large-scale linear and nonlinear programming. It also has free license for academic usage.

5.5.5 Xpress

Xpress contains its own modeling language called Xpress-Mosel. It can be used for linear and mixed integer problems, convex quadratic constrained and unconstrained problems, second-order cone problems as well as mixed integer counterparts. It offers free academic license.

5.5.6 MATLAB/Simulink

MATLAB is a multi-disciplinary computational environment which can solve all kinds of linear, nonlinear, mixed-integer and quadratic problems using Optimization Toolbox.

5.5.7 LINGO

LINGO is a comprehensive optimization AML tool for building models capable of solving linear, mixed-integer linear and nonlinear, nonlinear (both convex and nonconvex problems), constrained and unconstrained quadratic, stochastic, second-order cone as well as semidefinite problems.

5.5.8 HOMER

HOMER offers modeling, optimization and parametric sensitivity of grid-connected and standalone RES focusing on electrical energy conversion. Storage technologies include batteries, flywheels and hydrogen without any TES. The only available thermal components are simplified models of CHP, boiler and biomass. Different kinds of electrical and thermal demand profile/data can be used as input to show daily or seasonal variations [503].

5.5.9 SynCity

SynCity adopts the same approach for mathematical programming as GAMS to optimize carbon emission, required energy and total cost of a district. The tool includes built-in models which receive neighborhood layout as the input. Time and location of demands for electricity, fuel consumption for transportation and heating are calculated based on the simulated daily activities of people. The tool proposes optimal solution for network configuration, activity locations and

transportation map. The tool takes the concept of “energy hub” for design, operation and energy consumption optimization at site and district levels [504].

5.5.10 Neplan

Neplan is used for designing, modeling and optimization of distribution networks of water, electricity, gas and thermal piping. The tool can analyze energy flow, energy loss and hydraulics for a district to size the heating units, circulating pump and heat exchangers. Another major advantage of the tool is its interface for geographic information system (GIS).

5.5.11 MODEST

MODEST (model for optimization of dynamic energy systems and time-dependent components and boundary conditions) is among the available tools for cost optimization of DHSs [450]. MODEST is an optimization tool intended to model costs and essentially minimize an objective function on the basis of a linear-programming technique [448]. This tool has been extensively used for DHS design such as Linkoping, Sweden and Gjovik, Norway [449] as well as Stockholm, Sweden cases [450].

5.5.12 GenOpt

Unlike other optimization software, GenOpt has been developed to minimize an objective function which is evaluated by an external simulation program. It can be coupled to any simulation program which reads its input from text files and writes its output to text files. Since one of the main application fields for GenOpt is building energy use or operation and cost optimization, it has been designed such that it addresses the special properties of optimization problems in this area. In particular, GenOpt is designed for optimization problems with the following properties:

- The cost function may have to be defined based on approximate numerical solutions of differential algebraic equations, which may fail to be continuous;
- Evaluating the cost function requires much more computational time than determining the values for the next iteration;
- Analytical properties of the cost function (such as formula for the gradient) are not available.

GenOpt has the following advantages:

- GenOpt can be coupled to any simulation program which calculates the cost function without having to modify or recompile either of the programs, provided that the simulation program reads its input from text files and writes its output to text files;
- The user can select an optimization algorithm from an algorithm library, or implement a customized algorithm without having to recompile and understand the whole optimization environment;
- GenOpt does not require an expression for the gradient of the cost function.

With GenOpt, it is easy to couple a new simulation program, specify the optimization variables and minimize the cost function. Therefore, in designing complex systems, as well as

system analysis, a generic optimization program such as GenOpt offers valuable assistance. However, the efficiency and success of an optimization is strongly affected by properties and formulation of the cost function, by selection of an appropriate optimization algorithm and by selection of initial values of parameters prior to optimization.

A great advantage of GenOpt is the possibility of linking it to TRNSYS. TRNSYS has a dedicated interface for GenOpt, which is named TRNOPT. However, it only allows the variables of the simulation model which are defined in the “dck” file format (the main TRNSYS input file, created with the Simulation Studio interface) to be set as optimization parameters for running GenOpt. Therefore, within TRNOPT, it is not possible to deal with variables located in the BUI file (the input file created by TRNBuild, the TRNSYS interface for editing the Type 56 for multi-zone buildings) and to define the equations implementing relationships among different optimization variables.

To do so, it is necessary to create simulation templates by directly editing the “bui” and the “dck” simulation input files with variables readable by GenOpt. Moreover, it is required to create (1) the configuration file, which refers to the call of the TRNSYS software, (2) the command file, in which the variables are defined as optimization parameters, and (3) the initialization file, which contains specifications concerning the locations of input, configuration and command files and the position of the objective function value. The whole simulation-optimization framework is shown in Figure 5.18.

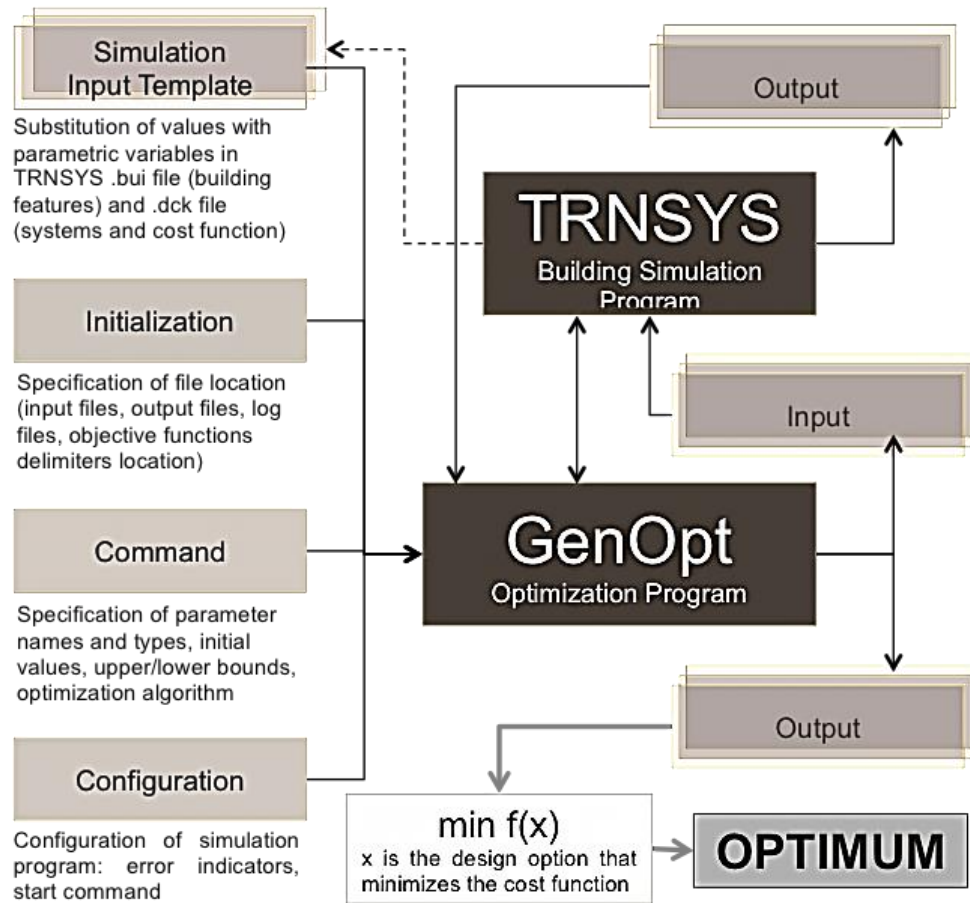


Figure 5.18: TRNSYS-GenOpt coupling framework

5.6 Problem classification

In this section, the most recent studies regarding district optimization are critically reviewed. As illustrated in Figure 5.19, district optimization problems can be classified into four main topics of (1) optimal superstructures, (2) optimal operation and planning along a representative period including some demand side models, (3) distributed integration and (4) subsystem building blocks.

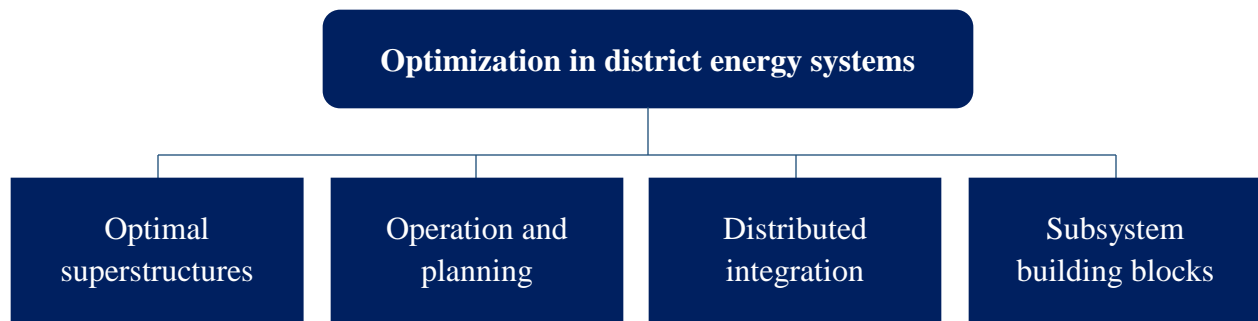


Figure 5.19: Classification of district optimization problems

A summary of optimization methods, objective functions, type of district energy and the commercial solver is shown in Table 5.12 for some recent district optimization studies. According to the table, determination of the optimal design and operation of district systems is usually an MILP formulation. In such formulation, decision vector contains both binary and continuous variables and a linear relationship holds among them. Binary variables characterize the existence of a component (also pipeline and wire) or the operation status (ON/OFF) of a generation plant, while all other decision variables are continuous. However, various solvers were used to simulate the performance. Table 5.13 presents the energy sources and technologies in separate groups. Gas boilers and CHP are among the most common technologies. Gas boilers are essential for providing backup energy to the system in the presence of an intermittent distributed system and/or storage system. In the following sections, each topic is briefly discussed.

Table 5.12: Summary of optimization approach in some recent district optimization studies

Ref.	Optimization type	Method/Algorithm	Objective(s)	DH type	Solver
Superstructures					
[505]	Single-objective	MILP	Total annualized cost of micro-grid	Centralized	GAMS
[495]	Multi-objective	MILP	Both economic and environmental aspects	Decentralized	Not mentioned
[494]	Single-objective Multi-objective	MILP	Annual cost and carbon dioxide emission	Decentralized	MATLAB Gurobi
[506]	Single-objective	MILP	Selection of new users	Centralized	CPLEX
[469]	Single-objective	MILP	Costs savings and reduction in CO ₂ emissions	Decentralized	CPLEX AIMMS
Operation and planning					
[507]	Single-objective	MILP	Operating costs for heat production	Centralized	CPLEX
[508]	Single-objective	LP	Costs of the net acquisition for heat and power in deregulated power market	Centralized	LP2
[360]	Single-objective	MILP	Dispatching strategy for the different power sources	Centralized	MATLAB
[259]	Single-objective	Newton's method	Total mass flow rate total thermal conductance	Centralized	Not mentioned
Distributed integration					
[171]	Single-objective	NLP	Cost per unit of thermal energy used	Centralized	Not mentioned
[17]	Single-objective	LP	Overall net acquisition cost for energy	Centralized	LP2 EnergyPro
[509]	Single-objective	MILP	Profit of CHP plant by selling electricity	Centralized	GAMS
[510]	Multi-objective	NLP	Costs of power and heat supply and CO ₂ emission equivalents	Decentralized	Not mentioned
Subsystem building blocks					
[511]	Single-objective	Calculus-based	Pipe investment cost	Centralized and Decentralized	Not used
[512]	Single-objective	Genetics algorithm	Calibration	Centralized	MATLAB

Table 5.13: Summary of technologies under consideration in some recent district optimization studies

Ref.	SH	CHP	HP	PV	GB	OB	WB	TS	CH	BA	OT
[505]	✓	✓		✓	✓						✓
[495]	✓	✓			✓			✓	✓		
[494]				✓	✓			✓	✓		
[469]		✓		✓	✓				✓		
[507]					✓	✓	✓	✓			
[508]	✓	✓			✓	✓	✓	✓			
[360]	✓	✓			✓			✓			
[171]		✓					✓				
[17]	✓	✓						✓		✓	
[509]		✓		✓	✓				✓		
[510]	✓	✓	✓	✓	✓		✓	✓		✓	
[513]	✓	✓			✓			✓			✓
[514]								✓	✓		
[515]	✓	✓	✓	✓	✓						✓
[498]		✓			✓			✓	✓		
[516]		✓						✓	✓		✓
[517]		✓		✓	✓			✓	✓		✓
[271]	✓	✓			✓			✓	✓		
[518]	✓	✓		✓	✓			✓		✓	
[499]				✓				✓		✓	✓
[519]		✓									✓
[520]	✓				✓						✓
[521]		✓					✓				
[479]					✓						
[522]		✓					✓	✓	✓		✓
[523]		✓									
[524]		✓			✓			✓			
[525]				✓						✓	✓
[526]				✓						✓	✓
[527]			✓								

Keys: SH: Solar heat, HP: heat pump, PV: photovoltaic units, GB: gas boiler, OB: oil boiler, WB: biomass wood boiler, TS: thermal storage, CH: chiller, BA: battery, OT: other (fuel cell, geothermal, wind).

5.6.1 Optimal superstructures

A superstructure is a flowsheet (or a scheme) gathering all the different feasible configurations, among which the optimal one can be chosen. Several studies concentrated on the optimal superstructure of a poly-generation energy system at the district level. The main outputs for the optimization problem in this category include the existence and size of each component/technology. This is usually followed by an optimal operation for a case study in which the objective is to decide which engine, chiller, CHP, etc., at which capacity and at which point during the time horizon should operate. In this section, a review on the most recent studies is carried out.

A MILP model has been introduced to find the optimal selection of the system components among several candidate technologies (micro CHP units, PV arrays, boilers, central power grid), including the optimal design of a heating piping network, which allows heat exchange among the different nodes [505]. However, its application was limited to 10 buildings and the district had no loops. Similarly, a model was proposed for determination of the energy generation components among various candidates, the site and size of each selected technology, optimal running schedule as well as optimal layout of heating network [495]. A comparison was made between three different scenarios: CON (conventional), DES + HN (heating network), DES + TS (thermal storage). However, such a model was only validated by measured data at three typical substations in a sample DH network, which was not typical for most systems all over the world.

A model has been proposed to minimize the total annual cost and CO₂ emission and achieve the optimal design and operation to meet the yearly energy demands for heating, cooling and power [494]. Different weights were used for the objective function to evaluate environmental and economic benefits. However, the model was validated with four simple buildings.

Selection of the set of new users to be connected to an existing district network has been optimized during time horizons of five and ten years [506]. The model maximized revenues and minimized operating and investment costs using fundamental of graph theory. The model was tested for a DH network in Emilia-Romagna, Italy, with 33 users (20 existing and 13 new). However, loops and multiple sources were not considered in the model. Cost of pumping, insertion of new tees, size of heat exchangers and optimal piping diameters were not included. Consumption variation of existing users is of paramount importance which was not analyzed in the model.

A model to optimize a tri-generation system based on combined cooling, heating and power (CCHP) in a district consisting of seven buildings in Tehran, Iran has been developed [469]. Four separate scenarios (i.e. conventional, CCHP without network, CCHP with network and CCHP/PV with network) were compared based on several component candidates to achieve minimum equivalent CO₂ emission and cost. The PV units were installed and operated with high subsidy and grid-selling price resulting in much lower energy cost in comparison to other scenarios. However, no thermal/electrical storage was considered in the model to shift energy purchases. Moreover, no loop equation was included in the model.

5.6.2 Operation and planning

The second category of studies focused on the optimal operation status and load planning of each component for an existing neighborhood at each point of time. In this category, the exchange of electricity, heating and cooling using the distribution network is the main output. The models typically quantify the economic and environmental impacts due to the overall operation of the energy system in comparison with individual buildings or a reference/base system. The reference scenario usually describes a conventional energy supply corresponding to the system. The electrical demand is supplied by the grid network and thermal demand is provided by gas-fired boilers. Normally, no renewable technology, CHP/CCHP system or piping network is introduced in the reference model. The layout of the network and the heating, cooling and power units are usually predefined for operational optimization, while the optimization procedure aims to find which engine, heating and cooling plant, and at which capacity should operate at any time.

A new process integration technique has been introduced [507] which allows (1) modeling of DHSs with loops (closed paths for fluid flow), without introducing any simplification or modification to their physical structure, (2) modeling of DHSs containing multiple sources of thermal energy production and (3) redesign of the DHS structure, particularly adding or removing consumers. The method was applied to a DHS in Kiruna, Sweden. However, this complex model takes a long time for simulation which was not addressed in the study by comparing the running time to that of the conventional models. Moreover, the results were not compared with simplified models to examine the accuracy. For example, it was stated that the model was able to analyze flow distribution of the DHS and identify the location of bottlenecks in the network. But no information was provided for comparison of these characteristics with conventional design techniques. Moreover, a constant return temperature was considered in the entire network.

An energy integration system named smart hybrid renewable energy for communities (SHREC) has been proposed consisting of heating and power markets under the context of district heating network and electricity grid [508]. The design included CHP, heat-only boiler, condensing plant, heat pump, renewable energy and energy storage system to be used in a community in southern Finland. The model was successful regarding heat losses from the storage tank and smooth operation of CHPs. The latter was achieved due to the integration of power ramping constraint to the model.

A different configuration for using RES in district heating networks has been investigated [360]. Renewable share in a DHS can be obtained from different sources such as burning renewable fuel, using geothermal source, using a renewable electric energy and converting it into heat through a reversible heat pump, inserting a solar heating contribution to the heating network, etc. However, due to the variable and non-controllable nature of renewable heating which must be handled by fulfilling users demand and coordinating its output with other controllable sources, TES is often necessary for exploiting RES at their best. The definition of a management strategy to run a plant at its minimal cost or using the largest possible share of renewable is not easy to achieve even with a limited number of components.

Newton's method has been used to minimize the cost of a DHS (a multi-floor building) based on separate mass flow rate (pumping cost) and thermal conductance (heat exchanger cost) [259]. In each case, the value of another objective was assumed to be constant. The model considered both the inner (user side) and outer loops. The problem can be formulated almost easily for large networks; however, the running time is questionable. Therefore, a tool is required for the model to be applicable in larger districts.

5.6.3 Distributed integration

Distributed integration deals with the connection of energy resources to the energy system to serve as reliable, sufficient, economic and environmentally friendly suppliers. In this context, among district energy production technologies, operation of CHP systems received attention.

A quasi-steady state model has been proposed based on thermodynamics, combustion processes and heat transfer to accurately estimate the performance of a biomass CHP plant integrated with a DHS [171]. Optimization was carried out to calibrate the model based on an existing plant. However, heat storage was not included which could considerably enhance the benefits of the CHP plant as it increases the equivalent utilization period. Moreover, the behavior of the integrated network was not considered. Besides, the model prediction is valid only for certain measurement accuracies (specific steam and flue gas mass flow rates and temperatures, and for a specific DH network).

In a study, a CHP based DHS with RES was investigated [17]. A modeling and optimization method was developed for planning and operating of such CHP-DHSs. The objective of the optimization was to minimize the overall costs of the net acquisition for heat and power in a deregulated power market. A planning model consisting of energy balances and constraints for system control and operation as well as an efficient algorithm was developed. The same system was also optimized with a higher share of RES and a larger TES to simulate the future situation. It should be noted that intermittent solar generation was included in the model. To make the model more accurate and realistic, constraints on the energy storage and power ramping were also included. This large CHP-DHS planning problem was solved using an efficient LP solver. The results indicated that the developed modeling and optimization method was efficient and flexible for planning and operating CHP-DHSs, for optimizing the combination of system components and for sizing problems. It was also found that the storage efficiencies should be well-considered when optimizing the operation of CHP-DHSs. The optimal operation of the TES was influenced by both the heat demand and power price. It was concluded that TES would be used more intensively in the future with more fluctuating CHP load and a higher share of RES.

In a study, the optimal integration of a CHP plant as a utility producer at the neighborhood level was investigated [509]. The optimum operation for the combination of CHP with PV was also investigated for predominantly cold climates. The fluctuations in energy rates, ambient conditions and demand level were considered. Moreover, the day-ahead price was considered in the economic study. When the day-ahead electricity rates rise, operation of the gas turbine is

economically beneficial since a huge profit is earned by selling electricity to the grid. For a CHP alone system (without PV), the net profit is approximately halved while the gas turbine should run continuously to supply the neighborhood demand.

A decomposed optimization solution has been proposed to a multi-objective problem with integrated economic and ecological objective functions to reduce computational complexity of similar problems [510]. The optimization model comprised of three stages: (1) heating network design, (2) generation plants, storage systems and renovation measures, and (3) operation of the generation plants and storage systems. The Pareto frontiers for a network were compared with individual buildings for an existing district system in Lampertheim, Germany. The meshed network was not considered in the model and electricity interchange among subnetwork buildings were prohibited. There was also no discussion on how the proposed decomposed optimization has reduced the computational complexity of the system.

5.6.4 Subsystem building blocks

The last category consists of optimization studies focusing on specific technical aspects of components or building blocks of a system. In this category, the focus is typically on determining the optimal piping and hydraulic resistance in a network.

An analytical model has been proposed to find the optimal pressure drop and related minimum annual cost for the distribution network in a DHS based on operating variables and different strategies [511]. In this model, all terms were rewritten based on only one parameter (pressure drop per length) and simple calculus methods were applied to find the optimum value. The model considered different types of annual cost for piping network beside investment including repairing, depreciation, distribution, management, labor, pumping and heat loss. However, the model requires several parameters (especially for regression) to be useful.

Optimization (using GA) was used to calibrate a model for steady-state distribution of thermal energy through pipes in a network [512]. The mathematical model was simple and taking advantage of temperature and flow measurements for three cases resulted in reduced uncertain parameters (aggregated heat conduction coefficient) and more accurate model. However, the proposed procedure is only applicable when data for at least three operation modes are available. Moreover, hydraulic losses were not included in the model.

5.7 Computational time deduction

Due to the complexity of building and district heating systems (several components, highly nonlinear relations between system inputs and outputs, etc.), the optimization process could be very time consuming where in some cases the optimization lasts several days. The mechanism of the optimization process (Figure 5.20) can be described as a repeated communication (several cycles) between a system model, an optimization algorithm and processing units which compute the values of the objective function(s). The whole process is realized based on a calculation machine. The total optimization time is the summation of the time consumed by each unit.

Therefore, to reduce the calculation time, it is necessary to act at the level of each or some of these units by:

- Reducing the simulation period of the modeled system (e.g. 12 days simulation period instead of 12-month period)
- Parallelizing the calculations using different machines
- Using an efficient and convenient algorithm
- Simplifying the model
- Reducing the number of decision variables to consider only the main effective ones
- Using a powerful calculation machine

In the following sections, some common methods are presented to reduce optimization computational time.

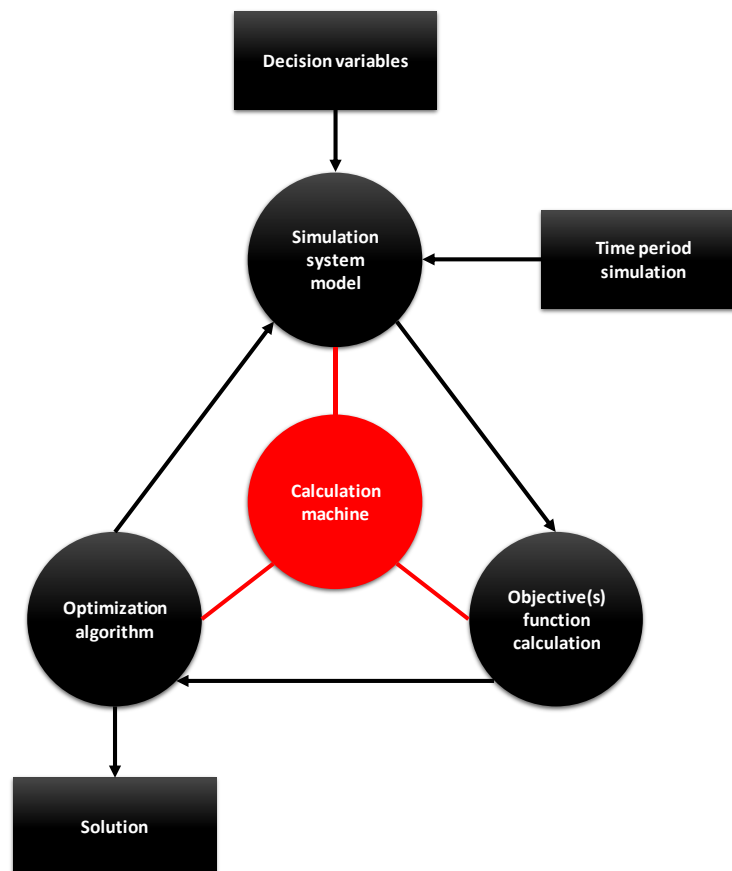


Figure 5.20: Flowchart of the general optimization process and the interaction between the computation and management units

5.7.1 Simulated period reduction

To design a building or a district heating system, it is common to consider at least one year of weather data and energy demand profiles (i.e. heating/cooling) of the desired city (in which the system and buildings are installed) to compute the objective function(s). In fact, the simulation

period should include all boundary condition patterns which the system will face during its operation. Assuming cyclic weather conditions over years, one-year simulation fulfils this condition. However, for optimizations that consider the system degradation over time for some extended systems, the simulation period could be equal to the entire system life period.

Reducing the simulation period for computing the objective function(s) is a promising method to significantly reduce the computational time of optimization (see Figure 5.21). However, to obtain a satisfactory solution, the reduced simulation period should include all boundary conditions patterns for at least one year. It is necessary to mention that the solution of an optimization process based on a reduced period is not equal to the solution which would be obtained using a complete simulation period; however, it can achieve an acceptable tradeoff between accuracy and calculation time.

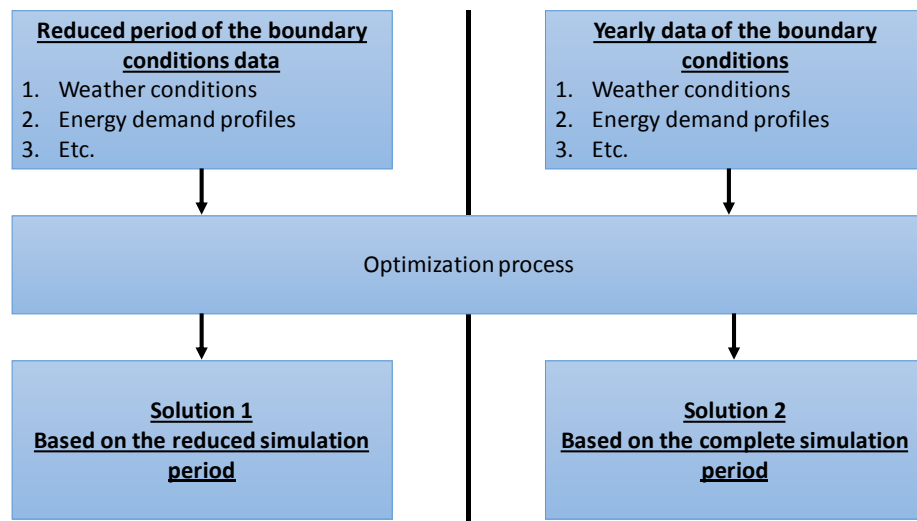


Figure 5.21: Representation of the two approaches for system optimization (the only difference is the period of boundary conditions data, note that the solutions are different).

According to the literature, such approaches were used very few times for buildings and districts. In a study, the computation and optimization time in DHSs was reduced by limiting the investigation to a certain period of time instead of dealing with yearly dataset [528]. K-means clustering algorithm was utilized to determine typical periods which allow achieving the accurate representation of the yearly consumption profiles, while significantly reducing the number of data points. To make sure that the global optimum was reached, five performance indicators were proposed which represented five ϵ -constraints in ϵ -constraints optimization technique. The accuracy of the models was verified by two case studies and it was concluded that the method is scalable and efficient.

There is no generic approach to determine the optimal period to be considered for any system. In fact, this period depends on the considered system and weather data. For energy performance evaluation of solar thermal systems, some methods have been proposed to test the system in a short period of time and then extrapolate the results to the whole year [529-531]. The

proposed methods are based on a reference model of solar combisystems and an algorithm which iteratively selects a limited number of days (6 or 12 depending on the considered methodology). For the considered system, these days reflect the entire year weather data in a way that energy consumption of the system during the reduced period is equivalent to its annual energy consumption. These methods could be extrapolated to system optimization applications to reduce the calculation time. In fact, for future work, these methods could be a hot topic for building and district heating optimization.

5.7.2 Parallelism models

Nowadays, calculation machines can fulfill different tasks simultaneously. Since some operations during the optimization process can be independently carried out, a way to reduce the calculation time is to divide these operations among calculation units. Different approaches were suggested to parallelize the optimization process. However, only the master-slave model has been used for building and district applications. This model is divided into a calculation management unit called master and several other calculation units called slaves. The master is in charge of data processing as well as interpretation of the results computed by each slave (Figure 5.22).

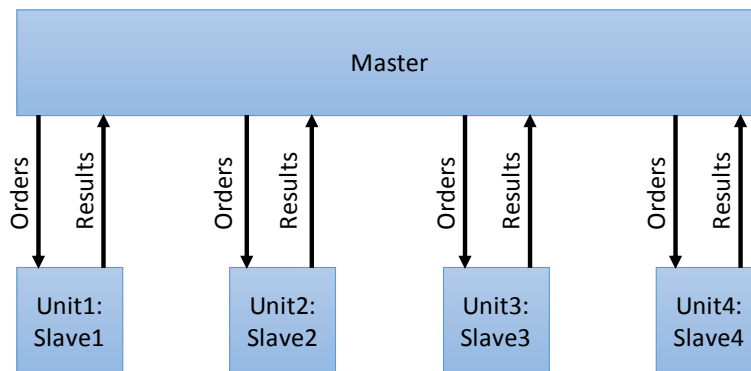


Figure 5.22 Representation of a master-slave model and the interaction between the units

The task to divide between the master and slaves can follow different patterns. For selected algorithms where the objective function should be computed several times for each iteration before going forward to the next one, parallelizing the objective function calculation could be the best approach. In this case, each slave computes the objective function for a specific value of the decision vector of variables and the master supervises the process and selects the best solution prior to going forward to the next iteration. Another approach which allows using several optimization algorithms, uses a specific optimization algorithm for each slave to look for the minimum (Figure 5.23). The master in this case selects the best solution for each iteration and transmits it to each slave as the initial point of the next iteration. The approach which divides tasks according to the objective function is widely used for multi-objective functions. In this case, each slave is responsible for the minimization of a specific function.

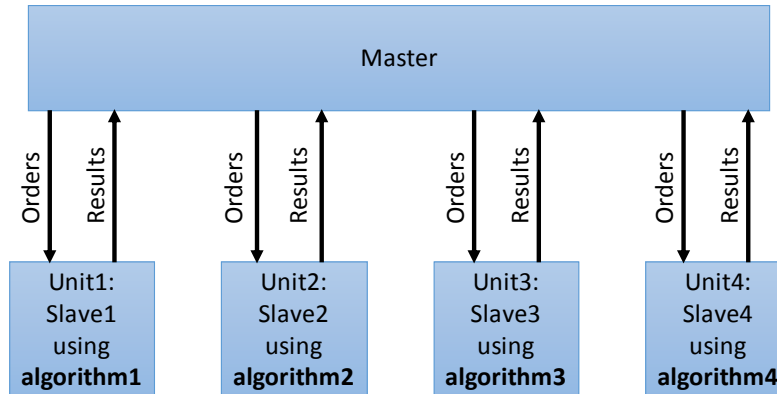


Figure 5.23 Master-slave model: parallelism approach based on dividing tasks according to optimization algorithms

In a study, a parallel master-slave model of micro-PSO was developed [532]. The proposed algorithm was implemented in five different test problems and two different computer-sets. It was concluded that by reducing the search space into subspaces of smaller dimension and by searching subspaces individually to find the suboptimal components by small subswarms, the run-time can be reduced, and the solution quality can be improved. In another study, master-slave swarm shuffling evolution algorithm was used for estimation of parameters in hydrological models [533]. The self-adaptive shuffling evolution strategies were combined with particle swarm and the searching direction of particles were controlled. It was concluded that the method can improve the accuracy and reduce the verification period. Decomposition of the optimization problem for a DHS to a master and slave problem has also been investigated [270]. The multi-objective evolutionary algorithms were used to minimize the costs and emissions. Fluid temperature in pipes, insulation thickness around the pipes, temperature difference between supply and return pipes, and type and size of the used technology in the system were used as the decision parameters in the master problem. The financial considerations were left to the slaves. A case study was carried out and it was concluded that the results could be improved if the objectives of the slaves cover emission and costs as well.

5.7.3 Surrogate modeling

A current trend in energy building design optimization is to reduce computational time using surrogate models (SM) to mimic time-costly transient simulation models. For instance, SM can be used to reduce the computational time for optimization of two objective functions to minimize cost and environmental impact of a building envelope [534].

SM may be classified based on their employed techniques: radial basis function, Kriging (KR), artificial neural network (ANN), support vector regression (SVR), multivariate adaptive regression splines (MARS), etc. Radial basis function surrogate modeling was used in a multi-objective optimization to maximize solar yield and minimize investment costs of a solar domestic hot water system [535]. KR is a non-parametric technique, suitable for the identification of long-term temporal and spatial trends [536]. Furthermore, one of its special features is the ability to

predict not only numerical values, but also uncertainty boundaries. KR is commonly used to predict building energy performance [537-540]. ANN is a parametric technique which has the ability to learn complex patterns [541] and simulate nonlinear systems [542]. Moreover, ANN is efficient in building studies [543]. It is the dominant technique for building energy performance analysis [544]. However, in the case of time-consuming transient simulation models, KR requires a far lower training time compared to ANN since less samples would be needed. Besides, the main advantage of SVM over ANN is related to the fact that the statistical learning process is cast as a convex optimization problem [545]. SVM was used to perform a model-based multi-objective optimization to minimize thermal discomfort (in terms of PMV) and annual energy consumption [546]. MARS is an adaptive non-parametric regression method [547]. MARS has found surprisingly little application in building-related studies to date [548]. For instance, MARS has been compared to other SM in a model-based multi-objective optimization problem, using a PSO algorithm to minimize the energy consumption of an HVAC system [549]. Besides, sequential design strategies for SM have been studied in the context of deterministic computer experiments, to perform either prediction or optimization [550]. For instance, a hybrid technique (MARS and artificial bee colony) was used in adaptive design of an SM to predict heating and cooling loads of buildings [548]. Besides, a covariate matrix adaption evolutionary strategy (CMA-ES-SA) optimization was applied to minimize cooling and heating demands of a building [551].

5.7.4 Satisfaction functions

In a multi-objective optimization, Pareto front can be a useful tool for decision makers to choose a solution; however, it is rather impractical for more than two performance criteria. There are many different multi-criteria decision-making analysis (MCDA) methods which can be used to post-process optimal solutions. Among these MCDA methods are technique for order of preference by similarity to ideal solution (TOPSIS) [552, 553], analytical hierarchy process (AHP) [554-556], elimination and choice expressing the reality (ELECTRE) [557], complex proportion assessment (COPRAS) [556, 558], stochastic multi-criteria acceptability analysis (SMAA) [559] and stochastic multi-criteria acceptability analysis [560]. Furthermore, it is not common in energy building design literature to use decision making tools before post-processing (i.e. integrated in the optimization algorithm). However, this could help reduce calculation time if the optimal solutions of little interest were not considered.

A new algorithm can be developed to reduce the calculation time. To do so, the new individuals of the adaptive sequential design are filtered with satisfaction functions [561]. It means that only the useful part of the Pareto front will be determined. In the case of a two-objective Pareto front, Figure 5.24 illustrates MCDA method with satisfaction functions. For each objective, the decision-maker first defines the shape of the corresponding satisfaction function. The illustrative figure shows that there is no individual in the area corresponding to 100% satisfaction for both criteria. However, the first individual can be obtained with a 90% satisfaction. On the other hand, some individuals have zero satisfaction and are ultimately of no value to the decision-maker. The "useful" area of the Pareto front can be reduced by requiring a minimum level of satisfaction for

the new points. The advantage is to accelerate convergence by limiting the scope of the optimal solutions to a useful area for the decision-maker.

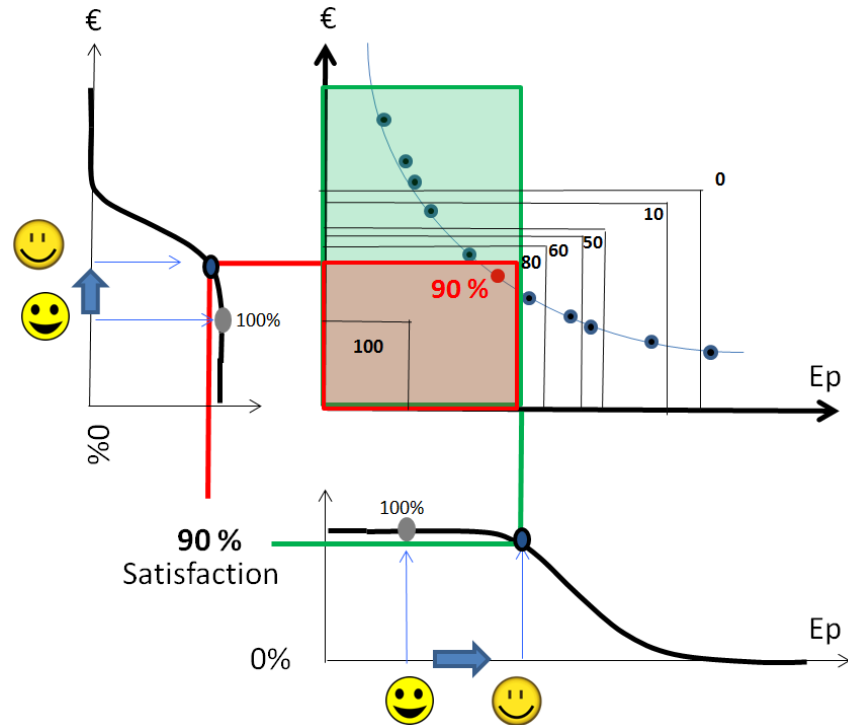


Figure 5.24: Illustration of decision making aid with satisfaction functions

5.8 Examples

5.8.1 Building level

5.8.1.1 Building life cycle optimization

The energy building design for nZEB is challenging in many ways. One challenge is to meet the large amount of energy requirements using RES [562-564]. That is problematic because RES highly depends on the climate of the building site. This means that the energy supply from RES does not always match the energy demands [565]. Therefore, designers cannot easily size, for example, the required installed power of the RES and the storage capacities (thermal and electrical) to meet the energy needs.

Another challenge is to reduce the relatively high value of embodied energy compared to nZEBs annual energy consumption [566-569]. Once the operational energy needs of a building during its lifetime are balanced by the use of RES, then the embodied energy (i.e. the energy used during its construction) becomes significant [570-572]. This leads nZEB designers to perform LCA which is a more comprehensive approach including embodied energy assessment. Considering the building lifetime, designers should also account for the climate change. To do so, more dynamic simulations on possible climate scenarios are required. These extra simulations add to the computational time.

Another issue is the complexity of modeling an nZEB as a whole (envelope, systems, etc.) which further increases computational time. Therefore, nZEB optimization should reduce the required computational time [573]. However, nZEB designers should consider many performance criteria, such as the cost, thermal comfort, embodied energy, CO₂ emissions, energy consumption, RES production, durability, etc. All of these factors lead to the need for a global approach of nZEB optimization [400]. Thus, designers should perform a multi-objective optimization that will result in many possible optimal solutions, which can be presented by a Pareto front.

5.8.1.1.1 Background

To address the issues for the life cycle optimization of nZEBs, an energy building design optimization methodology has been developed. To reduce the required computational time, a KR model was trained to surrogate nZEB performance criteria during the optimization process. The error estimation of the KR model was used for an adaptive sequential design to improve the model accuracy. A GA method (NSGA-II) was implemented to find the global optimal solutions. Finally, some network visualization was developed for MCDA. This approach can help designers find one solution in the case of multi-objective optimization. Moreover, the partitions can provide useful information regarding the characteristics of the optimal solutions.

5.8.1.1.2 System description

The case study concerns the design optimization of two buildings located in Chambéry (Savoie, France). The two residential buildings (34 apartments) have been modeled using TRNSYS. Each building was modeled with only two zones (i.e. heated and unheated).

In terms of climate change, some scenarios have been developed to predict the future global surface warming (see Figure 5.25). In this example, A2 scenario was selected according to which both irradiance and temperature clearly tend to increase over the next years. Maximum temperature will rise 12 degrees, whereas the rising rate of irradiance will be lower. Consequently, the climate change will decline heating demands from 1995 to 2050 by 30% (6427 kWh/year) (Figure 5.26). Therefore, it is necessary to consider the climate change for life cycle optimization.

In order to use future climate conditions, morphing methodology [574] was used for climate change transformation of weather data. The climate change world weather file generator (CCWorldWeatherGen) [575] was used. Based on global grid of scenario A2 for 2020, 2050 and 2080, it transformed a present day weather file to the future weather data.

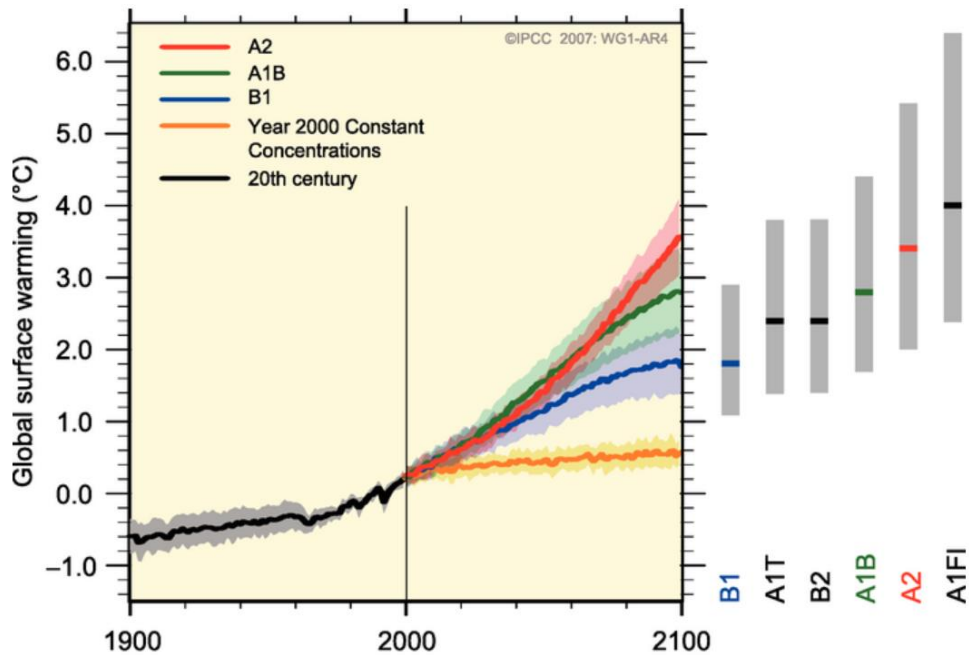


Figure 5.25: The future climate change scenarios [576]

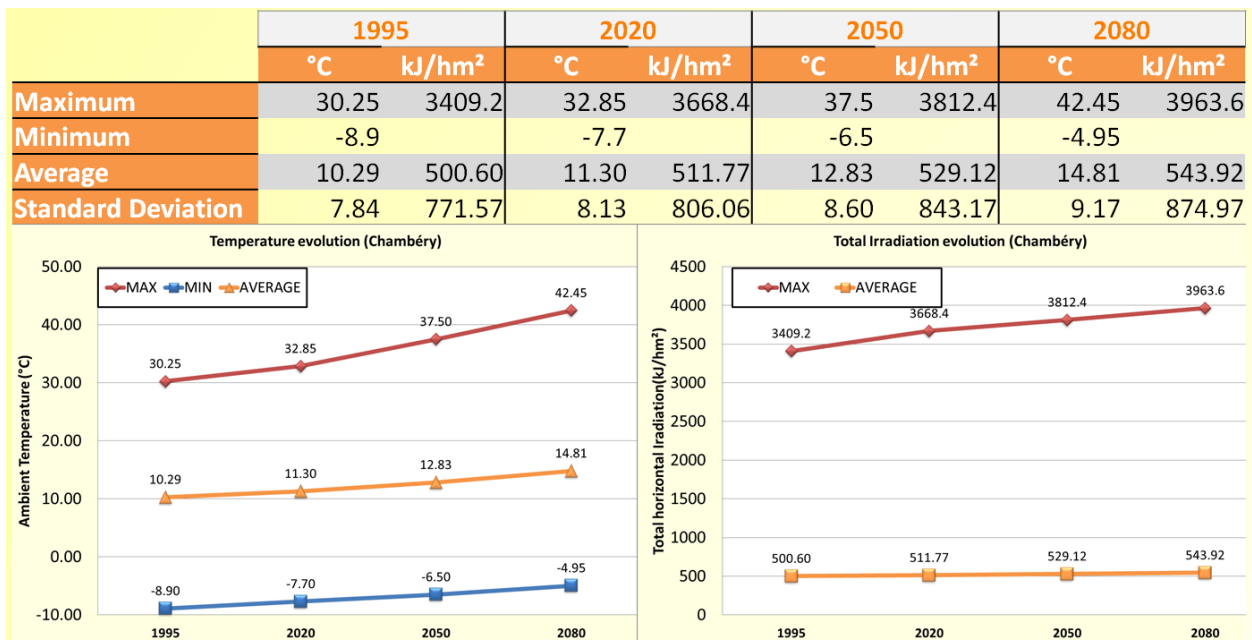


Figure 5.26: The heat demand (kWh) and internal temperature (max and mean) variations

Optimization has been carried out with the initial configuration of the two buildings (concrete, external insulation, collective gas boiler, solar hot water system, exhaust mechanical ventilation system). Other configurations can be considered for optimization, too. They concern heating and DHW systems as well as the envelope. In total, 64 possible combinations were identified for systems by considering building characteristics and the geographical location:

- Combined solar systems with different auxiliary heating systems
- Collective solar water heaters with different auxiliary heating systems
- Boilers using different sources of energy (gas, electricity and wood). Systems using oil as primary energy were not considered due to operating costs and excessive CO₂ emissions.
- Individual systems (one boiler per apartment) and collective systems (one boiler for the whole building)
- Collective or individual thermodynamic water heaters
- Heating network
- Air-to-water and water-to-water heat pumps
- Compact multifunction systems (ventilation with heat recovery, heat pumps, production of hot water, coupling with solar collectors, etc.)

Regarding the envelope alternatives, the main possible combinations were:

- Type of insulation (exterior, interior, distributed)
- Nature of the insulation (glass wool, Rockwool, polyurethane, wood-wool, polystyrene) according to the nature of the wall (façade, roof, etc.)
- Type of windows (double/single glazing, PVC, etc.), surfaces and orientations

It is not possible to combine all system-related configurations with those of the envelope. Clearly, modeling associated with system variants is much more time-consuming than that of the envelope. For instance, once the geometry and the thermal zones have been modeled on a configuration, changing the insulation position is simple. The main difficulty is to automatically change the thermal bridges. Besides, it is important to limit the number of systems by defining levels of relevance. Therefore, 9 systems were selected:

- Collective gas boilers (with/without solar DHW)
- Individual gas boilers (with/without solar DHW)
- Water-to-water heat pumps
- Collective pellet boilers (with/without solar DHW)
- Individual electric heating with solar DHW
- Heating network

5.8.1.1.3 Methodology

The main idea behind the methodology is to decrease computational time by performing multi-objective optimization with minimum calls for transient simulations. As the SM needs to be calibrated, the methodology (see Figure 5.27) is based on an adaptive sequential design which combines:

- Time consuming transient simulations (TRNSYS software) feed a database. The objective functions $f(x, y)$ are calculated with the simulations results. The decision parameters are denoted by x while y shows the remaining variables.
- The database $\{x, f(x)\}$ is used to calibrate the surrogate models.

- Each SM (i.e. KR model) calculates one objective function $f^*(x)$ with the decision parameters x as inputs.
- Multi-objective optimization is performed with the SM of $f^*(x)$.

The main challenge is determining new points x_{new} to properly calibrate the SM to find optimal solutions. The objective is to reduce the error of the SM, particularly in the Pareto area. Overall, the new individuals can be chosen based on four strategies:

- **Strategy 1:** the maximal error in the whole research space (in the range of each decision parameter)
- **Strategy 2:** the maximal error in the Pareto area only
- **Strategy 3:** hybrid strategy (first Strategy 1 and then Strategy 2)
- **Strategy 4:** same as Strategy 3 but with the maximal error in the Pareto area only and a minimum satisfaction level. The satisfaction functions (as mentioned in Section 5.7.4) are determined by decision makers.

In this example, Strategy 1 was used. The stopping criterion for the adaptive design was achieved when no improvement in the Pareto front occurred.

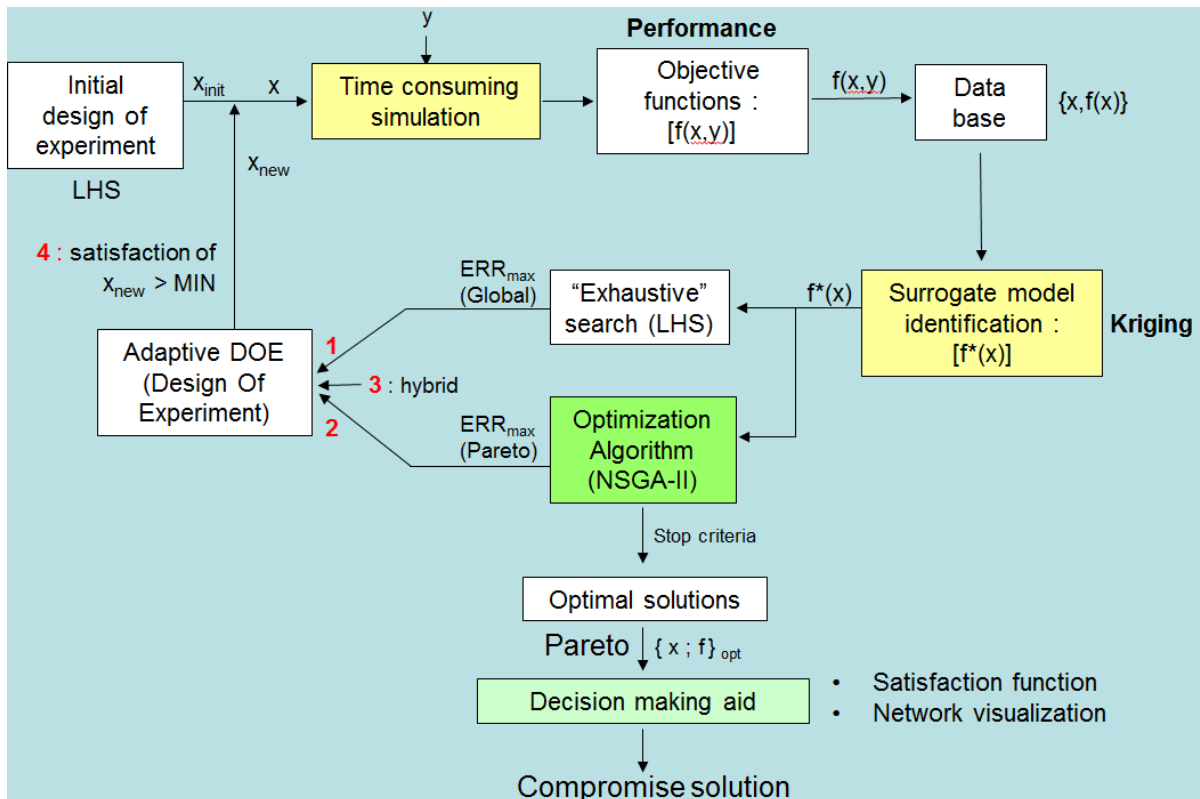


Figure 5.27: General presentation of the adaptive sequential design (LHS: Latin hypercube sampling)

5.8.1.1.3.1 The objective functions

Four main classes of performance were considered namely environment, cost, reliability and comfort. The life cycle of the building was considered for energy consumption and comfort taking climate change into account. Consumption was calculated for several years, which made it possible to evaluate the overall consumption after defining assumptions of energy retrofits. The life cycle was also addressed in the LCC. Finally, the performance criterion was limited to LCA in terms of CO₂ emissions (construction and energy consumption) for two reasons. The first is simply related to the importance of this criterion with respect to the greenhouse effect. The second reason concerns the interoperability difficulties between the selected LCA software (EQUER) and TRNSYS simulation tool. LCA can only be carried out *a posteriori* on some optimal solutions. Therefore, seven objective functions (Table 5.14) were considered which can be evaluated using the satisfaction functions defined by the decision maker.

Table 5.14: The objective functions

Environment	Primary energy consumption (E_p): boiler and electrical appliances (pumps, controller and fan)
	CO ₂ emissions over the lifetime (CO_2): they depend on both the decision parameters (systems and envelope) and energy consumption
Cost	Life cycle cost (LCC)
Durability	Number of hours when the temperature in the solar collector exceeds a limit value (T_{max})
	Number of boiler operating cycles (N_{cycle})
Comfort	Thermal comfort in the summer (T_{int}) corresponding to the number of hours when the internal temperature exceeds comfort temperature
	Compliance with the setting temperature for hot water (T_{ecs}) corresponding to the number of hours when the hot water temperature exceeds a temperature level

5.8.1.1.3.2 Decision parameters

The decision parameters for the building envelope and the systems depend closely on the configurations. Each parameter has a min/max variation range. Table 5.15 shows the considered nine decision parameters.

Table 5.15: The decision parameters

Envelope	Wall insulation of façade (LA : 0.1-0.5 m)
	Wall insulation of top floor; ceiling with attic/terrace (IB/IC : 0.1-0.5 m)
	Wall insulation of ground floor (ID : 0.1-0.5 m)
Systems	Collector area (S : 12-56 m ²) and slope ($Slope$: 20-50°)
	Storage volume (V : 1-4 m ³)
	Boiler output rate (P : 70-250 kW)
	Heating system temperature (T : 35, 45, and 60 °C)

5.8.1.1.3.3 Satisfaction functions

In this example, satisfaction functions were used for decision making aid (as shown in Figure 5.27). In the case study of the two buildings, a sigmoid-type satisfaction function was considered for each of the seven performance functions: E_p (primary energy), CO_2 (emissions), LCC (life cycle cost), N_{cycle} (boiler durability), T_{max} (solar system durability), T_{int} (summer comfort) and T_{ecs} (water temperature).

An overall satisfaction was considered by calculating a weighted (using AHP method) average of the satisfaction functions. This overall satisfaction of an individual also considered that a solution with a high standard deviation $\sigma(S_k)$ between the satisfaction functions must be penalized. Overall satisfaction was calculated by:

$$S_g(j) = (\bar{S}_k)_j - \alpha \cdot \sigma(S_k)_j \quad (5.23)$$

where α is a fixed parameter penalizing the dispersion of the satisfactions S_k for each individual j (α was considered -0.2).

5.8.1.1.4 Results

The KR models for each performance function were developed using MATLAB. The optimization was also performed in MATLAB based on GA (using NSGA-II). Transient simulations were performed in TRNSYS where the building was modeled using Type 56 with respect to the envelope. The resulting Pareto front consists of 62 individuals. These optimal solutions can be classified according to the overall satisfaction defined above. Individual 2 had the most efficient solution (see Figure 5.28).

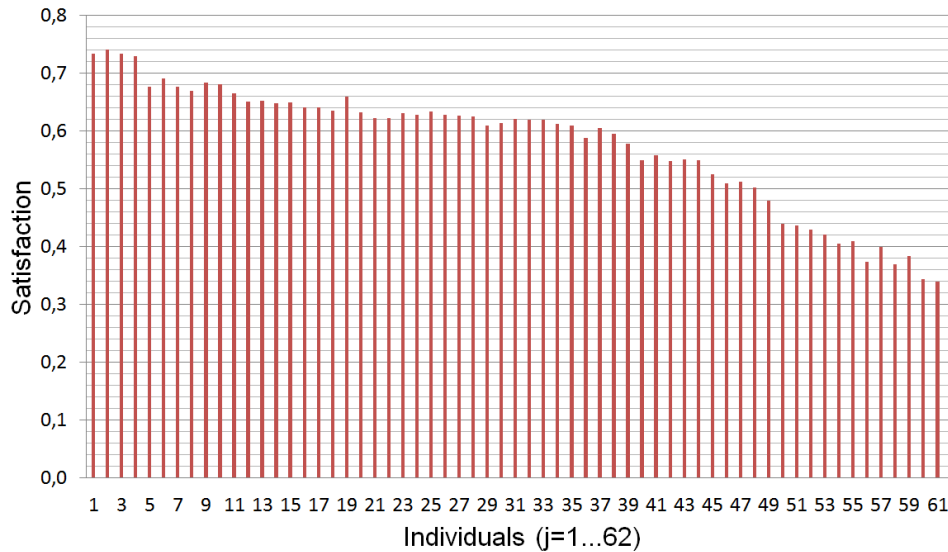


Figure 5.28: The satisfaction functions [0, 1] for all the optimal solutions

The defined overall satisfaction obviously simplifies the problem by transforming a multi-criteria optimization into a single criterion. However, if it is desirable to keep the seven satisfaction functions for the decision maker choice, it will be very difficult to interpret conventional graphical representations of the heat map, matrix scatter plot or radar type. To tackle this issue, network visualization can be used with Gephi software (ForceAtlas 2 algorithm). Each link between the node of a solution and the node of a criterion corresponds to the satisfaction level of the solution (an individual) for that criterion. The closer the individual node is to the criterion node, the better is the satisfaction level. Besides, the diameter of the node of an individual defines the overall satisfaction level. However, the diameters of the nodes representing the criteria are constant. As

shown in Figure 5.29, individual 2 had the largest diameter and therefore had the best overall performance. It is quite close to all the nodes representing the performance functions, excluding the performance related to the comfort (T_{int}). The automatic partition achieved by the Gephi software reveals three large classes (represented by three different colors) in a logical manner. For instance, LCC , E_p and CO_2 belong to the same classification. These three criteria were closely related in the case of the building under consideration, which did not have PV production (it is not an nZEB building). The second and third classifications are respectively related to the two functions for durability (T_{max} and N_{cycle}), and the two functions for comfort (T_{ecs} and T_{int}).

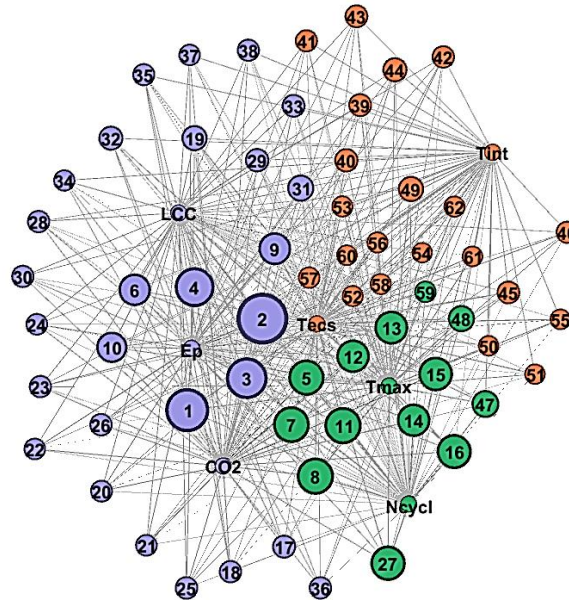


Figure 5.29: Links between the 62 individuals of the Pareto front and the performance criteria where a short distance between an individual node and criterion node means that high level of satisfaction

Another possible representation is to connect the nodes of the optimal solutions with the nodes of the associated values for each decision parameter. For instance, the variation range shown in Table 5.15 can be divided into three for each of the nine decision parameters (+/+/+++). In Figure 5.30, it is easy to see that the best solutions were obtained for:

- A large storage volume ($V+++$)
- A large thermal solar collector area ($S+++$)
- A large slope of collector area ($slope+++$), corresponding to the range 40-50°
- High insulation resistance for the envelope ($IA+++$, $IB+++$, $IC+++$), excluding the ground floor ($ID++$) which should not be very insulated for cost issue
- A low heating system temperature ($T+$), which reduces heat losses
- A non-oversized boiler output ($P+$)

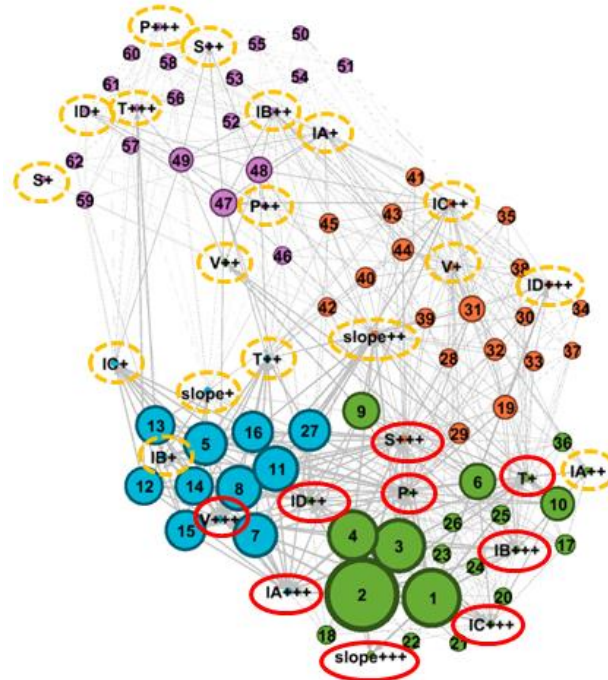


Figure 5.30: The 62 optimal solution nodes linked to the corresponding values of the decision parameters where variation range was divided into 3 partitions of +/+/+++

Comparing solutions 1 and 2 (Figure 5.31), the difference in decision parameters is only related to the insulation thickness at the ground floor (ID_{++} for solution 2 and ID_{+++} for solution 1). A lower thickness for the ground floor results in a lower investment cost and therefore a better *LCC* for solution 2. Figure 5.31 shows that the distance between the criterion *LCC* and the node for solution 2 is shorter than that of solution 1. Therefore, solution 2 had better overall satisfaction.

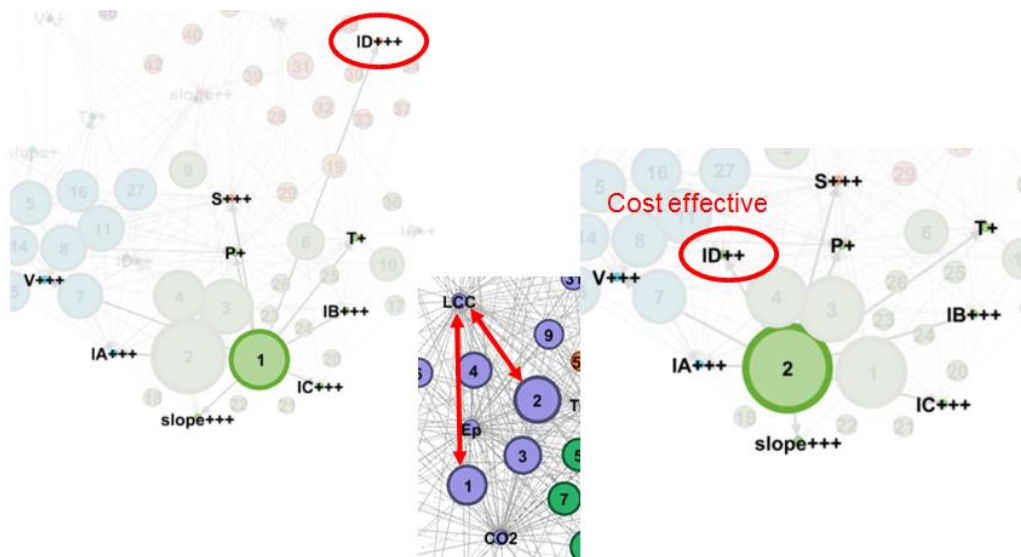


Figure 5.31: Comparison of solutions 1 and 2

Through this example, we can see that network modeling offers a new MCDA method. It is particularly powerful when there are many decision parameters and optimal solutions.

5.8.1.2 Single family house envelope optimization

In the context of the European Union efforts to reduce the growing energy expenditure, it is widely recognized that the building sector has an important role, accounting 40% of the total energy consumption in the EU and 36% of its CO₂ emissions [577]. The energy performance of building directive (EPBD) recast [464] imposes adoption of measures to improve energy efficiency for all new buildings to be nZEB by 2020. This practice represents the first effective way for the implementation of the greenhouse emission reduction policy requirements [578]; however, the challenge of refurbishment of the existing building stock should also be addressed in order to reach the objective of reducing GHG emissions in the building sector by 90% by 2050 compared to 1990 [579]. Moreover, measures related to environmental sustainability could not be pursued without considering the financial feasibility, as nowadays the design of an nZEB is not yet profitable in terms of costs; however, it is recognized that improving energy performance of building is a cost-effective way of addressing the problem of climate change and improving energy security, given the great European energy saving potential [580-582].

Furthermore, even if the results in terms of energy efficiency are evaluated at a global (or at least European) scale, it is remarkable that an efficient nZEB design is strictly related to the local scale. The optimal design solutions, from both energy and cost points of view, depend on many variables such as climatic data, available technologies and materials, population lifestyle, the age of the building and its use (commercial buildings, residential, etc.) [583]. Consequently, EPBD recast has set out that member states ensure that minimum energy performance requirements are set with a view of achieving cost optimal levels for buildings, building units and building elements using a comparative methodology framework established by the European Commission.

This methodology, which is defined in the guidelines [466] accompanying the regulation [584] supplementing the EPBD and in the EU Standard 15459 [467], consists of different steps. First, a reference building (RB) must be identified as a representative model of the national building stock. Secondly, a set of energy efficiency measures (EEMs) must be defined to improve energy performance of the building. EEMs can be combined in packages of measures. Then the energy consumptions related to the various packages of EEMs are calculated through energy simulations, and the costs of the different packages are estimated to identify the one having the lowest global cost and, consequently, representing the cost optimal level. Finally, the distance between the cost optimal performance and the nZEB target can be assessed and evaluated, orienting policies for reducing the distance.

The main challenge of this calculation methodology is to find a balance between two contradictory requirements. On the one hand, all measures with a possible impact on the primary or final energy use of a building should be considered. On the other hand, the calculation exercise should remain manageable and proportionate, as applying several variants to an RB can quickly result in thousands of calculations. Test runs performed for the European Commission [585] revealed that the number of packages/variants arbitrarily selected among the all possible design solutions and applied to each RB should certainly not be lower than 10. Therefore, this approach

clearly cannot guarantee the absolute cost-optimal solution since it explores only some of the available combinations of design options. Clearly, more packages (and variation of the measures included in the analyzed package) result in more accurate calculated economic optimum.

Furthermore, the methodology requires the calculation of investment and replacement costs related to all the building envelope and HVAC system variables as well as the operation cost, such as maintenance and energy costs. Due to the high number of independent variables involved in the calculation, the cost-optimal level is a complex optimization problem, whose objective function is the global cost function. To achieve the optimal solution with less time and computational labor while exploring many design options, a simulation-based optimization method may be used [394]. It consists of a computer-automated model where a building simulation program is coupled to an optimization engine. In this way, the optimization problem is solved using iterative methods driven by optimization algorithms [586] which construct sequences of progressively better approximations to a solution, which is a point satisfying an optimality condition within the search-space.

5.8.1.2.1 Background

Coupling of TRNSYS simulation program with GenOpt (see Section 5.5.12) creates a system of tools and approaches capable of supporting the application of the cost-optimal methodology with high accuracy. In this example, simulation-based optimization methods are investigated with application of the cost-optimal methodology in the French context. The idea is to provide a method which can increase the number of the analyzed design options. The method should be able to (1) deal with a huge number of simulations corresponding to several packages of EEMs, (2) maintain a manageable calculation, and (3) focus on design options which minimize the global cost function. In particular, this example addresses:

- Setting up a simulation-based optimization method for cost optimal analysis,
- Analyzing data related to the French market and creating the cost functions for each selected design variable,
- Finding the French cost-optimal range for the single-family house typology,
- Identifying the most cost-effective measures on envelope system for a given technical system and evaluating the impact of the energy system on the envelope design from a financial point of view.

5.8.1.2.2 System description

The case-study building (CSB) was a two-story high-performance single-family house (see Figure 5.32) located in Amberieu-en-Bugey, in the French Rhône-Alpes region. In terms of sustainable urban design, this building type is less sustainable, since it leads to higher consumption of resources (energy and land) compared to other residential typologies. In the future, the design of new buildings should consider the district perspective and the benefits in terms of resource savings related to more densely populated areas. However, the CSB was selected as a reference since it represents a consistent part of the current French building stock. In fact, 72% of the French useful building areas have residential functionality and around 55% of the total French residential

building stock (25.8 million of dwellings) is composed of two-story single-family houses, of which 60% is located in the H1 climate zone (according to the French regulation, the H1 zone is the northeastern France, including the Rhône-Alpes region).



Figure 5.32: Pictures of the reference building

The CSB benefited from low consumption due to its high efficiency energy system. It is composed of a mechanical dual flow ventilation system combined with controlled air-handling units with thermodynamic recovery. It incorporates an air-to-air reversible heat pump, whose global COP can reach 8 depending on the air flow rate, the compressor speed and the heating power. In winter, the system uses the energy from the exhaust air to heat the fresh air before sending it in the main rooms. In summer, the fresh air is cooled and dehumidified. When the outdoor temperature is cool, an over-ventilation system limits the operation of the heat pump and consequently the energy consumption. Before entering the system, the external air is pre-treated by a Canadian well.

5.8.1.2.3 Methodology

According to the guideline accompanying the regulation supplementing 2010/31/EU, a set of EEMs must be defined and applied to the established RB. The measures selected for this example concern the building envelope system (ES) and the building technical systems (TS).

5.8.1.2.3.1 Building envelope systems

The implementation of envelope-related EEMs may consist of changing the whole envelope technology (e.g. a light-wooden or a massive envelope system) or varying the properties of one or more layers within a defined technology (e.g. wall layer thickness). These EEMs within the same envelope system are expressed in this example through parameters, identifying the geometry features and the construction features which can influence the final energy need of the building. These are referred to the insulation thickness, the window type and dimensions, the solar protection dimension and the amount of internal mass, as represented in Figure 5.33. The range and the step of their variation were set according to regulation requirements (e.g. the minimum window area is set to the limit imposed by the French national regulation), technical feasibility (e.g. the maximum insulation thickness is set to the current technical practice) and market criteria (e.g. the window types are selected among those available on the French market). Table 5.16 reports all the parameters settings for each ES. Window types are reported in Table 5.17. The same parameters

of ES1 were considered also for ES2 and ES3, the only differences in parameters settings are due to technical feasibility and modeling limits of the EIFS package.

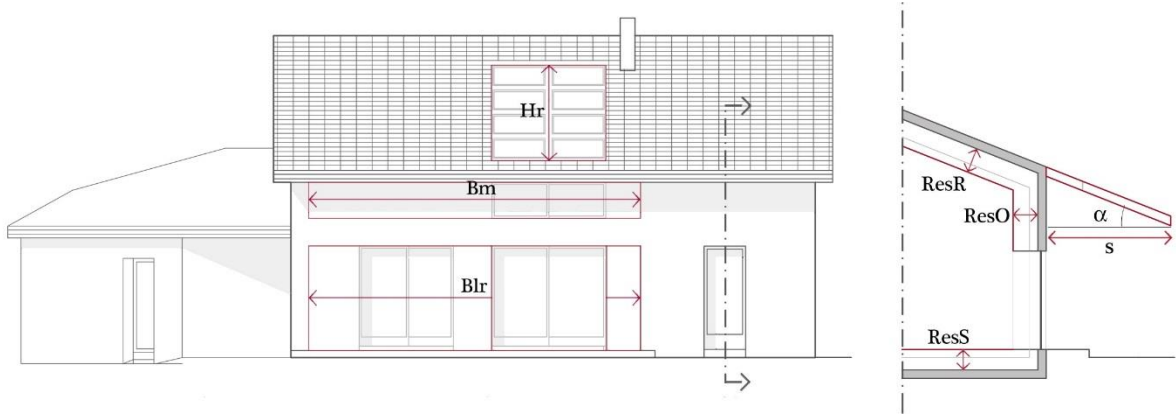


Figure 5.33: Representation of parameters on the south front and section

Table 5.16: Definition, variability range and step for parameters of the envelope systems

	Parameter name and description	Unit	Min	Max	Step	RB
ES1	<i>ResO</i> : Thermal resistance of wall internal insulation	[m ² Kh/kJ]	0.25	5.00	0.25	1.75
	<i>ResR</i> : Thermal resistance of roof insulation layer	[m ² Kh/kJ]	0.25	5.00	0.25	3.50
	<i>ResS</i> : Thermal resistance of slab insulation layer	[m ² Kh/kJ]	0.25	3.00	0.25	2.50
	<i>WT</i> : Window type of north, east and west walls	[-]	1	4	1	3
	<i>WTS</i> : Window type of south wall	[-]	1	4	1	3
	<i>WTR</i> : Window type of roof	[-]	1	4	1	3
	<i>Blr</i> : Ground floor south window width ($h = 2.15$ m)	[m]	2.20	7.80	0.20	4.20
	<i>Bm</i> : First floor south window width ($h = 0.80$ m)	[m]	0.20	7.80	0.20	2.20
	<i>Hr</i> : Roof window height ($w = 2.28$ m)	[m]	0.00	4.72	0.59	4.72
ES2	<i>ResO</i> : Thermal resistance of wall external insulation	[m ² Kh/kJ]	0.25	2.25	0.25	-
	Other parameters are the same as ES1					
ES3	<i>ResO</i> : Thermal resistance of wall additional insulation	[m ² Kh/kJ]	0.25	2.25	3.00	-
	<i>ResR</i> : Thermal resistance of roof additional insulation	[m ² Kh/kJ]	0.25	3.00	0.25	-
	Other parameters are the same as ES1					

Table 5.17: Description of window types used for parameters WT, WTR and WTS

	Type	Description	U-value [W/(m ² K)]	g-value
All	1	4/16/4 Double glazing	2.00	0.70
	2	4/16/4 Double glazing, low emissivity with Argon	1.43	0.58
ESs	3	4/16/4/16/4 Triple glazing	0.70	0.50
	4	4/16/4/16/4 Triple glazing, with Argon	0.40	0.40

5.8.1.2.3.2 Building technical systems

Concerning the building technical systems, four alternatives were selected as EEMs, among those commonly used in France, and modeled in TRNSYS. The TSs include the primary system and the terminals for heating, cooling and ventilation, as reported in Table 5.18. The TS1 is the one having the highest efficiency (variable *COP* up to 8) and corresponds to the one currently used in the CSB and was described earlier. The TS2 is a typical French all-electrical system which is very common in existing residential buildings. It was simply modeled assuming an efficiency of one. The TS3 includes a gas condensing boiler whose design power varies from 4 to 15 kW. Its

efficiency was modeled according to Table 5.18 as a function of its design capacity and operating capacity. Finally, for the pellet boiler TS4 a simple model having a medium efficiency of 0.85 was considered. The efficiency (in terms of EER) of the cooling system of TS2, TS3 and TS4 was assumed to be equal to 3.

Table 5.18: Energy efficiency measures concerning building technical systems (TSs)

Heating and cooling		Ventilation
TS1	Air-to-air reversible heat pump with Canadian well for pretreating air	Mechanical unit with heat recovery
TS2	All-electrical system with electric radiators and cooling fans	Natural
TS3	Gas condensing boiler with radiant heating floor and cooling fans	Natural
TS4	Wood-pellet boiler for heating and cooling fans	Natural

5.8.1.2.3.3 Packages

The correct application of the methodology implies the creation of many packages of EEMs to be applied to the RB. The three envelope systems were combined with the four energy systems in 12 ES/TS combination (see Table 5.19), which were denoted with two numbers indicating ES and TS, respectively. Furthermore, the parameters may assume different values according to their variation range and step. Each set of parameter values within each ES/TS combination is considered a package of EEMs.

Table 5.19: Combination of envelope and technical systems

	TS1	TS2	TS3	TS4
ES1	1.1	1.2	1.3	1.4
ES2	2.1	2.2	2.3	2.4
ES3	3.1	3.2	3.3	3.4

5.8.1.2.3.4 Financial calculations

The financial calculation was carried out according to the global cost method, which is described in the European Standard EN 15459 (see Section 5.3.2). In this example, according to the guidelines [466] accompanying Directive 2010/31/EU, the real interest rate (R_R) is set to 4%. The rate of evolution of prices is set equal to the inflation rate of 2% from the guideline. The calculation period (τ) is equal to 30 years and the related present value factor (f_{pv}) is equal to 17.29.

The choice of the energy system for a building influences the global cost calculation not only for the investment cost, but also for the energy cost. All detailed costs related to the energy system are reported in Table 5.20. The investment cost of each TS is split into supply cost and installation cost, which is expressed in terms of workdays. The investment cost in the third column (C_I) results from multiplying the unit cost (C_U , taken from the estimates provided by the consultancy firm) by the number of units. In some cases, the number of units varies for each simulation run in function of the maximum power (P_{max}) required to satisfy the energy needs calculated by TRNSYS for that building configuration, which depends on the variation of parameters affecting the overall building energy performance. However, when the TS has a variable power, the cost is fixed for all building configurations.

The replacement costs (C_R) calculation results from multiplying the investment cost (C_I) by the discount rate R_d as reported in the Table 5.20. The final value ($V_{f,t}$), reported in the last column

of Table 5.20, is calculated as remaining lifetime at the end of the calculation period (e.g. the remaining lifetime is 10 years when lifespan is 20 years and the calculation period is 30 years) divided by lifespan and multiplied by the replacement cost and referred to the starting year by the appropriate discount rate. When the lifespan of a component is 15 years the final value is equal to 0, as the life of the replaced component end together with the calculation period (30 years).

Table 5.20: Investment, installation and replacement costs of the technical systems

Description	C_U [€]	Number of units	C_I [€]	i [yr]	R_d	C_R [€]	$V_{f,r}$ [€]
All-in-one system	Supply	14,000	1	14,000	20	0.46 6,440	2,170
TS1	Installation	450	2 (workdays)	900	20	0.46 414	140
Radiator ¹	Supply	300	$\text{Var}=\text{int}(P_{\max,\text{heat}}/0.5)+1$	$n*300$	20	0.46 $\text{Var}=C_I*0.46$	$\text{Var}=C_I*0.16$
TS2	Installation	450	2 (workdays)	900	20	0.46 414	140
Condensing boiler ²	Supply (boiler)	7,178	1	7,178	20	0.46 3,301	1,112
and radiant floor	Supply (floor)	978	1	978	20	0.46 450	152
TS3	Installation	450	5 (workdays)	2,250	20	0.46 1,035	349
Pellet boiler ³ and pipes	Supply	7,788	1	7,788	20	0.46 3,582	1,207
TS4	Installation	450	2 (workdays)	900	20	0.46 414	140
Fans ⁴	Supply	1,500	$\text{Var}=\text{int}(P_{\max,\text{cool}}/2.5)+1$	$n*1,500$	15	0.56 $\text{Var}=C_I*0.56$	0
TS2, TS3, TS4	Installation	450	0.5 (workdays)	225	15	0.56 126	0

¹ $P = 0.5$ kW

² $P = 4-15$ kW

³ $P = 2-10$ kW

⁴ $P = 2.5$ kW

Details about calculation of maintenance and energy costs, which are considered as annual costs, are reported in Table 5.21. The energy prices are set according to the current French price levels of a major energy provider and among the electricity fees, the double-time band one is chosen, as it is the most common in residential buildings. The annual energy costs, resulted from multiplying the calculated energy consumption by the energy unit cost, is then multiplied by the present value factor (equal to 17.29 for 30 years of calculation period) to obtain the total energy costs over the calculation period referred to the starting year of calculation. Maintenance costs are calculated as a percentage (values are taken from Appendix A of the European Standard EN 15459) of the investment cost of the TS and then multiplied by the present value factor for 30 years.

Table 5.21: Annual costs calculation assumptions

Type		Unit cost [€/kWh]	Total cost (30 years)
Maintenance	TS1	2.5% C_I	6,441
	TS2	1.5% C_I	$C_I(\text{rad} + \text{fan}) * 0.015 * 17.29$
	TS3	2% C_I	$C_I(\text{boiler} + \text{floor} + \text{fan}) * 0.02 * 17.29$
	TS4	2% C_I	$C_I(\text{boiler} + \text{pipes} + \text{fan}) * 0.02 * 17.29$
Electricity cost	Night (10pm – 7am)	0.0567	$Q_{\text{electricity_night}} * 0.0567 * 17.29$
	Day (7am – 10pm)	0.0916	$Q_{\text{electricity_day}} * 0.0916 * 17.29$
	Contract and taxes	0.0228	$Q_{\text{electricity_tot}} * 0.0228 * 17.29$
Gas	Night and day	0.0570	$Q_{\text{gas_tot}} * 0.0570 * 17.29$
	Contract and taxes	0.0228	$Q_{\text{gas_tot}} * 0.0228 * 17.29$
Pellet	Material	0.0700	$Q_{\text{pellet_tot}} * 0.0700 * 17.29$

5.8.1.2.4 Results

According to the cost-optimal methodology, the results should be analyzed with the following principles:

- All the selected packages of EEMs should be assessed with respect to their financial and environmental impacts.
- The financial optimum is provided by the package with the lowest cost.
- At the same cost level, the package with the lowest energy use should be selected.

Therefore, results are shown in cost-optimal diagrams where the global cost (the objective function) is reported versus the primary energy consumption. The French primary energy conversion factors used for the calculation are 2.58 for electricity, 1 for gas and 0.6 for pellet (considering the French low consumption buildings label conversion coefficient for biomass). All values on the cost-optimal diagrams are normalized to the gross floor area of the heated volume, which is equal to 155 m².

Figure 5.34 reports all the resulted clouds of points and their corresponding cost optimal points. The red line corresponds to the estimated primary energy consumption limit for heating, cooling and ventilation for the French new buildings set by the thermal regulation RT 2012. It is interesting to note that, from the global cost minimization perspective, a higher efficiency of the energy system moves the envelope design towards a less performing envelope design. The two clouds related to combinations 1.1 and 1.3 are partially overlapped and the two optimal points are very close to each other, both leading to high energy performances and low values for insulation parameters. However, the reasons for the low primary energy needs are different. For combination ES/TS 1.1, it is due to the high system efficiency (the medium *COP* is around 4), while for the case of ES/TS 1.4 the 0.6 primary energy conversion coefficient moves the cloud towards lower primary energy consumptions. This advantageous conversion coefficient was established in the context of the French BBC (low consumption buildings) labels, to consider the benefit derived from the use of RES such as biomass. However, the new French thermal regulation RT2012 sets a value of one for all the coefficients of the sources other than electricity since these benefits are not countable yet. Considering a conversion coefficient equal to one, the cost optimal performance of ES/TS 1.4 would be equal to 78.1 kWh/m²year, which is not acceptable for RT 2012 regulation. The same analysis applies for ES2 and ES3, as the clouds acceptable for the French regulation are all related to TS1 and TS4 (the all-in-one system and pellet stove system, respectively), when considering the primary energy conversion coefficient of 0.6 for pellets. In this context, the resulted optimal configuration accepted by the French regulation is referred to ES/TS 3.4, indicating the combination of ES3 (wooden structure) with TS4 (wood-pellet boiler).

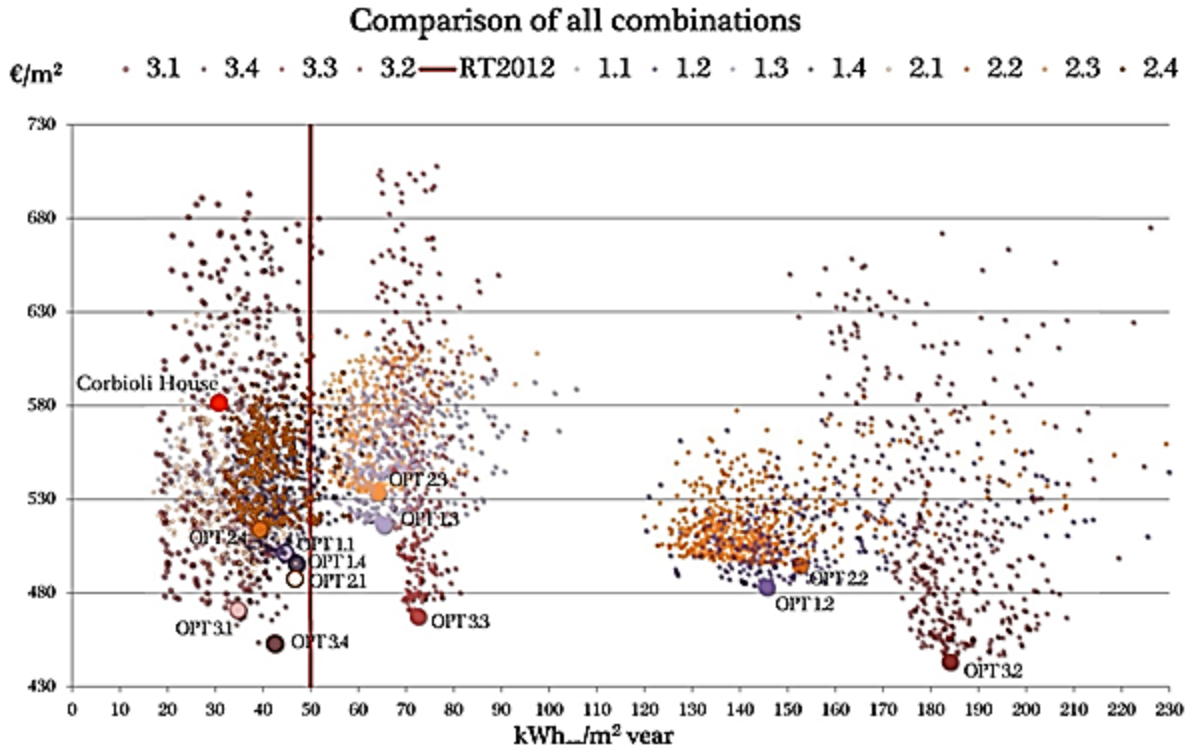


Figure 5.34: All the resulted cost-optimal clouds, with indicated cost optimal levels

However, if the new primary energy conversion coefficients of RT2012 are applied, the only acceptable clouds of points are the ones related to the TS1. In these conditions, the points having the lowest global costs (with respect to points on the same vertical line) are included in the cloud of ES/TS 3.1, which is related to the wooden structure.

Since the regulation is moving towards lower consumption limits, this example highlights that the all-in-one technical system (composed by the most currently advanced energy systems for high-performing buildings) is the best choice both from technical and financial points of view. Therefore, the cost-optimal configuration of the RB should use this type of energy system together with a light wooden envelope, whose decision parameters corresponds to the resulted optimal values.

Table 5.22 reports the parameter values, the energy performance, the global cost and the part of global cost related to energy of four relevant cost-optimal points, each representing a step of the RB optimization. The first column is for the RB, whereas the second column represents the cost-optimized ES/TS 1.1 building configuration (which uses the same energy system and envelope system as the RB, with different parameter values). The third column reports the optimal building configuration which substitutes the light envelope (ES3) to the massive internal insulated envelope (ES1). The last column indicates values related to the ES/TS 3.4 optimal configuration. The energy performance in brackets is obtained for the primary energy conversion factor of one for biomass.

As shown, the OPT 3.1 building configuration leads to the lowest energy performance with a little increase of global cost, fully meeting the regulation requirements. It is composed by low insulation for roof and outwall (it is important to remember that the wooden structure is internally insulated and that the insulation parameter only refers to the additional external insulation layer) and quite consistent insulation (23 cm) for slab. The optimal windows are high performing (type 3) and their dimensions are higher than in the RB.

Table 5.22: Set of parameter values related to relevant cost optimal points

Parameter name and description	Unit	RB	OPT 1.1	OPT 3.1	OPT 3.4
<i>ResO</i> : Thermal resistance of wall internal insulation	[m ² .K.h/kJ]	1.75	0.25	0.25	0.25
<i>ResR</i> : Thermal resistance of roof insulation layer	[m ² .K.h/kJ]	3.50	0.75	0.50	0.50
<i>ResS</i> : Thermal resistance of slab insulation layer	[m ² .K.h/kJ]	2.50	0.75	2.00	0.25
<i>WT</i> : Window Type of North - East -West walls	[-]	3	1	3	4
TS1 <i>WTS</i> : Window Type of South wall	[-]	3	1	3	1
<i>WTR</i> : Window Type of Roof	[-]	3	1	3	4
<i>Blr</i> : Ground floor south window width ($h = 2.15$ m)	[m]	4.20	2.20	2.20	2.20
<i>Bm</i> : First floor south window width ($h = 0.80$ m)	[m]	2.20	1.60	7.80	7.80
<i>Hr</i> : Roof window height ($w = 2.28$ m)	[m]	4.72	0.00	0.00	0.59
Energy performance	[kWh/m ² y]	32.1	45.1	37.1	42.4 (70.7)
Cost related to energy (including technical system)	[€/m ²]	202	209	202	178
Global cost (objective function)	[€/m ²]	582	499	470	453

5.8.2 District level

5.8.2.1 Hybrid community district heating system

In older DHS generations (the first to third generation), high heat loss in the system due to the use of a high-temperature distribution network was considered as a major issue among design engineers. In this regard, more focus was given to enhancing the system efficiency by controlling the system heat loss and subsequently, system optimization was done. As a result, most optimization studies focused on achieving the optimal design by minimizing the system heat loss. However, the new DHS generation (the 4GDHS) utilizes a low temperature distribution network; therefore, achieving higher system efficiency is possible by adopting an appropriate control strategy as well as equipment size optimization. In general, two major design methods can be considered for designing a 4GDHS. In the first method (conventional design method), component sizing is carried out based on the peak load estimated for a typical design day. However, in the second method, optimal equipment size is defined during the design stage using the available optimization tool. Since the conventional design methods mostly result in over-sizing of the equipment and poor system efficiency, the second method (using optimization tool) has received attention among design engineers to design 4GDHSs.

5.8.2.1.1 Background

Previously, DHS optimization was mainly focused on finding the optimal equipment size at the design stage for a given scenario using static optimization algorithms [587-590]. Both user defined codes and commercial simulation software were used to model district components and the interaction between them. In either case, both simulation and optimization processes operate exclusively from one another. In effect, the result of the simulation tool is then processed as the

input file for the optimization tool. By using the non-interactive model, i.e., separate simulation and optimization models (static model), there exists a higher probability of decreasing the effectiveness of the optimization tool towards predicting the optimal equipment size.

In dynamic optimization, on the other hand, the optimization and simulation should be performed simultaneously. Due to the complexity of coupling simulation and optimization tools in dynamic optimization problems, user-defined codes are used for system modeling (modeling the district components and the interaction between them) [591-594]. Since dynamic optimization of the system using detailed user-defined codes are computationally expensive (and in many cases unfeasible), different simplification approaches have been adopted by designers to decrease the computational time. These simplifying approaches are utilized for simplification of district energy models, using the decreased input file by using the representative weather or demand file for the design period instead of using the whole year profile, or a combination of the two.

In this example, a dynamic optimization model is developed which explores optimal equipment size using detailed demand profile. The developed model predicts the detailed demand profile of a DHS. It uses the predicted data along with detailed energy model of the DHS and detailed model of the equipment and interaction between them to dynamically optimize the entire model and subsequently the optimal equipment size is obtained. The equipment size obtained from the model is later compared with the one obtained from the conventional method as well as using a static optimization tool. In this regard, data from an existing H-CDHS with an integrated TES system have been used to optimize its boiler house to minimize its overall cost and CO₂ emission.

5.8.2.1.2 Methodology

TRNSYS was selected as the simulation platform to define the relationship between various system components and to couple the prediction and optimization tools. Besides, a previously developed simplified load prediction method was used to dynamically predict the system demand load [278]. Results obtained from the prediction tool were fed to the TRNSYS file using a text format. The optimization process was then performed for an operational mode by coupling the simulation (TRNSYS software) and optimization tools (MATLAB/Simulink).

5.8.2.1.2.1 Load prediction

To accurately optimize an H-CDHS, the first step is to predict the hourly energy demand profile of the entire H-CDHS, including the energy consumption data and its corresponding losses. There are different ways to obtain a community's energy demand profile: (1) direct measurement, (2) a comprehensive energy simulation tool used when data is absent, or (3) simplified prediction methods for high-level computational costs.

In this example, the simplified 4-step prediction model (presented earlier in Section 4.3) was used to predict energy demand profile of the community [278]. The procedure was previously validated in Section 4.5 using both an inter-model comparison and a series of measured data. Using the validated model, the community demand profile was predicted for two different scenarios:

- **Scenario 1:** optimizing the existing district by considering the demographic distribution regarding users' energy consumption habits.
- **Scenario 2:** optimizing the community as a newly built district using design criteria and thermostat control to simulate the overall energy behavior.

Before performing the optimization scenarios, in the first step, the community demand profile was predicted. To predict the community demand profile, occupants were divided into four different groups based on their energy consumption habits (i.e. non-typical high usage (NTHU), non-typical medium usage (NTMU), non-typical low usage (NTLU) and typical thermostat control usage (TTCU)). Once consumption habits of these groups were available, the prediction model was trained using the proportion of each group within the community.

In Scenario 1, the proportion of the different occupant types within the community remained constant and the results served as a basis of comparison for the optimization process. Leaving occupants demographic distribution untouched, the district energy demand profile for Scenario 1 was predicted using the weather data file measured on site. Scenario 1 has been used (1) to validate the accuracy of the energy simulation tool (TRNSYS), (2) to compare the effect of optimized equipment size and control strategy on energy consumption pattern of the existing community's CO₂ emission and cost, and (3) to calculate the potential cost and emission reductions.

Conversely, in Scenario 2, both weather file and occupants' demographic distribution were replaced by design condition. In Scenario 2, redefining the weather file (i.e. TMY3) as the prediction model input and training it based on the design condition, typical thermostat control usage (TTCU) profile, can show the potential savings in the initial investment cost of major equipment (boilers and thermal storage) post-optimization. The assumption works better for newly built communities (design stage) with unknown energy use behavior of occupants. Having no data regarding potential district users, the district load was determined based on the energy required to keep the buildings at a thermostat set point defined by a code for each building type. After obtaining both scenarios typical usage behavior, a prediction model was trained based on the fraction of each community group's data. Using the design weather data (i.e. TMY) and onsite measured weather data, the demand heating profile for both scenarios was predicted.

5.8.2.1.2.2 *Energy modeling*

To predict the district energy demand profile and the interaction between its different components, TRNSYS was used and the majority of district network components and their interaction was defined. To represent other components, such as biomass boilers and building stock, existing types in TRNSYS were modified. In general, TRNSYS has three major loops:

- **Generation loop**

The first loop (generation loop) consists of the auxiliary gas and biomass boilers, a controller, and a heat exchanger, which feeds energy into the system, as shown in Figure 5.35. Since no specific biomass boiler type exists in TRNSYS, Type 700 was modified to represent the biomass

boiler by adjusting its efficiency, partial efficiency and the control signal. After adjusting the boilers' type, two controllers were assigned to the generation loop to adjust the flow pattern between the generation/consumption loops and the storage loop. The first controller compared the predicted demand load of the network with the total capacity of the boiler house and the need for the TES system as a backup. The second controller decides which boiler (biomass or gas) should provide the required energy.

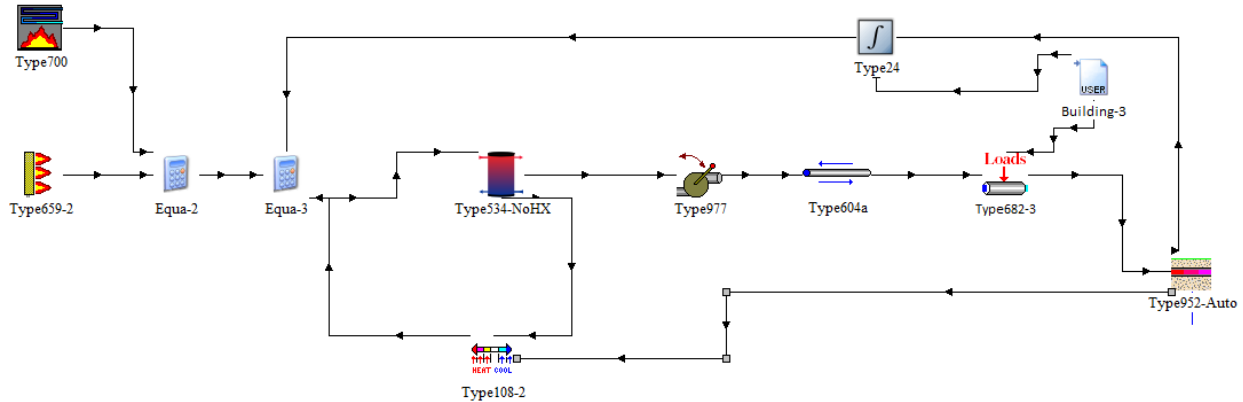


Figure 5.35: Simultaneous charging and discharging configuration

- **Consumption loop**

The consumption loop was constructed with Type 682, which represents the demand profile of all units (Figure 5.35). This type reads the predicted demand profile through an external link containing the predicted results. The distribution network heat loss was modeled using Type 952.

- **Storage loop**

The storage loop was formed with two different configurations, the first of which was modeled by simultaneously charging and discharging the thermal storage (see Figure 5.35).

In other words, both the boiler house and distribution network were connected to the TES system. While the boiler house provided energy to the TES system, the latter supplied the energy to the distribution network. The second configuration was modeled using a step-wise energy storing procedure (Figure 5.36). Here, a controller monitored the direction of the flow to/from the TES tank. As a result, the tank could be either charged or discharged. More detailed explanation on the controller will follow in the next section.

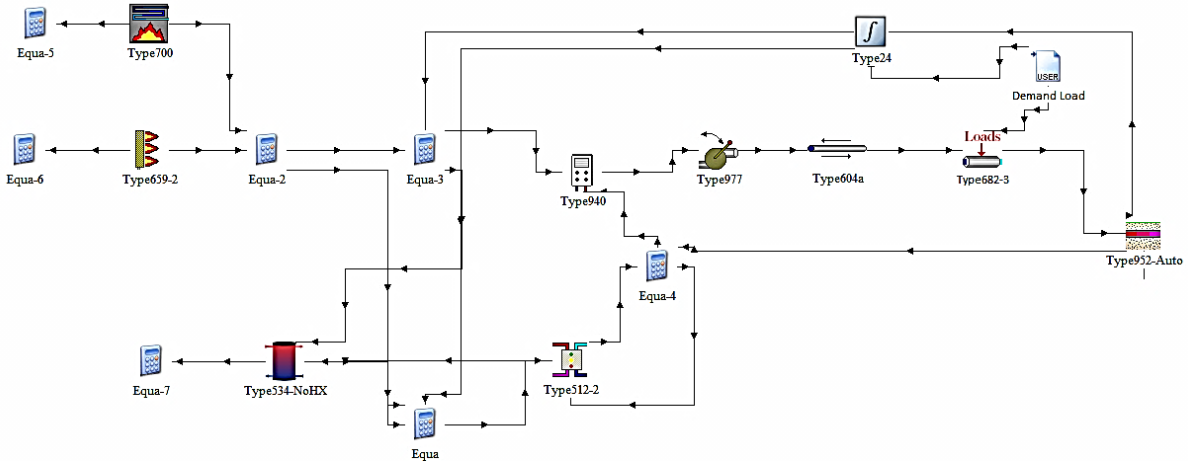


Figure 5.36: Step-wise charging and discharging configuration

Comparing the preliminary results obtained from the total heat loss of different configurations, it is inferred that the step-wise charging and discharging configuration had a lower heat loss than simultaneous charging/discharging configuration due to the TES system size and flow direction. Moreover, the step-wise charging and discharging configuration has a higher overall energy efficiency compared with the simultaneous charging/discharging due to the ON/OFF frequency of the generation loop in this configuration. As a result, the second configuration has been used as a base for optimization in this example.

5.8.2.1.2.3 Optimization formulation

For the design stage, a dynamic multi-objective optimization method was chosen to size the main components of the district network boiler house in the two defined scenarios. The model was based on mixed linear complementarity problem (MLCP) to minimize the objective functions (investment and operational cost or LCC and CO₂ emission). To improve model accuracy, other input data and model characteristics, including minimum and maximum output level constraints and partial load efficiencies, were defined on an hourly basis. The system operational and fuel costs were also considered.

A controller type (Ctrl-3) (see Figure 5.36) was developed and used in developing the TRNSYS model to compare the energy generated at each time-step with that in the boiler house (Ctrl-2) (see Figure 5.36) in accordance with the network demand load (Type 24) and flow direction. By comparing the demand load and generation capacity, controller first fed the network and then it decided whether to use the disparity between generation and demand to charge or discharge the TES. This implies that the controller regulated flow direction based on the general heat balance equation, while other constraints (e.g. minimum operative temperature ($T_{TS}(t)$) were set for the TES to ensure a minimum required temperature for DHW usage:

$$\sum_{n=1}^N Q_{Gen}(t,n) + Q_{TS,Ch}(t) - Q_{TS,Dis}(t) \geq Q_{Net}(t) \quad (5.24)$$

$$Q_{Net}(t) = Q_{BLDG}(t) + Q_{Losses}(t) \quad (5.25)$$

$$\text{If } : Q_{Gen}(t,n) \geq Q_{Net}(t) \rightarrow \begin{cases} Q_{Net}(t) \longrightarrow Loop_{DN}(t) \\ Q_{Gen}(t) - Q_{Net}(t) \longrightarrow Q_{TS,Ch}(t) \end{cases} \quad (5.26)$$

$$\text{If } : Q_{Gen}(t,n) < Q_{Net}(t) \rightarrow \begin{cases} Q_{Gen}(t) \longrightarrow Loop_{DN}(t) \\ Q_{TS,Dis}(t) : -Q_{Net}(t) - Q_{Gen}(t) \longrightarrow Loop_{DN}(t) \end{cases} \quad (5.27)$$

The general equations used for TES modeling, such as total energy at different time-steps and boundary conditions applied to it were:

$$Q_{TS}(t) = Q_{TS}(t-1) + Q_{TS,Ch}(t)\eta_{Ch} - Q_{TS,Loss}(t) - \left(\frac{Q_{TS,Dis}(t)}{\eta_{Dis}} \right) \quad (5.28)$$

$$Q_{TS}(t) \geq 0 \quad (5.29)$$

$$Q_{TS,Loss}(t) = UA[T_{TS}(t) - T_{OA}(t)] \quad (5.30)$$

$$T_{TS}(t) = T_{TS}(t-1) - \left[\frac{Q_{TS,Dis}(t)}{\eta_{Dis} \cdot V \cdot C_{p,w} \cdot \rho_w} \right] + \left[\frac{Q_{TS,Ch}(t)\eta_{Ch}}{V \cdot C_{p,w} \cdot \rho_w} \right] \quad (5.31)$$

$$T_{TS}(t) \geq 70 \quad (5.32)$$

After setting up the controllers, the optimization objective function was set up in the aim of optimizing the size of the biomass boiler(s) and TES system, and minimize the current net cost and CO₂ emissions:

$$\text{Min}\{Obj(C, E)\} \quad (5.33)$$

where C and E are the cost and emission objectives. To make the objective function linear and convert it from 2D to 1D, the optimization was employed using:

$$Obj(C, E) = \alpha \left(\frac{C}{C_0} \right) + \beta \left(\frac{E}{E_0} \right) \quad (5.34)$$

where α and β are the cost and emission importance factors in final objective function. The cost associated function considers the initial cost of the entire H-CDHS in addition to the present worth of the life cycle operational cost. To define the initial cost, the main boiler house equipment was divided into two modular modifiable parts (boilers and TES) and fixed non-modifiable equipment

(pumps and underground distribution pipelines). Only the modular modifiable equipment cost was considered in the initial cost function. The initial cost of fixed non-modifiable equipment was excluded. For operational costs, the present fuel life cycle value required for generating heat, the selling price of energy and the buyout price of energy for surrounding houses for a 30-year period were considered.

$$PV_{OC} = OC_{Annual} \left[\frac{(1+i)^n - 1}{i(1+i)^n} \right] \quad (5.35)$$

where i and n are the annual interest rate and year number, respectively, and OC_{Annual} is the annual operation cost. The cost function was defined as:

$$C = IC + \left[\sum_{n=1}^N \sum_{m=1}^M FC_{n,m} (1+i)^{-n} \right] - \left[\sum_{n=1}^N IN (1+i)^{-n} \right] + \left[\sum_{n=1}^N \sum_{m=1}^M E_{tax,n,m} (1+i)^{-n} \right] \quad (5.36)$$

where IC is the linearized initial cost of the boiler house, n is the number of the year, FC is fuel costs of different boilers, m is the boiler number, IN is the annual income from selling heat to off-site users, and E_{tax} are the energy taxes. The initial investment cost included the fixed and proportional variable expenses. The fixed component included the market value of the smallest size of the equipment available on the market while the proportional cost was determined by linearizing the extra cost associated with the higher capacity of the equipment:

$$IC = \left[\sum_{m=1}^M (IC_m + LC_m ExCap_m) \right] + LC_{TS} Cap_{TS} \quad (5.37)$$

The second objective function was defined to minimize the total CO₂ emission. The emission associated function was calculated as:

$$E = \sum_{n=1}^N \sum_{m=1}^M (E_{n,m} V_{n,m} PRFE_n + IE_{Aux} V_{Aux} PRFIE) \quad (5.38)$$

where $E_{n,m}$ represents the fuel emissions (kg CO₂/kg fuel) used for each boiler (n) in a year (m) of the operation, IE_{Aux} is the emission of the imported energy fed to the system from outside in month (m) of the operation (kg CO₂/kg fuel), $PRFE_n$ is the primary resource factor of the fuel, and $V_{n,m}$ is the fuel volume (m³) used in each month (m) by the boiler (n). When calculating the costs, the wood price was discounted to consider the governmental incentive on the price of wood pellets to encourage the small community to use biomass boilers.

5.8.2.1.3 Results

In this section, the results for each scenario is presented. Scenario 1 was defined based on the current situation of the H-CDHS regarding occupants behavior. Keeping a similar occupancy distribution to that of a real case scenario, the potential annual cost saving and CO₂ emission of the district over its life cycle was determined using the optimal equipment size and flow control (Table 5.23).

Table 5.23: Optimization results for Scenario 1

Technology	Existing situation	Scenario 1
Biomass boiler	870 kW	477 kW
Auxiliary boiler	1.3 MW	0.609 MW
Thermal storage	50 m ³	16.3 m ³
Peak heating load	1300kW	978 kW
Biomass percentage of peak	66.9%	49%
Percentage from biomass	NA	95%

The optimization results for this scenario clearly show that the boiler capacity, biomass or auxiliary boiler are about 40% of the peak demand load. Considering that only one boiler operates at a time, this fact is only achieved by utilizing a TES system, which balances the demand and supply heat between the generation and consumption loops.

Comparing the optimized model results with field measurements show a dramatic drop in CO₂ emission (171.9 tons of CO₂/year) as well as a considerable reduction in the total cost of the system (79,056 £/year). These cost and CO₂ reductions are partially due to the lower efficiency of the oversized equipment working under partial load while other parts can be associated to the non-optimal control strategy of the system and missing TES.

Since specific weather data and occupants' behavior were considered in the Scenario 1 with existing data for 2016-17, the demand energy load of the community could change anytime based on the number of tenants or weather conditions. Consequently, after optimizing the system and determining the optimal equipment size, two new cases (high and low usage) were defined to study the effects of change in community demand load on boiler house performance. These cases included a change in the fraction of occupant types in the community compared with the existing condition. In the high usage case, the fraction of NTLU and NTMU users dropped, adding to NTHU and TTCU users to represent a higher demand load (see Table 5.24). In low usage case, the number of NTHU users dropped and added to the lower energy consumers such as NTLU and NTMU (see Table 5.24).

Table 5.24: Fraction of the occupants' types in different scenarios

	Scenario 1	High usage	Low usage
NTLU	16%	10%	23%
NTMU	24%	15%	39%
NTHU	53%	65%	33%
TTCU	5%	10%	5%
Peak Load	978 kW	1,086 kW	884 kW

By changing the fraction of occupants, the energy demand profiles of the newly defined cases were predicted and fed to the energy model (see Figure 5.36). The boiler house equipment size remained similar to the Scenario 1. After modeling these newly defined cases, the system performance under new conditions was determined. Comparing the percentage of the biomass boiler and TES, which can cover the demand load of the community between the Scenario 1 and high usage case (see Table 5.25), shows that in the High scenario with 12% higher pick, the percentage coverage time by biomass boiler dropped by a negligible percentile of 1.1%.

Table 5.25: Performance of the optimized system under new demand profile load

Technology	Low scenario	Scenario 1	High scenario
Biomass boiler	477 kW	477 kW	477 kW
Auxiliary boiler	609 MW	609 MW	609 MW
Thermal storage	16.3 m ³	16.3 m ³	16.3 m ³
Peak load	884 kW	978 kW	1,086 kW
Biomass percentage of peak	54%	49%	44%
Percentage from biomass	97.8%	95.0%	93.9%

In Scenario 2, the weather file was changed, and the occupant distribution was altered to the TTCU to represent the design criteria for newly build buildings. Table 5.26 presents the optimal equipment sizes, resulting from the optimization of the boiler house for Scenario 2.

Table 5.26: Optimization results for Scenario 2

Technology	Existing situation	Scenario 2
Biomass boiler	870 kW	661 kW
Auxiliary boiler	1.3 MW	0.738 MW
Thermal storage	50 m ³	32.8 m ³
Peak heating load	1,300 kW	1,189 kW
Biomass percentage of peak	66.9%	55.6%
Percentage from biomass	N/A	98.8%

Similar to Scenario 1, the capacity of the boiler optimal size, biomass and auxiliary boiler was used less than 60% of their capacity to respond to the peak demand load. While using static optimized sizing tools such as Biomass Boiler Sizing Tool (version 6.8.2) for a same coverage percentage (98.8% coverage) suggested the biomass boiler with the capacity size of 62% of the peak load and 40.5 m³ TES tank. Table 5.27 presents the equipment size and cost associated with each design method.

Table 5.27: Comparison of the equipment size, cost for different design strategies

Technology	Conventional	Static optimization tool		Proposed dynamic optimization	
		Size	Size reduction [%] *	Size	Size reduction [%] *
Biomass boiler [kW]	870	737	15.3%	661	24.0%
Auxiliary boiler [MW]	1.3	0.891	31.5%	0.738	43.2%
Thermal storage [m ³]	50	40.5	19.0%	32.5	35.0%
Cost [£]	734,440	602,224	18.0%	538,372	26.7%

*Reductions calculated comparing with conventional method

Considering that only one boiler operated at a time, 98.8% coverage by biomass boiler was achieved using only TES to balance between the generation and consumption loop. As shown in Table 5.27, this solution can reduce the size of both auxiliary and main biomass boilers into a fraction of their original size and, as a result, decrease the system heat loss while improving the district's energy efficiency. The reduction in major equipment size of the district using the proposed dynamic optimization method caused a £196068 or 26.7% drop only in the initial investment cost of the system. Moreover, knowing that the partial capacity efficiency of the biomass boiler is lower than its efficiency in the full capacity, two scenarios could be assumed for a non-optimal size equipment. First, the biomass boiler operates at its full capacity all the time while keeping the generation efficiency at maximum value. This can result in generation of an

excessive amount of unused heat, which eventually is accounted as loss. Second, the boiler operates at partial load only to meet the network demand. This decreases generation efficiency due to a lower partial capacity efficiency of the boilers [595]. In both scenarios, the overall system efficiency drops.

5.8.2.2 Piecewise linear characterization curves for energy optimization

The application of energy system optimization at the district level can lead to tangible infrastructural decisions by designers. Considering this, energy systems must be realistically represented such that results can reliably direct the decision-making process. Most current models use MILP to optimize energy systems at the district level. In addition to allowing fast solutions of large-scale problems, MILP models can efficiently represent energy distribution networks. However, they are unable to handle nonlinear characteristics of energy supply technologies. Cooling technologies particularly exhibit nonlinearity in their operation, when operating below nominal load and at different external/internal temperatures. For instance, in a study [596], commercial properties were not considered for optimization in MILP due to the need to model cooling technologies. Metaheuristic techniques are used to include system nonlinearities, but can become intractable for large-scale problems, taking far longer than MILP to reach a reasonable solution [597].

By describing a nonlinear curve of an energy supply technology as multiple connected linear pieces, it is possible to compromise between model fidelity and computational efficiency. Bicubic and cubic technology part-load curves could be represented in piecewise form [598]. In fact, piecewise curves could contain up to ten pieces without significantly affecting computational time. An important factor is the location at which pieces meet (the “breakpoints”) [598]. Piecewise linearization was undertaken to compare MILP and metaheuristics for operation schedule optimization [597]. Six breakpoints were applied to linearize part load curves, specifically located at discontinuities and the point of maximum efficiency. The subsequent piecewise MILP model led to an objective function value similar to the same system optimized metaheuristically with nonlinear curves.

5.8.2.2.1 Background

In this example, a more complex case is presented while investigating breakpoint positioning. A sequential least-squares programming (SLSQP) algorithm is used to minimize the error between piecewise and nonlinear technology part-load consumption curves. This nonlinear optimization is compared to both placing pieces equidistantly along the x-axis and to a single value for efficiency (SVE). At full load, all curves converge on the nominal efficiency of a technology; however, at any part-load value it is possible to quantify the error between the “actual” nonlinear case and “expected” linearized cases. The minimization of this error is compared to computational time penalty when applied to a district energy system case study.

5.8.2.2.2 System description

A district planning case is considered, due to the non-negligible requirement for electricity, heating and cooling when combining different building types. This district is notional and consists

of 10 domestic properties, one large hotel, one large office, and one power plant (Figure 5.37). Within the district, a range of technologies is available to meet demand of each energy type (Table 5.28). Distribution networks exist for low voltage electricity, gas, and heat. Table 5.29 provides further information on attributes of each property type. Multiple technologies exist to meet each type of energy demand. In this case study, the technology choice facilitates the need for optimization, due to different energy interdependencies. Grid electricity (GE) and the boiler (NB), air source heat pump (AHP), and electric chiller (EC) can provide their respective energy demands without interdependency but have relatively high generation costs. Solar photovoltaic (PV) and solar thermal (ST) panels benefit from government subsidies, such as the feed-in tariff, but have fixed output once maximum capacity has been selected and the available roof space is limited. CHP produces both heat and power simultaneously, giving a low generation cost but a high initial capital investment (including a district heat network), while the heat recovery absorption refrigerator (HRAR) can be powered by either waste heat or gas. Finally, storage facilities exist for each energy type. By temporally decoupling supply and demand, storage reduces the effect of interdependencies. CHP can produce electricity without worrying about heat demand, and the PV and ST supply can be maximized knowing that all production can be effectively used on-site.

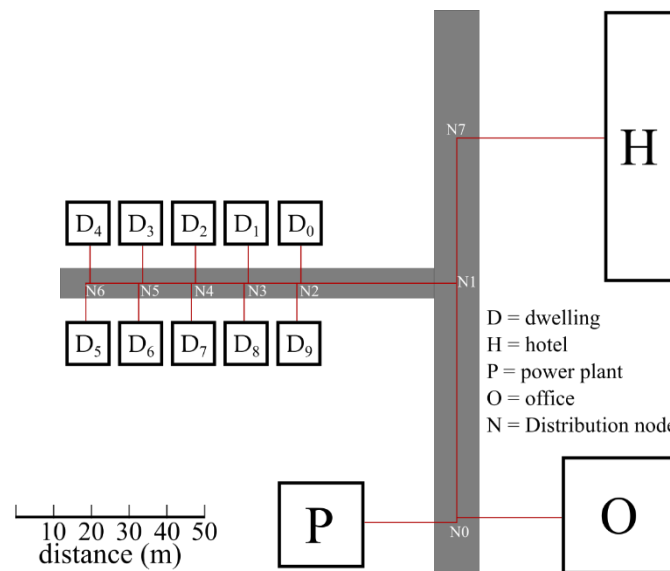


Figure 5.37: Graphical representation of the case study district network

Table 5.28: Model supply technologies and their consumption/production energy

Technology	AHP	EC	HRAR	CHP	NB	PV	ST	B	TES
Consumption	E	E	G, H	G	G	S	S	E	H/C
Production	C	C	C	E, H	H	E	H	E	H/C

Technology keys: AHP: air source heat pump, EC: electric chiller, HRAR: heat recovery absorption refrigerator, CHP: combined heat and power, NB: boiler, PV: photovoltaic, ST: solar thermal

Consumption/production keys: E: electricity, G: gas, S: solar radiation, C: cooling, H: heating

Table 5.29: Characteristics of the buildings in the case study district

		Dwelling	Hotel	Office	Plant
Annual energy demand (MWh)	Electricity	7.2	1,595.5	481.3	0
	Heat	17.5	1,641.6	86.5	0
	Cooling	0.0	1,757.9	99.1	0
Available roof area (m ²)		130	1300	900	0
Available technologies		NB, PV, ST, B, TES	mCHP, NB, PV, HRAR, AHP, EC, ST, B, TES	NB, PV, ST, HRAR, AHP, EC, B, TES	CHP, GE

Keys: AHP: air source heat pump, EC: electric chiller, HRAR: heat recovery absorption refrigerator, CHP: combined heat and power, NB: boiler, PV: photovoltaic, ST: solar thermal

To create a notional district, data on energy demand, technology characteristic curves and costs have been brought together from multiple sources:

- The district is located in the southeastern England, UK. However, due to availability, U.S. Department of Energy representative building demand data [599] is used to acquire hourly heat, cooling and electricity demand of representative buildings. Seattle, Washington climate conditions were chosen for climate similarity with London, UK.
- Characteristic curves for technologies are based on recommendations from society of heating, air conditioning and sanitary engineers of Japan (SHASE) [600]. It is assumed that energy supply technologies do not vary drastically between countries.

Costs curves are calculated based on values given in the SPON'S mechanical and electrical services price book [601]. Storage device costs have been aggregated from online suppliers.

5.8.2.2.3 Methodology

5.8.2.2.3.1 Piecewise linearization

Typically, in energy modeling, the efficiency of a technology is given as a single value based on nominal conditions [494, 602, 603]. In reality, efficiency varies depending on the output of the technology as a function of its maximum capacity, among other factors [604]. This nonlinearity can be addressed by metaheuristic optimization, which allows nonlinear inputs. However, given the non-deterministic nature of metaheuristic methods, mathematical programming (usually in the form of MILP) is still the dominant energy modeling method. To integrate nonlinear technology characteristics with MILP, it is possible to approximate a nonlinear curve by segmenting it into several straight lines. These straight lines create a linear but discontinuous curve which can be handled in a linear program. For application within the MILP environment, two approaches are discussed in this section: special ordered sets and constraint bound.

Special ordered sets of type 2 (SOS2) [605] are often used in MILP to piecewise linearize. Sampling points ('breakpoints') x_i ($i = 1, \dots, n$) are defined along a curve, including the start and end of the curve, with corresponding y-axis values $f(x_i)$ ($i = 1, \dots, n$) (Figure 5.38). A continuous decision variable, α_i is associated with each breakpoint i , such that $\alpha_i \in [0,1]$ ($i = 1, \dots, n$). By defining the α variables to be SOS2, constraints are applied so only two adjacent α variables can be non-zero at any time. For any decision variable x , the corresponding decision variable value of $f(x)$ is calculated by interpolating from adjacent breakpoints $(x_i, f(x_i))$ and $(x_{i+1}, f(x_{i+1}))$, based on

the relative weighting applied by α_i and α_{i+1} . In energy planning, part-load efficiency is a function of two decision variables of load rate and maximum capacity. If maximum capacity is a discontinuous variable, then an SOS2 can be described for discrete values of capacity.

If maximum capacity is a continuous variable, more complex methods are required, but special ordered sets are still applicable. The 3D surface describing the relationship between maximum capacity (x), load-rate (y) and consumption ($f(x, y)$) can be discretized. The most common approach is to have n breakpoints x_1, \dots, x_n on the x axis and m sampling points y_1, \dots, y_m on the y axis [606] where $f(x, y)$ is evaluated for each breakpoint. Any point (\bar{x}, \bar{y}) can be evaluated within the rectangle bounded by (x_i, y_j) , (x_{i+1}, y_j) , (x_i, y_{j+1}) , and (x_{i+1}, y_{j+1}) , which contains two triangles created by its diagonal $[(x_i, y_j), (x_{i+1}, y_{j+1})]$ (Figure 5.39). By convex combination of the function values evaluated at the vertices of the triangle containing (\bar{x}, \bar{y}) , $f(\bar{x}, \bar{y})$ can be ascertained.

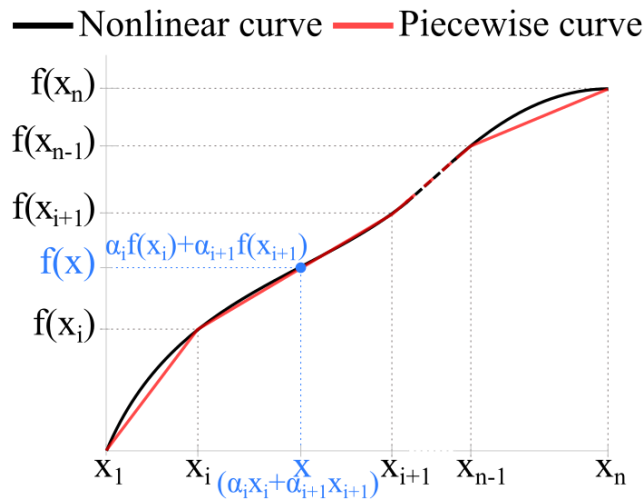


Figure 5.38: Graphical representation of SOS2 piecewise linearization where $f(x)$ is the sum of weighted values $\alpha_i f(x_i)$ and $\alpha_{i+1} f(x_{i+1})$, with all other values of α being zero

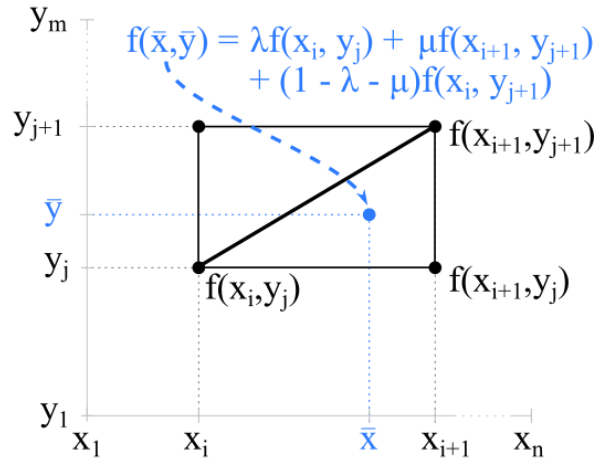


Figure 5.39: Graphical representation of 3D piecewise linearization where $f(\bar{x}, \bar{y})$ is the sum of weighted decision variables λ and μ applied to $f(x_i, y_j)$, $f(x_{i+1}, y_{j+1})$ and $f(x_{i+1}, y_j)$

In creating special ordered sets, many new decision variables are defined, more so when a 3D surface exists. This inevitably increases computational time, perhaps beyond what is feasible for a given problem. In certain cases, it is also possible to force a continuous decision variable to follow a piecewise curve, by applying constraints of the form $y = m x + C$, as depicted in Figure 5.40a. The constraint lines intersect the nonlinear curve where the gradient (m) equals the curve instantaneous gradient. In the case of energy systems, the global minimum will only exist where each technology has chosen to minimize its consumption at every given value of energy output. This means that the consumption curve given in Figure 5.40a will always follow the lower bound, which describes the piecewise curve. However, if the gradient of the technology characteristic curve is not strictly increasing/decreasing, this method cannot function. Figure 5.40b shows that certain lines describing the piecewise curve will override others at incorrect segments of load rate, due to the changing direction of gradient. Here, the consumption curve does not describe the piecewise curve. Although limited in its use cases, this method can also be extended easily to the 3D case, where the constraints are of the form $f(x, y) = m y + C x$, given a maximum capacity (x) and load-rate (y). On inspection of the characteristic curves used in this example, most met the gradient criterion for this method. The only technology which did not was the CHP, which has an undulating gradient when describing both its gas consumption and its heat output. However, as will be discussed in the next section, it is possible to account for this when optimizing the piecewise curves, to allow the bound by constraints method to viably be used for solving the given problem.

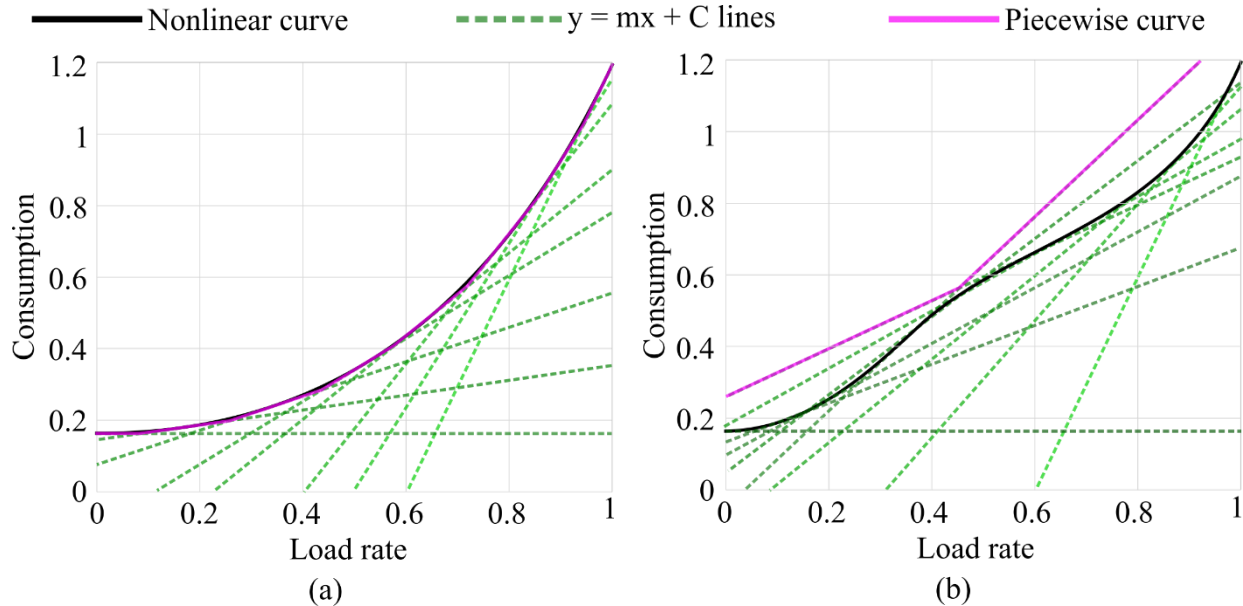


Figure 5.40: Application of bounding a technology nonlinear curve under multiple straight lines to create a piecewise linear curve where (a) shows its effective use on a curve of continuously decreasing gradient, while (b) shows its ineffectiveness when applied to a more complex curve

5.8.2.2.3.2 Optimization

For a limited number of breakpoints, there will be at least one optimal placement to describe a piecewise curve which best fits the nonlinear curve. The process of locating these breakpoints optimally can be simplified by automation. The piecewise curve with least error relative to the nonlinear curve, for a given number of breakpoints, can be ascertained when optimizing. Additionally, the constraint that the gradient must be strictly increasing or decreasing can be applied, creating piecewise curves which meet the requirements set out earlier.

Breakpoint allocation is undertaken during model pre-processing, by parameter optimization. Heuristic algorithms have been used to piecewise linearize [607, 608]. In this example, SLSQP [609] is used to minimize the *RMSE* between each nonlinear curve and its piecewise counterparts. To improve the chances of reaching the global optimum, 20 runs were undertaken for each minimization. This process took 17.1 seconds to optimize 108 piecewise curves describing characteristics of 8 technologies (27 nonlinear curves, three to six breakpoints). For the case of the EC, Figure 5.41a shows the resulting 5-breakpoint curve. Curve fit is better when breakpoints are optimized, most notably in the trough. Any form of piecewise linearization is an improvement on the SVE case, although there is continual improvement on error minimization when optimizing breakpoint location, as Figure 5.41b depicts for the EC.

Some technologies, such as the boiler, have a relatively static efficiency over the operating range. In this case, there is little advantage to piecewise linearize, and even less reason to undertake parameter optimization. Cooling technologies tend to function more nonlinearly. This nonlinearity can be a barrier to including cooling in a linear program [596], although it is usually considered to be caused by system temperatures rather than variable load-rate. From Figure 5.41a it is evident

that the EC acts nonlinearly with variable load rate. However, Figure 5.42 shows this nonlinearity is not as pronounced for other cooling supply technologies, unless operating at low load rates. Below a distinct discontinuity, the energy consumption becomes constant, irrespective of output. For the CHP, there is a reasonable disparity between the realistic operation and SVE, particularly when considering the heat to power ratio (Figure 5.43). The CHP characteristic curves are also not strictly increasing/decreasing which is not apparent for the other technologies. The result of this difference can be seen in the difference between the two optimized curves. However, the difference is relatively small, becoming non-negligible only for parts of the heat to power (HTP) ratio curve.

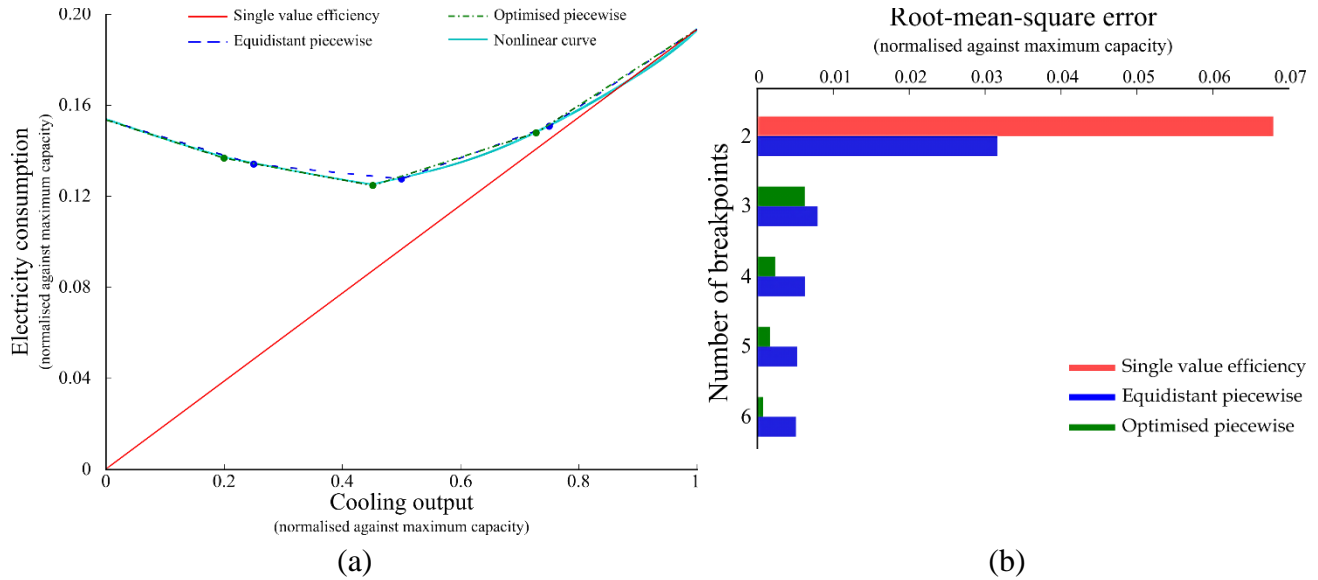


Figure 5.41: Comparison of different methods to describe electricity consumption of an EC, from nonlinear to SVE where (a) shows consumption curve and piecewise linearization with five breakpoints, (b) shows root-mean-square error between the methods and the nonlinear curve

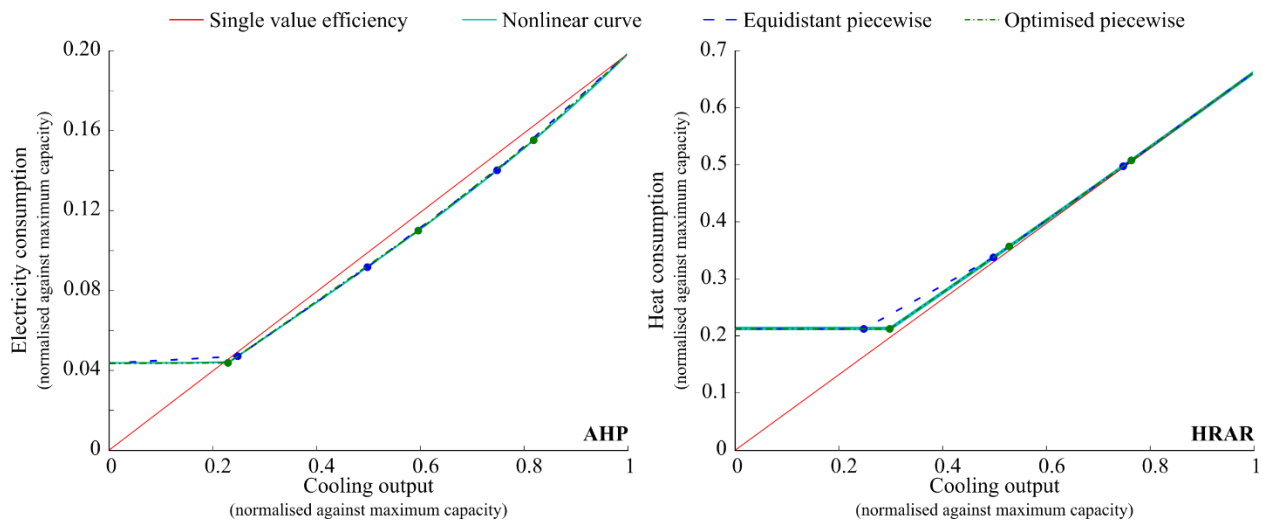


Figure 5.42: Comparison of different methods for describing the primary fuel consumption of an AHP and HRAR, from nonlinear to SVE, at different load rates where piecewise curves have five breakpoints

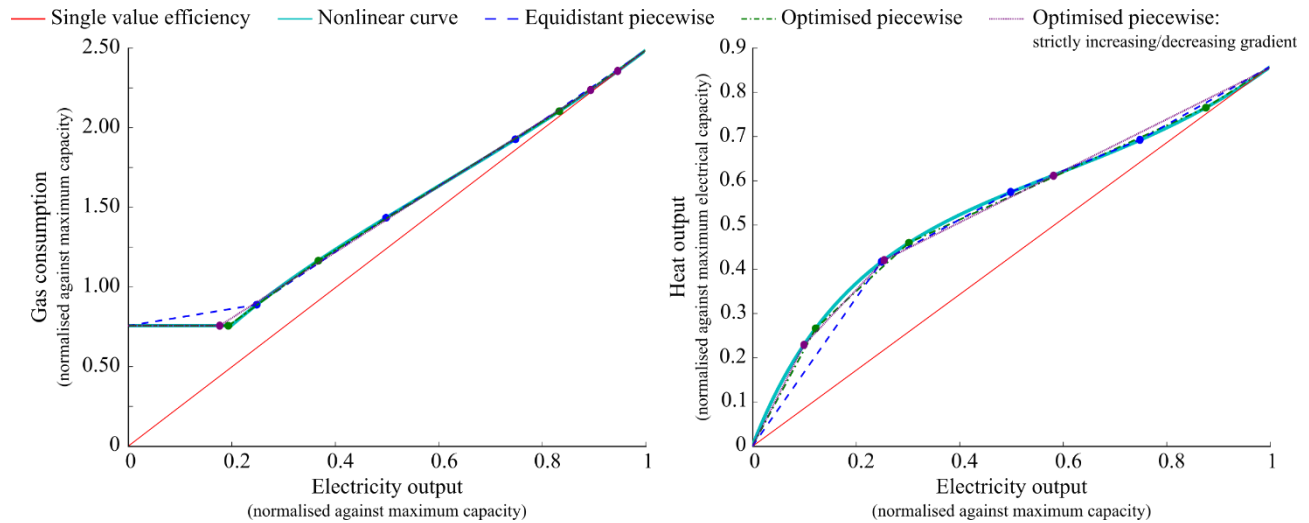


Figure 5.43: Comparison of different methods for describing the gas consumption and heat output of a CHP, from nonlinear to SVE, at different load rates where five breakpoints are given for piecewise curves

As with cooling, the performance of TES is primarily temperature dependent [17]. Varying load rates also have an effect, due in part to the use of pumps during charging/discharging [610], but also due to thermal stratification required for minimal heat loss. If the flow rate of charging/discharging is too high, it will likely disrupt the stratified layers in the tank, leading to mixing and associated exergetic losses [611]. As temperature dependence is not considered in this example, nonlinear characteristics of storage technologies are not included. However, thermal energy flow is limited for the tanks to simulate avoiding mixing effects.

5.8.2.2.3.3 Model configuration

The case study was modeled in Calliope [612], an open-source modeling framework which uses a python-based toolchain [613]. MILP optimization was run via CPLEX [614], with a 3% mixed integer optimality gap tolerance. Multiple model configurations were run, for different demand seasons, linearization techniques and breakpoints of piecewise linearization (Figure 5.44). The objective function was combined minimization of capital and operational costs.

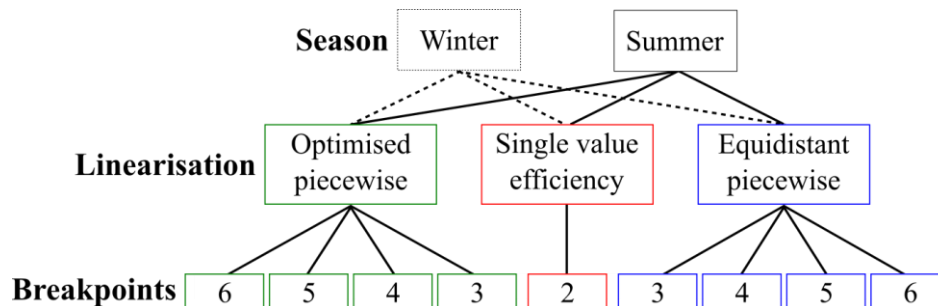


Figure 5.44: Configurations of modeling runs

5.8.2.2.3.4 Case study simplification

The initial district was to be modeled over all hourly time steps in a year. This created a problem of a size that could not be handled by the testing hardware. To maintain model tractability, individual weeks were considered instead. Two separate weeks were chosen based on maximum heat requirement (week 1) and maximum cooling requirement (week 28). The initial network in Figure 5.37 was also aggregated to the network seen in Figure 5.45, reducing decision variables from 8,649,607 to 410,905. To do so, all dwellings were merged into a single domestic property, and the hotel and office were merged into a commercial property. Total energy demand and available roof area remained constant. These simplifications were necessary to run the model multiple times and all the configurations given in Figure 5.43 could be analyzed in a timely fashion.

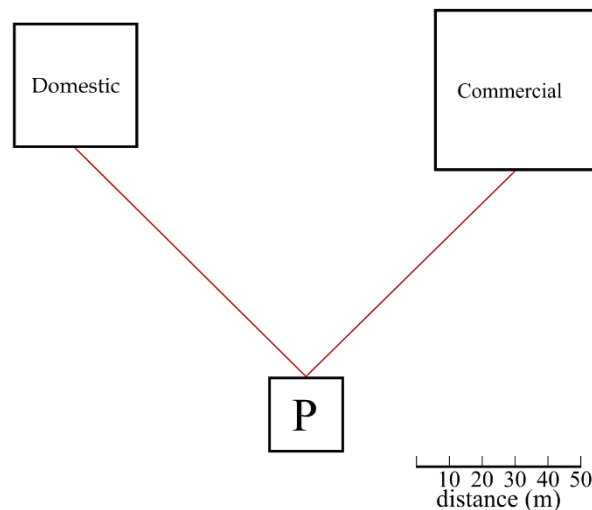


Figure 5.45: Graphical representation of the simplified case study district network

Initially, SOS2 was chosen as the method for representing the piecewise curves. However, model convergence was poor, particularly when within 10% of the relaxed LP solution. To ensure that all relevant technologies could be piecewise linearized, constraint bounds were applied. This leads to a greater error in describing the CHP curve, particularly at a greater number of breakpoints. After four breakpoints, it is not possible to reduce HTP curve error further, leading to double the error between SOS2 and constraint bounds at six breakpoints (Figure 5.46). However, both methods still provide a low error, lower than their equidistant counterparts. The technology characteristics considered for piecewise linearization were (1) CHP HTP and gas consumption, (2) EC and AHP electricity consumption, and (3) HRAR heat consumption. Other available characteristics were the boiler gas consumption and the pumps associated with distributing thermal energy from supply to demand. These characteristics were ignored due to the linearity of the former and the small scale of the latter.

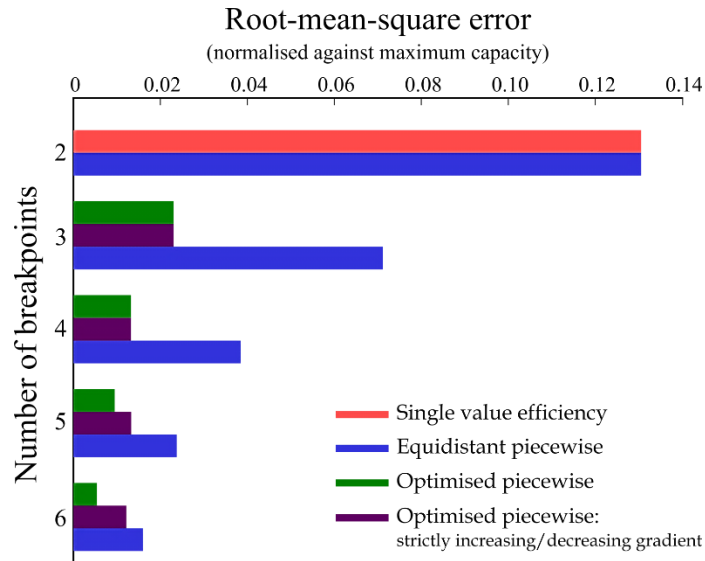


Figure 5.46: Root-mean-square error between linearization methods and the nonlinear characteristic curve of CHP HTP, for full range of breakpoints

5.8.2.2.4 Results

Application of piecewise curves increases the objective function value by as much as 5.2%. Table 5.30 shows that differences in objective function values are small when increasing the number of piecewise breakpoints, with optimized curve averages of £4,036 +1%/-0.5% in winter and -£2,394 +0%/-0.6% in summer. The summer negative cost represents the ability for the system to gain more revenue from subsidies and export than it spends on investment and operation in that period. There are no equidistant solutions beyond three breakpoints due to model infeasibility. It is not possible to place constraints on breakpoint location when placing equidistantly. Thus, the strictly increasing/decreasing gradient requirement for being bound by constraints cannot be met for CHP HTP and gas consumption.

Table 5.30: Objective function value in GBP for all run configurations

Breakpoints	2		3		4		5		6	
	Linearization	SVE	O	E	O	E	O	E	O	E
Winter										
Result		3,989	4,036	4,048	4,074	Fail	4,019	Fail	4,016	Fail
+NL		+465	+23	+12	+40	N/A	+32	N/A	+32	N/A
Summer										
Result		-2,507	-2,380	-2,377	-2,398	Fail	-2,398	Fail	-2,401	Fail
+NL		+294	-17	-28	-2	N/A	-1	N/A	0	N/A

Keys: O: optimized, E: equidistant, +NL: monetary cost due to applying nonlinear consumption curves ex-post

Each linear model run has been compared to its nonlinear counterpart, by applying the relevant nonlinear consumption curves to the technology outputs obtained using the linear optimization. In doing so, there is a potential difference between “expected” (MILP objective function value) and “actual” (nonlinear consumption curves applied ex-post) system costs (+NL). Although the optimal SVE objective function value is lower than piecewise models, the “actual” system costs end up being higher. +NL is 12% in both seasonal weeks for SVE, decreasing to less

than 1% when including piecewise curves. In summer, this effect is most pronounced, where +NL reduces to zero at six breakpoints.

While the accuracy of the objective function value is improved, piecewise linearized cases take much longer to solve than the SVE case (Table 5.31). This is more the case in the summer week, which peaks at 17,521 seconds (three breakpoints, equidistant), two orders of magnitude longer than the basic model. Even at the least number of breakpoints, the solution time is 2.5x and 14.9x longer than the basic model in winter and summer, respectively.

Table 5.31: Model runtime in seconds for all configurations, including pre-processing and subsequent MILP solving in CPLEX

Breakpoints	2		3		4		5		6	
Linearization	SVE	O	E	O	E	O	E	O	E	
Winter	366	926	610	880	Fail	847	Fail	1,408	Fail	
Summer	300	4,483	17,521	7,202	Fail	15,230	Fail	6,816	Fail	

Keys: O: optimized, E: equidistant

There is generally an increase in solution time with increased number of breakpoints, the only anomaly being the drastic decrease in model solution time between having five and six breakpoints in summer. Here, the model solves in less than half the time with an additional breakpoint. In this instance, the five-breakpoint case had solved within 10% of the relaxed LP 200 seconds sooner than the six-breakpoint case but failed to converge on the last few percent for an extended period. Equidistant breakpoints decrease the solution time by a small amount in the winter week and increase it substantially in the summer week. As mentioned, it is the final few percent of convergence that leads to the vastly inflated solution time.

The change of objective function value when applying piecewise characteristic curves results from changes in both investment and operation. Varying the “penalty” for part load operation leads to different technology choices. For instance, in meeting cooling demand in the SVE case, the EC is chosen to operate as the only technology throughout. When applying piecewise curves, Figure 5.47 shows that AHP is better suited for part load requirements, leaving the EC for almost exclusive use at its full load. Generally, there is more use of technologies in full/zero load configurations when piecewise curves are included. This means that a greater variety of technologies are purchased to avoid running any one of them at part load.

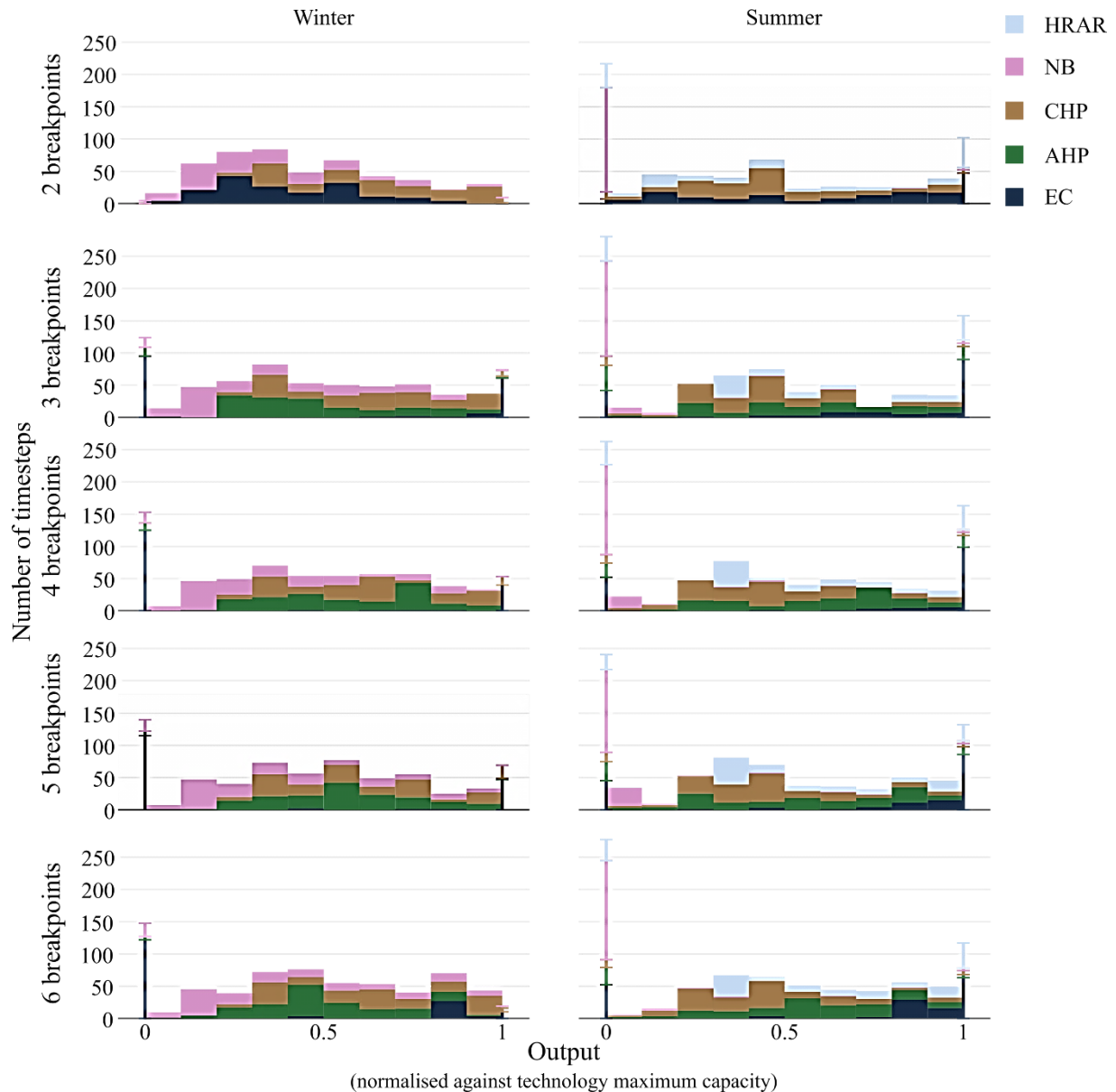


Figure 5.47: Technology output histograms for SVE and optimized piecewise model runs where full and zero loads are given as single points, with all other part load operation given in 10% increments

Purchased technology capacities also vary (Figure 5.48). In both seasons, EC capacity is reduced in the piecewise results and AHP is purchased to account for the deficit. In the winter week, boiler size is also reduced, balanced by a larger heat storage capacity (Table 5.32). Storage is used more in piecewise models, leading to lower cumulative system capacity. The results also show that the utility of the local distribution network is dictated by technology choices. For example, more power is distributed to the commercial properties in summer due to the purchase of a smaller CHP and heat networks are avoided. Besides, a small plant CHP is purchased in all cases, but it dumps heat in favor of distributing it. The system is limited in how much heat it can dump, so the plant CHP could be feasibly larger if that constraint were lifted.

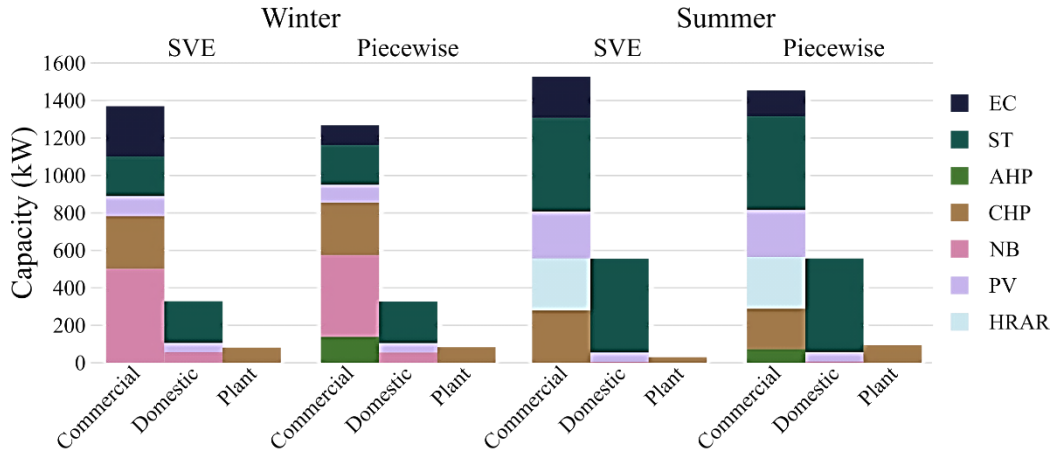


Figure 5.48: Energy supply technology investment portfolios at each location and in each season

Table 5.32: Capacity of distribution network to, and storage at, both demand locations

	Distribution						Storage					
	Gas		Heat		Power		Cooling		Power		Heat	
	SVE	P	SVE	P	SVE	P	SVE	P	SVE	P	SVE	P
Winter												
Commercial	1,304	1,224	0	0	71	75	0	24	7	0	0	59
Domestic	69	67	0	0	41	37	0	0	7	7	145	145
Summer												
Commercial	788	622	0	0	40	135	0	7	7	7	230	289
Domestic	6	9	8	0	40	43	0	0	7	7	5	8

Keys: P: piecewise

Chapter 6: Key performance indicators

In a scenario of rapid spread of nZEBs, energy storage systems (ESSs) allow decoupling of energy supply and demand, avoiding or minimizing the overload of the grid, with considerable advantages in terms of reducing the impact on the network. Therefore, it is important that the size of storage is correctly captured in design, guidelines, standards and policy. By this way, storage can be appropriately adopted in buildings/districts to enhance the overall system performance and achieve the aims of resilient energy systems with minimum emissions. Generally, energy storage consists of both explicitly designed and inherent storage systems for storing thermal or electrical energy. Examples of explicit storage include hot water tanks, PCMs, batteries, etc. On the other hand, inherent storages are incorporated in buildings and district systems due to their normal functional characteristics such as in building elements and spaces, and in the mass of water within a district heating distribution system.

In order to evaluate the effectiveness of energy storage technologies (both explicitly designed storage and inherent storage) in building/district applications, the key performance indicators (KPIs) represent important methods for analyzing interactions among economic, human activity, energy consumption and the reduced GHG emissions [30].

Prior to presenting further details about KPIs, some definitions are presented for the correct interpretation of this chapter as well as enabling comparison between energy storage technologies:

- **Innovative features:** describe the main innovative features of the storage technology compared to the commercially available solutions.
- **Operational constraints:** describe all the operational constraints which must be known for the operation of the storage.
- **Environmental aspects:** describe all specific environmental hazards during the life cycle of the storage system.
- **Storage system:** a system composed of a storage medium (a physical or chemical element in which the energy is stored) and other necessary accessories (e.g. envelope or accessories strictly necessary to operate the system). The main purpose of the storage system is to typically reduce nonrenewable based power generation and/or running cost of an nZEB or a group of low-energy buildings (district).
- **Energy source:** generator or environment from which the energy is transferred to the storage system.
- **Charging period:** the period during which energy is intentionally transferred from the energy source to the storage system.
- **Discharging period:** the period during which energy is intentionally transferred from the storage system to the energy user.
- **Energy user:** the thermal zone or to the building technical systems which are intended to use the energy.

- **Stand by period:** the period during which the storage system is intentionally not in the charging or discharging period.
- **Working cycle:** it is a process which includes a complete charge of the storage system, the discharge of the storage system and eventually a certain inactivity time. It is defined according to the typical use of the storage system.

In this chapter, first, the existing KPIs in literature are analyzed to evaluate their pros and cons. Subsequently, to allow a simplified but exhaustive analysis and comparison of Annex 31 case studies, a specific set of KPIs are proposed and defined. These optimized KPIs are later used at the end of this chapter to evaluate Annex 31 case studies. A set of advanced KPIs are also defined to shed light on their potential future applications.

6.1 Review of existing KPIs

Although some researchers outlined the fundamental characteristics of storage systems in order to establish comparison criteria for selecting the best technology [615-617], few of them focused on the application of storage systems in buildings [616, 617]. Of the latter, some studies [616] defined indicators to compare the efficiency and performances of TES systems integrated in the building structures (e.g. PCM façade), which hence cannot be extended to all available energy storage technologies, while others especially focused on an economically optimized decision of electrical energy storage capacity.

In general, even if some researchers used a set of fundamental indicators such as the *storage capacity*, the *efficiency* and the *cost*, their definition and calculation methods were not univocal. For instance, the *storage capacity*, one of the most used indicators, is defined as the energy which can be stored in reference conditions [618] or as the quantity of available energy retrievable without negatively affecting the storage device [619]. The *efficiency*, often called roundtrip efficiency [618], is the ratio between the amount of energy which comes out of storage and the amount put into the storage. This definition is often oversimplified since it does not consider the losses measured during the three main phases of charging, discharging and standby [619, 620].

Similarly, the cost is sometimes evaluated as the *capital cost*, without considering the *operating cost* [618], which can be further subdivided in labor associated with system operation, system maintenance and replacement, and finally decommissioning and disposal cost [31, 615, 621]. Another useful parameter which is often not univocally defined is the *lifetime* or *durability*, which typically refers to the number of times the storage unit can release the energy level by which it was designed after each recharge, expressed as the maximum number of cycles N_t (one cycle corresponds to one charge and one discharge) [621, 622]. This is usually the principal cause of aging. The rate of degradation depends on the type of storage technology, operating conditions and other variables. This is especially important for electrochemical batteries [615]. The *transportability* indicator is also an interesting parameter introduced recently [621], which can affect the cost of installation as well as the feasibility of dismissing. However, the study does not define the useful features to evaluate and quantify the indicator in a metric. Moreover, to be highly

efficient, a storage system needs to be precisely adapted to the type of application (low to mid power in isolated areas, network connection, building connection, etc.) and to the type of production (permanent, portable, renewable, etc.). In such regards, an indicator called feasibility and adaptation to the generating source is introduced but not well defined [619, 621]. Another attractive feature of energy storage is the *flexibility* or *modularity* that it can provide. Modularity allows for more optimal levels and types of capacity and/or discharge duration because modular resources allow utilities to increase or decrease the storage capacity, when and where needed, in response to changing conditions [615, 621, 623].

6.2 Main KPIs

Some of the existing KPIs that have been discussed earlier lack clear definition. Therefore, in this publication, some specific KPIs are clearly defined and used. These main KPIs allow the assessment of ESSs in buildings/districts which are presented and described in detail hereafter.

6.2.1 Storage capacity

This is the quantity of the energy contained in the storage system or available immediately after the full charging. The aim of the indicator is to easily evaluate the amount of energy which can be stored and released in reference conditions. It is defined based on two quantities:

- **Total capacity:** the total energy which can be stored in reference conditions, noted by C_t [Wh];
- **Maximum useful capacity:** the maximum useful energy which can be actually retrieved in reference conditions without negatively affecting the storage system (i.e. permanent damages), noted by $C_{us,max}$ [Wh].

The difference between C_t and $C_{us,max}$ is mainly related to the depth of discharge and to the discharging efficiency (both are defined later).

For TES systems, supply temperatures and flow rate should be indicated. Moreover, the average temperatures and flow rate of heating/cooling energy provided by the storage on the load side should be specified. For TES systems where useful energy is directly released in the internal environment of the building, the capacities should be referred to the nominal working temperature of the storage (maximum/minimum storage medium temperature for heating/cooling purposes, respectively) and the reference indoor temperature (e.g. 20 °C during the heating season and 26 °C in the cooling season for commercial/tertiary buildings) of the environment to be heated/cooled.

If the capacities change during the expected lifetime of the storage system (i.e. proportionally to the number of working cycles), the values should be specified for 0%, 30%, 50%, 70% and 100% of the durability (see the next indicator).

6.2.2 Recharging energy

The recharging energy C_r is the amount of energy which should be supplied to the storage to reach the total storage capacity (C_t), with respect to a specific charging period. The aim of this indicator is to quantify the amount of energy which should be provided to obtain the full charge of

the storage system. The relation between the C_r and $C_{us,max}$ is the charging/discharging efficiency. For TES systems, if the recharging energy is varying as a function of the charging duration, then the minimum and maximum values should be provided.

6.2.3 Maximum charging and discharging power

These indicators represent the maximum charging power ($P_{c,max}$) and maximum discharging power ($P_{d,max}$) [kW], which can be constantly released for the minimum charging/discharging periods ($D_{c,min}/D_{d,min}$) [h]. The indicators are useful to understand the capability of the ESS to manage peaks of generated power (e.g. by non-predictable RES) or needed by the building technical systems.

If the power is significantly changing during the charging/discharging periods as a function of the state of charge, a power profile or the $P_{c,max}$ and $P_{d,max}$ values at 100%, 70%, 50% and 30% of the useful capacity $C_{us,max}$ should be provided.

For electrical energy storages, the maximum discharging power is determined by the power electronics equipment used to manage the ESS. The maximum charging power may also be different from (generally lower than) the maximum discharging power.

6.2.4 Depth of discharge

The depth of discharge (DOD [%]) describes how deeply the storage can be discharged providing usable energy (considering the reference conditions for which it is designed) and without negatively affecting its properties (i.e. permanent damages). It is expressed as a percentage of the total capacity, reciprocal of state of charge. This means a DOD of 100% indicates that the ESS can be fully discharged, until the state of charge is 0%.

For TES systems, it should be referred to the nominal working temperature of the storage (maximum/minimum storage medium temperature for heating/cooling purposes, respectively) and the temperature of medium/environment to be heated/cooled.

Note that the difference between the ($C_t \times DOD$) and the $C_{us,max}$ is related to the discharging efficiency and, consequently, the losses during the discharging period. If the storage has no losses during the discharge, then $(C_t \times DOD) = C_{us,max}$.

6.2.5 Durability

This indicator refers to the assumed maximum number of working cycles (N_i) for which the storage system can release at least 75% of the designed useful capacity $C_{us,max}$, during a certain lifespan, expressed in years. The scope of the indicator is to estimate the useful working life of a certain technology, based on the intensity of use within an expected lifespan. It must be referred to the DOD if it influences the durability. Note that the durability is a specific characteristic of the storage system and not of the energy source.

6.2.6 Specific cost of the storage

The aim of this indicator (SC_s) is to consider the overall cost of a certain ESS, normalized to the total amount of energy it can deliver during its expected lifetime. In detail, SC_s [€/kWh] is the

ratio of the sum of the total turn-key costs (CO_t), the O&M costs (CO_{OM}) during the expected lifetime and, if available, the decommissioning cost (CO_{DC}), over the product between the average useful capacity C_{us} and the durability (total number of cycles N_t).

$$SC_s = \frac{CO_t + CO_{OM} + CO_{DC}}{C_{us} \times N_t} \quad (6.1)$$

If C_{us} decreases as the number of working cycles increases, the average C_{us} should be considered for the maximum number of working cycles. Note that this indicator does not consider the costs related to the charging/discharging and self-discharge losses. These are subsequently considered in the specific cost of the stored energy (SC_{se}), which is presented later.

It is worth also noting that the cost is normalized only to the useful energy ($C_{us,max}$ in the denominator). However, as described earlier, some ESSs (in particular electrical energy storages) provide two contributions, in terms of energy and power. This could lead to a disparity in treating thermal and electrical storage devices. The need for a unique set of indicators pushes towards the usage of the proposed formula based on the deliverable energy only.

6.2.7 Maximum self-discharge rate

The indicator SD [%] is the portion of the energy which was initially stored (C_t) and has been dissipated over a certain standby period of the storage (no charge or discharge power applied). The value should be provided for standby periods equal to 1h, 10h, 100h and 1000h. The aim of the indicator is to quantify the unwanted discharge occurring during the inactivity time (i.e. standby period), the period during which no energy/power is intentionally requested from/sent to the ESS.

For TES systems, the self-discharge should be seen as thermal losses (or gains for cold storages such as ice/chilled water). The losses released to the environment to be heated/cooled during the standby period should also be considered.

Note that for electrical energy storage devices, this indicator is important; however, under proper design and sizing, self-discharge should never occur. In fact, should it occur, it would mean that the chosen technology and the application (the timeframe of the application, rather than the energy or the power involved) are not matching.

6.2.8 Storage size/weight

The storage size (S_t) is the volume [m^3] occupied by a storage system of a given useful capacity ($C_{us,max}$), and the storage weight (W_t) is defined as its total mass [kg]. If additional elements are required to operate the storage (envelope or accessories strictly necessary to operate the system), the volume and weight of such elements should also be specified. If the ESS is modular, the two parameters should be indicated for each module of the ESS. This allows evaluation of the capability to transport or install the ESS in narrow spaces.

6.2.9 Energy storage factor

This indicator (ES [%]) is the fraction of the total energy demand (calculated over a representative period, e.g. one day or one season) for a certain purpose (e.g. heating, cooling, DHW

production) and/or of the RES based power generation, related to the building/district in which the storage technology is installed, that is released by the energy storage. The scope of the indicator is to consider which part of the total energy is required by the building/district (or by a specific function such as heating or artificial lighting) and/or of the RES generation during a certain period is stored and later released from the storage system.

ES is the ratio of the product of $C_{us,max}$ and the number of the measured/expected equivalent cycles during the reference period (N_{RP}) over the total energy demand for a certain purpose (e.g. heating, cooling, DHW), ED_t [kWh], or the RES generation (G_{RES}) [kWh].

$$ES_D = \frac{C_{us,max} \times N_{RP}}{ED_t} \quad (6.2)$$

$$ES_{RES} = \frac{C_{us,max} \times N_{RP}}{G_{RES}} \quad (6.3)$$

Note that the preferred periods and timeframes to be considered are typical and worst-case summer, spring and winter days, heating/cooling seasons and an entire year. In all cases, data can be used from the typical meteorological year (in the decision making/design phase) or measured data (in the monitoring phase).

6.2.10 Generated energy/cost saving

This indicator is the expected energy saving (E_{sav} [kWh]) and/or cost saving (CO_{sav} [€]), generated using the ESS inside an nZEB or a group of buildings during a certain reference period (e.g. a day, a season, a year), which must be characterized by a specific number of equivalent working cycles. The comparison should be made with an nZEB or district with the same characteristics but without the storage system. The indicator highlights the economic benefit generated by the storage system thanks to different mechanisms, such as:

- Shifting the building electric load from peak-hours (high tariff) to off-peak hours (low tariff).
- Increasing the self-consumption of onsite RES production, decreasing both the energy exported to the grid and the energy imported from the grid.
- Reducing the heating/cooling energy demand.
- Bulk energy arbitrage which involves the possibility of purchasing inexpensive electricity available during low demand periods to charge the storage plant, so that the low-priced energy can be used or sold later when the price for electricity is higher.
- Avoiding cost or revenue increase of central generation capacity: for areas where the supply of electric generation capacity is tight, energy storage could be used to offset the needs such as (1) purchase and install new generation and/or (2) “rent” generation capacity in the wholesale electricity marketplace.
- Reducing reliability-related financial losses: storage reduces financial losses associated with power outages. This benefit is very end-user-specific and applies to commercial

and industrial (C&I) customers, primarily those for which power outages cause moderate to significant losses.

Note that analogous to the energy storage factor, the preferred periods and timeframes to be considered are typical (e.g. worst-case summer, spring and winter days, heating/cooling seasons and an entire year). In all cases, data can be used from the typical meteorological year (in the decision making/design phase) or measured data (in the monitoring phase).

6.3 Related KPIs

The following indicators can be calculated based on the main indicators previously presented.

6.3.1 Fastest charge/discharge durations

These are the fastest charge and discharge durations ($D_{c,min}$ and $D_{d,min}$) in hours, where the former is calculated as the ratio of C_r/C_t and the latter is the average maximum charging/discharging power which can be released constantly ($P_{c,max}/P_{d,max}$) during the charging/discharging durations, in the reference operating conditions.

$$D_{c,min} = \frac{C_r}{P_{c,max}} \quad (6.4)$$

$$D_{d,min} = \frac{C_t}{P_{d,max}} \quad (6.5)$$

where $D_{c,min}$ and $D_{d,min}$ refer to the same reference conditions defined for $P_{c,max}$ and $P_{d,max}$, respectively.

The indicators are useful to know the minimum timeframe in which an ESS can be charged or discharged. If the powers ($P_{c,max}/P_{d,max}$) significantly change during the charging/discharging periods as a function of the state of charge, the durations should be calculated according to the power profile, at 100%, 70%, 50% and 30% of the useful capacity $C_{us,max}$.

6.3.2 Charging efficiency

It is the efficiency of the charging phase of the storage system and is calculated as:

$$\eta_c = \frac{C_t \times DOD}{C_r} \quad (6.6)$$

where DOD is assumed equal to 100% for the first charging cycle (empty storage).

6.3.3 Discharging efficiency

It is the efficiency of the discharging period of the storage system and is calculated as:

$$\eta_d = \frac{C_{us,max}}{C_t \times DOD} \quad (6.7)$$

where DOD is 100% for the first charging cycle (empty storage).

6.3.4 Total charging/discharging efficiency

The indicator η_{cd} is the ratio of the useful capacity $C_{us,max}$ over the recharged energy C_r to reach 100% of storage capacity, referred to specific charge/discharge durations. The obtained value indicates the total efficiency of a complete working cycle (charging/discharging).

The value could be differentiated for the first recharging cycle (empty storage) and the subsequent cycles (thus considering the DOD) and must be calculated/measured immediately after the full charging period.

$$\eta_{cd} = \frac{C_{us,max}}{C_r} \quad (6.8)$$

Note that if a standby period is also included, the indicator should be called roundtrip efficiency.

6.3.5 Mass and volume densities of energy

It represents the maximum amount of useful energy ($C_{us,max}$) per unit of mass or volume of the storage unit, calculated as the ratio of $C_{us,max}$ and S_t or W_t . Such indicators demonstrate the importance of specific mass and volume for certain applications, in kWh/kg and kWh/m³, respectively.

6.3.6 Specific cost of the stored energy

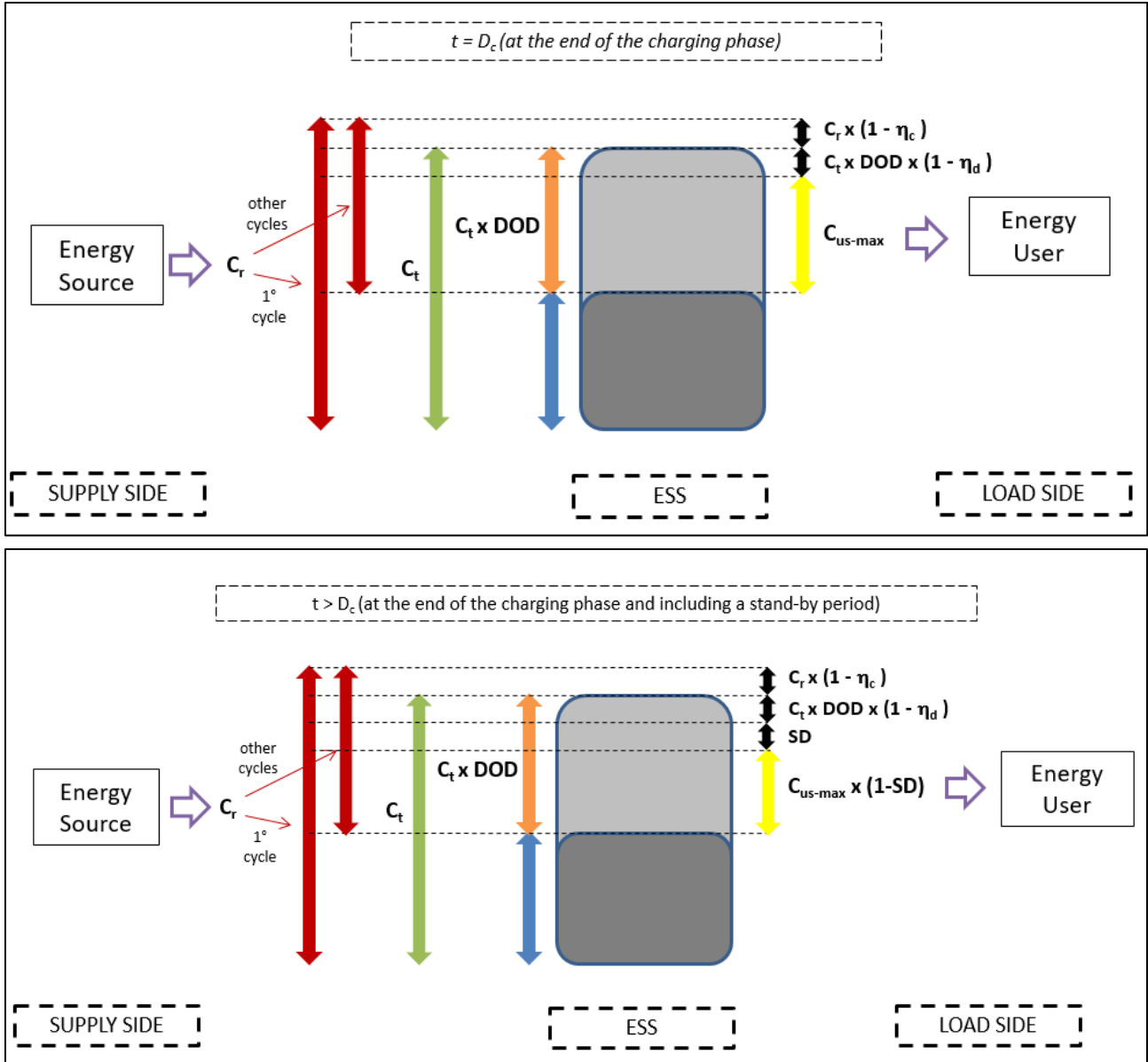
The indicator SC_{se} specifies the cost of each kWh released from the ESS [€/kWh]. It is useful to know the overall cost of the energy (i.e. generation/purchasing cost and additional cost due to the energy storage use) provided by a certain ESS applied in building/district.

$$SC_{se} = \frac{CO_t + CO_{OM}}{C_{us,max} \times N_t} + \frac{CGE}{\eta_{cd}(1 - SD_{ave})} \quad (6.9)$$

where CGE is the specific generation/purchasing cost [€/kWh] of the energy sent to the storage and is dependent to the generation technology/energy supply and SD_{ave} [%] is the average self-discharge for each working cycle, considering the type of use of the storage technology.

6.4 Schematic representation

Figure 6.1 shows a schematic representation of an ESS and the main abovementioned indicators.



t : time and D_c : duration of charging

Figure 6.1: Schematic representation of an energy storage system and the main KPIs

Following observations are made to clarify the mentioned concepts:

- The C_r considers the amount of energy which must be provided to the storage system to reach the 100% of C_t .
- The C_r could be different for the first working cycle (when the storage is completely empty) and the normal recharging cycles, if the DOD is lower than 100%. The C_r refers to the quantity of energy which should be provided to bring the state of charge (SOC [%]) from $100 - DOD$ to 100%.
- The C_t is the total energy stored at the end of the complete charging period.

- The $C_t \times DOD$ considers the total energy stored at the end of the complete charging period (C_t), net of the fraction which cannot be safely and/or effectively retrieved from the storage system.
- The $C_{us,max}$ considers the total energy stored at the beginning of the discharging period, which is the $C_t \times DOD$ deducted from the losses during the eventual inactivity time and the losses during the discharging period. It represents the final useful energy which can be effectively used.

6.5 Advanced KPIs

What has been presented so far will be used at the end of this chapter to evaluate and compare the Annex 31 case studies. However, other KPIs also exist which can be used to assess the advanced features of energy storages, with specific reference to the benefits generated by the storage on the district scale or national grid. In short, the mentioned main and related KPIs are intended to easily compare ESSs mainly under a user-side perspective, while the advanced KPIs presented in this section primarily highlight (but not only) the grid-side perspective. The advanced KPIs could be either evaluated by specific measurements only or obtained from modeling results, but typically require a deeper and more detailed analysis compared to the effort needed to determine the main and related KPIs described earlier.

It is important to ensure that the value associated with storage is properly captured in the design and operation of low carbon buildings and districts. Therefore, these values should be clearly defined and quantified, and incorporated in the assessment of various design options so that an optimal system is achieved. Consequently, modeling tools should support quantification of the KPIs associated with explicit and inherent storages so that a storage is correctly comprehended in modeling tools which support policy formulation, design and regulatory processes.

The following are the potential advantages of a storage system:

- **Short-term demand response:** local load shedding or grid surplus absorption for short-term supply response (< 15 mins).
- **Long-term supply balancing:** load shaping for grid supply/demand system balancing optimization (> 15 mins).
- **Supply optimization:** local building or district supply optimization (in terms of cost, CO₂, renewable energy, etc.).
- **Plant optimization:** which applies at all levels (e.g. smaller generator if a storage is used).
- **Enhanced service:** in terms of reduced fluctuations (e.g. thermal comfort).
- **Enhanced resilience:** to loss of service.

On the other hand, potential storage disadvantages include:

- **Increased energy use:** due to the losses in storage cycle.
- **Discomfort:** for instance due to lack of service or parasitic losses.

- **Undesirable life cycle change:** due to the indirect increase in the embodied energy, carbon emission, environmental impacts, etc.

It is important to recognize in the KPIs that energy systems are dynamic and subject to stochastic and seasonal variations in demands and supply characteristics. Therefore, KPIs should be quantified for appropriate periods (e.g. time of day, typical summer period, typical winter period, annualized) and the quantification should consider the statistical uncertainties. Some advanced KPIs and the associated quantifications are discussed in this section. It is important to note that the presented equations are simplistic and illustrative. Therefore, more detailed models are expected to be used in practice.

6.5.1 KPIs capturing storage advantages

6.5.1.1 Short-term demand response

Storage, whether explicit or inherent, allows the possibility to provide short-term response services to the grid through reduction or increase in the load based on a signal from the grid operator or local measurements of frequency or voltage condition. This functionality is often termed ‘demand or frequency response’ and typically requires the system to respond with an ON (load absorb/charging) or OFF (load shed/discharging) within a time of the order of seconds (depending on the size of the network and its reactance). This type of demand response (DR) is currently deployed for curtailment of renewable generators such as local PV when there is an oversupply. It can also be used to start up fossil fuel backups if there is a renewable shortfall. In the future, DR actions associated with storage would be used to minimize CO₂ emissions. Infrastructure similar to that used for 'smart meters' or 'storage heaters' on 'white meter' tariffs could potentially be used to aggregate consumers to provide this service in the future. Local intelligence (or in the cloud) would allow individual systems to provide a response if capacity was available without compromising delivery of services to the customer. The aggregator would require some assessment of the likely response at any time to quantify the service they could provide to the grid. Performance metrics important for this short-term response service are presented in Table 6.1.

Table 6.1: Short-term demand response KPIs

No.	Parameter	Symbol	Unit
1	Time to response	t_{DR}	s
2	Current power (grid side)	P_i	kW
3	Maximum power (grid side)	P_{max}	kW
4	Average power (grid side)	P_{ave}	kW
5	State of charge (energy)	SOC	kWh
6	State of temperature	SOT	°C
7	Service delivery temperature	SDT	°C
8	Service demand (projection)	SD	kWh (t)
9	Storage service temperature (projection)	ST	°C (t)
10	Storage load duty schedule (projection)	SLD	kW (t)
11	Load grid to heat conversion rate (projection)	GTH	% (t)
12	Load shed relative power (grid side)	$\%P_{dis}$	%
13	Load shed ramp rate	$P_{r,dis}$	kW/s
14	Load shed duration	t_{dis}	h
15	Load shed energy	E_{dis}	kWh
16	Percentage of load shed energy	$\%E_{dis}$	%
17	Load shed net energy cost	CO_{dis}	€
18	Load shed recovery time	RT_{dis}	h
19	Maximum power (grid side for load absorb)	$P_{DR} (=P_{max})$	kW
20	load absorb relative power (grid side)	$\%P_{ch}$	%
21	Load absorb ramp rate (grid side)	$P_{r,ch}$	kW/s
22	Load absorb duration	t_{ch}	h
23	Load absorb energy (grid side)	E_{ch}	kWh
24	Percentage of load absorb energy	$\%E_{ch}$	%
25	Load absorb net energy cost	CO_{ch}	€
26	Load absorb recovery time	RT_{ch}	h

The obtained response is primarily characterized from the grid side by the time to respond, the current power consumption (or the average power for aggregated loads), the maximum power consumption, the power ramp rates, the available durations (and associated energy) for power absorb (charge) or load shed (discharge) operations, the energy and financial costs associated with these response events, and the recovery time required before a repeat response is available. The response available as a fraction of the total load may also be a useful parameter.

The duration of the required absorb or shed response is a key parameter. Very short responses of the order of seconds or a few minutes would in many circumstances be invisible to the end user due to the large system time constant.

Longer responses would require the available durations to be assessed by 'local' intelligence (i.e. the storage or enhanced heating/cooling system controls) based on individual system parameters such as the current stored energy, storage temperature, service demands and storage temperature projections including system losses, storage normal duty cycle and grid to heat conversion rate (e.g. for a heat pump), etc. (parameters 5 to 11 in Table 6.1). The individual system would then only provide a response if there was no impact on comfort.

6.5.1.2 Long-term supply balancing

The load shaping functionality is similar to the short-term DR but acts over longer periods in the order of 2 to 48 hours ahead based on forecasted grid conditions. Pricing signals are applied, either by standard schedules for peak and base tariffs or increasingly, time of use (TOU) hourly or half-hourly electricity cost schedules. In both cases, the intent is to reduce peak demands and provide less variation in demands to reduce the need to invest for peak capacity and to increase the utilization factors and return on investment for the existing capacity. Historically, there has been a need to shift the demand to night time to fill in the overnight demand gap and reduce the morning and evening peaks which has been enabled by the systems such as ‘storage heaters’ and thermal storages on ‘white meter’ tariffs in the UK. In the future, it is expected that the availability of TOU tariffs might increase where each 30-minute timeslot in a 24 or 48-hour period is given an independent price, re-forecasted periodically, allowing for storage to enable load shifting to low tariff periods. Storage used in this way can also enable surplus grid scale renewable energy to supply the grid which would otherwise be curtailed. Most of the performance parameters which were important for short-term DR are also important for load shaping; however, some further metrics are also useful (Table 6.2).

Table 6.2: Load shaping for demand to supply optimization KPIs

No.	Parameter	Symbol	Unit
1	Tariff base and peak or TOU (projection)	CO_{TOU}	€/MWh (t)
2	Load flexibility ratio (absorb time/shed time)	LF	-
3	Percentage of load flexibility	$\%LF$	%
4	Forward projection of DR (vector)	V	-
5	Periods with shed flexibility over x hours (e.g. 4, 8, etc.)	$FLEX(x)$	%

The load flexibility in support of demand optimization has two dimensions. The first is the ability to absorb low tariff electricity during periods of availability, for which the time taken for complete charging (t_{ch} , parameter 22 in Table 6.1) is important since if it is too slow, then opportunities will be missed. The second is the ability to coast through periods of high cost (t_{dis} , parameter 14 in Table 6.1) since if this is too short, then high cost electricity cannot be avoided. A load flexibility ratio is defined as the ratio of charge time to coast time to help characterize storage flexibility.

The percentage of the load which can be shifted to periods of low tariff for defined high and low period situations would provide a useful but tariff specific output, so the tariff used must be clearly stated. The load shed duration could be used to provide alternative tariff independent metrics derived from an analysis of load shed durations for a range of potential flexibility periods.

The current logic applied to the tariff periods is generally a simplistic switch ON of off-peak charging when low tariff periods commence and OFF when the off-peak period ends with maximum charging controlled thermostatically. If the storage reaches its lower control limit during peak times, then peak electricity is used to boost. In the future, TOU tariffs will potentially support more sophisticated local optimization through some forward projection of performance (e.g. a multi-parameter vector) and option selection.

6.5.1.3 Supply optimization

Local supply optimization would take information regarding future RES availability, grid energy tariff pricing, grid associated carbon emissions, weather and end user demand forecasts over a future time horizon as inputs. The information is used to optimize the TES usage to achieve the best possible performance for a selected objective function. The required functionality for this service could potentially be built upon smart meter platforms or similar infrastructure. The parameters described in the previous sections should provide inputs to the optimization.

A set of performance metrics quantifying the benefits of the storage can be envisaged (in Table 6.3) such as saving in grid supplied energy ($\%GE_{sav}$), reduction in carbon emissions ($\%CO_{2sav}$), reduction in total energy cost ($\%CO_{sav}$), reduction in life cycle cost ($\%LCC_{sav}$) and reduction in life cycle energy ($\%LCE_{sav}$). In reality, the objective function for the optimization is likely to be some combination of these.

Table 6.3: Local building or district supply optimization KPIs

No.	Parameter	Symbol	Unit
1	Percentage of grid supplied energy reduction (modeling)	$\%GE_{sav,m}$	%
2	Percentage of carbon emission saving (modeling)	$\%CO_{2sav,m}$	%
3	Percentage of cost reduction (modeling)	$\%CO_{sav,m}$	%
4	Percentage of LCC saving (modeling)	$\%LCC_{sav,m}$	%
5	Percentage of energy saving (modeling)	$\%E_{sav,m}$	%
6	Percentage of grid supplied energy reduction (actual)	$\%GE_{sav,a}$	%
7	Percentage of carbon emission saving (actual)	$\%CO_{2sav,a}$	%
8	Percentage of cost reduction (actual)	$\%CO_{sav,a}$	%
9	Percentage of LCC saving (actual)	$\%LCC_{sav,a}$	%
10	Percentage of life cycle energy saving (actual)	$\%LCE_{sav,a}$	%

Design estimations of performance should be clearly differentiated from actual measured performance to allow insight into performance gaps which may exist due to practical problems. Based on evidence from the building industry, there is large scope for such performance gaps unless the prevalent industry issues are addressed [390]. Actual verification of system performance would appear to be essential for validation [391].

6.5.1.4 Plant optimization

Storage has significant capital cost reduction and revenue enhancing benefits at both larger and smaller scale. At larger scale, the savings in capital cost required for generation, transmission and distribution expansions associated with increased electrification of heat and transport, and increased implementation of variable renewable generation technologies is substantial. Storage can also enable increased revenue from renewable generation through avoidance of curtailment. The need for flexible backup generation to accommodate variable renewables can potentially be avoided through TES.

At the smaller scale, newly installed TES systems can allow peak loads to be satisfied by a significantly less expensive smaller thermal or electrical generator (e.g. with a heat pump) running for longer hours achieving better asset utilization. Where heat or electrical generation capacity is already installed, storage can allow larger loads to be served with longer operating hours,

increasing asset utilization and maximizing revenues. The TES allows the system to operate in a more continuous mode rather than short cycling. This improves operational efficiency and can reduce maintenance requirements and extend the asset lifetime. TES allows demands to be served immediately from storage rather than waiting for the heat generation system to come up to operating speed, which often requires considerable time. To capture these benefits in generic terms, the metrics presented in Table 6.4 are proposed.

Table 6.4: Plant optimization KPIs

No.	Parameter	Symbol	Unit
1	Percentage of source system size reduction	%SSSR	%
2	Percentage of apparent peak load reduction	%APLR	%
3	Percentage of total capital cost reduction	%TCCR	%
4	Percentage of increased source system utilization	%ISSU	%
5	Percentage of reduced unit service cost	%RUSC	%
6	Percentage of reduction in system response time	%RSTT	%
7	Percentage of reduction in source system short cycling	%RSSC	%

6.5.1.5 Enhanced service

Storage has the potential to provide capacity within a system by reducing the fluctuations that would otherwise not be seen by building occupants. This capacity potentially provides a comfort benefit or extends the period that the system can withstand a loss of service improving its resilience. These properties are captured in several DR and load shifting KPIs provided earlier; however, there remains a potential to express these more directly in thermal comfort and resilience metrics as shown in Table 6.5.

Table 6.5: Enhanced service KPIs

No.	Parameter	Symbol	Unit
1	Percentage of reduction or increase in discomfort	%RD	%
2	Comfort after loss of service	CLS	h
3	Parasitic losses from storage (internal gains)	LOSS	kW

6.5.2 KPIs capturing storage disadvantages

Negative aspects of storage should be explicitly captured in KPIs and be considered in design, too. These include the potential for increased energy use through the incorporation of storage systems, having an energy penalty due to charging, discharging and standby losses. These losses should be closely scrutinized at the design and post design stages. This increase in energy use is captured in parameters 25 and 17 in Table 6.1; however, experience from the building domain suggests that often these parameters are underestimated as parasitic losses due to pipe connection points, pumps and other service connections are neglected from calculations. Underestimating these energy costs could significantly undermine the benefits and must be avoided.

Parasitic losses also have the potential to cause discomfort and further unintended secondary energy use. For instance, parasitic losses from TES systems in the summer can cause overheating which stimulates the use of cooling systems. Experience from implementation of solar thermal systems in Passivhaus dwellings in the UK has revealed that gains associated with the TES systems

cause overheating particularly due to poor insulation on connecting pipework rather than the storage itself [390].

Manufacturing the storage systems and the infrastructure required for their implementation should be carefully considered as part of a comprehensive LCA including production, disposal, recycling, etc. These considerations are covered by the KPIs described above but should be managed throughout the design and post design phases to ensure that positive intended outcomes are achieved from storage.

6.6 Description of case studies

This section contains the description of demonstration case studies of Annex 31 related to energy storage solutions designed for the application at the building/district level. To facilitate the analysis and the comparison of different case studies, first, a simplified project form is illustrated which was defined to collect the required information. Thereafter, the information for each case study is presented in detail. Finally, the specific KPIs are calculated for each case study.

Title of the project: Keywords:		
Contact person: Address: Phone: Email:		
Institutions involved: Industry collaboration:		
Type of activity: (mark the appropriate)	X X	Demonstration in laboratory (TRL* ≤ 6) Demonstration in operational environment (TRL ≥ 7)
Type of project: (mark the appropriate)	X X	Demonstration of a stand-alone energy storage technology/solution Demonstration of an energy storage technology/solution applied in a building

*TRL: technology readiness level

Description of the energy storage solution (max 4000 characters)

Technology type:

- Mechanical
- Electrical
- Electrochemical
- Thermal
- Potential

Storage medium:

Describe the storage medium and the required accessories included in the storage system.

Innovative features:

Describe the main innovative features of the storage technology compared to the commercial available solutions.

Operational constraints:

Describe all the operational constraints that must be known for the operation of the storage.

Environmental aspects:

Describe all specific hazards for the environment during the life cycle of the storage system.

Description of the demonstration activity (max 4000 characters)

Brief description of the demonstration activity, with particular reference to:

- Purpose of the demonstration
- Demonstration context (e.g. description of the building in which the energy storage is installed)
- Obtained or expected results
- Budget and funding of the demonstration activity

References

Web sites, published works, etc. related to the demonstration activity.

In this section, based on the previously defined project form, a description of each case study included in the Annex 31 activities is reported. All the case studies are related to demonstration activities realized/monitored by Annex members in laboratory or in operational environment.

6.6.1 HIKARI project, France

Title of the project: HIKARI
Keywords: ZEB, PCM, storage

Contact person: David Corgier
Address: Savoie Technolac BP 209, 73 374 Le Bourget du Lac, France
Phone: +33 6 42 84 20 34 **Email:** david.corgier@cmdl.fr

Institutions involved: ENTPE
Industry collaboration: BOUYGUES IMMOBILIER/ CMDL MANASLU Ing

Type of activity:	Demonstration in laboratory (TRL \leq 6)
X	Demonstration in operational environment (TRL \geq 7)

Type of project:	Demonstration of a stand-alone energy storage technology/solution
X	Demonstration of an energy storage technology/solution applied in a building

Description of the energy storage solution

The different energy storages are hereunder described:

1. Hot water storage:

- 28 m³ water tanks made of 7 tanks in series
- Lifetime: infinite
- Energy storage: 650 kWh (in winter season)

2. Cold water storage:

- 4 tanks with a total volume of 90 m³ in parallel filled with PCM,
- PCM reference: ECIOJOLE 108 from JX Nippon Oil (melting temperature range 8 °C)
- Lifetime: to be evaluated
- Energy storage: 700 kWh
- Cost: €300,000 for the PCM material and €200,000 for the tank

3. Battery system:

- 50 kW in charging and discharging,
- SCIB and Lead Acid coupled technology,
- Capacity: 100 kWh
- Lifetime: to be evaluated
- Cost: €350,000

Description of the demonstration activity

- Purpose of the demonstration: demonstration of a positive energy plot made of 3 buildings.
- Demonstration context: The city of Lyon and Grand Lyon have launched in 2011 a tender to study, to build and to monitor during a period of 24 months a 12,000 m² plot. This latest should be representative of the future targeting a positive energy balance over the year.

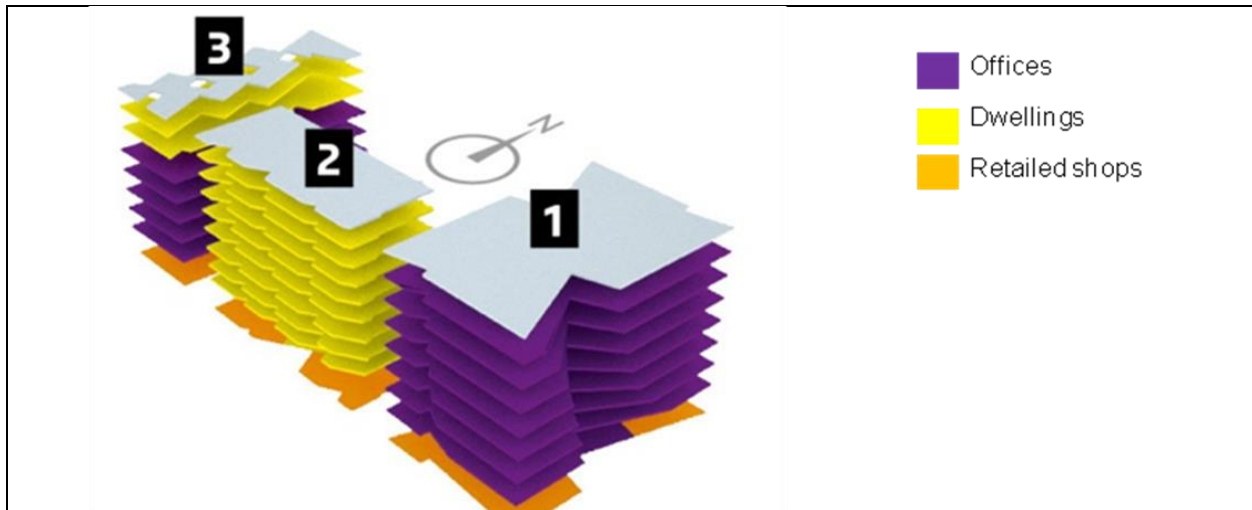


Figure 6.2: HIKARI project description with surface sharing

The surface sharing for each building for dwellings, office area and retail shops is hereunder described in Table 6.6.

Table 6.6: HIKARI surface sharing between buildings and activities

Building name (see Figure 6.2)	Offices	Dwellings	Retail shops	Total
1 – HIGASHI	5,434 m ²	N/A	567 m ²	6,001 m²
2 – MINAMI	N/A	2,959 m ²	289 m ²	3,248 m²
3 – NISHI	2,338 m ²	570 m ²	153 m ²	3,061 m²
Total	7,772 m²	3,529 m²	1,009 m²	12,310 m²

- Obtained or expected results: to evaluate the actual performance of the buildings and equipment within a 2-year operating period to validate the design concept and quality of execution and facility management.
- Budget and funding of the demonstration activity: Construction budget 33 million euros, with a NEDO participation around 5 million euros, demonstration activity: €350,000, with an ADEME funding of 50% in cooperation with ENTPE

References

Website [624]

6.6.2 LOCCIONI project, Italy

Title of the project:	Leaf Lab Thermal Storage
Keywords:	Sensible thermal storage

Contact person:	Antonio Giovannelli
Address:	Via Collefreddo 8/9 Maiolati Spontini (AN) Italy 60030
Phone:	+39 0731 816 537
Email:	a.giovannelli@loccioni.com

Institutions involved:	
Industry collaboration:	Loccioni Group (www.loccioni.com)

Type of activity:	Demonstration in laboratory (TRL \leq 6)
	X Demonstration in operational environment (TRL \geq 7)

Type of project:	Demonstration of a stand-alone energy storage technology/solution
	X Demonstration of an energy storage technology/solution applied in a building

Description of the energy storage solution

A 450 m³ insulated water storage used as thermal storage by charging energy with heat pumps, powered by a solar PV system.

- Long lifetime: it is only an underground water storage and the heat pumps are the same for building conditioning
- Limited cost: the storage concrete structure was realized during the building construction (not many additional costs)
- Large storage capacity: 523.25 kWh
- CO₂ emission reduction by using the energy generated through solar PV system
- Costs reduction by reducing the grid energy consumption

Description of the demonstration activity

- The storage system is charged by using the same heat pumps used for the building conditioning that allow to increase/decrease the temperature of the water in the storage. It is possible to charge the storage when exceeding photovoltaic energy is available to use this energy for cooling/heating the building during the following days.
- The new building (Leaf Lab) is an nZEB with a PV system (240 kW_p) on the roof and heat pumps coupled with the groundwater for conditioning.
- The ESS allows to avoid the energy consumption from the grid during the first two or three days of the week by charging the storage during the weekend. Obviously, the number of days without energy consumption from the grid depends on the amount of stored energy and external conditions.

References

Publications [625-627]

6.6.3 Electrically heated floor, Canada

Title of the project:	Load management using electrically heated floor
Keywords:	Load management, electrically heated floor, floor heating system

Contact person:	Fariborz Haghighat
Address:	1455 De Maisonneuve Blvd. W., Montreal, QC, Canada, H3G 1M8
Phone:	+1 514-848-2424 (3192) Email: fariborz.haghighat@concordia.ca

Institutions involved:	Concordia University (Montreal, QC, Canada)
Industry collaboration:	Hydro-Québec, Ouellet Canada

Type of activity:	X	Demonstration in laboratory (TRL \leq 6)
		Demonstration in operational environment (TRL \geq 7)

Type of project:		Demonstration of a stand-alone energy storage technology/solution
	X	Demonstration of an energy storage technology/solution applied in a building

Description of the energy storage solution	
	<ul style="list-style-type: none">• The energy storage solution is an electrically heated floor (EHF). It consists of wires embedded in a concrete layer with an insulation layer at the bottom. Currently, the system is installed for comfort reasons (to have hot feeling under foots). The objective of this research is to develop its storage capability.• The storage capacity is limited to the maximal floor surface temperature allowed by ASHRAE (29 °C). A lifetime of approximately 20 years is expected.• Actual costs of the material are around \$2.5 (CAD)/cm/m² for the insulation, \$2.5 (CAD)/cm/m² for the concrete and \$65 (CAD)/m² for the EHF turnkey cost. Therefore, for a conventional assembly in Québec, the cost is about \$115 (CAD)/m².

Description of the demonstration activity	
	<ul style="list-style-type: none">• The goal of this project is to study whether EHF can store enough energy to significantly reduce the peak consumption. Moreover, in all houses with low thermal mass, especially in Canada, the only place with thermal mass is the basement floor. Thus, one goal of this project is to study the possibility for storing and release energy in the basement floor.• A first simulation study has been done on a building (without basement) in Canada. Considering that peak periods are mainly during morning and evening, it was assumed that the peak period is from 6:00 AM to 8:00 PM to not create a new peak during the afternoon. The results for January show that 84% of the energy for space conditioning was consumed during the night, with the rest of the consumption only during the afternoon.

References	
	Publications [392, 628]

6.6.4 PCM wall, Turkey

Title of the project:	Enhancing thermal properties of concrete mixes by using phase change materials for energy efficient buildings
Keywords:	Passive thermal energy storage in buildings, microencapsulated PCM, composite wall

Contact person:	Halime Paksoy
Address:	Çukurova University, Adana, 01330, Turkey
Phone:	+90 322 3386418
Email:	hopaksoy@cu.edu.tr

Institutions involved:	Cukurova University, Erciyes University, Niğde University
Industry collaboration:	Kambeton Prefabricated Panel Production Company

Type of activity:	Demonstration in laboratory (TRL \leq 6)
X	Demonstration in operational environment (TRL \geq 7)

Type of project:	Demonstration of a stand-alone energy storage technology/solution
X	Demonstration of an energy storage technology/solution applied in a building

Description of the energy storage solution	
<ul style="list-style-type: none"> • Innovative features: new microencapsulated PCM (mPCM) which is durable to be mixed was developed. The core material in the microcapsule was fatty acid based mixture with melting temperature of 22 °C. The fatty acids, which are bio-based and have limited flammability are more advantageous compared to paraffinic PCMs. The developed mPCM was added in concrete to build a novel composite prefabricated panel. The composite panels with sizes $2 \times 2 \times 0.12 \text{ m}^3$ had two layers each of which had 0.06 m thickness. One of the layers contained 10% mPCM-concrete mixture and the other layer was prepared without PCM. • Capacity and expected lifetime: south and west walls of the test building were built with the composite panel. Total mass of mPCM used was 17 kg. With a latent heat storage capacity of 85 kJ/kg, the total added storage capacity of the composite panels was 1,445 kJ. • Costs (actual and/or expected): mPCM was synthesized in the laboratory and does not have an actual cost. Other microencapsulated products (e.g. Micronal) had an approximate cost of 5 €/kg. • Environmental impact: with the expected energy savings in heating and cooling, CO₂ emissions will also be reduced. The assessment will be done once the measurements are completed. The used fatty acid has vegetable origin and is not a fossil fuel derivative as paraffins. This is also an important feature in terms of carbon footprint of the building and storage technology. 	

Description of the demonstration activity

- **Purpose of the demonstration:**

- (1) developing new mPCM and preparation methods to be used for thermal enhancement of concrete mixes,
- (2) incorporating the developed materials in prefabricated panels with a new approach,
- (3) demonstrating thermal performance of the novel prefabricated panels in test buildings

- **Demonstration context:**

Three buildings shown in Figure 6.3 were built in Adana, Turkey using the novel composite panels. One of the layers contained 10% of mPCM-concrete mixture and the other layer was prepared without PCM. The dimensions of the buildings were $2 \times 2 \times 2 \text{ m}^3$. One of the buildings was the reference, the second one had PCM without microencapsulation and the third one had microencapsulated PCM. South and west walls were built using the composite panels.



Figure 6.3: Picture of test buildings for demonstration of the novel composite walls in Adana, Turkey

T-type thermocouples were placed inside and outside of the test buildings for temperature measurements at 11 different points and connected to a data acquisition system, which recorded at 5-minute intervals. All the instrumentation was connected to a data-server system with internet connection in a separate control building. Temperature distribution on the wall surfaces was also investigated with an infrared camera (Testo 875-2i). Thermal camera images were used to observe thermal effects of mPCMs in the vertical section of panels. Pyranometer (EKO MS-410 Class 1) was placed on the test building to collect total solar irradiation data with 10 minutes intervals.

- **Obtained or expected results:**

Thermal camera image comparison of reference and composite mPCM panels is shown in Figure 6.4. Images were taken on November 5, 2014 at noon. Maximum values of solar irradiation were observed at this time frame can reach above 900 W/m^2 . As can be seen in right image of the figure, there is an increasing temperature gradient in the reference panel. The highest temperature was measured as $35 \text{ }^\circ\text{C}$, on the left side where the sun is shining and, the lowest temperature was around $27 \text{ }^\circ\text{C}$, on the right side facing inwards. In the left image, the highest temperature was also measured as $35 \text{ }^\circ\text{C}$ on left side. Moreover, along the first 6 cm of the composite panel, where no mPCM was used, similar temperature gradient as the base case is observed; however, in the second half of the composite panel, temperature increase is slowed down, and the lowest temperature was around $22 \text{ }^\circ\text{C}$, on the right side facing inwards. This difference of $5 \text{ }^\circ\text{C}$ between inside surface of reference and composite walls is attributed to the heat stored by mPCM which melts isothermally during this process.

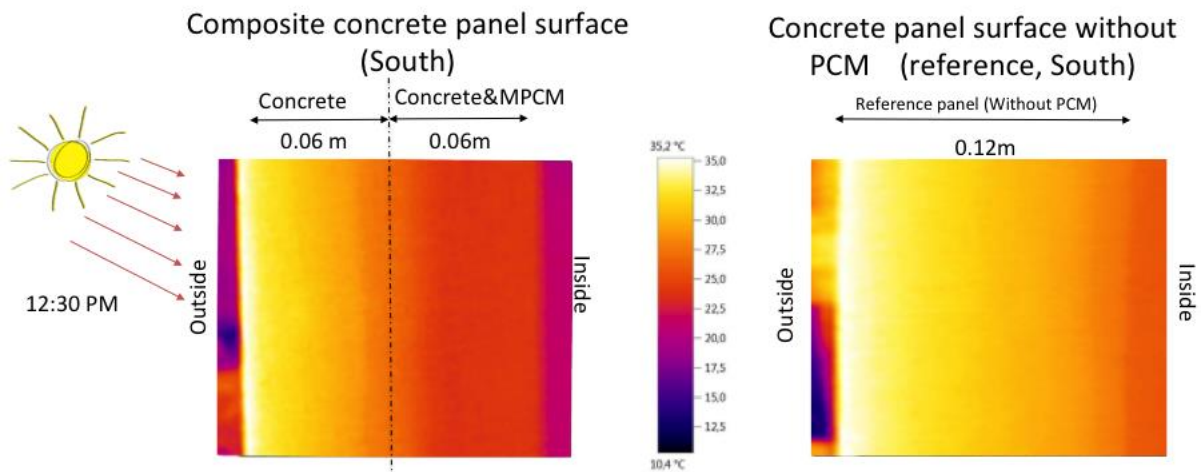


Figure 6.4: Thermal camera images of mFDM panel (left) and the reference case (right)

- **Budget and funding of the demonstration activity:**

Project grant from Turkish Scientific Research Council with two full time PhD students.

References

Publication [629]

6.6.5 KOMCEE, Japan

Title of the project:	21 KOMCEE “Komaba Centre for Educational Excellence”
Keywords:	ZEB, active thermal storage, ground source heat pump, ground water heat pump

Contact person:	Ryozo Ooka		
Address:	IIS, The University of Tokyo, 4-6-1 Komaba, Meguro-ku, Tokyo, Japan		
Phone:	+81-3-5452-6435	Email:	ooka@iis.u-tokyo.ac.jp

Institutions involved:	The University of Tokyo
Industry collaboration:	

Type of activity:	Demonstration in laboratory (TRL \leq 6)
	X Demonstration in operational environment (TRL \geq 7)

Type of project:	Demonstration of a stand-alone energy storage technology/solution
	X Demonstration of an energy storage technology/solution applied in a building

Description of the energy storage solution	
Hot/cold water storage	
<ul style="list-style-type: none">• 300 m³ water tank constructed within the ground pit of the building• Perfect mixing type• Lifetime: infinite• Energy storage: 3,500 kWh at maximum (temperature difference: 10 K)	

Type of project:	X	Demonstration of a stand-alone energy storage technology/solution Demonstration of an energy storage technology/solution applied in a building
------------------	---	---

Description of the energy storage solution

Market development of solar thermal systems in France is penalized by the investment cost compared to other solutions which use fossil fuels or electricity. Moreover, standard solar systems are more suitable for new systems rather than renovation (additional space required for storage), which is the major energy issue in the building sector. The research activities should encourage the development of innovative solutions leading to lower cost suitable for renovation. In this context, integrated collector storages (ICS) are very interesting since they allow financial savings compared to conventional solar thermal systems due to their simplicity, passive operation and faster installation. The ICS exist since the end of 19th century. Currently, about ten companies produce ICS of various geometries, using water as the storage medium [630]. The ICS are suitable both for new buildings and renovation in existing buildings. In ICS, the storage is not located inside the building (few spaces available in existing buildings and square meters cost in new buildings). Therefore, ICS are promising systems for the development of solar thermal market. However, the main drawback of such systems is related to the high thermal losses since the storage is generally not insulated behind the collector absorber. Consequently, the ICS are rather used in hot climates.

The work focused on a new concept of ICS using PCMs within a parallelepiped cavity (honeycomb), using thermosyphon heat pipes to transfer solar energy from the flat plate collector to the storage (see Figure 6.6). The storage cavity is fully thermally insulated to minimize heat losses. The interest of the heat pipes is their passive operation and “thermal diode” behavior. The use of PCM allows reducing the thickness of the storage cavity as compared to water. Architectural integration is thus greatly improved knowing that it is a major problem for most currently available ICS. Moreover, using PCM inside the storage excludes the freezing problem. Finally, a coil type heat exchanger allows discharging the energy contained in the ICS.

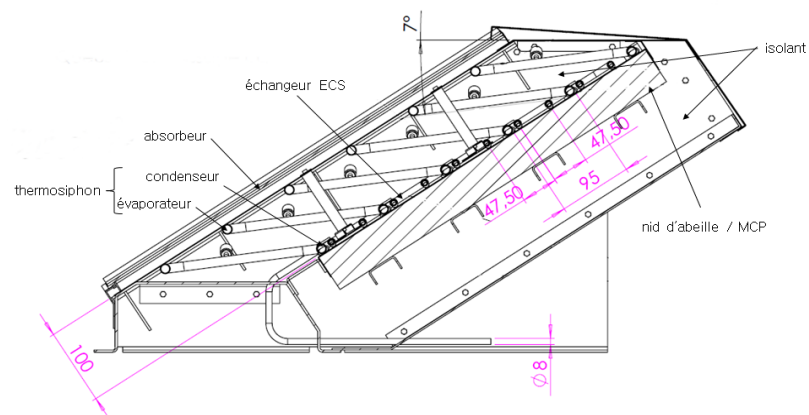


Figure 6.6: The new concept of integral collector storage

Description of the demonstration activity

This new type of ICS has been tested in real conditions at National Solar Energy Institute (INES). The aim of this test was to study the dynamic behavior of ICS in real conditions. This experimental study will also be used to validate a numerical model.

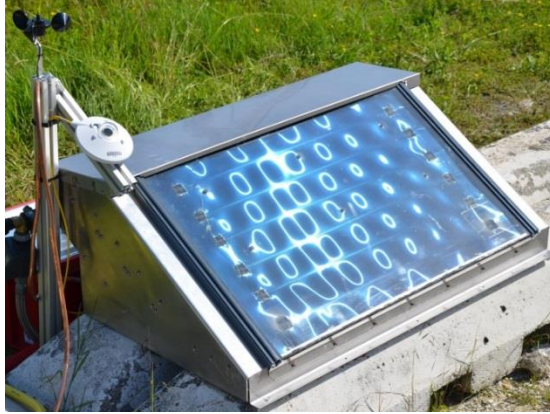


Figure 6.7: Picture of the integral collector storage

Temperature measurements have been carried out using thermocouples at different points within the ICS: the absorber, heat pipe, storage cavity and air-gap.

A pyranometer has also been installed near the collector to measure the irradiance of the collector. An acquisition unit stores all the data. The water discharge rate was 9.3 liters per minute for 19 minutes at 6 AM. This choice has been made to completely discharge the collector to focus only on the storage phase. Complementary tests with more realistic water withdrawal are currently being conducted. The results for the first week of observation are shown in Figure 6.8.

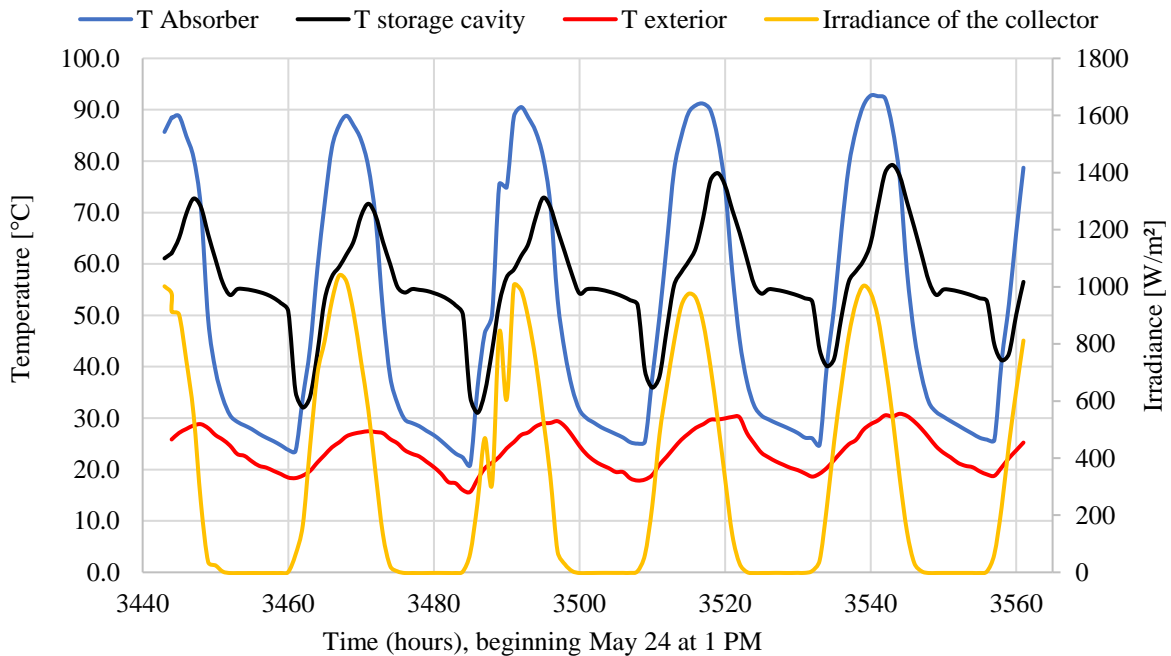


Figure 6.8: Temperature and solar radiation profile (from May 24 to 29)

The results shown in Figure 6.8 are for the first five days of experimentation. During these days, the collector irradiance exceeded 1,000 W/m² (tilt of 30°). The average absorber temperature reached 90 to 95 °C during noon, following the solar radiation fairly well. Concerning the storage, its temperature increased along the day to a peak at about 70 °C during the afternoon. This allowed validating the correct operation of the heat pipes. A stabilization period of several hours appeared at the beginning of each night at about 55 °C, which is the phase change temperature of the PEG 6000, showing its crystallization. A similar phenomenon was observed during the morning when it is melting. The melting was faster due to the solar gains rate. Finally, the water withdrawal decreased the storage temperature (which dropped to about 35 °C before rising again). This experimental study is funded by the ADEME in the framework of the agreement n° 1205C0129 (project CSIS).

References

Publications [631-633]

6.6.7 WWHC District, UK

Title of the project: West Whitlawburn Housing Co-operative biomass district heating with thermal storage
Keywords: Sensible thermal storage, district heating, housing, fuel poverty, biomass, heat pump, renewable, 4th generation, performance gap, design tool

Contact person: Andrew Lyden
Address: 16 Richmond Street, Glasgow G1 1XQ
Phone: +44 7540395205 **Email:** andrew.lyden@strath.ac.uk

Institutions involved: University of Strathclyde
Industry collaboration: West Whitlawburn Housing Co-operative

Type of activity:
 Demonstration in laboratory (TRL ≤ 6)
 Demonstration in operational environment (TRL ≥ 7)

Type of project:
 Demonstration of a stand-alone energy storage technology/solution
 Demonstration of an energy storage technology/solution applied in a building

Description of the energy storage solution

A thermal storage (a hot water tank) has been included in a DHS serving 600 dwellings mainly in high rise and tenement blocks which uses a biomass boiler as the main heat source. The purpose of the thermal storage is both to allow for heat generated by the biomass to meet daily demand peaks which exceed the boiler capacity, and to reduce the boiler cycling such that it can run at a steadier output which optimizes performance. This thermal storage differs from a separate much smaller buffer tank, primarily utilized for protection from rapid cycling which can cause damage to the boiler. District heating provides the boiler with a smoother, diversified load but this is still subject to daily peaks. The thermal storage allows for the separation of the stochastic district heating load and the required output from the biomass

boiler which can be run at a more fixed value optimizing efficiency and maintenance schedules and minimizing the use of backup gas boilers. The biomass-supplied heat is supported by a Government renewable heat incentive (RHI) payment so the thermal storage increases the financial returns from the system and reduces the overall cost of heating.

The capacity of the hot water tank is 50 m³ and runs at high and low temperatures of 85 °C and 70 °C, respectively. This means that there is an energetic capacity of 871 kWh or 58 kWh/K. The expected lifetime of the thermal storage has not been analyzed.

The current biomass and thermal storage operation is configured to fill and empty the storage depending on its mean temperature. Figure 6.9 shows a 9-hour period of the thermal storage mean temperature and the biomass flow rate. When the thermal storage reaches a temperature of 85 °C and the biomass output exceeds the load, the boiler switches OFF (evident by the flow rate drop in Figure 6.9). The thermal storage then meets the load until the mean temperature drops to 70 °C when the biomass turns back ON. The thermal storage then returns to the high mean temperature (85 °C). This operation mode allows the biomass to operate at a fixed point, feeding both the load and the storage, separating the district load and the boiler load. Options for more advanced control schemes will be investigated. Figure 6.10 shows an excerpt of the nodal analysis of the thermal storage at 7 different heights in the tank.

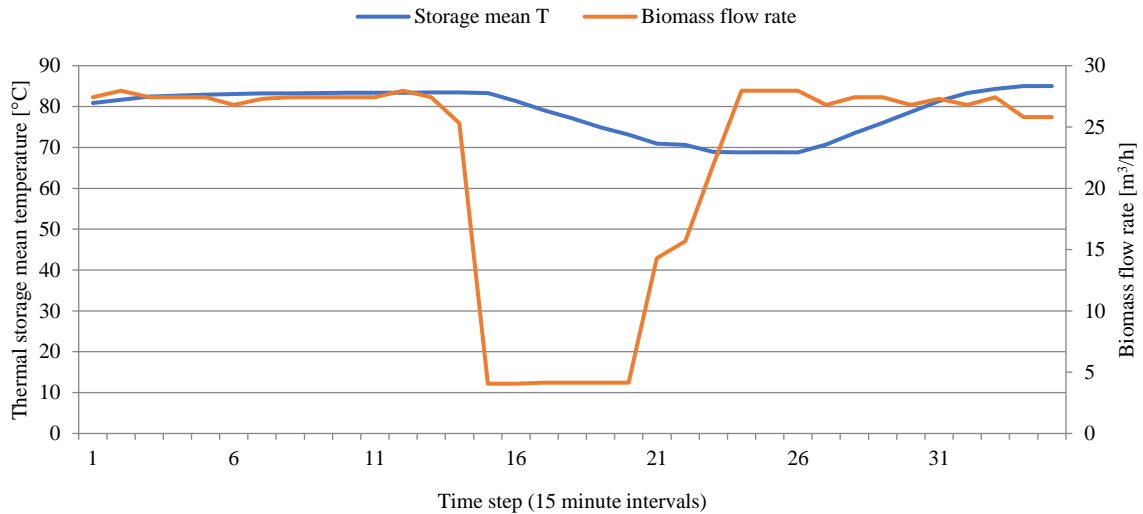


Figure 6.9: Current biomass and thermal storage operation

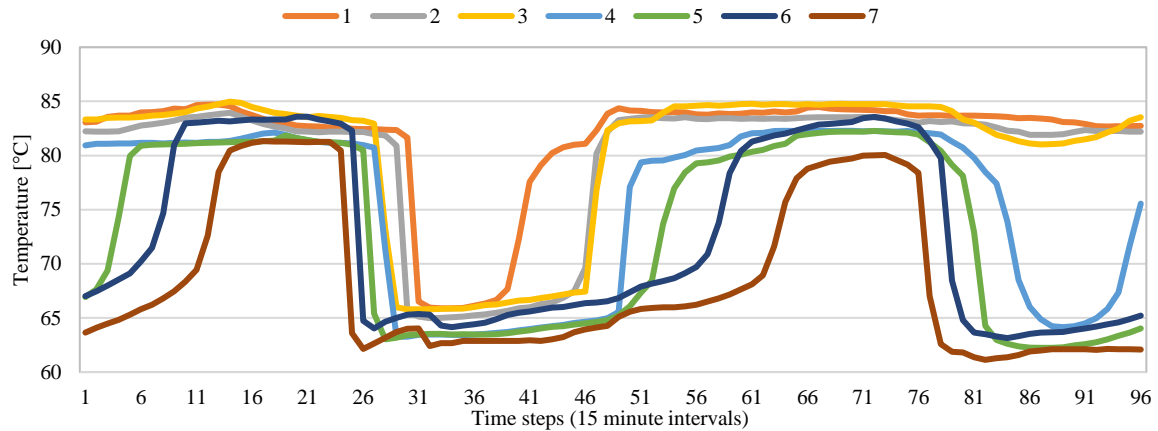


Figure 6.10: Temperature levels in thermal storage

The negative environmental impact of a hot water tank is seen as minimal, with the physical dimensions of the storage tank not particularly taller than the boiler house and lower than the flues meaning the visual impact is the same as the boiler house. There should be a positive environmental impact due to the higher usage of the biomass boiler, displacing the use of gas boilers. Here, it is presumed that gas has a worse environmental impact than biomass. The biomass boiler should also be working more efficiently due to the thermal storage, resulting in a higher heat output per input mass unit of biomass.

Description of the demonstration activity

- **Purpose and context**

West Whitlawburn Housing Co-operative (WWHC) is a fully mutual, tenant owned and controlled housing co-operative with charitable status, located in the south of Glasgow in Cambuslang, South Lanarkshire. It is an area of multiple deprivations and its aim was to provide affordable, sustainable and community-controlled energy to the households.

WWHC own and manage 644 properties: 432 multi-story flats, 112 low-rise tenement flats and 100 houses (Figure 6.11). Previously, heat was supplied via electric storage and panel heaters in the individual dwellings. Due to the build construction types of the multi-story and low-rise tenement flats, gas heating could not be installed. All these properties have had fabric upgrades including building, windows and roofs. The largest investment was adding substantial external cladding to multi-story flats.



Figure 6.11: Picture of WWHC multi-story flats

The solution to tackle the rising problem of fuel poverty in the community was decided to be a biomass based DHS with a centralized energy center supplying domestic heat and hot water to dwellings via a district heating network. To allow for optimal performance of the biomass boiler, a thermal storage was included. Work on this scheme was completed in December 2014, though extensive remedial work has been necessary which began in June 2015 and is ongoing.

There is a 740 kW Viessman Pyrotec biomass boiler (Figure 6.12) which operates with the 50 m³ water tank and three 1.2 MW gas boilers (Figure 6.13) which help with peak demand, provide backup in the event of a breakdown, and ensure demand is met during maintenance.



Figure 6.12: Picture of Viessman Pyrotec (740 kW)



Figure 6.13: Picture of the thermal storage with 50,000 liters capacity (left) and the boiler house (right)

The system is being used as a base for academic research and knowledge transfer to industry. Monitoring data is being gathered on the system operation and this is informing the creation of models which will be used to develop design and control strategy improvements to optimize performance. These will be tested on the system and the results will be reported.

- **Research focus and results**

A methodology and supporting software tool for optimizing the design of biomass heating systems and thermal storage has recently been developed and released for industry use [317], called the Biomass Design Support Tool. This is being retrospectively applied to the WWHC system with the aim of further developing and extending this methodology and toolset to better support delivery of biomass plus storage systems which operate effectively without gaps between design and operational performance. The biomass design tool suggests that the system performance should be much better than is being seen (e.g. for the current system around 95% of the heat should be from biomass while in reality it was 77% from March 2016 to February 2017).

Energy performance certificates are a requirement for flats in the UK. These have been improved due to the installation of the DHS. The multi-story flats have moved from D to C and A for energy efficiency and environmental impact, respectively.

The community looked at an individual flat and found there to be a 34% reduction in consumption and 16% reduction in cost for that particular tenant.

The secondary aim of the research is to develop a methodology and supporting toolset for the incorporation of heat pumps and thermal storage within single building or 4GDHS which maximize the use of renewable generation (wind and solar). The methodology should address design and operation and avoid performance gaps. Several large-scale district systems have been announced in Scotland [634] but these do not yet consider optimization of thermal storage, use of renewables, performance gaps, or 4GDHS concepts.

The third aim of the research is to establish a methodology for realistically capturing demand behaviors for use in design and control of district level systems with storage. This will be incorporated into the methodology and toolsets to be developed for design.

- **Budget and funding of the demonstration activity**

Funding for the WWHC district heating network came from various sources and different times. A substantial amount was contributed by Npower, through the Energy Company Obligation (ECO), who became WWHC's utility partner. An overall of £6.75 million capital funding package was obtained by funding from Npower through ECO, the Warm Homes Fund, and European Regional Development grant funding. Further funding came from the Big Lottery Community Spaces funding to extend the district heating network.

References

Websites [317, 634-636] and publications [232, 637]

6.6.8 Tsukuba-Mirai, Japan

Title of the project:	Tsukuba-Mirai Technology Center of SANKEN Environmental Engineering
Keywords:	Stratified water thermal storage, solar collector

Contact person:	SANKEN Environmental Engineering
Address:	
Phone:	Email:

Institutions involved:	
Industry collaboration:	SANKEN Environmental Engineering

Type of activity:	X	Demonstration in laboratory (TRL \leq 6)
		Demonstration in operational environment (TRL \geq 7)

Type of project:	X	Demonstration of a stand-alone energy storage technology/solution
		Demonstration of an energy storage technology/solution applied in a building

Description of the energy storage solution

The system is consisted of 28 flat plate solar collectors with total space of 96 m² and a stainless-steel tank with 4 m³ of volume. The stratified water TES system is connected to the solar collector directly. The charging and discharging operations depend on inside temperature of the storage.

Description of the demonstration activity

The objective of this project is to make the most of the solar thermal energy usage with the stratified TES tank. The annual solar thermal energy usage in 2013 was 59.1 GJ. COP of the solar thermal system (including pumps) in winter, especially November to March, was 36-40 and the coefficient of utilization of solar energy was 89-96%. The COP in July and October was 22-23 and the coefficient was 72-80%.

Energy costs: 17 yen/kWh in summer, 16 yen/kWh in other seasons.

Cost per stored kWh annual thermal: 0.55 yen/kWh to discharge annual thermal energy from tank.

References

Website [638]

6.6.9 Nagoya University, Japan

Title of the project:	Building for researches and experiments at Nagoya University
Keywords:	Stratified water thermal storage, demand prediction

Contact person:	Hideki Tanaka
Address:	
Phone:	Email:

Institutions involved:	Nagoya University
Industry collaboration:	None

Type of activity:	X	Demonstration in laboratory (TRL \leq 6)
		Demonstration in operational environment (TRL \geq 7)

Type of project:	X	Demonstration of a stand-alone energy storage technology/solution
		Demonstration of an energy storage technology/solution applied in a building

Description of the energy storage solution	
	<ul style="list-style-type: none">• The storage total capacity is 3,535 kWh• Design temperature degree 13 K (5–18 °C: cooling, actual charge temp: 5.3 °C)• Actual temperature degree 12.7 K• Storage tank volume: 126 m³ × 2 tanks

Description of the demonstration activity	
	<p>The project has three main purposes:</p> <ol style="list-style-type: none">1) Reduction of the peak-time demand.2) Energy saving by the utilization of groundwater and heat pump.3) Load forecasting for optimal operations of the TES system. <p>Especially, energy saving by 20% compared to an ordinary building. The building has total floor space of 7,000 m² and air-conditioned area of 3,200 m². The designed COP of the heat source machine (heat pump) was 6.3. The system COP (SCOP) was designed to 2.33 in a design stage and measured to 2.02 in practice. Annual primary energy consumption per square meter was 1.93 GJ/m² (reference case: 2.32 GJ/m² of common buildings in Japan).</p>

References	
	None

6.6.10 T-building, Japan

Title of the project:	T-building
Keywords:	Several stratified water thermal storages, utilization of middle temperature chilled and hot water for space cooling and heating

Contact person:	Ryozo Ooka
Address:	IIS, The University of Tokyo, 4-6-1 Komaba, Meguro-ku, Tokyo, Japan
Phone:	+81-3-5452-6435
Email:	

Institutions involved:	
Industry collaboration:	MORI building, NIHON SEKKEI, SHINRYO CORPORATION

Type of activity:	X	Demonstration in laboratory (TRL \leq 6)
		Demonstration in operational environment (TRL \geq 7)

Type of project:	X	Demonstration of a stand-alone energy storage technology/solution
		Demonstration of an energy storage technology/solution applied in a building

Description of the energy storage solution

The capacities of three thermal storage tanks are 1,600 m³, 2,000 m³ and 900 m³ for ST1, ST2 and ST3, respectively.

Measured data:

ST1: 20,556 kWh for cooling and 24,722 kWh for heating

ST2: 17,222 kWh for cooling

ST3: 19,167 kWh for cooling

Description of the demonstration activity

The purpose of this project is to minimize daily primary energy consumption. The optimal operations could reduce the primary energy consumption in summer and intermediate day by 6.2% and 19.4%, respectively.

Measured data:

Annual SCOP for cooling system at 6 °C water was 1.81.

The SCOP for cooling system at middle temperature was 2.05.

The SCOP for heating system at middle temperature was 1.28.

The SCOP for hot water system at 44 °C was 0.94 due to the utilization of boilers.

References

Publication: presented in a Japanese conference.

6.7 KPI calculation for the Annex 31 case studies

In general, where possible the KPIs were calculated considering the results of monitoring activities. If the indicator is derived from predicted or simulated data, it was marked with an asterisk. In few cases, some indicators were not calculated since the available information at this state was not considered sufficiently reliable.

Table 6.7: KPI values for HIKARI project, France, storage 1: chilled water storage (thermal storage)

No.	KPI	Value	Comment
1a	Storage total capacity	700 kWh _t	
1b	Storage useful capacity	686 kWh _t	
2	Recharging energy	714 kWh _t	
3a	Maximum charge power	45 kW _t	
3b	Maximum discharge power	70 kW _t	
4	Depth of discharge (DOD)	100%	
5	Durability (number of cycles)	Over 20 years	With 1 cycle per day. To be confirmed by long-term monitoring.
6	Specific cost of the storage	0.1 €/kWh _t 0.3 €/kWh _e	€500,000 (€150,000 for the tank and €350,000 for the materials and baskets). O&M costs are negligible. The value for €/kWh _e assumes chiller EER of 3.
7	Maximum self-discharge rate	0.5%	
8a	Storage size	92 m ³	
8b	Storage weight	90,000 kg	
9a	Energy storage factor on demand	20 – 80%	
9b	Energy storage factor on RES production	Not applicable	No RES are connected to the storage.
10	Generated energy/cost saving	N/A	

Table 6.8: KPI values for HIKARI project, France, storage 2: electrical energy storage (electrochemical storage)

No.	KPI	Value	Comment
1a	Storage total capacity	100 kWh _e	
1b	Storage useful capacity	95 kWh _e	To be verified by monitoring
2	Recharging energy	102 kWh _e	To be verified by monitoring
3a	Maximum charge power	50 kW _e	
3b	Maximum discharge power	50 kW _e	
4	Depth of discharge (DOD)	80%	
5	Durability (number of cycles)	6,000	With a remaining capacity of 82% (to be confirmed by long-term monitoring)
6	Specific cost of the storage	1.05 €/kWh _e + O&M costs	Total cost of €500,00. O&M costs will be accounted after long-term monitoring.
7	Maximum self-discharge rate	Negligible	To be confirmed by monitoring
8a	Storage size	28 m ³	
8b	Storage weight	7,300 kg	
9a	Energy storage factor on demand	N/A	
9b	Energy storage factor on RES production	Not applicable	No RES connected to the storage
10	Generated energy/cost saving	N/A	

Table 6.9: KPI values for LOCCIONI project, Italy

No.	KPI	Value	Comment
1a	Storage total capacity	6,800 kWh	523.25 kWh/K. Maximum charging temperature: 45 °C (winter), 4 °C (summer)
1b	Storage useful capacity	6,800 kWh	
2	Recharging energy	N/A	To be defined by monitoring
3a	Maximum charge power	430 kW	
3b	Maximum discharge power	390 kW	
4	Depth of discharge (DOD)	100%	To be confirmed by monitoring
5	Durability (number of cycles)	Over 30 years	With 1 cycle per day. To be confirmed by monitoring
6	Specific cost of the storage	N/A	
7	Maximum self-discharge rate	0.5%/24 h	To be confirmed by monitoring
8a	Storage size	450 m ³	
8b	Storage weight	550,000 kg	
9a	Energy storage factor on demand	25%	From Dec. 2016 to Mar. 2017
9b	Energy storage factor on RES production	Not applicable	
10	Generated energy/cost saving	Variable	

Table 6.10: KPI values for electrically heated floor, Canada

No.	KPI	Value	Comment
1a	Storage total capacity	85.86 kWh	For the coldest day of Jan. 2009 (Jan. 15, 2009)
1b	Storage useful capacity	41.5 kWh	For the coldest day of Jan. 2009 (Jan. 15, 2009)
2	Recharging energy	107.42 kWh	For the coldest day of Jan. 2009 (Jan. 15, 2009)
3a	Maximum charge power	12,478 W	For the coldest day of Jan. 2009 (Jan. 15, 2009)
3b	Maximum discharge power	6,727 W	For the coldest day of Jan. 2009 (Jan. 15, 2009)
4	Depth of discharge (DOD)	62%	For the coldest day of Jan. 2009 (Jan. 15, 2009)
5	Durability (number of cycles)	4,240	Concrete durability of 20 years, and 1 cycle per day for 7 months per year
6	Specific cost of the storage	0.048 €/kWh	
7	Maximum self-discharge rate	53%	For the coldest day of Jan. 2009 (Jan. 15, 2009)
8a	Storage size	11,85 m ³	
8b	Storage weight	26,070 kg	
9a	Energy storage factor on demand	41.5%	For the coldest day of Jan. 2009 (Jan. 15, 2009)
9b	Energy storage factor on RES production	Not applicable	
10	Generated energy/cost saving	Variable	

Table 6.11: KPI values for PCM wall, Turkey

No.	KPI	Value	Comment
1a	Storage total capacity	384 Wh	
1b	Storage useful capacity	384 Wh	
2	Recharging energy	N/A	To be defined by monitoring
3a	Maximum charge power	3 W	Outside temperature higher than 25 °C during 57 days in the fall
3b	Maximum discharge power	1 W	Outside temperature higher than 25 °C during 57 days in the fall
4	Depth of discharge (DOD)	100%	
5	Durability (number of cycles)	10 years	1 cycle per day
6	Specific cost of the storage	25€/kg - 0.28 €/kWh	
7	Maximum self-discharge rate	N/A	To be defined by monitoring
8a	Storage size	0.04 m ³	
8b	Storage weight	16 kg	
9a	Energy storage factor on demand	N/A	To be defined by monitoring
9b	Energy storage factor on RES production	Not applicable	
10	Generated energy/cost saving	N/A	To be defined by monitoring

Table 6.12: KPI values for KOMCEE, Japan

No.	KPI	Value	Comment
1a	Storage total capacity	1,732 kWh	
1b	Storage useful capacity	1,160 kWh	
2	Recharging energy	1,765.6 kWh	
3a	Maximum charge power	357.2 kW	
3b	Maximum discharge power	250 W	
4	Depth of discharge (DOD)	65.7%	
5	Durability (number of cycles)	N/A	To be defined by monitoring
6	Specific cost of the storage	N/A	
7	Maximum self-discharge rate	53%/96 h	
8a	Storage size	298.2 m ³	
8b	Storage weight	298,200 kg	
9a	Energy storage factor on demand	N/A	To be defined by monitoring
9b	Energy storage factor on RES production	N/A	To be defined by monitoring
10	Generated energy/cost saving	N/A	To be defined by monitoring

Table 6.13: KPI values for integral solar collector, France

No.	KPI	Value	Comment
1a	Storage total capacity	16.9 kWh	
1b	Storage useful capacity	16.9 kWh	
2	Recharging energy	N/A	To be defined by monitoring
3a	Maximum charge power	4 kW	(4 m ² at 1000 W/m ²)
3b	Maximum discharge power	25 W	
4	Depth of discharge (DOD)	100%	
5	Durability (number of cycles)	1,825	(PCM - PEG 6000 - lifetime is around 5 years [639])
6	Specific cost of the storage	0.020 €/kWh	PCM + Honeycomb: 157 €/m ²
7	Maximum self-discharge rate	3%	
8a	Storage size	0.160 m ³	Modular elements, can be added to infinity
8b	Storage weight	192 kg	
9a	Energy storage factor on demand	100%	
9b	Energy storage factor on RES production	70%	
10	Generated energy/cost saving	N/A	To be defined by monitoring

Table 6.14: KPI values for biomass district heating with thermal storage, UK

No.	KPI	Value	Comment
1a	Storage total capacity	871 kWh	Return temperature into storage is 85 – 70 °C
1b	Storage useful capacity	871 kWh	Charge/discharge efficiency is considered negligible
2	Recharging energy	871 kWh	
3a	Maximum charge power	740 kW	
3b	Maximum discharge power	1,896 W	
4	Depth of discharge (DOD)	100%	
5	Durability (number of cycles)	N/A	To be defined by monitoring
6	Specific cost of the storage	N/A	
7	Maximum self-discharge rate	N/A	To be defined by monitoring
8a	Storage size	Missing information	
8b	Storage weight	Missing information	
9a	Energy storage factor on demand	15.83%	Monitored for 1 day (Mar. 26, 2016)
9b	Energy storage factor on RES production	16.04%	Monitored for 1 day (Mar. 26, 2016)
10	Generated energy/cost saving	N/A	To be defined by monitoring

Table 6.15: KPI values for Tsukuba-Mirai, Japan

No.	KPI	Value	Comment
1a	Storage total capacity	160 kWh	Reference temp: 23 °C, operation: Feb. 11, 2017 7:59 AM to 3:35 PM
1b	Storage useful capacity	136 kWh	Ambient tank temperature: 7 °C, discharge operation: Feb. 12, 2017 7:46 AM to 6:31 PM
2	Recharging energy	166 kWh	
3a	Maximum charge power	32 kW	
3b	Maximum discharge power	47 kW	
4	Depth of discharge (DOD)	N/A	To be defined by monitoring
5	Durability (number of cycles)	N/A	To be defined by monitoring
6	Specific cost of the storage	0.0075 €/kWh	150 million yen was required for primary cost of the tank with 1600 kWh capacity
7	Maximum self-discharge rate	6%/16 h	Average temperature in tank: about 61 °C, ambient temperature: 7 °C, reference period: Feb. 11, 2017 3:35 PM to Feb. 12, 2017 7:45 AM
8a	Storage size	4 m ³	
8b	Storage weight	4,290 kg	
9a	Energy storage factor on demand	N/A	To be defined by monitoring. Utilization rate of stored energy in winter was 93%.
9b	Energy storage factor on RES production	N/A	To be defined by monitoring
10	Generated energy/cost saving	N/A	To be defined by monitoring

Table 6.16: KPI values for Nagoya University, Japan

No.	KPI	Value	Comment
1a	Storage total capacity	3,535 kWh	Design temperature: 13 K (5 -18 °C, cooling)
1b	Storage useful capacity	4,470 kWh	Actual temperature: 17.7 K (5.3 - 23 °C, cooling), discharge ratio by limiting temperature of charging and discharging: 13.8%
2	Recharging energy	4,470 kWh	
3a	Maximum charge power	260 kW	
3b	Maximum discharge power	280 kW	
4	Depth of discharge (DOD)	N/A	To be defined by monitoring
5	Durability (number of cycles)	N/A	To be defined by monitoring
6	Specific cost of the storage	N/A	To be defined by monitoring
7	Maximum self-discharge rate	Cooling: 0% Heating: 29%	
8a	Storage size	252 m ³	
8b	Storage weight	252,000 kg	
9a	Energy storage factor on demand	N/A	To be defined by monitoring
9b	Energy storage factor on RES production	N/A	To be defined by monitoring
10	Generated energy/cost saving	N/A	To be defined by monitoring

Table 6.17: KPI values for T-building, Japan

No.	KPI	Value	Comment
1a	Storage total capacity	Cooling: 20,556 kWh Heating: 24,722 kWh	Cooling reference temperature: 19 °C, water temperature in TES: 12 °C, temperature difference: 7 °C Heating reference temperature: 31 °C, water temperature in TES: 39 °C, temperature difference: 8 °C
1b	Storage useful capacity	Cooling: 20,556 kWh Heating: 24,722 kWh	Cooling reference temperature: 19 °C, water temperature in TES: 12 °C, temperature difference: 7 °C Heating reference temperature: 31 °C, water temperature in TES: 39 °C, temperature difference: 8 °C
2	Recharging energy	N/A	To be defined by monitoring
3a	Maximum charge power	Cooling: 1,722 kW Heating: 1,709 kW	
3b	Maximum discharge power	Cooling: 3,106 kW Heating: 6,782 kW	
4	Depth of discharge (DOD)	100%	
5	Durability (number of cycles)	N/A	To be defined by monitoring
6	Specific cost of the storage	N/A	
7	Maximum self-discharge rate	Cooling: 11.9%	Reference period: Apr. 1, 2015 to Mar. 31, 2016
8a	Storage size	2,706 m ³	
8b	Storage weight	2,706,000 kg	
9a	Energy storage factor on demand	70%	
9b	Energy storage factor on RES production	N/A	To be defined by monitoring
10	Generated energy/cost saving	N/A	To be defined by monitoring

The proposed simplified project form eased the collection of necessary information about the different case studies among the Annex 31 members. The features and the performances of the analyzed ESSs are heterogeneous. The total storage capacity ranges from less than 1 kWh to over 10,000 kWh. In 6 demonstrations, a sensible thermal storage is used, whereas in 3 a latent thermal storage and in one case a sensible thermal storage and an electrochemical storage are coupled. To provide a general overview of the completeness of the information retrieved, Table 6.18 presents the percentage of the analyzed case studies in which (with the available data) such indicators could be calculated.

Table 6.18: Percentage of the case studies in which the KPI was correctly calculated using the available information

No.	KPI	Completeness
1a	Storage total capacity	100%
1b	Storage useful capacity	100%
2	Recharging energy	80%
3a	Maximum charge power	100%
3b	Maximum discharge power	100%
4	Depth of discharge (DOD)	70%
5	Durability (number of cycles)	50%
6	Specific cost of the storage	50%
7	Maximum self-discharge rate	70%
8a	Storage size	90%
8b	Storage weight	90%
9a	Energy storage factor on demand	60%
9b	Energy storage factor on RES production	20%
10	Generated energy/cost saving	10%

As it can be observed, several indicators were easily calculated in all cases, using the information already monitored/retrieved. Other KPIs could not be determined for several applications, with particular reference to durability, specific cost of the storage, energy storage factors and generated energy/cost saving. The reason was that the requested information for their calculation were not monitored/available.

The detailed analysis of the encountered problems allowed identifying the main barriers:

- The determination of some quantities requires a long-term testing phase (e.g. in the case of durability) but many of the analyzed demonstrations are very recent; however, a reliable indication about durability should always be provided, by means of accelerated aging tests carried out by ESS manufacturers in the typical operating conditions of building applications.
- Other KPIs (e.g. energy storage factors) involve a comprehensive monitoring of the energy flows in the building where the ESS is installed and not just of the ESS itself. Such

quantities are sometimes neglected in the specific monitoring activity of the ESS or are acquired with an insufficient level of detail. In such cases, a comprehensive monitoring campaign aimed at recovering the data needed to calculate the proposed KPIs should be always designed.

- Problems encountered in the calculation of economic parameters (e.g. specific cost of the storage and generated cost of saving) are often related to the uncertain/enhanced costs of demonstration activities. This reveals the need to strengthen the capability to precisely determine the actual cost/benefit ratio related to the application of ESSs in buildings, by separating the extra costs due to experimental activities to the other expenses. This effort is fundamental for the selection of the most appropriate technology and to trigger the commercial penetration of ESS in the building sector.

Chapter 7: Conclusion

7.1 Concluding remarks

Effective utilization of RES and the development of optimized districts hold greater potential in meeting the increasing energy demand as well as reducing the GHG emissions from buildings/districts. However, the main drawback of RES is their intermittent nature, while for DHSs, the main challenge is the effective energy management between the supply and demand. In this context, TES systems could play a vital role in addressing the drawbacks of both RES and DHSs. Although TES is a significant technology, determining its optimal operation and integrating it with buildings/districts are stalled by the high computational demand (or even lack of) tools and optimization techniques.

Annex 31 aimed to reduce the existing gap in developing effective tools for modeling and optimization for building/district with energy storage systems. The main focus of the annex was held on emphasizing the need for the development of simplified modeling and optimization tools related to predicting, operating and evaluating the performance of buildings and districts when energy storage is included. In addition, the current state-of-the-art regarding energy storage in buildings/districts were presented. The basic introduction on energy consumption pattern in buildings/districts, necessity of energy storage and the various energy storage technologies were briefly discussed in Chapters 1 and 2 of Annex 31. In Chapters 3 and 4, fundamentals along with the general capabilities and limitations of the available modelling and optimization tools for analyzing/determining the optimal operation of TES systems at building and district levels were critically assessed. Exclusive examples/case studies related to simplified modeling at the building scale were given in Chapter 3 and two levels of model validation at the district level were illustrated in Chapter 4. Chapter 5 was dedicated to critically review the types of optimization methods (deterministic, stochastic, hybrid), algorithms (MILP, MINLP, DP, etc.), objective functions and the optimization tools (AIMMS, GAMS, AMPL, etc.). The methodologies to reduce the optimization computational time at building and district levels were discussed in detail. Further, two unique examples with one addressing the issues for the life cycle optimization of nZEBs and other proposing a dynamic optimization model to explore the optimal equipment size using detailed demand profile at the district scale were presented. In Chapter 6, the existing KPIs from the literature were analyzed to evaluate their pros and cons. Subsequently, a specific set of KPIs were defined to conduct a simplified but exhaustive analysis and comparison of Annex 31 case studies. A set of advanced KPIs were also defined to shed light on their potential future applications.

In summary, Annex 31 discussed the multi-disciplinary field of energy storage at building/districts covering a wide spectrum of challenges in modeling, optimization and performance evaluation. Since among energy storage systems, sensible and latent thermal systems received considerable attention, the majority of this publication was dedicated to them. Several up-to-date challenges in the field of energy storage were also presented as examples in each chapter to enlighten the concept and to present the current state-of-the-art.

7.2 Achievements

The main achievements of Annex 31 can be summarized as:

- Effective integration of TES systems with buildings and districts were discussed distinctly with some real case examples.
- Computationally efficient modeling and optimization tools were developed to assess the performance of buildings and districts with energy storage.
- KPIs which consider storage capacity, recharging energy, maximum charging and discharging power, depth of discharge, durability, specific cost of storage, maximum self-discharge rate, storage size/weight, energy storage factor, and generated energy/cost saving were developed for assessing the impacts of energy storage systems integrated with buildings and districts.
- The dissemination of knowledge and experience acquired in Annex 31 will guide researchers toward the integration of optimally sized energy storage systems with buildings and districts.

7.3 Recommendations for the future work

The following points present the recommendations for the future research for each title presented in this publication:

- **Building level modeling:** the existing comprehensive models are already well-established and saturated. However, the discrepancies between the simulations and real case scenarios can be further reduced. In this context, it is recommended to upgrade the existing models so that users can easily model the buildings within the urban setting (as opposed to the existing stand-alone approach).
- **District level modeling:** despite development of several tools for district level modeling, existing models lack the capability of modeling the entire DHS elements (i.e. energy resources, distribution network as well as demand profile prediction). In addition, data collection and processing for large-scale communities (city or regional level) are very computationally intensive or even not feasible. Therefore, developing a smart systematic approach which can easily gather data from different sources (i.e. city databanks, utility industries, etc.) and then model the entire district system is required.
- **Optimization:** Existing optimization approaches are either focused on energy mapping or equipment sizing. Hence, a simplified dynamic optimization approach which can simultaneously optimize both of them at the design stage is currently missing.
- **Key performance indicators:** more precise and standardized monitoring procedures are needed to have a comprehensive view of the benefits related to energy storage in buildings/districts. In this sense, the developed KPIs allow to push for more detailed and widespread assessments in the future.

References

- [1] B.R. Keeble, The Brundtland report: 'Our common future', *Medicine and War*, 4 (1) (1988) 17-25.
- [2] K. Li, H. Su, J. Chu, Forecasting building energy consumption using neural networks and hybrid neuro-fuzzy system: A comparative study, *Energy and Buildings*, 43 (10) (2011) 2893-2899.
- [3] Y. Li, L. Fu, S. Zhang, X. Zhao, A new type of district heating system based on distributed absorption heat pumps, *Energy*, 36 (7) (2011) 4570-4576.
- [4] A. Keçebaş, Effect of reference state on the exergoeconomic evaluation of geothermal district heating systems, *Renewable and Sustainable Energy Reviews*, 25 (2013) 462-469.
- [5] *Energy Technology Perspectives*, International Energy Agency, 2012.
- [6] T. Laajalehto, M. Kuosa, T. Mäkilä, M. Lampinen, R. Lahdelma, Energy efficiency improvements utilising mass flow control and a ring topology in a district heating network, *Applied thermal engineering*, 69 (1) (2014) 86-95.
- [7] A. Fragaki, A.N. Andersen, D. Toke, Exploration of economical sizing of gas engine and thermal store for combined heat and power plants in the UK, *Energy*, 33 (11) (2008) 1659-1670.
- [8] M. Noussan, G.C. Abdin, A. Poggio, R. Roberto, Biomass-fired CHP and heat storage system simulations in existing district heating systems, *Applied Thermal Engineering*, 71 (2) (2014) 729-735.
- [9] G. Taljan, G. Verbič, M. Pantoš, M. Sakulin, L. Fickert, Optimal sizing of biomass-fired Organic Rankine Cycle CHP system with heat storage, *Renewable Energy*, 41 (2012) 29-38.
- [10] M. Wigbels, W. Althaus, M. Lucht, Nonlinear Optimisation in CHP Applications, Fraunhofer Institut für Umwelt-, Sicherheits- und Energietechnik UMSICHT, (2002).
- [11] A. Christidis, C. Koch, L. Pottel, G. Tsatsaronis, The contribution of heat storage to the profitable operation of combined heat and power plants in liberalized electricity markets, *Energy*, 41 (1) (2012) 75-82.
- [12] B. Rolfsman, Combined heat-and-power plants and district heating in a deregulated electricity market, *Applied energy*, 78 (1) (2004) 37-52.
- [13] G. Krajačić, N. Duić, Z. Zmijarević, B.V. Mathiesen, A.A. Vučinić, M. da Graça Carvalho, Planning for a 100% independent energy system based on smart energy storage for integration of renewables and CO₂ emissions reduction, *Applied thermal engineering*, 31 (13) (2011) 2073-2083.
- [14] A. Hawkes, M. Leach, Modelling high level system design and unit commitment for a microgrid, *Applied energy*, 86 (7-8) (2009) 1253-1265.
- [15] A. Chesi, G. Ferrara, L. Ferrari, S. Magnani, F. Tarani, Influence of the heat storage size on the plant performance in a smart user case study, *Applied energy*, 112 (2013) 1454-1465.
- [16] S. Hameer, J. Van Niekerk, A thermodynamic model for comparing thermal energy storage system to electrochemical, chemical, and mechanical energy storage technologies, in, 3rd Southern African Solar Energy Conference, South Africa, 11-13 May, 2015.
- [17] H. Wang, W. Yin, E. Abdollahi, R. Lahdelma, W. Jiao, Modelling and optimization of CHP based district heating system with renewable energy production and energy storage, *Applied Energy*, 159 (2015) 401-421.
- [18] S. Ashok, R. Banerjee, Optimal cool storage capacity for load management, *Energy*, 28 (2) (2003) 115-126.

- [19] V. Verda, F. Colella, Primary energy savings through thermal storage in district heating networks, *Energy*, 36 (7) (2011) 4278-4286.
- [20] J. Vetterli, M. Benz, Cost-optimal design of an ice-storage cooling system using mixed-integer linear programming techniques under various electricity tariff schemes, *Energy and buildings*, 49 (2012) 226-234.
- [21] H. Ren, W. Gao, Y. Ruan, Optimal sizing for residential CHP system, *Applied Thermal Engineering*, 28 (5-6) (2008) 514-523.
- [22] T. Fang, R. Lahdelma, Optimization of combined heat and power production with heat storage based on sliding time window method, *Applied energy*, 162 (2016) 723-732.
- [23] O.P. Palsson, H.F. Ravn, Stochastic heat storage problem—solved by the progressive hedging algorithm, *Energy conversion and management*, 35 (12) (1994) 1157-1171.
- [24] J.R. Nielsen, H. Quicklund, Two-step decision and optimisation model for centralised or decentralised thermal storage in DH&C systems, in, 2005.
- [25] K.M. Powell, Dynamic optimization of energy systems with thermal energy storage, (2013).
- [26] H. Yun, W. Li, Optimization and analysis of distributed energy system with energy storage device, *Energy Procedia*, 12 (2011) 958-965.
- [27] K.M. Powell, W.J. Cole, U.F. Ekarika, T.F. Edgar, Optimal chiller loading in a district cooling system with thermal energy storage, *Energy*, 50 (2013) 445-453.
- [28] M. Martin, P. Thornley, The potential for thermal storage to reduce the overall carbon emissions from district heating systems, Tyndall Centre for Climate Change Research, (2013).
- [29] H. Tanaka, T. Tomita, M. Okumiya, Feasibility study of a district energy system with seasonal water thermal storage, *Solar Energy*, 69 (6) (2000) 535-547.
- [30] Building Energy Performance Metrics - Secure Sustainable Together Supporting Energy Efficiency Progress in Major Economies, in, International Energy Agency, 2015.
- [31] H. Ibrahim, A. Ilinca, J. Perron, Energy storage systems—characteristics and comparisons, *Renewable and sustainable energy reviews*, 12 (5) (2008) 1221-1250.
- [32] T. Kousksou, P. Bruel, A. Jamil, T. El Rhafiki, Y. Zeraoui, Energy storage: Applications and challenges, *Solar Energy Materials and Solar Cells*, 120 (2014) 59-80.
- [33] L.F. Cabeza, E. Galindo, C. Prieto, C. Barreneche, A.I. Fernández, Key performance indicators in thermal energy storage: Survey and assessment, *Renewable Energy*, 83 (2015) 820-827.
- [34] F. Wang, G. Maidment, J. Missenden, R. Tozer, -A review of research concerning the use of PCMS in air conditioning and refrigeration engineering, in: *Advances in building technology*, Elsevier, 2002, pp. 1273-1280.
- [35] F. Setterwall, K. Alexanderson, Phase Change Materials and Chemical Reactions for Thermal Energy Storage: State of the Art 1996, 1996.
- [36] S. Hasnain, Review on sustainable thermal energy storage technologies, Part I: heat storage materials and techniques, *Energy conversion and management*, 39 (11) (1998) 1127-1138.
- [37] S. Hasnain, Review on sustainable thermal energy storage technologies, Part II: cool thermal storage, *Energy conversion and management*, 39 (11) (1998) 1139-1153.
- [38] M.M. Farid, A.M. Khudhair, S.A.K. Razack, S. Al-Hallaj, A review on phase change energy storage: materials and applications, *Energy conversion and management*, 45 (9) (2004) 1597-1615.
- [39] A. Gil, M. Medrano, I. Martorell, A. Lázaro, P. Dolado, B. Zalba, L.F. Cabeza, State of the art on high temperature thermal energy storage for power generation. Part 1—Concepts,

- materials and modellization, *Renewable and Sustainable Energy Reviews*, 14 (1) (2010) 31-55.
- [40] E. Hahne, Thermal energy storage: some views on some problems, in: *Proceedings of the 8th International Heat Transfer Conference*, 1986, pp. 279-292.
- [41] K. Lovegrove, A. Luzzi, H. Kreetz, A solar-driven ammonia-based thermochemical energy storage system, *Solar energy*, 67 (4) (1999) 309-316.
- [42] M. Kubota, K. Yokoyama, F. Watanabe, M. Hasatani, Heat releasing characteristics of CaO/CaCO₃ reaction in a packed bed for high temperature heat storage and temperature upgrading, in: *Proceedings of the 8 th International Conference on Thermal Energy Storage (Terrastock 2000)*, 2000.
- [43] K. Visscher, SolarCombi systems, heading for 100% solar fraction, ECN presentation given at VSK Utrecht, (2004).
- [44] S. Shiizaki, I. Nagashimga, K. Iwata, T. Hosoda, H. Kameyama, Development of plate fin reactor for heat recovery system using methanol decomposition, in: *Proceedings of the 8th International Conference on Thermal Energy Storage (Terrastock 2000)*, 2000.
- [45] H. Liu, J. Jiang, Flywheel energy storage—An upswing technology for energy sustainability, *Energy and buildings*, 39 (5) (2007) 599-604.
- [46] B. Lehmann, V. Dorer, M. Koschenz, Application range of thermally activated building systems tabs, *Energy and buildings*, 39 (5) (2007) 593-598.
- [47] V. Basecq, G. Michaux, C. Inard, P. Blondeau, Short-term storage systems of thermal energy for buildings: a review, *Advances in Building Energy Research*, 7 (1) (2013) 66-119.
- [48] A.R. Corporation, U.D.O.o.P. Development, Solar dwelling design concepts, For sale by the Superintendent of Documents, US Govt. Print. Off., 1976.
- [49] G. Reynders, J. Diriken, D. Saelens, Generic characterization method for energy flexibility: Applied to structural thermal storage in residential buildings, *Applied energy*, 198 (2017) 192-202.
- [50] L. Navarro, A. de Gracia, S. Colclough, M. Browne, S.J. McCormack, P. Griffiths, L.F. Cabeza, Thermal energy storage in building integrated thermal systems: A review. Part 1. active storage systems, *Renewable Energy*, 88 (2016) 526-547.
- [51] J. Heier, C. Bales, V. Martin, Combining thermal energy storage with buildings—a review, *Renewable and Sustainable Energy Reviews*, 42 (2015) 1305-1325.
- [52] E. Dotzauer, Simple model for prediction of loads in district-heating systems, *Applied Energy*, 73 (3) (2002) 277-284.
- [53] J. Ortiga, J.C. Bruno, A. Coronas, I.E. Grossman, Review of optimization models for the design of polygeneration systems in district heating and cooling networks, *Computer Aided Chemical Engineering*, 24 (2007) 1121-1126.
- [54] N. Eriksson, Predicting demand in districtheating systems: A neural network approach, in, 2012.
- [55] T. CIBSE, Degree-days: theory and application, London: The Chartered Institution of Building Services Engineers, 16 (2006).
- [56] M. Pirouti, A. Bagdanavicius, J. Ekanayake, J. Wu, N. Jenkins, Energy consumption and economic analyses of a district heating network, *Energy*, 57 (2013) 149-159.
- [57] V. Verda, G. Baccino, A. Sciacovelli, S.L. Russo, Impact of district heating and groundwater heat pump systems on the primary energy needs in urban areas, *Applied thermal engineering*, 40 (2012) 18-26.
- [58] *Energy Use Data Handbook*, in, Natural Resources Canada, 2013.

- [59] M.S. Al-Homoud, Computer-aided building energy analysis techniques, *Building and Environment*, 36 (4) (2001) 421-433.
- [60] T. Sharp, Energy benchmarking in commercial office buildings, in: *Proceedings of the ACEEE*, 1996, pp. 321-329.
- [61] A. Dalla Rosa, J.E. Christensen, Low-energy district heating in energy-efficient building areas, *Energy*, 36 (12) (2011) 6890-6899.
- [62] A. Dalla Rosa, R. Boulter, K. Church, S. Svendsen, District heating (DH) network design and operation toward a system-wide methodology for optimizing renewable energy solutions (SMORES) in Canada: A case study, *Energy*, 45 (1) (2012) 960-974.
- [63] 2008 commercial and institutional consumption of energy survey summary, in, *Natural Resources Canada*, 2008.
- [64] C.S. Barnaby, J.D. Spitler, Development of the Residential Load Factor Method for Heating and Cooling Load Calculations, *ASHRAE Transactions*, 111 (1) (2005).
- [65] D.B. Crawley, L.K. Lawrie, F.C. Winkelmann, W.F. Buhl, Y.J. Huang, C.O. Pedersen, R.K. Strand, R.J. Liesen, D.E. Fisher, M.J. Witte, EnergyPlus: creating a new-generation building energy simulation program, *Energy and buildings*, 33 (4) (2001) 319-331.
- [66] S. Klein, W. Beckman, J. Mitchell, J. Duffie, N. Duffie, T. Freeman, J. Mitchell, J. Braun, B. Evans, J. Kummer, TRNSYS 16—A TRaNsient system simulation program, user manual, Solar Energy Laboratory. Madison: University of Wisconsin-Madison, (2004).
- [67] M. de Guadalfajara, M.A. Lozano, L.M. Serra, Evaluation of the potential of large solar heating plants in Spain, *Energy Procedia*, 30 (2012) 839-848.
- [68] M. Guadalfajara, M.A. Lozano, L.M. Serra, Comparison of simple methods for the design of central solar heating plants with seasonal storage, *Energy Procedia*, 48 (2014) 1110-1117.
- [69] Y. Zhang, K. Soga, R. Choudhary, S. Bains, GSHP application for heating and cooling at 'City Scale' for the city of westminster, in: *Proceedings World Geothermal Congress*, 2015.
- [70] Y. Zhang, K. Soga, R. Choudhary, Shallow geothermal energy application with GSHPs at city scale: study on the City of Westminster, *Géotechnique Letters*, 4 (2) (2014) 125-131.
- [71] E.-J. Kim, G. Plessis, J.-L. Hubert, J.-J. Roux, Urban energy simulation: Simplification and reduction of building envelope models, *Energy and Buildings*, 84 (2014) 193-202.
- [72] S. Wang, X. Xu, Simplified building model for transient thermal performance estimation using GA-based parameter identification, *International Journal of Thermal Sciences*, 45 (4) (2006) 419-432.
- [73] G. Gross, F.D. Galiana, Short-term load forecasting, *Proceedings of the IEEE*, 75 (12) (1987) 1558-1573.
- [74] Z. Tang, C. de Almeida, P.A. Fishwick, Time series forecasting using neural networks vs. Box-Jenkins methodology, *Simulation*, 57 (5) (1991) 303-310.
- [75] N. Amjady, Short-term hourly load forecasting using time-series modeling with peak load estimation capability, *IEEE Transactions on Power Systems*, 16 (4) (2001) 798-805.
- [76] C.-M. Lee, C.-N. Ko, Short-term load forecasting using lifting scheme and ARIMA models, *Expert Systems with Applications*, 38 (5) (2011) 5902-5911.
- [77] O.P. Palsson, Stochastic modeling, control and optimization of district heating systems, Ph. D. thesis, IMSOR, DTU, 1993.
- [78] E.S. Gardner, Exponential smoothing: The state of the art, *Journal of Forecasting*, 4 (1) (1985) 1-28.
- [79] S. Makridakis, Empirical-evidence versus personal-experience, John Wiley & Sons LTD Baffins Lane Chichester, W Sussex, England PO19 1UD, 1983.

- [80] G. Zhang, B.E. Patuwo, M.Y. Hu, Forecasting with artificial neural networks:: The state of the art, *International journal of forecasting*, 14 (1) (1998) 35-62.
- [81] H.S. Hippert, C.E. Pedreira, R.C. Souza, Neural networks for short-term load forecasting: A review and evaluation, *IEEE Transactions on power systems*, 16 (1) (2001) 44-55.
- [82] B.-J. Chen, M.-W. Chang, Load forecasting using support vector machines: A study on EUNITE competition 2001, *IEEE transactions on power systems*, 19 (4) (2004) 1821-1830.
- [83] D.B. Crawley, J.W. Hand, M. Kummert, B.T. Griffith, Contrasting the capabilities of building energy performance simulation programs, *Building and environment*, 43 (4) (2008) 661-673.
- [84] S.E. Mattsson, H. Elmqvist, Modelica-An international effort to design the next generation modeling language, *IFAC Proceedings Volumes*, 30 (4) (1997) 151-155.
- [85] M. Wetter, W. Zuo, T.S. Nouidui, X. Pang, Modelica buildings library, *Journal of Building Performance Simulation*, 7 (4) (2014) 253-270.
- [86] J. Van Roy, B. Verbruggen, J. Driesen, Ideas for tomorrow: New tools for integrated building and district modeling, *IEEE Power and Energy Magazine*, 11 (5) (2013) 75-81.
- [87] C. Nytsch-Geusen, J. Huber, M. Ljubijankic, J. Rädler, Modelica BuildingSystems– eine Modellbibliothek zur Simulation komplexer energietechnischer Gebäudesysteme, *Bauphysik*, 35 (1) (2013) 21-29.
- [88] M. Wetter, C.v. Treeck, IEA EBC Annex 60, New generation computational tools for building and community energy systems based on the Modelica and Functional Mockup Interface standards, (2014).
- [89] IBPSA Project 1: BIM/GIS and Modelica Framework for building and community energy system design and operation, in, <https://ibpsa.github.io/project1/>.
- [90] A. Bastani, F. Haghighat, J. Kozinski, Designing building envelope with PCM wallboards: Design tool development, *Renewable and Sustainable Energy Reviews*, 31 (2014) 554-562.
- [91] A. Bastani, F. Haghighat, Expanding Heisler chart to characterize heat transfer phenomena in a building envelope integrated with phase change materials, *Energy and Buildings*, (2015).
- [92] A. El-Sawi, F. Haghighat, H. Akbari, Assessing long-term performance of centralized thermal energy storage system, *Applied Thermal Engineering*, 62 (2) (2014) 313-321.
- [93] F. Nasiri, F. Mafakheri, D. Adebajo, F. Haghighat, Modeling and analysis of renewable heat integration into non-domestic buildings-The case of biomass boilers: A whole life asset-supply chain management approach, *Biomass and Bioenergy*, 95 (2016) 244-256.
- [94] B. Talebi, P.A. Mirzaei, A. Bastani, F. Haghighat, A review of district heating systems: modeling and optimization, *Frontiers in Built Environment*, 2 (2016) 22.
- [95] D. Olsthoorn, F. Haghighat, P.A. Mirzaei, Integration of storage and renewable energy into district heating systems: A review of modelling and optimization, *Solar Energy*, 136 (2016) 49-64.
- [96] P. Weitzmann, J. Kragh, P. Roots, S. Svendsen, Modelling floor heating systems using a validated two-dimensional ground-coupled numerical model, *Building and Environment*, 40 (2) (2005) 153-163.
- [97] D. Cvetković, M. Bojić, Optimization of thermal insulation of a house heated by using radiant panels, *Energy and Buildings*, 85 (2014) 329-336.
- [98] D. Wang, Y. Liu, Y. Wang, J. Liu, Numerical and experimental analysis of floor heat storage and release during an intermittent in-slab floor heating process, *Applied Thermal Engineering*, 62 (2) (2014) 398-406.
- [99] T. SEL, T. CSTB, Multizone Building modeling with Type56 and TRNBuild, in, TRNSYS, 2004.

- [100] S. Aongya, *Contrôle du Chauffage Pour la Gestion de la Demande Résidentielle—Rapport Technique sur la Création d’un Modèle Résidentiel Fonctionnel*, Hydro-Quebec: Shawinigan, QC, Canada, (2010).
- [101] A. Bastani, F. Haghighat, C.J. Manzano, Investigating the effect of control strategy on the shift of energy consumption in a building integrated with PCM wallboard, *Energy Procedia*, 78 (2015) 2280-2285.
- [102] ASHRAE Guideline 14–2014, Measurement of Energy and Demand Savings, in, American Society of Heating, Refrigeration and Air Conditioning Engineers, Atlanta, GA, 2014.
- [103] S. Seddegh, X. Wang, A.D. Henderson, Numerical investigation of heat transfer mechanism in a vertical shell and tube latent heat energy storage system, *Applied thermal engineering*, 87 (2015) 698-706.
- [104] N. Tay, M. Belusko, F. Bruno, An effectiveness-NTU technique for characterising tube-in-tank phase change thermal energy storage systems, *Applied Energy*, 91 (1) (2012) 309-319.
- [105] M.M. Joybari, F. Haghighat, Natural convection modelling of melting in phase change materials: Development of a novel zonal effectiveness-NTU, in: 9th International Conference on Indoor Air Quality Ventilation and Energy Conservation In Buildings (IAQVEC 2016), Incheon Songdo, South Korea, 2016.
- [106] A.A. Al-Abidi, S. Mat, K. Sopian, M. Sulaiman, A.T. Mohammad, Experimental Investigation of Melting in Triplex Tube Thermal Energy Storage, (2013).
- [107] X. Sun, Q. Zhang, M.A. Medina, K.O. Lee, Experimental observations on the heat transfer enhancement caused by natural convection during melting of solid–liquid phase change materials (PCMs), *Applied Energy*, 162 (2016) 1453-1461.
- [108] N. Tay, F. Bruno, M. Belusko, Experimental validation of a CFD and an ε -NTU model for a large tube-in-tank PCM system, *International Journal of Heat and Mass Transfer*, 55 (21) (2012) 5931-5940.
- [109] RT31 Data sheet, in, Rubitherm Technologies GmbH, 2013.
- [110] A.R. Darzi, M. Farhadi, K. Sedighi, Numerical study of melting inside concentric and eccentric horizontal annulus, *Applied Mathematical Modelling*, 36 (9) (2012) 4080-4086.
- [111] V.R. Voller, C. Prakash, A fixed grid numerical modelling methodology for convection-diffusion mushy region phase-change problems, *International Journal of Heat and Mass Transfer*, 30 (8) (1987) 1709-1719.
- [112] S. Mat, A.A. Al-Abidi, K. Sopian, M. Sulaiman, A.T. Mohammad, Enhance heat transfer for PCM melting in triplex tube with internal–external fins, *Energy Conversion and Management*, 74 (2013) 223-236.
- [113] A.A. Al-abidi, S.B. Mat, K. Sopian, M. Sulaiman, A.T. Mohammed, CFD applications for latent heat thermal energy storage: a review, *Renewable and sustainable energy reviews*, 20 (2013) 353-363.
- [114] S. Seddegh, X. Wang, A.D. Henderson, Z. Xing, Solar domestic hot water systems using latent heat energy storage medium: A review, *Renewable and sustainable energy reviews*, 49 (2015) 517-533.
- [115] F. Agyenim, N. Hewitt, P. Eames, M. Smyth, A review of materials, heat transfer and phase change problem formulation for latent heat thermal energy storage systems (LHTESS), *Renewable and sustainable energy reviews*, 14 (2) (2010) 615-628.
- [116] S.S.M. Tehrani, R.A. Taylor, P. Saberi, G. Diarce, Design and feasibility of high temperature shell and tube latent heat thermal energy storage system for solar thermal power plants, *Renewable energy*, 96 (2016) 120-136.

- [117] Q. Li, S.S.M. Tehrani, R.A. Taylor, Techno-economic analysis of a concentrating solar collector with built-in shell and tube latent heat thermal energy storage, *Energy*, 121 (2017) 220-237.
- [118] M. Farid, Y. Kim, T. Honda, A. Kanzawa, The role of natural convection during melting and solidification of PCM in a vertical cylinder, *Chemical Engineering Communications*, 84 (1) (1989) 43-60.
- [119] M. Farid, A. Mohamed, Effect of natural convection on the process of melting and solidification of paraffin wax, *Chemical engineering communications*, 57 (1-6) (1987) 297-316.
- [120] M.M. Farid, R.M. Husian, An electrical storage heater using the phase-change method of heat storage, *Energy Conversion and Management*, 30 (3) (1990) 219-230.
- [121] N. Amin, F. Bruno, M. Belusko, Effective thermal conductivity for melting in PCM encapsulated in a sphere, *Applied Energy*, 122 (2014) 280-287.
- [122] E. Sparrow, J. Broadbent, Inward melting in a vertical tube which allows free expansion of the phase-change medium, *ASME Journal of Heat Transfer*, 104 (2) (1982) 309-315.
- [123] C. Liu, D. Groulx, Experimental study of the phase change heat transfer inside a horizontal cylindrical latent heat energy storage system, *International Journal of Thermal Sciences*, 82 (2014) 100-110.
- [124] J. Yang, L. Yang, C. Xu, X. Du, Experimental study on enhancement of thermal energy storage with phase-change material, *Applied Energy*, 169 (2016) 164-176.
- [125] B.J. Jones, D. Sun, S. Krishnan, S.V. Garimella, Experimental and numerical study of melting in a cylinder, *International Journal of Heat and Mass Transfer*, 49 (15) (2006) 2724-2738.
- [126] C.-Y. Li, S.V. Garimella, J.E. Simpson, Fixed-grid front-tracking algorithm for solidification problems, part I: Method and validation, *Numerical Heat Transfer, Part B: Fundamentals*, 43 (2) (2003) 117-141.
- [127] *The Copper Tube Handbook*, Copper Development Association Inc., New York, NY, USA, 2011.
- [128] Rubitherm Technologies GmbH, in: *Organic PCM*, <http://www.rubitherm.eu/en/index.php/productcategory/organische-pcm-rt/>, Berlin, Germany, 2017.
- [129] M.M. Joybari, F. Haghighat, S. Seddegh, Numerical investigation of a triplex tube heat exchanger with phase change material: Simultaneous charging and discharging, *Energy and Buildings*, 139 (2017) 426-438.
- [130] S. Seddegh, X. Wang, A.D. Henderson, A comparative study of thermal behaviour of a horizontal and vertical shell-and-tube energy storage using phase change materials, *Applied Thermal Engineering*, 93 (2016) 348-358.
- [131] G. Hed, R. Bellander, Mathematical modelling of PCM air heat exchanger, *Energy and Buildings*, 38 (2) (2006) 82-89.
- [132] E. Halawa, W. Saman, Thermal performance analysis of a phase change thermal storage unit for space heating, *Renewable Energy*, 36 (1) (2011) 259-264.
- [133] D.N. Nkwetta, F. Haghighat, Thermal energy storage with phase change material—a state-of-the-art review, *Sustainable Cities and Society*, 10 (2014) 87-100.
- [134] D.N. Nkwetta, P.-E. Vouillamoz, F. Haghighat, M. El-Mankibi, A. Moreau, A. Daoud, Impact of phase change materials types and positioning on hot water tank thermal

- performance: Using measured water demand profile, *Applied Thermal Engineering*, 67 (1-2) (2014) 460-468.
- [135] M. Pomianowski, P. Heiselberg, Y. Zhang, Review of thermal energy storage technologies based on PCM application in buildings, *Energy and Buildings*, 67 (2013) 56-69.
- [136] P. Ma, L.-S. Wang, N. Guo, Modeling of TABS-based thermally manageable buildings in Simulink, *Applied energy*, 104 (2013) 791-800.
- [137] M. Gwerder, B. Lehmann, J. Tödtli, V. Dorer, F. Renggli, Control of thermally-activated building systems (TABS), *Applied energy*, 85 (7) (2008) 565-581.
- [138] D. Saulles, *Free cooling systems: design and application guidance*, Bracknell, England: Building Services Research and Information Association, (1996).
- [139] J. Turnpenny, D. Etheridge, D. Reay, Novel ventilation cooling system for reducing air conditioning in buildings.: Part I: testing and theoretical modelling, *Applied Thermal Engineering*, 20 (11) (2000) 1019-1037.
- [140] B. Zalba, J.M. Marín, L.F. Cabeza, H. Mehling, Free-cooling of buildings with phase change materials, *International Journal of Refrigeration*, 27 (8) (2004) 839-849.
- [141] X. Chen, Q. Zhang, Z.J. Zhai, Energy saving potential of a ventilation system with a latent heat thermal energy storage unit under different climatic conditions, *Energy and Buildings*, 118 (2016) 339-349.
- [142] J. Holman, *Heat Transfer*, 9th Edition ed., McGrawHill, New York, USA, 2002.
- [143] A. Maccarini, M. Wetter, A. Afshari, G. Hultmark, N.C. Bergsøe, A. Vorre, Energy saving potential of a two-pipe system for simultaneous heating and cooling of office buildings, *Energy and Buildings*, 134 (2017) 234-247.
- [144] M. Deru, K. Field, D. Studer, K. Benne, B. Griffith, P. Torcellini, B. Liu, M. Halverson, D. Winiarski, M. Rosenberg, *US Department of Energy commercial reference building models of the national building stock*, (2011).
- [145] H.S. Carslaw, J.C. Jaeger, *Conduction of heat in solids*, Oxford: Clarendon Press, 1959, 2nd ed., (1959).
- [146] L. Ingersol, O. Zobel, A. Ingersol, *Heat conduction, with Engineering and Geological Applications*, MacGraw-Hill, New York, (1948).
- [147] L.R. Ingersoll, O.J. Zabel, A.C. Ingersoll, *Heat conduction with engineering, geological, and other applications*, (1954).
- [148] P. Eskilson, *Thermal analysis of heat extraction boreholes*, Univ. Lund, 22 (1986).
- [149] H. Zeng, N. Diao, Z. Fang, A finite line-source model for boreholes in geothermal heat exchangers, *Heat Transfer—Asian Research*, 31 (7) (2002) 558-567.
- [150] L. Lamarche, B. Beauchamp, A new contribution to the finite line-source model for geothermal boreholes, *Energy and Buildings*, 39 (2) (2007) 188-198.
- [151] J. Claesson, S. Javed, An analytical method to calculate borehole fluid temperatures for time-scales from minutes to decades, in: *ASHRAE Transactions*, 2011, pp. 279-288.
- [152] M. Philippe, M. Bernier, D. Marchio, Validity ranges of three analytical solutions to heat transfer in the vicinity of single boreholes, *Geothermics*, 38 (4) (2009) 407-413.
- [153] L. Lamarche, Short-term behavior of classical analytic solutions for the design of ground-source heat pumps, *Renewable energy*, 57 (2013) 171-180.
- [154] D. Marcotte, P. Pasquier, F. Sheriff, M. Bernier, The importance of axial effects for borehole design of geothermal heat-pump systems, *Renewable Energy*, 35 (4) (2010) 763-770.
- [155] W. Choi, R. Ooka, Y. Nam, Impact of long-term operation of ground-source heat pump on subsurface thermal state in urban areas, *Sustainable Cities and Society*, (2018).

- [156] G. Hagen, Ueber die Bewegung des Wassers in engen cylindrischen Röhren, *Annalen der Physik*, 122 (3) (1839) 423-442.
- [157] J.L. Poiseuille, *Recherches expérimentales sur le mouvement des liquides dans les tubes de très-petits diamètres*, Imprimerie Royale, 1844.
- [158] W. Choi, R. Ooka, Effect of disturbance on thermal response test, part 2: Numerical study of applicability and limitation of infinite line source model for interpretation under disturbance from outdoor environment, *Renewable Energy*, 85 (2016) 1090-1105.
- [159] R. Ooka, W. Choi, Y. Nam, Environmental Impact Assessment of Long-term Operation of Ground Source Heat Pump Using Numerical Simulation, in: *IEA ECES Greenstock 2015*, Beijing, China, 2015.
- [160] M.A. Ancona, M. Bianchi, L. Branchini, F. Melino, District heating network design and analysis, *Energy Procedia*, 45 (2014) 1225-1234.
- [161] H. Gopalakrishnan, D. Kosanovic, Economic optimization of combined cycle district heating systems, *Sustainable Energy Technologies and Assessments*, 7 (2014) 91-100.
- [162] D.D. Andrews, A. Krook-Riekkola, E. Tzimas, J. Serpa, J. Carlsson, N. Pardo-Garcia, I. Papaioannou, Background report on EU-27 district heating and cooling potentials, barriers, best practice and measures of promotion, in: *Publications Office of the European Union*, 2012.
- [163] M. Gong, S. Werner, Exergy analysis of network temperature levels in Swedish and Danish district heating systems, *Renewable energy*, 84 (2015) 106-113.
- [164] T. Srinivas, B.V. Reddy, Comparative studies of augmentation in combined cycle power plants, *International Journal of Energy Research*, 38 (9) (2014) 1201-1213.
- [165] H. Fang, J. Xia, Y. Jiang, Key issues and solutions in a district heating system using low-grade industrial waste heat, *Energy*, 86 (2015) 589-602.
- [166] D. Chasapis, V. Drosou, I. Papamechael, A. Aidonis, R. Blanchard, Monitoring and operational results of a hybrid solar-biomass heating system, *Renewable Energy*, 33 (8) (2008) 1759-1767.
- [167] D. McIlveen-Wright, F. Pinto, L. Armesto, M. Caballero, M. Aznar, A. Cabanillas, Y. Huang, C. Franco, I. Gulyurtlu, J. McMullan, A comparison of circulating fluidised bed combustion and gasification power plant technologies for processing mixtures of coal, biomass and plastic waste, *Fuel processing technology*, 87 (9) (2006) 793-801.
- [168] E. Pihl, S. Heyne, H. Thunman, F. Johnsson, Highly efficient electricity generation from biomass by integration and hybridization with combined cycle gas turbine (CCGT) plants for natural gas, *Energy*, 35 (10) (2010) 4042-4052.
- [169] F. Nemry, A. Uihlein, C.M. Colodel, C. Wetzel, A. Braune, B. Wittstock, I. Hasan, J. Kreißig, N. Gallon, S. Niemeier, Options to reduce the environmental impacts of residential buildings in the European Union—Potential and costs, *Energy and Buildings*, 42 (7) (2010) 976-984.
- [170] L. Hong, H. Lund, B. Möller, The importance of flexible power plant operation for Jiangsu's wind integration, *Energy*, 41 (1) (2012) 499-507.
- [171] K. Sartor, S. Quoilin, P. Dewallef, Simulation and optimization of a CHP biomass plant and district heating network, *Applied Energy*, 130 (2014) 474-483.
- [172] R. Klaassen, M.K. Patel, District heating in the Netherlands today: A techno-economic assessment for NGCC-CHP (Natural Gas Combined Cycle combined heat and power), *Energy*, 54 (2013) 63-73.

- [173] C. Liao, I.S. Ertesvåg, J. Zhao, Energetic and exergetic efficiencies of coal-fired CHP (combined heat and power) plants used in district heating systems of China, *Energy*, 57 (2013) 671-681.
- [174] R. Lund, B.V. Mathiesen, Large combined heat and power plants in sustainable energy systems, *Applied Energy*, 142 (2015) 389-395.
- [175] J. Taillon, R.E. Blanchard, Exergy efficiency graphs for thermal power plants, *Energy*, 88 (2015) 57-66.
- [176] I. Yabanova, A. Keçebaş, Development of ANN model for geothermal district heating system and a novel PID-based control strategy, *Applied Thermal Engineering*, 51 (1) (2013) 908-916.
- [177] A. Keçebaş, I. Yabanova, Thermal monitoring and optimization of geothermal district heating systems using artificial neural network: A case study, *Energy and Buildings*, 50 (2012) 339-346.
- [178] M.A. Alkan, A. Keçebaş, N. Yamankaradeniz, Exergoeconomic analysis of a district heating system for geothermal energy using specific exergy cost method, *Energy*, 60 (2013) 426-434.
- [179] L. Ozgener, Coefficient of performance (COP) analysis of geothermal district heating systems (GDHSs): Salihli GDHS case study, *Renewable and Sustainable Energy Reviews*, 16 (2) (2012) 1330-1334.
- [180] E. Eudp, J.E. Thorsen, J. Bennetsen, O. Juhl, S. Lang, F. Rosenberg, Miscellaneous investigations, *Network*, (May) (2011) 1-97.
- [181] H. Lund, P.A. Østergaard, Sustainable Towns: the case of Frederikshavn aiming at 100 Per cent Renewable Energy, in, 2008.
- [182] P.A. Østergaard, H. Lund, A renewable energy system in Frederikshavn using low-temperature geothermal energy for district heating, *Applied Energy*, 88 (2) (2011) 479-487.
- [183] P.A. Østergaard, B.V. Mathiesen, B. Möller, H. Lund, A renewable energy scenario for Aalborg Municipality based on low-temperature geothermal heat, wind power and biomass, *Energy*, 35 (12) (2010) 4892-4901.
- [184] Z. Oktay, I. Dincer, Exergoeconomic analysis of the Gonen geothermal district heating system for buildings, *Energy and Buildings*, 41 (2) (2009) 154-163.
- [185] L. Ozgener, A. Hepbasli, I. Dincer, Effect of reference state on the performance of energy and exergy evaluation of geothermal district heating systems: Balçova example, *Building and environment*, 41 (6) (2006) 699-709.
- [186] T. Fruergaard, T.H. Christensen, T. Astrup, Energy recovery from waste incineration: Assessing the importance of district heating networks, *Waste Management*, 30 (7) (2010) 1264-1272.
- [187] M. Münster, H. Lund, Comparing Waste-to-Energy technologies by applying energy system analysis, *Waste management*, 30 (7) (2010) 1251-1263.
- [188] H. Cheng, Y. Hu, Municipal solid waste (MSW) as a renewable source of energy: Current and future practices in China, *Bioresource technology*, 101 (11) (2010) 3816-3824.
- [189] M. Münster, H. Lund, Use of waste for heat, electricity and transport—Challenges when performing energy system analysis, *Energy*, 34 (5) (2009) 636-644.
- [190] M. Grosso, A. Motta, L. Rigamonti, Efficiency of energy recovery from waste incineration, in the light of the new Waste Framework Directive, *Waste Management*, 30 (7) (2010) 1238-1243.

- [191] T. Urbaneck, T. Oppelt, B. Platzer, H. Frey, U. Uhlig, T. Göschel, D. Zimmermann, D. Rabe, Solar district heating in East Germany—transformation in a cogeneration dominated city, *Energy Procedia*, 70 (2015) 587-594.
- [192] C. Flynn, K. Sirén, Influence of location and design on the performance of a solar district heating system equipped with borehole seasonal storage, *Renewable Energy*, 81 (2015) 377-388.
- [193] B. Sibbitt, D. McClenahan, R. Djebbar, J. Thornton, B. Wong, J. Carriere, J. Kokko, The performance of a high solar fraction seasonal storage district heating system—five years of operation, *Energy Procedia*, 30 (2012) 856-865.
- [194] E. Rodriguez-Ubinas, L. Ruiz-Valero, S. Vega, J. Neila, Applications of phase change material in highly energy-efficient houses, *Energy and Buildings*, 50 (2012) 49-62.
- [195] D. Trier, Towards solar district heating with more than 70% solar fraction, *Energy Procedia*, 70 (2015) 580-586.
- [196] F.A. Boyaghchi, M. Chavoshi, V. Sabeti, Optimization of a novel combined cooling, heating and power cycle driven by geothermal and solar energies using the water/CuO (copper oxide) nanofluid, *Energy*, 91 (2015) 685-699.
- [197] I.-L. Svensson, J. Jönsson, T. Berntsson, B. Moshfegh, Excess heat from kraft pulp mills: Trade-offs between internal and external use in the case of Sweden—Part 1: Methodology, *Energy Policy*, 36 (11) (2008) 4178-4185.
- [198] S.J. Cooper, G.P. Hammond, J.B. Norman, Potential for use of heat rejected from industry in district heating networks, GB perspective, *Journal of the Energy Institute*, 89 (1) (2016) 57-69.
- [199] E. Dotzauer, Experiences in mid-term planning of district heating systems, *Energy*, 28 (15) (2003) 1545-1555.
- [200] BCS, Waste Heat Recovery: Technology Opportunities in US Industry., in: Inc.: Laurel, MD, USA, U.S. Department of Energy, 2008.
- [201] G. Faninger, Combined solar–biomass district heating in Austria, *Solar Energy*, 69 (6) (2000) 425-435.
- [202] D. Mangold, T. Schmidt, H. Müller-Steinhagen, Seasonal thermal energy storage in Germany, in: *International Conference on Thermal Energy Storage*, Sapporo, Japan, 1997.
- [203] W. Weiss, Solar heating systems-status and recent development, *Renewable Energy World*, 7 (4) (2004) 214-225.
- [204] D. Lindenberger, T. Bruckner, H.-M. Groscurth, R. Kümmel, Optimization of solar district heating systems: seasonal storage, heat pumps, and cogeneration, *Energy*, 25 (7) (2000) 591-608.
- [205] V. Lottner, M. Schulz, E. Hahne, Solar-assisted district heating plants: Status of the German programme Solarthermie-2000, *Solar Energy*, 69 (6) (2000) 449-459.
- [206] D. Bauer, R. Marx, J. Nußbicker-Lux, F. Ochs, W. Heidemann, H. Müller-Steinhagen, German central solar heating plants with seasonal heat storage, *Solar Energy*, 84 (4) (2010) 612-623.
- [207] S. Furbo, J. Fan, B. Perers, W. Kong, D. Trier, N. From, Testing, development and demonstration of large scale solar district heating systems, *Energy Procedia*, 70 (2015) 568-573.
- [208] A. Argiriou, N. Klitsikas, C. Balaras, D. Asimakopoulos, Active solar space heating of residential buildings in northern Hellas—a case study, *Energy and buildings*, 26 (2) (1997) 215-221.

- [209] T. Schmidt, D. Mangold, H. Müller-Steinhagen, Central solar heating plants with seasonal storage in Germany, *Solar energy*, 76 (1) (2004) 165-174.
- [210] J.E. Nielsen, IEA-SHC Task 45: Large solar heating/cooling systems, seasonal storage, heat pumps, *Energy Procedia*, 30 (2012) 849-855.
- [211] Solar Heating and Cooling, Retrieved February 14, 2016 from <http://www.iea-shc.org/>, in, International Energy Agency, 2016.
- [212] N. Le Truong, L. Gustavsson, Solar heating systems in renewable-based district heating, *Energy Procedia*, 61 (2014) 1460-1463.
- [213] J.E. Mock, J.W. Tester, P.M. Wright, Geothermal energy from the earth: its potential impact as an environmentally sustainable resource, *Annual review of Energy and the Environment*, 22 (1) (1997) 305-356.
- [214] B. Rezaie, M.A. Rosen, District heating and cooling: Review of technology and potential enhancements, *Applied Energy*, 93 (2012) 2-10.
- [215] J. Zhang, F. Haghghat, Development of Artificial Neural Network based heat convection algorithm for thermal simulation of large rectangular cross-sectional area Earth-to-Air Heat Exchangers, *Energy and Buildings*, 42 (4) (2010) 435-440.
- [216] A. Hepbasli, L. Ozgener, Development of geothermal energy utilization in Turkey: a review, *Renewable and Sustainable Energy Reviews*, 8 (5) (2004) 433-460.
- [217] H. Esen, M. Inalli, M. Esen, Technoeconomic appraisal of a ground source heat pump system for a heating season in eastern Turkey, *Energy Conversion and Management*, 47 (9) (2006) 1281-1297.
- [218] M. Eriksson, L. Vamling, Future use of heat pumps in Swedish district heating systems: Short-and long-term impact of policy instruments and planned investments, *Applied energy*, 84 (12) (2007) 1240-1257.
- [219] L. Dai, S. Li, L. DuanMu, X. Li, Y. Shang, M. Dong, Experimental performance analysis of a solar assisted ground source heat pump system under different heating operation modes, *Applied Thermal Engineering*, 75 (2015) 325-333.
- [220] H. Esen, M. Inalli, M. Esen, K. Pihtili, Energy and exergy analysis of a ground-coupled heat pump system with two horizontal ground heat exchangers, *Building and environment*, 42 (10) (2007) 3606-3615.
- [221] A. Keçebaş, İ. Yabanova, Economic analysis of exergy efficiency based control strategy for geothermal district heating system, *Energy conversion and management*, 73 (2013) 1-9.
- [222] Z. Oktay, C. Coskun, I. Dincer, Energetic and exergetic performance investigation of the Bigadic geothermal district heating system in Turkey, *Energy and Buildings*, 40 (5) (2008) 702-709.
- [223] Y. Kalinci, A. Hepbasli, I. Tavman, Determination of optimum pipe diameter along with energetic and exergetic evaluation of geothermal district heating systems: modeling and application, *Energy and Buildings*, 40 (5) (2008) 742-755.
- [224] L. Ozgener, A. Hepbasli, I. Dincer, Energy and exergy analysis of geothermal district heating systems: an application, *Building and Environment*, 40 (10) (2005) 1309-1322.
- [225] A.N. Ajah, A.C. Patil, P.M. Herder, J. Grievink, Integrated conceptual design of a robust and reliable waste-heat district heating system, *Applied thermal engineering*, 27 (7) (2007) 1158-1164.
- [226] M. Grosso, L. Rigamonti, Experimental assessment of N₂O emissions from waste incineration: the role of NO_x control technology, in: turning waste into ideas. ISWA/APESB

- 2009 World Congress: Book of abstracts, edited by José MP Vieira, Paulo J. Ramisio, and Ana IE Silveira, 2009.
- [227] M. Waldner, R. Halter, A. Sigg, B. Brosch, H. Gehrman, M. Keunecke, Energy from Waste—Clean, efficient, renewable: Transitions in combustion efficiency and NO_x control, *Waste management*, 33 (2) (2013) 317-326.
- [228] M. Münster, P. Meibom, Long-term affected energy production of waste to energy technologies identified by use of energy system analysis, *Waste Management*, 30 (12) (2010) 2510-2519.
- [229] A. Tabasová, J. Kropáč, V. Kermes, A. Nemet, P. Stehlik, Waste-to-energy technologies: Impact on environment, *Energy*, 44 (1) (2012) 146-155.
- [230] R. Kothari, V. Tyagi, A. Pathak, Waste-to-energy: A way from renewable energy sources to sustainable development, *Renewable and Sustainable Energy Reviews*, 14 (9) (2010) 3164-3170.
- [231] R. Lund, S. Mohammadi, Choice of insulation standard for pipe networks in 4 th generation district heating systems, *Applied Thermal Engineering*, 98 (2016) 256-264.
- [232] H. Lund, S. Werner, R. Wiltshire, S. Svendsen, J.E. Thorsen, F. Hvelplund, B.V. Mathiesen, 4th Generation District Heating (4GDH): Integrating smart thermal grids into future sustainable energy systems, *Energy*, 68 (2014) 1-11.
- [233] H. Li, S. Svendsen, Energy and exergy analysis of low temperature district heating network, *Energy*, 45 (1) (2012) 237-246.
- [234] E. Zvingilaite, T.S. Ommen, B. Elmegaard, M.L. Franck, Low temperature district heating consumer unit with micro heat pump for domestic hot water preparation, in: 13th International Symposium on District Heating and Cooling, 2012, pp. 136-143.
- [235] T. Ommen, W.B. Markussen, B. Elmegaard, Lowering district heating temperatures—Impact to system performance in current and future Danish energy scenarios, *Energy*, 94 (2016) 273-291.
- [236] P.D. Lund, J. Lindgren, J. Mikkola, J. Salpakari, Review of energy system flexibility measures to enable high levels of variable renewable electricity, *Renewable and Sustainable Energy Reviews*, 45 (2015) 785-807.
- [237] H.Í. Tol, S. Svendsen, Effects of boosting the supply temperature on pipe dimensions of low-energy district heating networks: A case study in Gladsaxe, Denmark, *Energy and Buildings*, 88 (2015) 324-334.
- [238] H. Tol, S. Svendsen, Improving the dimensioning of piping networks and network layouts in low-energy district heating systems connected to low-energy buildings: A case study in Roskilde, Denmark, *Energy*, 38 (1) (2012) 276-290.
- [239] O. Paulsen, J. Fan, S. Furbo, J.E. Thorsen, Consumer unit for low energy district heating net, in: The 11th International Symposium on district heating and cooling, 2008.
- [240] J. Xu, R. Wang, Y. Li, A review of available technologies for seasonal thermal energy storage, *Solar Energy*, 103 (2014) 610-638.
- [241] M. Harris, Thermal Energy Storage in Sweden and Denmark, Potentials for Technology Transfer', Lund University IIIIEE, Lund, Sweden, (2011).
- [242] D. Vanhoudt, J. Desmedt, J. Van Bael, N. Robeyn, H. Hoes, An aquifer thermal storage system in a Belgian hospital: Long-term experimental evaluation of energy and cost savings, *Energy and Buildings*, 43 (12) (2011) 3657-3665.

- [243] P. Sørensen, L. Holm, N. Jensen, Water storages, solar thermal and heat pumps in district heating, in: Eurosun—1st international conference on solar heating, cooling and buildings, 2008.
- [244] T. Pauschinger, Solar district heating with seasonal thermal energy storage in germany, Solar District Heating guidelines, p. Fact Sheet, 30 (2011).
- [245] S. Chapuis, M. Bernier, Seasonal storage of solar energy in borehole heat exchangers, (2009).
- [246] J. Dalenbäck, Solar District Heating, in, 2012.
- [247] M. Fisch, M. Guigas, J. Dalenbäck, A review of large-scale solar heating systems in Europe, Solar energy, 63 (6) (1998) 355-366.
- [248] M. Lundh, J.-O. Dalenbäck, Swedish solar heated residential area with seasonal storage in rock: Initial evaluation, Renewable Energy, 33 (4) (2008) 703-711.
- [249] T. Yoon, Y. Ma, C. Rhodes, Individual Heating systems vs. District Heating systems: What will consumers pay for convenience?, Energy Policy, 86 (2015) 73-81.
- [250] A. Di Giorgio, F. Liberati, Near real time load shifting control for residential electricity prosumers under designed and market indexed pricing models, Applied Energy, 128 (2014) 119-132.
- [251] L. Brand, A. Calvén, J. Englund, H. Landersjö, P. Lauenburg, Smart district heating networks—A simulation study of prosumers' impact on technical parameters in distribution networks, Applied Energy, 129 (2014) 39-48.
- [252] B. Di Pietra, F. Zanghirella, G. Puglisi, An evaluation of distributed solar thermal “net metering” in small-scale district heating systems, Energy Procedia, 78 (2015) 1859-1864.
- [253] L. Brange, J. Englund, P. Lauenburg, Prosumers in district heating networks—a Swedish case study, Applied Energy, 164 (2016) 492-500.
- [254] A. Hepbasli, Thermodynamic analysis of a ground-source heat pump system for district heating, International Journal of Energy Research, 29 (7) (2005) 671-687.
- [255] I.B. Hassine, U. Eicker, Impact of load structure variation and solar thermal energy integration on an existing district heating network, Applied Thermal Engineering, 50 (2) (2013) 1437-1446.
- [256] M. Kuosa, M. Aalto, M.E.H. Assad, T. Mäkilä, M. Lampinen, R. Lahdelma, Study of a district heating system with the ring network technology and plate heat exchangers in a consumer substation, Energy and Buildings, 80 (2014) 276-289.
- [257] H. Madsen, K. Sejling, H.T. Søggaard, O.P. Pálsson, On flow and supply temperature control in district heating systems, Heat Recovery Systems and CHP, 14 (6) (1994) 613-620.
- [258] J. Dahm, District Heating Pipelines in the Ground-Simulation Model, in, TRNSYS, 1999.
- [259] W. Wang, X. Cheng, X. Liang, Optimization modeling of district heating networks and calculation by the Newton method, Applied Thermal Engineering, 61 (2) (2013) 163-170.
- [260] I.B. Hassine, U. Eicker, Simulation and optimization of the district heating network in Scharnhäuser Park, in: 2nd European conference on Polygeneration, 2011, pp. 1-18.
- [261] M. Kuosa, K. Kontu, T. Mäkilä, M. Lampinen, R. Lahdelma, Static study of traditional and ring networks and the use of mass flow control in district heating applications, Applied Thermal Engineering, 54 (2) (2013) 450-459.
- [262] H. Pálsson, Methods for planning and operating decentralized combined heat and power plants, RISO-REPORTS-RISO R, (2000).
- [263] C. Arsene, A. Bargiela, D. Al-Dabass, Modelling and simulation of water systems based on loop equations, IJ of Simulation, 5 (1–2) (2004) 61-72.

- [264] H. Chenoweth, C. Crawford, Pipe network analysis, *Journal (American Water Works Association)*, (1974) 55-58.
- [265] R.P. Donachie, Digital program for water network analysis, *Journal of the Hydraulics Division*, 100 (3) (1974) 393-403.
- [266] A.G. Collins, R.L. Johnson, Finite-element method for water-distribution networks, *Journal (American Water Works Association)*, (1975) 385-389.
- [267] M. Cali, R. Borchiellini, District heating networks calculation and optimization, (2002).
- [268] Termis District Energy Optimization Software, available online at: <http://software.schneider-electric.com/products/termis/>, in, Schneider Electric Corporate.
- [269] U. Eicker, POLYCITY–Europäische Energieforschung für Kommunen, *Solares Bauen. Sonderheft der Sonnenenergie*, (2004).
- [270] C. Weber, F. Maréchal, D. Favrat, Design and optimization of district energy systems, *Computer Aided Chemical Engineering*, 24 (2007) 1127-1132.
- [271] D. Buoro, P. Pinamonti, M. Reini, Optimization of a Distributed Cogeneration System with solar district heating, *Applied Energy*, 124 (2014) 298-308.
- [272] I.B. Hassine, U. Eicker, Control aspects of decentralized solar thermal integration into district heating networks, *Energy Procedia*, 48 (2014) 1055-1064.
- [273] T. Nuytten, B. Claessens, K. Paredis, J. Van Bael, D. Six, Flexibility of a combined heat and power system with thermal energy storage for district heating, *Applied energy*, 104 (2013) 583-591.
- [274] A. Hlebnikov, N. Dementjeva, A. Siirde, Optimization of Narva District Heating Network and Analysis of Competitiveness of Oil Shale CHP Building in Narva, *Oil Shale*, 26 (2009).
- [275] S.M. Sanaei, T. Nakata, Optimum design of district heating: Application of a novel methodology for improved design of community scale integrated energy systems, *Energy*, 38 (1) (2012) 190-204.
- [276] F. Haghighat, H. Brohus, J. Rao, Modelling air infiltration due to wind fluctuations—a review, *Building and Environment*, 35 (5) (2000) 377-385.
- [277] F. Haghighat, T. Unny, M. Chandrashekar, Stochastic modeling of transient heat flow through walls, *Journal of solar energy engineering*, 107 (3) (1985) 202-207.
- [278] B. Talebi, F. Haghighat, P.A. Mirzaei, Simplified model to predict the thermal demand profile of districts, *Energy and Buildings*, 145 (2017) 213-225.
- [279] Y. Shimoda, T. Fujii, T. Morikawa, M. Mizuno, Residential end-use energy simulation at city scale, *Building and environment*, 39 (8) (2004) 959-967.
- [280] S. Heiple, D.J. Sailor, Using building energy simulation and geospatial modeling techniques to determine high resolution building sector energy consumption profiles, *Energy and buildings*, 40 (8) (2008) 1426-1436.
- [281] A. Mavrogianni, M. Davies, M. Kolokotroni, I. Hamilton, A GIS-based bottom-up space heating demand model of the London domestic stock, in: *Proceedings of 11th international IBPSA conference, building simulation*, 2009.
- [282] A. Galante, M. Torri, A methodology for the energy performance classification of residential building stock on an urban scale, *Energy and Buildings*, 48 (2012) 211-219.
- [283] P. Caputo, G. Costa, S. Ferrari, A supporting method for defining energy strategies in the building sector at urban scale, *Energy Policy*, 55 (2013) 261-270.
- [284] A. Mastrucci, O. Baume, F. Stazi, U. Leopold, Estimating energy savings for the residential building stock of an entire city: A GIS-based statistical downscaling approach applied to Rotterdam, *Energy and Buildings*, 75 (2014) 358-367.

- [285] M. Aksoezen, M. Daniel, U. Hassler, N. Kohler, Building age as an indicator for energy consumption, *Energy and Buildings*, 87 (2015) 74-86.
- [286] S.K. Firth, K.J. Lomas, A. Wright, Investigating CO2 emission reductions in existing urban housing using a community domestic energy model, in: *Building Simulation*, 2009, pp. 2098-2105.
- [287] I. Ballarini, S.P. Corgnati, V. Corrado, Use of reference buildings to assess the energy saving potentials of the residential building stock: The experience of TABULA project, *Energy Policy*, 68 (2014) 273-284.
- [288] I. Theodoridou, A.M. Papadopoulos, M. Hegger, A typological classification of the Greek residential building stock, *Energy and Buildings*, 43 (10) (2011) 2779-2787.
- [289] A.A. Famuyibo, A. Duffy, P. Strachan, Developing archetypes for domestic dwellings—an Irish case study, *Energy and Buildings*, 50 (2012) 150-157.
- [290] É. Mata, A.S. Kalagasidis, F. Johnsson, Building-stock aggregation through archetype buildings: France, Germany, Spain and the UK, *Building and Environment*, 81 (2014) 270-282.
- [291] P. Tuominen, R. Holopainen, L. Eskola, J. Jokisalo, M. Airaksinen, Calculation method and tool for assessing energy consumption in the building stock, *Building and Environment*, 75 (2014) 153-160.
- [292] L. Filogamo, G. Peri, G. Rizzo, A. Giaccone, On the classification of large residential buildings stocks by sample typologies for energy planning purposes, *Applied Energy*, 135 (2014) 825-835.
- [293] J.A. Fonseca, A. Schlueter, Integrated model for characterization of spatiotemporal building energy consumption patterns in neighborhoods and city districts, *Applied Energy*, 142 (2015) 247-265.
- [294] R. Nouvel, C. Schulte, U. Eicker, D. Pietruschka, V. Coors, CityGML-based 3D city model for energy diagnostics and urban energy policy support, *IBPSA World*, 2013 (2013) 1-7.
- [295] K.M. Powell, A. Sriprasad, W.J. Cole, T.F. Edgar, Heating, cooling, and electrical load forecasting for a large-scale district energy system, *Energy*, 74 (2014) 877-885.
- [296] F.G.H.K.L.G.B. S.Narmasara, SIMPLIFIED BUILDING MODEL OF DISTRICTS in: Fifth German-Austrian IBPSA Conference RWTH Aachen University, 2014, pp. 152-159.
- [297] H. Gadd, S. Werner, Daily heat load variations in Swedish district heating systems, *Applied Energy*, 106 (2013) 47-55.
- [298] M.T. Ali, M. Mokhtar, M. Chiesa, P. Armstrong, A cooling change-point model of community-aggregate electrical load, *Energy and Buildings*, 43 (1) (2011) 28-37.
- [299] Y.-S. Lee, L.-I. Tong, Forecasting energy consumption using a grey model improved by incorporating genetic programming, *Energy Conversion and Management*, 52 (1) (2011) 147-152.
- [300] A. Goia, C. May, G. Fusai, Functional clustering and linear regression for peak load forecasting, *International Journal of Forecasting*, 26 (4) (2010) 700-711.
- [301] A. Mavrogianni, M. Davies, M. Kolokotroni, I. Hamilton, A GIS-based bottom-up space heating demand model of the London domestic stock, in: *Proceedings 11th International IBPSA Conference*, *Building Simulation*, 2009.
- [302] A. Mavrogianni, M. Davies, Z. Chalabi, P. Wilkinson, M. Kolokotroni, J. Milner, Space heating demand and heatwave vulnerability: London domestic stock, *Building Research & Information*, 37 (5-6) (2009) 583-597.

- [303] L. Pedersen, J. Stang, R. Ulseth, Load prediction method for heat and electricity demand in buildings for the purpose of planning for mixed energy distribution systems, *Energy and Buildings*, 40 (7) (2008) 1124-1134.
- [304] H.A. Nielsen, H. Madsen, Modelling the heat consumption in district heating systems using a grey-box approach, *Energy and Buildings*, 38 (1) (2006) 63-71.
- [305] J. Tanimoto, A. Hagishima, H. Sagara, A methodology for peak energy requirement considering actual variation of occupants' behavior schedules, *Building and Environment*, 43 (4) (2008) 610-619.
- [306] U. Eicker., POLYCITY – Europäische Energieforschung für Kommunen., in: S.B.S.d. Sonnenenergie (Ed.), Oktober 2004.
- [307] P. Sehrawat, K. Kensek, Urban energy modeling: GIS as an alternative to BIM, in: *Proceedings of ASHRAE/IBPSA Conference*, 2014.
- [308] F. Koene, L. Bakker, D. Lanceta, S. Narmsara, S. P, I. Fraunhofer, Simplified building model of districts, *Proceedings of BauSIM*, (2014).
- [309] K. Orehounig, G. Mavromatidis, R. Evins, V. Dorer, J. Carmeliet, Predicting energy consumption of a neighborhood using building performance simulations, *Building Simulation and Optimization*, (2014).
- [310] ENVI-met, available online at: <http://www.envi-met.com/introduction/>, in.
- [311] Radiance tool, available online at: <https://www.radiance-online.org/>, in, RADSITE.
- [312] P. Mancarella, MES (multi-energy systems): An overview of concepts and evaluation models, *Energy*, 65 (2014) 1-17.
- [313] I. Van Beuzekom, M. Gibescu, J. Sloopweg, A review of multi-energy system planning and optimization tools for sustainable urban development, in: *PowerTech*, 2015 IEEE Eindhoven, IEEE, 2015, pp. 1-7.
- [314] D. Connolly, H. Lund, B.V. Mathiesen, M. Leahy, A review of computer tools for analysing the integration of renewable energy into various energy systems, *Applied energy*, 87 (4) (2010) 1059-1082.
- [315] Balmorel energy system model, available online at: <http://www.balmorel.com/>, in.
- [316] BCHP Screening Tool User Manual, available online at: https://www1.eere.energy.gov/manufacturing/tech_assistance/pdfs/bchp_user_manual.pdf, %20<http://eber.ed.ornl.gov/bchpsc/>, in, U.S. Department of Energy.
- [317] Biomass Decision Support Tool, available online at: <https://www.carbontrust.com/resources/tools/biomass-decision-support-tool/>, in, Carbon Trust.
- [318] J. Allegrini, K. Orehounig, G. Mavromatidis, F. Ruesch, V. Dorer, R. Evins, A review of modelling approaches and tools for the simulation of district-scale energy systems, *Renewable and Sustainable Energy Reviews*, 52 (2015) 1391-1404.
- [319] Y. Ruan, J. Cao, F. Feng, Z. Li, The role of occupant behavior in low carbon oriented residential community planning: A case study in Qingdao, *Energy and Buildings*, 139 (2017) 385-394.
- [320] D. Robinson, F. Haldi, J. Kämpf, P. Leroux, D. Perez, A. Rasheed, U. Wilke, CitySim: Comprehensive micro-simulation of resource flows for sustainable urban planning, in: *Proc. Building Simulation*, 2009, pp. 1614-1627.
- [321] 2050 Energy Calculator, available online at: <http://2050-calculator-tool.decc.gov.uk/#/home>, in, Department of Energy and Climate Change.

- [322] C. Marnay, M. Stadler, A. Siddiqui, N. DeForest, J. Donadee, P. Bhattacharya, J. Lai, Applications of optimal building energy system selection and operation, Proceedings of the Institution of Mechanical Engineers, Part A: Journal of Power and Energy, 227 (1) (2013) 82-93.
- [323] G. Mendes, C. Ioakimidis, P. Ferrão, On the planning and analysis of Integrated Community Energy Systems: A review and survey of available tools, Renewable and Sustainable Energy Reviews, 15 (9) (2011) 4836-4854.
- [324] K.-O. Vogstad, Utilising the complementary characteristics of wind power and hydropower through coordinated hydro production scheduling using the EMPS model, in: Proc. 2000 Nordic Wind Energy Conference, 2000.
- [325] H. Lund, N. Duić, G. Krajac, M. da Graça Carvalho, Two energy system analysis models: a comparison of methodologies and results, Energy, 32 (6) (2007) 948-954.
- [326] EnergyPlan: Advanced energy system analysis computer model, available online at: <http://www.energyplan.eu/>, in, Department of Development and Planning, Aalborg University.
- [327] V.M. Kiss, Modelling the energy system of Pécs–The first step towards a sustainable city, Energy, 80 (2015) 373-387.
- [328] EnergyPRO, available online at: <https://www.emd.dk/energypro/>, in, EMD International A/S.
- [329] A. Mirakyan, R. De Guio, Integrated energy planning in cities and territories: a review of methods and tools, Renewable and Sustainable Energy Reviews, 22 (2013) 289-297.
- [330] I. Beausoleil-Morrison, M. Kummert, F. Macdonald, R. Jost, T. McDowell, A. Ferguson, Demonstration of the new ESP-r and TRNSYS co-simulator for modelling solar buildings, Energy Procedia, 30 (2012) 505-514.
- [331] ESP-r, available online at: <http://www.esru.strath.ac.uk/Programs/ESP-r.htm>, in, University of Strathclyde.
- [332] L. Drouet, J. Thénié, An Energy-Technology-Environment Model to Assess Urban Sustainable Development Policies-Reference Manual, in, Technical report, Ordecys Technical Reports, 2009.
- [333] ETEM: Energy Technology Environment Model, available online at: <http://apps.ordecys.com/etem>, in, ORDECSYS Applications.
- [334] B.H. Bakken, H.I. Skjelbred, Planning of distributed energy supply to suburb, in: Power Engineering Society General Meeting, 2007. IEEE, IEEE, 2007, pp. 1-8.
- [335] B.H. Bakken, H.I. Skjelbred, O. Wolfgang, eTransport: Investment planning in energy supply systems with multiple energy carriers, Energy, 32 (9) (2007) 1676-1689.
- [336] Generation and Transmission Maximization (GTMax) Model, available online at: <https://ceesa.es.anl.gov/projects/Gtmax.html>, in, Center for Energy, Environmental, and Economic Systems Analysis.
- [337] N. Duić, M. da Graça Carvalho, Increasing renewable energy sources in island energy supply: case study Porto Santo, Renewable and Sustainable Energy Reviews, 8 (4) (2004) 383-399.
- [338] D. Neves, C.A. Silva, S. Connors, Design and implementation of hybrid renewable energy systems on micro-communities: a review on case studies, Renewable and Sustainable Energy Reviews, 31 (2014) 935-946.
- [339] Z. Chmiel, S.C. Bhattacharyya, Analysis of off-grid electricity system at Isle of Eigg (Scotland): Lessons for developing countries, Renewable Energy, 81 (2015) 578-588.

- [340] S. Sinha, S. Chandel, Review of recent trends in optimization techniques for solar photovoltaic–wind based hybrid energy systems, *Renewable and Sustainable Energy Reviews*, 50 (2015) 755-769.
- [341] HOMER Pro, available online at: <https://www.homerenergy.com/products/pro/index.html>, in, HOMER Energy.
- [342] E.I. Baring-Gould, Hybrid2: The hybrid system simulation model, Version 1.0, user manual, in, National Renewable Energy Lab., Golden, CO (United States), 1996.
- [343] A. Mills, S. Al-Hallaj, Simulation of hydrogen-based hybrid systems using Hybrid2, *International Journal of Hydrogen Energy*, 29 (10) (2004) 991-999.
- [344] O. Ulleberg, A. Morkved, Renewable energy and hydrogen system concepts for remote communities in the West Nordic Region: the Nolsoy case study, *Institute for Energy Technology*, 2008.
- [345] S. Phrakonkham, J.-Y. Lechenadec, D. Diallo, C. Marchand, Optimisation Software Tool Review and the Need of Alternative Means for Handling the Problems of Excess Energy and Mini-Grid Configuration: A Case Study from Laos, in: *ASEAN Symposium on Power and Energy Systems*, 2009, pp. pp. 53-58.
- [346] S. Sinha, S. Chandel, Review of software tools for hybrid renewable energy systems, *Renewable and Sustainable Energy Reviews*, 32 (2014) 192-205.
- [347] iHOGA, available online at: <https://ihoga.unizar.es/en/>, in, University of Zaragoza.
- [348] M. Ragwitz, A. Brakhage, L. Kranzl, M. Stadler, C. HUBER, R. Haas, E. Tsioliaridou, J. Pett, P. Gürtler, K. Joergensen, Final report of work phase 6 of the project Invert, Vienna University of Technology:[Accessed November 2013], (2005).
- [349] R. Baetens, R. De Coninck, J. Van Roy, B. Verbruggen, J. Driesen, L. Helsen, D. Saelens, Assessing electrical bottlenecks at feeder level for residential net zero-energy buildings by integrated system simulation, *Applied Energy*, 96 (2012) 74-83.
- [350] R. Baetens, R. De Coninck, F. Jorissen, D. Picard, L. Helsen, D. Saelens, Openideas-an open framework for integrated district energy simulations, in: *Building simulation*, 2015.
- [351] L.G. Swan, V.I. Ugursal, Modeling of end-use energy consumption in the residential sector: A review of modeling techniques, *Renewable and sustainable energy reviews*, 13 (8) (2009) 1819-1835.
- [352] G. Comodi, L. Cioccolanti, M. Gargiulo, Municipal scale scenario: analysis of an Italian seaside town with MarkAL-TIMES, *Energy Policy*, 41 (2012) 303-315.
- [353] M.R.F. Zonooz, Z.M. Nopiah, A.M. Yusof, K. Sopian, A review of MARKAL energy modeling, *European Journal of Scientific Research*, 26 (3) (2009) 352-361.
- [354] F.J. Born, Aiding renewable energy integration through complimentary demand-supply matching, (2001).
- [355] R.D. Prasad, R. Bansal, A. Raturi, Multi-faceted energy planning: A review, *Renewable and Sustainable Energy Reviews*, 38 (2014) 686-699.
- [356] Y. Cai, G.H. Huang, Q. Lin, X. Nie, Q. Tan, An optimization-model-based interactive decision support system for regional energy management systems planning under uncertainty, *Expert Systems with Applications*, 36 (2) (2009) 3470-3482.
- [357] D. Henning, Cost minimization for a local utility through CHP, heat storage and load management, *International Journal of Energy Research*, 22 (8) (1998) 691-713.
- [358] D. Henning, MODEST—an energy-system optimisation model applicable to local utilities and countries, *Energy*, 22 (12) (1997) 1135-1150.
- [359] NEPLAN, Smarter tools, available online at: <https://www.neplan.ch/>, in, Switzerland.

- [360] E. Carpaneto, P. Lazzeroni, M. Repetto, Optimal integration of solar energy in a district heating network, *Renewable Energy*, 75 (2015) 714-721.
- [361] S.W. Hadley, The oak ridge competitive electricity dispatch (orced) model, in, Oak Ridge National Lab.(ORNL), Oak Ridge, TN (United States), 2008.
- [362] F. Bava, S. Furbo, Development and validation of a detailed TRNSYS-Matlab model for large solar collector fields for district heating applications, *Energy*, 135 (2017) 698-708.
- [363] Polysun simulation software, available online at: <http://www.velasolaris.com/>, in, Vela Solaris.
- [364] K. Blok, D. de Jager, C. Hendriks, N. Kouvaritakis, L. Mantzos, Economic evaluation of sectoral emission reduction objectives for climate change—Comparison of topdown and bottom-up analysis of emission reduction opportunities for CO₂ in the European Union, Ecofys, AEA and NTUA, Report for European Commission, DG Environment, Brussels, September, (2001).
- [365] ProDRisk, available online at: <https://www.sintef.no/en/software/prodrisk/>, in, SINTEF.
- [366] T. Lambert, Micropower System Modeling with Homer”, in *Integration of Alternative Sources of Energy* by Felix A. Farret and M. Godoy Simoes, (2006).
- [367] J. Choi, R. Yun, Operation strategy and parametric analysis of a CHP and a tri-generation system for integrated community, *International Journal of Air-Conditioning and Refrigeration*, 23 (01) (2015) 1550001.
- [368] S. Herbergs, H. Lehmann, S. Peter, The computer-modelled simulation of renewable electricity networks, Institute for Sustainable Solutions and Innovations, Aachen, Germany, (2005).
- [369] STREAM - an energy scenario modelling tool, available online at: <http://www.streammodel.org/>, in, Technical University of Denmark.
- [370] S.A. Kalogirou, Use of TRNSYS for modelling and simulation of a hybrid pv–thermal solar system for Cyprus, *Renewable energy*, 23 (2) (2001) 247-260.
- [371] TRNSYS, Transient System Simulation Tool, available online at: <http://www.trnsys.com/>, in.
- [372] R. Dufo-López, I.R. Cristóbal-Monreal, J.M. Yusta, Optimisation of PV-wind-diesel-battery stand-alone systems to minimise cost and maximise human development index and job creation, *Renewable Energy*, 94 (2016) 280-293.
- [373] J.F. Manwell, A. Rogers, G. Hayman, C.T. Avelar, J.G. McGowan, U. Abdulwahid, K. Wu, Hybrid2 - a hybrid system simulation model: theory manual, in, National Renewable Energy Laboratory, 2006.
- [374] Create Your Own Microgrid Control Strategies with HOMER Pro APIs, available online at: <http://microgridnews.com/create-microgrid-control-strategies/>, in: HOMER Microgrid News and Insight, HOMER Energy.
- [375] J.F. Manwell, J.G. McGowan, Lead acid battery storage model for hybrid energy systems, *Solar Energy*, 50 (5) (1993) 399-405.
- [376] H. Energy, HOMER Pro Version 3.7 User Manual, no. August, (2016) 416.
- [377] J.F. Manwell, J.G. McGowan, Extension of the kinetic battery model for wind/hybrid power systems, in: *Proceedings of EWEC*, 1994, pp. 284-289.
- [378] J.F. Manwell, J.G. McGowan, U. Abdulwahid, K. Wu, Improvements to the Hybrid2 battery model, in: *Windpower 2005 Conference*, 2005.
- [379] J. Copetti, F. Chenlo, Lead/acid batteries for photovoltaic applications. Test results and modeling, *Journal of power sources*, 47 (1-2) (1994) 109-118.

- [380] J. Schiffer, D.U. Sauer, H. Bindner, T. Cronin, P. Lundsager, R. Kaiser, Model prediction for ranking lead-acid batteries according to expected lifetime in renewable energy systems and autonomous power-supply systems, *Journal of Power sources*, 168 (1) (2007) 66-78.
- [381] J. Groot, M. Swierczynski, A.I. Stan, S.K. Kær, On the complex ageing characteristics of high-power LiFePO₄/graphite battery cells cycled with high charge and discharge currents, *Journal of Power Sources*, 286 (2015) 475-487.
- [382] S. Saxena, C. Hendricks, M. Pecht, Cycle life testing and modeling of graphite/LiCoO₂ cells under different state of charge ranges, *Journal of Power Sources*, 327 (2016) 394-400.
- [383] J. Wang, P. Liu, J. Hicks-Garner, E. Sherman, S. Soukiazian, M. Verbrugge, H. Tataria, J. Musser, P. Finamore, Cycle-life model for graphite-LiFePO₄ cells, *Journal of Power Sources*, 196 (8) (2011) 3942-3948.
- [384] M. Stadler, Integrated building energy systems design considering storage technologies, Lawrence Berkeley National Laboratory, (2009).
- [385] H. Lund, G. Salgi, The role of compressed air energy storage (CAES) in future sustainable energy systems, *Energy Conversion and Management*, 50 (5) (2009) 1172-1179.
- [386] D. Steen, M. Stadler, G. Cardoso, M. Groissböck, N. DeForest, C. Marnay, Modeling of thermal storage systems in MILP distributed energy resource models, *Applied Energy*, 137 (2015) 782-792.
- [387] I. Ridjan, B.V. Mathiesen, D. Connolly, N. Duić, The feasibility of synthetic fuels in renewable energy systems, *Energy*, 57 (2013) 76-84.
- [388] H. Lin, A. Lai, R. Ullrich, M. Kuca, K. McClelland, J. Shaffer-Gant, S. Pacheco, K. Dalton, W. Watkins, Cots software selection process, in: *Commercial-off-the-Shelf (COTS)-Based Software Systems, 2007. ICCBSS'07. Sixth International IEEE Conference on, IEEE, 2007*, pp. 114-122.
- [389] P. Tuohy, J.M. Kim, A. Samuel, A. Peacock, E. Owens, M. Dissanayake, D. Corne, J. Chaney, L. Bryden, S. Galloway, Orchestration of renewable generation in low energy buildings and districts using energy storage and load shaping, *Energy Procedia*, 78 (2015) 2172-2177.
- [390] P.G. Tuohy, G.B. Murphy, Are current design processes and policies delivering comfortable low carbon buildings?, *Architectural Science Review*, 58 (1) (2015) 39-46.
- [391] P.G. Tuohy, G.B. Murphy, Closing the gap in building performance: learning from BIM benchmark industries, *Architectural Science Review*, 58 (1) (2015) 47-56.
- [392] H. Thieblemont, F. Haghghat, A. Moreau, Thermal energy storage for building load management: application to electrically heated floor, *Applied Sciences*, 6 (7) (2016) 194.
- [393] Canada's energy future: Energy supply and demand projections to 2035, available online at: <https://www.neb-one.gc.ca/nrg/ntgrtd/ft/2013/ppndcs/ppndcs-eng.html>, in, National Energy Board, 2013.
- [394] A.-T. Nguyen, S. Reiter, P. Rigo, A review on simulation-based optimization methods applied to building performance analysis, *Applied Energy*, 113 (2014) 1043-1058.
- [395] S. Attia, M. Hamdy, W. O'Brien, S. Carlucci, Assessing gaps and needs for integrating building performance optimization tools in net zero energy buildings design, *Energy and Buildings*, 60 (2013) 110-124.
- [396] T. Weise, *Global Optimization Algorithms-Theory and Application*, in, 2008.
- [397] N. Sharma, Stochastic techniques used for optimization in solar systems: A review, *Renewable and Sustainable Energy Reviews*, 16 (3) (2012) 1399-1411.
- [398] X.-S. Yang, *Nature-inspired metaheuristic algorithms*, Luniver press, 2010.

- [399] A. Zhou, B.-Y. Qu, H. Li, S.-Z. Zhao, P.N. Suganthan, Q. Zhang, Multiobjective evolutionary algorithms: A survey of the state of the art, *Swarm and Evolutionary Computation*, 1 (1) (2011) 32-49.
- [400] R. Evins, A review of computational optimisation methods applied to sustainable building design, *Renewable and Sustainable Energy Reviews*, 22 (2013) 230-245.
- [401] T. Wakui, R. Yokoyama, K.-i. Shimizu, Suitable operational strategy for power interchange operation using multiple residential SOFC (solid oxide fuel cell) cogeneration systems, *Energy*, 35 (2) (2010) 740-750.
- [402] T. Ikegami, K. Kataoka, Y. Iwafune, K. Ogimoto, Optimal demand controls for a heat pump water heater under different objective functions, in: *Power System Technology (POWERCON), 2012 IEEE International Conference on*, IEEE, 2012, pp. 1-6.
- [403] A. Ashouri, S.S. Fux, M.J. Benz, L. Guzzella, Optimal design and operation of building services using mixed-integer linear programming techniques, *Energy*, 59 (2013) 365-376.
- [404] S. Fazlollahi, G. Becker, F. Maréchal, Multi-objectives, multi-period optimization of district energy systems: II—Daily thermal storage, *Computers & Chemical Engineering*, 71 (2014) 648-662.
- [405] Z. Zhou, P. Liu, Z. Li, W. Ni, An engineering approach to the optimal design of distributed energy systems in China, *Applied Thermal Engineering*, 53 (2) (2013) 387-396.
- [406] T. Wakui, T. Kinoshita, R. Yokoyama, A mixed-integer linear programming approach for cogeneration-based residential energy supply networks with power and heat interchanges, *Energy*, 68 (2014) 29-46.
- [407] A.H. Land, A.G. Doig, An automatic method for solving discrete programming problems, *50 Years of Integer Programming 1958-2008*, (2010) 105-132.
- [408] R.J. Dakin, A tree-search algorithm for mixed integer programming problems, *The computer journal*, 8 (3) (1965) 250-255.
- [409] E.D. Andersen, K.D. Andersen, Presolving in linear programming, *Mathematical Programming*, 71 (2) (1995) 221-245.
- [410] G. Cornuéjols, Valid inequalities for mixed integer linear programs, *Mathematical Programming*, 112 (1) (2008) 3-44.
- [411] A.M. Geoffrion, Generalized benders decomposition, *Journal of optimization theory and applications*, 10 (4) (1972) 237-260.
- [412] M.A. Duran, I.E. Grossmann, An outer-approximation algorithm for a class of mixed-integer nonlinear programs, *Mathematical programming*, 36 (3) (1986) 307-339.
- [413] P. Belotti, C. Kirches, S. Leyffer, J. Linderoth, J. Luedtke, A. Mahajan, Mixed-integer nonlinear optimization, *Acta Numerica*, 22 (2013) 1-131.
- [414] B. Richard, *Dynamic programming*, Princeton University Press, 89 (1957) 92.
- [415] G.P. Henze, R.H. Dodier, M. Krarti, Development of a predictive optimal controller for thermal energy storage systems, *HVAC&R Research*, 3 (3) (1997) 233-264.
- [416] G.P. Henze, Parametric study of a simplified ice storage model operating under conventional and optimal control strategies, in: *ASME Solar 2002: International Solar Energy Conference*, American Society of Mechanical Engineers, 2002, pp. 83-95.
- [417] A.L. Facci, L. Andreassi, S. Ubertini, E. Sciubba, Analysis of the influence of thermal energy storage on the optimal management of a trigeneration plant, *Energy procedia*, 45 (2014) 1295-1304.
- [418] H.-J. Chen, D.W. Wang, S.-L. Chen, Optimization of an ice-storage air conditioning system using dynamic programming method, *Applied thermal engineering*, 25 (2) (2005) 461-472.

- [419] S. Bradley, A. Hax, T. Magnanti, Applied mathematical programming, (1977).
- [420] G.P. Henze, C. Felsmann, G. Knabe, Evaluation of optimal control for active and passive building thermal storage, *International Journal of Thermal Sciences*, 43 (2) (2004) 173-183.
- [421] R.H. Byrd, H.F. Khalfan, R.B. Schnabel, Analysis of a symmetric rank-one trust region method, *SIAM Journal on Optimization*, 6 (4) (1996) 1025-1039.
- [422] E.R. Berndt, B.H. Hall, R.E. Hall, J.A. Hausman, Estimation and inference in nonlinear structural models, in: *Annals of Economic and Social Measurement*, Volume 3, number 4, NBER, 1974, pp. 653-665.
- [423] R. Fletcher, A new approach to variable metric algorithms, *The computer journal*, 13 (3) (1970) 317-322.
- [424] D.F. Shanno, Conditioning of quasi-Newton methods for function minimization, *Mathematics of computation*, 24 (111) (1970) 647-656.
- [425] C.G. Broyden, The convergence of a class of double-rank minimization algorithms 1. General considerations, *IMA Journal of Applied Mathematics*, 6 (1) (1970) 76-90.
- [426] D. Goldfarb, *Mathematics of Computation*, American Mathematical Society, 24 (1970) 23.
- [427] J.A. Nelder, R. Mead, A simplex method for function minimization, *The computer journal*, 7 (4) (1965) 308-313.
- [428] A. Hajiah, M. Krarti, Optimal control of building storage systems using both ice storage and thermal mass–Part I: Simulation environment, *Energy conversion and management*, 64 (2012) 499-508.
- [429] A. Hajiah, M. Krarti, Optimal controls of building storage systems using both ice storage and thermal mass–Part II: Parametric analysis, *Energy conversion and management*, 64 (2012) 509-515.
- [430] N.A. Barricelli, Symbiogenetic evolution processes realized by artificial methods, *Methodos*, 9 (35-36) (1957) 143-182.
- [431] A.S. Fraser, Simulation of genetic systems by automatic digital computers I. Introduction, *Australian Journal of Biological Sciences*, 10 (4) (1957) 484-491.
- [432] J.H. Holland, *Adaptation in natural and artificial systems*, Ann Arbor, MI: University of Michigan Press and, (1992).
- [433] E.S. Barbieri, F. Melino, M. Morini, Influence of the thermal energy storage on the profitability of micro-CHP systems for residential building applications, *Applied Energy*, 97 (2012) 714-722.
- [434] S. Sanaye, A. Shirazi, Thermo-economic optimization of an ice thermal energy storage system for air-conditioning applications, *Energy and Buildings*, 60 (2013) 100-109.
- [435] S. Sanaye, A. Fardad, M. Mostakhdemi, Thermo-economic optimization of an ice thermal storage system for gas turbine inlet cooling, *Energy*, 36 (2) (2011) 1057-1067.
- [436] T. Takahashi, K. Kawai, H. Nakai, Y. Ema, Development of the automatic modeling system for reaction mechanisms using REX+ JGG, *Physics Procedia*, 46 (2013) 239-247.
- [437] Y. Akimoto, J. Sakuma, I. Ono, S. Kobayashi, Adaptation of expansion rate for real-coded crossovers, in: *Proceedings of the 11th Annual conference on Genetic and evolutionary computation*, ACM, 2009, pp. 739-746.
- [438] K. Uemura, N. Nakashima, Y. Nagata, I. Ono, A new real-coded genetic algorithm for implicit constrained black-box function optimization, in: *Evolutionary Computation (CEC), 2013 IEEE Congress on*, IEEE, 2013, pp. 2887-2894.
- [439] R. Eberhart, J. Kennedy, *Particle swarm optimization*, in: *IEEE International Conference on Neural Networks*, Perth, Australia, 1995.

- [440] W.-S. Lee, Y.T. Chen, T.-H. Wu, Optimization for ice-storage air-conditioning system using particle swarm algorithm, *Applied Energy*, 86 (9) (2009) 1589-1595.
- [441] J. Wang, Z.J. Zhai, Y. Jing, C. Zhang, Particle swarm optimization for redundant building cooling heating and power system, *Applied Energy*, 87 (12) (2010) 3668-3679.
- [442] Y. Shi, R. Eberhart, A modified particle swarm optimizer, in: *Evolutionary Computation Proceedings, 1998. IEEE World Congress on Computational Intelligence., The 1998 IEEE International Conference on, IEEE, 1998*, pp. 69-73.
- [443] N. Higashi, H. Iba, Particle swarm optimization with Gaussian mutation, in: *Swarm Intelligence Symposium, 2003. SIS'03. Proceedings of the 2003 IEEE, IEEE, 2003*, pp. 72-79.
- [444] A. Stacey, M. Jancic, I. Grundy, Particle swarm optimization with mutation, in: *Evolutionary Computation, 2003. CEC'03. The 2003 Congress on, IEEE, 2003*, pp. 1425-1430.
- [445] V. Miranda, N. Fonseca, EPSO-best-of-two-worlds meta-heuristic applied to power system problems, in: *Evolutionary Computation, 2002. CEC'02. Proceedings of the 2002 Congress on, IEEE, 2002*, pp. 1080-1085.
- [446] U. Nations, Kyoto protocol to the united nations framework convention on climate change, (1998).
- [447] E. Commission, An EU Energy Security and Solidarity Action Plan, *Second Strategic Energy Review, SEC (2008) 2794SEC (2008), 2795 (2008)*.
- [448] M. Åberg, D. Henning, Optimisation of a Swedish district heating system with reduced heat demand due to energy efficiency measures in residential buildings, *Energy Policy*, 39 (12) (2011) 7839-7852.
- [449] A. Gebremedhin, Introducing district heating in a Norwegian town—potential for reduced local and global emissions, *Applied energy*, 95 (2012) 300-304.
- [450] M. Danestig, A. Gebremehdin, B. Karlsson, Stockholm CHP potential—An opportunity for CO₂ reductions?, *Energy Policy*, 35 (9) (2007) 4650-4660.
- [451] M.F. Torchio, G. Genon, A. Poggio, M. Poggio, Merging of energy and environmental analyses for district heating systems, *Energy*, 34 (3) (2009) 220-227.
- [452] G. Genon, M.F. Torchio, A. Poggio, M. Poggio, Energy and environmental assessment of small district heating systems: Global and local effects in two case-studies, *Energy Conversion and Management*, 50 (3) (2009) 522-529.
- [453] S. Mudgal, L. Lyons, F. Cohen, R. Lyons, D. Fedrigo-Fazio, Energy performance certificates in buildings and their impact on transaction prices and rents in selected EU countries, Paris: European Commission (DG Energy), (2013).
- [454] A. Bagdanavicius, N. Jenkins, G.P. Hammond, Assessment of community energy supply systems using energy, exergy and exergoeconomic analysis, *Energy*, 45 (1) (2012) 247-255.
- [455] H. Torio, D. Schmidt, Development of system concepts for improving the performance of a waste heat district heating network with exergy analysis, *Energy and Buildings*, 42 (10) (2010) 1601-1609.
- [456] C.T. Yucer, A. Hepbasli, Thermodynamic analysis of a building using exergy analysis method, *Energy and Buildings*, 43 (2) (2011) 536-542.
- [457] I.O.f. Standardization, ISO 14040: Environmental Management: Life Cycle Assessment: Principles and Framework, in, 1997.
- [458] C. Scheuer, G.A. Keoleian, P. Reppe, Life cycle energy and environmental performance of a new university building: modeling challenges and design implications, *Energy and buildings*, 35 (10) (2003) 1049-1064.

- [459] F. Calise, Thermoeconomic analysis and optimization of high efficiency solar heating and cooling systems for different Italian school buildings and climates, *Energy and Buildings*, 42 (7) (2010) 992-1003.
- [460] Y. Hang, L. Du, M. Qu, S. Peeta, Multi-objective optimization of integrated solar absorption cooling and heating systems for medium-sized office buildings, *Renewable energy*, 52 (2013) 67-78.
- [461] B.H. Gebreslassie, G. Guillén-Gosálbez, L. Jiménez, D. Boer, Solar assisted absorption cooling cycles for reduction of global warming: A multi-objective optimization approach, *Solar Energy*, 86 (7) (2012) 2083-2094.
- [462] R. Mora, G. Bitsuamlak, M. Horvat, Life-Cycle Performance Framework for Building Sustainability: Integration Beyond Building Science, (2010).
- [463] J.F. Nicol, M.A. Humphreys, Thermal comfort as part of a self-regulating system, (1973).
- [464] EPBD Recast: Directive 2010/31/EU of the European Parliament and of the Council of 19 May 2010 on the energy performance of buildings (recast), in: *Official Journal of the European Union*, 2010.
- [465] T. Boermans, K. Bettgenhäuser, A. Hermelink, S. Schimschar, Cost optimal building performance requirements, Calculation methodology for reporting on national energy performance requirements on the basis of cost optimality within the framework of the EPBD, "European Council for an Energy Efficient Economy, Sweden, (2011).
- [466] E. Commission, Commission Delegated Regulation (EU) No 244/2012 of 16 January 2012 supplementing Directive 2010/31, EU of the European Parliament and of the Council on the energy performance of buildings.
- [467] E.C.f. Standardization, Energy performance of buildings – Economic evaluation procedure for energy systems in buildings, EN 15459:2007, in, 2007.
- [468] S. Nielsen, B. Möller, GIS based analysis of future district heating potential in Denmark, *Energy*, 57 (2013) 458-468.
- [469] M. Ameri, Z. Besharati, Optimal design and operation of district heating and cooling networks with CCHP systems in a residential complex, *Energy and Buildings*, 110 (2016) 135-148.
- [470] D. Wei, A. Chen, B. Sun, C. Zhang, Multi-objective optimal operation and energy coupling analysis of combined cooling and heating system, *Energy*, 98 (2016) 296-307.
- [471] R. Wu, G. Mavromatidis, K. Orehounig, J. Carmeliet, Multiobjective optimisation of energy systems and building envelope retrofit in a residential community, *Applied Energy*, 190 (2017) 634-649.
- [472] P. Penna, A. Prada, F. Cappelletti, A. Gasparella, Multi-objectives optimization of Energy Efficiency Measures in existing buildings, *Energy and Buildings*, 95 (2015) 57-69.
- [473] E. Sciubba, G. Wall, A brief commented history of exergy from the beginnings to 2004, *International Journal of Thermodynamics*, 10 (1) (2007) 1-26.
- [474] C.T. Yucer, A. Hepbasli, Exergoeconomic analysis of a central heating system from the generation stage to the building envelope, *Energy and Buildings*, 47 (2012) 592-599.
- [475] A. Hepbasli, A review on energetic, exergetic and exergoeconomic aspects of geothermal district heating systems (GDHSs), *Energy Conversion and Management*, 51 (10) (2010) 2041-2061.
- [476] H. Lund, B. Möller, B.V. Mathiesen, A. Dyrelund, The role of district heating in future renewable energy systems, *Energy*, 35 (3) (2010) 1381-1390.

- [477] N. Yamankaradeniz, Thermodynamic performance assessments of a district heating system with geothermal by using advanced exergy analysis, *Renewable Energy*, 85 (2016) 965-972.
- [478] H. Gopalakrishnan, D. Kosanovic, Operational planning of combined heat and power plants through genetic algorithms for mixed 0–1 nonlinear programming, *Computers & Operations Research*, 56 (2015) 51-67.
- [479] T. Fang, R. Lahdelma, Genetic optimization of multi-plant heat production in district heating networks, *Applied Energy*, 159 (2015) 610-619.
- [480] A. Molyneaux, G. Leyland, D. Favrat, Environomic multi-objective optimisation of a district heating network considering centralized and decentralized heat pumps, *Energy*, 35 (2) (2010) 751-758.
- [481] S. Fazlollahi, G. Becker, A. Ashouri, F. Maréchal, Multi-objective, multi-period optimization of district energy systems: IV—A case study, *Energy*, 84 (2015) 365-381.
- [482] D. Scardigno, E. Fanelli, A. Viggiano, G. Braccio, V. Magi, A genetic optimization of a hybrid organic Rankine plant for solar and low-grade energy sources, *Energy*, 91 (2015) 807-815.
- [483] V. Baudoui, *Optimisation robuste multiobjectifs par modèles de substitution*, Toulouse, ISAE, 2012.
- [484] A. Rysanek, R. Choudhary, Optimum building energy retrofits under technical and economic uncertainty, *Energy and Buildings*, 57 (2013) 324-337.
- [485] M. Ferrara, E. Fabrizio, J. Virgone, M. Filippi, Energy systems in cost-optimized design of nearly zero-energy buildings, *Automation in Construction*, 70 (2016) 109-127.
- [486] M. Ferrara, J. Virgone, F. Kuznik, M. Filippi, Modelling zero energy buildings: Parametric study for the technical optimization, *Energy Procedia*, 62 (2014) 200-209.
- [487] M. Thalfeldt, E. Pikas, J. Kurnitski, H. Voll, Facade design principles for nearly zero energy buildings in a cold climate, *Energy and Buildings*, 67 (2013) 309-321.
- [488] M. Ferrara, M. Filippi, E. Sirombo, V. Cravino, A simulation-based optimization method for the integrative design of the building envelope, *Energy Procedia*, 78 (2015) 2608-2613.
- [489] R. Azari, Integrated energy and environmental life cycle assessment of office building envelopes, *Energy and Buildings*, 82 (2014) 156-162.
- [490] M. Ferrara, E. Fabrizio, J. Virgone, M. Filippi, A simulation-based optimization method for cost-optimal analysis of nearly Zero Energy Buildings, *Energy and Buildings*, 84 (2014) 442-457.
- [491] M. Ferrara, F. Dabbene, E. Fabrizio, Optimization algorithms supporting the cost optimal analysis: the behavior of PSO, in: *15th International Conference of IBPSA-Building Simulation*, 2017.
- [492] V. Monetti, E. Fabrizio, M. Filippi, Impact of low investment strategies for space heating control: Application of thermostatic radiators valves to an old residential building, *Energy and Buildings*, 95 (2015) 202-210.
- [493] F. Ascione, N. Bianco, R.F. De Masi, C. De Stasio, G.M. Mauro, G.P. Vanoli, Multi-objective optimization of the renewable energy mix for a building, *Applied Thermal Engineering*, 101 (2016) 612-621.
- [494] L. Li, H. Mu, N. Li, M. Li, Economic and environmental optimization for distributed energy resource systems coupled with district energy networks, *Energy*, 109 (2016) 947-960.
- [495] Q. Wu, H. Ren, W. Gao, J. Ren, Multi-objective optimization of a distributed energy network integrated with heating interchange, *Energy*, 109 (2016) 353-364.

- [496] E.D. Mehleri, H. Sarimveis, N.C. Markatos, L.G. Papageorgiou, Optimal design and operation of distributed energy systems: Application to Greek residential sector, *Renewable Energy*, 51 (2013) 331-342.
- [497] Y. Yang, S. Zhang, Y. Xiao, An MILP (mixed integer linear programming) model for optimal design of district-scale distributed energy resource systems, *Energy*, 90 (2015) 1901-1915.
- [498] Z. Zhou, P. Liu, Z. Li, E.N. Pistikopoulos, M.C. Georgiadis, Impacts of equipment off-design characteristics on the optimal design and operation of combined cooling, heating and power systems, *Computers & Chemical Engineering*, 48 (2013) 40-47.
- [499] H. Ren, Q. Wu, W. Gao, W. Zhou, Optimal operation of a grid-connected hybrid PV/fuel cell/battery energy system for residential applications, *Energy*, 113 (2016) 702-712.
- [500] G. Fraisse, Y. Bai, N. Le Pierrès, T. Letz, Comparative study of various optimization criteria for SDHWS and a suggestion for a new global evaluation, *Solar Energy*, 83 (2) (2009) 232-245.
- [501] G. Fraisse, C. Ménézo, K. Johannes, Energy performance of water hybrid PV/T collectors applied to combisystems of Direct Solar Floor type, *Solar Energy*, 81 (11) (2007) 1426-1438.
- [502] Department of Energy: Building Energy Software Tools Directory, available online at: http://apps1.eere.energy.gov/buildings/tools_directory/subjects_sub.cfm, in.
- [503] R. Sen, S.C. Bhattacharyya, Off-grid electricity generation with renewable energy technologies in India: An application of HOMER, *Renewable Energy*, 62 (2014) 388-398.
- [504] N. Ouhajjou, W. Loibl, S. Fenz, A.M. Tjoa, Stakeholder-oriented energy planning support in cities, *Energy Procedia*, 78 (2015) 1841-1846.
- [505] E.D. Mehleri, H. Sarimveis, N.C. Markatos, L.G. Papageorgiou, A mathematical programming approach for optimal design of distributed energy systems at the neighbourhood level, *Energy*, 44 (1) (2012) 96-104.
- [506] C. Bordin, A. Gordini, D. Vigo, An optimization approach for district heating strategic network design, *European Journal of Operational Research*, 252 (1) (2016) 296-307.
- [507] M. Vesterlund, J. Dahl, A method for the simulation and optimization of district heating systems with meshed networks, *Energy Conversion and Management*, 89 (2015) 555-567.
- [508] H. Wang, E. Abdollahi, R. Lahdelma, W. Jiao, Z. Zhou, Modelling and optimization of the smart hybrid renewable energy for communities (SHREC), *Renewable Energy*, 84 (2015) 114-123.
- [509] A.D. Ondeck, T.F. Edgar, M. Baldea, Optimal operation of a residential district-level combined photovoltaic/natural gas power and cooling system, *Applied Energy*, 156 (2015) 593-606.
- [510] T. Falke, S. Krengel, A.-K. Meinerzhagen, A. Schnettler, Multi-objective optimization and simulation model for the design of distributed energy systems, *Applied Energy*, 184 (2016) 1508-1516.
- [511] P. Jie, X. Kong, X. Rong, S. Xie, Selecting the optimum pressure drop per unit length of district heating piping network based on operating strategies, *Applied Energy*, 177 (2016) 341-353.
- [512] J. Wang, Z. Zhou, J. Zhao, A method for the steady-state thermal simulation of district heating systems and model parameters calibration, *Energy Conversion and Management*, 120 (2016) 294-305.
- [513] D. Buoro, M. Casisi, A. De Nardi, P. Pinamonti, M. Reini, Multicriteria optimization of a distributed energy supply system for an industrial area, *Energy*, 58 (2013) 128-137.

- [514] R. Khir, M. Haouari, Optimization models for a single-plant District Cooling System, *European Journal of Operational Research*, 247 (2) (2015) 648-658.
- [515] C. Weber, N. Shah, Optimisation based design of a district energy system for an eco-town in the United Kingdom, *Energy*, 36 (2) (2011) 1292-1308.
- [516] K.M. Powell, J.S. Kim, W.J. Cole, K. Kapoor, J.L. Mojica, J.D. Hedengren, T.F. Edgar, Thermal energy storage to minimize cost and improve efficiency of a polygeneration district energy system in a real-time electricity market, *Energy*, 113 (2016) 52-63.
- [517] M. Rivarolo, A. Cuneo, A. Traverso, A. Massardo, Design optimisation of smart poly-generation energy districts through a model based approach, *Applied Thermal Engineering*, 99 (2016) 291-301.
- [518] S. Barberis, M. Rivarolo, A. Traverso, A. Massardo, Thermo-economic analysis of the energy storage role in a real polygenerative district, *Journal of Energy Storage*, 5 (2016) 187-202.
- [519] J. Pirkandi, M.A. Jokar, M. Sameti, A. Kasaeian, F. Kasaeian, Simulation and multi-objective optimization of a combined heat and power (CHP) system integrated with low-energy buildings, *Journal of Building Engineering*, 5 (2016) 13-23.
- [520] X. Jiang, Z. Jing, Y. Li, Q. Wu, W. Tang, Modelling and operation optimization of an integrated energy based direct district water-heating system, *Energy*, 64 (2014) 375-388.
- [521] I. Karschin, J. Geldermann, Efficient cogeneration and district heating systems in bioenergy villages: an optimization approach, *Journal of Cleaner Production*, 104 (2015) 305-314.
- [522] M. Uris, J.I. Linares, E. Arenas, Size optimization of a biomass-fired cogeneration plant CHP/CCHP (Combined heat and power/Combined heat, cooling and power) based on Organic Rankine Cycle for a district network in Spain, *Energy*, 88 (2015) 935-945.
- [523] N.A. Diangelakis, C. Panos, E.N. Pistikopoulos, Design optimization of an internal combustion engine powered CHP system for residential scale application, *Computational Management Science*, 11 (3) (2014) 237-266.
- [524] U.S. Kim, T.C. Park, L.-H. Kim, Y.K. Yeo, Optimal operation of the integrated district heating system with multiple regional branches, *Korean journal of chemical engineering*, 27 (1) (2010) 6-18.
- [525] T. Maatallah, N. Ghodhbane, S.B. Nasrallah, Assessment viability for hybrid energy system (PV/wind/diesel) with storage in the northernmost city in Africa, Bizerte, Tunisia, *Renewable and Sustainable Energy Reviews*, 59 (2016) 1639-1652.
- [526] W.M. Amutha, V. Rajini, Cost benefit and technical analysis of rural electrification alternatives in southern India using HOMER, *Renewable and Sustainable Energy Reviews*, 62 (2016) 236-246.
- [527] X.-l. Li, L. Duanmu, H.-w. Shu, Optimal design of district heating and cooling pipe network of seawater-source heat pump, *Energy and Buildings*, 42 (1) (2010) 100-104.
- [528] S. Fazlollahi, S.L. Bungener, P. Mandel, G. Becker, F. Maréchal, Multi-objectives, multi-period optimization of district energy systems: I. Selection of typical operating periods, *Computers & Chemical Engineering*, 65 (2014) 54-66.
- [529] M. Albaric, B. Mette, J. Ullman, H. Drück, P. Papillon, Comparison of two different methods for solar combisystems performance testing, in: *Eurosun conference*, 2010.
- [530] M. Albaric, J. Nowag, P. Papillon, Thermal performance evaluation of solar combisystems using a global approach, in: *Eurosun conference*, 2008.

- [531] M.Y. Haller, R. Haberl, T. Persson, C. Bales, P. Kovacs, D. Chèze, P. Papillon, Dynamic whole system testing of combined renewable heating systems—The current state of the art, *Energy and Buildings*, 66 (2013) 667-677.
- [532] K.E. Parsopoulos, Parallel cooperative micro-particle swarm optimization: A master–slave model, *Applied Soft Computing*, 12 (11) (2012) 3552-3579.
- [533] Y. Jiang, X. Li, C. Huang, Automatic calibration a hydrological model using a master–slave swarms shuffling evolution algorithm based on self-adaptive particle swarm optimization, *Expert Systems with Applications*, 40 (2) (2013) 752-757.
- [534] J. Carreras, C. Pozo, D. Boer, G. Guillén-Gosálbez, J.A. Caballero, R. Ruiz-Femenia, L. Jiménez, Systematic approach for the life cycle multi-objective optimization of buildings combining objective reduction and surrogate modeling, *Energy and Buildings*, 130 (2016) 506-518.
- [535] R. Bornatico, J. Hüsey, A. Witzig, L. Guzzella, Surrogate modeling for the fast optimization of energy systems, *Energy*, 57 (2013) 653-662.
- [536] V.M. Zavala, E.M. Constantinescu, T. Krause, M. Anitescu, Weather forecast-based optimization of integrated energy systems, in, Argonne National Lab.(ANL), Argonne, IL (United States), 2009.
- [537] C.J. Hopfe, M.T. Emmerich, R. Marijt, J. Hensen, Robust multi-criteria design optimisation in building design, *Proceedings of Building Simulation and Optimization*, Loughborough, UK, (2012) 118-125.
- [538] E. Tresidder, Y. Zhang, A.I. Forrester, Acceleration of building design optimisation through the use of kriging surrogate models, *Proceedings of building simulation and optimization*, (2012) 1-8.
- [539] L. Van Gelder, P. Das, H. Janssen, S. Roels, Comparative study of metamodelling techniques in building energy simulation: Guidelines for practitioners, *Simulation Modelling Practice and Theory*, 49 (2014) 245-257.
- [540] P. Eguía, E. Granada, J. Alonso, E. Arce, A. Saavedra, Weather datasets generated using kriging techniques to calibrate building thermal simulations with TRNSYS, *Journal of Building Engineering*, 7 (2016) 78-91.
- [541] M. Beccali, M. Cellura, V.L. Brano, A. Marvuglia, Forecasting daily urban electric load profiles using artificial neural networks, *Energy conversion and management*, 45 (18-19) (2004) 2879-2900.
- [542] A. Kanarachos, K. Geramanis, Multivariable control of single zone hydronic heating systems with neural networks, *Energy Conversion and Management*, 39 (13) (1998) 1317-1336.
- [543] L. Magnier, F. Haghghat, Multiobjective optimization of building design using TRNSYS simulations, genetic algorithm, and Artificial Neural Network, *Building and Environment*, 45 (3) (2010) 739-746.
- [544] F. Ascione, N. Bianco, C. De Stasio, G.M. Mauro, G.P. Vanoli, Artificial neural networks to predict energy performance and retrofit scenarios for any member of a building category: A novel approach, *Energy*, 118 (2017) 999-1017.
- [545] S. Boyd, L. Vandenberghe, *Convex optimization*, Cambridge university press, 2004.
- [546] B. Eisenhower, Z. O'Neill, S. Narayanan, V.A. Fonoberov, I. Mezić, A methodology for meta-model based optimization in building energy models, *Energy and Buildings*, 47 (2012) 292-301.
- [547] J.H. Friedman, Multivariate adaptive regression splines, *The annals of statistics*, (1991) 1-67.

- [548] M.-Y. Cheng, M.-T. Cao, Accurately predicting building energy performance using evolutionary multivariate adaptive regression splines, *Applied Soft Computing*, 22 (2014) 178-188.
- [549] A. Kusiak, M. Li, F. Tang, Modeling and optimization of HVAC energy consumption, *Applied Energy*, 87 (10) (2010) 3092-3102.
- [550] J.P. Kleijnen, Regression and Kriging metamodels with their experimental designs in simulation: a review, *European Journal of Operational Research*, 256 (1) (2017) 1-16.
- [551] A. Ramallo-González, D. Coley, Using self-adaptive optimisation methods to perform sequential optimisation for low-energy building design, *Energy and Buildings*, 81 (2014) 18-29.
- [552] Q. Jin, F. Favoino, M. Overend, Design and control optimisation of adaptive insulation systems for office buildings. Part 2: A parametric study for a temperate climate, *Energy*, 127 (2017) 634-649.
- [553] E. Wang, N. Alp, J. Shi, C. Wang, X. Zhang, H. Chen, Multi-criteria building energy performance benchmarking through variable clustering based compromise TOPSIS with objective entropy weighting, *Energy*, 125 (2017) 197-210.
- [554] J. Si, L. Marjanovic-Halburd, F. Nasiri, S. Bell, Assessment of building-integrated green technologies: A review and case study on applications of Multi-Criteria Decision Making (MCDM) method, *Sustainable Cities and Society*, 27 (2016) 106-115.
- [555] F. Roberti, U.F. Oberegger, E. Lucchi, A. Troi, Energy retrofit and conservation of a historic building using multi-objective optimization and an analytic hierarchy process, *Energy and Buildings*, 138 (2017) 1-10.
- [556] E. Mulliner, N. Malys, V. Maliene, Comparative analysis of MCDM methods for the assessment of sustainable housing affordability, *Omega*, 59 (2016) 146-156.
- [557] T. Catalina, J. Virgone, E. Blanco, Multi-source energy systems analysis using a multi-criteria decision aid methodology, *Renewable Energy*, 36 (8) (2011) 2245-2252.
- [558] R. Volvačiovas, Z. Turskis, D. Aviža, R. Mikštienė, Multi-attribute selection of public buildings retrofits strategy, *Procedia Engineering*, 57 (2013) 1236-1241.
- [559] J. Iwaro, A. Mwashia, R.G. Williams, R. Zico, An Integrated Criteria Weighting Framework for the sustainable performance assessment and design of building envelope, *Renewable and Sustainable Energy Reviews*, 29 (2014) 417-434.
- [560] K. Kontu, S. Rinne, V. Olkkonen, R. Lahdelma, P. Salminen, Multicriteria evaluation of heating choices for a new sustainable residential area, *Energy and Buildings*, 93 (2015) 169-179.
- [561] M.S. Cherif, H. Chabchoub, B. Aouni, Quality control system design through the goal programming model and the satisfaction functions, *European Journal of Operational Research*, 186 (3) (2008) 1084-1098.
- [562] N. Kalkan, E. Young, A. Celiktas, Solar thermal air conditioning technology reducing the footprint of solar thermal air conditioning, *Renewable and Sustainable Energy Reviews*, 16 (8) (2012) 6352-6383.
- [563] G. Comodi, A. Giantomassi, M. Severini, S. Squartini, F. Ferracuti, A. Fonti, D.N. Cesarini, M. Morodo, F. Polonara, Multi-apartment residential microgrid with electrical and thermal storage devices: Experimental analysis and simulation of energy management strategies, *Applied Energy*, 137 (2015) 854-866.
- [564] A.J. Marszal, P. Heiselberg, Life cycle cost analysis of a multi-storey residential net zero energy building in Denmark, *Energy*, 36 (9) (2011) 5600-5609.

- [565] S. Cao, A. Hasan, K. Sirén, Analysis and solution for renewable energy load matching for a single-family house, *Energy and buildings*, 65 (2013) 398-411.
- [566] R. Giordano, V. Serra, E. Demaria, A. Duzel, Embodied energy versus operational energy in a nearly zero energy building case study, *Energy Procedia*, 111 (2017) 367-376.
- [567] R. Giordano, V. Serra, E. Tortalla, V. Valentini, C. Aghemo, Embodied energy and operational energy assessment in the framework of nearly zero energy building and building energy rating, *Energy Procedia*, 78 (2015) 3204-3209.
- [568] G.A. Blengini, T. Di Carlo, The changing role of life cycle phases, subsystems and materials in the LCA of low energy buildings, *Energy and buildings*, 42 (6) (2010) 869-880.
- [569] T. Ramesh, R. Prakash, K. Shukla, Life cycle energy analysis of buildings: An overview, *Energy and buildings*, 42 (10) (2010) 1592-1600.
- [570] Y. Chen, S.T. Ng, Factoring in embodied GHG emissions when assessing the environmental performance of building, *Sustainable Cities and Society*, 27 (2016) 244-252.
- [571] R. Fieldson, D. Rai, B. Sodagar, Towards a framework for early estimation of lifecycle carbon footprinting of buildings in the UK, *Construction Information Quarterly*, 11 (2) (2009) 66-75.
- [572] T. Ibn-Mohammed, R. Greenough, S. Taylor, L. Ozawa-Meida, A. Acquaye, Operational vs. embodied emissions in buildings—A review of current trends, *Energy and Buildings*, 66 (2013) 232-245.
- [573] M. Wetter, E. Polak, A convergent optimization method using pattern search algorithms with adaptive precision simulation, *Building services engineering research and technology*, 25 (4) (2004) 327-338.
- [574] S.E. Belcher, J.N. Hacker, D.S. Powell, Constructing design weather data for future climates, *Building Services Engineering Research and Technology*, 26 (1) (2005) 49-61.
- [575] Climate change world weather file generator (CCWorldWeatherGen), available online at <http://www.energy.soton.ac.uk/ccworldweathergen/> in, Sustainability energy research group (SERG), University of Southampton.
- [576] Climate Change 2007: Working Group I: The Physical Science Basis, available online at https://www.ipcc.ch/publications_and_data/ar4/wg1/en/spmsspmpm-projections-of.html, in, Intergovernmental panel on climate change (IPCC).
- [577] T. Constantinescu, Cost optimality discussing methodology and challenges with the recast energy performance of building directive, *The Buildings Performance Institute Europe (BPIE)*, Brussels, (2010).
- [578] B. Atanasiu, S. Attia, Principles for nearly zero-energy buildings: Paving the way for effective implementation of policy requirements, *Principles for nearly Zero-energy Buildings: Paving the way for effective implementation of policy requirements*, (2011) 124.
- [579] C.o.t.E. Communities, Communication from the Commission to the European Parliament, the Council, the European Economic and Social Committee and the Committee of the Regions: Key Competences for a Changing World: Draft 2010 Joint Progress Report of the Council and the Commission on the Implementation of the " Education & Training 2010 Work Programme", Office for Official Publications of the European Communities, 2009.
- [580] W. Eichhammer, T. Fleiter, B. Schlomann, S. Faberi, M. Fioretto, N. Piccioni, S. Lechtenböhmer, A. Schüring, G. Resch, Study on the energy savings potentials in EU member states, candidate countries and EEA countries, (2011).

- [581] P. Tuominen, K. Klobut, A. Tolman, A. Adjei, M. de Best-Waldhober, Energy savings potential in buildings and overcoming market barriers in member states of the European Union, *Energy and Buildings*, 51 (2012) 48-55.
- [582] T. Boermans, J. Grözinger, Economic effects of investing in EE in buildings—the BEAM2 Model, in: Background paper for EC Workshop on Cohesion policy, 2011.
- [583] J. Kurnitski, F. Allard, D. Braham, G. Goeders, P. Heiselberg, L. Jagemar, R. Kosonen, J. Lebrun, L. Mazzarella, J. Railio, How to define nearly net zero energy buildings nZEB, *Rehva Journal*, 48 (3) (2011) 6-12.
- [584] Commission Delegated Regulation (EU) No 244/2012 of 16 January 2012 supplementing Directive 2010/31, EU of the European Parliament and of the Council on the energy performance of buildings.
- [585] B. Atanasiu, I. Kouloumpi, K.E. Thomsen, S. Aggerholm, A. Enseling, T. Loga, K. Witczak, Implementing the cost-optimal methodology in EU countries: Lessons learned from three case studies, (2013).
- [586] V. Machairas, A. Tsangrassoulis, K. Axarli, Algorithms for optimization of building design: A review, *Renewable and Sustainable Energy Reviews*, 31 (2014) 101-112.
- [587] M. Vesterlund, A. Toffolo, J. Dahl, Optimization of multi-source complex district heating network, a case study, *Energy*, 126 (Supplement C) (2017) 53-63.
- [588] H. Wang, H. Wang, Z. Haijian, T. Zhu, Optimization modeling for smart operation of multi-source district heating with distributed variable-speed pumps, *Energy*, 138 (Supplement C) (2017) 1247-1262.
- [589] M. Rivarolo, A. Cuneo, A. Traverso, A.F. Massardo, Design optimisation of smart poly-generation energy districts through a model based approach, *Applied Thermal Engineering*, 99 (Supplement C) (2016) 291-301.
- [590] Z. Zhou, P. Liu, Z. Li, E.N. Pistikopoulos, M.C. Georgiadis, Impacts of equipment off-design characteristics on the optimal design and operation of combined cooling, heating and power systems, *Computers & Chemical Engineering*, 48 (Supplement C) (2013) 40-47.
- [591] P.E. Campana, S.J. Quan, F.I. Robbio, A. Lundblad, Y. Zhang, T. Ma, B. Karlsson, J. Yan, Optimization of a residential district with special consideration on energy and water reliability, *Applied Energy*, 194 (Supplement C) (2017) 751-764.
- [592] G. Schweiger, P.-O. Larsson, F. Magnusson, P. Lauenburg, S. Velut, District heating and cooling systems – Framework for Modelica-based simulation and dynamic optimization, *Energy*, 137 (Supplement C) (2017) 566-578.
- [593] M. Sameti, F. Haghighat, Optimization approaches in district heating and cooling thermal network, *Energy and Buildings*, 140 (Supplement C) (2017) 121-130.
- [594] M. Ameri, Z. Besharati, Optimal design and operation of district heating and cooling networks with CCHP systems in a residential complex, *Energy and Buildings*, 110 (Supplement C) (2016) 135-148.
- [595] S.M. Camporeale, B. Fortunato, M. Torresi, F. Turi, A.M. Pantaleo, A. Pellerano, Part Load Performance and Operating Strategies of a Natural Gas—Biomass Dual Fueled Microturbine for Combined Heat and Power Generation, *Journal of Engineering for Gas Turbines and Power*, 137 (12) (2015) 121401-121401-121413.
- [596] M. Jennings, D. Fisk, N. Shah, Modelling and optimization of retrofitting residential energy systems at the urban scale, *Energy*, 64 (2014) 220-233.

- [597] B. Pickering, S. Ikeda, R. Choudhary, R. Ooka, Comparison of metaheuristic and linear programming models for the purpose of optimising building energy supply operation schedule, in: 12th REHVA World Congress, 2016.
- [598] A. Bischi, L. Taccari, E. Martelli, E. Amaldi, G. Manzolini, P. Silva, S. Campanari, E. Macchi, A detailed MILP optimization model for combined cooling, heat and power system operation planning, *Energy*, 74 (2014) 12-26.
- [599] E. Wilson, Commercial and Residential Hourly Load Profiles for all TMY3 Locations in the United States, O. o. EE a. R. Energy, Ed., ed. US Department of Energy Open Data Catalog: US Department of Energy, (2014).
- [600] Computer Aided Simulation for Cogeneration Assessment & Design III, in, The Society of Heating Air-Conditioning and Sanitary Engineers of Japan (SHASE), Tokyo, 2003.
- [601] Aecom, Spon's Mechanical and Electrical Services Price, CRC Press, 2017.
- [602] J. Keirstead, N. Samsatli, N. Shah, SynCity: an integrated tool kit for urban energy systems modelling, *Energy efficient cities: Assessment tools and benchmarking practices*, 21 (2010).
- [603] A. Omu, R. Choudhary, A. Boies, Distributed energy resource system optimisation using mixed integer linear programming, *Energy Policy*, 61 (2013) 249-266.
- [604] S. Ikeda, R. Ooka, Metaheuristic optimization methods for a comprehensive operating schedule of battery, thermal energy storage, and heat source in a building energy system, *Applied Energy*, 151 (2015) 192-205.
- [605] E.M.L. Beale, J.A. Tomlin, Special facilities in a general mathematical programming system for non-convex problems using ordered sets of variables, *OR*, 69 (447-454) (1970) 99.
- [606] C. D'Ambrosio, A. Lodi, S. Martello, Piecewise linear approximation of functions of two variables in MILP models, *Operations Research Letters*, 38 (1) (2010) 39-46.
- [607] A. Horner, J. Beauchamp, Piecewise-linear approximation of additive synthesis envelopes: a comparison of various methods, *Computer Music Journal*, 20 (2) (1996) 72-95.
- [608] P. Siriruk, Fitting piecewise linear functions using particle swarm optimization, *Suranaree J. Sci. Technol*, 19 (4) (2012) 259-264.
- [609] D. Kraft, A software package for sequential quadratic programming, *Forschungsbericht-Deutsche Forschungs- und Versuchsanstalt für Luft- und Raumfahrt*, (1988).
- [610] S. Ikeda, R. Ooka, Optimal operation of energy systems including energy storage equipment under different connections and electricity prices, *Sustainable Cities and Society*, 21 (2016) 1-11.
- [611] A.C. Celador, M. Odriozola, J. Sala, Implications of the modelling of stratified hot water storage tanks in the simulation of CHP plants, *Energy Conversion and Management*, 52 (8-9) (2011) 3018-3026.
- [612] S. Pfenninger, Dealing with multiple decades of hourly wind and PV time series in energy models: A comparison of methods to reduce time resolution and the planning implications of inter-annual variability, *Applied energy*, 197 (2017) 1-13.
- [613] S. Pfenninger, J. Keirstead, Renewables, nuclear, or fossil fuels? Scenarios for Great Britain's power system considering costs, emissions and energy security, *Applied Energy*, 152 (2015) 83-93.
- [614] IBM ILOG CPLEX Optimisation Studio, in, IBM Corp., Armonk, NY, US, 2016.
- [615] J. Eyer, G. Corey, Energy storage for the electricity grid: Benefits and market potential assessment guide, *Sandia National Laboratories*, 20 (10) (2010) 5.

- [616] J.A. Tenorio, J. Sánchez-Ramos, Á. Ruiz-Pardo, S. Álvarez, L.F. Cabeza, Energy efficiency indicators for assessing construction systems storing renewable energy: application to phase change material-bearing façades, *Energies*, 8 (8) (2015) 8630-8649.
- [617] E. Oh, S.-Y. Son, Electric energy storage design decision method for demand responsive buildings, *Energy and Buildings*, 126 (2016) 139-145.
- [618] P. Komarnicki, P. Lombardi, Z. Styczynski, *Electric Energy Storage Systems: Flexibility Options for Smart Grids*, Springer, 2017.
- [619] H. Ibrahim, A. Ilinca, J. Perron, Comparison and analysis of different energy storage techniques based on their performance index, in: *Electrical Power Conference, 2007. EPC 2007*. IEEE Canada, IEEE, 2007, pp. 393-398.
- [620] G. Robin, M. Ruellan, B. Multon, H.B. Ahmed, P.-Y. Glorennec, Solutions de stockage de l'énergie pour les systèmes de production intermittente d'électricité renouvelable, in: *Colloque SeaTechWeek 2004 (Semaine Internat. des Technologies de la Mer)*, 2004, pp. 9p.
- [621] H. Ibrahim, A. Ilinca, Techno-economic analysis of different energy storage technologies, in: *Energy Storage-Technologies and Applications*, InTech, 2013.
- [622] J.M. Bonneville, *Stockage cinétique*, Institut de recherche de l'Hydro-Québec, 1975.
- [623] E.-D. EPRI, *Handbook of Energy Storage for Transmission and Distribution Applications*, EPRI & US Department of Energy: Palo Alto, CA, (2003).
- [624] Lyon Smart Community - Toshiba, available online at: <http://www.toshiba.fr/generic/smart-community/>, in.
- [625] A. Mavrigiannaki, N. Kampelis, D. Kolokotsa, D. Marchegiani, L. Standardi, D. Isidori, C. Christalli, Development and testing of a micro-grid excess power production forecasting algorithms, *Energy Procedia*, 134 (2017) 654-663.
- [626] A. Arteconi, E. Ciarrocchi, Q. Pan, F. Carducci, G. Comodi, F. Polonara, R. Wang, Thermal energy storage coupled with PV panels for demand side management of industrial building cooling loads, *Applied Energy*, 185 (2017) 1984-1993.
- [627] A. Arteconi, J. Xu, E. Ciarrocchi, L. Paciello, G. Comodi, F. Polonara, R. Wang, Demand side management of a building summer cooling load by means of a thermal energy storage, *Energy Procedia*, 75 (2015) 3277-3283.
- [628] H. Thieblemont, F. Haghghat, A. Moreau, A. Bastani, F. Kuznik, Alternative Method to Integrate Electrically Heated Floor in TRNSYS: Load Management, in: *CLIMA 2016 - 12th REHVA World Congress*.
- [629] K. Cellat, B. Beyhan, H. Paksoy, C. Gungor, Y. Konuklu, O. Karahan, C. Dündar, Passive Thermal Storage in Buildings with a Novel Composite Panel with Microencapsulated Phase Change Material, in: *Greenstock 2015, 13th International conference on Energy Storage*, Beijing, China, 2015.
- [630] Sun and Wind Energy, available online at: <http://www.sunwindenergy.com/1+2/2013>, in.
- [631] G. Fraisse, M. Pailha, New concept of Integrated Collector Storage using phase change material and thermosyphon heat pipes, in: *EUROSUN*, Palma (Mallorca), 2016.
- [632] M. Tasset, M. Pailha, G. Fraisse, D. Cloet, Experimental study of a solar collector integrating phase change materials and heat pipes, in: *JNES*, Perpignan, France.
- [633] M. Pailha, M. Tasset, G. Fraisse, D. Cloet, Prototype of integrated collector storage using phase change material and thermosyphon heat pipes, in: *Solar World Congress*, Abu Dhabi, 2017.

- [634] £43m for low-carbon infrastructure projects, available online at: <https://news.gov.scot/news/gbp-43m-for-low-carbon-infrastructure-projects>, in, Scottish Government.
- [635] West Whitlawburn Co-operative Ltd, available online at <http://www.wwhc.org.uk/>, in, Scotland.
- [636] The UK's first water source heat pump for district heating unveiled at EuroHeat & Power Congress, available online at: <http://www.neatpumps.com/news/the-uks-first-water-source-heat-pump-for-district-heating-unveiled-at-euroheat-power-congress.aspx>, in, Star Renewable Energy.
- [637] CIBSE AM15 biomass heating, in, CIBSE, 2014.
- [638] Company homepage, available online at: <http://skk.jp/>, in, Sanken Environmental Engineering.
- [639] R. Sharma, P. Ganesan, V. Tyagi, T. Mahlia, Accelerated thermal cycle and chemical stability testing of polyethylene glycol (PEG) 6000 for solar thermal energy storage, Solar Energy Materials and Solar Cells, 147 (2016) 235-239.